The geochemistry of the Atlanta Lobe of the Idaho Batholith in the western United States, Cordillera

Thesis

The Geochemistry of the Atlanta Lobe of the Idaho Batholith in the Western United States Cordillera

A thesis submitted for the Degree of Doctor of Philosophy

by

Christopher Brian Clarke B.A. *OXON.*

Department of Earth Sciences

The Open University

May, 1990

ABSTRACT

Isotope, major and trace element studies of the Late Cretaceous and Tertiary granitoids of the Atlanta lobe of the Idaho batholith in the western United States cordillera have led to new insights on the nature of the lower crust and have placed constraints on granitoid magma genesis during a transition from a compressional to an extensional regime.

The Cretaceous (~90-75Ma), calc-alkaline, tonalitic to granitic, metaluminous to peraluminous granitoids are characterised by high LILE/HFSE and LREE/HREE ratios, low Rb/Sr and Sm/Nd ratios and ε_{Nd} and ε_{Sr} of -4.9 to -11.6 and 35 to 120 respectively. Only the tonalites and silicic granodiorites to granites underwent significant degrees of within suite fractional crystallization, the former dominated by hornblende and plagioclase and the latter by alkali feldspar, quartz, plagioclase and biotite. The Cretaceous magmas have been successfully modelled as 25%-45% partial melts of tonalitic to gabbroic, biotite, garnet and hornblende-bearing meta-igneous sources. Thermal conditions suggest that anatexis was induced by both Sevier tectonic crustal thickening and ponding of subduction-related basalts at the base of the crust. The inferred source regions were relatively trace element enriched, with high Sr and LILE/HFSE ratios; this volcanic-arc signature was presumably attained during generation of the source region by subduction related processes. Little intra-crustal reprocessing of the source region can have occurred, but unsupported Sr and Pb isotope ratios suggest that minor depletion of Rb, U, and Th by high-grade metamorphism may have occurred. Small differences between the trace element compositions of the Cretaceous intrusive phases are thought to reflect minor heterogeneities within the source regions. Small volume leucogranites with distintive REE and isotope compositions are interpreted as upper crustal, partial melts of Archaean and Proterozoic metasediments.

Inferred garnet-bearing granulitic residues after partial melting cause Sm/Nd ratios to be significantly reduced from source to magma, but correcting for this produces T_{DM}^{Nd} in agreement with Pb-Pb ages of ~1.5Ga. This mid-Proterozoic age of the lower crust indicates that major age province boundaries with the Wyoming and Snake River Plain Archaean provinces exist to the east and close to the southern margin of the Atlanta lobe.

The Tertiary bimodal granitoids consist of a 55Ma-47Ma, metaluminous dioritic suite characterised by high Sr and Ba, low LILE and moderate LREE/HREE ratios, and a 48Ma-42Ma, peraluminous granitic suite are characterised by lower Ba and Sr abundances and LREE/HREE ratios, higher HFSE and Rb, U and Th abundances, with large LILE variation and minor to large negative Eu/Eu* anomalies. ε_{Nd} and ε_{Sr} of -4 to -11.8 and 25 to 65 respectively, in the dioritic suite, systematically vary with major and trace elements and are interpreted to reflect AFC processes, with dioritic initial magmas derived from the sub-continental mantle lithosphere and high proportions of old continental crust assimilants. The

Tertiary granitic suite have higher ε_{Sr} and lower ε_{Nd} and Pb isotope ratios than the Cretaceous granitoids, but similar mid-Proterozoic T_{DM}^{Nd}. They are modelled as anatectic melts at the base of a thinned, isotopically distinct region of a trace element enriched lower crust similar to the source of the Cretaceous granitoids to leave a mafic granulitic residue without garnet leading to distinctly higher Y and Yb abundances in the Tertiary granitoids.

The Cretaceous to Tertiary transition from lower crustal granitoids generated in a tectonically thickened crust with ponding of subduction-related basalts, to generation of granitoids in an attenuated lithosphere, due to rapid uplift, thermal and gravitational relaxation and extension in the latest Cretaceous, is reflected in the change to increasing HREE abundances, the incorporation of mantle-derived material and the epizonal levels of emplacement and association with the coeval Challis volcanics.

ACKNOWLEDGEMENTS

I am grateful and indebted to many people, who in many ways have made this project possible and I am sure they need no reminding who they are, but in particular I would like to thank the following people.

Prof. Chris Hawkesworth and Prof. Bill Leeman who originated this project are thanked for their untold advice without which, to be perfectly candid and quite frank I may not have had a barking clue. Bill Leeman provided serious geologic and logistic help in the field, a matching funds grant and together with Connie and 'Little' Chris are thanked for good old U.S. hospitality. Chris Hawkesworth has 'played a key role' in all aspects of this project, has been a constant source of inspiration, shown extreme patience, understanding and intuition and provided 'notional new insights' on the science in this work.

In the field Ron Worl of the U.S. Geological Survey provided a gassed up jeep, a field H.Q., many maps, mailing labels and introduction to many 'Friends of the Idaho batholith' on the 1987 'Hailey Troops' field trip. Larry Snee and John Sutter, the 'sports fans' for sampling techniques and 50 mph mineral identification. Reed Lewis for passing on long and painstakingly acquired knowledge of the Atlanta lobe granites, and his even more ancient sour-dough pancake recipe. Brian 'you winging Brit' Mahoney provided companionship, vital potions and top bar-room sharking tips. Norio Honjo 'Man' for the record breaking Texas to Idaho return express and for paying the speeding fines.

At the Open University, Peter van Calsteren, Mabs Kunka and the rest of the isotope lab'. crew provided invaluable technical assistance, advice and encouraged the consumption of copious quantities of wine and cakes. Janet Hergt ran several vital samples in her own valuable time. D. Wright (Mr.), Drs. Andy Tindle and D. Ormerod, Eira Parker and Janet Dryden provided computing and Mac advice. Ian Chaplain, Brian 'Oi' Ellis and Michelle made excellent, 'short order' thin sections and provided crushing facilities with which I made full use. Dr. Nick 'D.D.' Rogers performed... and kindly carried out INAA analyses. Dr Tim Brewer carried out XRF analyses at Nottingham University and together with the S238 and S236 summer school course teams are thanked for the sober introduction to personal tutorial skills. John Holbrook and the O.U. overseas travel committee arranged funding for conferences and field work, and a D.S extension grant is gratefully acknowledged. For academic discussion the whole O.U. department of Earth Sciences should be thanked for providing such an erudite assembly and academic hot bed of stimulation, as of course should Jimmy Hill.

Among the real players at the O.U. who have constantly posed the proverbial question, "Wanna get loaded?", the following should be mentioned: Dave 'Chukka' Jackson for the

free and convenient taxi service; T. 'Earman' Elliott for spicing it up large top tips; Jon 'Giraffeman' Davis for L.A. driving skills and contraceptive hints; Steve 'Mad Dog' Hallinan for assuring me of my own sanity (together with the Samaritans); 'Big Jim' Miller and 'Big' Shan de Silva for having been there, seen that, done that...; Sian 'Citronella' May for rescuing me from the threshold of a real job; Matty Watkinson (Dr.) for morality; Nick 'Broughie' Brough for pessimism; Sarah 'Fergie' Everett and the Old Vicarage for several stone grooves, Franchi (Ian) and the 'footie boys' for footie; Richard 'Lord-Melchett' for not handling his beers; Janet 'Madge' Hergt for breakfast (fnarr, fnarr); Mabs for Cleopatra hair and foster mothering; Simon 'Zigi, Gizmo, Niger, Gear-Freak' Inger for having more nick names than me; Seife 'Don`t take no shit my man' Berhe for jive; Paul 'Gamo' and Sasha for the Derick Battey award, Andrew 'Jail-Bird' Morse for beers; Fiona 'Big Fifi' McGibbon for photo albums and gardening tips; Nick 'Dick Dodger' Rogers for cocktail advice and rumours; the 'Biology Greboes' for scape-goats.

These are the people at the O.U., now what about my other friends? -they are too numerous to mention individually, but I graciously acknowledge my debt to you and promise to buy you are a beer when I get a proper job.

Finally my parents, brothers and families are sincerely thanked for encouragement, financial support, patience and an infectious belief of my ability to succeed in my chosen work. I dedicate this work to you all, but particularly my mother whom I hope would have been proud.

CONTENTS

LIST OF FIGURES

Chapter 3 Field study and petrography

Chapter 4 Major and trace element geochemistry

Chapter 5 Isotope geochemistry

LIST OF TABLES

Appendix A

LIST OF PLATES

Chapter 3

CHAPTER 1

Introduction

This thesis is mainly concerned with gaining an understanding of the processes of intra-crustal differentiation by the geochemical study of selected granitoids. The continental crust is generated by a flux of material from the mantle into the crust, and it differentiates by intra-crustal processes whereby material is selectively redistributed by element fluxes from the lower to upper crust and reworking of both these crustal reservoirs.

Reprocessing of the upper crust can occur by sedimentary, magmatic and metamorphic processes, whereas the lower crust is largely unaffected by sedimentary processes and thus may be characterised by an absence of the effects of such processes.

During orogenic events or prolonged periods of orogenesis, the above processes occur as a response to what is often intense tectonic and thermal activity, the topographic manifestations of which were first recognised by early workers as mountain building events (Holmes, 1964). However, the associated sedimentary, magmatic and metamorphic processes had significant effects on the geochemical evolution of the crust. In order to understand quantitatively the effects of orogenic events throughout the geological record, detailed study of the products of these processes, namely the rocks, must be undertaken.

Since granitoids are common products of magmatism affecting the continental crust, there is a two-fold purpose for obtaining an understanding of their petrogenesis. The first is to gauge the effects of granitoid magmatism on evolution of the continental crust and secondly as a means of sampling unexposed levels of the crust and monitoring the combined effects of magmatic, sedimentary and metamorphic processes and addition of new material from the mantle to the crust in these source regions.

This thesis seeks to model the petrogenesis of the Idaho batholith granitoids and use the findings to constrain both the processes and effects of granitoid magmatism on evolution of the continental crust and to document, specifically, the evolution of the continental crust in the northwestern United States. The aim of this chapter is to outline the reasons for studying the Idaho batholith and to define the major objectives of the thesis. In addition the field area

will be located and put into context with the geological, geographical and demographic elements of the western United States cordillera of the present day. The detailed geological development of the Idaho batholith region is dealt with in chapter 2.

1.1 Location of the study area

1.1.1 Circum-Pacific magmatism

A near continuous ring of oceanic and continental magmatic arcs surround the Pacific ocean and are coincident, or were once coincident, with destructive plate margins where the various oceanic plates of the Pacific ocean floor underwent subduction (figure 1.1). Granitoids are particularly a feature of the continental arcs, but are also present in the oceanic arcs.

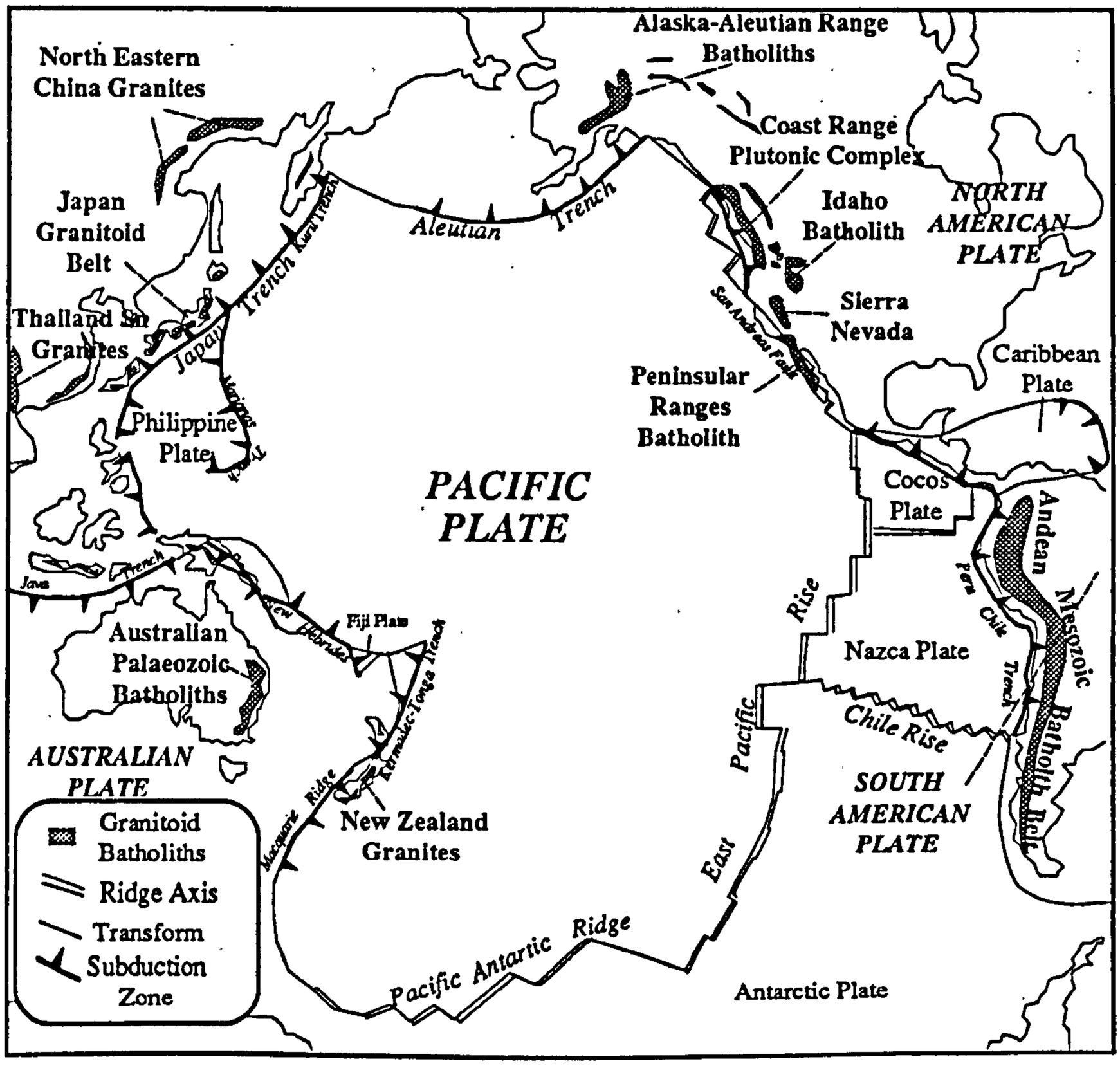

Figure 1.1 Map of the circum-Pacific magmatic arcs highlighting those with significant amounts of granitoid intrusions and showing the major plate margins.

Oceanic island arcs which have significant proportions of granitoids include the Aleutians, New Zealand, the Japan arc and the Thailand-Malaysia arcs. The continental arcs, such as the Andes and the great North American Mesozoic batholiths were generated where subduction occurred beneath a continental margin (figure 1.2). The Idaho batholith is one of the circum-Pacific Mesozoic batholiths of the western United States cordillera, of which other examples include the Sierra Nevada, the Peninsular Ranges, the Coast Ranges and the Alaska-Aleutian batholiths (figure 1.2).

1.1.2 The western United States Cordillera

The western United States is a mosaic of tectonically distinct regions which boast a diverse range of igneous rock types. The major elements of the western United States (figure 1.2) have resulted from a series of compressional and extensional continental margin orogenic events from the mid-Proterozoic until the present day.

The Colorado Plateau is an area of thick, stable, flat lying, undeformed continental crust in the southern Cordilleran Interior (figure 1.2). It is underlain by Proterozoic basement 1.7Ga-1.8Ga old (Bennett and DePaolo, 1987) and has been undergoing rapid isostatic uplift since the Miocene (Oldow et al., 1989).

The Basin and Range tectonic province, extends from the Great Basin in the north to the Sonoran Desert and Rio Grande Rift in the south, and surrounds the Colorado Plateau (figure 1.2). In contrast it has undergone large amounts of extension during the Miocene (Oldow et al.,1989) thought to be the result of post-orogenic thermal and tectonic relaxation of crust previously tectonically thickened in the Mesozoic and Early Tertiary (Gaudemer et al., 1988).

Other areas of extension are the core complexes of the Omenica-Okanogan crystalline belt in the northern cordillera which extended in early Tertiary times (58Ma-52Ma, Oldow,1989). Less extreme, but coeval extension migrated as far south as the Idaho batholith region and it may represent an early episode of extension related to the Basin and Range (Bennett, 1986).

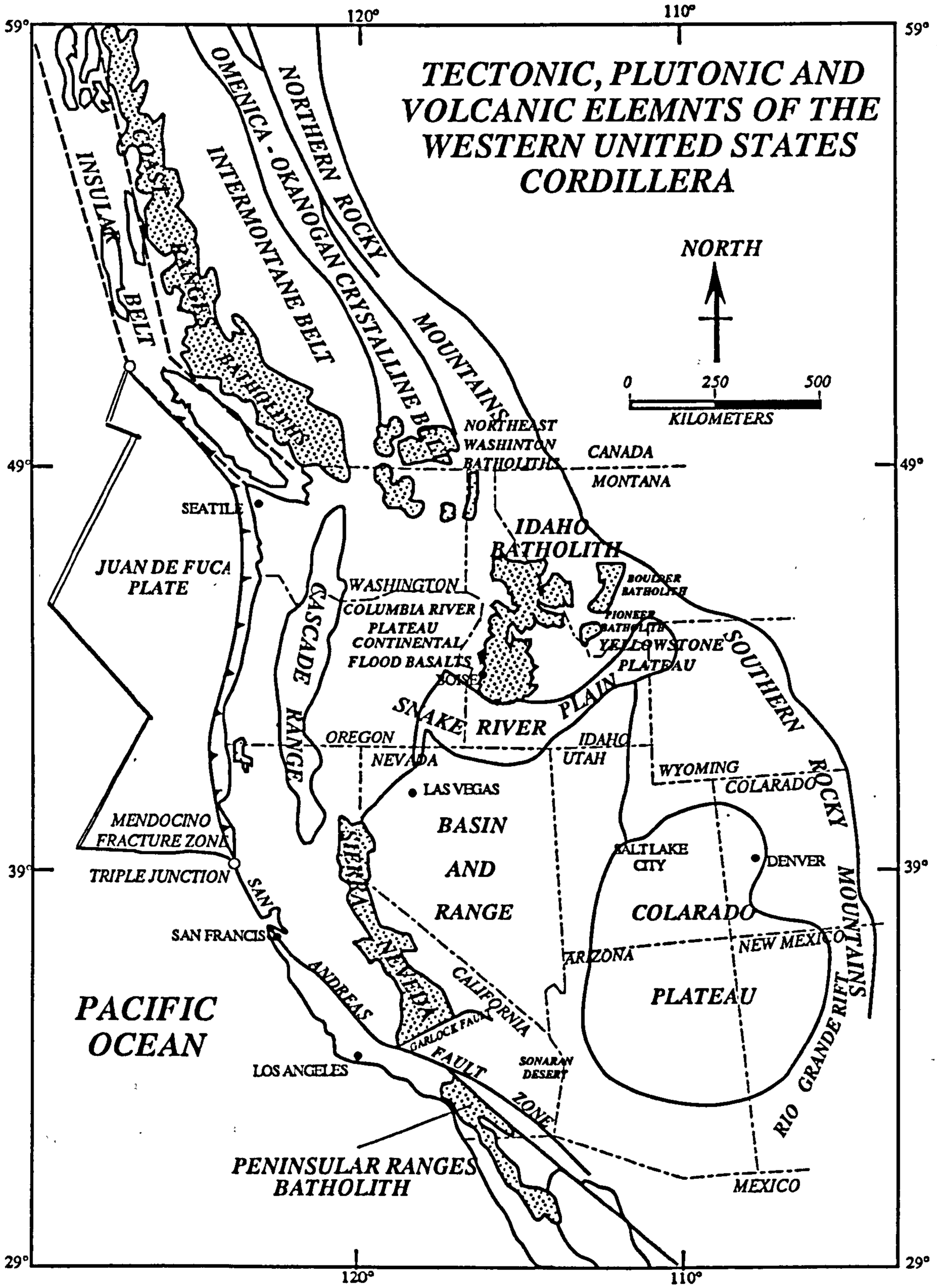

Figure 1.2 Map of the western United States cordillera showing the major tectonic and igneous provinces.

The Northern Rocky Mountains or Sevier Belt marks the eastern limit of the northern cordillera (figure 1.2) and is a classic example of upper crustal, 'thin-skinned' thrust tectonics formed as a result of the Sevier orogeny compressional events (Oldow et al.,1989). The deformation is controlled by stratigraphically defined décollement levels within the sedimentary cover. Such deformation results in a significant amount of crustal thickening, and it almost certainly extended further south into the Basin and Range province where it has been obscured by later extensional events.

The Southern Rocky Mountains of Wyoming, Colorado, Utah and New Mexico mark the eastern limit of the central and southern cordillera (figure 1.2) and in contrast with the Northern Rocky Mountains are the result of 'thick-skinned' or basement thrust tectonics. In essence they are basement uplifts on medium angle reverse faults which are best explained by intra-crustal decoupling at middle to lower crustal levels (Oldow et al., 1989). They occurred under the influence of the Laramide orogeny in the Late Cretaceous and Eocene which was likely to have been a response to the shallow subduction of the Farallon Plate beneath the North American continent, but the details are not fully understood (Lipman et al., 1971; Bird, 1984 and Oldow et al., 1989). A significant amount of crustal thickening occurred during this event and granitoid magmatism has been attributed to partial melting in response to increased thicknesses of crustal material with high heat producing element contents (Patiño Douce et al., 1990).

The southwestern United States cordillera is dominated by strike-slip fault motions, such as on the San Andreas fault (figure 1.2) as a result of the East Pacific Rise being consumed beneath the North American continent and the migration of the Mendocino and Rivera triple junctions north and south along a transform fault (Lipman, 1971 and figure 2.12).

The Cascades arc of andesitic, calc-alkaline volcanoes is presently active from northern California (Mount Lassen) to the Canadian border (figure 1.2). 17 Ma ago it was 100km wide and extended south to Mexico, but the southern margin of activity has migrated north

with the Mendocino triple junction (compare figures 1.2 and 2.12) to its present day position.

The Columbia River Plateau of Washington and Oregon is covered by extensive, sub-alkaline, continental flood basalts (figure 1.2) erupted rapidly over the short period of time 17Ma -14Ma (Carlson and Hart, 1987). The flows emanated from fissures associated with large, north-south orientated dyke swarms, travelled large distances and represent a significant addition to the crust in this region.

The Snake River Plain-Yellowstone Plateau province developed as a large bimodal basaltic-rhyolitic volcanic centre near the Oregon, Idaho and Nevada state borders (figure 1.2), and it has since migrated to its present position on the Yellowstone Plateau (Armstrong et al., 1975). This has been interpreted as the result of the North American continent migrating over the central plume of a hot-spot (Morgan, 1972), but following recent work on the size of the heads of hot-spots or plumes (White and McKenzie, 1989) it may also be due to propagation of a rift or fracture (Leeman 1972).

The major cordilleran granitoid batholiths of western North America may be divided into two groups; the Coastal batholiths and the batholiths of the Cordilleran Interior. The Coastal batholiths are large, calc-alkaline bodies and include the Peninsular Ranges, the Sierra Nevada, the Coast Range and the Alaska-Aleutian Range (figure 1.2). The batholiths of the Cordilleran Interior include the enormous Idaho batholith, but the generally small Boulder, Pioneer, Northeast Washington and Ruby Mountains batholiths are more typical. Although both suites of rocks are related to subduction, a fundamental difference between the groups is that the Inner Cordilleran batholiths are intruded into crust underlain by basement of at least Proterozoic age, whereas the Coastal batholiths were intruded into Palaeozoic to Mesozoic accreted island arc terranes and associated metasedimentary and meta-volcanic sequences. The batholiths of both groups were intruded between the Late Jurassic to the Eocene, but in general most of the Interior Cordilleran granitoids are slightly younger (Roddick, 1983). Compositions typically range from tonalite to granite, but more mafic

types occur in the Coastal batholiths and leucogranites and peraluminous, muscovite-bearing granites are more common in the Inner Cordillera.

The general features and characteristics of the granitoid batholiths of the Cordilleran Interior and those peculiar to the Idaho batholith are:

i) they lie in an area of Mesozoic crustal thickening (Patiño Douce et al., 1990);

ii) they probably contain high proportions of ancient crustal material (up to 100%);

iii) they are influenced by subduction, but not continental collision (the Idaho batholith may be a special case, since there was a transpressional island arc accretion event on the margins of the batholith just prior to intrusion; Lund and Snee, 1988);

iv) plutonism occurred after crustal contraction and thickening;

v) the volume of the batholiths is small compared with the Coastal batholiths except in the case of the Idaho batholith.

vi) they have only a small proportion of mantle-derived volcanic or dyke rocks associated with them (Patiño Douce et al., 1990), but again the Idaho batholith may be an exception as Hyndman (1988) argued that 50% of the northern lobe of the Idaho batholith was mantle-derived material. There is, however, no such evidence for mantle-derived material in the southern lobe of the batholith which is the focus of this study.

1.1.3 The Idaho batholith region

The northwestern Cordilleran Interior is dominated by the large, 40000km^2, Late Cretaceous, Idaho batholith, which extends 480km north-south, is approximately 100km wide and is located 600km east of the Pacific coast in Idaho and western Montana (figures 1.2 and 1.3). This section is concerned with outlining the major geographical and geological features of the area rather than with a detailed geological description which follows in chapter 2. The map in figure 1.3 shows the major geological features of the region and the following points may be highlighted.

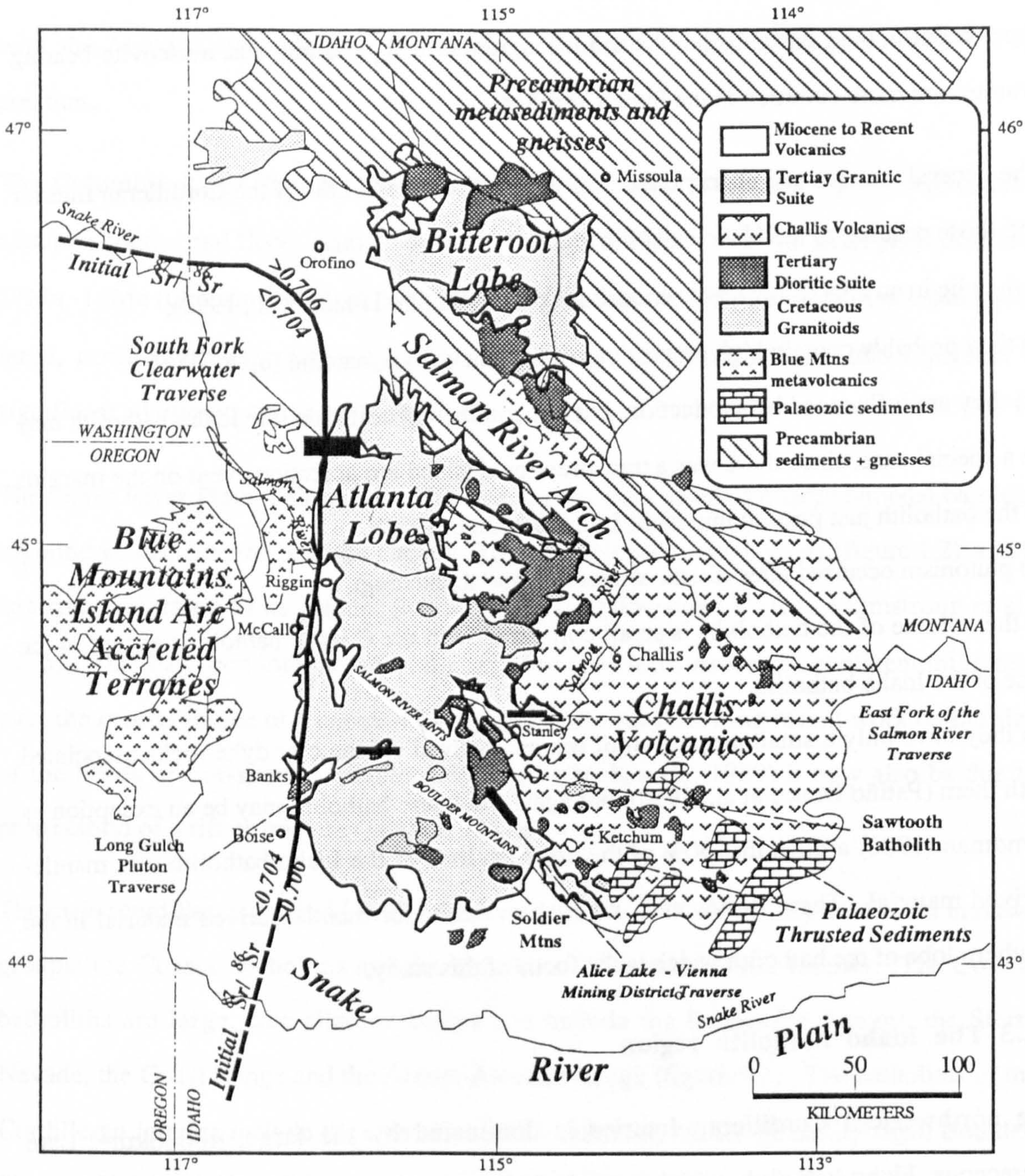

Figure 1.3 Map of the Idaho batholith region defining the names of the geological and geographical features of the field area. Black boxes represent are sample collection traverses.

i) The Idaho batholith is split into the northern Bitteroot lobe and the southern Atlanta lobe, although Hyndman et al. (1989) prefer the terms Bitteroot batholith and Atlanta batholith. The former notation is adopted here and it is only the Atlanta lobe which has been studied in this thesis.

ii) The two lobes are separated by Precambrian metasediments and orthogneisses of the Salmon River Arch (Armstrong, 1975). Similar Belt/Purcell and Salmon River Group

metasediments (see figure 2.6) outcrop to the north of the Bitteroot lobe in the Belt basin (figure 1.3).

iii) To the west of the batholith lies the Blue Mountain accreted island arc terranes of Permian -Jurassic age (Vallier and Brooks, 1987) comprising metavolcanic and volcaniclastics (figure 1.3). The accreted terrane consists of the tectonically juxtaposed Huntington arc, the Wallowa/Seven Devils arc, the Riggins group and two metasedimentary volcaniclastic sequences (Manduca, 1988).

iv) The Columbia River Plateau flood basalts also lie to the west of the batholith and obscure many of the intrusive contacts along the western margin of the Atlanta lobe.

v) To the east of the batholith are the Tertiary, andesitic-rhyolitic Challis volcanics (McIntyre et al., 1982). These are equivalent to the Tertiary bimodal dioritic and granitic intrusive phases of the Idaho batholith (see figure 3.8), which outcrop both within the batholith and as small satellite stocks to the east (Bennett and Knowles, 1985).

vi) Also to the east of the batholith are Palaeozoic carbonates, sandstones and shales preserved as northwest vergent thrust slices, emplaced during the Cretaceous Sevier orogeny (Link et al., 1988).

vii) The Miocene basalts and rhyolites of the Snake River Plain lie immediately to the south of the batholith and obscure the intrusive contacts here.

viii) The initial $^{87}Sr/^{86}Sr$ 0.704-0.706 line (Armstrong et al., 1977) which separates regions underlain by old continental crust from younger accreted terranes, is shown for reference (see chapters 2, 3 and 5) and the region of the Atlanta lobe which lies within 5-10km of this line is referred to as the western border zone.

The towns and settlements referred to in the text are marked in figure 1.3, the major ones being Stanley, McCall and Banks. The Idaho batholith region has numerous rivers, and the two largest are the Salmon River and the Snake River (figure 1.3). The drainage within the batholith are tributaries to these, and provided particularly good sections for sample collection. The Atlanta lobe is a mountainous area with a maximum elevation of 3859m and an average base level of 1500m. The mountain ranges referred to in the text include the

Sawtooth Range, the Soldier Mountains, the Boulder Mountains and the Salmon River Mountains.

1.2 Why study the Idaho batholith ? -a statement of the problem

As previously stated the reason for studying granitoids in general is both to gauge the effects and processes by which granitoid magmatism plays a role in evolution of the continental crust, and as a means of monitoring the evolution of the crust in a particular region, especially of the lower crust which cannot be directly sampled. The principal question is why the Idaho batholith in particular was chosen as a field area in which to approach such problems, and the more geological answers are outlined here.

The largest scale crustal magmatic events occur during the generation of continental margin batholiths similar to the Andinotype of Pitcher (1987). In order to study anatectic processes it is to these destructive plate margins that the research effort must be directed. However, the contribution to the magmas from crustal and sub-crustal sources is still controversial in most continental margin batholiths due to the young ages of the source materials and hence similarity of their isotopic compositions. The relative contributions of mantle and crustal-derived material may be judged with much greater certainty where subduction related granitoids have been generated in areas of older continental crust such as the western United States Cordilleran Interior and particularly the Idaho batholith region.

The identification and characterisation of anatectic melts generated in the deep crust, such as those from the Idaho batholith, facilitates determination of the contribution from lower crustal material to mantle derived magmas in other areas, and is therefore a useful tool in determining the elemental fluxes from the mantle to the crust. Although recent studies in the Andes (Hildreth and Moorbath, 1988) for example, have addressed the effect of lower crustal contaminants on mantle-derived melts, they still remain contraversial and relatively little is known of the effect of such processes in the lower crust in other regions. The Idaho batholith offers an opportunity to gauge these effects.

The Atlanta lobe of the Idaho batholith was chosen for the additional reasons that geochemical and isotope studies had not previously been carried out within the lobe, and yet recent mapping by the U.S. Geological Survey (Fischer et al., 1989) had established a first order understanding of the lithology, intrusive relationships and geochronology (see chapter 3).

In contrast to this, extensive geochemical and isotopic studies have been undertaken in the northern, Bitteroot lobe (Fleck and Criss, 1985; Shuster and Bickford, 1984; and Hyndman, 1988), across the island arc/continental margin suture zone (Armstrong et al., 1977; Manduca, 1988) and in the Snake River Plain (Leeman et al., 1985), with which the findings in this thesis may be contrasted.

Although complex, the western United States cordillera is probably one of the most extensively studied igneous and tectonic provinces in the world so that a reliable tectonic framework already existed. This both helped in the interpretation of the results of this work and allowed the results to be used to refine further regional tectonic and magmatic models for this area.

More practically the granitoids of the Atlanta lobe, though geographically remote, are deeply eroded, well exposed and freshly preserved, facilitating a comprehensive geochemical study. In addition the existence of separate Cretaceous and Tertiary phases of granitoid magmatism in close proximity, allows the temporal change in magmatic styles and evolution of the source regions to be evaluated in the context of the changing compressional to extensional tectonic regime.

Recent studies have placed the Idaho batholith region in a crustal formation province of Archaean age (Bennett and DePaolo, 1987; Ernst, 1988 and chapter 2), but they were based on few data from the Atlanta lobe. Therefore identification of the chemical characteristics, and in particular the age of the source of the granitoids is important in developing models for the growth of the continental crust in the western United States cordillera.

1.3 Aims of Research

In addition to the more general reasons for studying the Idaho batholith, a number of priority objectives were identified which together may answer the problems outlined in the previous section. The objectives of this thesis are:

i) to characterise the Cretaceous and Tertiary granitoids in terms of their mineralogy, major and trace elements and Sr, Nd and Pb isotopic compositions;

ii) to model the partial melting processes in order to constrain the major and trace element composition of the sources of the granitoids and whether they were derived from the lower crust, upper crust or the mantle;

iii) to evaluate the age of the granitoid source regions and place the region into a crust formation age province;

iv) to model the internal evolution of the granitoid batholith and decide whether the various granitoids are directly related to each other principally by fractional crystallization or magma mixing type processes;

v) to identify the differences between the Cretaceous and Tertiary granitoids and relate these to temporal changes in the tectonic regime, the conditions of magma generation and the composition of the source regions;

vi) to assess the effects, if any, of the major Tertiary hydrothermal systems (Criss and Taylor, 1983) on the geochemistry of the Atlanta lobe granitoids;

vii) to present a geotectonic model for the evolution of the northwestern United States cordillera which can account for the generation of the large volumes of granitoid magma in the context of the pre-existing tectonic framework.

1.4 Previous work

Although there has been no previous research by Open University scientists on the Idaho batholith, there is a tradition of geochemical studies associated with subduction processes at

destructive plate margins and the study of granitoids. Recent related theses from this department include: 'A geochemical traverse across the north Chilean Andes' by Rogers (1985); 'Granite Petrogenesis and crustal evolution studies in the Damara Pan-African Orogenic belt' by McDermott (1986) and 'Granite petrogenesis in the Cordillera Real, Bolivia and crustal evolution in the central Andes' by Miller (1988). W.P. Leeman has carried out much work on the basalts and rhyolites of the Snake River Plain-Yellowstone Plateau Province in southern Idaho and has had an interest in the Atlanta lobe granitoids which he encouraged, logistically and academically in this study.

More specifically to the Idaho batholith, there have been many previous studies indirectly related to this which are summarised at the beginning of the relevant sections. There are, however, several very significant studies that are more directly relevant to this work and have set the scene for this investigation, and these include:

i) Armstrong et al. (1977) recognised an age independent step in initial $^{87}Sr/^{86}Sr$ on the western border of the batholith and suggested that this reflected the suture between Precambrian crust and accreted Permian -Jurassic island arc terranes.

ii) Fleck and Criss (1985) and Criss and Fleck (1987) better defined this boundary and suggested a petrogenetic model for the Bitteroot lobe granitoids involving mixing components derived from the mantle, upper crust and lower crust.

iii) Lewis et al., (1987) and Kilsgaard and Lewis (1985) described the lithologies, mineralogy, and geochronology of the Cretaceous granitoids of the Atlanta lobe;

iv) Bennett (1980) and Bennett and Knowles (1985) identified and described the Tertiary bimodal suite granitoids in terms of their mineralogy, major element chemistry and intrusive relationships;

v) Criss et al. (1982) and Criss and Taylor (1983) identified the large Tertiary hydrothermal systems of the Atlanta lobe and mapped these by extensive $\partial^{18}O$ and ∂D analyses.

In addition various geological maps have been invaluable to this work, but the Hailey 1°x2° and the Challis 1°x2° quadrangles (Fischer et al., 1989) were used as the standard reference maps for the study area.

CHAPTER 2

The Geological History of the Western United States Cordillera

2.1 Introduction to the geology of the western United States cordillera.

The aim of this chapter is to outline the geological history of the western United States cordillera from the Archaean until the Recent, with particular focus on the northwestern region, in order to place the Atlanta lobe of the Idaho batholith within the context of cordilleran evolution as a whole. The geological history is concerned mainly with documenting the lithology and stratigraphy of the western United States cordillera viewed as a complex, three dimensional jigsaw puzzle. The tectonic, metamorphic, and magmatic processes that created and juxtaposed the blocks of this collage are interpretations that follow the factual description of the geology of the western United States cordillera. Detailed description of the variations in chemistry and isotopes, and arguments concerning the depth, origin and conditions for generation of the Idaho batholith magmas are contained in the later relevant sections. The reason that it is imperative to pay particular interest in the pre-batholithic lithologies and stratigraphy, of the northwestern region is so that we can estimate, the characteristics which the magmas of the Idaho batholith could inherit from likely source regions.

At the simplest scale, the geology of the western United States cordillera is a jigsaw of just three pieces. The outcrop patterns of the rocks of the western United States cordillera allow only the upper layer of the three dimensional structure to be seen. Nonetheless, from a map of the metamorphic recrystallization ages figure 2.1, (Ernst, 1988) it can be seen that the western United States cordillera breaks down into provinces on the basis of the oldest rocks in particular regions. To the northwest in the Wyoming Archaean province high grade meta-igneous rocks outcrop (Wooden and Mueller, 1988). Surrounding that province are Proterozoic, high to intermediate grade, metasediments and meta-igneous rocks together with age equivalent unmetamorphosed sediments. The western margin of the cordillera,

which truncates the Proterozoic rim to the north, has outcrops of Phanerozoic, low to high grade metamorphic rocks with a diverse range of compositions becoming younger westward, (figure 2.1).

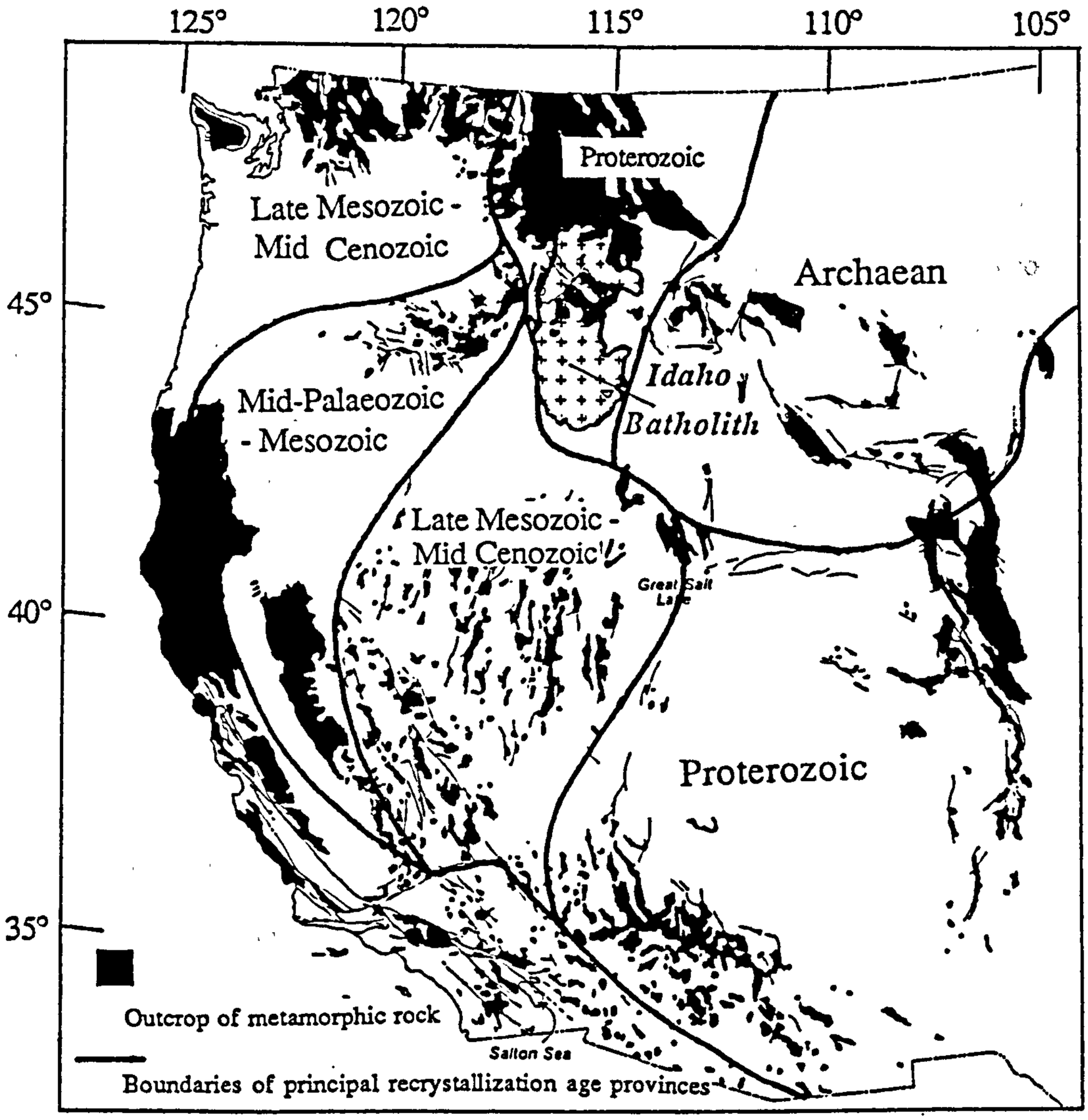

Figure 2.1 Map of approximate ages of principal recrystallization events characteristic of the dominant metamorphic assemblages of the western United States cordillera, taken from, Ernst, 1988. Note the spatial distribution of recrystallization ages, with the Archaean in the northwest, the Proterozoic to the south, and the Palaeozoic and Mesozoic along the west coast.

In order to build a complete picture of the geology of the western United States cordillera in the following sections, indirect methods must be used to assess the nature of the rocks at depth, together with the simple outcrop information described above.

The processes responsible for the post-Archaean growth of the western United States cordillera have primarily been the addition of subduction related volcanic island arcs and calc-alkaline batholiths, and recycling in the forearc, backarc and trench environments (Ernst, 1988). Crustal growth of the cordillera has taken place in three major phases of continental accretion:

i) The Late Archaean (3.3-2.5Ga) aggregation and cratonization of the North American continental nucleus.

ii) The Early and Middle Proterozoic (2.3-1.4Ga) growth of a thick rim of sialic continental crust, by accretion of autochthonous magmatic arcs.

iii) The Palaeozoic and dominantly Mesozoic westward growth of the continental crust by accretion of largely locally derived island arc terranes, but also minor exotic Phanerozoic microcontinental fragments (Ernst, 1988).

This basic sequence of crustal growth is overprinted by second order processes of metamorphism and rearrangement of slivers of the continental margin by transcurrent movements. Furthermore, intra-plate orogeny leading to uplift and erosion resulted in redistribution of material as sediments. Subsequently, in the Cenozoic, intra-plate bimodal volcanism associated with major crustal extension added material to the crust and caused offsetting of tectonic belts.

Since the Precambrian the western United States continental margin has developed through a series of configurations analogous to various present day continental margins. A passive Atlantic-type margin was in existence during the Palaeozoic, evolving to a Japanese-type plate margin with development of off-shore magmatic arcs in the Late Palaeozoic. An Andean-type convergent plate margin associated with accretion of allochthonous terranes evolved during the Early Mesozoic, was followed by strike slip motion in the southwestern cordillera and continued subduction in the northwest.

The development of the Idaho batholith in the northwestern United States cordillera, occurred during a tectonically complicated period in the Late Mesozoic and Early Cenozoic, associated with eastward subduction, island arc accretion and transpressive motion, crustal thickening and finally crustal relaxation and attenuation.

2.2 The Archaean : the nucleus of the western United States cordillera.

The Wyoming Archaean craton formed the nucleus for the subsequent growth of the whole of the western United States cordillera. The present location of Archaean rocks is mainly confined to Wyoming and the neighbouring parts of Idaho, Utah, Montana and South Dakota, (figure 2.2).

Archaean rocks outcrop to the east and southeast of the Atlanta lobe of the Idaho batholith. Archaean gneisses form the cores of the Pioneer and Albion range metamorphic complexes to the southeast (Armstrong and Hills, 1967), and the northern boundary of the Archaean craton with younger Proterozoic rocks is exposed in uplifted blocks in southern Montana, striking southwest towards the southern margin of the Idaho batholith (Hedge, 1986), figure 2.2.

The lithologies of the Archaean rocks range from gneisses of amphibolite to granulite facies indicating a high temperature and moderate pressure metamorphic environment. Assemblages in the sillimanite to orthoclase zones are common in the more hydrous intermediate, andesitic compositions, whereas granulite facies rocks are often developed from anhydrous mafic to ultramafic precursors (Hyndman et al., 1988). The Wyoming craton is classified as a type III craton, one that is typifyed by rapid development of high U/Pb ratios and rapid differentiation of the crust without early metamorphism leading to development of high $^{207}Pb/^{206}Pb$ ratios (Mueller and Wooden, 1988).

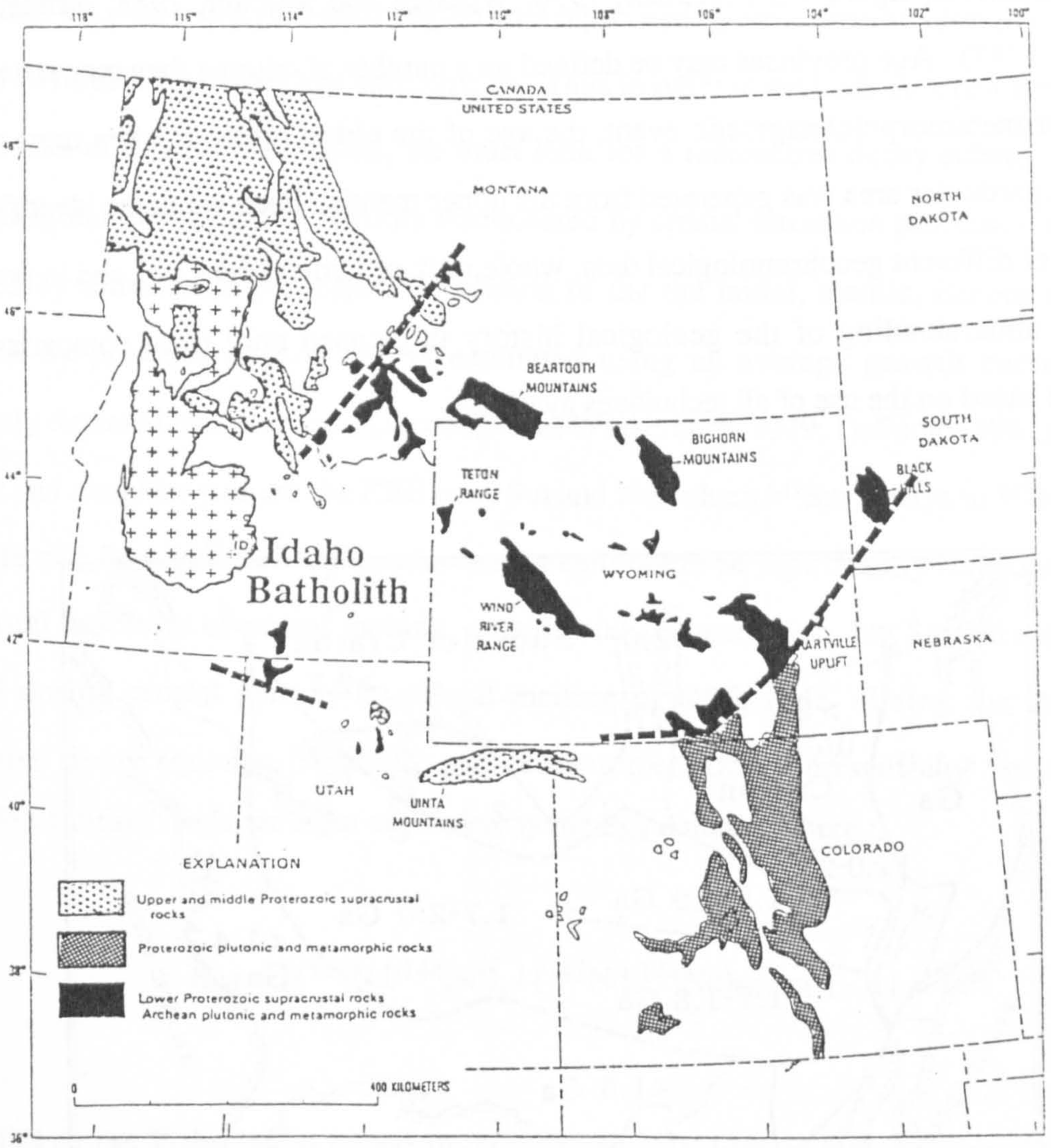

Figure 2.2 Map of the outcrop pattern of Archaean and Proterozoic basement and supra-crustal rocks, taken from Hedge, 1986. The dashed line delineates the probable boundaries of the Wyoming Archaean craton, which demonstrates that all but the southern margin of the Atlanta lobe lies in a region where there is no surface evidence for Archaean basement. Compare with the interpreted distribution of the Archaean age basement in figure 2.3.

The 2.8Ga andesitic amphibolites of the Beartooth Mountains of northern Wyoming, show high field strength element depletions and isotopic signatures analogous to typical modern convergent continental plate margin andesites (Mueller and Wooden, 1988). This suggests that subduction was an important continental forming processes in the Late Archaean, at least on the margins of the Wyoming Archaean craton.

The Wyoming Archaean age province has been delineated mainly on the basis of U-Pb, Sm-

Nd, and Rb-Sr isotope variations of both young igneous rocks, old metamorphic rocks and crustal xenoliths, figure 2.3 (Zartman, 1974; Wooden and Mueller, 1988; Bennett and DePaolo, 1987). Age provinces may be defined on a number of criteria; they may reflect the last major metamorphic/magmatic event, the age of the oldest rocks or when most of the crust in a particular area was generated from the upper mantle. Each would be identified on the basis of different geochronological data, whole rock or mineral ages etc., and in practice a proper understanding of the geological history is gleaned only from comparison of provinces based on the use of all techniques available.

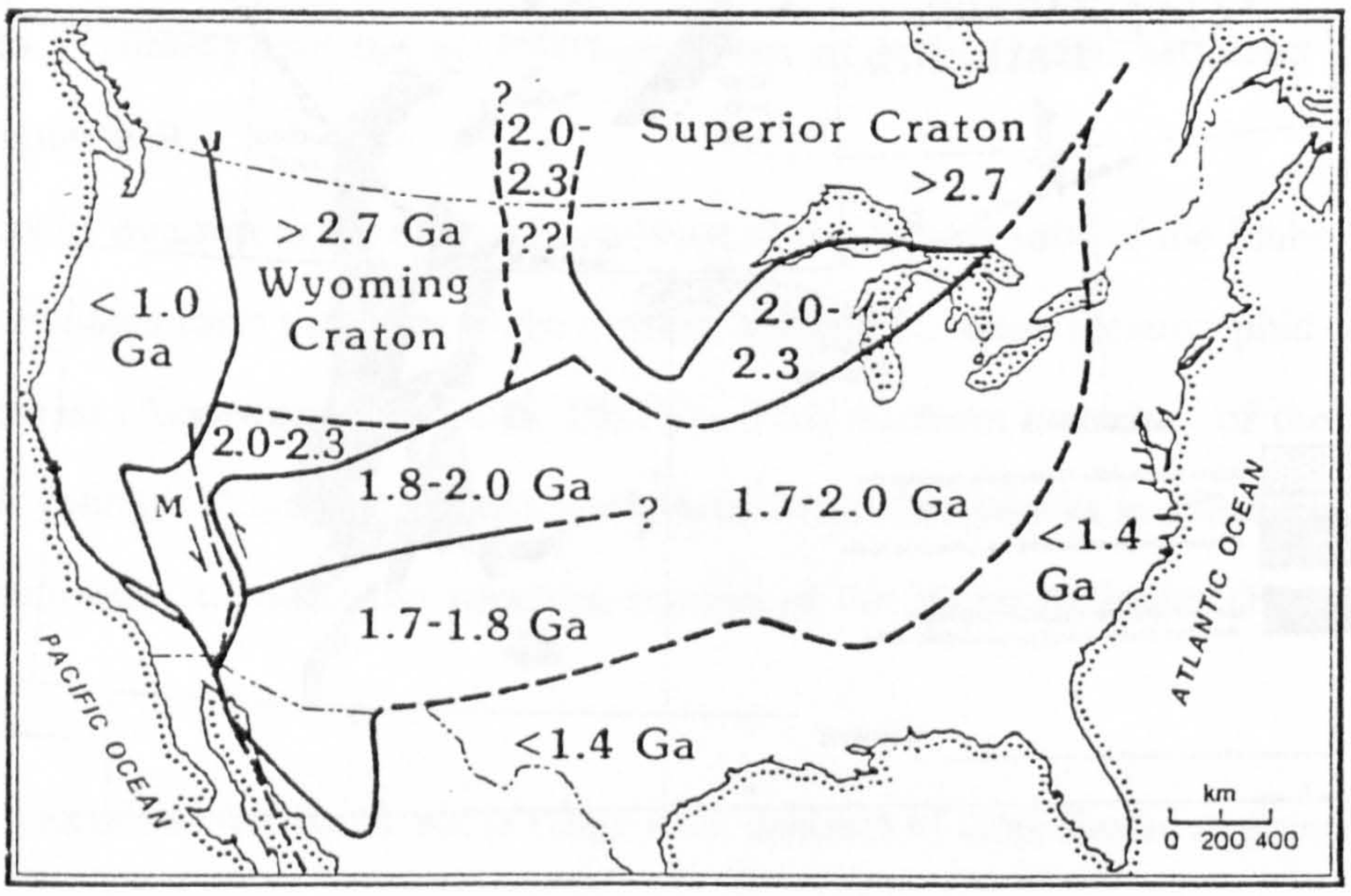

Figure 2.3 Map of North America, showing the distribution of Nd-model age provinces, taken from Bennett and DePaolo, 1987. The Nd-model ages from each province represent the average crust formation age of the continental basement from each area.

Perhaps the most fundamental age province, is that based on the average time since the crust was extracted from the underlying mantle. This is the "crust formation age" of Bennett and DePaolo (1987), and strictly speaking it probably applies to the time when the crust, and the underlying continental mantle lithosphere were derived from the convecting upper mantle. Fractionation of incompatible from compatible elements into fluids and melts, and the upwards migration of these established the separate crustal and mantle reservoirs enriched

and depleted in certain elements. The process of crustal extraction from the mantle may occur more than once in a particular region, and reprocessing and differentiation in the crust can lead to further depletions and enrichments. Thus in order to evaluate the crust-formation age of rocks in a particular region, we must look for a radioactive decay scheme whose parent/daughter elemental ratio is only fractionated by crustal formation processes, and not modified by intracrustal processes. Evolution of the the initial, mantle, isotope ratio is modified by previous events, and is estimated using an average growth curve for a previously depleted model mantle (Jacobsen and Wasserburg, 1979; DePaolo, 1981). Such a parent and daughter pair are the REE pair, Sm and Nd, where ^{147}Sm decays to ^{143}Nd with a half life of 1.06×10^{11}a. Sm/Nd ratios are thought not to be significantly fractionated by intracrustal processes of partial melting, erosion and sedimentation, but Sm/Nd ratios are reduced during crustal genesis by partial melting of the mantle. Using the standard radioactive decay equation (Appendix A), measurement of the present day Sm/Nd and $^{143}Nd/^{144}Nd$ ratios, the latter often expressed by the ε_{Nd} notation where :

$$\varepsilon_{Nd} = \{(^{143}Nd/^{144}Nd)_t / (^{143}Nd/^{144}Nd)_{CHUR,\,t} - 1\} \times 10^4$$

and CHUR refers to the initial chondrite-normalised $^{143}Nd/^{144}Nd$ isotope ratio (DePaolo and Wasserburg, 1976), allows extrapolation back to the time when crustal rocks or their precursors were separated from the mantle (figure 2.4). This age is known as the depleted mantle Nd model age (T_{DM}^{Nd}) and major age provinces have been defined on this basis within the western United States cordillera (Bennett and DePaolo, 1987) where DM refers to a depleted mantle and:

$$T_{DM}^{Nd} = 1/\lambda \ln\left\{\frac{^{143}Nd/^{144}Nd_{sample} - ^{143}Nd/^{144}Nd_{DM}}{^{147}Sm/^{144}Nd_{sample} - ^{147}Sm/^{144}Nd_{DM}} + 1\right\}$$

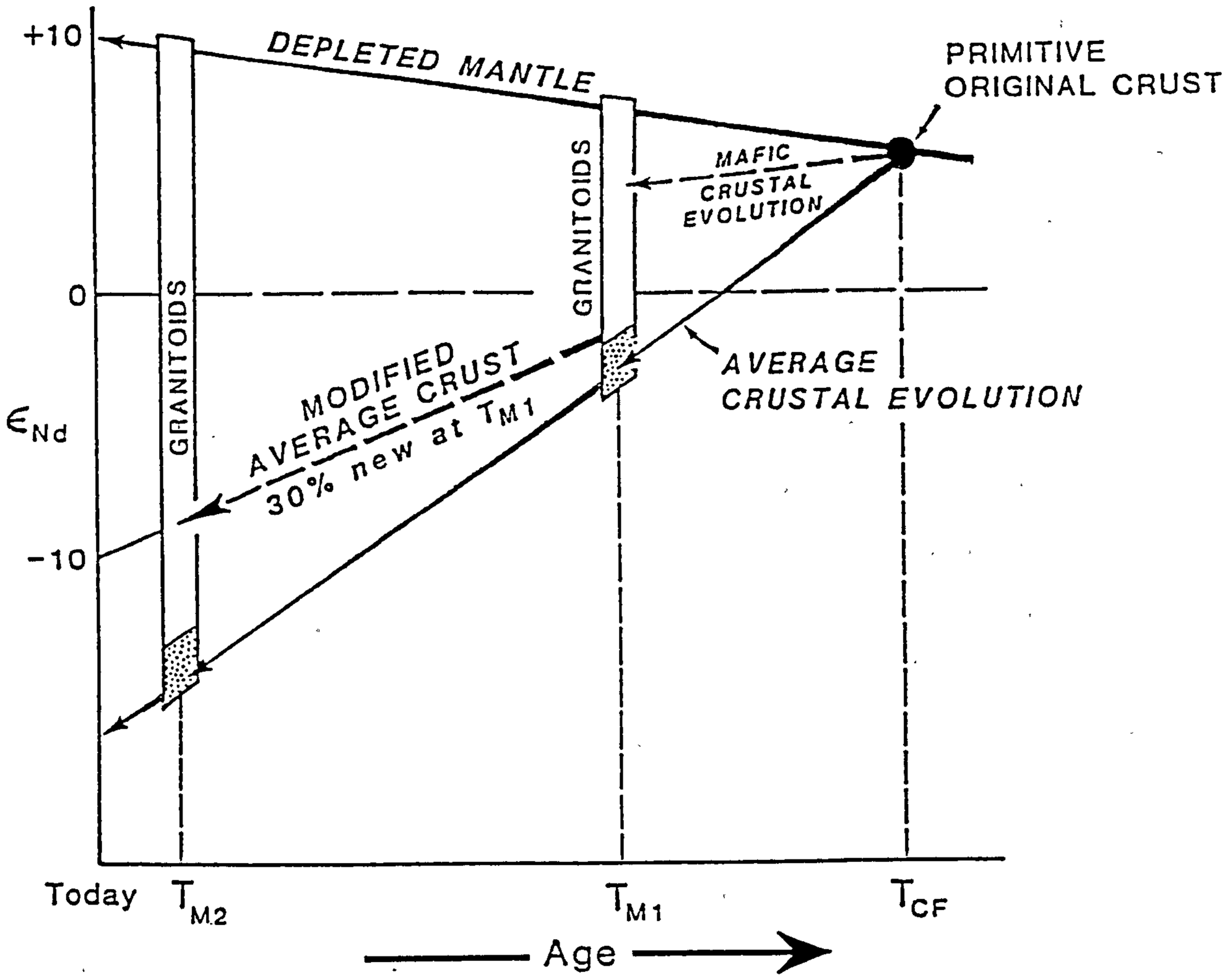

Figure 2.4 Model for Nd isotope systematics of a typical continental crustal segment modified from Bennett and DePaolo, 1987. Primitive crust originally separates from the depleted mantle during a magmatic event at T_{CF}. The primitive crust has reduced Sm/Nd ratios due to fractionation during partial melting of the mantle and so evolves towards negative ε_{Nd} values. A second magmatic event at T_{M1} generates granitoids in the crust with a possible range of initial ε_{Nd} between the depleted mantle values and the original evolved crustal isotopic composition, as shown by the parallelograms. The actual value of initial ε_{Nd} of the granitoids is dependent on the proportions of the mantle versus evolved crustal component. A similar granitoid forming event at T_{M2} due to heating of the crust by mantle derived magmas has an even larger range of possible initial ε_{Nd} values depending on the proportions of old crust and newly separated mantle component. The age that the original, primitive crust separated from the mantle, (the depleted mantle Nd-model age, T_{Nd}) can be calculated by extrapolation back to the depleted mantle model evolution curve having analysed a granitoid for Sm/Nd ratios and ε_{Nd}. However it is only granitoids derived wholly from remobilised ancient crust that will yield the true crust formation age, and so peraluminous crustal melt granitoids are preferred. Substantial additions (>30%), of new mantle-derived crustal material having higher ε_{Nd} values and Sm/Nd ratios can alter the crustal evolution curves which may lead to older or younger Nd-model ages than the true age of crust formation.

However, care must still be taken while interpreting Nd model ages, because processes such as mixing older crust with newly separated crust from the mantle during younger can alter both the ε_{Nd} values and the Sm/Nd ratios. When this happens extrapolation back to the mantle curve can produce Nd model ages that are often older than crystallization ages, determined by other methods, of even the most refractory isotope systems (figure 2.4). This is discussed later in more detail, where it is especially relevant to the development of the Proterozoic crust around the Archaean nucleus in the western United States cordillera, but it emphasises that a better understanding of the Sm-Nd data is gained by sampling rocks of different ages, where these ages are constrained by independent methods.

Model ages calculated using the Rb-Sr decay scheme do not yield reliable crust formation ages because Rb/Sr ratios are significantly fractionated by intra-crustal processes. Nonetheless, Rb-Sr whole rock dating remains the basis for accurate determination of crystallization ages. The U-Pb system offers several methods for gaining model ages. Without going into the details of U-Pb isotope systematics (see appendix A), measurement of the radiogenic $^{207}Pb^*/^{206}Pb^*$ ratio in minerals that contain little or no U, such as alkali-feldspar, yield the $^{207}Pb^*/^{206}Pb^*$ ratio of their source region, and this can be interpolated to give the age of the source (Faure, 1977). However for this method to yield ages of crustal formation, we must assume that the U/Pb ratios are not significantly fractionated within the continental crust. A second U-Pb method of obtaining old model ages is dating suites of inherited zircon grains in granites or sediments. Upper intercept ages on concordia diagrams represent the mean age of crystallization of these older zircons and thus the age the source from which the granite or sediment was derived. In addition, direct isochron ages by several methods can be made on any available metamorphic rocks and crustal xenoliths, which were originally stabilised as basement subsequent to crustal formation, provided that later metamorphic events have not reset the ages. Ultimately then, the crustal formation provinces are distinguished on the basis of different Nd isotopic evolution paths interpreted using all the independent age data available.

In the region of the Idaho batholith in the northwestern United States cordillera estimates of the crustal formation age have been made by a number of different methods noted above (compare figures 2.1, 2.2, 2.3, 2.5, and 2.8). Archaean crustal xenoliths of felsic granulite from the Snake River Plain, to the south of the Idaho batholith, give Nd model ages (T^{Nd}_{CHUR}) of 3.1-3.4Ga, dating the age of separation of components from the mantle to form the ancestral Wyoming craton (Leeman et al., 1985). Bennett and DePaolo (1987), have defined a Nd model age province greater than 2.7Ga delineating the boundaries of the Wyoming Archaean province (figure 2.3). Concordant Pb-Pb and Sm-Nd metamorphic recrystallization ages from the Snake River Plain xenoliths yield an average age of 2.8Ga, (Leeman et al., 1985) and metamorphic ages within the craton as a whole, are generally greater than 2.5Ga (Mueller and Wooden, 1988). The metamorphic ages record the time of cratonization which is greater than at least 2.6Ga (Ernst, 1988) which places a minimum limit on the age of crustal formation.

The region of the Idaho batholith has been placed within the Wyoming Archaean province by many authors constructing maps of age, isotopic and model age provinces of the western United States cordillera, as in figure 2.5 (Condie, 1981; 1986, Bennett and DePaolo, 1987; Ernst, 1988; Bickford, 1988). However, there is not a single recorded Archaean metamorphic model age, recorded from the granitoids of the Idaho batholith nor the country rocks within 50-100km. Although few model ages have previously been available from the Idaho batholith region, upper intercept Pb concordia ages from xenocrystic zircon cores and monazites from both the batholith magmas and xenolith suites yield ages between 1700-2349Ma (Chase et al., 1978; Bickford et al., 1980; Shuster and Bickford, 1985). These zircons are thought to have been inherited from a lower crustal source which can now be placed in a Proterozoic age province (figure 2.2). This evidence hints that age province boundaries must exist between the Idaho batholith and the Wyoming Archaean province in eastern Idaho and near the northern margin of the Snake River Plain.

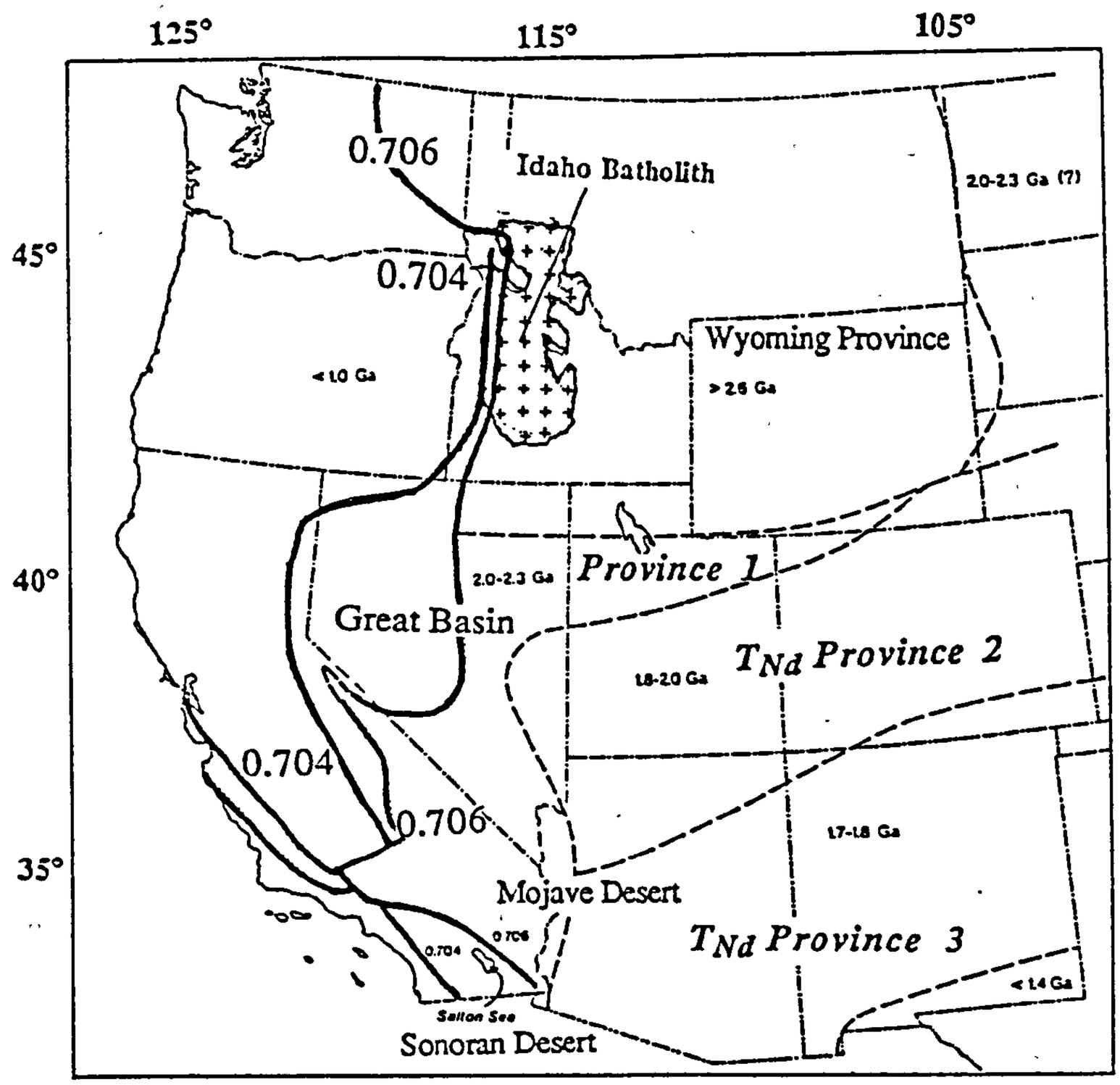

Figure 2.5 Map of isotopic and crystallization age provinces of the western United States, taken from Ernst, 1988. Ages are depleted mantle Nd-model ages separated by dashed lines. Bold lines are $^{87}Sr/^{86}Sr$ = 0.704 and 0.706; the initial ratio limits of Mesozoic and Cenozoic granitoids. Mid-Proterozoic and older basement, lies inboard of the 0.706 line. The region of the Idaho batholith has been placed within the Wyoming Archaean province although there is no evidence of Archaean basement in this region.

2.3 The Proterozoic

The Proterozoic rocks of the western United States cordillera outcrop to the south and southeast of the Wyoming Archaean province, (figures 2.1, 2.3, 2.5). On a broad scale, the Early and Middle Proterozoic stratigraphy is represented by repeated cycles of bimodal volcanics, overlain by quartzites and shales (Condie, 1982). In the northwestern cordillera, in the vicinity of the Idaho batholith, large thicknesses of Middle to Late Proterozoic sedimentary and volcanic basin sequences were deposited. The Proterozoic basement of the

western United States cordillera decreases in age to the south and west of the Wyoming Archaean province from Early Proterozoic in the central Great Basin and Mojave Desert, to the Mid-Late Proterozoic Sonoran Desert (Bennett and DePaolo, 1977) as shown in figure 2.5. This represents the growth of new crust during the Proterozoic, by successive island arc accretion with the addition of new mantle derived material and a relatively small proportion of reworked crustal material.

2.3.1 The Proterozoic lithologies and stratigraphy of the Idaho batholith region and the western United States cordillera.

The early Proterozoic basement complex is not exposed in the northwestern cordillera, in the region of the Idaho batholith, and its characteristics can only be inferred by indirect methods on rocks derived from this basement. Large thicknesses of Proterozoic sediments were discordantly deposited upon the Early Proterozoic basement in the northwestern United States and Canada. In the region of the Idaho batholith many of the surrounding, older, country rocks are obscured by more recent deposits, so that the relationships and stratigraphy must be inferred from adjacent areas. This is particularly true of the Atlanta lobe of the Idaho batholith, where Columbia River Plateau flood basalts lie to the west, the Snake River Plain lies to the south and the Challis volcanic field lies to the east, figures 1.2 and 1.3.

The Lemhi group and Yellowjacket formations of quartzites and argillites were deposited during the Lower and Middle Proterozoic in central Idaho and southwestern Montana (Hyndman, 1988). Intrusion of granitic gneisses, dated at ≈1500Ma using Rb-Sr techniques, into the Proterozoic basement of the Salmon River arch figure 1.3 in central Idaho, were thought by Armstrong (1975) to form the Proterozoic basement complex to the later developed Belt sedimentary basin in this region. Hyndman (1983,1988) postulates that the 1.5Ga age is hardly old enough to form the basement to the Middle Proterozoic sediments of the Belt basin, and argues that resetting was likely if Mesozoic granitoids originally extended across the Salmon River arch. However, augen gneiss intruding the basal metasedimentary unit in the Salmon river arch yields U-Pb zircon ages of 1370Ma

(Evans and Fischer, 1986) and so the oldest metasediments exposed in this area are regarded by Lund and Snee (1988) to be equivalent to Middle Proterozoic Belt metasediments and volcanics. The overlying 3000m of Concord and Quartzite Butte units are also equivalent with the Middle Proterozoic Belt supergroup and the upper, Moores and Umbrella units, of 6500m of metasediments correlate with the Upper Proterozoic Windermere group that was previously thought to be missing (Lund, 1984; Lund and Snee, 1988; Hyndman, 1988). Figure 2.6 outlines the generalised stratigraphy of the Idaho area.

In northern Idaho, the Middle Proterozoic Belt supergroup rocks are shallow marine, clastics, carbonates and volcanics, approximately 15-20km thick, which have been correlated with the deposits in the Belt-Purcell basin of Canada (Aitken and McMechan, 1989). The Upper Proterozoic Windermere supergroup, usually developed to thicknesses greater than 3km, was deposited between 0.78-0.57Ga. It consists predominantly of clastics, rift-related basalts and diamictites, and it marks the establishment of the southwest trending cordilleran miogeosyncline (Oldow et al., 1988). This formation extends, some 3000km discontinuously, from British Columbia to Death Valley.

The tectonic setting for the deposition of the Proterozoic sediments and volcanics requires the development of a large basin in the northwestern United States and Canada. Traditionally this has been interpreted to be a passive margin sequence, but more recently, Winston (1986) postulated an intra-cratonic basin environment because he identified a western source of clastics, east-west normal growth faults, and rift conglomerates. Rifting at ≈1450Ma is suggested by Burchfield and Davis (1975) and Dickinson (1977) to produce the great Belt Middle-Proterozoic basin. The Archaean basement of southwestern Montana contains numerous dolerite dykes dated at 1.1-1.0Ga and 1.5-1.4Ga, (Daniel and Berg, 1981) which may indicate two distinct rifting events during the development of the Belt basin. The Windermere group was deposited during episodic rifting followed by subsidence of the miogeosyncline which persisted until the Palaeozoic.

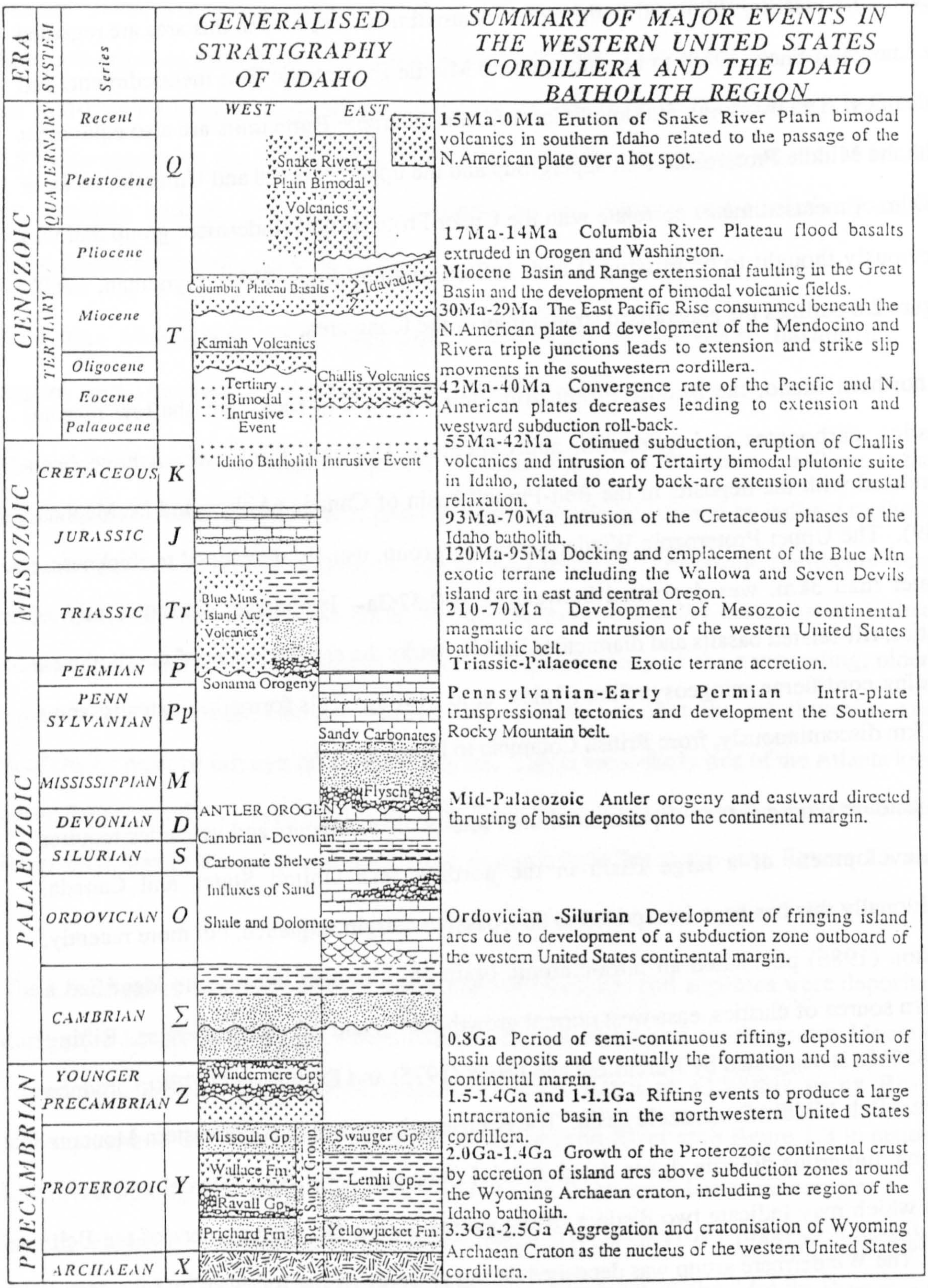

Figure 2.6 Generalised stratigraphic section for the Idaho batholith region correlated with the orogenic, major magmatic and deformational events in the western United States cordillera.

Thick dolerite sills intruding the Proterozoic of western Montana and northern Idaho are dated at 800Ma (Daniel and Berg, 1981), and together with the presence of pillow basalts and greywackes argue for an extensional tectonic setting, where crustal thinning led to volcanism, and subsidence and sedimentation resulted in thick sedimentary basin deposits.

2.3.2 The Proterozoic growth of continental crust of the western United States cordillera.

The Proterozoic crustal development of the western United States cordillera has been primarily deduced by the use of Pb, Nd and Sr isotope in rocks of the Proterozoic basement, and in the Mesozoic and Tertiary granitoids and lower crustal xenoliths which sample the basement.

On the basis of Nd isotope mapping Bennett and DePaolo (1987) have identified three provinces, incrementally increasing in model Nd age southwards from the Archaean craton; Province 1 (T_{DM}^{Nd}≈2.0-2.3Ga), Province 2 (T_{DM}^{Nd}≈1.8-2.0), and Province 3 (T_{DM}^{Nd}≈1.7-1.8Ga) figure 2.3, 2.5. In fact, comparison of data indicate that there is good agreement in the regional variation of initial isotope ratios, model ages, times of intrusion and recrystallisation of metamorphic facies (Ernst, 1988). For example, comparison of figures 2.1, 2.3, and 2.5, shows that the boundaries for the Nd age provinces are subparallel to those for the crystallization age provinces, though the actual ages differ, and boundaries between provinces of similar isotopic signatures also have a similar distribution. The reason that the Nd model ages are often older than the crystallization ages may be because subsequent metamorphic events have completely obliterated any evidence of the original crystallization age, or the rocks analysed may represent a mixture of Archaean crustal material and a newly extracted mantle component, and thus have intermediate ε_{Nd} values which extrapolate to older Nd model ages than the time of the actual crust formation event, (see figure 2.4).

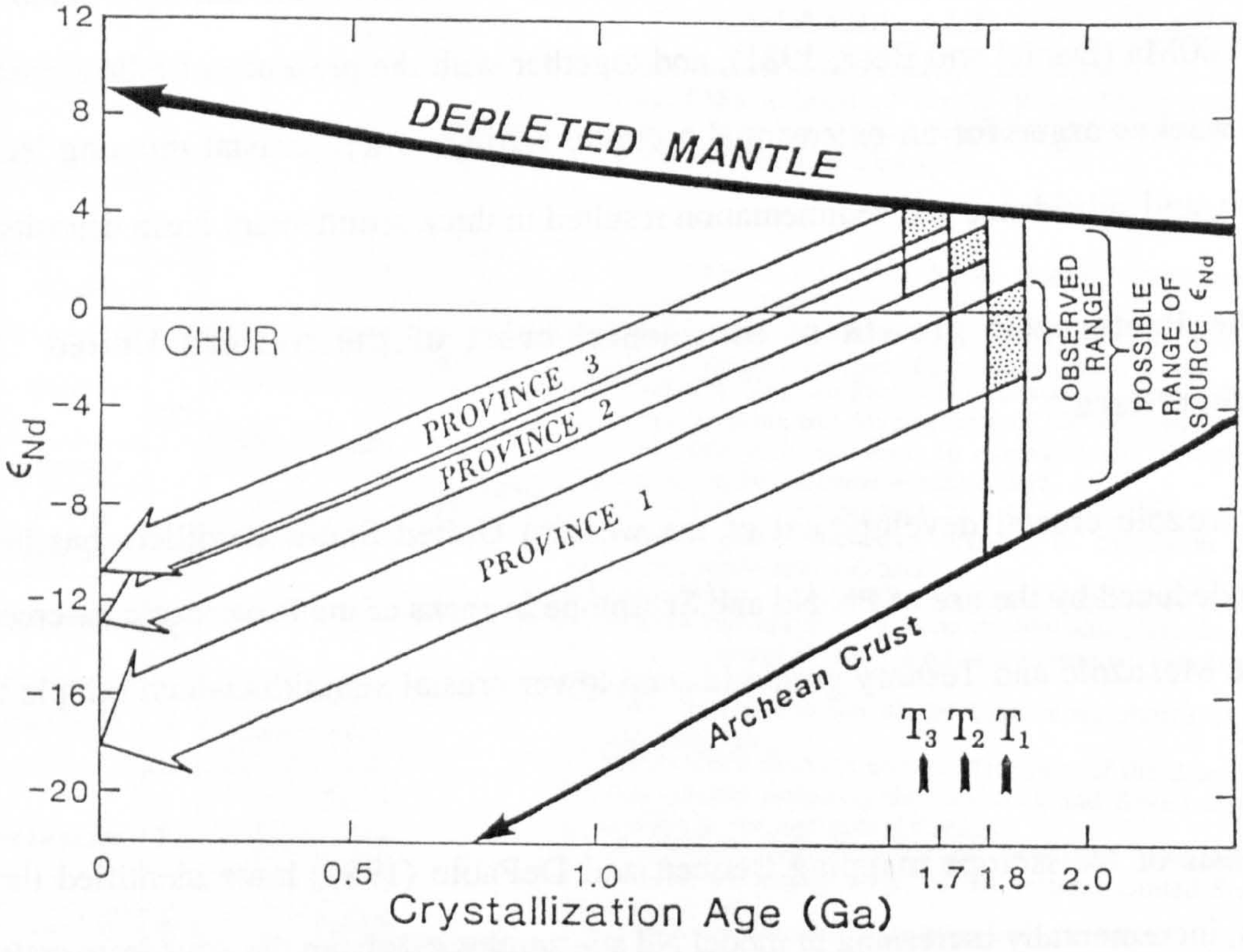

Figure 2.7 Model of the progressive Proterozoic Nd isotopic evolution of the western United States continental crust, from Bennett and DePaolo, 1987. The parallelograms indicate the possible range of ε_{Nd} values for each new portion of crust, with the shaded part indicating the restricted range of observed initial ε_{Nd} values, suggesting that averaged over a crustal province constant proportions of old crust and new mantle derived material is involved. Province 1 is derived from a mixture of Archaean crust and material derived from the depleted mantle at 1.9Ga. The model of Bennett and DePaolo, 1987, shows that although each succeeding continental segment is formed from the same percentage of pre-existing crust and new, mantle derived material, the Nd isotopic composition of the progressively younger crust gradually becomes more similar to the depleted mantle isotopic composition as the Archaean component is screened and diluted from the region of crustal accretion. In province 3, the crystallization ages of the oldest rocks are thus equal to the Nd-model ages.

Figures 2.3 and 2.5 illustrate that there is a distinct gap in crust formation age between the Archaean age province, and the oldest Proterozoic age province, Province 1 of Bennett and DePaolo (1987) and that the Proterozoic age provinces show a gradual decrease in Nd model ages to the south. The favoured interpretation is that continuous continental accretion occurred between 2.0-1.7Ga during the Proterozoic in the western United States cordillera. Province 1, which is nearest to the Archaean craton, incorporated the largest proportion of up to 20% reworked ancient Archaean material with an evolved Nd isotopic signature, (Bennett and DePaolo, 1987; Ernst, 1988) and it is therefore characterised by Nd model ages

which are much older than the crystallization ages. The gradual decline in Nd model ages between the Proterozoic provinces 1, 2, and 3, as they become more distal from the Archaean craton, was then attributed to the incorporation of decreasing amounts of reworked Archaean material. In practise it is more likely that reworked material incorporated during later crust forming events would be derived from neighbouring Proterozoic rocks to the north which have not had enough time to develop significantly contrasting isotopic signatures. Thus in the more southerly Proterozoic continental crust of the western United States cordillera, the crystallization ages of the Proterozoic basement become nearly equivalent to the Nd model ages, figure 2.7 (Bennett and DePaolo, 1987; Ernst, 1988; Bickford, 1988). Therefore, the position of the boundaries between the Proterozoic crustal formation provinces 1-3 are rather arbitrarily identified within an age spectrum of 2.0-1.7Ga.

A striking feature of the western United States is how the various age province boundaries coincide with the well established initial Sr isotope 0.704 - 0.706 line identified in Mesozoic and younger magmatic rocks (Kistler and Peterman, 1978) and regions with similar Pb isotope ratios (Zartman, 1974: Wooden et al., 1988). The common position of the boundaries is no coincidence (figure 2.8). If reservoirs are created at different times and then isolated from one another they evolve characteristic isotope signatures. Igneous rocks which sample these source rocks inherit the signature and effectively map out provinces that have a common chemical evolution. It is then no surprise that significant isotopic discontinuities occur between provinces where there have been significant time intervals between crustal formation events and no sharp changes in isotopic signatures occur between the continuously produced Proterozoic rocks in the western United States.

This leads to the general conclusion that most of the Proterozoic continental crust in the western United States was generated by separation of mantle components above a subducting, palaeo-Pacific, oceanic, lithospheric slab: subsequent sedimentary, metamorphic, and igneous processes then reprocessed them into the Proterozoic basement of western United States cordillera (Bennett and DePaolo, 1987; Ernst, 1988). Moreover, only

a small proportion (<20%) of the material added to the new crust was derived from pre-existing crust, either reworked older parts of the continent to the north or accreted as exotic terranes (Bennett and DePaolo, 1987; Ernst, 1988).

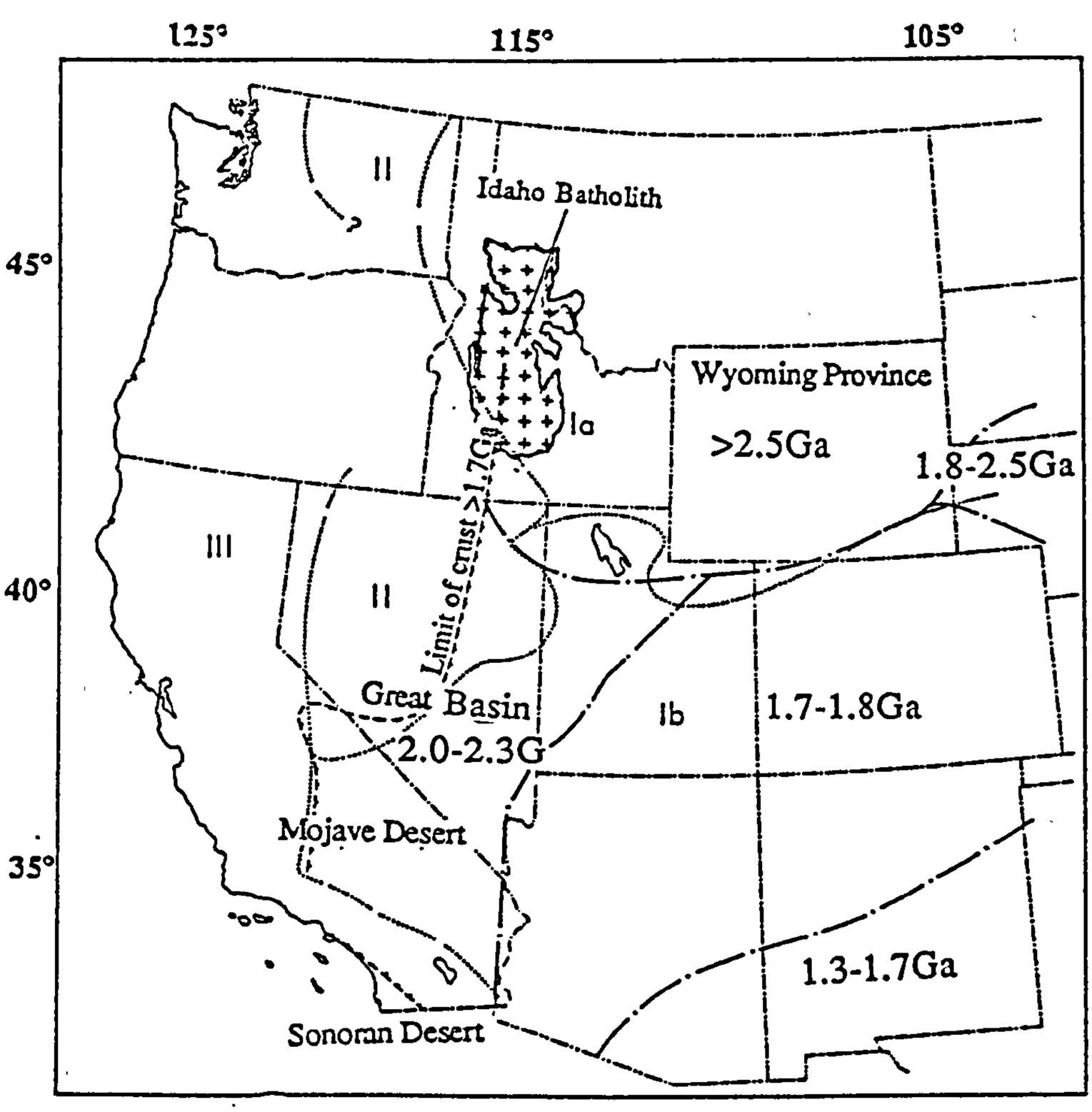

Figure 2.8 Map showing the basement provinces of the western United States, from Ernst, 1988. Pb isotopic provinces and areas characterized by radiometric, mainly Rb/Sr and U/Pb bulk rock ages of crystallization delineated by dot and dashed lines. Regions I, II, and III, separated by dotted lines, are typified by lead from post-Palaeozoic igneous rocks occurring in regions principally of Precambrian basement, derivative sedimentary strata and young "eugeoclinal" mixed provenance, respectively.

Within each province, Condie (1982) recognised a similar succession of bimodal volcanic assemblages overlain by quartzites and shales. The basalts are derived from depleted upper mantle and the intrusive and extrusive silicic magmas were attributed to a lower crustal source. Growth of the Proterozoic continent southwards is interpreted in terms of

successive marginal basin closures and the accretion of magmatic arcs to the continental margin as the active margin migrated southwards. This led to the development of a band of continental crust 1300km wide on the southwestern margin of North America, over 300Ma, from approximately 2.0-1.7Ga ago.

Figure 2.3 (Bennett and DePaolo, 1987) shows that the Archaean cratons in the northern United States and Canada are nearly continuously surrounded by crust with 2.0-2.3 Ga Nd model ages except in the Idaho batholith region. Although it has been previously shown that the 2.0-2.3Ga Nd model age province does not represent the actual time of crust formation, there was certainly material extracted from the mantle at 2.0Ga which was mixed with reworked Archaean crust in the above Nd model age province. If mixing of the crustal and mantle components was not 100% efficient, during magma generation and ascent, then we may expect there to be some remaining evidence of the earliest, 1.9-2.0Ga, Proterozoic orogenic episode. Equivalent 2.1Ga bulk rock crystallization ages and Nd model ages are obtained from orthogneisses in the Yukon Territory (Dunsel et al., 1985 and Aleinkoff et al., 1981) and from the Shuswap complex in British Columbia (Armstrong, 1986 and Bennett and DePaolo, 1987). Furthermore, in northern California, Silver et al. (1961) and Wooden (1985) have determined upper intercept U-Pb zircon ages of 1.8-1.95Ga. The Nd isotopic evolution of the Idaho batholith region is discussed later in the light of new Nd data presented. However, the 1700-2349Ma zircon upper intercept ages (Chase et al., 1978; Bickford et al., 1980; Shuster and Bickford, 1985), within the Idaho batholith and the surrounding country rocks, suggest that a Proterozoic crust should exist around the Wyoming Archaean continental nucleus and perhaps has been truncated by later faulting and shuffling of crustal blocks.

2.4 The Palaeozoic

Up to 12km of Palaeozoic miogeosynclinal sequences deposited in regions surrounding the Idaho batholith, are divided into an early, Cambrian-Devonian sequence and a later, Carboniferous sequence by the Middle-Palaeozoic Antler orogeny which changed the sedimentary patterns. In the Idaho batholith region there is little evidence of the Palaeozoic

sediments, presumably because of post-Palaeozoic uplift and erosion to the level of the presently exposed Proterozoic sedimentary successions, now seen to the north and northeast of the Idaho batholith (figure 2.2). It is unlikely that Palaeozoic rocks can have been a source for the magmas of the Idaho batholith, but they were probably present at the time of emplacement, and thus they need to be considered in any discussion of possible emplacement depths.

In the Cambrian to Lower Devonian, carbonate shelves dominated in the western North American continental margin. Carbonates and dolomites are interspersed with influxes of sand, shale and argillite from the west and northwest, into south-central Idaho (Dickinson, 1977), and these are now preserved as thrust slices in southeast Idaho. A passive margin was the tectonic environment for the deposition of the Early Palaeozoic rocks which exhibit a low angle unconformity with the Late Proterozoic Windermere supergroup in the western United States cordillera. During the Ordovician and Silurian fringing island arcs developed outboard of the continental margin (Oldow et al., 1988).

There are few rocks which represent Mid-Palaeozoic times in the northwestern cordillera. In Idaho, Mississippian flysch was shed off the newly formed Antler highland, to the east of the present position of the Idaho batholith (Oldow et al., 1988). The Mid-Palaeozoic continental margin tectonics were dominated by the coeval Ellesmerian orogeny to the north of the Idaho region, and the Antler orogeny to the south, resulting in major shortening of the continental eugeosyncline. The Late Devonian and Early Mississippian saw the eastward directed thrusting of the Antler basin onto the northeast-southwest trending continental margin and the development of synorogenic clastic rock types.

The Late Palaeozoic carbonates grade westward into sandy carbonates and clastics in south-central Idaho and may have extended north into the Idaho batholith region (Dickinson, 1977). In the western United States cordillera a period of intra-plate transpressional tectonics, forming the ancestral Rocky Mountains occurred during the Pennsylvanian and Early Permian. The Sonama orogeny of the Late Permian to earliest Triassic saw the emplacement of the Golconda allochthon (figure 2.9) simultaneously in western Nevada and

northeast Oregon, due to the development of an active subduction zone along the continental margin (Oldow et al., 1988).

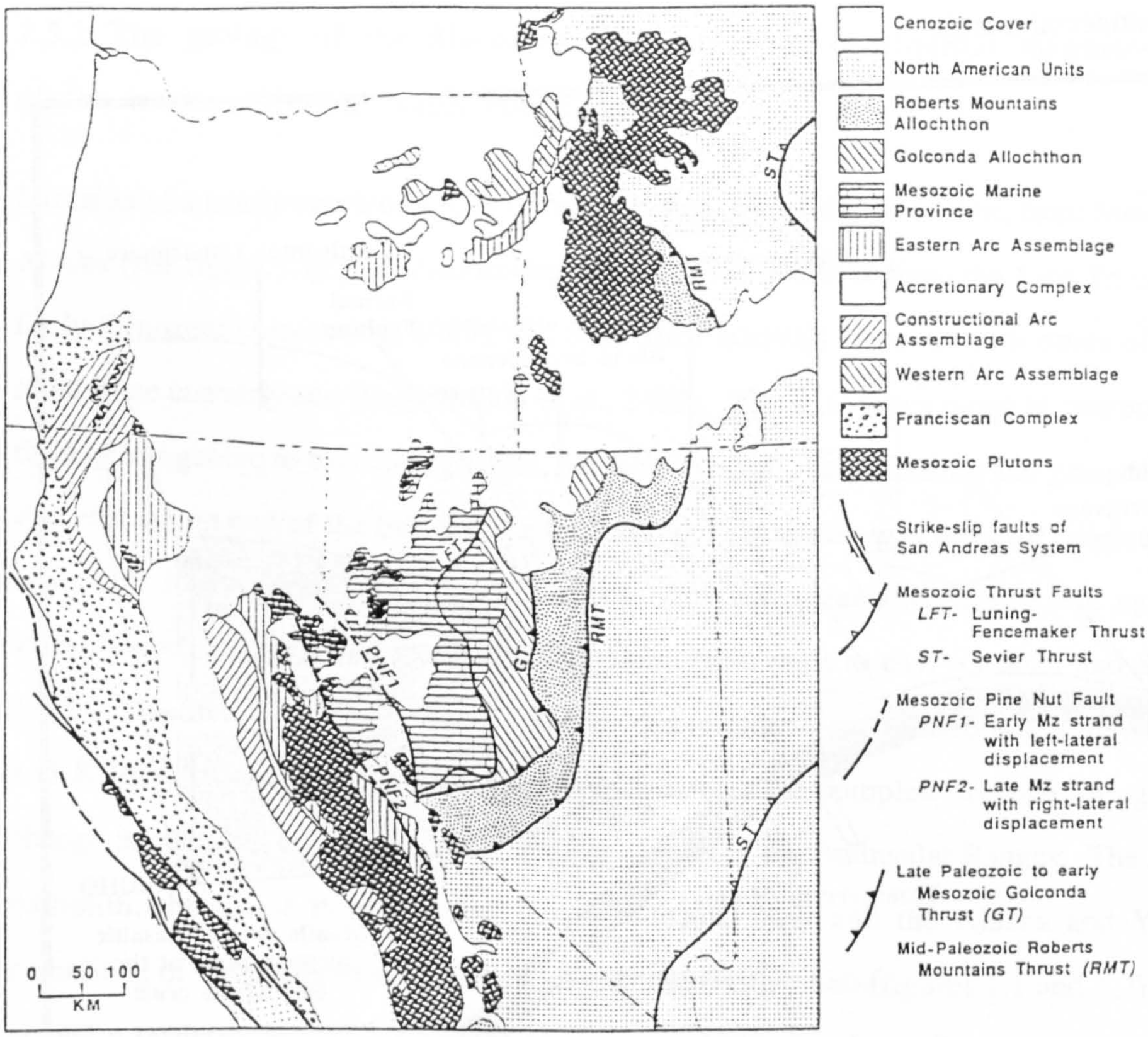

Figure 2.9 Generalised geological map (from Oldow et al.,1988) illustrating the distribution of the major Mesozoic allocthons and the Mesozoic granitoid plutons from the western United States cordillera.

Development of a double fringing magmatic arc (Stikinia and Quesnellia terranes), outboard of the western margin of the cordillera, occurred during the Permian and Middle to Upper Triassic as a result of the development of the new destructive plate margin outboard of the western margin of the North American continent (Oldow et al., 1988).

2.5 The Mesozoic

The geological history of the western United States cordillera, from the Triassic to the Palaeocene, records the addition of material, principally by two related processes: intrusion of a semi-continuous belt of Mesozoic granitoid batholiths running north-south along the western margin of the North American continental crust, and accretion of island arc terranes to the continental margin.

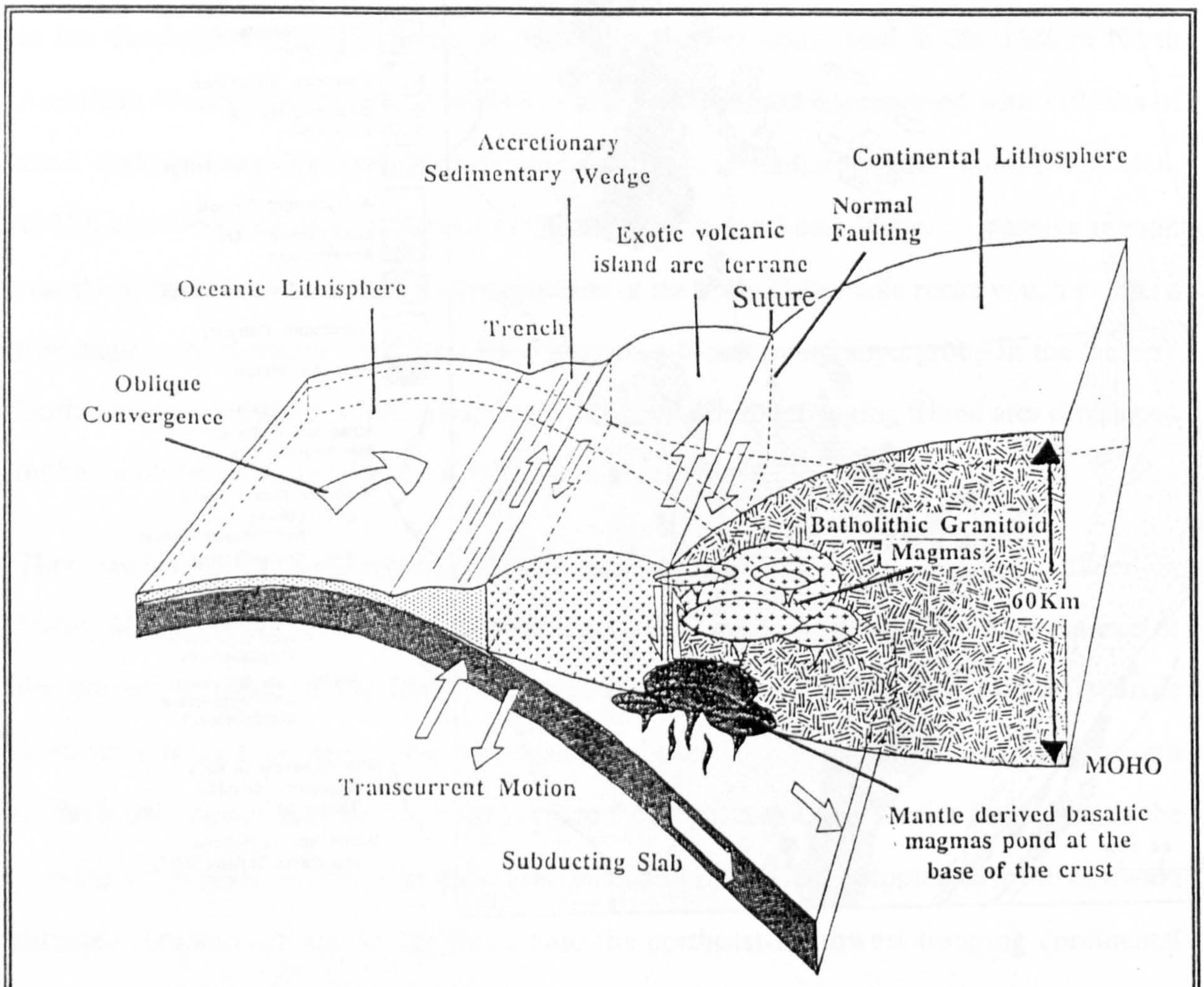

Figure 2.10 Hypothetical model of convergence at a destructive plate boundary associated with the transpressive accretion of an exotic island arc to the continental margin and the generation and emplacement of granitoid magmas of batholithic proportions. Such a tectonic setting is envisioned for the generation of the Atlanta lobe of the Idaho batholith.

Both processes of crustal growth are a result of oblique convergence of the Pacific plate and the North American continental plate, and the associated development of an eastward dipping

subduction zone beneath the North American continent (figure 2.10) (Engebretson et al., 1985). The belt of Mesozoic batholiths represent the exposed roots of an ancient 'Andean'-type continental margin formed above the subduction zone (Hamilton, 1988).

2.5.1 The geology of the Mesozoic, 'Andean-type', continental magmatic arc of the western United States cordillera.

Intrusion of a nearly continuous belt of calc-alkaline, composite batholiths, from Mexico to Alaska (see figure 1.1), occurred during discrete time intervals from the Late Triassic to Early Cenozoic (Armstrong, 1988), and these time intervals correlate with times of more rapid plate convergence (Engebretson et al., 1985). The rock types range in composition from quartz gabbro to two mica granites, but they are dominantly tonalites and granodiorites. At the southern end of the belt the Peninsular Ranges batholith was intruded continuously from 130-80Ma (Silver et al., 1975), and it shows a systematic decrease in age and variations in chemical and isotopic composition from west to east (Gromet and Silver, 1987). The Sierra Nevada batholith was intruded intruded between 210-80Ma, (Evernden and Kistler, 1970), with an analogous but spatially more complex decrease in age and change in chemical composition towards the east, as in the Peninsular Ranges. The Idaho batholith, the Coast Plutonic Complex, the Insular Belt and the Alaska and Yukon batholiths, of the northern end of the Mesozoic batholithic belt (figures 1.1 and 1.2) were coevally intruded between 90-70Ma (Armstrong, 1988; Lund and Snee, 1988; Bennett, 1980). Ages and chemical compositions change from west to east across the batholiths, but reversals occur which complicate the simple patterns.

In general the batholiths contain a greater proportion of ancient continental material to the east, as a result of the intrusion of the batholiths across boundaries between young accreted island arc terranes to the west, and thick Proterozoic continental crust to the east (Oldow et al., 1988). This is particularly well illustrated by the rapid increase from juvenile mantle type initial $^{87}Sr/^{86}Sr$ ratios of ≤ 0.704, of batholiths intruded to the west, in the young

accreted terranes, to the initial $^{87}Sr/^{86}Sr$ ratios ≥ 0.706 of the granitoids intruded in regions to the east where ancient continental basement exists (Kistler and Peterman, 1978; Armstrong, 1977) as shown in figure 2.5. The spatial distribution of the belt today has significant offsets which may be in part a result of changes in dip of the subducting oceanic slab, the region of thickening of the continental crust (Oldow et al., 1988), but also due to post-emplacement distortions of the crust.

Despite the enormous volume of Mesozoic batholithic material emplaced within the western United States cordillera very little of the contemporaneous, volcanic material is preserved as would have been expected by analogy with modern Andean-type continental margins. Estimation of emplacement depths of 8-24km for the Peninsular Ranges and Sierra Nevada and Idaho batholiths (Ague and Brimhall, 1988; Zen and Hammarstrom, 1984) suggest that only small amounts of contemporaneous volcanic material was added to the crustal pile and was likely to have been redistributed by erosion and sedimentation.

2.5.2 Mesozoic exotic terrane accretion

Accretion of exotic oceanic island arc terranes during the Triassic to the Palaeocene, repeatedly occurred by the docking of terranes with the north-south trending continental margin of the western United States cordillera, as a result of the component of oblique convergence, normal to the North American continental margin. Post-docking, predominantly dextral and sinistral shear motions of the terranes along major transcurrent faults, subparallel to the continental margin, accommodated the component of oblique convergence parallel to the continental margin. The resistance of the North American continental plate to large amounts of instantaneous shortening prohibited further motion of the terranes normal to the continental margin, and so promoted these large transcurrent motions developed along major shear zones (Oldow et al., 1988; Engebretson et al., 1985). Kinematic models for oblique convergence involving components of transcurrent and compressive motions, such as the one described above, have become known as "transpressive" motions in the modern American literature (figure 2.10). Recognition of these transpressive motions is important when estimating the amount of crustal thickening

that has taken place by shortening and over-thrusting in compressive orogenic belts, because substantial volumes of material may be transferred in and out of the crustal cross section. To consider the geology and tectonic development of the western United States cordillera during the Mesozoic, Oldow and others (1988) have delineated four tectonic provinces with distinct geological characteristics, (figure 2.11).

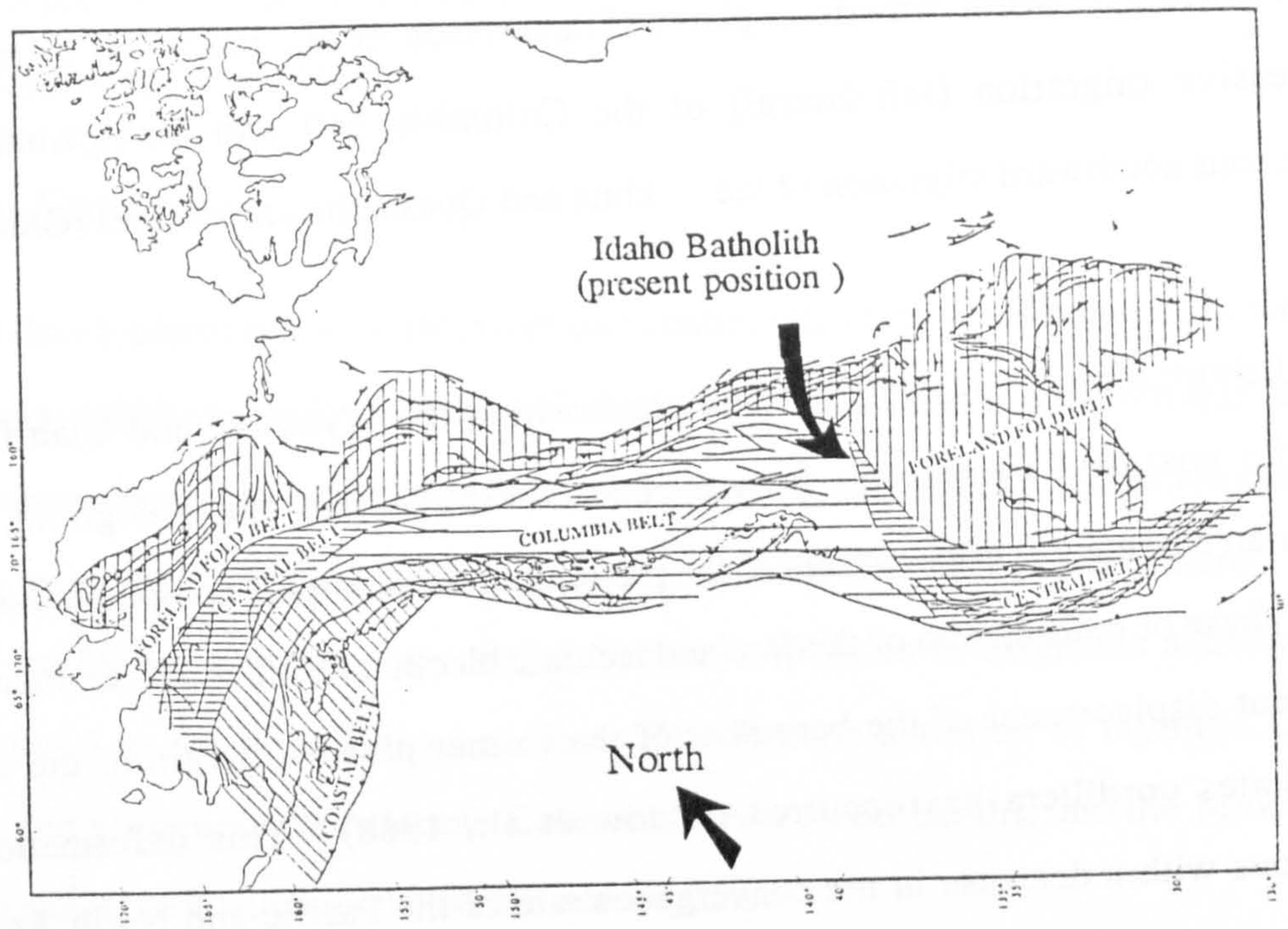

Figure 2.11 Map of the tectonic belts of the western United States cordillera (after Oldow et al., 1988). The Idaho batholith lies just to the west of the juncture between the Central and Foreland belts in the northern United States.

i) The Foreland Fold Belt, of deformed rocks, of unambiguous North American origin, in the eastern cordillera.

ii) The Central Belt of accreted terranes of North American affinity, and remobilised metamorphic basement.

iii) The Columbia Belt of exotic island arc terranes accreted in the northern cordillera.

iv) The Coastal Belt of exotic island arc terranes in northwestern Canada.

The latter three tectonic blocks represent transpressional terranes, while the first two are present in Idaho and important in the generation of the Idaho batholith.

The general situation in the Early Mesozoic is thought to be a westerly facing double arc system, the Stikinia and Quesnellia volcanic arc terranes, of the Columbia tectonic belt, which started to impinge on the margin of the North American continent in the Late Triassic to Early Jurassic (Oldow et al., 1988). Late Jurassic increased rates of oblique convergence of the Pacific and North American plates (Engebretson et al., 1985) led to southward transpressive migration (left-lateral) of the Columbia belt and amalgamation and simultaneous southward migration of the Stikinia and Quesnellia arc terranes (Oldow et al., 1988).

Foreland shortening of 100-150km, took place within the Wyoming and Utah fold belt during the post-Mid Cretaceous (Royse et al., 1975; Villien and Kliegfield, 1986). Precambrian basement is often present as the protolith in metamorphic complexes associated with this phase of deformation of the foreland tectonic block, indicating that shortening and transcurrent displacement of the basement of the former passive margin of the western United States cordillera has occurred (Oldow et al., 1988). This deformation was synchronous with a decrease in the convergence rate of the Pacific and North American plates, the change to generally northward migration of transpressive terranes of the Late Mesozoic, and the docking of terranes, particularly those of the Central Belt at latitudes equal to, and south of Idaho, in present day eastern Oregon and California. The amount of northward migration of accreted terranes decreases in a step-wise manner towards the east, whereas the age of accretion becomes younger towards the west (Oldow et al., 1988). At the time of docking of the Central tectonic belt, the Columbia belt and Coastal belt were still migrating north to their present position in northwest Canada and Alaska.

A broad zone of Mesozoic regional metamorphism with a strongly developed foliation developed in the Proterozoic lithologies to the north of the Idaho batholith, just pre-dates the intrusion of the earliest phases of the Idaho batholith (Lund and Snee, 1988). Radiometric ages of 118Ma and the strong foliation distinguishes this Mesozoic metamorphic event from

the Proterozoic burial metamorphism. The Mesozoic Barrovian sequence of metamorphic mineral assemblages has been preserved to the northwest of the batholith (figure 3.1). Metamorphic grade decreases away from the batholith from sillimanite zone adjacent to the batholith, through the garnet, biotite and chlorite zones of the amphibolite to greenschist facies (Hyndman et al., 1988). In general there is a decrease in metamorphic grade from the northwest to southeast in the country rocks of northern Idaho, which is probably related to shallower depths of emplacement of the Bitteroot lobe of the Idaho batholith towards the southeast (Hyndman et al., 1988).

2.6 The Cenozoic

The major development of the North American continental crust of the present day western United States cordillera, took place by periods of crustal accretion in the Archaean, Early-Middle Proterozoic and the Mesozoic. Subsequently, magmatic activity, and extensional and strike slip tectonics have created the present day western United States cordillera. In the region of the Idaho batholith, three major Cenozoic episodes of magmatic activity have added material to the crustal cross-section. The Eocene andesitic to rhyolitic Challis volcanics and plutonics, the Miocene Columbia River flood basalts, and the Miocene to Recent Snake River Plain bimodal basalts and rhyolites.

Subduction and arc magmatism continued all along the western margin of the cordillera in the Early Cenozoic. Changes in tectonic regime and magmatic activity were due to episodic changes in plate motions. The controlling factor up to 55Ma were variations in rates of convergence, change in direction of convergence occurred at 42Ma (Engebretson, 1985), and change in the nature of the boundaries at 29-30Ma (Atwater and Molnar, 1973). Figure 2.12 shows reconstructions of the Pacific and North American plate interactions and the regions of major magmatic activity from the Early Cretaceous to the Late Miocene. A break in magmatic activity occurred between 70-55Ma along the whole margin of the western United States cordillera, due to an increased rate of convergence leading to a lower angle of subduction and a lull in the generation of arc related magmas (Lipman, 1971).

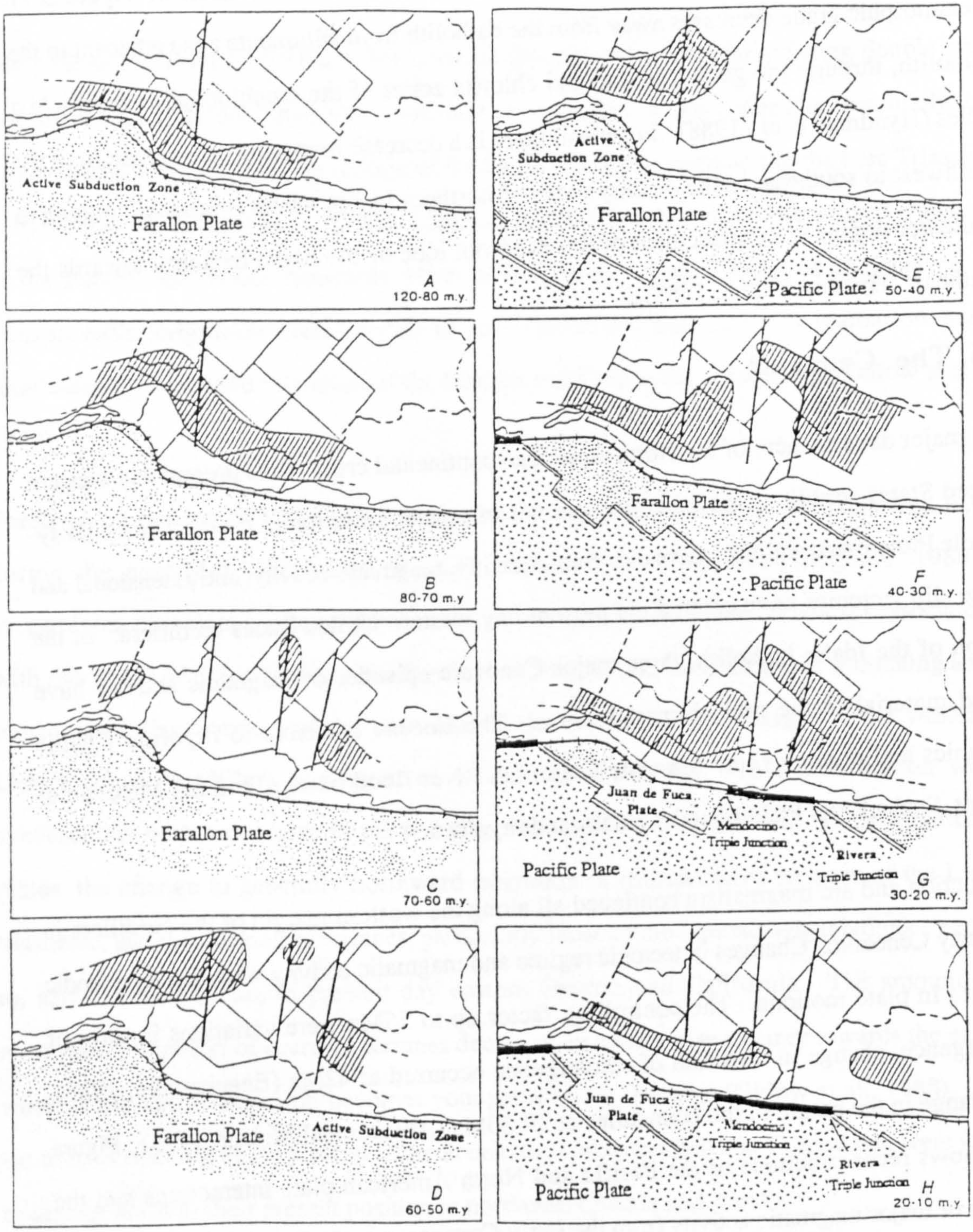

Figure 2.12 Generalised distribution in the western United States of andesitic volcanic suites, thought to be related to subduction, (from Lipman 1980). North lies to the left, and ruled fields represent the distribution of active volcanism during a particular time frame. Notice the generation of the Mendocino and Rivera triple junctions in the Early Cenozoic as the east-Pacific rise was consumed beneath the overiding American continental plate.

The Challis volcanics, erupted on the eastern margin of the Idaho batholith, consist of early, mafic-intermediate lava flows and tuff breccias, and later, voluminous, explosive and more silicic, dacitic to rhyodacitic lavas and ash flow tuffs (Moye et al., 1988). Volcanism spans the period of 51-44Ma, which also brackets the time of epizonal intrusion of a bimodal suite of dioritic to granitic plutons into the Cretaceous phases of the Idaho batholith (Bennett, 1980), interpreted to be the intrusive equivalents of the Challis volcanics. Increased rates of convergence were associated with the growth of this extensive calc-alkaline to potassic volcanic belt from 50-45Ma, including the eruption of the Clarno and Absaroka volcanics (Bennett, 1986; Hyndman, 1980; Moye et al., 1988).

The change to a more orthogonal, and decreased rate of, convergence, between the Pacific and North American plates, between 42-40Ma, led to a steeper angle of subduction, subduction zone roll back, and the onset of back arc spreading as the first major extensional event during the Cenozoic (Engebretson, 1985; Oldow, 1988). A westward step of the subduction zone, in the northwestern United States cordillera, at 40 Ma occurred due to the accretion of the Oregon and Washington, Coast ranges, (Duncan, 1982), and the development of a broad Cascades arc.

Early Cenozoic magmatic activity in the Great Basin encroached from the north and south in a step wise fashion, following the similar migration of early extension into the Great Basin eventually to form the Basin and Range tectonic and magmatic province in the Late Cenozoic, figure 2.12 (Lipman 1981). This intense Late Cenozoic extension is concentrated in areas of previous shortening, and is associated with development of the Mendocino and Rivera triple junctions, as the east Pacific rise was consumed beneath the overiding North American continent, figure 2.12 (Engebretson, 1985). The change to dominantly strike slip motions in the southwest cordillera is the controlling factor in an overall decrease in magmatic activity and the eruption of bimodal volcanics, which were thought to become gradually more basaltic as the fertile crustal sources were exhausted (Oldow et al., 1988).

In Oregon, Washington and Idaho, the Columbia River Plateau flood basalts were erupted between 17-14Ma (Christiansen and Lipman, 1972; Carlson and Hart, 1987). The sub-alkaline magmas are probably related to southwest-northeast extension behind the Cascades magmatic arc and they are synchronous with large bimodal eruptions near the Oregon, Idaho and northern Nevada state borders (Oldow et al., 1988). Similar eruptive centres migrated northeastwards to form the Snake River Plain-Yellowstone Plateau province (Armstrong et al., 1975). It has been speculated that this linear province may represent the track of the North American continent over the central plume of a hot spot now centred beneath Yellowstone, although this origin is uncertain (Leeman, 1982; Thompson, 1989).

In general the Cenozoic magmatic activity in the western United States cordillera has decreased and become more basaltic with time, and spatially more voluminous and tholeiitic towards the northwest. The development of silicic magmas is greatest in the Cordilleran Interior where thick continental basement exists.

2.7 Evolution of the continent-island arc juncture in west-central Idaho, and intrusion of the Idaho batholith.

The following section puts the Mesozoic tectonic development of Idaho and the intrusion of the Idaho batholith in context of the above generalised tectonic framework of the western United States cordillera.

Amalgamation of the Olds Ferry, Wallowa-Seven Devils and Baker terranes of the Blue Mountains province in Oregon occurred in the latest Jurassic (Avé Lallemant, 1989). The rocks of the Blue Mountains of east-central Oregon were juxtaposed with the North American continental margin in the late Early to early Late Cretaceous (120-95Ma) (Lund and Snee, 1988; Snee et al., 1989; Lund, 1984; Allen-Manduca, 1988).

Continued right-lateral movement on a transcurrent fault along the previously developed suture between the Blue Mountains and the North American continent, led to multiple phase deformation and metamorphism in the greenschist to upper amphibolite facies, within both

the western terrane of arc volcanics, and the eastern terrane of Mid-Proterozoic to Palaeozoic continental metasediments (Lund, 1984). Lund and Snee (1988) have dated these events at 118-93 Ma and have recognised inverted metamorphic sequences, decreasing in grade structurally down and away from the suture. These sequences are interpreted as flower structures, with the deepest crustal levels exposed at the suture as a consequence of dominant vertical movement at the suture, and lateral transport away from the juncture Lund and Snee (1988) Allen Manduca (1988).

The final metamorphic event and the synchronous emplacement and deformation of tonalitic plutons along the suture is dated at 93-88Ma (Lund and Snee, 1988). Coeval, undeformed plutons intrude both terranes a few kilometers both east and west of the suture, cutting across earlier fabrics. The suture can be recognised within a few tens of meters on the basis of initial $^{87}Sr/^{86}Sr$ isotope ratios of the tonalites intruding it (Armstrong, 1975; Fleck and Criss, 1985). To the west of the suture initial $^{87}Sr/^{86}Sr$ ratios are ≤ 0.704, whereas to the east, the initial $^{87}Sr/^{86}Sr$ ratios are ≥ 0.706, with a transition zone on the scale of a few tens of metres, representing the contrasting isotopic signatures from a young island arc, and mature Proterozoic continental crust respectively (Fleck and Criss, 1985).

Rapid uplift, associated with cooling and erosion of the plutons, occurs between 88-78Ma (Lund and Snee, 1988). Emplacement depths are estimated to be more than 25km, due to the presence of primary magmatic epidote (Zen and Hammarstrom, 1984), and estimation of the geothermal gradient, and measurement of hornblende closure temperatures, has allowed Lund and Snee (1988) to estimate uplift rates of 4mm/yr between 84-81Ma and 2mm/yr for 81-78Ma. These extremely rapid uplift rates are put in perspective by the 5mm/yr measured uplift rates of the Nanga Pargat massif in the Himalayas (Zeitler, 1985).

At 85Ma a decrease in convergence rates of the Pacific and North American plates occurred at the time the main phases of the Idaho batholith were intruded, as the focus of magmatic arc activity migrated east. The main phases of tonalite, granodiorite and two-mica granite of the Idaho batholith were intruded east of the continent-island arc juncture between 85-70Ma (Criss et al., 1982; Armstrong, 1977; Criss and Fleck, 1987; Fleck and Criss, 1985; Snee et

al., 1986; Lund and Snee, 1988; Chase et al., 1978; Bickford et al., 1981; Shuster and Bickford, 1985; Bennett, 1980;Lewis et al., 1987). Uplift of the southern Idaho batholith continued throughout the Upper Cretaceous and Early Eocene (Vallier and Brooks, 1987). Intrusion of the Eocene bimodal, dioritic and granitic suites occurred within, and to the east of the Cretaceous main phases of the Idaho batholith. Emplacement of these rocks, which are exposed at the surface with the main Cretaceous phases of the Idaho batholith today, was at upper crustal levels, proving that by the Eocene the Idaho batholith had risen by 15-20km.

CHAPTER 3

Field Study and Petrography

3.1 Introduction

The granitoids of the Atlanta lobe of the Idaho batholith are part of the great chain of Mesozoic, subduction-related, composite batholiths of the western United States cordillera, and they outcrop over an area of approximately 40000km^2 in west-central Idaho. This chapter contains information on the field relations and petrography of the tonalitic to granitic (sensu-stricto) Cretaceous, main phases of the southern, "Atlanta lobe" (Armstrong, 1975b) of the Idaho batholith. It also documents the field relations of a suite of bimodal Eocene plutons with compositions ranging from diorite to granite.

The major objectives of this chapter are listed below:

i) To describe the field relationships and the petrography of the Cretaceous, 'Main phase' granitoids, of the Idaho batholith, and the Tertiary bimodal intrusive suite;

ii) To classify the Idaho batholith granitoids into useful groups of genetically related rock suites;

iii) To determine the crystallization sequences for each group of genetically related rocks, and to discuss the emplacement depth responsible for such crystallizing assemblages;

iv) To identify any petrographic textural features which may be indicative of such physical processes as crystal separation, in-situ growth, or crystal accumulation.

v) To summarise the geochronology of the granitoids of the Atlanta lobe of the Idaho batholith.

In order to model the chemical variations within the Idaho batholith granitoids in the later chapters, it is necessary to identify the crystallizing phases that maybe responsible for the chemical fractionation. It is also necessary to demonstrate that subsequent metamorphic reactions, metasomatism, or alteration, has not changed or developed new mineralogical

assemblages and hence disrupted any simple relationships between crystallizing assemblages and chemical variations, by the recognition of undisputed igneous textures. Moreover, it is important to recognise texturally whether the phases crystallized during the ascent of the magma (cumulus), or crystallized after the magma was emplaced and ceased to behave as a fluid (inter-cumulus), both from the view point of chemical modelling, and estimation of source versus emplacement depths. The high viscosities of silicic magmas and the probability that such magmas exist as crystal-rich mushes (Wickham, 1987), make recognition of cumulus versus inter-cumulus phases particularly problematic in coarse grained granitic rocks.

3.1.1 Previous work

Ross (1928) and Anderson (1952) recognised several phases of Mesozoic granitoids and an episode of Tertiary plutonism during early reconnaissance and mapping of the Atlanta lobe of the Idaho batholith. Further mapping by Schimdt (1964) Reid (1963) and Kiilsgaard et al. (1970) in restricted areas, discovered the extensive nature of the Cretaceous intrusive phases and separated out some small Tertiary epizonal stocks. Subsequently much work has been carried out by various workers, and in association with the United States geological survey, it has been condensed into two geological maps which cover the study area: the Challis 1° x 2° geological map (Fischer et al., 1983; 1987); and the geological map of south-central Idaho, the Hailey 1° x 2° sheet compiled by Johnson et al. (1988). Although these maps were published after the field work of this project was completed, early editions allowed the outcrop patterns and major divisions of lithology to be used as the basis in the field during this study. Extensive geochronological work in association with the above mapping projects has been important in separating the Cretaceous main phases of the Idaho batholith from the Tertiary intrusive phases, that were not previously thought to be so voluminous. Lewis et al. (1987) provide a comprehensive list of geological studies of the Cretaceous batholith, and Bennett and Knowles (1985) have compiled a list of studies on the Tertiary intrusives.

A common observation made of the Idaho batholith, which appears in many of the field reports and maps, is the lack of numerous, small, well-defined, granitoid plutons with sharp intrusive contacts, in contrast with other large composite batholiths such as the Sierra Nevada (Hamilton, 1988). The discrete Cretaceous intrusive phases of the Idaho batholith are extremely large, outcropping over areas of approximately 1000-10000km^2 (Lewis et al., 1987), and even where well exposed they display gradational contacts between different lithologies. Consequently problems have arisen in constructing maps of the boundaries between the main phases, and interpretation of the genetic relationship between the main phases is difficult to establish. Grouping of rocks into single intrusive units or 'facies', on a pluton by pluton scale, is only possible in limited areas where extensive geochemical and geochronological data exist. The absence of an unambiguous field-based framework on which to fall back on, as the, "bottom line" in more complex geochemical arguments requires a greater number of assumptions and generalisations become necessary. However, the monotonous intrusive nature of the batholith has been interpreted to indicate that the main rock types of the batholith have a monogenetic origin, and represent a single comagmatic series or super unit (Hyndman, 1984). The study by Fischer et al. (1983) subdivides the Cretaceous batholith into six major lithological groups, and Lewis (1984) Lewis and Kiilsgaard (in press) have separated the Tertiary intrusive rocks into a bimodal suite of epizonal granites and a more mafic dioritic to quartz-monzodioritic suite. These subdivisions have been adopted as the basis for the classification of the granitoids of the Idaho batholith, but are modified where necessary (see section 3.2).

Petrographic descriptions of the granitoids of the Atlanta lobe are reported in Kiilsgaard and Lewis (1985) and in Lewis et al. (1987). Little detailed, thin section, textural analysis of the granitoids has been reported, except for the tonalites of the western border zone and in the northern Bitteroot lobe of the batholith (Hyndman, 1984; Toth, 1987; Wiswal and Hyndman, 1987).

Studies of the metamorphism, deformation and some limited geochemistry, have been carried out on the only exposed pre-batholithic country rocks associated with the Idaho batholith, to the northwest of the Atlanta lobe, in the Salmon River Arch and to the north of the Bitteroot lobe in northern Idaho (figure 3.1). Although these rocks outcrop over 100km to the north of the most northerly samples from this study (see figure 3.3) they are the only country rocks exposed, and so a brief review of the work completed on these rocks by, Hyndman (1983; 1988b), Armstrong (1975b), Wiswall and Hyndman (1987), and Hamilton (1988), will be contained in this chapter. The importance of this is to constrain the emplacement depth, and to put a minimum limit on the depth of the source, and thus the part of the stratigraphic section that may be considered as possible source rocks.

A geological traverse along a southwest to northeast cross-section from the Proterozoic metamorphic country rocks of the Salmon River Arch across the border zone and into the interior of the Bitteroot lobe of the Idaho batholith (figure 3.1a,b) has revealed variations in the lithologies and metamorphic grade of the country rock, which led to suggestions on the depth of emplacement of the Bitteroot lobe (Hyndman, 1984). Across approximately 15km of section, the dominant muscovite-biotite-quartz-feldspar schist and gneiss with local kyanite and almandine give way towards the batholith, to granitic augen-gneiss and ultramafic breccia. At the contact these are replaced by diopside-hornblende-plagioclase gneiss and mica-quartz-feldspar schist with the development of sillimanite, i.e. within the upper amphibolite facies. Further south in the Salmon River Arch, Wiswall (1979b), has reported similar Proterozoic Belt supergroup, metasedimentary anatectic migmatites, in the upper amphibolite facies, which are interpreted to outcrop below the lacolithic lobe of the batholith in this area (Hyndman and Wiswall, 1987). Additional rock types intruding the basal metasedimentary pile are hornblende-quartzmonzonite augen gneiss, dioritic orthogneiss and meta-anorthosites, together with pods of amphibolite, meta-gabbro and pyroxenite.

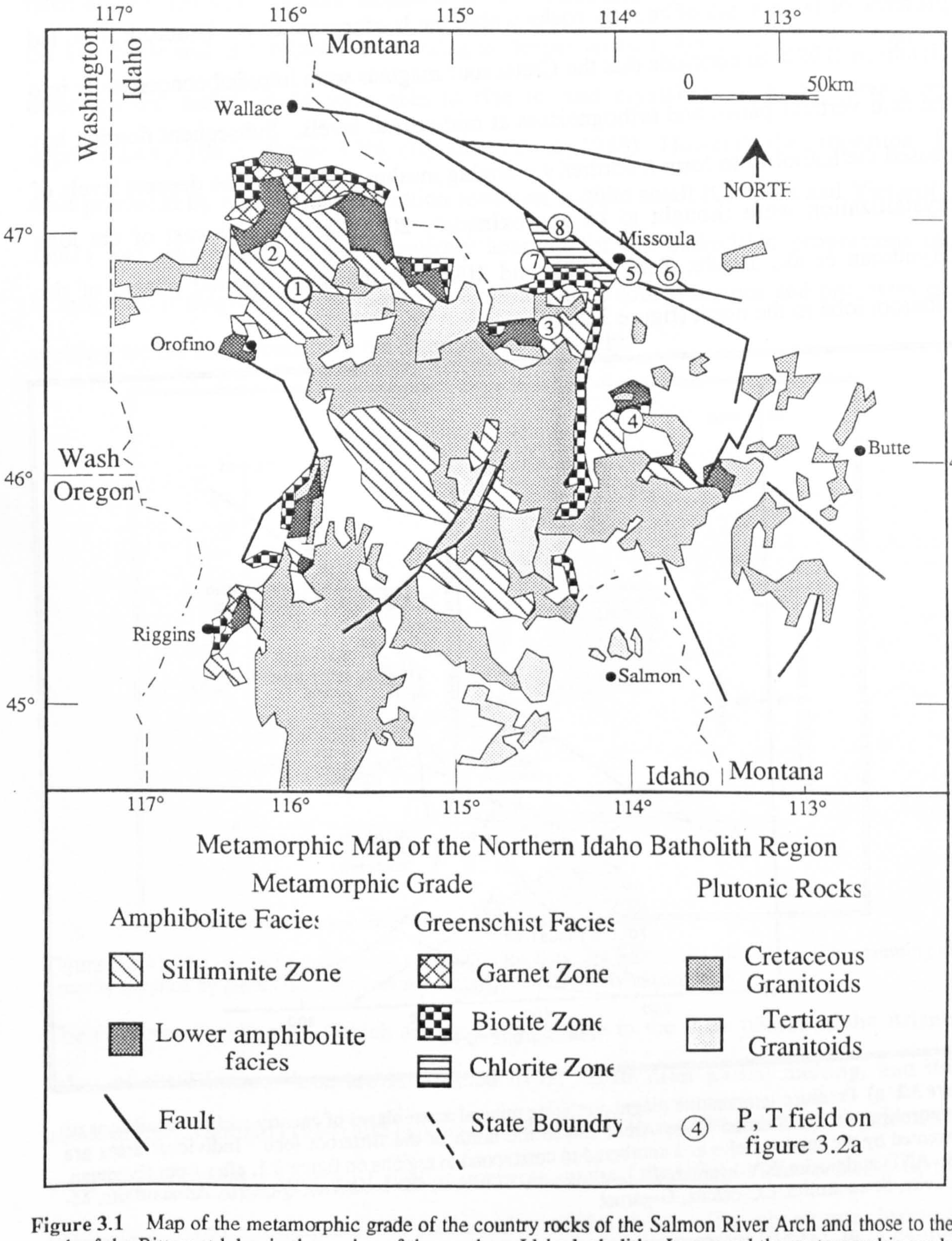

Figure 3.1 Map of the metamorphic grade of the country rocks of the Salmon River Arch and those to the north of the Bitteroot lobe, in the region of the northern Idaho batholith. In general the metamorphic grade declines from the silliminite zone of the upper amphibolite facies adjacent to either lobe of the batholith away in a roughly concentric manner. Map modified after Hyndman et al.(1988b) and circled numbers refer to pressure/temperature fields shown on figure 3.2a.

An internal foliation within the granitoids which varies from vertical at the margins to near horizontal in the interior, the high metamorphic grade of the country rocks and the presence of large septa of country rocks within the border zone of the Bitteroot lobe, led Hyndman (1984) to conclude that the Cretaceous magmas were intruded concordantly into the near vertical para-, and orthogneisses at mid-crustal levels. Subsequent doming has caused the batholith to form a northerly plunging mushroom shape. The deepest levels of crystallization were thought to be approximately 20km in the southwest of the lobe (Hyndman et al., 1988b; Zen, 1988), and 10km for the main internal phases of the Bitteroot lobe to the north (figure 3.2a,b).

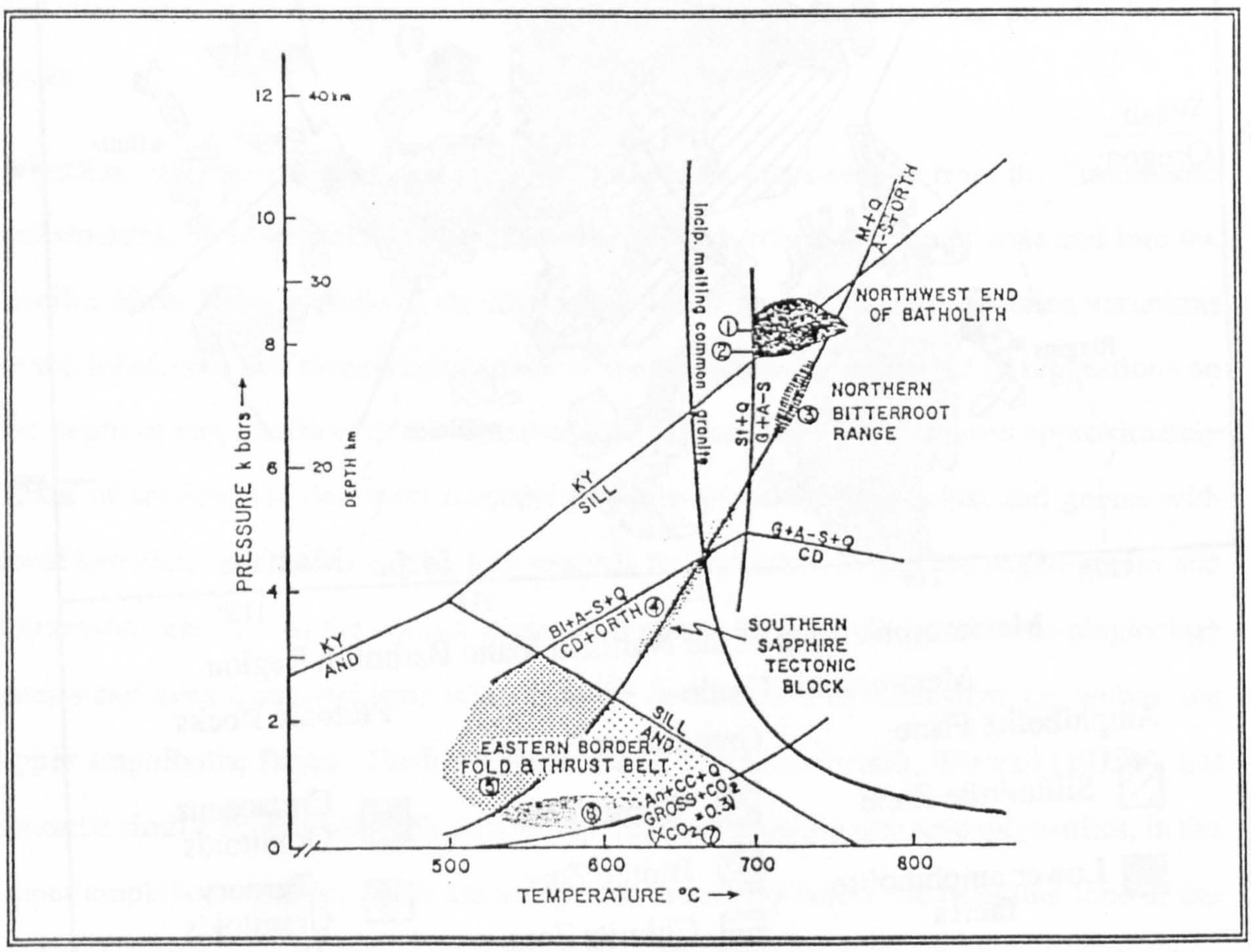

Figure 3.2 a) Pressure-temperature diagram relating mineral assemblages of country rocks to conditions of metamorphism in the Salmon River Arch, and to the north of the Bitteroot lobe. Individual areas are represented by the shaded fields and numbered to correspond to regions on figure 3.1, after from Hyndman, 1988. AND-andalusite, KY-kyanite, SILL-sillmanite, BI-biotite, CD-cordierite, Q-quartz, An-anorthite, M-muscovite, St-staurolite, CC-calcite, G-garnet

Hyndman et al. (1988) interpreted the migmatites to represent the upper level of a quartzo-feldspathic paragneiss or orthogneiss source region for the Cretaceous magmas of the

Bitteroot lobe. Partial melting by dehydration of muscovite at 20-25 km was wrongly thought by Hyndman et al. (1988) to produce water saturated magmas that could have risen to only 15km, before intersection with the solidus and crystallization occurred. To the southeast end of the batholith, melting at deeper levels (≈40km), resulted in hotter, drier, partial melts which were able to rise to, and crystallize at higher levels of approximately 10km, (figure 3.2b), (Hyndman et al., 1988). However, the proportion of melt produced by muscovite dehydration reactions is quite small (Clemens and Vielzeuf, 1987) and thus it is unlikely to entirely account for the batholithic proportions of homogeneous magmas of the Atlanta lobe. Alternative source regions and processes of melting are the main concern of the latter part of this study.

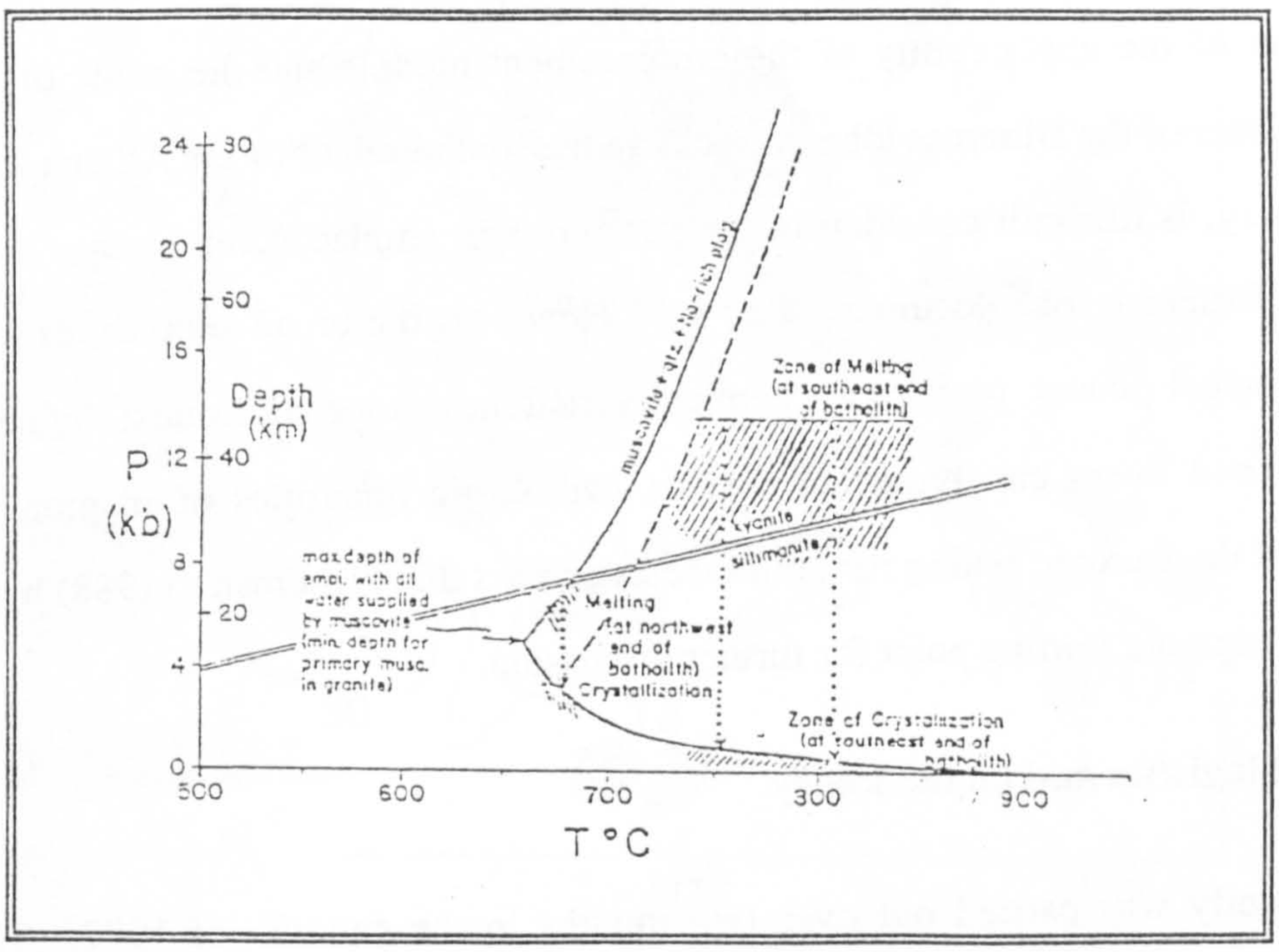

Figure 3.2 b) Melting and emplacement relations in the Bitteroot lobe of the Idaho batholith, assuming all water is supplied by muscovite dehydration reactions, taken from Hyndman, 1988.

The common "schlieren", (which are surprisingly rare in the main phases of the Atlanta lobe) of the Bitteroot lobe are interpreted to be restite after partial melting, and this encouraged Hyndman (1984) and Hyndman et al. (1988) to suggest that large degree melts were derived from a source of similar composition and that little differentiation of the magmas allowed entrainment and preservation of the restite. The above conclusion is

further supported by the extensive nature, and monotonous composition of the internal phases of the batholith.

The conclusions regarding the metamorphism and structural levels of emplacement of the Bitteroot lobe appear to be broadly correct, substantiated by the reported factual evidence in comparison with experimental studies. However, the rather speculative conclusions regarding the depth and nature of the source are directly contradicted by the extreme contrast between the ε_{Sr} values of the exposed orthogneisses, paragneisses and schists, with the main phases of the Bitteroot lobe (Criss and Fleck, 1987). Fleck and Criss (1985) suggest that the internal phases of the Bitteroot lobe, with an initial $^{87}Sr/^{86}Sr$ ratio of, ≈0.708, probably incorporates a major component of Proterozoic lower crust.

Assessment of the applicability of the emplacement models and the grade of regional metamorphism of the Bitteroot lobe, to rocks in the southern half of the Atlanta lobe, over 300km, away, is difficult considering the variations in emplacement depth over 100km across the Bitteroot lobe documented above. However, the broad similarities in pluton size, lithological phases, petrology, chemical variation, isotope signatures; the need for a coeval thermal event capable of producing batholithic quantities of magma and the similarity of the tectonic setting for both lobes, suggests that Hyndman's (1988) hypothesis make an acceptable starting point for further discussion.

3.1.2. Field logistics and methodology

The field study was carried out over two months in the summer of 1987. The area investigated, and from which the samples were taken is shown in figure 3.3, which covers most of the central and eastern parts of the Atlanta lobe of the Idaho batholith. Exposure is generally very extensive but varies considerably from region to region. In the southern parts of the batholith, low, deeply weathered, rounded hills covered in scrubby sage-brush make for very little exposure in this desert-like environment. To the north of the field area, extensive tracts of national pine forest, the high peaks (3650m) and deep river canyons (plate 3.1) of the granitoid terrain, allow excellent, almost 100% exposure of the granitoids in some of the highland areas.

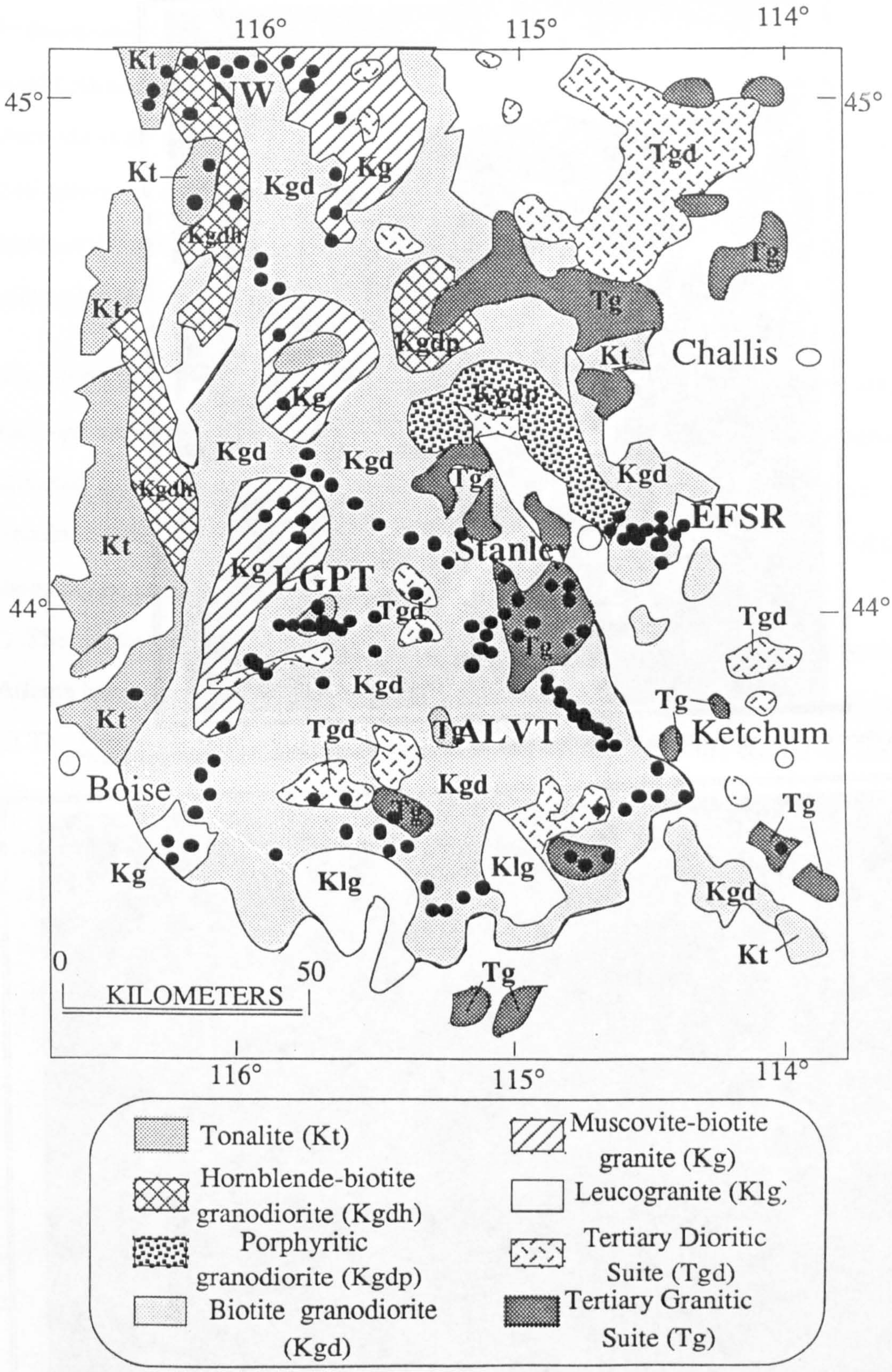

Figure 3.3 Simplified geological map of the study area of the Atlanta lobe of the Idaho batholith showing the general distribution of the Cretaceous and Tertiary phases, the sample localities(•), and the detailed traverses, EFSR, ALVT, NW and LGPT.

Plate 3.1 A deep canyon on the South Fork of the Payette River exposes granitoids at a range of levels.

Plate 3.2 Jagged peaks of the Tertiary, epizonal, granite plutons in the Sawtooth batholith are well exposed but logistically difficult to study and sample. A dominantly vertical jointing pattern gives rise to the rugged topography.

Unfortunately the road access varies inversely with exposure, but spectacular, canyon side road cuts and temporary, but migrational, logging roads, allowed most of the study to be undertaken by week-long jeep trips into the wilderness areas from the towns of Ketchum and Stanley in central Idaho (figure 3.3). In addition, a number of multi-day treks to less accessible areas, particularly the jagged peaks of the Tertiary intrusives (plate 3.2), were undertaken to fill in the gaps in traverses.

The field study was targeted on a number of small scale traverses, or restricted areas, but a back-ground sample set was collected with a much lower sample density between the targeted areas, because of the unusually extensive nature of the intrusive units. Four detailed traverses were made in the Cretaceous main phases of the batholith, and these are listed below and shown in figure 3.3 and 3.4a,b,c.

i) The northwest traverse, (NW); from the northwestern border to the interior of the Atlanta lobe, figure 3.3.

ii) The East Fork of the Salmon River traverse, (EFSR); from the central eastern border along the Salmon river to the interior of the batholith near Stanley, figure 3.4a.

iii) The Long Gulch pluton traverse, (LGPT); in the south-central area of the Atlanta lobe, figure 3.4b.

iv) The Alice Lake to Vienna Mining District traverse, (ALVT); in the south eastern region of the Atlanta lobe, figure 3.4c.

Additional samples of Cretaceous main phases of the Atlanta lobe were collected towards the southern margin of the Atlanta lobe and in the central areas of the lobe where the same lithologies occur over particularly extensive areas. The Tertiary bimodal suite of granitoids have been studied in several areas where they outcrop as small, distinct, individual plutons (figure 3.5). The Sawtooth batholith, in the southeastern region of the lobe, the Long Gulch pluton in the south-central Atlanta lobe, numerous plutons in the Cape Horn Lakes area, and various stocks in the south of the lobe, collected by Leeman, 1986 and Lewis, 1986, have been studied.

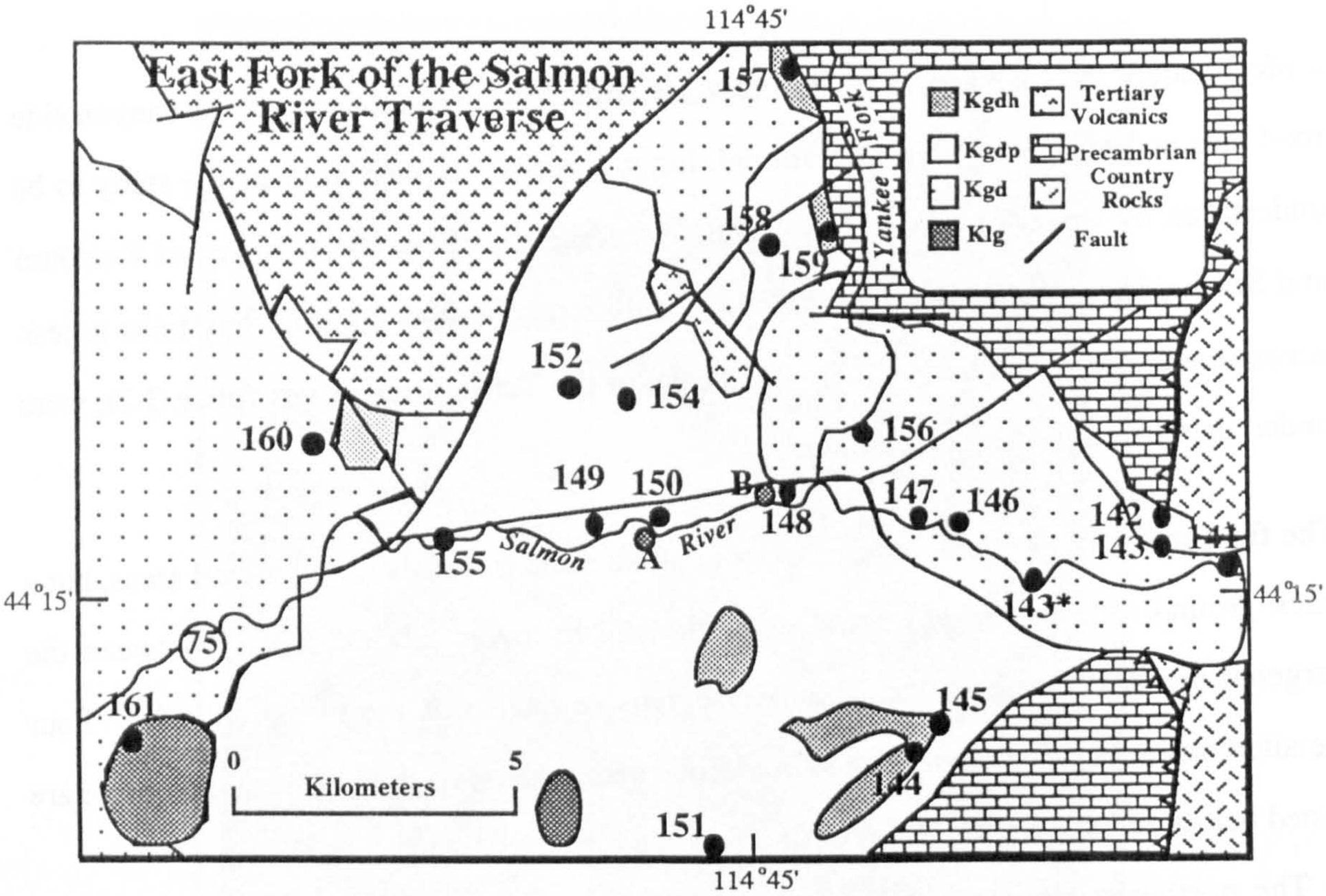

Figure 3.4a Map of the East Fork of the Salmon River traverse, showing the distribution of lithologies and sample localities. Kgdh-hornblende-biotite granodiorite, Kgdp-Porphyritic granodiorite, Kgd-biotite granodiorite, Klg-leucogranite.

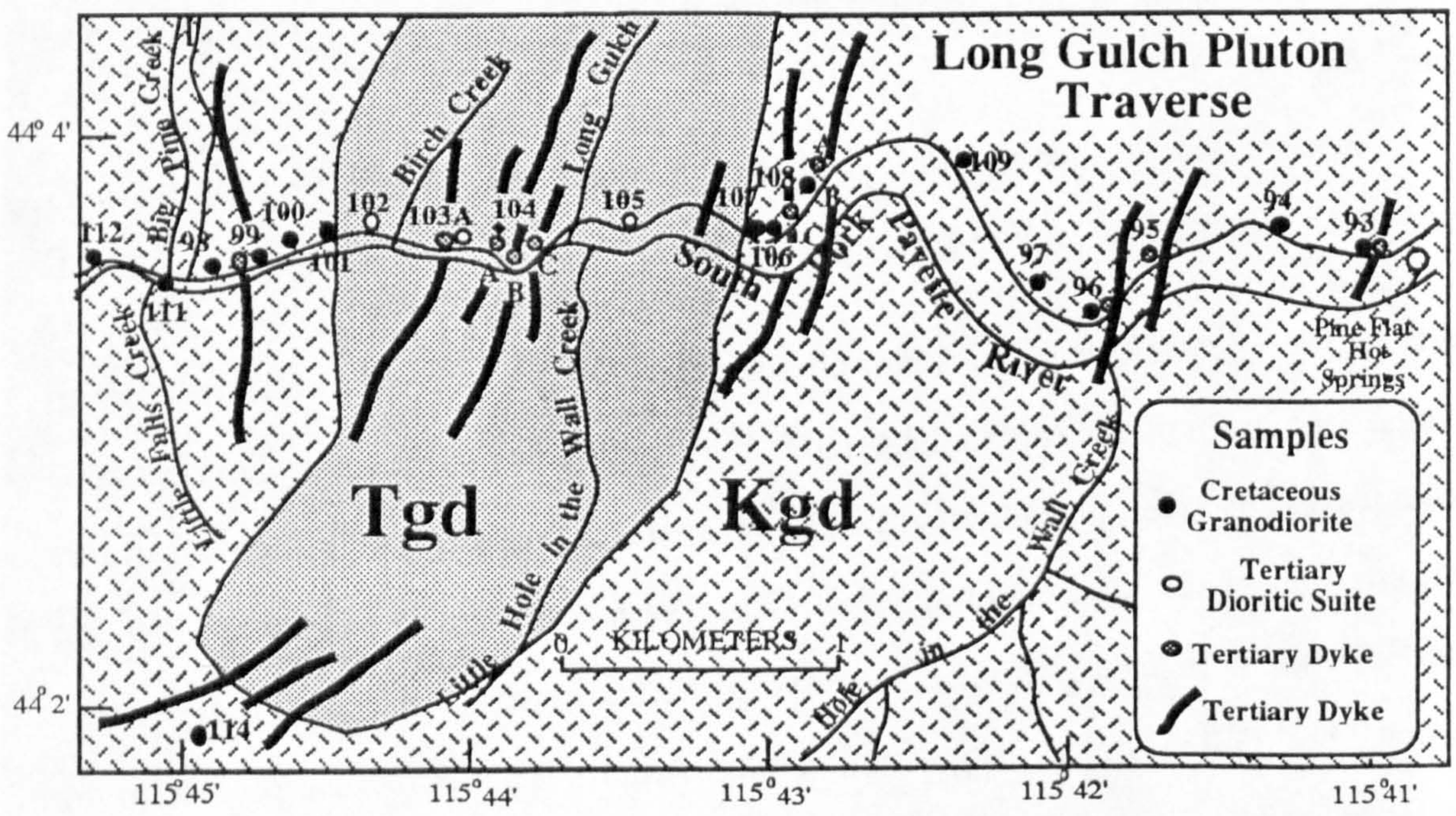

Figure 3.4b Map of the Long Gulch pluton traverse, showing the distribution of lithologies and sample localities.

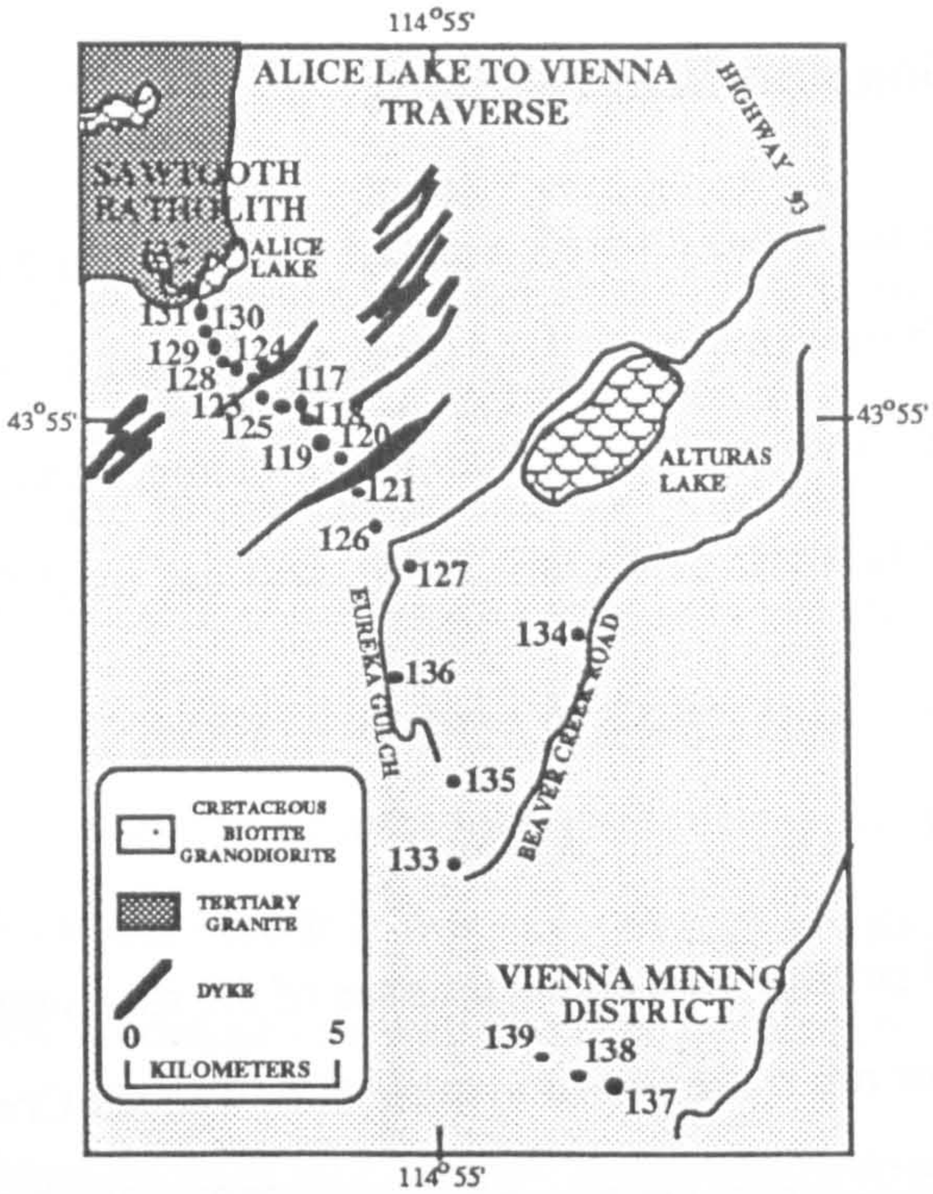

Figure 3.4c Map of the Alice Lake to Vienna Mining District traverse, showing the distribution of lithologies and sample localities.

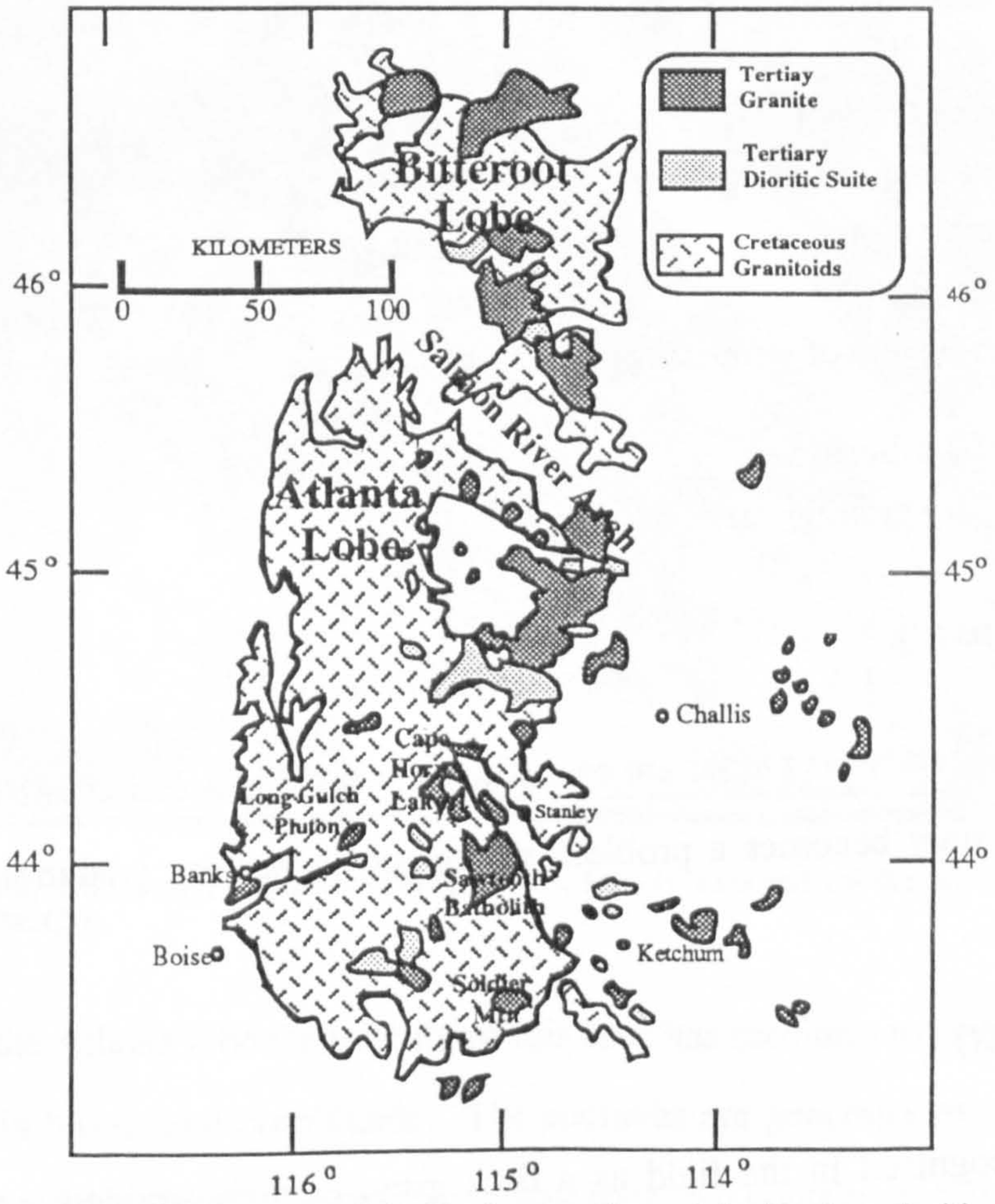

Figure 3.5 Map showing the distribution of the Tertiary granite and the Tertiary dioritic suite in the region of the Idaho batholith.

3.2 Field classification and field relations

The granitoids of the Idaho batholith are classified according to the recommendations of Strekeisen (1976) as shown in figure 3.7. Estimated modal mineralogies from thin sections, agree well with those calculated from major element data, using the GRANITE NORM fortran program (Harris, pers com.,1988), and are used for the purpose of the above classification.

3.2.1 Field classification

The main lithological and petrogenetic characteristics of the six Cretaceous rock types, and the two Tertiary rock types are summarised in table 3.1. The six Cretaceous main phases, (K), are:

Tonalite	**(Kt)**
Hornblende-biotite granodiorite	**(Kgdh)**
Porphyritic granodiorite	**(Kgdp)**
Biotite granodiorite	**(Kgd)**
Muscovite-biotite granite	**(Kg)**
Leucogranite	**(Klg)**

The Tertiary bimodal suite of granitoids (T) are split into:

Tertiary dioritic suite	**(Tgd)**
Tertiary granitic suite	**(Tg)**

3.2.2 Field relationships

In the field, all six Cretaceous phases are easily identified. Classification into one or other lithological group only becomes a problem where rock types are gradational into one another.

3.2.2 i) Tonalite (Kt)

The tonalite is recognised in the field as a dark grey, medium-grained, equigranular, homogeneous rock. The tonalites outcrop extensively along the western border zone of the

Atlanta lobe and develop a weak to strong, yet pervasive foliation and exclusively to this region, within the Atlanta lobe, are spatially associated with migmatites (plate 3.3). Studies by Allen-Manduca (1988) and Lund and Snee (1984) in the northwest of the lobe, reveal that foliation in this region strikes approximately north-south, subparallel to the margin of the batholith, and to the suture with the Blue Mountain accreted island arc terrane to the west. Similar north-south striking foliations are seen further to the south, in border zone tonalites, in the vicinity of the town of Banks, (figure 3.3). Tonalite crops out close to the eastern border of the Atlanta lobe particularly along the East Fork of the Salmon River (figure 3.4a) but here it is less extensive, discontinuous, and it only rarely develops a weak foliation in comparison with that near the western margin.

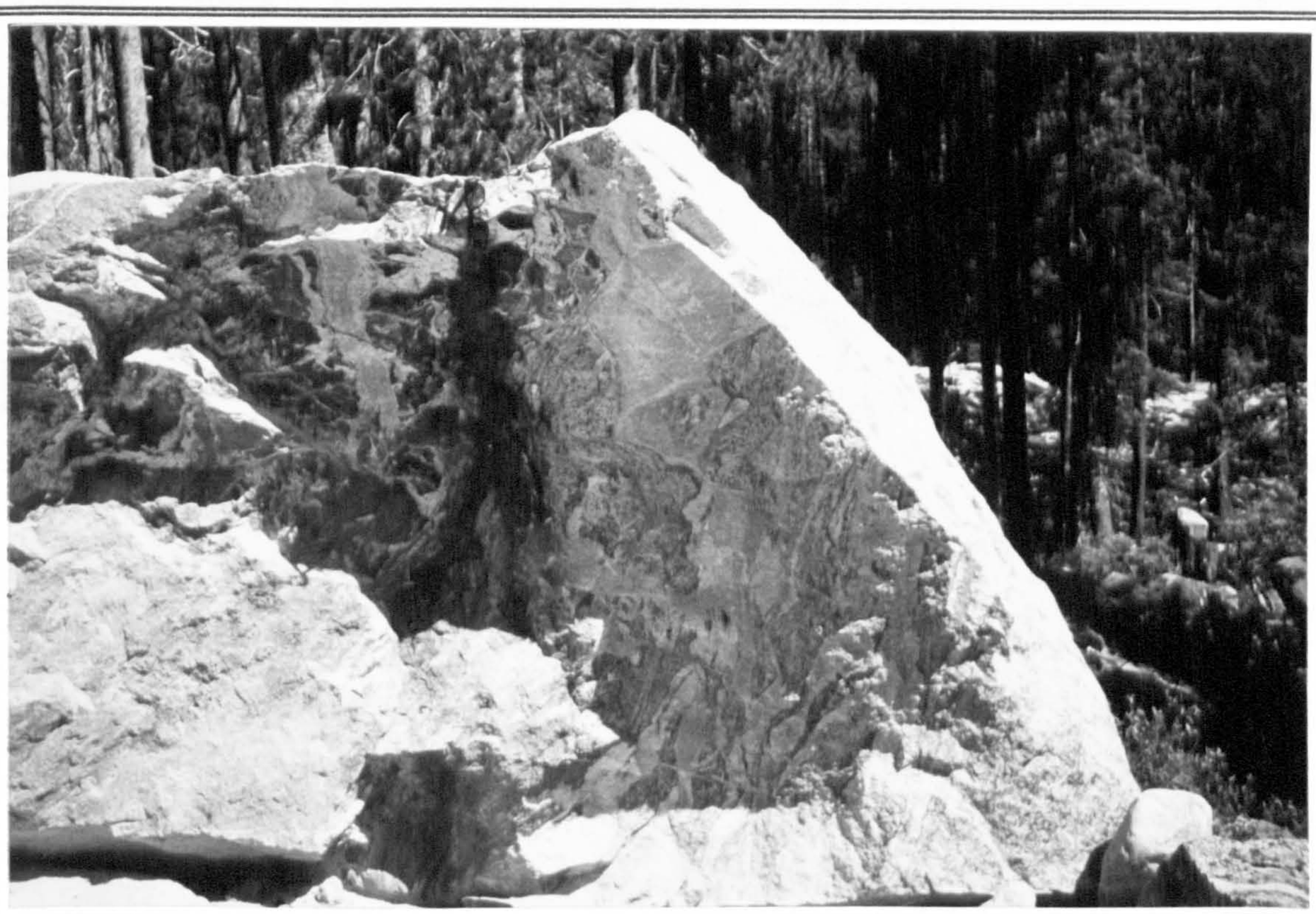

Plate 3.3 Foliated, migmatitic, tonalitic, orthogneisses, locally exposed on the western border of the batholith, west of McCall.

Unusually for the Atlanta lobe the tonalite of this area has medium- to fine-grained, mafic enclaves, rich in biotite and hornblende. The enclaves are generally rounded, and have well defined boundaries with the surrounding host rock, but contain modally only 5%-10% more hornblende and biotite than the matrix. The enclaves are interpreted to be igneous

autoliths of slightly more mafic liquids that became separated into viscous blobs and entrained in convecting, slightly more silicic magmas. Smaller areas of tonalite have been identified in the interior of the Atlanta lobe, some of which have been sampled in the southern region. The tonalite appears gradational into the hornblende-biotite granodiorite, and it can only be distinguished from the porphyritic granodiorite by the lack of alkali feldspar megacrysts. Rarely it is preserved as xenoliths within the biotite granodiorite as near Banks, on the western margin (Lewis et al., 1987).

3.2.2 ii) Hornblende-biotite granodiorite (Kgdh)

In the field, the lighter grey colour, the smaller proportion of hornblende, and higher proportions of alkali feldspar than plagioclase, distinguishes the hornblende-biotite granodiorite from the tonalite. The hornblende-biotite granodiorite outcrops most extensively in association with the tonalite on the eastern and western borders of the batholith, and it is homogeneous, medium-grained and equigranular, except for a north-south striking foliation concordant with the tonalites near the western border. Lewis et al. (1987) report the rock outcropping on the high ridges in the interior of the batholith and suggest that it may represent an early crystallized roof phase. Intrusive relationships with the tonalite and the porphyritic granodiorite are ambiguous due to their gradational nature, but cross-cutting contacts with the biotite granodiorite and the leucogranite show that it pre-dates the latter two rock types.

3.2.2 iii) Porphyritic granodiorite (Kgdp)

A discontinuous belt of alkali feldspar megacryst bearing rocks has been mapped by Fischer et al. (in press) and Lewis et al. (1987) in the northeastern region of the Atlanta lobe (figure 3.4a). The porphyritic granodiorite is characterised by large (1cm-10cm), brown-pink, alkali feldspar megacrysts in an equigranular, grey, medium-grained matrix, which has a variable composition between tonalite and granodiorite, depending on the proportions of hornblende and the proportion of alkali feldspar megacrysts (plate 3.4).

Only rarely in this belt, as on the East Fork of the Salmon River, is hornblende absent when there are alkali feldspar megacrysts developed.

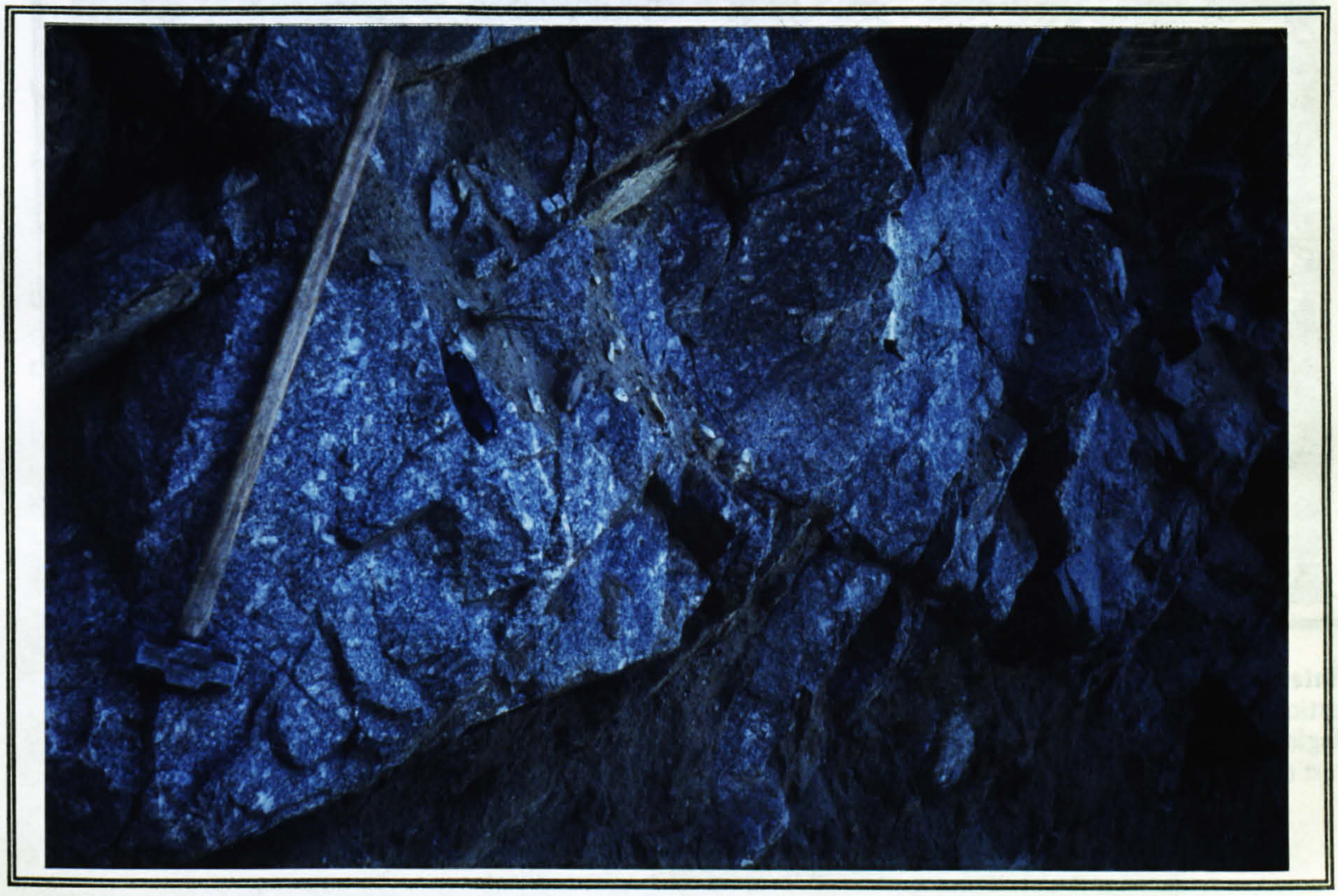

Plate 3.4 Pink alkali feldspar megacrysts developed in mafic, hornblende bearing, porphyritic granodiorite, characteristic of the belt of porphyritic granodiorites on the East Fork of the Salmon River west of Stanley.

Moreover, in this area, numerous pegmatite dikes with similar large pink alkali feldspars, biotite and quartz intrude the porphyritic granodiorite: some alkali feldspar megacrysts are in crystalline continuity with the pegmatites, and in some cases the crystals grow across the vein. Plate 3.5 shows the concentration and association of leucogranite and pegmatite veins in the east of the batholith. Elsewhere in the Atlanta lobe, alkali feldspar megacrysts occur within the biotite granodiorite and hornblende-biotite granodiorite, but do not have the characteristic brownish-pink colour and they are never so numerous and pervasive throughout the rock unit as the in the eastern belt (plate 3.6) -apart from some high ridges in the interior (Lewis et al., 1987).

Plate 3.5 Aplite and pegmatite dykes cut deeply weathered biotite granodiorite and also cut the large, vertical leucogranite dyke in the left of the picture. The youngest rock type cutting all others is a plagioclase and hornblende bearing, porphyritic, mafic dyke. Located on the East Fork of the Salmon River west of Stanley.

Plate 3.6 White alkali feldspar megacrysts are locally exposed throughout the interior of the Atlanta lobe in the more leucocratic phases. Here the megacrysts are exposed in biotite granodiorite.

3.2.2 iv) Biotite granodiorite (Kgd)

Biotite-granodiorite is light grey, equigranular to locally porphyritic, with alkali feldspar phenocrysts, medium- to coarse-grained, and contains biotite as the only mafic mineral. The biotite granodiorite cross cuts the tonalite and the hornblende-biotite granodiorite, and contains rare xenoliths of tonalite. The biotite granodiorite is often transitional into the muscovite-biotite granite, over distances of 10m-2000m before a large enough proportion of thick books of muscovite are present to place it within the muscovite-biotite granite category. The biotite granodiorite is the most extensive rock unit within the Atlanta lobe of the batholith, and it outcrops continuously over vast areas of up to 10000km^2 in the interior of the lobe (figure 3.3). The biotite granodiorite is surprisingly homogeneous, neither containing enclaves or developing any foliation, except some primary flow foliation near the contacts with earlier phases seen on the East Fork of the Salmon River traverse.

3.2.2 v) Muscovite-biotite granite (Kg)

The muscovite-biotite granite (two-mica granite of Lewis et al., 1987), outcrops as a north-south trending body in the central parts of the Atlanta lobe. It is a white, coarse-grained, equigranular rock, which outcrops over large areas, and effectively makes up the core of the lobe (figure 3.3). It shows transitional contacts with the biotite granodiorite over distances of up to 2km and is roughly enclosed by the biotite granodiorite, with the proportion of muscovite increasing towards the core suggesting that these two rock types are intruded during a continuous event, but that the muscovite-biotite granite is slightly younger. The contacts of these latter two rock types with the tonalite and hornblende-biotite granodiorite, are much better defined and may indicate that the east and west border zone tonalite and hornblende-biotite granodiorite represent a slightly earlier phase of emplacement. The intrusive relationships with the tonalite, and the hornblende-biotite granodiorite in the interior of the Atlanta lobe are unclear, but they may represent roof phases of the batholith that have been locally preserved in down thrown fault blocks within the batholith.

3.2.2 vi) Leucogranite (Klg)

Characteristically, the leucogranite crops out in the Atlanta lobe as very small and irregular plutons, particularly near the eastern margin (figure 3.3), but also as veins, dykes and sills throughout the lobe. The intrusive relationships are very clear, owing to the small scale of the intrusions and the linear nature of the veins and sills (plate 3.7).

Plate 3.7 A large 10m wide leucogranite dyke cutting biotite granodiorite on the South Fork of the Payette River on the Long Gulch Pluton traverse. The dyke is fine grained with a minor chilled margins.

The leucogranite cross-cuts and post-dates all other Cretaceous phases of the Idaho batholith. The leucogranites were classified as alaskites by Cater et al. (1973) when they

outcropped in dykes and sills, but in this study they were classified in the field, as aplites, where they are often associated with pegmatites in the same vein or dyke. The leucogranite is white, equigranular and fine-grained with accessory amounts of biotite as the only mafic mineral. The leucogranite when associated with pegmatites is interpreted to be a late stage, volatile rich phase of the Cretaceous batholith, and some concentration of alkali feldspar megacrysts near the margins of the leucogranite veins may suggest an associated, late, subsolidus origin for the alkali feldspar megacrysts. Geochemical evidence is presented later which suggests that some of the leucogranites are mid- to upper crustal melts.

3.2.2 vii) Tertiary dioritic suite (Tgd)

The granites and diorites of the Tertiary bimodal intrusive suite occur in approximately equal proportions in the Atlanta lobe; they have contrasting field relations, but they are often exposed in close proximity. The Tertiary dioritic suite range from gabbros to granites (Lewis, 1984). Diorites to quartzmonzodiorites and granodiorites are most common, but large variations in composition and texture occur within individual plutons over short distances (~10m). The plutons occur as small, individual stocks with sharp contacts and minimal contact aureoles with rocks of the Cretaceous batholith. The rocks of the Tertiary dioritic suite sampled in this study, come from the Jackson peak area, and the Cape Horn Lakes area to the west and north of the Sawtooth batholith respectively, although numerous small stocks outcrop throughout the lobe particularly to the north and east of the study area (figure 3.5). Intimately associated with rocks of the Tertiary dioritic suite are hypabyssal sills, dykes and small bodies of rhyodacite to dacite. Volcanic equivalents of these rocks are dacitic to rhyodacitic ash flows and tuffs preserved in the Custer graben of the trans-Challis fault system (figure 3.6). Together these three rock groups represent the magma chamber, conduits and extrusive products of a monogenetic suite. The dioritic suite is recognised in the field by the association of mafic phases, medium-grain size, seriate to porphyritic textures and the common occurrence of small (~5cm) scale, fine grained enclaves rich in hornblende and biotite.

3.2.2 viii) Tertiary granites (Tg)

The Tertiary granites are recognised primarily in the field by the common, but not ubiquitous pink alkali feldspar and the vertical jointing leading to a distinctive jagged topography. There is a restricted range in mineralogy, which consists of sub-equal amounts of quartz, plagioclase, and alkali feldspar, always with biotite and occasionally with hornblende. Common miarolitic cavities occur filled with smokey quartz, and rare fluorite and topaz, suggesting an epizonal depth of emplacement (Bennett, 1980). The rock is typically homogeneous, medium- to coarse-grained, equigranular to porphyritic with no foliation developed and a lack of entrained enclaves. Hypabyssal equivalents of the granites are numerous rhyolite dykes, the extrusive equivalents of which are the rhyolitic flows and tuffs of the Challis volcanics, preserved in the Custer graben, (figure 3.6) (Bennett and Knowles 1985).

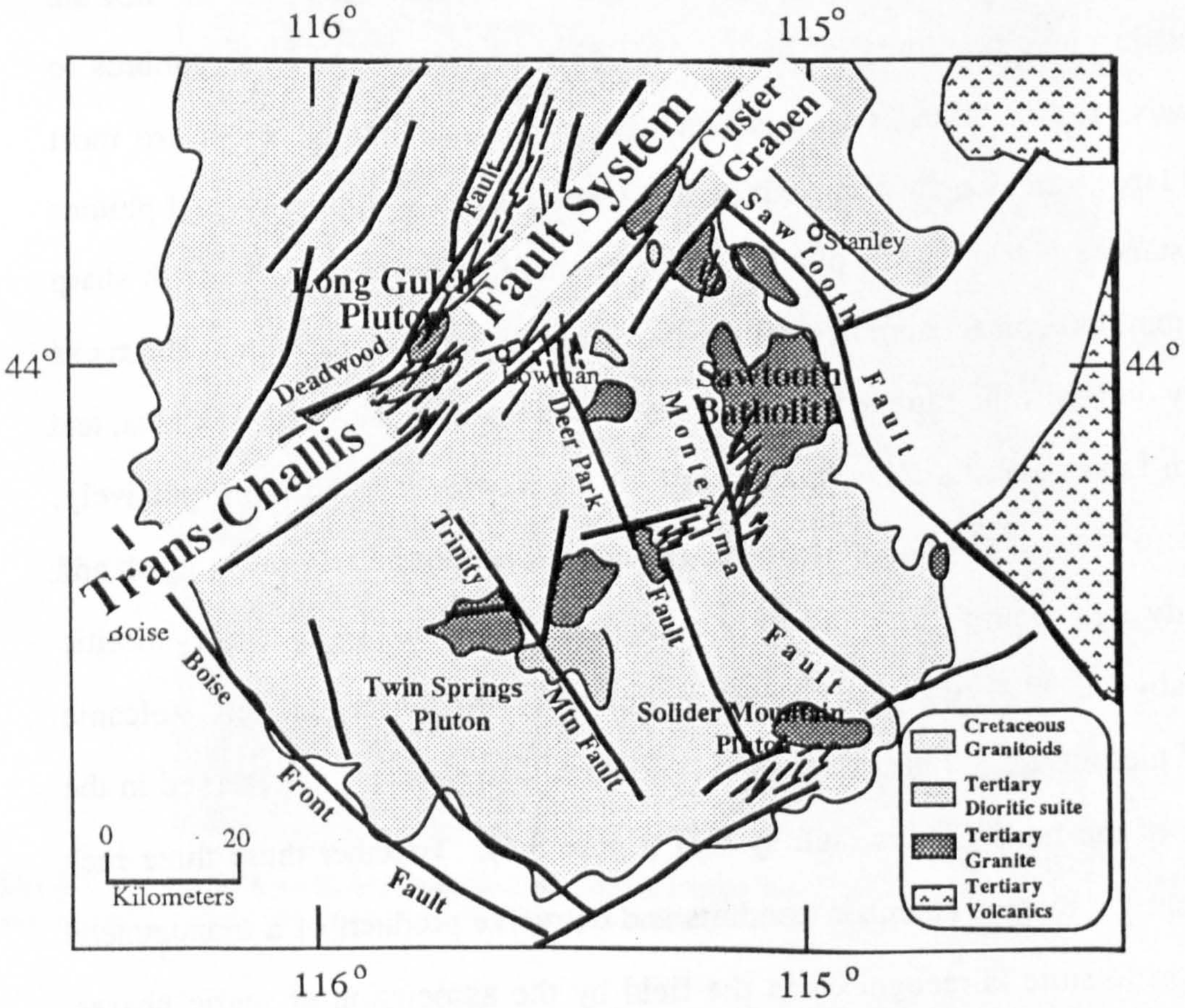

Figure 3.6 Map showing the relationship between the Tertiary granitoids, the northwest trending faults of the trans-Challis fault system, the northeast trending faults and the Tertiary dyke swarms.

To the north of the Sawtooth batholith, hypabyssal rhyolite dykes intruding the Tertiary granite are continuous with rhyolite flows and tuffs, (Kiilsgaard and Bennett, 1985). The Sawtooth batholith has been sampled in this study, and represents one of the largest occurrences of Tertiary granite in the lobe. In contrast, the Long Gulch pluton is a typically small pluton of the dioritic suite, which has also been accurately sampled, as have some Tertiary granites from the south of the lobe.

The exposure of the Tertiary bimodal suite, and particularly the epizonal granites, is intimately related to extensional faulting in the Atlanta lobe of the Idaho batholith (figure 3.6). Many Tertiary plutons and their extrusive equivalents are exposed within the northeast trending system of horsts and grabens of the trans-Challis fault system (Bennett and Knowles, 1985).

Plate 3.8 Panoramic view of the Sawtooth batholith as an up-thrown block due to the intersection of the Sawtooth and Montezuma faults. The range front, Sawtooth fault is covered by trees and glacial drift in the foreground. The view is from the northwest of Stanley looking southeast with a base level to peak difference of approximately 1700m.

The Tertiary granite is exposed in the up-thrown horst blocks, and rhyolitic flows are confined to the grabens in the north of the lobe. In the south of the lobe the mode of exposure of the Tertiary granitoids is more complex, with a series of northwest trending normal faults which terminate against the northeast trending trans-Challis faults (figure 3.6). Tertiary granites and the dioritic suite are exposed in the horsts of a basin and range type horst and graben system, which is exposed to the east of the area, except that the northwest trending extensional faults have produced, uplifted and down-thrown rhomboid shaped blocks (Bennett and Knowles, 1985). This is the case for the Sawtooth batholith where the northwest trending, unexposed, 'range front' Sawtooth fault (plate 3.8) and Montezuma fault, intersect the trans-Challis faults to produce the the up-thrown Sawtooth block (figure 3.6). The Long Gulch pluton is exposed in the trans-Challis fault system and is associated with a northeast trending Tertiary dyke swarm of mafic to felsic compositions. The dykes are fine-grained to porphyritic, and range in size from 0.5m to 20m, showing sharp contacts. The mafic dykes are chilled and flow banded, whereas the more felsic porphyritic dykes are unchilled. This indicates that the Tertiary granitoids were still at elevated temperatures, but cool enough to behave as brittle solids when the dykes intruded along cracks parallel to the fault system and normal to the direction of extension. Figure 3.6, shows the relationship of the dyke swarms to the Tertiary granitoids, and the orientation of faults; while plate 3.9 shows the intrusive contacts of the dykes with the Tertiary granites.

3.2.2 ix) Other rock types

The Atlanta lobe of the Idaho batholith is notorious for the lack of country rocks exposed, and indeed within the interior of the batholith, other rock types apart from Cretaceous and Tertiary granitoids, are very limited. An exception to this, are small, ten meter scale, metasedimentary blocks most commonly occurring on high ridge crests and peaks in the eastern half of the Atlanta lobe (Kiilsgaard and Lewis, 1985). Biotite schists are the most common lithology, but quartzites were also observed, and carbonate rich quartzite, quartz-diopside marble and calc-silicate gneiss have been reported by Kiilsgaard

Plate 3.9 Chilled and flow banded margin of a dacitic to rhyolitic dyke within the Long Gulch Pluton

and Lewis (1985). These lithologies are interpreted to be equivalents of the lower Palaeozoic succession of carbonates and quartzites deposited and preserved in southeastern Idaho, but direct correlation with the sedimentary sequences is impossible due to the small scale of outcrop and the subsequent metamorphism and deformation. Kiilsgaard and Lewis (1985) claim that localised weakly developed foliation in the granitoids close to the contact with the metasedimentary blocks and slivers, is concordant with the foliation developed within the metasediments. They therefore argue that these represent the roof, or close to the top of the Atlanta lobe. These 'roof pendants' (Kiilsgaard and Lewis, 1985) are observed in contact with all rock types of the Atlanta lobe including the Tertiary bimodal suite.

3.3 Classification and Petrography

This section aims to describe and interpret the petrography, to group the rocks into lithological associations, to constrain further emplacement depths and discover the order of crystallization. Seventy-five thin-sections have been studied which is approximately half the sample set, the summaries of which are in table 3.1.

3.3.1 The Cretaceous phases

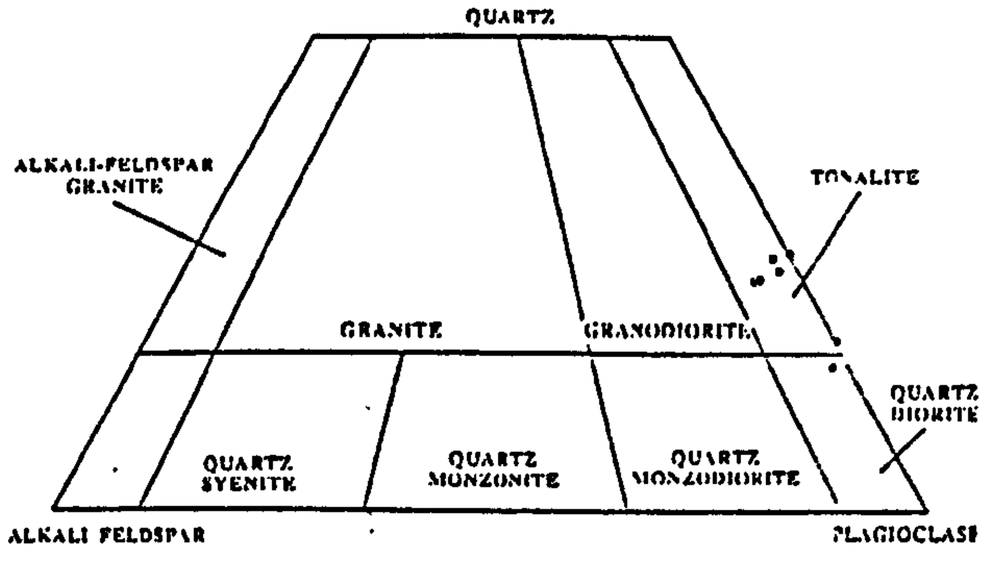

Tonalite (Kt)

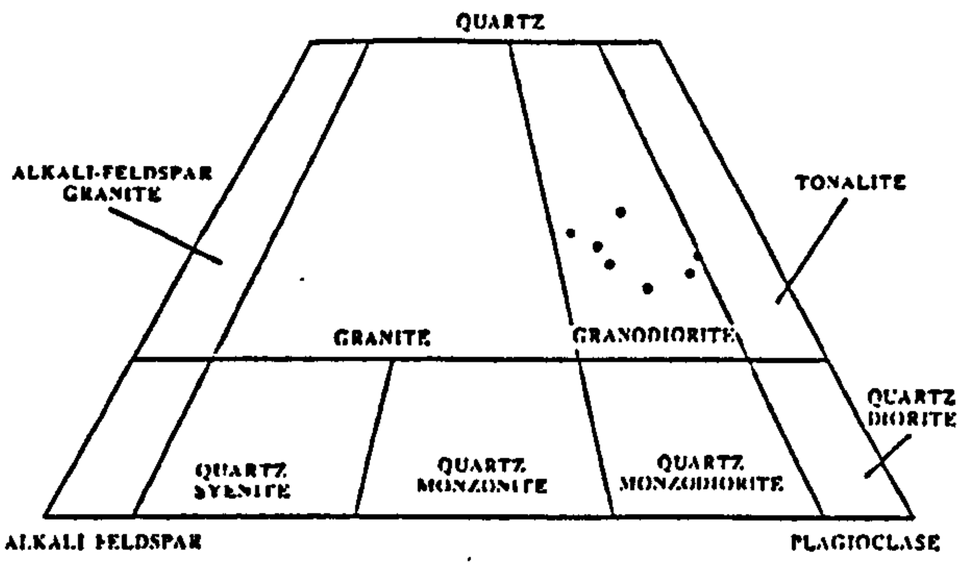

Hornblende-biotite granodiorite (Kgdh)

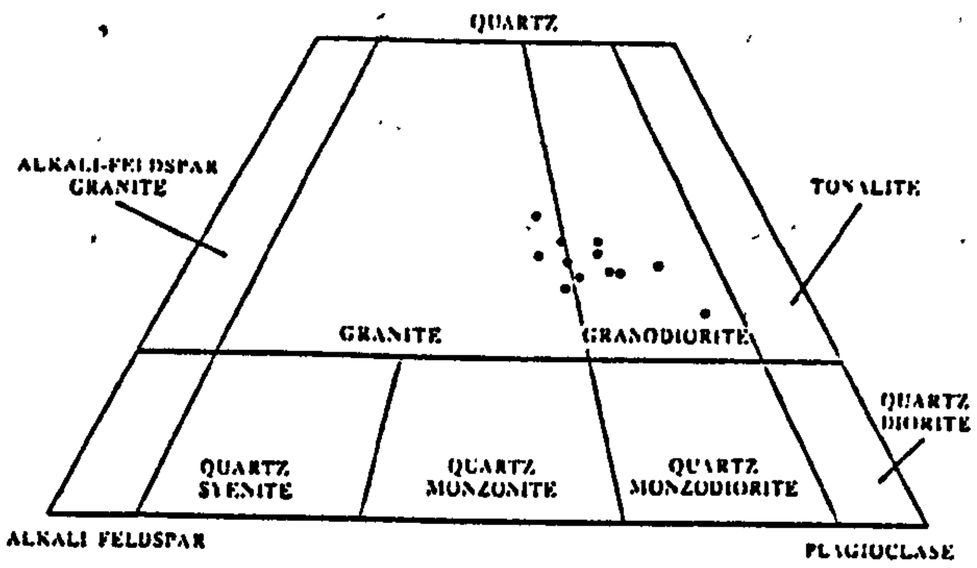

Porphyritic granodiorite (Kgdp)

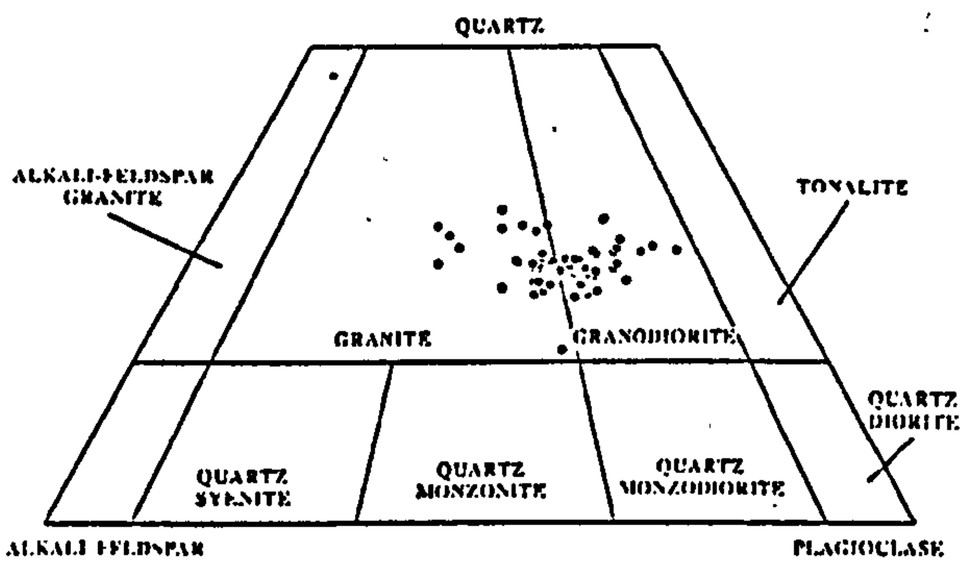

Biotite granodiorite (Kgd)

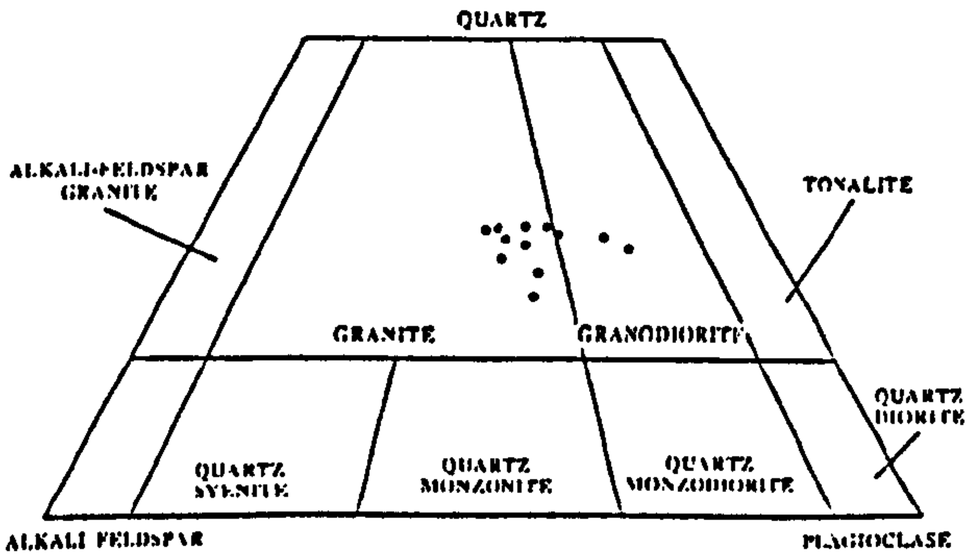

Muscovite-biotite granite (Kg)

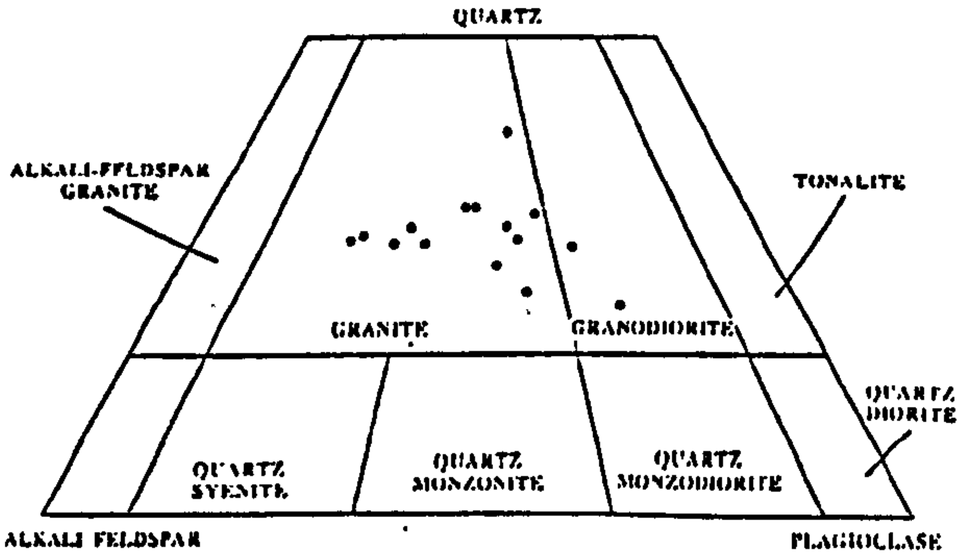

Leucogranite (Klg)

Figure 3.7 Strekeisen classification diagram for modal proportions based on the GRANITE NORM calculation (Harris, pers.com) of the six Cretaceous phases in the Atlanta lobe.

3.3.1 i) Tonalite (Kt)

In thin section the tonalite is medium grained, equigranular to rarely porphyritic, intermediate rock with up to 30% mafic minerals. Modal estimates are 40%-50% plagioclase, 20%-30% quartz, 15%-30% hornblende and biotite, and <10% alkali feldspar, which agrees well with the GRANITE NORM (Harris, pers com.,1989), and plot as tonalites on the Strekeisen diagram, (figure 3.7).

The dominant phase in the tonalite is andesitic plagioclase, which is generally subhedral to anhedral and shows no zoning, forming a hypidiomorphic to allotriomorphic interlocking texture with the other mineral phases of the rock. The plagioclase was a marginally early phase of the rock in comparison with the subordinate mineral phases (figure 3.8a). The only exception to the above is sample CBC87-145 from the EFSR traverse, which has the least evolved composition of any Cretaceous tonalite and contains large, euhedral, multiple zoned phenocrysts of plagioclase, with labradorite (An 55) cores, and andesine rims (An 35) (plate 3.10). The plagioclase may have a cumulate origin with the remaining phases being inter-cumulus, apart from the unusually large, very early apatites. The general lack of cumulus textures, however and the distribution of the plagioclase throughout the tonalite suggests that small amounts of physical separation of plagioclase has occurred.

Quartz is always present as interlocking grains with a distinctive lack of sutured boundaries, recrystallization textures or undulose extinction, except in samples that have further textural evidence for subsolidus deformation. Where rare interstitial alkali feldspar is observed, it is orthoclase and often inter-grown with vermicular quartz on the boundaries of feldspar grains.

The mafic phases of the rock are hornblende and biotite, the hornblende appearing as an early phase, often mantled by later biotite. The hornblende is variably preserved as pristine, euhedral crystals, to very skeletal remnants, being replaced by biotite, embayed by quartz and often over grown by epidote and rarely chloritised. The biotite is not chloritised, but it has euhedral inclusions of epidote. Other inclusions in hornblende and

biotite are zircon, allanite, apatite and opaque minerals, probably magnetite. Coarse sphene occurs in most tonalites as a euhedral early phase, often associated with epidote which appears later.

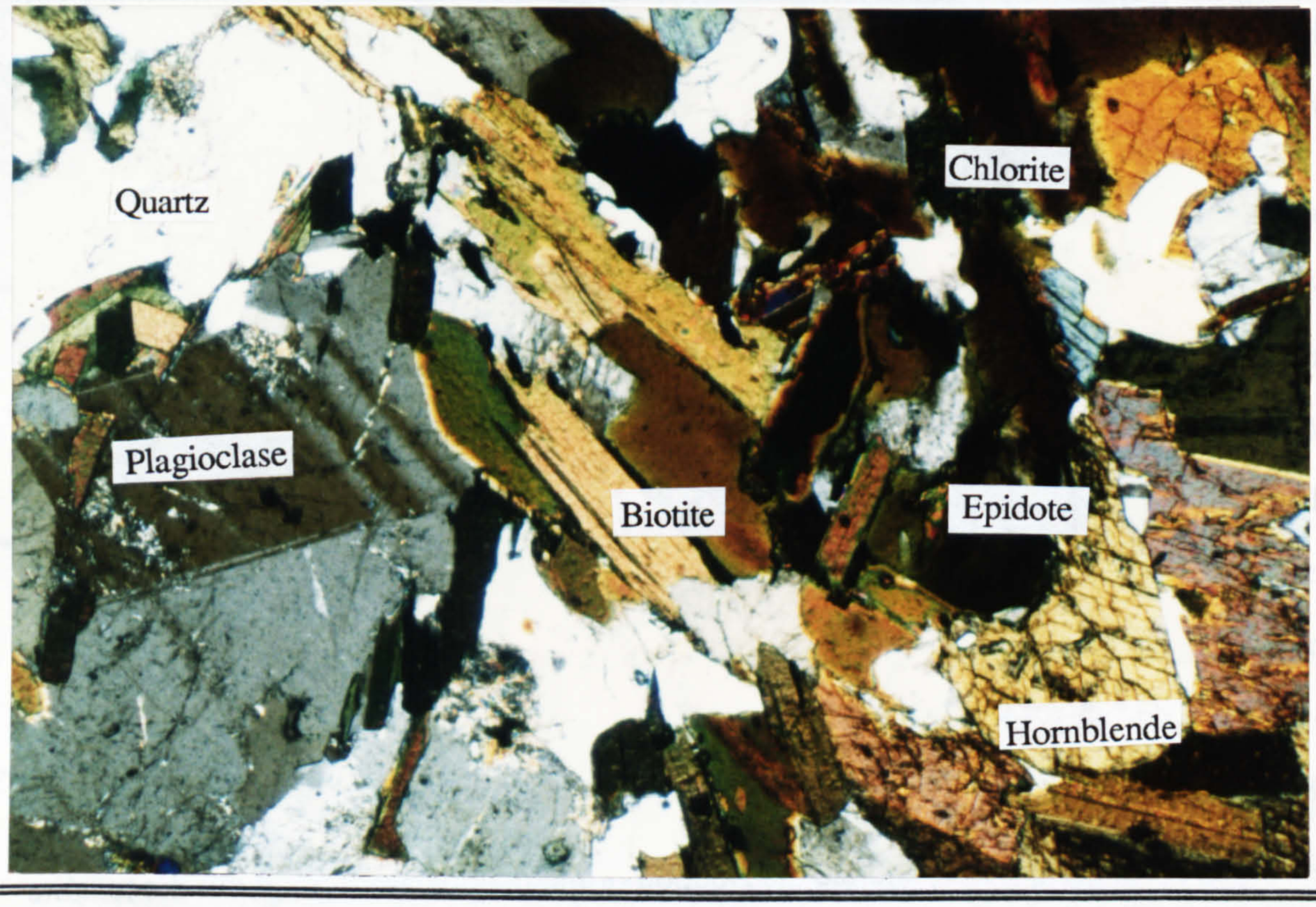

Plate 3.10 Photo micrograph of a tonalite under crossed polars at x10 magnification showing foliation defined by hornblende and biotite, zoned plagioclase, small grains of epidote and sphene and interlocking quartz.

The tonalite from the south and west of the Atlanta lobe preserves a pervasive foliation defined by biotite and hornblende, but with quartz, plagioclase and alkali feldspar undeformed and unoriented, indicating that the fabric is of primary igneous origin with the deformation synchronous with crystallization. Tonalite from the extreme western margin of the Atlanta lobe has developed a major gneissic foliation where layers rich in aligned hornblende and biotite, are separated by deformed quartz and plagioclase, elongate parallel to the major foliation. These are the oldest tonalites, and they crystallized prior to and during deformation, which allows the last deformational event associated with accretion of the Blue Mountain island arc to be dated at approximately 93Ma (Lund and Snee, 1988).

Tonalite on the eastern border of the Atlanta lobe is of similar age as the syn-deformational rocks from the west, but it shows no foliation indicating that the deformation was associated with transpressive movements near the continent/island arc suture.

In conclusion, the tonalite, which is the earliest phase of the Cretaceous batholith, is a noncumulative, typically foliated rock with igneous textures that suggest that plagioclase and hornblende may have been early crystallized phases, but the bulk of the rock crystallized simultaneously, with epidote crystallizing late. The textures which epidote displays suggests that it is at least in part primary, and the late appearance is in agreement with the fact that magmatic epidote should only crystallize out of magmas that already have a large proportion of crystals (Naney, 1983). Moreover, Zen (1988) states that primary epidote cannot crystallize from tonalitic magmas at pressures ≤6Kb, and due to the immobility of crystal mushes, this suggests that emplacement of the tonalites was between 20km-30km.

3.3.1 ii) Hornblende-biotite granodiorite (Kgdh)

The hornblende-biotite granodiorite is, in many respects, similar to the tonalite into which it is gradational. It has often mistakenly been collected in the field as tonalite because of the high mafic mineral content of up to 20% biotite and hornblende, but on closer examination, is modally classified as granodiorite (figure 3.7). In contrast, the more leucocratic granodiorite has only minor amounts of fine grained hornblende that is difficult to see in hand-specimen. The hornblende-biotite granodiorite is medium- to coarse-grained, equigranular, hypidiomorphic and it has an average modal composition of 40% plagioclase, 25% quartz, 20% alkali feldspar, and 15% biotite and hornblende. The plagioclase is subhedral to anhedral, with occasional early, euhedral grains zoned from An_{40} in the cores, to An_{30} on the rims; whereas the later, subhedral plagioclase is unzoned oligoclase. In the more leucocratic samples, myrmekite is developed in plagioclase and the proportion of alkali feldspar increases, becomes perthitic, and shows the tartan twinning of microcline. The quartz is early to late, intercertal but normally undeformed, except in the more leucocratic varieties. The proportion of hornblende is always less than

5% of the rock and it originally crystallized as euhedral grains quite early in the order of crystallization (figure 3.8b). However, the hornblende in the hornblende-biotite granodiorite, in contrast with that in the tonalite appears to be unstable, and is always to some extent chloritised, embayed or skeletal with quartz, and over-grown by biotite and epidote, (plate 3.11). The epidote does not show the primary magmatic textures noted in the tonalite, apart from in the more mafic rocks, suggesting a shallower depth of emplacement. In contrast to the hornblende the biotite is unaltered, rarely chloritised, and it defines the foliation prominent in the western area. The hornblende-biotite granodiorite is normally easily collected fresh, with the feldspars only occasionally altered. Sphene is prominent, coarse-grained and euhedral, often being partially or completely oxidised to an opaque phase. Apatite and allanite are common accessory phases, whereas zircon is far less common than in the tonalite.

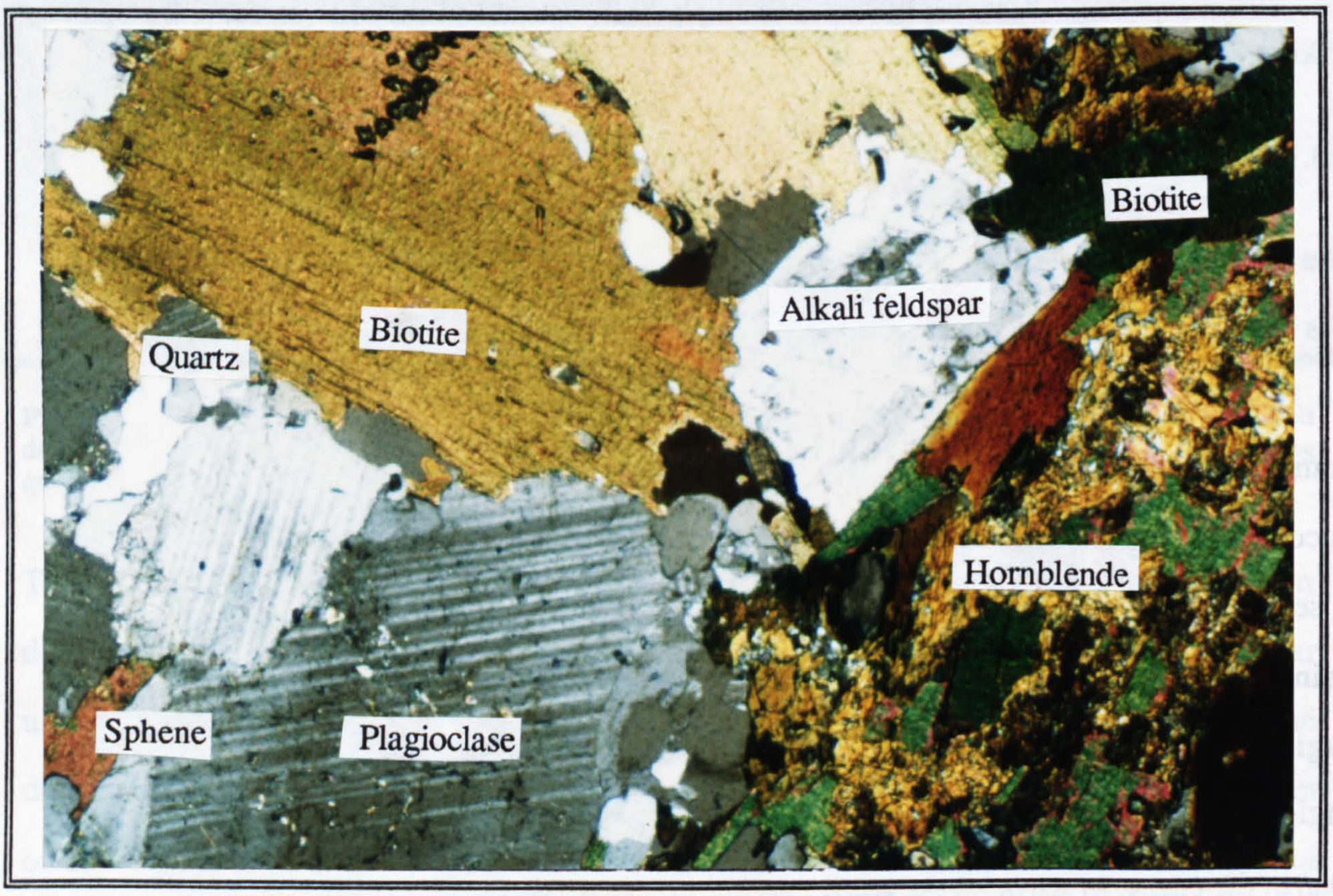

Plate 3.11 Hornblende-biotite granodiorite under crossed polars at x10 magnification.

In conclusion, the hornblende-biotite granodiorite ranges from near tonalitic compositions to granodioritic compositions, and it has a probable order of crystallization of early plagioclase and hornblende followed by later biotite, plagioclase quartz and alkali feldspar.

3.3.1 iii) Porphyritic granodiorite (Kgdp)

It is impossible to give an accurate, estimated, modal mineralogy, from thin section for the porphyritic granodiorite, because of the variable distribution of alkali feldspar megacrysts. The matrix of the unit most closely resembles the hornblende-biotite granodiorite if hornblende is present, and the biotite granodiorite if absent. The calculated GRANITE NORM mineralogy (Harris, pers com.,1988), from major element analyses, of large whole rock samples gives a mineralogy of 28% quartz, 15% alkali feldspar, 40% plagioclase, 3% hornblende and 12% biotite, which plot as variable compositions from granodiorite to granite on the Strekeisen diagram (figure 3.7c).

The matrix of the rock is medium- to coarse-grained, equigranular, with a hypidiomorphic texture. Biotite and hornblende are the mafic minerals but hornblende is extensively altered to biotite, epidote and embayed by quartz. The earliest phases are hornblende and subhedral plagioclase, with a typical composition of An_{30} (figure 3.8c). Biotite makes up to 15% of the rock and is commonly, but not extensively chloritised. Quartz is late, it has undulose extinction and subgrains indicating some mild, post-crystallization deformation, but it is also common as myrmekite, forming vermicular intergrowths with plagioclase. Alkali feldspar is nearly entirely absent from the ground-mass, but common accessory phases are coarse grained sphene, together with allanite, apatite and zircon.

The alkali feldspar megacrysts are pink orthoclase or microcline and are commonly perthitic. Seemingly euhedral alkali feldspar megacrysts have irregular boundaries in thin section, and they contain small embayed grains of plagioclase, and variably resorbed grains of all other phases of the rock. A more poikilitic texture is developed when anhedral alkali feldspar encloses large grains of the other phases and occurs as embayments into these, as well as having irregular boundaries that are both intercertal and appear to have grown into the surrounding mineralogy. Thin section studies have shown that this texture is more common than it was thought in the field, but is only common in areas where megacrysts are observed and and so the poikilitic megacrysts are believed to

have a common origin. Plate 3.12 shows the typical textural relationships of the alkali feldspar megacrysts and the ground-mass of the rock.

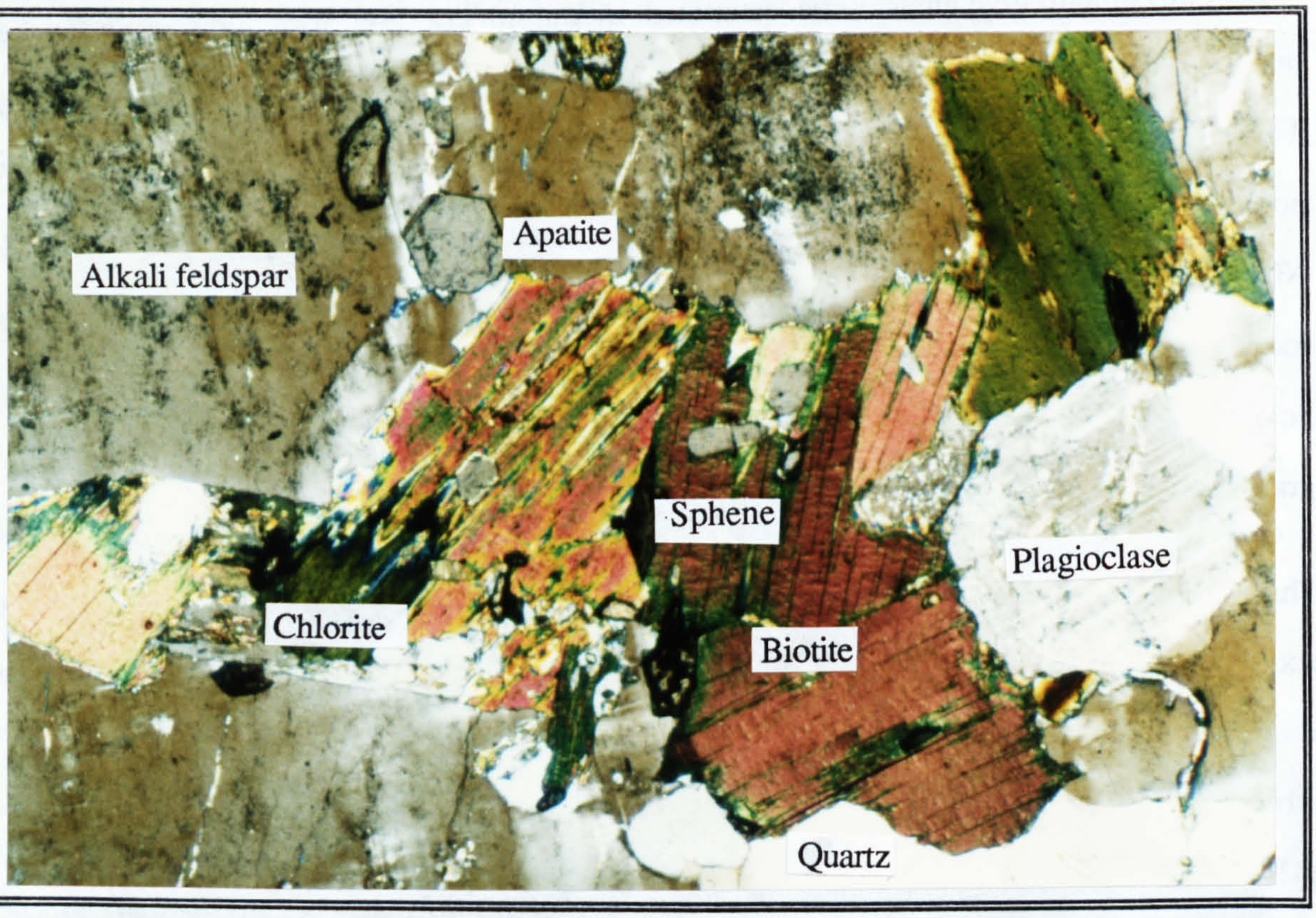

Plate 3.12 Photomicrograph of a porphyritic granodiorite under crossed polars at x10 magnification showing subhedral alkali feldspar megacrysts with inclusions embayments and a poikilitic texture.

Two origins have been suggested in the granite literature for alkali feldspar megacrysts:- subsolidus metasomatic growth and primary magmatic crystallization. Indeed, merely within the Idaho batholith, Hyndman (1984) argues for a magmatic origin, whereas Criss (1981) favours, "subsolidus deuteric porphyroblastic growth" and Kiilsgaard and Lewis (1985) think the megacrysts result from potassium metasomatism. There is no doubt that whatever their origin the alkali feldspar megacrysts have crystallized as a late phase on the textural evidence above.

A metasomatic, subsolidus origin for the megacrysts is supported by several lines of evidence, including, the late, poikilitic texture of the alkali feldspar, the embayed and replaced inclusions of the marginal phases, and the lack of orientation of the inclusions around the early cores of primary growing magmatic crystals. Moreover, the presence of numerous alkali-feldspar rich veins in the region of the belt of the porphyritic granodiorite

and the observation that the density of distribution of the alkali feldspar megacrysts is greatest near the alkali feldspar veins and leucogranite dykes, suggests that these may have acted as conduits for metasomatic fluids. In addition, Kiilsgaard and Lewis (1985) report the growth of alkali feldspar megacrysts across a vein, which also indicates a subsolidus origin.

However, the field evidence supports the origin of the alkali feldspar megacrysts as a primary, late magmatic phase. Such lines of evidence include the confinement of the alkali feldspar megacrysts just to a belt of granitoids, the similarity and extent of the megacrysts over large areas, and the absence of megacrysts from country rocks of the Salmon River Arch, even though the megacryst belt is present in the northern and southern lobes of the Idaho batholith (Hyndman, 1984). Textural evidence in support of a late primary magmatic origin is the poikilitic nature of the alkali feldspar megacrysts, the fact that they enclose all other mineral species, and the interpretation that replacement of the inclusions and surrounding phases by alkali feldspar took place late in the period of crystallization. Hyndman.(1984) argues that the total amount of alkali feldspar in the rock is too low for alkali feldspar to have precipitated as initial liquidus phenocrysts.

The large size of the alkali feldspar megacrysts and the absence of fine grained alkali feldspar from the matrix can be explained by experimental results, which show that in granodioritic magmas the nucleation rate of alkali feldspar is at a minimum when the growth rate of alkali feldspar is at a maximum (Fenn, 1977; Naney and Swanson, 1980). Furthermore, Swanson (1977) showed that at the degree of undercooling at which alkali feldspar reaches its maximum growth rate, plagioclase has a much lower growth rate which would enhance the probability of developing poikilitic textures. The likelihood of a primary, late magmatic phase of alkali feldspar forming a poikilitic texture is consistent with experimental data (Clemens and Wall, 1981) which show that a peraluminous melt becomes saturated in alkali feldspar only a few degrees above the solidus. Even at these low tempratures the magma contains only a small fraction of crystals, and thus leaves room for the growth of large alkali feldspar crystals. Large sizes of alkali feldspar crystals

will only be achieved if the growth rate is high or cooling rate very slow, because with the onset of cotectic crystallization of quartz, plagioclase and alkali feldspar, large volumes of crystals are produced rapidly through a small drop in temperature. In conclusion, therefore, the alkali feldspar megacrysts of the porphyritic granodiorite are believed to be of a late primary magmatic origin.

3.3.1 iv) Biotite granodiorite (Kgd)

The biotite granodiorite is the most voluminous Cretaceous phase of the Atlanta lobe of the Idaho batholith, and it is well known for its very monotonous composition. Thin section study of many samples of the biotite granodiorite produces an estimate for the average modal mineralogy of 30% quartz, 20% alkali feldspar, 40% plagioclase and 10% biotite, which is indeed very consistent for all samples. GRANITE NORMS (Harris, pers com., 1988), show a limited range in composition from granodiorite to granite (figure 3.7d).

The rock is commonly medium to coarse grained, equigranular to locally porphyritic, with a hypidiomorphic granular texture. The plagioclase is oligoclase, ranging in composition from An_{22}-An_{28} , but it is only rarely zoned, and then the plagioclase is uncommonly euhedral, indicating a slightly earlier time of crystallization (figure 3.8d). The plagioclase is typically subhedral, with common myrmekite, distorted twinning and the development of rare subgrains, suggesting some subsolidus deformation. After plagioclase, quartz is the second most abundant mineral in the rock unit, and as in the other granodiorites of the lobe, it shows undulose extinction, sutured grain boundaries and appears to have crystallized late. Alkali feldspar is the latest phase and is often intersertal or poikilitic when it is more abundant. The alkali feldspar is perthitic microcline and rarely it forms megacrysts, which were unnoticed in hand specimen because of their poikilitic nature. Biotite is the only mafic mineral and it is often chloritised and oxidised to opaque minerals. Accessory phases include muscovite and epidote as alteration products, hornblende, apatite and zircons with anhedral cores preserved in biotite. Rare veins filled

with quartz, chlorite and carbonate occur in the weathered rocks. Plate 3.13 shows the common mineralogy and texture of the biotite granodiorite.

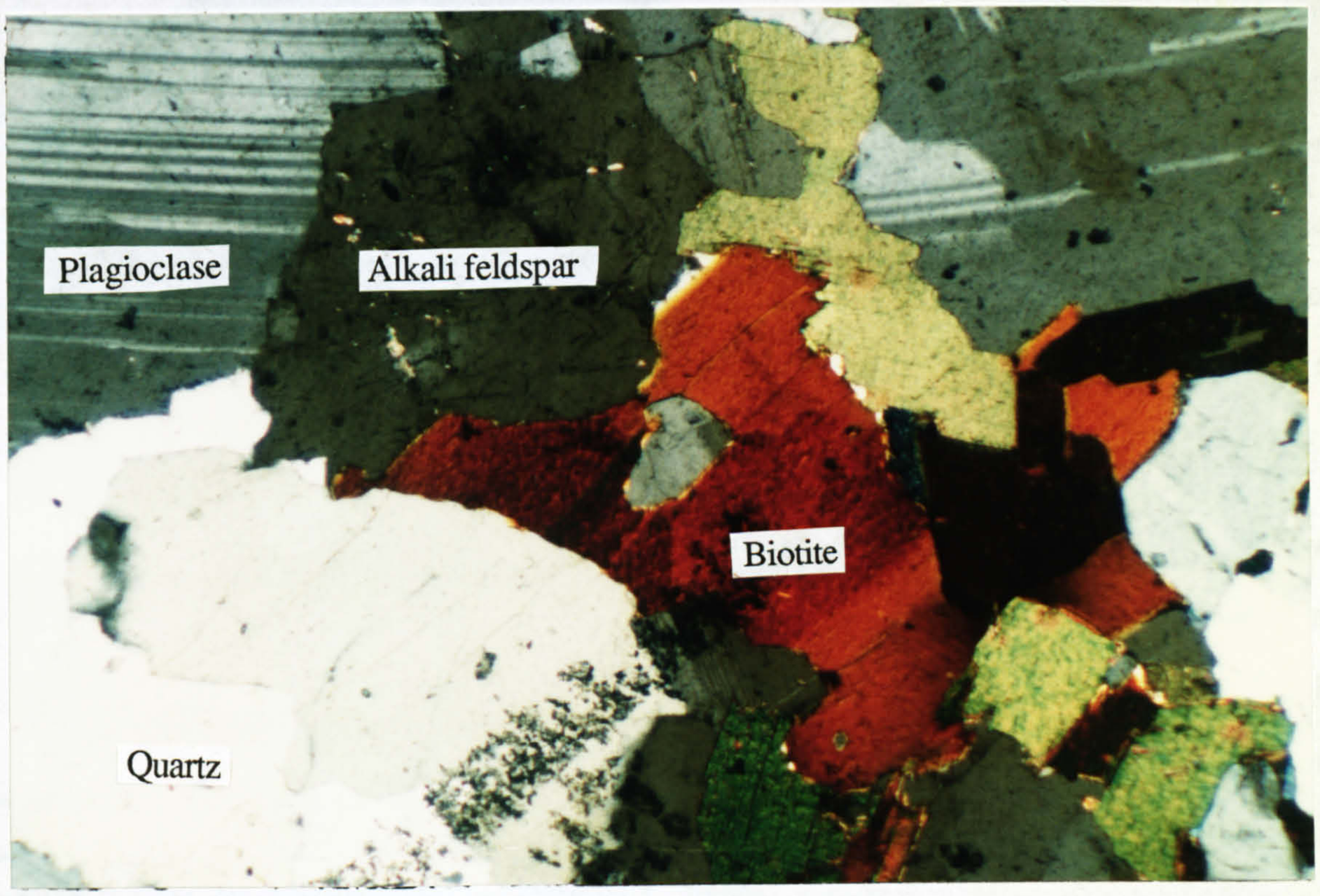

Plate 3.13 Photomicrograph of biotite granodiorite in crossed polars at x10 magnification showing unfoliated granular texture with biotite as the only mafic phase, two feldspars and quartz with undulose extinction.

To summarise, the biotite granodiorite has crystallized all phases simultaneously with just a small proportion of early plagioclase and biotite. It has undergone minor subsolidus deformation but it only develops a primary flow foliation, defined by biotite, near the boundary with other units on the East Fork of the Salmon River. In some areas sericitisation of the feldspars is common, but typically it was relatively easy to sample fresh rock.

3.3.1 v) Muscovite-biotite granite (Kg)

The muscovite-biotite granite varies modally between granite and granodiorite, and the average modal mineralogy of 35% quartz, 25% alkali feldspar, 35% plagioclase and 5% muscovite and biotite, agrees well with the calculated GRANITE NORMS (Harris, pers com.,1988) used to classify the rocks in (figure 3.7e). The muscovite-biotite granite is coarse-grained, equigranular, but are locally porphyritic or poikilitic, with either large subhedral alkali feldspar or anhedral alkali feldspar enclosing all other mineral species. The alkali feldspar is most commonly microcline which often shows granophyric textures and rarely is mildly perthitic with sinuous trails of albite. The alkali feldspar megacrysts are zoned and contain inclusions of quartz and plagioclase.

Unlike the late stage alkali feldspar, plagioclase is commonly euhedral to subhedral with few inclusions (figure 3.8e). The grains are simply zoned from core to rim with an average composition of An_{20} (oligoclase). The grains are well preserved, but locally show sericitised cores, and myrmekite is developed on the rims and within the smaller grains. Distinct from the sericite is coarse grained muscovite growing in crystallographic continuity with the cores of plagioclase crystals which may be primary rather than secondary. Primary muscovite is positively identified as large, subhedral, inclusion free grains often associated with biotite. Embayments of quartz in muscovite is evidence for an early origin for the muscovite (figure 3.8e). Secondary muscovite developed along grain boundaries occurs only in rocks where the biotite is chloritised to any extent. Muscovite may constitute up to 5%-7% of the rock with the proportion of biotite behaving inversely with the proportion of muscovite. Biotite is an early phase, enclosed by alkali feldspar and it contains no inclusions apart from tiny zircon and monazite grains which produce radiation damage pleochroic haloes. Accessory phases are present only where the rock is transitional into the biotite granodiorite.

Quartz appears as a late phase and forms large grains as well as smaller intercertal grains between other phases of the rock. It is distinctive because it alone has accommodated

small amounts of strain, as revealed by undulose extinction, strongly sutured or concertal grain boundaries and the development of subgrains on the boundaries of larger grains.

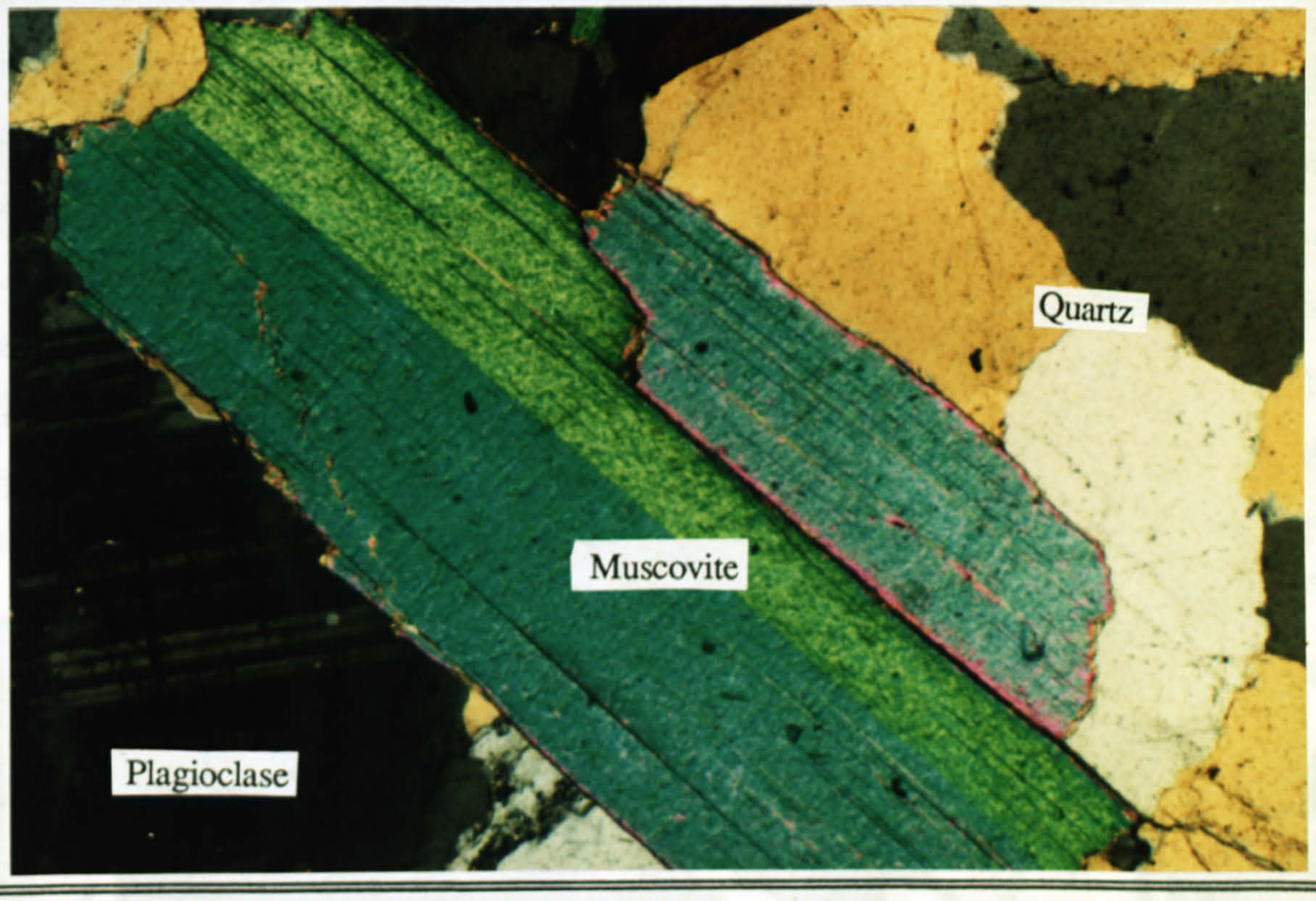

Plate 3.14 Photomicrograph of muscovite-biotite granite in crossed polars at x40 magnification showing unfoliated granular texture with primary muscovite showing high order birefringence colours, altered plagioclase cores and rare biotite grains.

In summary, the muscovite-biotite granite is coarse-grained, leucocratic, hypidiomorphic granular, subsolvus granite to granodiorite. The granophyric texture suggests that close to eutectic crystallization occurred although plagioclase, primary muscovite and biotite were crystallized early before simultaneous crystallization of all phases. The rock is fresh with minimal alteration and has undergone little subsolidus deformation.

3.3.1 vi) Leucogranite (Klg)

The leucogranite is characteristically fine- to medium-grained, allotriomorphic and leucocratic. Estimates of the modal mineralogy yield sub-equal proportions of quartz, alkali feldspar and plagioclase, but the GRANITE NORMS (Harris, pers com.,1988) are slightly higher in the proportions of quartz and alkali feldspar than those estimated from

thin section (figure 3.7f). The alkali feldspar is microcline, generally perthitic and variably altered. The plagioclase too is anhedral, but occasionally euhedral cores are preserved and extensively sericitised, with some completely replaced by muscovite. The plagioclase is unzoned and has a composition of An_{10} -An_{20}. Muscovite is always secondary and other alteration effects include the almost complete alteration of the trace amounts of biotite present to chlorite, opaques and epidote, and rare carbonate filled cracks. Sphene occurs rarely along grain boundaries and zircons are early inclusions within most phases. Rounded to subhedral normally inclusion-free grains of garnet up to 2mm occur quite regularly and are thought to have an igneous origin, with a spessartine to almandine composition which have often been recorded as being crystallized from aplites and pegmatites (Deer, Howie, and Zussman, 1966).

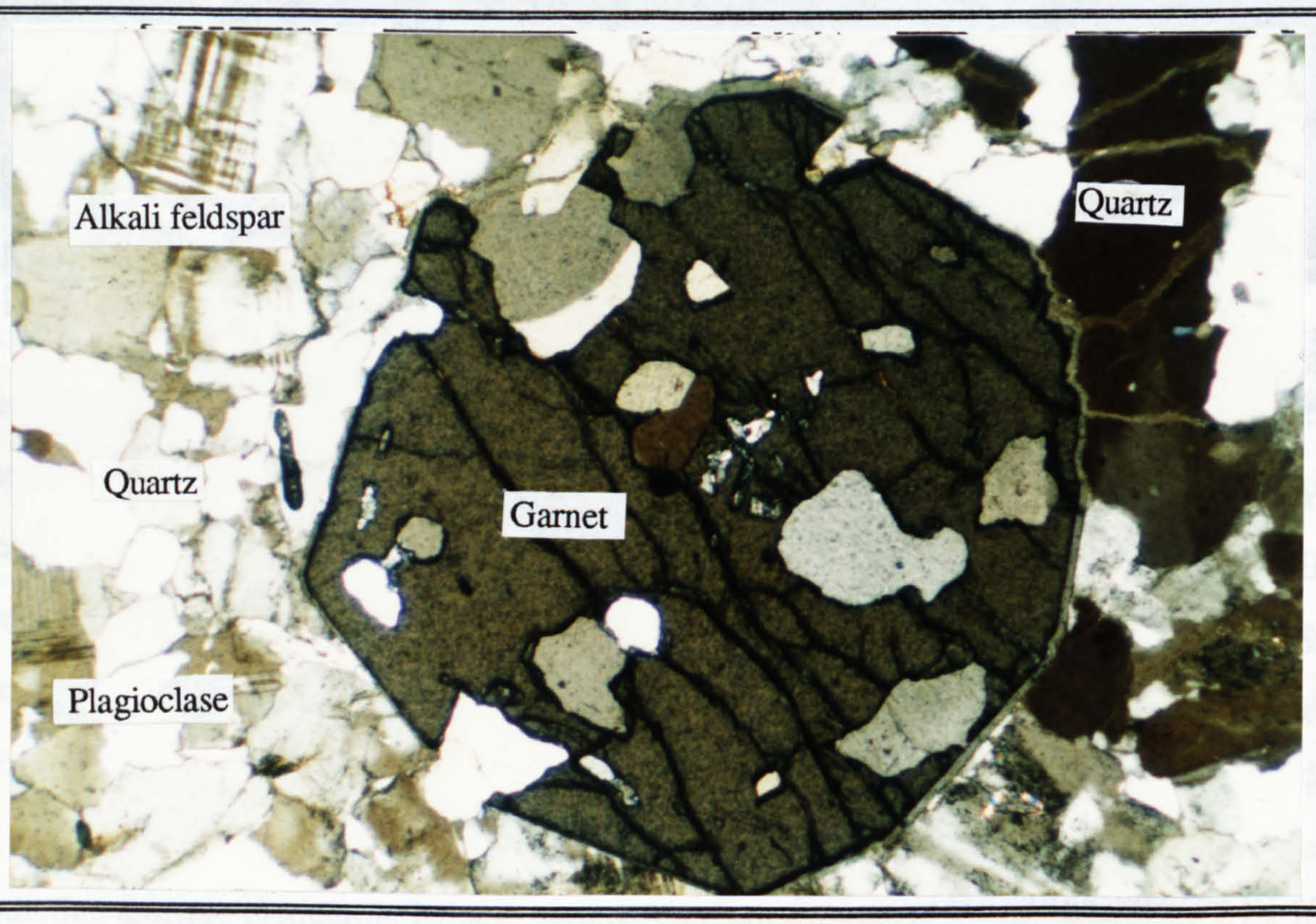

Plate 3.15 Photomicrograph of leucogranite in crossed polars at x40 magnification showing rare garnet grains distorted plagioclase twinning, interlocking texture and a distinct lack of mafic phases.

Although the overall texture is interlocking, the quartz grains have sutured boundaries and have recrystallized many smaller sub-grains and exhibit undulose extinction as a result of mild deformation. No foliation is seen, and the only other deformational features are

distorted plagioclase twins. In contrast to the other lithologies of the Atlanta lobe, no myrmekitic or granophyric textures are developed.

Often associated with the leucogranite are pegmatites of dominantly perthitic, euhedral, microcline meagacrysts and coarse-grained quartz. The pegmatites contain similar small garnets, to the leucogranite, and rarely develop coarse-grained biotite, but often have secondary, chloritised biotite along grain boundaries.

In conclusion, the leucogranite is a late phase of the Cretaceous Atlanta lobe granitoids which has crystallized all the mineral species rapidly and simultaneously (figure 3.8f), probably due to the loss of volatiles at high levels of emplacement. There is a hint that plagioclase may have been the earliest crystallizing phase, but extensive alteration and development of late secondary minerals suggests that the dykes and veins continued to act as conduits for percolating fluids after crystallization.

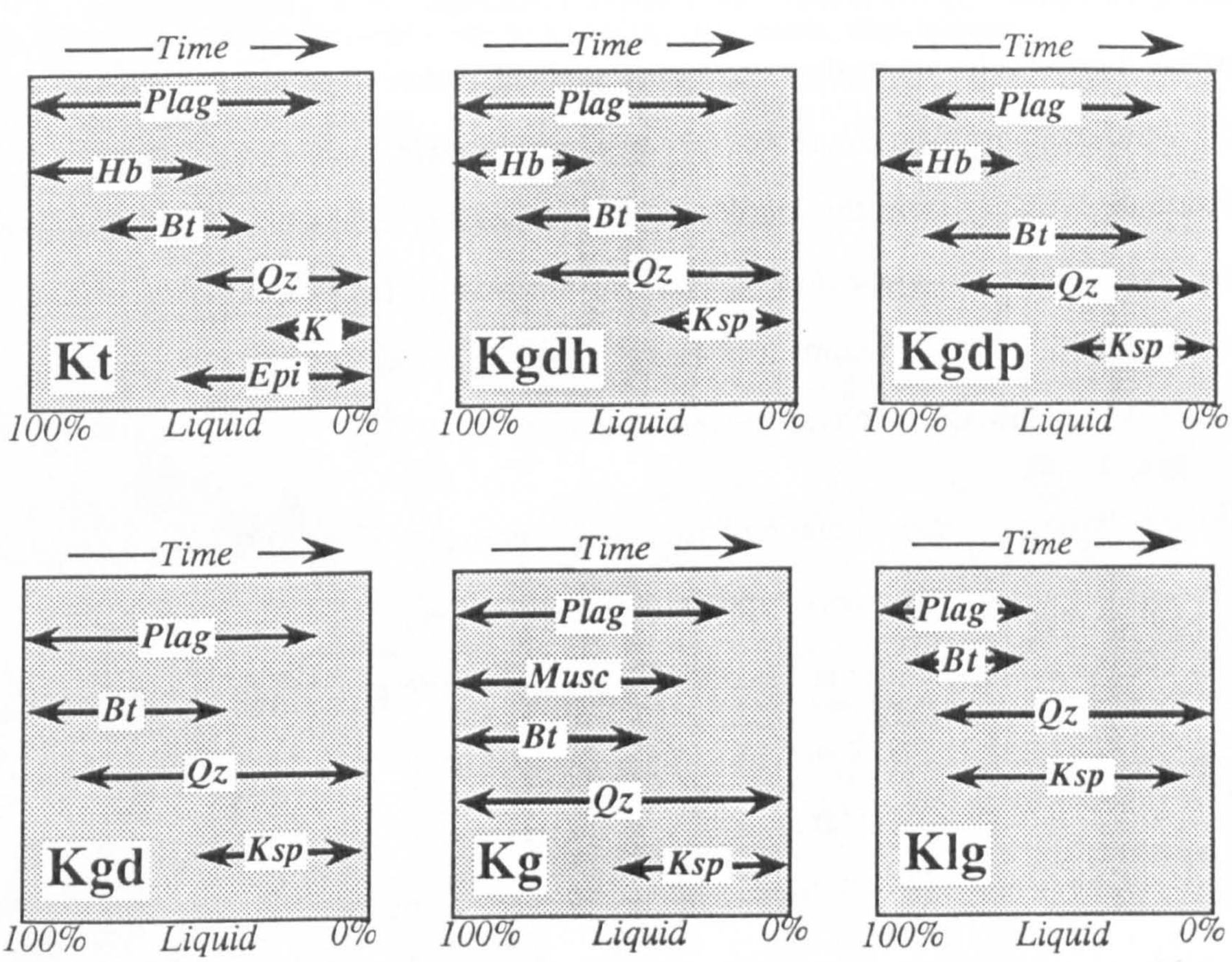

Figure 3.8 Diagram of relative sequence of crystallization of major mineral phases from each the Cretaceous granitoid rock types of the Atlanta lobe.

3.3.2 The Tertiary bimodal suite.

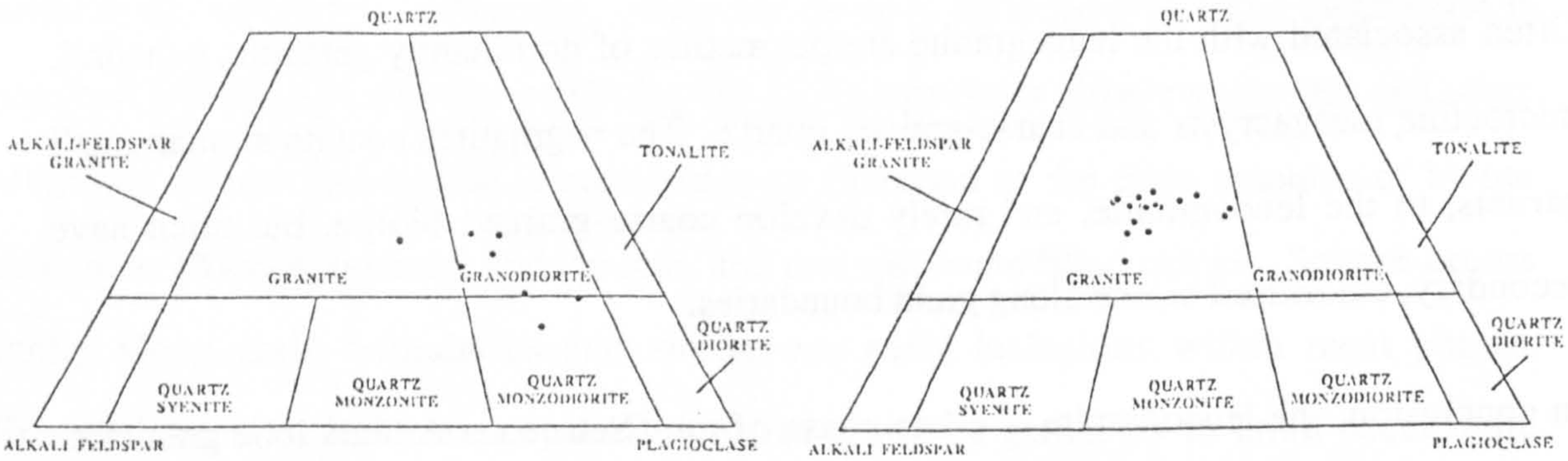

Tertiary Dioritic Suite (Tgd) Tertiary Granitic Suite (Tg)

Figure 3.9 Strekeisen classification diagrams for the Tertiary bimodal suite based on the GRANITE NORM calculation (Harris, pers. com.).

3.3.2 vii) Tertiary dioritic suite (Tgd)

The Tertiary dioritic suite are medium- to coarse-grained, seriate to porphyritic diorites to granites, although hornblende gabbros are reported (Lewis, pers com.). They are compositionally distinct from the mafic Cretaceous phases, by trending from dioritic compositions through the monzodioritic field to the granite field on Strekeisen plots (figure 3.9), due to the smaller amount of free quartz, evident modally from thin section, and calculated from GRANITE NORMS (Harris, pers com., 1988).

Hornblende is the most common mafic phase and it is normally euhedral, coarse-grained, but occasionally it has altered cores of clinopyroxene, probably aegirine-augite crystallized very early (figure 3.10). Biotite is the other ubiquitous mafic phase, and together with hornblende can make up to 50% of the rock. Plagioclase is on average andesine, but varies from An_{28}-An_{45}. A diagnostic feature of the dioritic suite, is the complex nature of the plagioclase zoning in comparison with that in the Cretaceous tonalites.

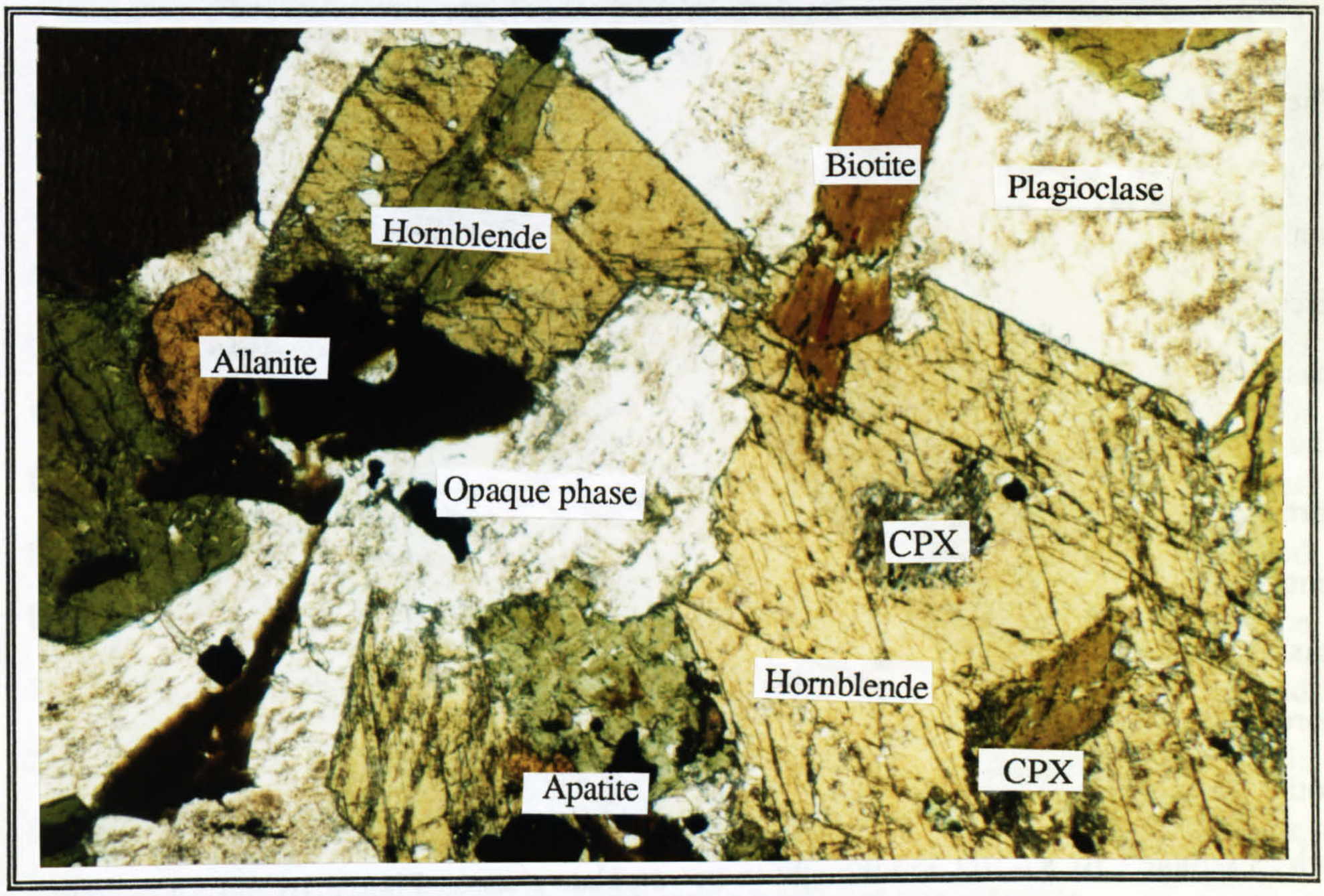

Plate 3.16 Photomicrograph in crossed polars of a quartz monzodiorite from the Tertiary dioritic suite showing complex zoning in the plagioclase, hornblende with cores of clinopyroxene, both of which are cumulate phases surrounded poikilitically by later plagioclase, quartz, alkali feldspar.

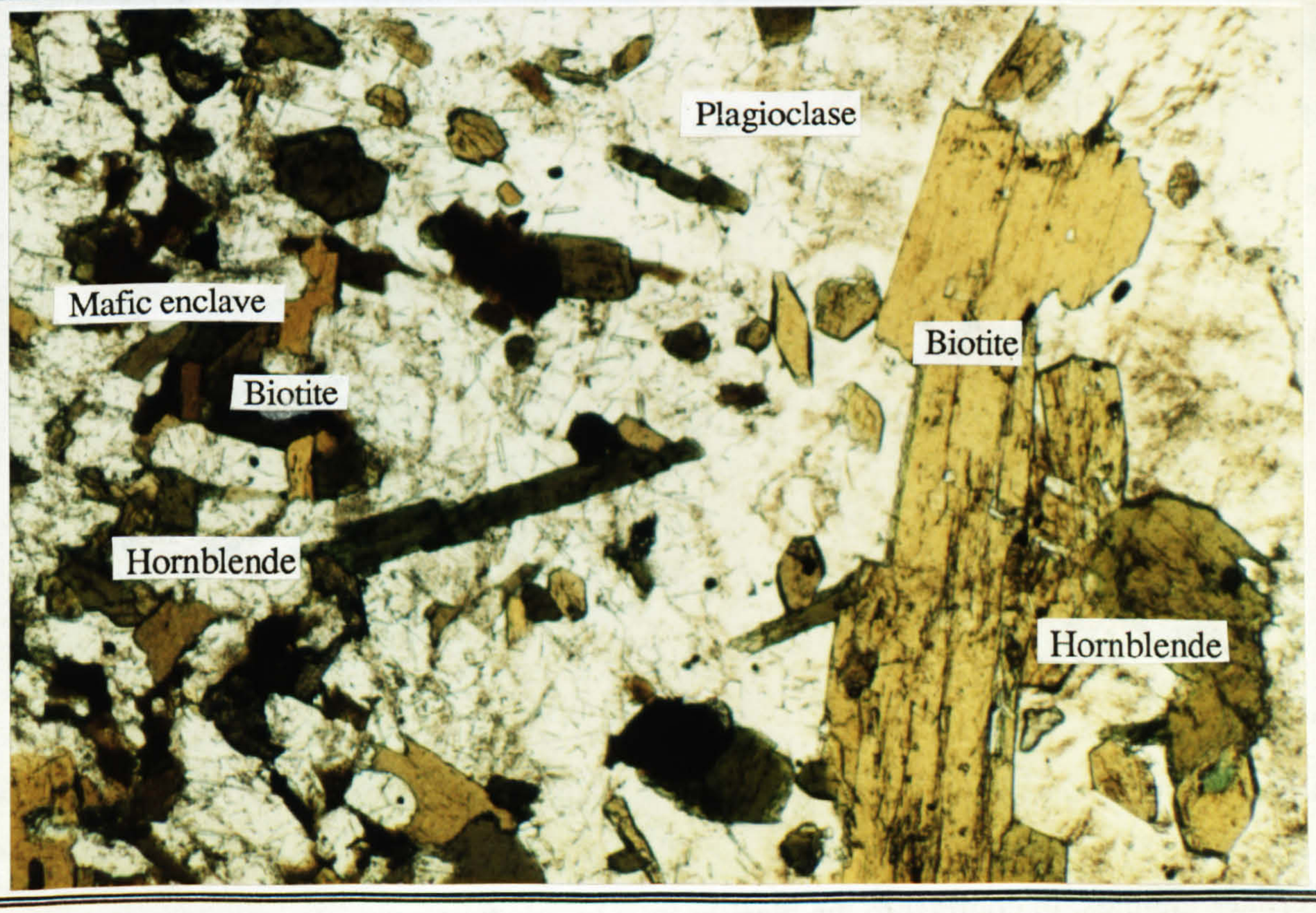

Plate 3.17 Photomicrograph of a quartz monzodiorite from the Tertiary dioritic suite in crossed polars showing a mafic enclave with a diffuse boundary interpreted as an entrained pod of an earlier crystallized slightly more mafic crystal mush.

The plagioclase is subhedral, crystallizing later than the hornblende, but before the interstial and often minor amounts of quartz and rare poikilitic alkali feldspar. Magnetite is a common opaque phase, and other accessory phases are rare apatite, sphene, allanite, zircon and monazite. Rounded mafic enclaves in the rock contain fine grained radiating masses of hornblende, biotite and plagioclase (An_{45}) with minor quartz and alkali feldspar. The borders of the enclaves are indistinct because earlier, coarse grained phenocrysts of hornblende, biotite and plagioclase are incorporated into the margins, but never into the centres of the enclaves. The enclaves are interpreted as representing early chilled crystal mushes from the walls of the pluton which have become entrained within later, slightly more felsic magmas. Occasional concentrations of euhedral, coarse-grained hornblende, biotite and plagioclase, surrounded poikilitically by plagioclase, alkali feldspar and quartz, such as sample CBC87-102, are thought to be cumulate phases. Plate 3.16 and 3.17 show a thin-section view of a typical seriate texture, a mafic enclave and the cumulate texture.

The dioritic suite have variable compositions, but monzodiorites are most common. The order of crystallization is clinopyroxene, hornblende, biotite, plagioclase and later quartz and alkali feldspar (figure 3.10).

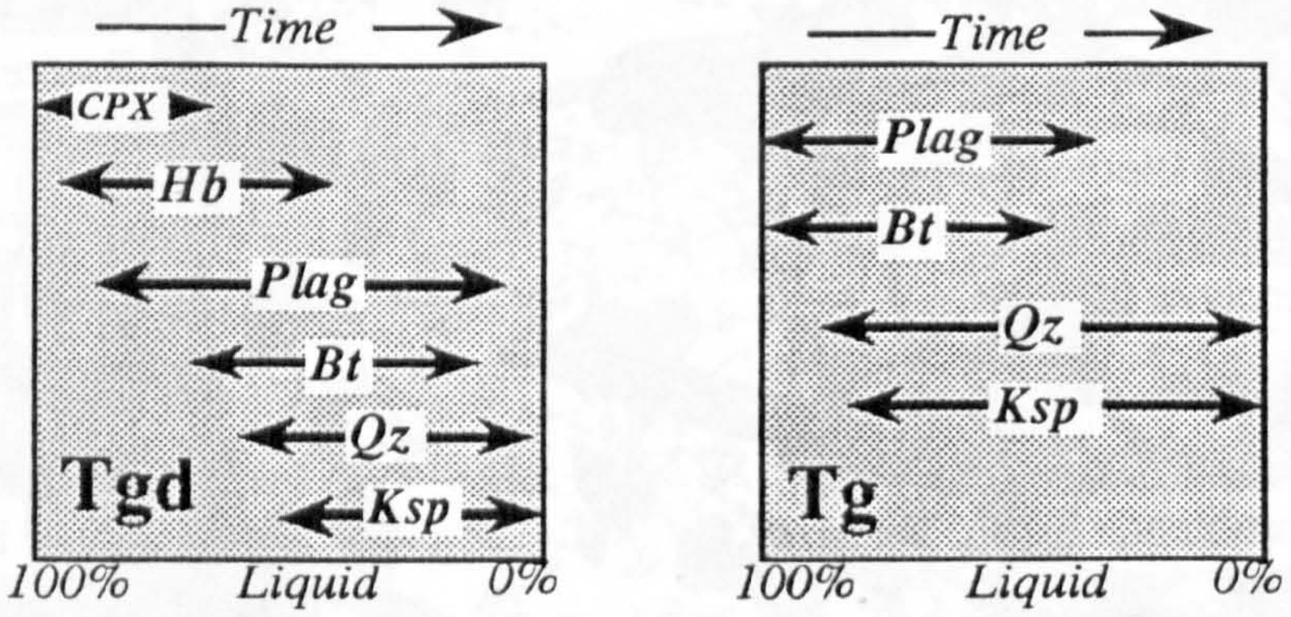

Figure 3.10 Inferred order of crystallization of the dioritic suite and granitic suite from petrographic studies.

3.3.2 viii) Tertiary granite (Tg)

The Tertiary granites, in contrast to the dioritic suite have a limited range of compositions generally plotting within the the granite field on Strekeisen diagrams (figure 3.8). The

rocks are coarse- to fine-grained, leucocratic, equigranular to poikilitic with no foliation developed. The fine-grained varieties are rare and are only found on the margins of plutons. The rock is dominated by pink, alkali feldspar which is both subhedral and more rarely poikilitic around minor plagioclase and biotite. The alkali feldspar is almost always perthitic, with the development of both albitic stringers and large patches of albite. Thin sections show that very minor amounts of early hornblende are more common than thought from hand specimen, but biotite is the only common mafic mineral, making up to 5% of the rock. Opaque phases are rare unless they are associated with the often chloritised biotite. The plagioclase is oligoclase, it is sub- to anhedral and crystallizes early to late (figure 3.10). Myrmekite and granophyric textures are commonly reported (Bennett and Knowles, 1985), but they are rare in the Tertiary granites from this study. The quartz is undeformed, but often dark due to the high radioactive element content of the rock. Common accessory phases are zircon, monazite, allanite and minor apatite.

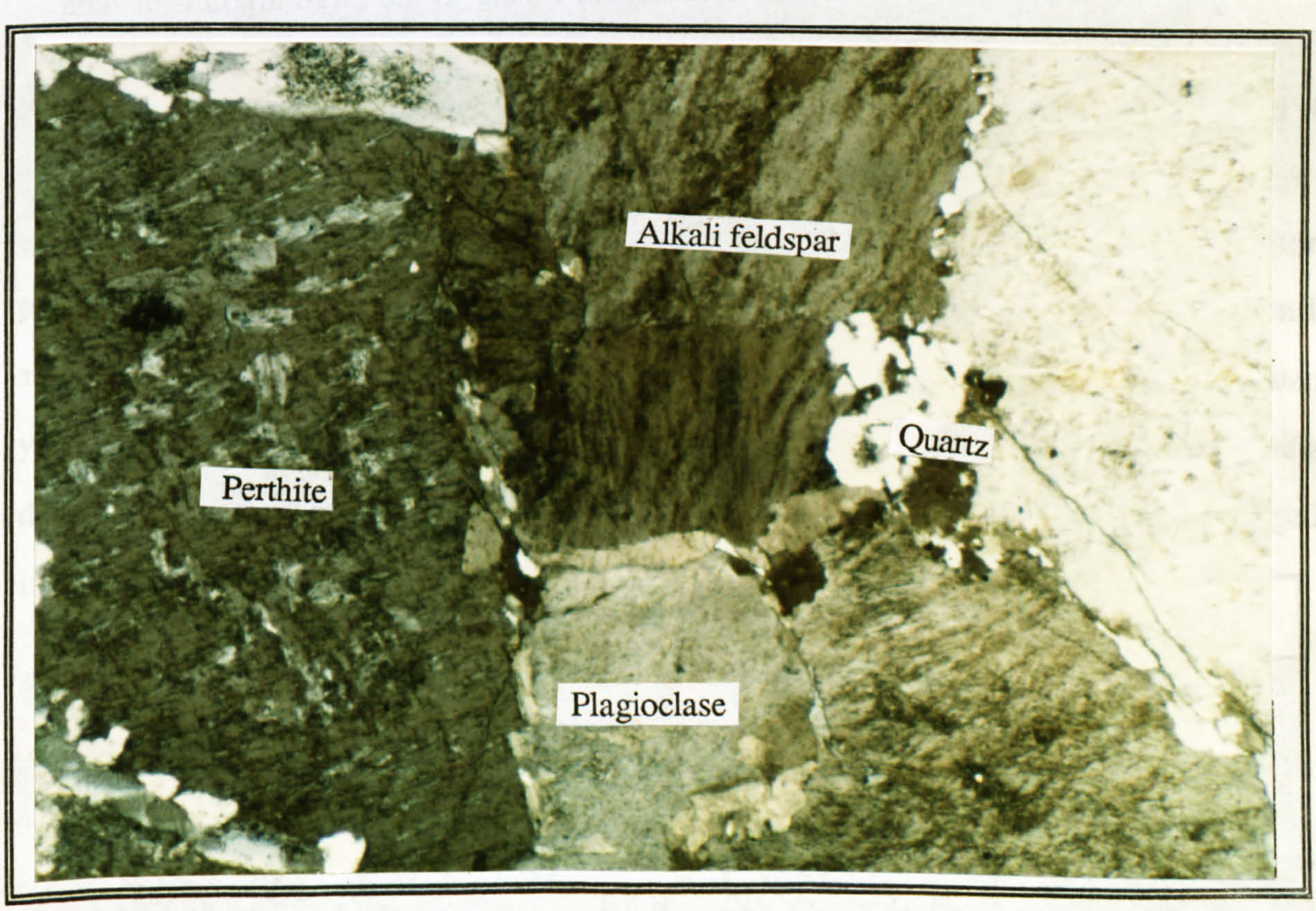

Plate 3.18 Photomicrograph of Tertiary granite in crossed polars showing early pink alkali feldspar and patches and stringers of perthite.

Microprobe analysis of biotite (Bennett and Knowles, 1985) indicate high fluorine contents and, together with the presence of fluorite and topaz in miarolitic cavities, suggest that the melts were dry and able to rise to high levels in the crust before intersection with the solidus. This is a false logic as F^- and OH^- ions behave similarly. The presence of large alkali feldspar phenocrysts in a finer grained ground mass of plagioclase and quartz in the Tertiary granites (unseen in this study) have been interpreted to represent high temperature crystallization, complicated by quenching at high levels of emplacement in the crust (Bennett and Knowles, 1985). In conclusion the Tertiary granites are hypersolvus, cotectically crystallized granites emplaced at high levels in the crust.

3.4 Geochronology of the Cretaceous and Tertiary granitoids

No attempt is made in this study to date the age of crystallization of the Cretaceous and Tertiary granitoids by radioactive decay techniques, owing to the large amount of data which already exists, and to projects concurrently being undertaken during the course of this research. However, the reported dates are summarised in this section, and are shown to agree well with the cross-cutting relationships (figure 3.11). Moreover, previously ambiguous relationships between rock types, based on field relations alone, are further delineated, so that the genetic relationships between the rock types can be better constrained for the purpose of later geochemical modelling. Much of the summarised data has been taken from Lewis et al. (1987), Criss et al. (1982), Bennett and Knowles (1985) Kiilsgaard and Lewis (1985), Criss and Fleck (1987) and Armstrong et al. (1977b).

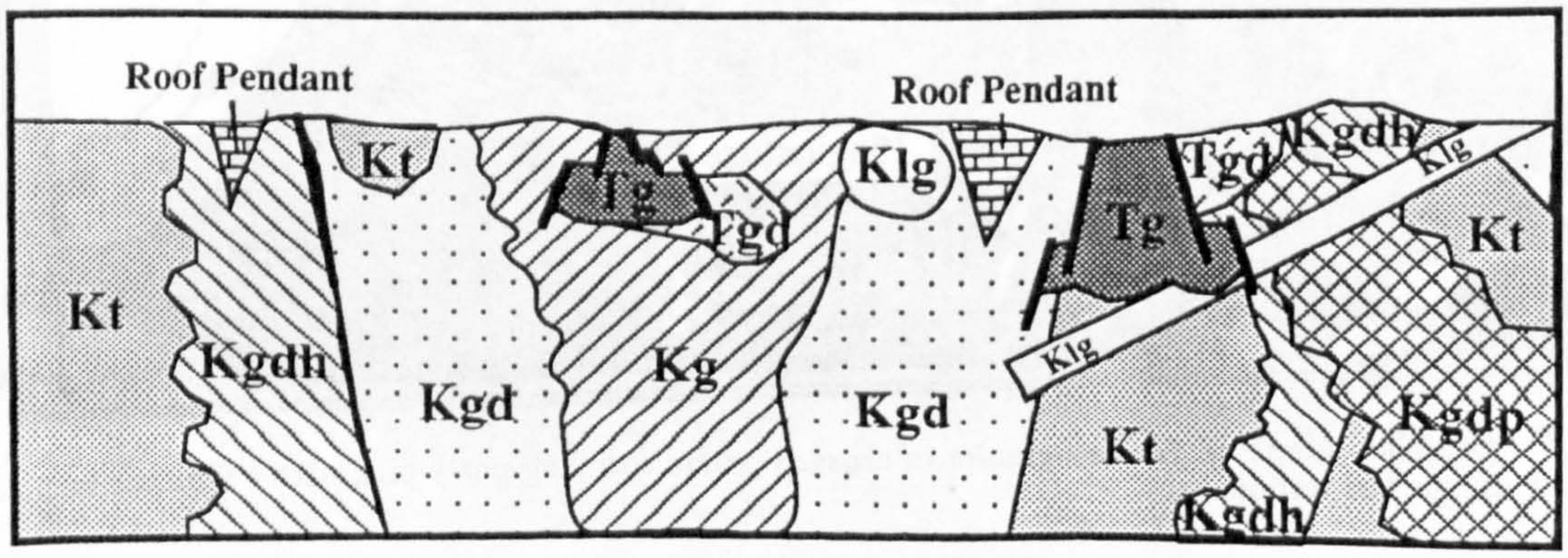

Figure 3.11 Schematic field cross-section to illustrate the cross-cutting relationships where they have been determined. Wavey lines indicate gradational contacts.

Extensive early work, by K-Ar methods of dating, of the Cretaceous phases of the northern and southern lobes of the Idaho batholith has largely been proved to be anomalous. This is due to the Eocene heating event associated with intrusion of the Tertiary bimodal suite, and regional uplift and doming causing whole or partial resetting of the K-Ar system (Criss et al., 1982). The K-Ar ages only represent a minimum age of emplacement, i.e. when the mineral dated (usually biotite or hornblende) cooled past its respective blocking temperature. Thus complex cooling histories, involving later thermal pulses and variable rates of uplift, as in the Atlanta lobe, make careful interpretation of the results necessary to elucidate the actual events being dated.

This problem is reflected in the large range of ages, 67Ma-82Ma, for the tonalite from the eastern and western borders of the lobe, even where Tertiary heating was not significant (Criss et al., 1982; Armstrong et al., 1977b). A porphyritic granodiorite has been analysed from the eastern side of the batholith by several techniques (Lewis et al., 1987) for the sake of comparison, and to gauge the results by other techniques. A U-Pb zircon age of 88±6 Ma, is interpreted to represent the age of emplacement, whereas the ages of 84.7±2.9Ma and 79.8±2.7Ma by K-Ar techniques on hornblende and biotite respectively, illustrate the possible complications due to slow cooling rates, and differences in blocking temperatures and uplift rates. Further more, the same unit 50km north, in the Yellowpine area, yields a younger biotite K-Ar age of 77.9±2.8Ma leading Lewis et al.(1987) to suggest regional differences over short distances, although it should be pointed out that they are analytically indistinguishable.

Biotite K-Ar ages from the more internal biotite granodiorite and muscovite-biotite granodiorite from the Atlanta lobe, yield a large, but overlapping range of ages of 54Ma-79Ma, (Lewis et al., 1987), because of similar complications to those above. In general the ages are significantly younger than the tonalites, hornblende-biotite granodiorite and porphyritic granodiorite, which outcrop near the eastern and western margin of the Atlanta lobe. K-Ar ages on biotites are mostly in the range of 70Ma-73Ma for the leucogranite, but those in the proximity of Tertiary granites yield ages of 64Ma-65Ma due to resetting

(Lewis et al., 1987). A summary of the K-Ar ages for the Atlanta lobe is shown in figure 3.12, after Lewis et al. (1987) who have interpreted the emplacement ages to be: 95Ma-85Ma for the tonalites and hornblende-biotite granodiorite; between 85Ma-75Ma for the biotite granodiorite; 78Ma-72Ma for the muscovite-biotite granite; and 75Ma-70Ma for the leucogranite. Although there is uncertainty in these ages, the order of emplacement, and the significant overlap in ages is in agreement with cross-cutting relationships and the gradual boundaries between lithologies(figure 3.11).

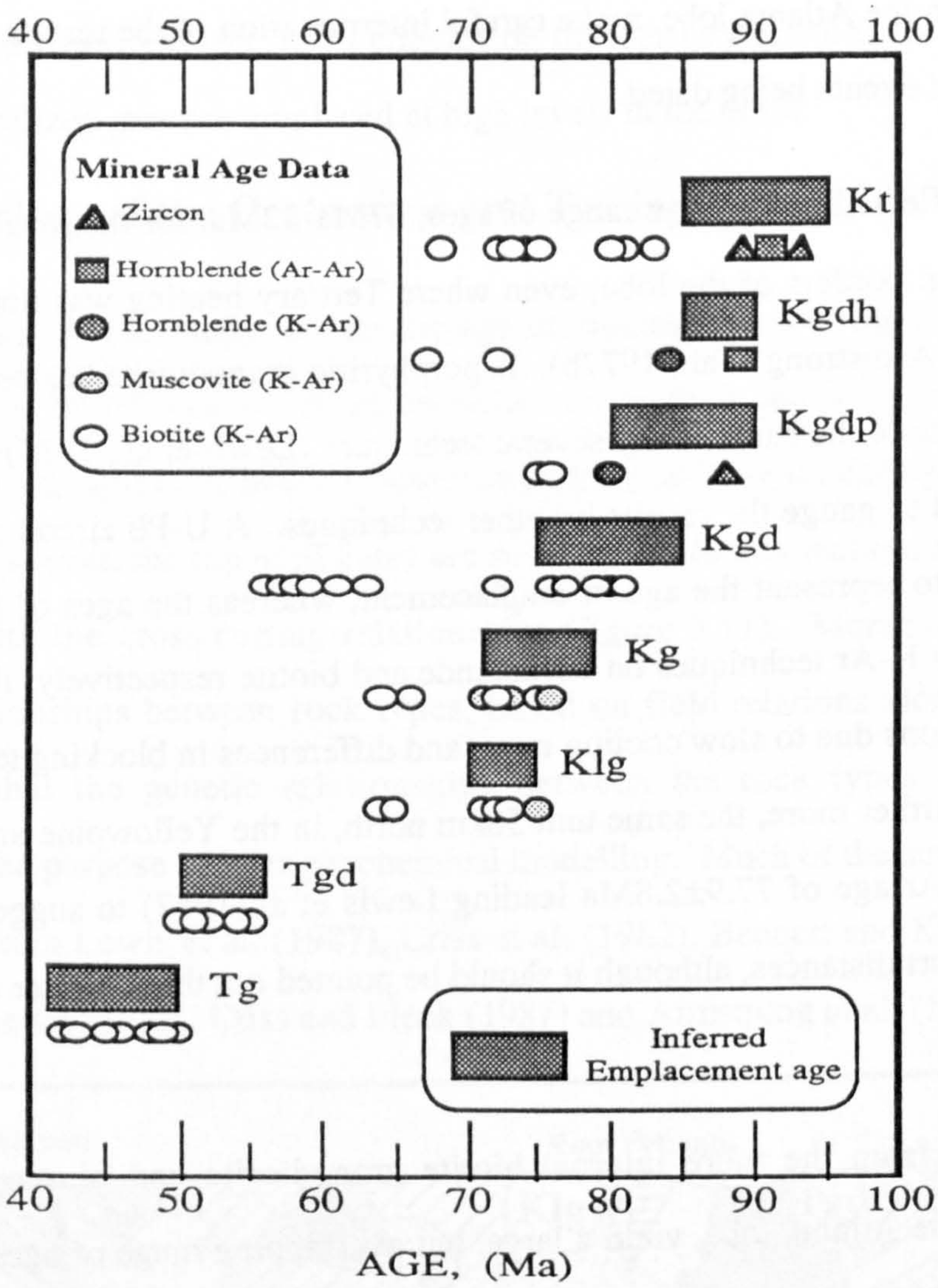

Figure 3.12 Summary of the radiometric geochronological data, and the interpreted ages of emplacement, of the Cretaceous and Tertiary phases of the Atlanta lobe of the Idaho batholith, modified from Lewis et al., 1987, with further data from Criss et al., 1982 and Lund and Snee, 1988.

K-Ar dates for the Tertiary bimodal suite are much more representative of the true age of emplacement because high levels of emplacement in the crust have allowed rapid cooling,

there has been no significant thermal events since the time of emplacement, and uplift rates and distances have been slower and so less significant. The ages are summarised in Bennett and Knowles (1985) and Fischer et al. (in press), but range from 50Ma-45Ma for emplacement of the dioritic suite, and the 49Ma-42Ma for the granites.

Alternative geochronological techniques yield comparable emplacement ages to the K-Ar method and significantly, produce the same order for emplacement of the individual rock types. Although many Rb-Sr isotope analyses have been completed, very little specifically geochronological work has been very successful (Criss and Fleck, 1987). Armstrong et al. (1977b) reported Rb-Sr whole rock and mineral dates between 69Ma to 99Ma for Cretaceous phases from the Atlanta lobe of the Idaho batholith, but the isochron relationships are confused in some cases and the errors are high. The incidental use of Rb-Sr isotopic data from this study, to construct whole rock isochrons from related lithologies even within restricted areas, were completely unsuccessful due to the large variation in initial ratios for individual samples from likely isochron suites. Criss and Fleck (1987) noted the same problem for numerous Rb-Sr isotopic measurements made in the Cretaceous granitoids of the Bitteroot lobe of the batholith, and suggested that hydrothermal alteration processes caused by the large hydrothermal systems set up around the intrusive Tertiary bimodal suite (Criss and Taylor, 1983), may have been responsible for changes to the $^{87}Sr/^{86}Sr$ ratios, or the Rb/Sr ratios or both. However, they concluded that the hydrothermal systems do not seem to have influenced the initial $^{87}Sr/^{86}Sr$ ratios even in areas of major ∂O^{18} and ∂D anomalies surrounding the Tertiary intrusive phases (Criss and Taylor, 1983) because altered and unaltered rocks have the same initial $^{87}Sr/^{86}Sr$ ratios. The variation of initial $^{87}Sr/^{86}Sr$ ratios is therefore attributed to the varying source characteristics. Furthermore, they stress the relatively small time difference between the age of hydrothermal alteration, and the age of emplacement of the Cretaceous phases of the Idaho batholith, so that changes in the measured Rb/Sr ratio produce only moderate complications in the Rb-Sr systematics.

A similar scenario is envisaged here for the Cretaceous phases of the Atlanta lobe of the Idaho batholith, where initial $^{87}Sr/^{86}Sr$ ratios vary within unaltered rocks over short

distances and there are no systematic changes in the $^{87}Sr/^{86}Sr$ ratios along traverses away from intrusions of the Tertiary bimodal suite, even in areas of established ∂O^{18} and ∂D anomalies (Criss and Taylor, 1983). Two traverses were made across Cretaceous granitoids which fall within the Tertiary hydrothermal alteration zones delineated by Criss and Taylor (1983) and by the altered nature of the rocks along cracks and fissures, and the presence of many mineralised veins and working and disused mines and mine prospects. The ALVT traverse was taken towards the southwest, away from the Sawtooth Tertiary granite batholith, and the Long Gulch pluton traverse was taken across the Long Gulch pluton. The hypothesis that the isotope variations inherited from within the source region are responsible for the lack of isochron relationships is further suggested by variable $^{143}Nd/^{144}Nd$ ratios for related granitoids over short distances that correlate with variations in the $^{87}Sr/^{86}Sr$ ratios (Chapter 5).

In the Atlanta lobe two U-Pb zircon lower intercept ages of 90Ma and 88Ma have been reported for the tonalite from the western and eastern borders respectively (Lewis et al., 1987). Moreover $^{40}Ar/^{39}Ar$ dating of the earliest tonalites from the western border yield ages of 93Ma for emplacement followed by rapid uplift (Lund and Snee,1988).

Comparison of isotope data from the Atlanta lobe, with radiometric ages and field relations from the northern, Bitteroot lobe (Criss and Fleck, 1987; Bickford et al., 1981; Toth, 1987; Hyndman, 1984), show that the lobes were emplaced coevally, but that the Cretaceous phases of the Bitteroot lobe were emplaced over a shorter time span between approximately 87Ma-75Ma. The order of emplacement, with the early tonalite and hornblende-biotite granodiorite towards the borders, and the later biotite granodiorite and muscovite-biotite granite in the core of the Bitteroot lobe, (Hyndman, 1984) suggest a strong genetic relationship between the two lobes of the Idaho batholith.

In summary the Cretaceous phases of the Atlanta lobe of the Idaho batholith were emplaced during three overlapping time intervals.

i) The tonalite, transitional into the hornblende-biotite granodiorite, was emplaced towards the western and eastern margin of the lobe between 95Ma-85Ma.

ii) The biotite granodiorite and muscovite-biotite granite, which form the core of the lobe, were intruded between 85Ma-72Ma, and although the contact between the rock types is transitional, the slightly younger range in K-Ar ages, and the more central location of the muscovite-biotite granite suggest that it is slightly younger.

iii) The leucogranite, the youngest Cretaceous phase, was emplaced at 75Ma-70Ma as small plutons and dykes which cross-cut all other phases of the Atlanta lobe.

There is a brief lull in magmatism between 70Ma-55Ma, before the earlier dioritic suite was emplaced between 55Ma-50Ma and the later epizonal granites between 49Ma-42Ma. Together these comprise the Tertiary bimodal suite. The overlapping ages of emplacement of all phases of Cretaceous granitoids, suggest that they are genetically related and may be classified as a single co-magmatic suite, which is further discussed and tested in the light of chemical and isotopic data in later sections.

Rock Unit	Kt	Kgdh	Kgdp	Kgd	Kg	Klg	Tgd	Tg
Rock Name	Tonalite	Hornblende-Biotite Granodiorite	Porphyritic granodiorite	Biotite Granodiorite	Muscovite-Biotite Granite	Leuco-granite	Tertiary Dioritic Suite	Tertiary Granitic Suite
Texture	Hypidiomorphic Equigranular	Hypidiomorphic Equigranular	Porphyritic to Poikilitic	Hypidiomorphic Equigranular	Hypidiomorphic Equigranular to Granular	Allotriomorphic Equigranular	Seriate to Porphyritic	Hypidiomorphic Equigranular
Grain Size	Medium	Medium-Coarse	Medium-Coarse	Medium-Coarse	Coarse	Fine to Medium	Medium	Fine-Coarse
Foliation	Pervasive, Strong by Hb and Bt	Strong to weak Hb Bt	Unfoliated	Rare Primary Flow foliation	Unfoliated	Unfoliated	Unfoliated	Unfoliated
% Mafic Phases	30% Hb and Bt	20% Hb and Bt	20% Hb and Bt	10% Bt	5% Bt	<2% Gt and Bt	50% CPX, Hb and Bt	5% Hb and Bt
%An in Plagioclase	An_{55}-An_{35} Unzoned	An_{40}-An_{30} Unzoned	An_{40}-An_{30} Rare zone	An_{28}-An_{22} Zoned	An_{20} Zoned	An_{20}-An_{10} Unzoned	An_{45}-An_{20} Complex zones	An_{20} Zoned
Accessory Phases	Epidote, Zircon, Magnetite, Sphene, Apatite, Allanite	Epidote, Zircon, Magnetite, Apatite, Allanite, Sphene	Zircon, Magnetite, Apatite, Allanite, Sphene	Hnbld ,Zircon, Magnetite, Apatite, Sphene	Zircon, Apatite, Allanite, Monazite	Sphene, Garnet, Biotite	Zircon, Magnetite, Sphene, Apatite, Allanite	Zircon, Apatite, Allanite,
Qz & Fsp Textures	Myrmekite	Myrmekite Perthite	Myrmekite Perthite	Myrmekite Perthite	Perthite Granophyre	Perthite	Myrmekite	Myrmekite Perthite Granophyre
Order of Crystal-lization	1.Pg, Hb, Bt 2. Qz, Ksp 3. Epi	1.Pg, Hb, 2. Bt, Qz 3. Ksp	1.Hb 2. Pg, Bt 3. Qz Ksp	1. Pg, Bt 2. Qz, Ksp	1.Pg, Bt, Mu 2. Qz, Ksp	1. Pg, 2.Bt,Qz,Ksp 3. Gt	1. Cpx 2..Hb 3. Pg, Bt 4. Qz Ksp	1. Pg, Bt, Qz, Ksp
Nature of Enclaves	Mafic Autoliths	Mafic Autoliths	Mafic Autoliths	Tonalite Xenoliths	None	None	Mafic Autoliths, Cumulates	None
Age	95Ma-85Ma	90Ma-85Ma	90Ma-80Ma	85Ma-75Ma	78Ma-72Ma	75Ma-70Ma	55Ma-50Ma	49Ma-42Ma
Depth of Emplacement	Catazonal >30km	Catazonal	Mesozonal	Mesozonal	Mesozonal	Mesozonal -Epizonal	Mesozonal -Epizonal	Epizonal
Distributio n and Nature of Plutons	Elongate, medium size plutons on eastern and western borders and ridges of the Atlanta lobe		North-South belt in east of Atlanta lobe	Large plutons in the internal core of the Atlanta lobe		Dykes, stocks and veins in eastern Atlanta lobe	Small stocks in east and external to Atlanta lobe, associated with dyke swarms and volcanics	
Contacts	Transitional with Kgdh	Transitional with Kgdp and Kt	Transitional with Kgdh and Kt	Transitional with Kg	Transitional with Kgd	Always Sharp	Sharp	Sharp

Table 3.1 Summary of the field relations, petrography and geochronology of the Cretaceous and Tertiary phases of the Idaho batholith.

CHAPTER 4

Major and Trace Element Geochemistry

4.1 Introduction

Major and trace element data are presented for over 160 samples of Cretaceous and Tertiary granitoids from the Idaho batholith region which have been analysed by X-ray wavelength dispersive techniques. A subset of representative samples has also been analysed for rare earth elements (REE), and Th, Ta, Hf, U, Co and Sc by instrumental neutron activation analysis (INAA). Appendix A documents the analytical techniques while Appendix B lists the major and trace element data.

The major objectives of this chapter are:

i) To describe the major and trace element variations of the Cretaceous granitoids of the Atlanta lobe and the Tertiary granitic and dioritic suites.

ii) To compare the selected granitoid classification schemes and to evaluate them in the context of the Atlanta lobe granitoids.

iii) To model the major and trace element variations by partial melting and fractional crystallization processes, and to identify suites of samples which require some form of crustal contamination model to account for their chemistry.

iv) To suggest the likely conditions and metamorphic reactions for production of the Atlanta lobe granitoids.

iv) To characterise the major and trace element compositions of the likely source rocks of the Atlanta lobe granitoids.

4.2 Major element geochemistry

The Cretaceous granitoids of the Idaho batholith are very typical of the calc-alkaline association. They grade from tonalite to granodiorite to granite, with only minor diorite and gabbro (Hyndman, 1984), as illustrated on the Strekeisen diagram (figure 3.7). The association with active subduction at the time of formation of the Idaho batholith (Lipman et al., 1972) is typical of the Mesozoic and Tertiary calc-alkaline granitoids of the western Americas. The Cretaceous granitoids of the Idaho batholith have less iron and more alumina than the tholeiitic association, and on ternary Na_2O+K_2O-FeO-MgO (AFM) diagrams (figure 4.1) they plot within the calc-alkaline field of Irvine and Barager (1971). The typical trend, convex towards more iron rich compositions, and an alkali-lime index in the range 60-64 indicates that the Cretaceous phases are all calc-alkaline (Peacock 1931).

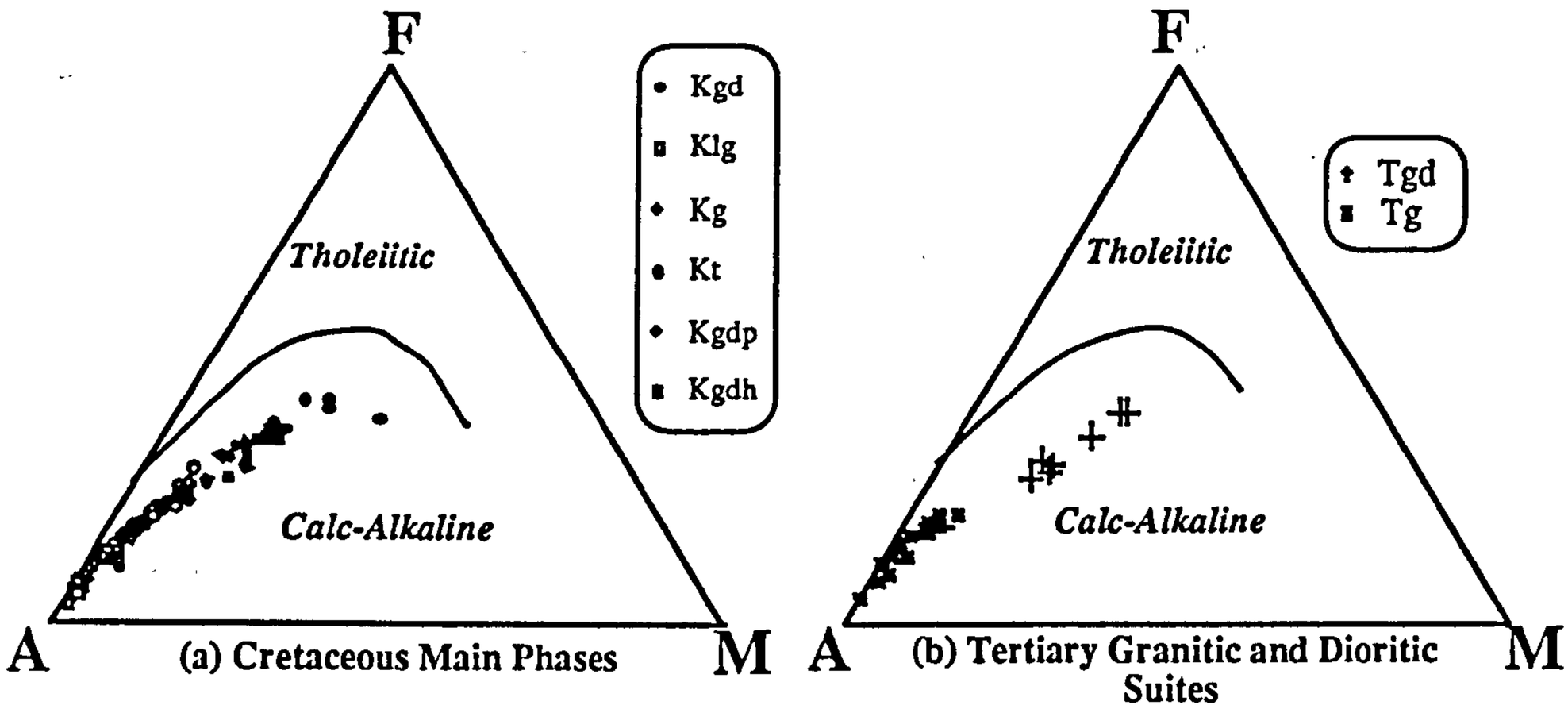

Figure 4.1 Ternary alkali vs. total iron vs. magnesia (AFM) diagrams, (a)Cretaceous granitoids, (b) Tertiary granitic and diorotic suites.

In contrast the Tertiary dioritic suite exhibits a distinctly flatter trend on the Strekeisen diagram (figure 3.7), trending across the quartz-monzodiorite field from dioritic to granitic (*sensu-stricto*) compositions. The granitic suite plots exclusively within the granite field (figure 3.7). However the Tertiary dioritic and granitic suites fall strictly within the field of the calc-alkaline trend, on the AFM diagram (figure 4.1) although some resemblance to the alkaline magma association trend is noted on Strekeisen diagrams (figure 3.9). Such an alkaline affinity may be linked to the westward jump of the subduction zone, and the change

to a more intra-plate tectonic setting in the Eocene (Lipman et al., 1972). The Tertiary bimodal suite has an alkali-lime index of 65-70 falling into the calc-alkaline association of Peacock (1931).

In summary all the Cretaceous granitoids in the area of study are calc-alkaline, but the Tertiary rocks show some evidence of a change to a more alkaline character. This may be due to a change in tectonic regime from dominantly compressional in the Late Cretaceous, to one of more extensional character in the Eocene, resulting in the emplacement of the intra-plate Tertiary granites at high levels in the crust. However, the role of the source composition in determining the composition of the granitoid magmas must be considered, as it probably has a more dominant effect than the tectonic setting, particularly in relation to trace element and isotopic compositions of the Idaho batholith magmas.

4.2.1 Harker diagrams

4.2.1 i) The Cretaceous Granitoids

Figure 4.2 shows Harker diagrams for the major element variation for the Cretaceous phases of the Atlanta lobe. Smooth inter-element variation patterns suggest that the major element chemistry reflects igneous processes. The lack of significant alteration textures noted during petrographic studies, together with the smooth inter-element variations are taken as evidence that the Cretaceous phases of the Atlanta lobe, sampled in this study, are largely unaffected by subsolidus alteration processes. Two rarely noted alteration textures are sericitisation of the more anorthite rich cores of zoned plagioclase and chloritisation of amphibole and biotite. Sericitisation of plagioclase and chloritisation of amphibole involve the loss of Ca. However, the co-variation of CaO with silica defines a tight trend and thus dispels the possibility of significant major element transport associated with subsolidus alteration processes on a scale greater than the sample size.

All six Cretaceous phases of the Atlanta lobe are plotted on figure 4.2 with silica as the index of evolution. They exhibit a wide range from 55-78 wt.% SiO_2 with no clear compositional gaps between the rock types although each rock type, apart from the porphyritic

granodiorite, forms a discrete group on the variation diagrams.

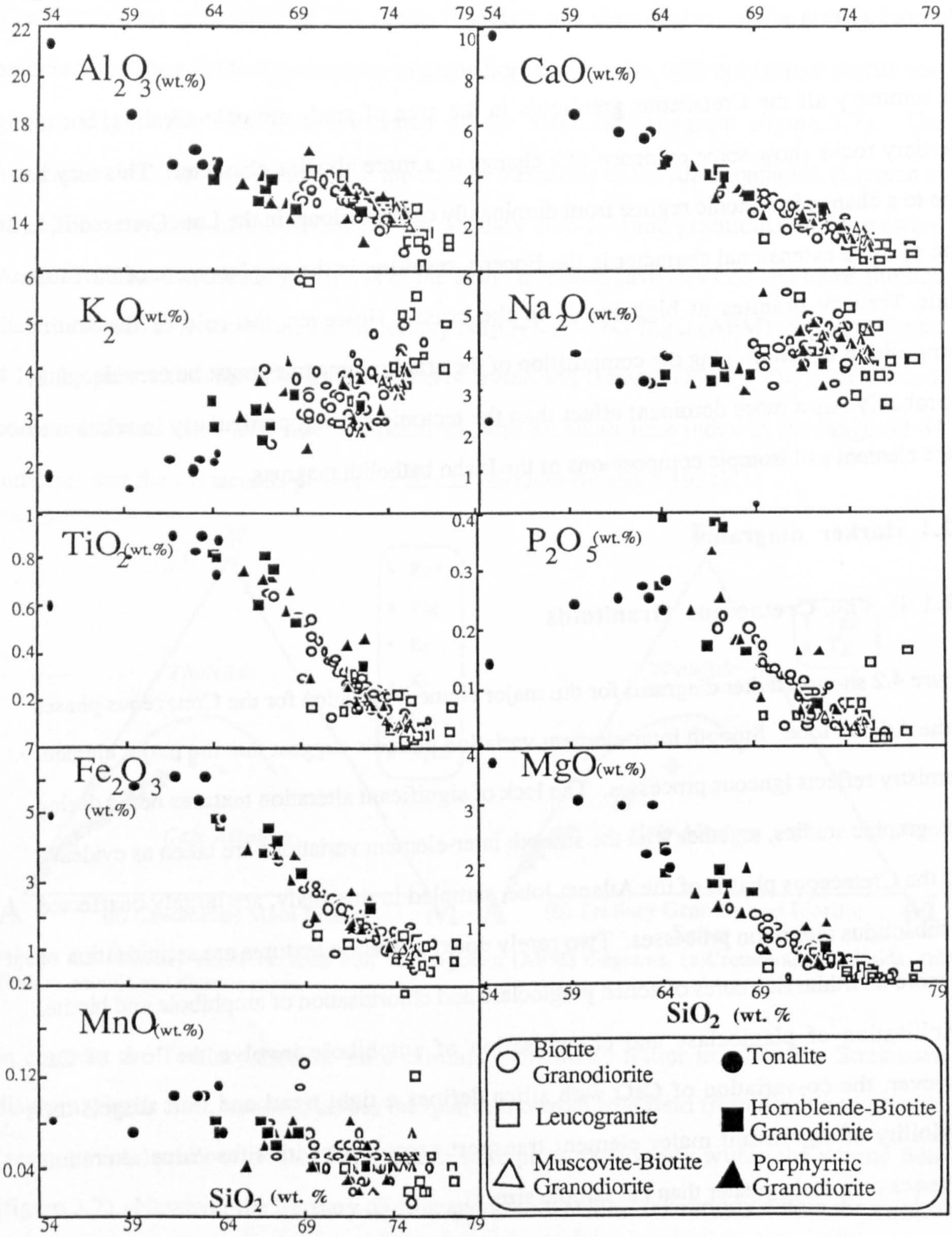

Figure 4.2 Major element Harker variation diagrams for the six Cretaceous phases of the Idaho batholith, all plotted as wt. % against silica.

Despite the discrete intrusive phases recognised in the field, where diffuse boundaries exist between rock types based on modal mineralogy, the boundaries are placed somewhat arbitrarily in terms of chemical composition. The continuous range in major element compositions of the Cretaceous phases with few intrusive contacts suggest they are genetically related.

The field terms for classification of the rocks work in terms of chemical composition. Silica contents increase from tonalite, in the order tonalite, hornblende-biotite granodiorite, porphyritic granodiorite, biotite granodiorite, muscovite-biotite granite to leucogranite. The tonalites range from 55-65 wt.% SiO_2, whereas the field related hornblende-biotite granodiorite is more restricted between 64-68 wt.% SiO_2. The porphyritic granodiorite has silica contents in the wide range of 65.5-73.5 wt.% SiO_2, perhaps indicating that late stage alkali feldspar megacrysts were developed in several different Cretaceous magma types. The silica content of the biotite granodiorite varies from 67.5-76 wt.% SiO_2, with the more silicic varieties plotting as granites on Strekeisen classification diagrams (figure 3.7). The muscovite-biotite granite is compositionally restricted between 73-75 wt.% SiO_2 and, surprisingly, the leucogranite ranges from 71-78 wt.% SiO_2, the latter being the only phase which may be affected by subsolidus silica mobility in late stage fluids.

Al_2O_3, CaO, TiO_2, Fe_2O_3, MgO, P_2O_5 and MnO exhibit clear decreases in concentration with increasing silica. CaO and MgO show a coherent linear decrease with increasing silica through all six Cretaceous rock types, whereas TiO_2, Fe_2O_3 and P_2O_5 decrease in concentration from the hornblende-biotite granodiorite to the leucogranite with increasing silica. The tonalite, in contrast exhibits an initial possible increase of TiO_2, Fe_2O_3 and P_2O_5 from 55wt.% SiO_2 with a peak at 63-64 wt.% SiO_2, before decreasing on the same trend defined by the other five phases. The P_2O_5 trend is more scattered than those for TiO_2 and Fe_2O_3 due to several samples of hornblende-biotite granodiorite and two leucogranite samples having particularly high concentrations of P_2O_5, which may in turn reflect modal variations in apatite. MnO shows a similar trend to those for TiO_2, Fe_2O_3 and P_2O_5, but it is more scattered because the low concentrations of MnO are nearer the detection limits.

Furthermore, two garnet-bearing leucogranite samples CBC87-42 and CBC87-72 have particularly high MnO contents, which may reflect the presence of garnet grains which presumably have high spessartine contents typical of garnets in granitic aplites and pegmatites (Deer, Howie and Zussman, 1966).

The concentration of Al_2O_3 decreases with increasing silica on a linear trend through the tonalite, hornblende-biotite granodiorite and less silica rich porphyritic granodiorite. At ≈69 wt.% SiO_2 there appears to be a slight increase in Al_2O_3 concentrations in the least evolved biotite granodiorite and the porphyritic granodiorite samples, which then exhibit a linear decrease through the biotite granodiorite and muscovite-biotite granite to the leucogranite. The significance of alumina saturation in granitoids and this break in the Al_2O_3 trend is discussed further in section 4.2.3. It should be noted, however, that K_2O shows the inverse relationship with increasing silica to that of Al_2O_3. K_2O increases with silica until 69 wt.% SiO_2 where there is a drop in K_2O concentration, followed by a linear increase through the more silica rich Cretaceous phases. Although the trend is more scattered than the alumina trend perhaps as a result of greater mobility of alkalis, a link may be inferred and a common process envisaged. The identification of such inflexion points on variation diagrams have often been interpreted in terms of changes in the residual and/or fractionating mineral assemblage and this is discussed in section 4.7. The porphyritic granodiorite shows no evidence of unexpectedly high contents of K_2O in relation to the other phases, and it exhibits no trend towards alkali feldspar on Strekeisen diagrams (see figure 3.7) which supports the petrographic conclusion that the alkali feldspar megacrysts are unlikely to have been the product of K-rich metasomatism.

Na_2O describes a more scattered trend which remains virtually constant up to 69 wt.% SiO_2 and then slowly increases to higher concentrations with increasing silica. The leucogranite shows a particularly wide range in Na_2O and K_2O concentrations which may reflect their greater mobility in late stage residual liquids.

4.2.1 ii) The Tertiary bimodal suite

Harker diagrams for the Tertiary bimodal suite are plotted for all the major elements in figure 4.3. Within the Tertiary granitic and the Tertiary dioritic suites the major elements behave in a coherent and systematic manner reflecting the control of igneous processes. Although the observed trends are coherent, it must be noted that the samples are taken from stocks and plutons that are geographically widely spaced and they are most unlikely to be the products of the same differentiating magma body. In order to formulate any sort of petrogenetic model it is necessary simply to assume that similar processes acted on the various magma batches of each suite to produce the observed chemical trends. The lack of alteration textures indicate that subsolidus transport of elements has probably not been significant on a scale greater than the size of individual whole rock samples although the alkalis, Na_2O and K_2O exhibit significant scatter, particularly in the Tertiary granite.

Although the Tertiary dioritic and granitic suites are distinctly bimodal in the field, on Harker diagrams and with the exception of CBC87-103 (a sample with granitic composition from the Tertiary dioritic suite) they exhibit only a small compositional gap. The Tertiary dioritic suite has a range in silica content of 56-67 wt.% SiO_2 (and CBC87-103 has 72 wt.% SiO_2). The Tertiary granites have higher, yet more restricted silica contents in the range 70-77 wt.% SiO_2.

Al_2O_3 decreases linearly through the Tertiary dioritic suite, but much more sharply within the Tertiary granites. K_2O mirrors the behaviour of Al_2O_3, with an initial increase through the dioritic suite, and then an even steeper increase in K_2O with increasing silica in the granites. Na_2O increases through both Tertiary groups, but again the trends are not obviously colinear: the Tertiary dioritic suite appears to trend to higher concentrations of Na_2O at a given silica value. The remaining major elements show coherent trends which decrease in concentration with increasing silica for both the Tertiary granitic suite and the dioritic suite. The dioritic suite, however, tend to exhibit steeper trends which suggests a different mineralogical control than that for the Tertiary granitic suite, and perhaps even an independent magmatic evolution.

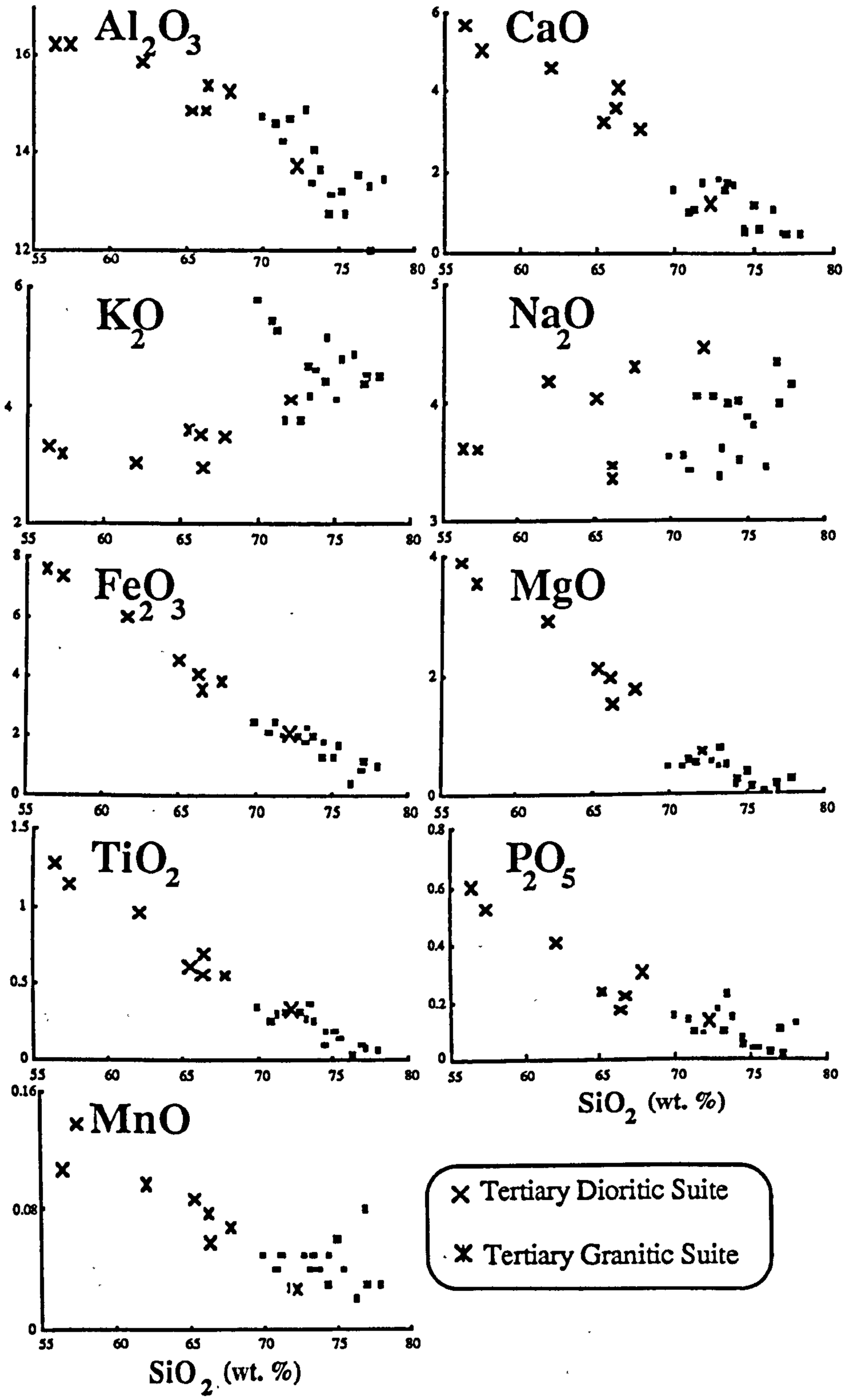

Figure 4.3 Major element Harker variation diagrams for the Tertiary bimodal suite. Crosses represent the dioritic suite and stars the granitic suite. All values are in wt. %

The slight overlap in arrays of samples from each of the Tertiary suites appear to trend to different parental liquids, which again may indicate that the Tertiary granitic and dioritic suites evolved independently. In addition, the two suites occur in discrete plutons that do

not grade into one another, even though they are intruded in close proximity, which suggests that they are not comagmatic, but that similar tectonic and structural elements account for their close spatial distribution.

In later geochemical modelling this question as to whether the Tertiary granitic and the Tertiary dioritic suites were derived from the same source by progressive differentiation processes will be pursued, although initial inspection of the chemical data combined with field evidence and petrography suggests that it is unlikely.

4.2.2 The significance of alumina saturation

The degree of alumina saturation as defined by Shand (1951) is the molecular ratio of alumina to the sum of lime and the alkalis i.e. mol.% Al_2O_3 / mol.% ($CaO+Na_2O+K_2O$) where:

Peraluminous granitoids	$Al_2O_3 > CaO+Na_2O+K_2O$
Metaluminous granitoids	$Na_2O+K_2O < Al_2O_3 < CaO+Na_2O+K_2O$
Peralkaline granitoids	$Al_2O_3 < Na_2O+K_2O$

Alumina saturation has often been used as a first order classification of granites. The degree of alumina saturation was one of a range of geochemical and mineralogical criteria Chappell and White (1974) used to classify the granitoids of the Lachland fold belt into two groups based on the inferred source characteristics (table 4.1). Metaluminous "I-type" granitoids were thought to have been derived from igneous sources and strongly peraluminous "S-type" granitoids from metasedimentary sources, but alumina saturation was just one of several criteria used to imply the nature of the source (see table 4.1) (Chappell and White 1973; White et al., 1986; Bowden et al., 1984).

I-type Granites	S-type Granites
Metaluminous to weakly peraluminous Mol % Al_2O_3 /(Na_2O+K_2O+CaO) < 1.1. Cordierite absent, sphene common.	Strongly peraluminous Mol % Al_2O_3 /(Na_2O+K_2O+CaO) > 1.1. Cordierite present, monazite common.
CIPW normative diopside or < 1% normative corundum. Magnetite common.	>1% normative corundum. Primary muscovite rare. Ilmenite common.
High Na (Na_2O>3.2% in felsic varieties, Na_2O>2.2% in mafic varieties).	Low Na, (Na_2O<3.2% when K_2O≈5% Na_2O<2.2% when K_2O≈2%.
Relatively high Ca and Sr. Regular inter-element variation within plutons and near linear variation diagrams.	Relatively low Ca and Sr. Variation diagrams more irregular.
Broad spectrum of compositions from mafic to felsic, shallow to deep level and mafic hornblende bearing xenoliths are common.	Restricted in composition to high SiO_2 types, shallow level and metasedimentary xenoliths common.
Low initial $^{87}Sr/^{86}Sr$ ratios (.704-.706).	High and variable initial $^{87}Sr/^{86}Sr$ ratios.

Table 4.1 Criteria for the classification of I- and S-type granites after Chappell and White (1974), White and Chappell (1983) and White et al. (1986).

Widespread abuse of this classification scheme has occurred by the isolated application of just some of the above criteria, used to infer granitoid igneous and sedimentary sources in the Lachland fold belt, to imply the nature of the sources of granitoids from other regions. Hyndman (1983) has shown that individual granitoids within the Bitteroot lobe have characteristics of both I-type and S-type granites and thus argued that the scheme is inapplicable to the Idaho batholith. This may be the case for most granitoids because the composition of source regions within the crust may vary from basaltic I-type, through intermediate compositions to a typical greywacke S-type source. Moreover a granitoid may be derived from a source composed of both sedimentary and igneous rocks, the characteristics of each blurred by homogenisation of the magmas.

Miller (1985) pointed out that only 2% of granitoids actually had the requisite criteria to be classified as S-type granites and so concluded that whereas peraluminous granitoids are derived from continental crust, they are not necessarily S-type. White and Chappell, (1974) only inferred granitoids to be S-type if they are highly peraluminous, cordierite-bearing and typically contain much metasedimentary restite.

In evaluating the Nd model age of segments of the continental crust, Farmer and DePaolo (1983, 1984) have shown that only strongly peraluminous granitoids were wholly derived from crustal sources, i.e. without the incorporation of significant juvenile mantle material. However, metaluminous granitoids may be derived from mafic continental crustal sources, but also without the addition of a mantle component (Bennett and DePaolo,1987). Thus the degree of alumina saturation cannot be simply linked to the presence or absence of a juvenile mantle component without taking into account other geochemical parameters.

The use of alumina saturation in a classification scheme to interpret the nature of the source region of granitoids is therefore not uncontroversial. Moreover, even the extent to which the degree of alumina saturation of granitoids reflects the alumina saturation of the source regions cannot be answered unambiguously.

Following the highly compelling work of White and Chappell (1974) on S-type and I-type granitoids, high degrees of alumina saturation have been extensively used to imply a sedimentary source for the granitoids. Nonetheless experimental work has shown that peraluminous magmas can be generated during partial melting of a variety of sources. Helz (1976) showed that melting various basaltic compositions at 5kb, within the hornblende stability field, produces granitic liquids that are relatively insensitive to the basalt source composition, even though at higher temperatures (1000°C-1045°C) the TiO_2, FeO and MgO contents of the melt rapidly increase. Furthermore Holloway and Burnham (1972) and Green and Ringwood (1968) found that liquid compositions were always peraluminous when they coexisted with a significant amount of hornblende. In addition, partial melting of ultramafic peridotite at P_{H_2O} = 10kb and T = 1025°C without the presence of hornblende can produce peraluminous melts (Kushiro and Yoder, 1972), as can anatexis of mafic rocks (Stern and Wyllie 1978).

Alternatively fractionation of a mineral assemblage with an alumina poor composition of for example hornblende, pyroxene, epidote or sphene, from a metaluminous melt can drive the evolving liquid composition towards that of a peraluminous granite.

Although experimental data show that high degrees of alumina saturation are not necessarily indicative of a peraluminous source composition, field evidence suggests that large volumes of strongly peraluminous granites unrelated to metaluminous granitoids are derived from peraluminous sources (Chappell and White, 1974). Moreover, melting experiments are carried out at temperatures often greater than that typical of high temperature regional metamorphism and so may not be strictly relevant to crustal anatexis.

Further control on alumina saturation of granitoids by tectonic setting was suggested by Pitcher (1979) and Brown et al. (1984) who noted that peraluminous granites are characteristic of orogenic belts located within ancient continental crust.

Finally a genetic link between high T and low P metamorphism and peraluminous granitoids has been shown by Le Fort (1981) and DePaolo and Farmer (1984), even though both crustal thickening (England and Thompson, 1984), and crustal thinning (Wickham and Oxburgh, 1985) can result in high temperature and low pressure metamorphism.

4.2.2 i) Alumina saturation in the Cretaceous granitoids

The six Cretaceous phases of the Idaho batholith are weakly metaluminous to weakly peraluminous. The tonalite, hornblende-biotite granodiorite and hornblende-bearing porphyritic granodiorite are metaluminous ($0.9 < A/CNK < 1.0$), whereas the biotite granodiorite, muscovite-biotite granite and leucogranite are peraluminous ($1.0 < A/CNK < 1.1$) except for a few samples of leucogranite and leucocratic biotite granodiorite (figure 4.4). However there are several reasons for suggesting that these peraluminous magma types are not necessarily derived from a metasedimentary source:

i) the association of metaluminous with peraluminous granitoids;

ii) the high pressure and high temperature metamorphism;

iii) the presence of magmatic epidote implying high pressure emplacement depths in the metaluminous phases;

iv) the weakly peraluminous nature of the biotite granodiorite, muscovite-biotite granite and leucogranite i.e. A/CNK <1.1;

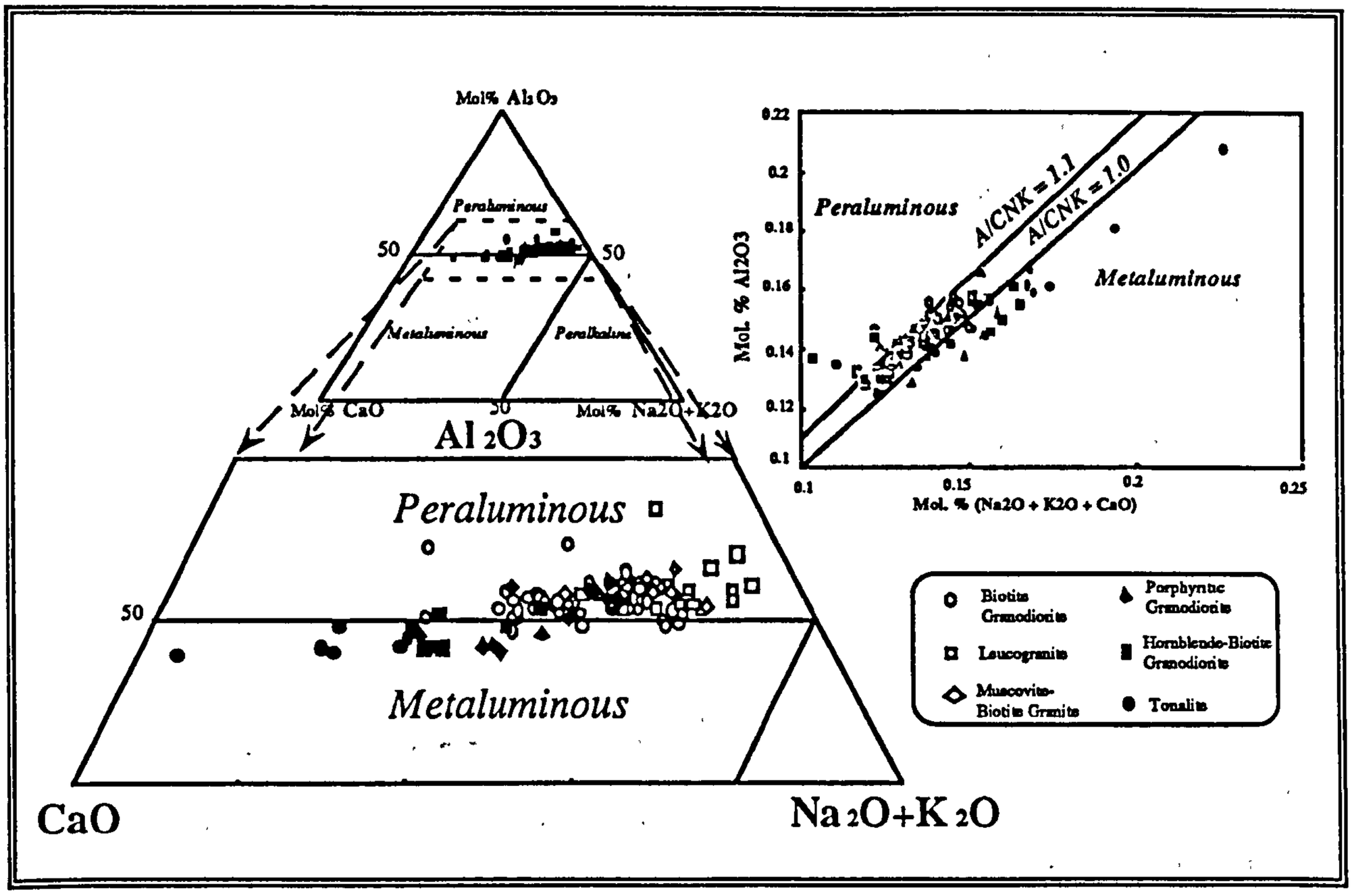

Figure 4.4 Alumina saturation diagrams for the Cretaceous phases: (a) Ternary lime, alumina, alkalis diagram; (b) alumina versus lime + alkalis with lines for the degree of alumina saturation.

Indeed the presence of abundant hornblende, sphene and epidote in the tonalite, hornblende-biotite granodiorite, and porphyritic granodiorite, combined with the slightly younger age and more central position of the peraluminous rock types within the Atlanta lobe, may imply that they were derived from metaluminous parental magmas. Crystal fractionation of a metaluminous assemblage or alternatively partial melting in the presence of hornblende are equally viable processes that could account for the evolution from metaluminous to peraluminous compositions.

The division between metaluminous and peraluminous granitoids correlates with the step to higher Al_2O_3 and to lower K_2O at ≈ 69 wt.% SiO_2 noted on the Harker diagrams (figure 4.2). If the peraluminous magmas are genetically related to the metaluminous magmas the increase in Al_2O_3 and the decrease in K_2O may represent a change in the fractionating crystal assemblage as the evolving magma became too peraluminous in composition for metaluminous mineral phases to crystallize from the magma. A petrographically noted

change which correlates with this inflexion point is the common presence of hornblende (where Ca/Al > than in plagioclase) in the samples with < 69wt.% SiO_2 and the general absence of hornblende in the more silicic rocks.

Alternative explanations for this break in slope on Harker diagrams, and the change from metaluminous to peraluminous compositions, are different source compositions or mineralogies and/or a nongenetic relationship between the metaluminous and peraluminous phases.

4.2.2 ii) Alumina saturation in the Tertiary dioritic and granitic suites

Within the Tertiary bimodal suite there is a distinct difference in alumina saturation between the Tertiary dioritic suite and granitic suite (figure 4.5). The Tertiary dioritic suite trend from strongly to weakly metaluminous compositions (0.8 < A/CNK < 1.0) whereas the Tertiary granites show no real trend and are weakly peraluminous (1.0 < A/CNK < 1.1) (figure 4.5). The basic conclusion that neither group of Tertiary granitoids are derived from mature, peraluminous metasedimentary sources can be made with some confidence because of the weakly peraluminous nature of the granite, the geographic if not genetic association with metaluminous granitoids, and the lack of field evidence for an S-type source.

Although peraluminous granitoids can be derived by fractionation of hornblende or other alumina poor phases from metaluminous magmas there is no evidence to suggest that the Tertiary granite was derived from the Tertiary dioritic suite.

In fact figure 4.5 indicates that although the Tertiary dioritic suite does evolve towards the composition of the Tertiary granite, it is not a colinear trend and might be explained by a change of the controlling mineral phases. Further trace element and isotopic data, in conjunction with the degree of alumina saturation will be used to decide whether both Tertiary granitoid groups ultimately had a common origin.

The Tertiary dioritic suite has many features similar to those of the Cretaceous phases but they tend to be more mafic, more strongly metaluminous and to show little increase in alkalis and LILE with increasing silica.

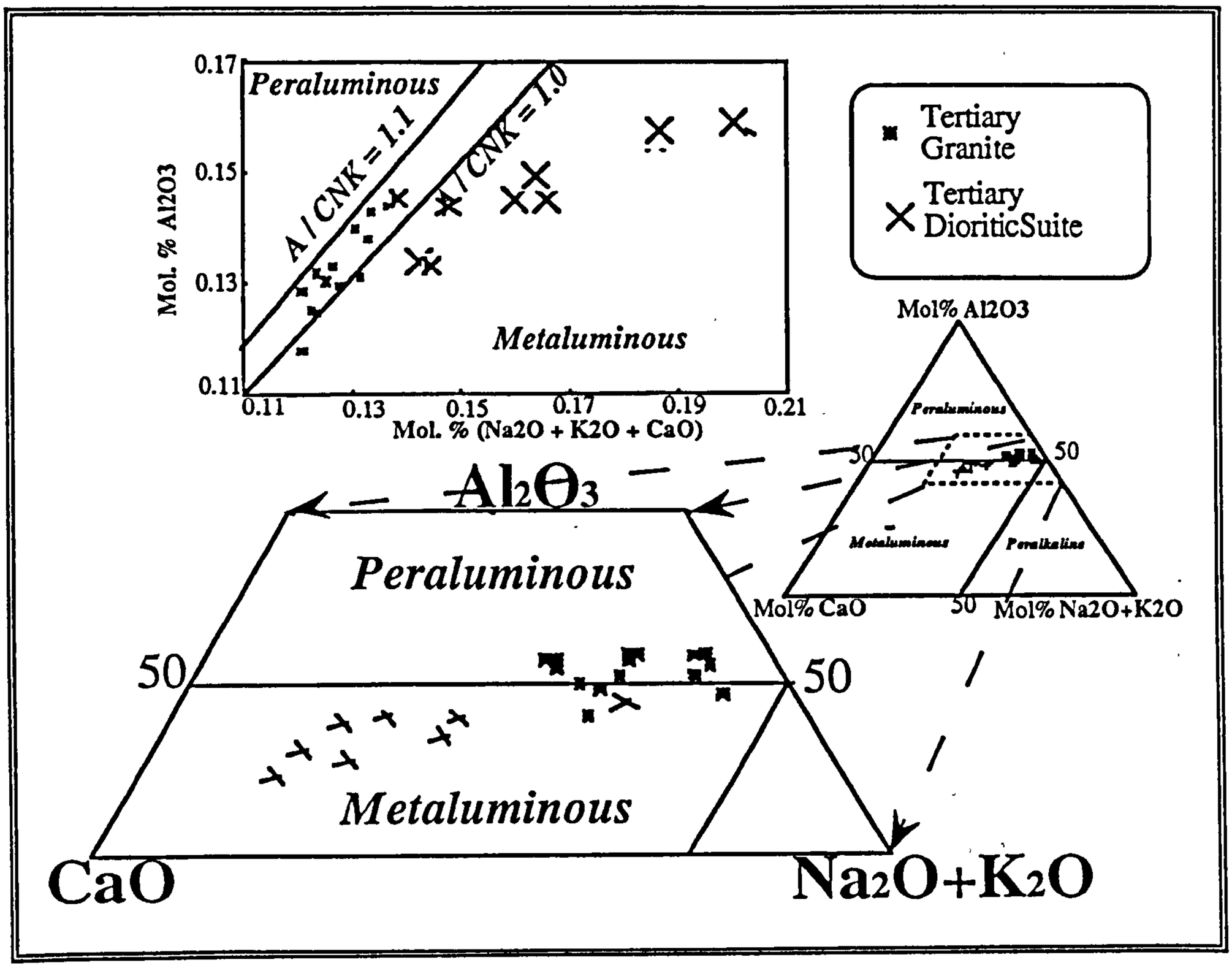

Figure 4.5 Alumina saturation diagrams for the Tertiary bimodal suite: (a) Ternary lime, alumina, alkalis diagram; (b) alumina versus lime + alkalis with lines for the degree of alumina saturation.

In common with the Cretaceous phases the dioritic suite have well defined trends of decreasing CaO, Fe_2O_3, TiO_2 and MgO with increasing silica, but without the maximum in Fe_2O_3, TiO_2 and P_2O_5 demonstrated by the more mafic Cretaceous phases. The variable mineral assemblages noted over small distances, mafic phenocryst phases, zoned plagioclase crystals and high Fe_2O_3, TiO_2 and MgO abundances may suggest that the dioritic suite evolved by fractional crystallization of mafic mineral phases such as clinopyroxene, hornblende and biotite and limited amounts of plagioclase. It is difficult to distinguish melting from fractional crystallization trends by major element modelling of the dioritic suite, but the possibility of AFC processes must be investigated in the light of isotopic data (chapter 5).

The Tertiary granitic suite is distinct from the remaining granitoids of the Atlanta lobe, particularly because of the high abundances of HFSE and LILE which give it a within-plate

character (figure 4.13). They are most easily distinguished from the dioritic suite on the basis of higher initial Sr isotopic ratios, although these overlap with those in the Cretaceous phases (compare figures 4.11 and 4.14). Moreover their higher HREE contents distinguish the Tertiary granites from the other Cretaceous and Tertiary phases of the Idaho batholith, which have particularly depleted Yb concentrations.

Bennett and Knowles (1985) noted, using field relations and limited major element and microprobe analysis, that the Tertiary granitic suite have many of the characteristics of anorogenic (A-type) granites (Collins et al., 1982) and that they may be genetically related to early intra-continental rifting or extension. A-type granite was used initially by Loiselle and Wones (1979) to describe "somewhat alkaline, anorogenic and anhydrous granites". Collins et al. (1982) have described a set of chemical criteria for the anorogenic granites of the Lachland fold belt of southeastern Australia, which were emplaced after the I-type granites of Chappell and White (1974). The chemical and other characteristics of A-type granites in comparison with I-type granites with the same silica content have been described by Collins et al. (1982) and listed below in table 4.3 which also compares the Tertiary granitic suite with the Cretaceous phases of the Idaho batholith.

A-type Granite	Tertiary granite
Higher abundances of large highly charged cations (Nb, Ga, Y and REE).	Higher HFSE, MREE and HREE
Lower Al, Mg and Ca. Al/Ga diagnostic.	Al, Mg, and Ca are lower.
Melts are dry emplaced high in the crust and associated with volcanics.	Epizonal emplacement, few hydrous phases and associated Challis volcanics (rhyolites).
Cl high in peralkaline and F high in metaluminous magmas reduces viscosity.	F high in biotite and fluorite present.
Post dates I-type granitoid magmatism.	Post dates intrusion of Cretaceous granitoids.
Associated with intracontinental extension.	Emplaced into an extensional fault system.
Preferred origin by partial melting a felsic granulite, itself the residue after generation of a previous granitoid from the lower crust.	Partial melting felsic granulite after production of the Cretaceous phases.was suggested by Bennett & Knowles (1985)

Table 4.2 Comparison of A-type granites with I-type granites and a parallel comparison of the Tertiary granitic suite with the Cretaceous phases of the Idaho batholith.

It can be seen that the Tertiary granitic suite has several of the features characteristic of anorogenic granites (table 4.3), (Collins et al.,1982). The granitic suite cannot be generated from the residue after production of the dioritic suite due to differences in Sr isotopic compositions. Bennett & Knowles (1985) suggested partial melting the residue after extraction of the Cretaceous magmas by intrusion of the hot, basaltic to dioritic parental magmas of the dioritic suite as a likely origin for generation of the Tertiary granitic suite. Problems anticipated in trace element modelling partial melting processes (section 4.8) will be generation of the high contents of incompatible elements such as Rb Th and U in the granitic suite from a previously depleted source.

Collins et al. (1982) argued that the residue after production of a near minimum melt from a dioritic lower crust was a felsic granulite and contained the mineral assemblage quartz + plagioclase + alkali feldspar ± clinopyroxene. Any remaining amphibole or biotite would be F rich (Holloway and Ford, 1975 and Munoz and Ludington, 1974). Additional minor residual mineral phases may include apatite, zircon ±sphene ± magnetite.

4.2.3 Comparison with experimental granitic systems

It is instructive to compare some of the experimental data for the granitic system with the granitoids of the Atlanta lobe. There are many problems in comparing natural rock data with experimental results, but an understanding of the possible partial melting or crystallization behaviour of the major mineralogical phases can be obtained, as well as an indication of the conditions under which these processes occurred.

The theory of "metasomatic granitisation" for the origin of granites was dispelled by Tuttle and Bowen's (1958) work on the quaternary system $NaAlSi_3O_8$-$KAlSi_3O_8$-SiO_2-H_2O (alkali feldspar-quartz -water or Q-Or-Ab-H_2O) which showed a direct correspondence between the composition of natural granites and rhyolites, and that at the thermal minimum in the Q-Or-Ab-H_2O system. This indicated that granite magmas can be the products of either partial melting of metasediments or meta-igneous rocks, or of fractional crystallization of basaltic or andesitic magmas.

Figure 4.6a illustrates the position of Tuttle and Bowen's (op. cit.) thermal minimum over a range of pressures (filled circles). At pressures less than 5kb they identified a thermal minimum in the quartz-alkali feldspar cotectic (720°C at P_{H_2O}=1kb) and a thermal valley within the alkali feldspar solid solution field. At higher pressures the latter is replaced by the two feldspar cotectic as the liquidus surface falls and the minimum is below the solvus of the system albite-orthoclase. Thus at pressures greater than 5kb a pseudobinary eutectic point migrates towards the albite end of the albite-orthoclase join (figure 4.6a) and the quartz field expands as P_{H_2O} increases.

In order that the experimental results might be more applicable to natural granites, Von Platen (1965) and Winkler (1974) investigated the addition of anorthite ($CaAl_2Si_2O_8$) to the system. Figure 4.6a also shows the shift in the thermal minimum (open circles) at 2kb (projected from the anorthite apex in the system $CaAl_2Si_2O_8$-$NaAlSi_3O_8$-$KAlSi_3O_8$-SiO_2-H_2O) as the albite/anorthite ratio is varied. Significant migration of the thermal minimum occurs up to albite/anorthite ≈ 8, but this effect must be extrapolated for higher pressures.

Manning (1980) showed that the thermal minimum migrates towards the albite-orthoclase join as the quartz field expands, and the liquidus temperature drops, as a function of increasing fluorine in the system Q-Or-Ab-H_2O at 1kb from 730°C at 0% F to 630°C at 4% F (figure 4.6a). This may be particularly relevant to the epizonal Tertiary granite which have high fluorine content in the micas (Bennett and Knowles, 1985).

There are several problems in comparing natural rock analyses with experimental data that must be borne in mind. Naturally occurring granites are generally not pure liquids, but crystal mushes, and so the measured whole rock compositions may lie on a mixing lines between the compositions of the liquid and that of the crystals. Measured rock compositions are not restricted to four components and CIPW normative calculations rarely yield modal mineralogies.

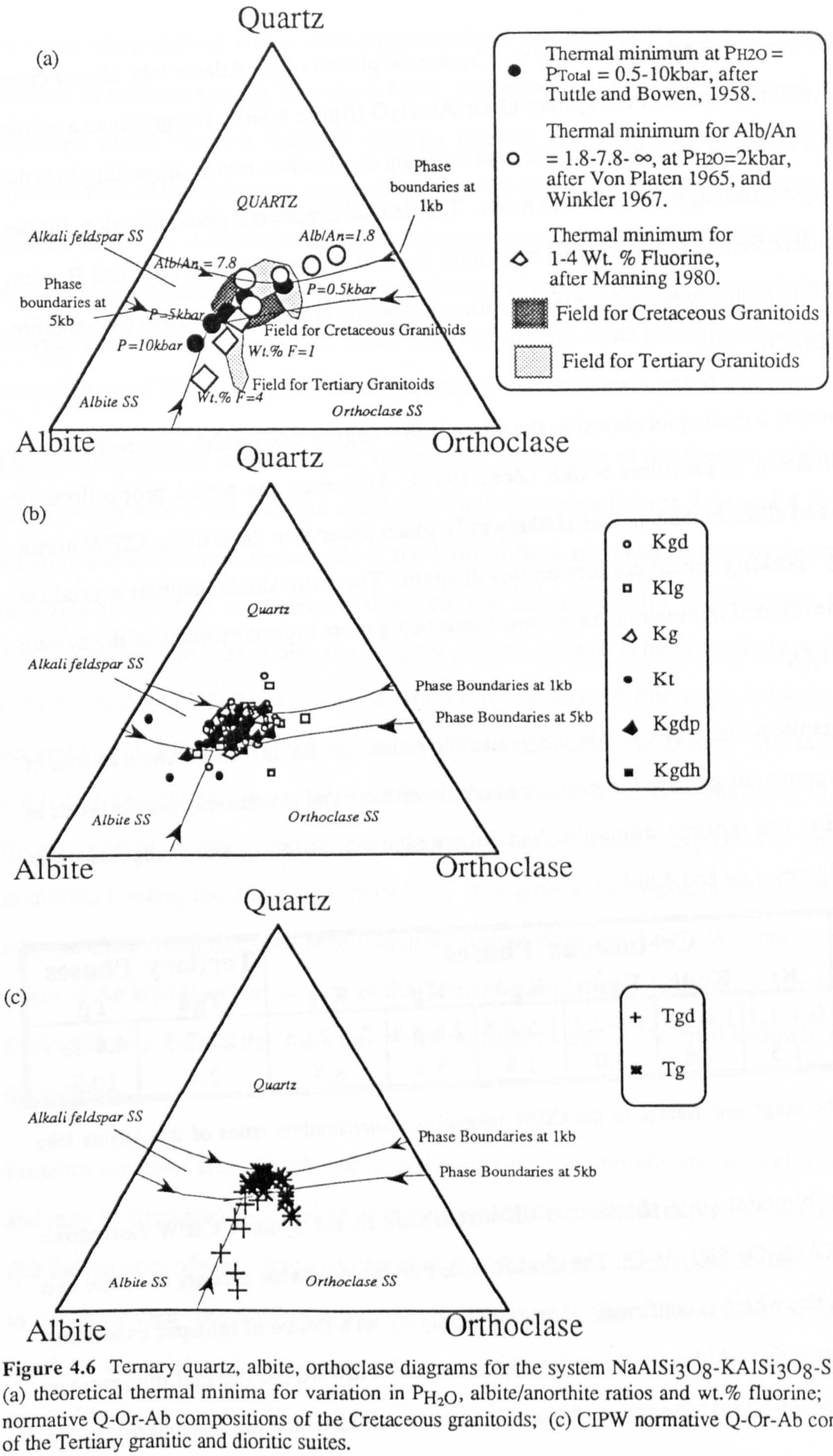

Figure 4.6 Ternary quartz, albite, orthoclase diagrams for the system $NaAlSi_3O_8$-$KAlSi_3O_8$-SiO_2-H_2O: (a) theoretical thermal minima for variation in P_{H_2O}, albite/anorthite ratios and wt.% fluorine; (b) CIPW normative Q-Or-Ab compositions of the Cretaceous granitoids; (c) CIPW normative Q-Or-Ab compositions of the Tertiary granitic and dioritic suites.

The CIPW normative compositions of the Cretaceous phases of the Atlanta lobe cluster close to the thermal minimum in the system Q-Or-Ab-H_2O (figure 4.6b). The group as a whole appear as a clump of data points rather than defining any distinct trend, suggesting that the magmas crystallized as near minimum melts. The field of Cretaceous granitoids plots further into the quartz field than the thermal minimum for mid-crustal depths (Tuttle and Bowen, 1958). This is probably because of the significant anorthite component of these calc-alkaline rocks (table 4.3).

The tonalites as a group plot closest to the albite corner (figure 4.6b) which may be the effect of crystallisation at pressures > 8kb (Zen, 1988). However, the actual proportions of oligoclase and albite in the tonalites is likely to be much lower than those in the CIPW norms and strictly speaking should not plot on this diagram. The more silicic magmas crystallize closer to the thermal minimum melt compositions being more typical magmas of the system Q-Or-Ab-H_2O.

The leucogranite plots further within the quartz and orthoclase fields than the main cluster of Cretaceous granitoids perhaps because it was emplaced later and at relatively higher levels in the crust; i.e. the thermal minimum had migrated towards the quartz-orthoclase join (compare figures 4.6a and 4.6b).

Suite	Cretaceous Phases						Tertiary Phases	
Ab/An	Kt	Kgdh	Kgdp	Kgd	Kg	Klg	Tgd	Tg
Range	0.4-2.7	1.4-2.5	1.4-2.3	1.5-6.5	2.8-8.8	3.4-23.5	1.7-7.5	4.4-23
Average	1.3	1.8	3.0	3.8	5.4	8.5	2.8	10.2

Table 4.3 The range and average of the CIPW normative albite/anorthite ratios of the Atlanta lobe granitoids.

The Tertiary bimodal suite shows two distinct trends in the system CIPW normative $NaAlSi_3O_8$-$KAlSi_3O_8$-SiO_2-H_2O. The dioritic suite trends along what appears to be the two feldspar cotectic, which is confirmed petrographically by an absence of feldspar exsolution textures (figure 4.6c). Although this suite appears to trend toward the thermal minimum at pressures ≈2kb, the low Ab/An ratios (table 4.3) probably indicate that the thermal minimum

for these compositions was shifted significantly to the right in figure 4.6c, and a better estimate of pressure may be between 5-10kb. The trend may either be interpreted as liquid evolution down the two feldspar cotectic towards the pseudoeutectic by fractional crystallization of two feldspars, or increasing degrees of partial melting along the trend in the opposite direction. A third possibility is feldspar accumulation and liquid evolution from an intermediate composition. It is hard without further discussion of other chemical data to pick between the first two possibilities and, moreover, there is some petrographic evidence for accumulation of feldspars by rare cumulate textures and complexly zoned feldspars.

The Tertiary granitic suite samples, in contrast, congregate at the thermal minimum for P_{H_2O}=1-2kb with a tail into the orthoclase field (compare figures 4.6a and 4.6c). This pressure estimate seems reasonable in the light of field and petrographic evidence which indicates an epizonal emplacement depth for the Tertiary granite. Furthermore the high Ab/An ratios (table 4.3) allows the Tertiary granitic suite to behave similarly to the ideal system Qz-Ab-Or-H_2O, so that no migration of the thermal minimum is likely to have occurred away from Tuttle and Bowen's (1958) experimental minimum. The tail into the orthoclase field may be due to accumulation of orthoclase or perhaps less likely to the high fluorine content in some Tertiary granitic suite magmas causing migration of the thermal minimum towards the albite-orthoclase join. The latter effect would usually cause a shift into the albite field not seen here (compare figures 4.6a and 4.6c). A more pronounced effect of the high fluorine contents of the Tertiary granitic suite, is that they may have been derived from dry melts that were able to rise to higher levels in the crust before intersecting the solidus.

Pressure estimates from CIPW norms and non-eutectic granitoids are not well constrained and may be erroneous, but if taken as best estimates, the available experimental data suggest that the majority of the Cretaceous phases of the Idaho batholith crystallized from melts close to minimum melt composition at pressures in the range 5-10kb. The tonalite may reflect the result of a partial melting process at $P_{H_2O} \geq 10$kb, whereas the leucogranite may have crystallized at pressures lower than 5kb. Evolution of the dioritic suite may have been

controlled by cotectic crystallization of two feldspars between 5-10kb, whereas the Tertiary granitic suite crystallized at minimum melt compositions between 1-2kb.

4.3 Petrogenetic processes and the origin of the Idaho batholith granitoids: statement of problem and philosophy

A striking feature of the major element content and variation within granitoid suites, particularly calc-alkaline batholiths, is their similarity. The typical characteristics are low contents of TiO_2, Fe_2O_3, MgO, CaO and P_2O_5 that decrease with increasing silica, K_2O and Na_2O abundances that increase with silica, and somewhat variable contents of alumina that decrease with silica. Moreover, that observation challenges any assumption that smooth and coherent major elements trends within a group of granitoids implies that they reflect the same petrogenetic processes during the same event. A more cautious assumption, that the major element variation is controlled by one or more of a number of igneous processes which often occur within granitoid suites, is more apt. The most regularly cited igneous processes which are used to explain and relate a range of compositions within a granitoid suite are partial melting, fractional crystallization, mixing between restite and minimum melt compositions, magma mixing and assimilation/fractional crystallization (AFC) models. Numerous variations may be applied to the model processes to account for subtle differences in the chemical variation, such as:

i) the choice of fractional crystallization or partial melting model, for example, equilibrium batch melting, Rayleigh crystallization, zone refining etc...;

ii) open system replenishment of magma chambers;

iii) separation of evolved liquids to successive magma chambers;

iv) source region heterogeneities.

It is apparent then that several models can be forced to fit the data by making favourable assumptions about the more poorly constrained parameters and thus modelling, especially of major elements, is only selective between extreme cases. Nonetheless a central theme in the discussion of the origin of the Atlanta lobe granitoids is to use geochemical data to interpret which process or processes were responsible for the chemical variation of the magmas. A

crucial factor related to the above is whether the different Cretaceous magma types recognised in the field are related to one another - perhaps by variable degrees of partial melting of a common source or by fractional crystallization from a common parental liquid.

The only way to determine which petrogenetic processes are more likely to account for the origin of the Idaho batholith magmas is by the combined examination of the field relations, the petrography, the trace element characteristics and the isotopic signatures. Combined modelling of the major and trace element and isotopic variation can only then be used to evaluate whether the favoured process, indicated by primary observation, can generate the observed features of the Atlanta lobe granitoids.

4.4 Identification of petrogenetic processes using field and petrographic evidence

The petrographic, geochronological and field evidence, in the form of diffuse boundaries, cumulate textures, the order of intrusion, the area of outcrop of individual magma types, the metamorphic grade of the country rocks and the proportion of mafic to felsic rock types may all constrain the likely petrogenetic models. It has already been suggested that "the Cretaceous phases are probably genetically related and classified as a comagmatic suite" (chapter 3), and other crucial pointers are as follows.

Xenoliths of meta-igneous or metasedimentary origin within granitoids are often used to imply the nature of the source, but they may also represent material incorporated into the magma during ascent, or emplacement, indicating the possibility of contamination. There is a distinct lack of xenoliths which might be representative of country rocks at the present level of exposure, either wholly or partly digested. Thus there is no *a priori* evidence for significant assimilation of country rocks. This suggests that crustal contamination of magmas by mid- to upper crustal metasediments or orthogneisses is minimal.

Migmatite terranes have been interpreted as the frozen partial melting textures that develop in a source region during generation of granitoid magmas by crustal melting. If a genetic link between the granitoids and the migmatites can be established the source composition of the granitoids can be inferred. There are no migmatites exposed in association with any of the Cretaceous phases of the Atlanta lobe, except with the tonalites near the western border. This may indicate that at least the more evolved magmas were separated from their source regions, and that at deeper levels of exposure some of the primary tonalitic liquids may still be in contact with their source rocks. However there are a number of problems with this interpretation:

i) the migmatites are very localised and on a scale too small to account for the batholithic volumes of magma;

ii) the isotopic composition of the possible source rocks at this level of exposure (para- and orthogneisses) are significantly different from the tonalites, which disproves a genetic link and precludes them as the source of the tonalites (Fleck and Criss,1985);

iii) very limited field examination of the migmatites in this study shows that partial melts in veins and blebs associated with the country rocks are of a highly silicic nature, of small volumes and thus do not resemble the tonalites, but are more similar to the leucogranites.

The preferred interpretation for the generation of the migmatites is that limited upper crustal melting occurred during the emplacement of the batholith. The interaction of hot tonalitic melts (1000°C-1100°C) with the country rocks is only observed on the borders of the batholith, but it could offer a preliminary explanation for the origin of the leucogranites which have an extremely wide range of major element, trace element and isotopic compositions.

Cumulate textures are rarely observed in coarse grained silicic plutonic rocks because they are notoriously difficult to identify, and because they are probably only rarely formed. The simultaneous crystallization of the dominant modal mineral phases from a granitoid magma with a composition close to the minimum melt composition results in early and late mineral phases of only slightly different compositions. Moreover, even in more mafic granitoid

magmas the physical separation of cumulate phases is likely to be a very sluggish and inefficient process due to the high viscosity of granitoid magmas. There is, however, no textural evidence of accumulation in the granitoids of the Atlanta lobe such as high melting point phases surrounded by near minimum melt compositions. Petrographic studies show that certain minerals are nucleated earlier than others, but there is simultaneous crystallization of most phases and no apparent separation of such phases. Therefore the restite plus minimum melt model and within suite fractional crystallization (where the least and most evolved samples of a suite represent the cumulates and evolved liquid respectively) are not thought to have been the dominant processes in the evolution of the Atlanta lobe magmas.

Large volumes of near homogeneous magmas represented by the extensive tracts of single rock types suggests that these may be individual batches of partial melt that have separated from their source, been emplaced in the crust coevally, and subsequently undergone only minor modification from the initial liquid composition. The large volume of the proposed magma bodies precludes the possibility that they represent some form of zoned magma chamber, or set of magma chambers, because of the physical problems in the homogeneous separation of early crystallized phases and evolved viscous melts over large distances.

The gradational boundaries between some of the Cretaceous rock types might indicate that one magma type evolved from the other by some form of crystal differentiation over the large distances implied by the size of the plutons and thus ultimately have the same parental magma. However an alternative explanation may simply be that the magmas were emplaced almost coevally, and specifically that the later magma was emplaced before the first crystallized.

Larsen (1948), used simple mixing calculations to demonstrated that a tonalite can yield ~50% of its mass as a leucocratic granodiorite by crystallization of a plagioclase and hornblende dominated assemblage. The volume of tonalitic magma interpreted to have existed from the present area of exposure of tonalite in the Atlanta lobe suggests that it was a minor magma type in contrast to the very much more voluminous biotite granodiorite and muscovite-biotite granite. In the simplest case there would, therefore, have been insufficient

tonalitic magma from which to generate the more silicic magmas, suggesting that the magma types were not simply related by fractional crystallization.

In opposition to this Hyndman (1988) suggested that numerous, syn-plutonic mafic dykes and the presence of tonalites at the deepest levels of exposure (25-30km) indicates that a larger proportion of of mafic rock types are present at deeper levels within the batholith. From an interpreted cross-section of the Bitteroot lobe, Hyndman (1988) estimated a ratio of mafic to silicic rock types at 52% : 48%. This represents sufficient volumes of more mafic parental magma from which the rest of the magma types may be derived.

Petrographic and field evidence, though equivocal, on balance indicates that the magma types are probably near liquid compositions reflecting partial melting processes with only minor modification by fractional crystallization.

4.5 Trace element variation

4.5.1 Introduction : the application of trace elements to the petrogenesis of granitoid systems.

Before characterising the trace element variations within the Atlanta lobe granitoids it is worth noting the difficulties in interpretation of trace elements in silicic liquids. As previously noted for the major elements, trace element variations are often the response to several superimposed petrogenetic processes, including the effects of partial melting in heterogeneous source regions, mobility in fluids and fractional crystallization. However, they are also particularly sensitive to the distribution of minor and accessory phases.

A large proportion of the trace element budget of a granitoid magma is hosted by minor and accessory phases, but fractionation such phases may be limited for reasons discussed below and so be of less importance than the concentration of trace elements imply. Mineral phases such as allanite, zircon, sphene and apatite and less dramatically hornblende and biotite can have the dominant control over LREE, Hf, Zr, Th, U, and Ta. For instance REE crystal/liquid partition coefficients for allanite are two orders of magnitude greater than those of sphene and apatite which, in turn, are at least an order of magnitude higher than those of

hornblende -the latter being the only common major mineral phase that hosts significant quantaties of REE in granitoids (Gromet and Silver, 1983).

The effect on the composition of partial melts, as a result of the presence of accessory phases during crustal melting is dependent on the solubility of accessory phases, the diffusivities of chemical species in accessory phases and the partition coefficients of the trace elements between the crystal and liquid (Watson and Harrison, 1984). For example, at a given temperature zircon is more soluble in magmas of intermediate composition than in more felsic or mafic magmas; apatite is insoluble during crustal melting (Watson and Harrison, 1984); and the partition coefficients of REE in sphene and allanite are higher in more silicic liquids (Gromet and Silver, 1983). Only by painstaking examination and much microprobe analysis of minor phases in granitoids, can the distribution of trace elements in accessory phases be gauged, and their effect on the fractionation of trace elements be interpreted. In this study, however only the occurrence and proportions of accessory phases have been noted for the simple reason that accessory phases may not cause significant alterations in trace element distribution patterns as granitic magmas evolve. Even though many trace elements are hosted by accessory phases, crystal/melt separation is sluggish in viscous magmas (Rice, 1981) and minor phases may only be able to be removed from liquids within larger host minerals (Miller and Mittlefehldt, 1982). Thus during partial melting, insoluble minor phases can be incorporated into melts with no significant source/liquid fractionation of the trace elements hosted by the accessory phases, so modelling with Kd`s will only be successful for major phases.

In highly silicic magmas the melt composition has the overriding control on trace element partition coefficients as opposed to the pressure and temperature conditions (Watson, 1979). The "liquid structure" of high viscosity silicic melts requires that trace elements find suitable sites, rather than reside anywhere within the melt and thus the trace element partition coefficients are different than those for unstructured liquids. Moreover, polymerisation and variable concentrations of complexing ligands causes partition coefficients to be high and have wide ranges (Mahood and Hildreth,1981).

Volatile components can also have a pivotal control on the behaviour of trace elements in granitoid magmas. However the effect of F and Cl in concentrating alkalis and LREE, and CO_2 rich fluids concentrating HREE are commonly noted in alkaline and peralkaline magmas,but will control partition coefficients in any melt (Flynn and Burnham, 1978).

4.5.2 Trace element variation diagrams

4.5.2 i) The Cretaceous phases

Trace element diagrams are plotted for Ba, Sr, Th, Nb, Y, Yb, Pb, Ce and La against silica as the index of differentiation in figure 4.7. All analyses are by X-ray wavelength dispersive techniques and they were carried out on the same sample set as the major element analyses. The exception are the Yb analyses which are for the subset analysed by INAA only.

Unlike the major element variations smooth and competent trends are rarely observed for the trace elements which exhibit much more scatter, but each phase clusters in overlapping groups with the adjacent phases. The large ion lithophile elements (LILE) Ba, Th and U (not shown) exhibit some extreme scatter which may be a result of their susceptibility to become mobile in late stage fluids. Distinct features noted in the major element trends seem to be coincident with those for Rb and Sr, which show the least scatter of the trace elements.

i) the tonalites form a discrete group which tend, particularly at low silica values, to exhibit a trend which is inclined relative to those for the other magma types (figures 4.7 and 4.2);

ii) distinct inflexions at 69 wt.% SiO_2 and 72 wt. % SiO_2 in the trends occur;

iii) the leucogranites exhibit high and variable trace element compositions;

The trace elements can be split into two groups depending on whether they exhibit similar trends to either Sr or Rb. Pb and Th can be grouped with Rb and behave incompatibly, increasing in abundance with increasing SiO_2. The inflexion points give the incompatible trace elements a "Z" shaped pattern with abundances slowly increasing through the tonalites, a drop in concentration at 69 wt.% SiO_2 before increasing in concentration from 72 wt. % SiO_2.

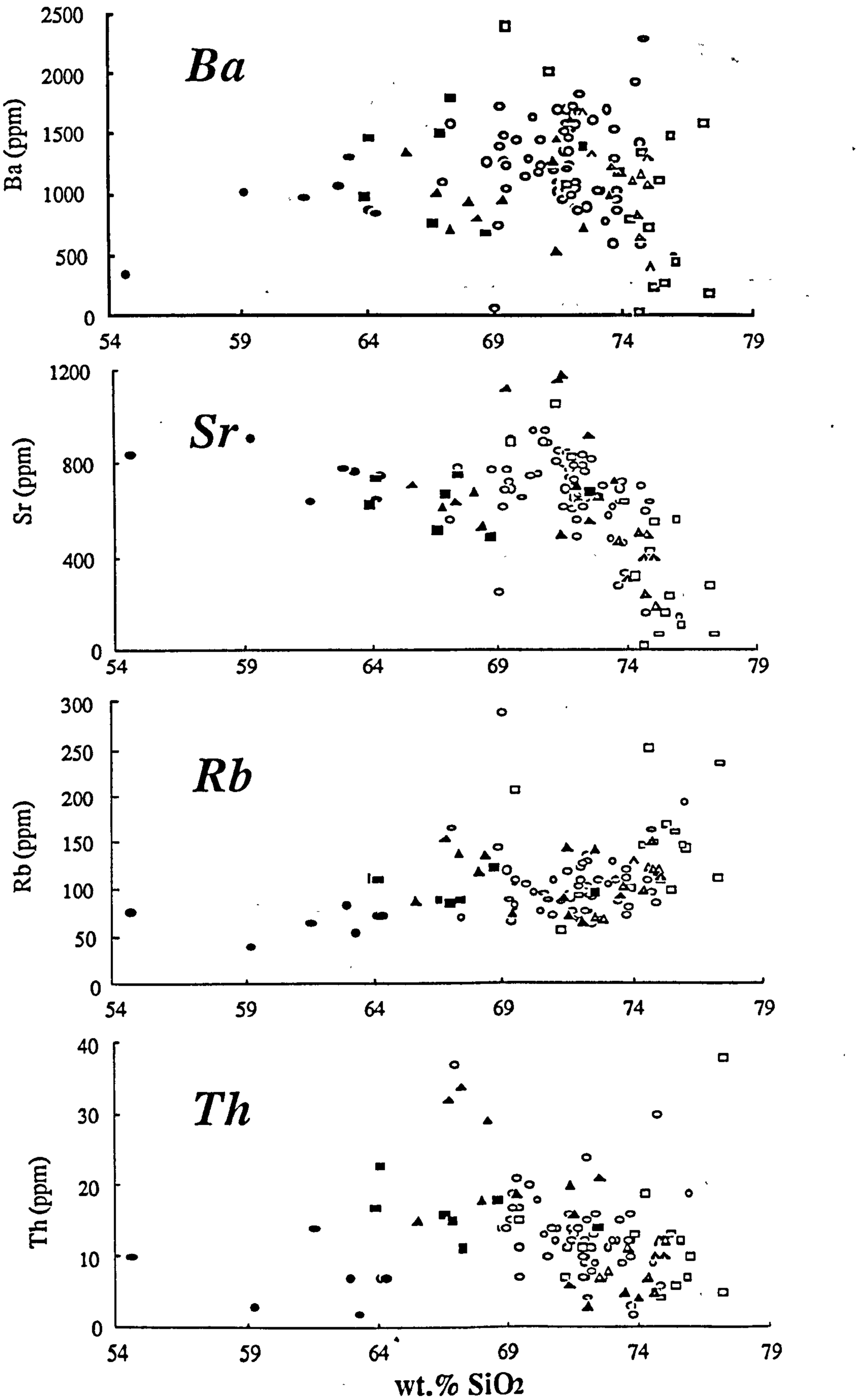

Figure 4.7 Trace element variation diagrams for the six Cretaceous rock types of the Atlanta lobe of the Idaho batholith.

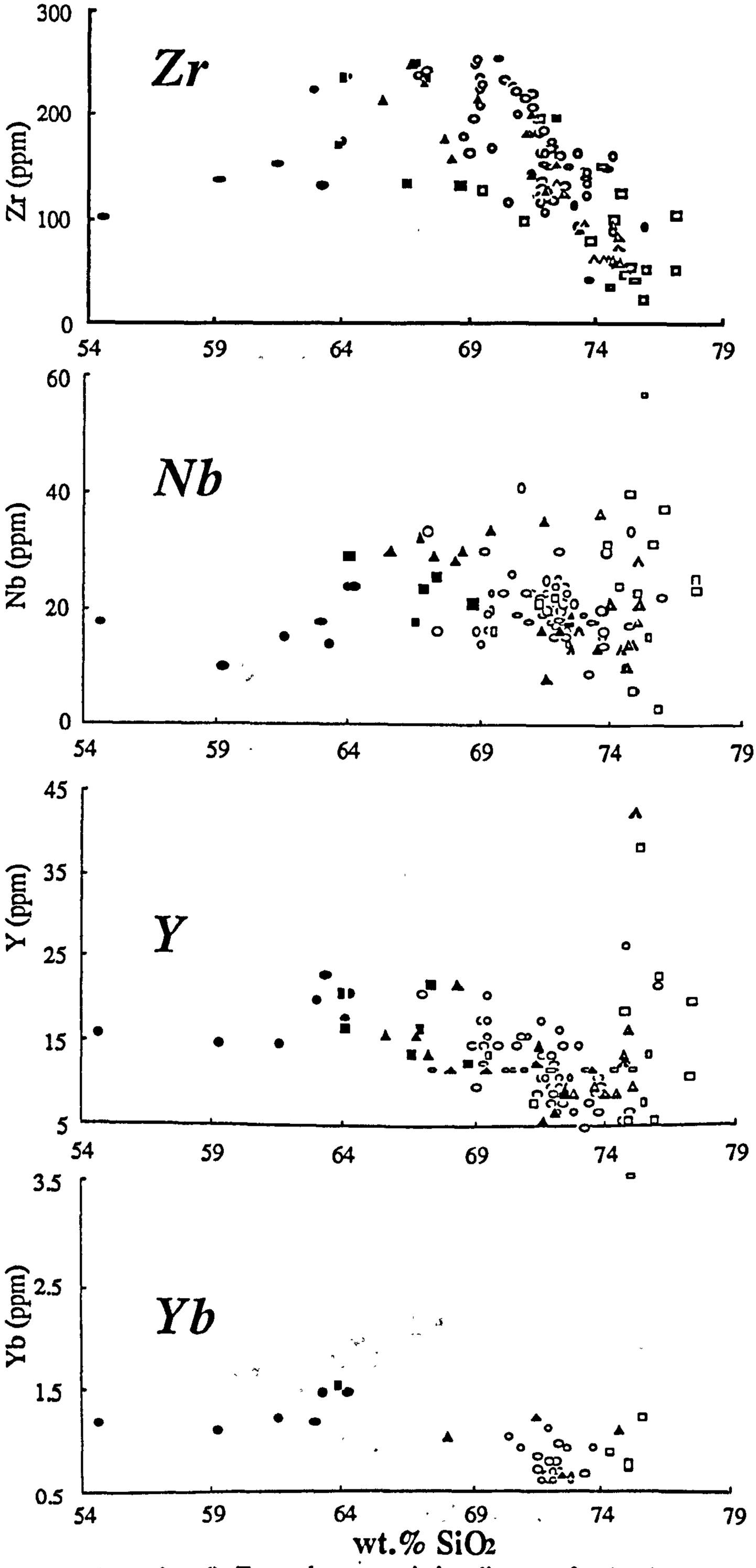

Figure 4.7 (continued) Trace element variation diagrams for the six Cretaceous rock types of the Atlanta lobe of the Idaho batholith.

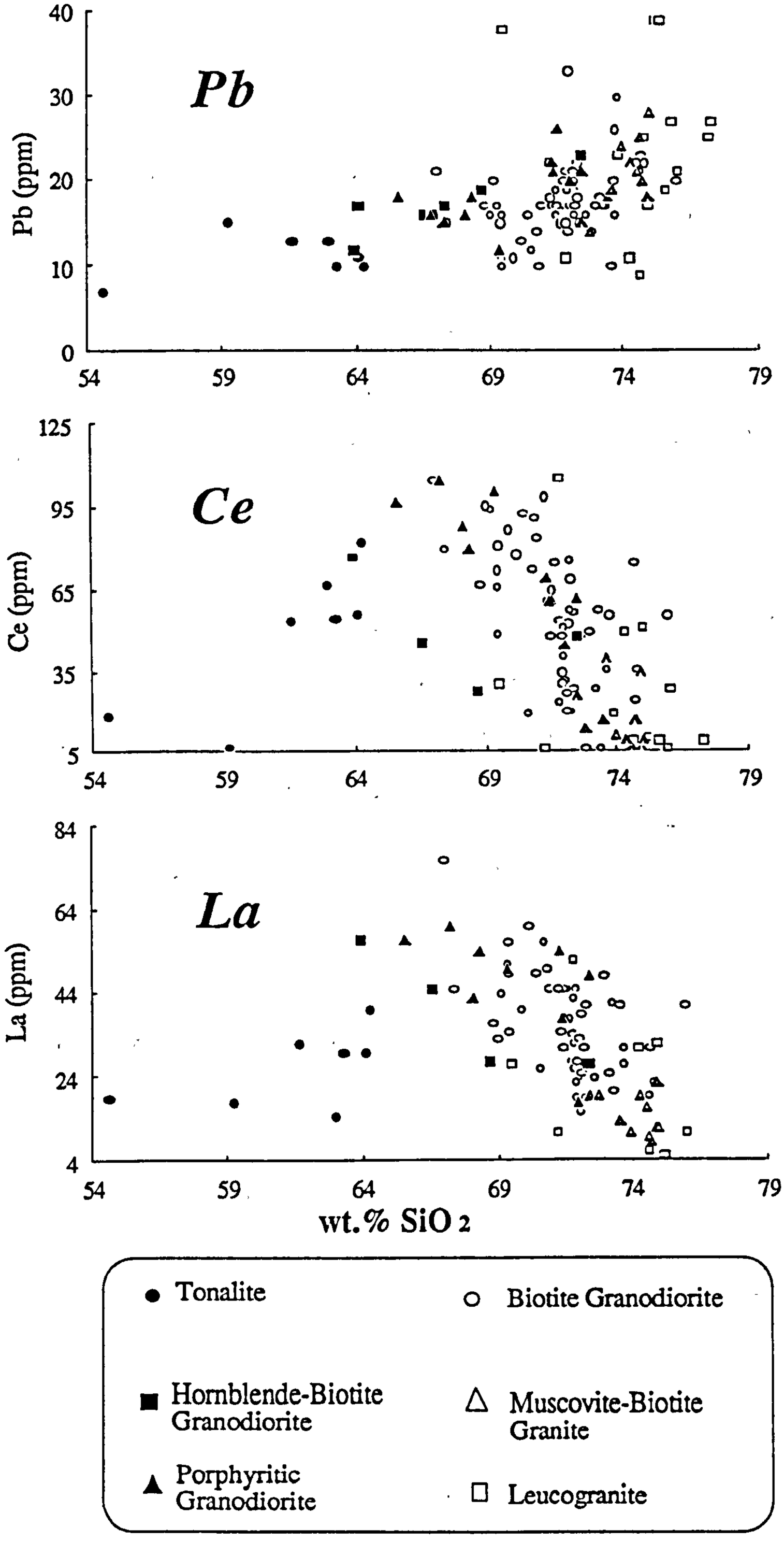

Figure 4.7 (continued) Trace element variation diagrams for the six Cretaceous rock types of the Atlanta lobe of the Idaho batholith.

The second group of trace elements Ba, Zr, Nb, Y, Yb, La and Ce though often defining very poor trends tend to behave compatibly like Sr, generally decreasing in concentration with increasing silica abundance with "S" shaped patterns as a result of the inflexion points. Sr illustrates this well with high values in the tonalite at 59-60 wt. % SiO_2, low values until 69 wt.% SiO_2 where a sharp increase in Sr abundance occurs followed by decreasing concentrations higher SiO_2. Ba has a similar yet more poorly defined trend than Sr whereas Zr, Nb, Y, Yb, La and Ce increase in the tonalites but otherwise behave similarly to Sr. The leucogranites exhibit increased concentrations of Y, Nb and Zr -the high field strength elements (HFSE) and the REE.

4.5.2 ii) The Tertiary bimodal suite

Trace element variation diagrams for the Tertiary dioritic and granitic suites are presented in figure 4.8. Each Tertiary suite exhibits distinct trace element variations and are described separately here. Ba, Sr, Zr, Rb, Th, U, Pb, Nb, Y and Ce data are X-ray wavelength dispersive analyses whereas Ta and Yb have been analysed by INAA.

The dioritic suite show little variation in abundance of Rb, Nb, Y, Yb, Pb and Ta with increasing silica, but Th and U increase slowly with increasing silica on very scattered trends. In contrast Ba and Sr behave compatibly, decreasing in concentration with increasing silica values along well defined arrays. Zr and Ce are also weakly compatible, falling in abundance with increasing silica. Only poorly defined trace element trends are noted amongst the granitic suite samples. Rb, Th, U, and Pb all show a large amount of scatter, but appear to increase in concentration with increasing silica. Nb, Y and Yb have high concentrations in the most silica rich rocks whereas Ba, Sr and Zr are compatible decreasing in concentration with increasing silica abundance.

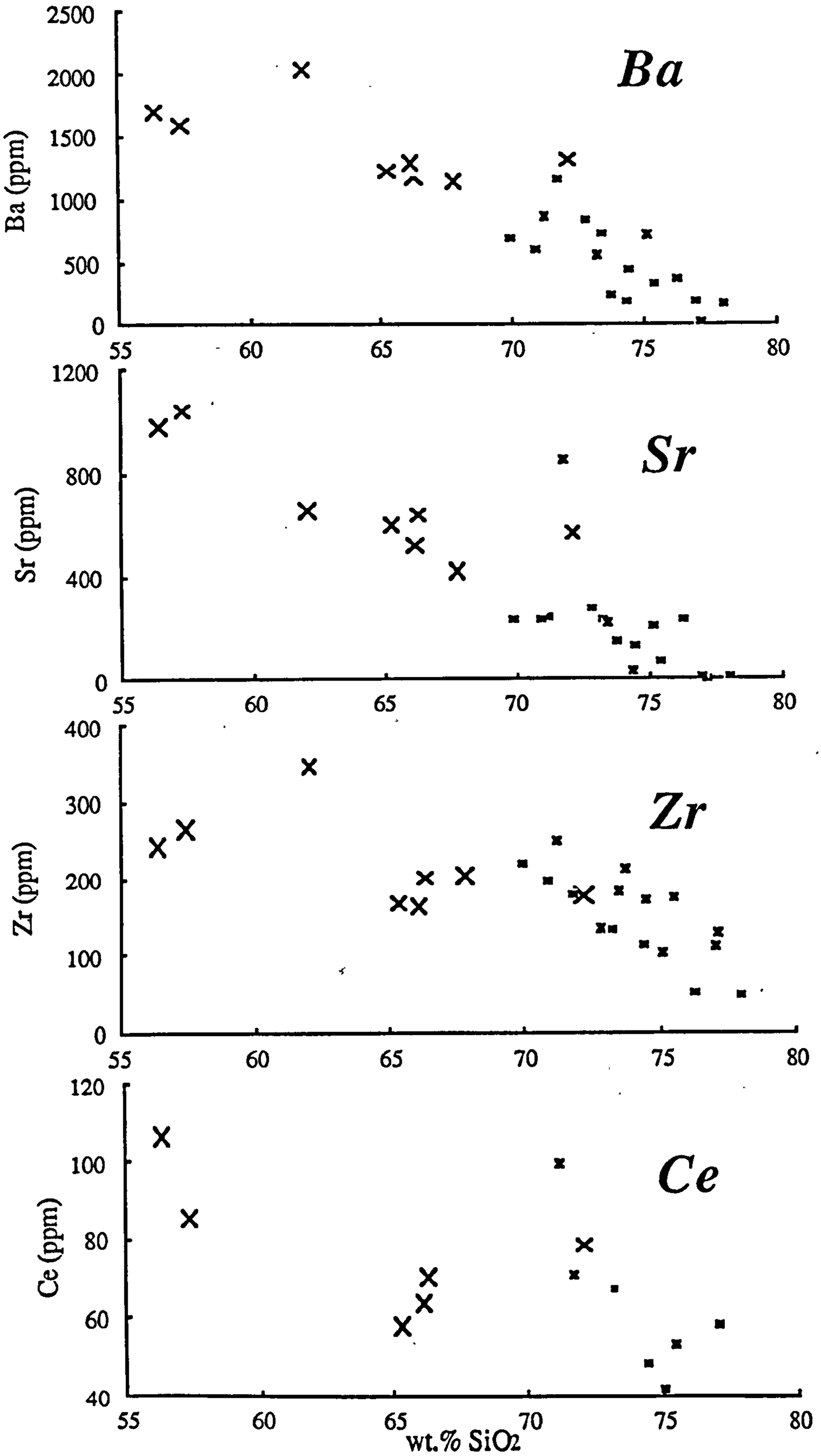

Figure 4.8 Trace element Harker variation diagrams for the Tertiary bimodal suite. x-dioritic suite, *-granitic suite.

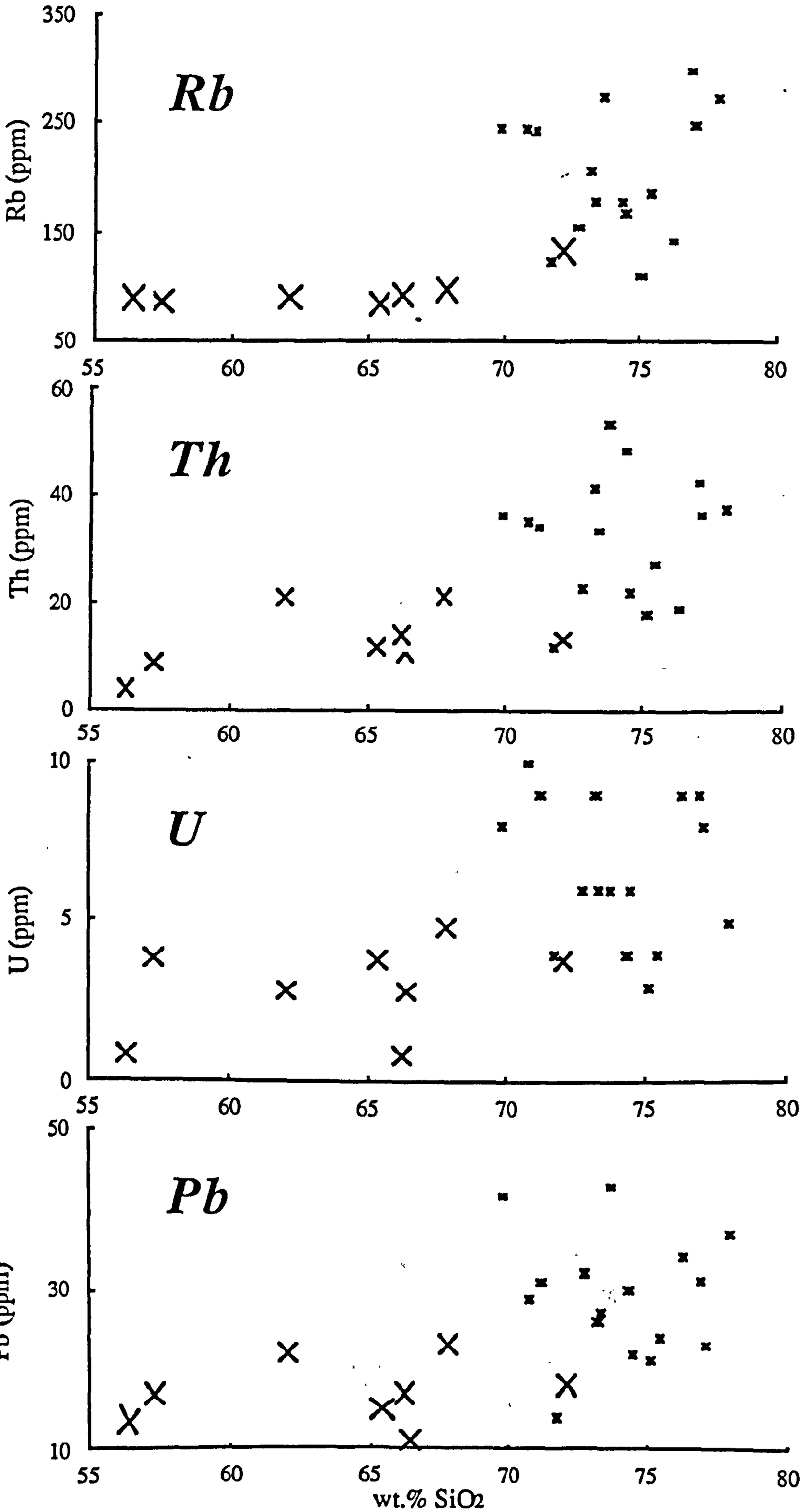

Figure 4.8(cont) Trace element Harker variation diagrams for the Tertiary bimodal suite.

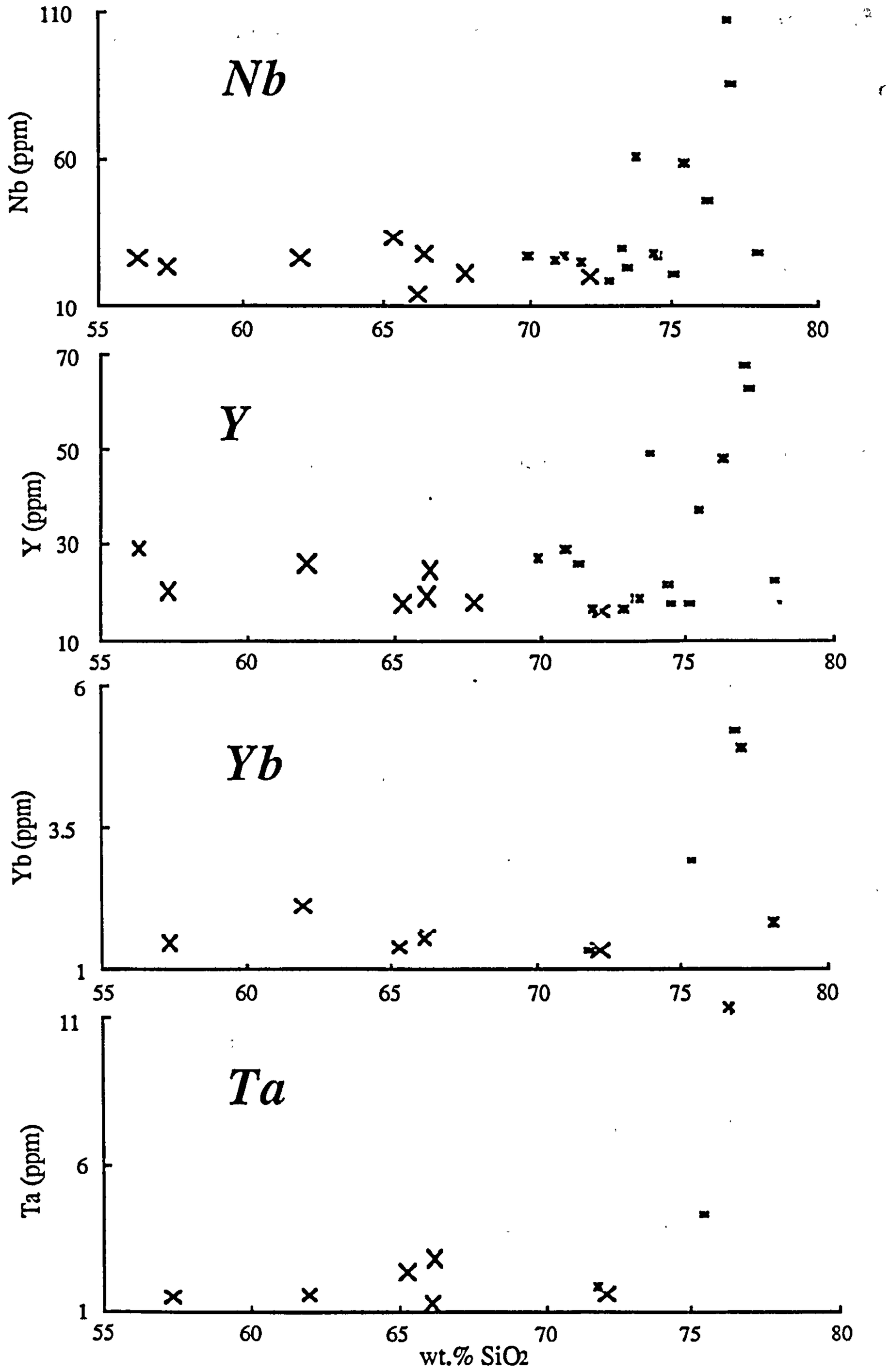

Figure 4.8(cont) Trace element Harker variation diagrams for the Tertiary bimodal suite. x-dioritic suite, *-granitic suite.

4.5.3 Trace element characterisation of the Atlanta lobe granitoids

Discriminant type diagrams are used to illustrate trace element and some limited Sr isotope data for each of the Cretaceous and Tertiary rock types in an attempt to group or separate the phases that have evolved by common petrogenetic processes.

4.5.3 i) The Cretaceous phases

Trace element distribution patterns are presented for an average analysis of all six Cretaceous phases of the Atlanta lobe in figure 4.9. Abundances are normalised to a hypothetical ocean ridge granite (HORG) generated by assuming 75% fractional crystallization of a mid-ocean ridge basaltic magma (Pearce, 1984).

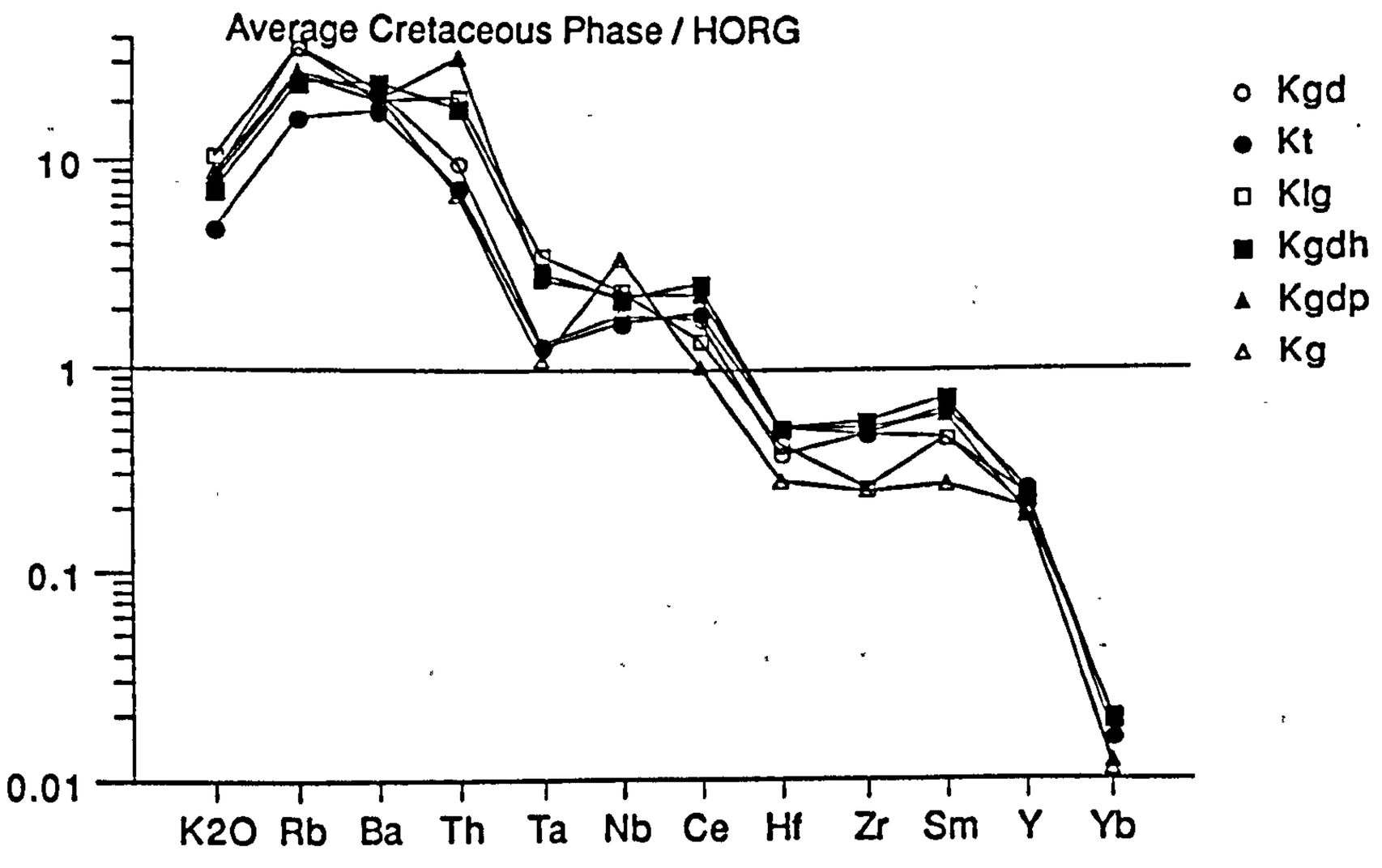

Figure 4.9 Hypothetical ocean ridge granite normalised trace element abundance "spider" diagrams for an average of each of the six Cretaceous phases of the Atlanta lobe.

The most striking feature of this diagram are the similarities of the trace element variations between the six Cretaceous phases showing enrichment in K, Rb, Ba and Th relative to Ta, Nb, Hf, Zr, Y, and Yb and the especially low values of Y and Yb relative to the normalising composition. The shape of the patterns most closely resembles those for volcanic island arc granites of Pearce et al. (1984), differing from syn-collision granites in having lower Rb

contents and higher abundances of Ce, Zr, Hf and Sm. This would appear to fit with the subduction-related tectonic setting postulated in the literature for the Late Cretaceous in the Idaho batholith region although the degree to which the tectonic setting or source region characteristics may determine the composition of crustally-derived granitoids is controversial.

Differences between the trace element variations in the different Cretaceous rock types are more a function of absolute abundance than differences in shape of the normalised patterns (figure 4.9), as indicated by their similar trace element ratios. There are nonetheless some features which are unique to individual rock types worth commenting upon. All rock types except the tonalites and hornblende-biotite granodiorites have lower Ba relative to Rb contents suggesting that biotite or alkali feldspar may have reduced Ba relative to Rb in the more evolved rocks. Only in the porphyritic granodiorite is Th enriched relative to Ba although data are limited for this group.

Systematic differences in trace element abundances and their ratios in 600 granitoid analysis taken from "known" tectonic environments were used by Pearce et al. (1984) in a series of discrimination diagrams in an attempt to attribute granitoids to one of four generalised tectonic settings. The classification scheme worked well for less common granitoid types such as ocean ridge and within-plate granites, but volcanic arc granites and syn-collision granites are indistinguishable unless the latter have exceptionally high Rb contents, and post-tectonic granites fall into almost any field.

The inferred subduction-related tectonic setting is most clearly shown on Rb versus Nb+Y discrimination diagrams (Pearce et al., 1984) where most Cretaceous phases fall within the volcanic arc granite field (VAG) (figure 4.10). The muscovite-biotite granites have high Nb contents whereas the leucogranites have high Rb and Nb+Y abundances which makes it the only magma type to plot in the within-plate granite field.

Although qualitative parallels in trace element variations can be drawn between various volcanic arc granites and the Idaho batholith there is no *a priori* reason why there should be a

strong link between the chemical and isotopic composition of silicic magmas and their tectonic setting. A silicic magma will form if a pre-existing volume of rock of suitable composition is subjected to the appropriate P-T-X_{H_2O} conditions at which melting may occur. Vastly different quantities of magma with a wide range of different compositions may be generated in the region being melted depending on how refractory the mineral assemblage was, the P-T-X_{H_2O} conditions and the average composition. Such discrimination diagrams are more likely to indicate the tectonic setting in which the source rocks of the granitoids were initially generated if subsequent reprocessing was minimal. Although, powerful constraints are placed on the likely tectonic setting in which the Idaho batholith was formed, by structural, stratigraphic and palaeomagnetic studies which all suggest a subduction-related continental margin magmatic arc, it is also likely that the pre-batholithic mid- to lower crust was generated within a subduction related environment during the Proterozoic.

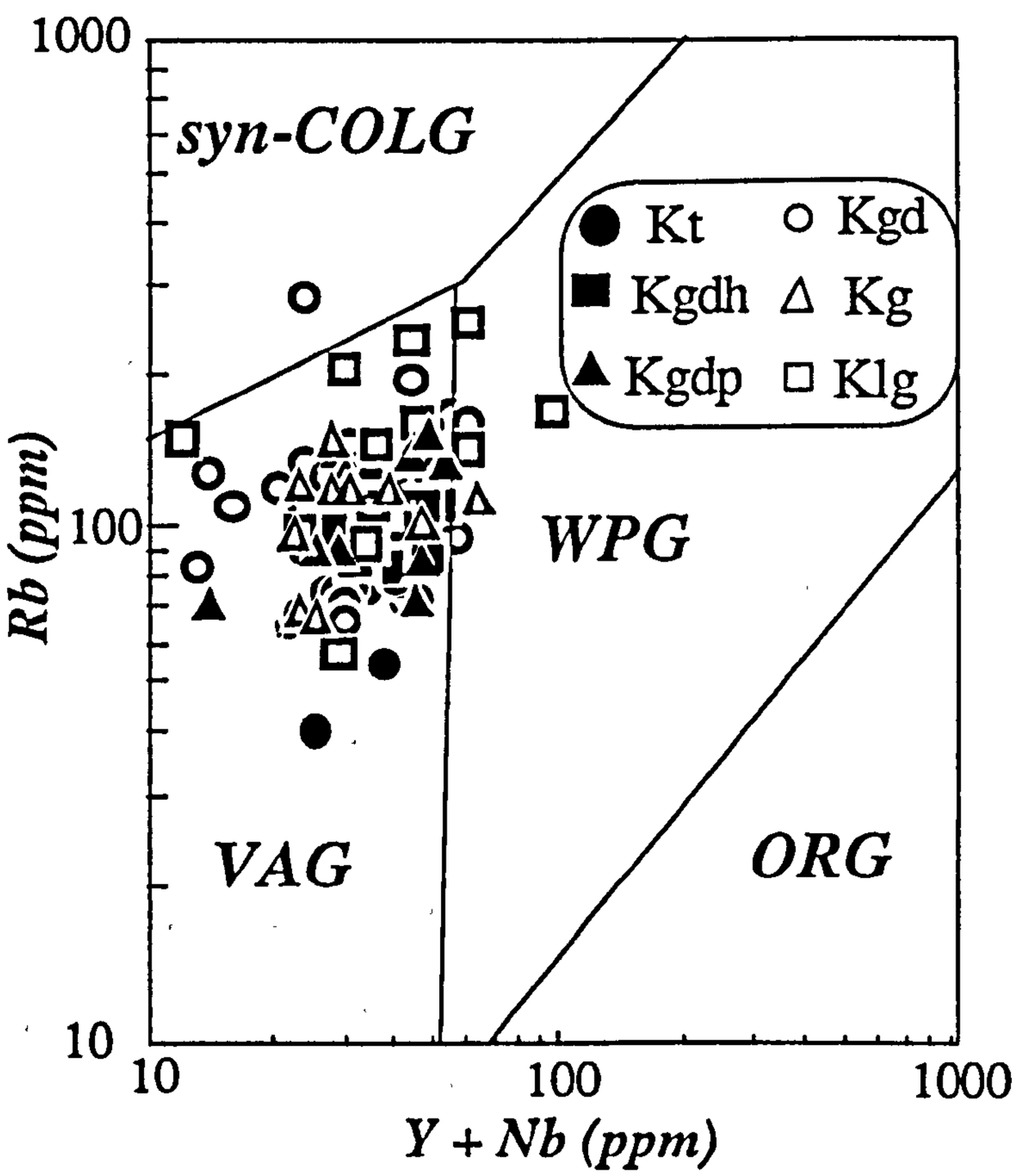

Figure 4.10 Granitoid tectonic discrimination diagram (Pearce et al., 1984) for the Cretaceous phases.

The range in Rb/Sr as a function of silica content has as much variation within each Cretaceous phase as across the whole suite (figure 4.11). The muscovite-biotite granite and leucogranite have much higher and more variable Rb/Sr ratios for a number of samples than the bulk of the Cretaceous phases. Small changes in wt. % SiO_2 can correlate with large variations in trace element concentration in well structured highly silicic liquids and it may be that these extremely high Rb/Sr ratios are merely a result of continued evolution of the whole Cretaceous suite by the same fractional crystallization or partial melting process, but this will be tested by modelling in section 4.8. The possibility of contamination of the muscovite-biotite granite by upper crustal partial melts and the previously suggested origin for the leucogranite by upper crustal melting must be examined isotopically. The possibility of heterogeneous source regions must also be taken into account.

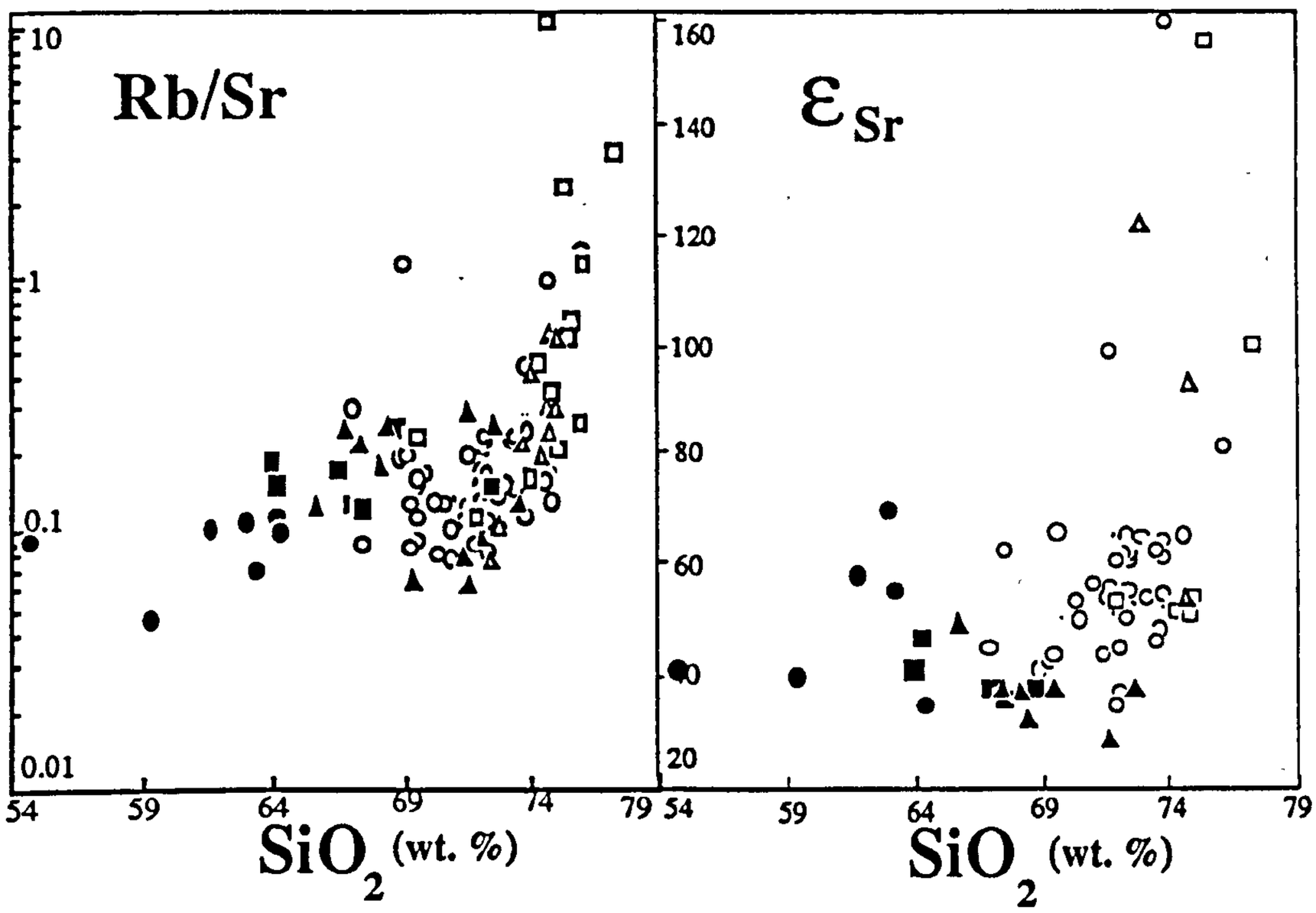

Figure 4.11 Rb/Sr (ppm) versus SiO_2 wt. % and ε_{Sr} versus SiO_2 wt. % for the Cretaceous phases. See figure 4.10 for legend.

Figure 4.11 shows ε_{Sr} plotted against silica. The majority of data have ε_{Sr} in the range 25-70 and exhibit no correlation with silica which rules out progressive contamination or mixing of components with different ε_{Sr} and silica contents to account for the variation. Several leucogranite muscovite-biotite granite and biotite granodiorite samples have ε_{Sr} in the range

80-160 which are also the rocks with the highest Rb/Sr ratios. This restates the possibility that these rocks either underwent limited contamination or they were generated by upper crustal melting.

In summary the major element, trace element and isotopic signatures of the Cretaceous phases of the Atlanta lobe are equivocal in deciding whether the chemical variations are due to variable degrees of partial melting or fractional crystallization processes. A limited number of samples may have incorporated some upper crustal components by melting and contamination. Major and trace element variation diagrams are most successful in identifying changes in the petrogenetic evolution of the Cretaceous magma types and it will only be by modelling these variations that identification of the petrogenetic processes will be made.

4.5.3 ii) The Tertiary dioritic and granitic suites

Both suites of Tertiary granitoids show enrichments in the LILE (K_2O, Rb, Ba, and Th), the HFSE (Nb and Ta) and the LREE (Ce) relative to a hypothetical ocean ridge granite, as are typical of granitoids from most continental settings (figure 4.12). However the variations within the two Tertiary granitoids suites are clearly different from one another.

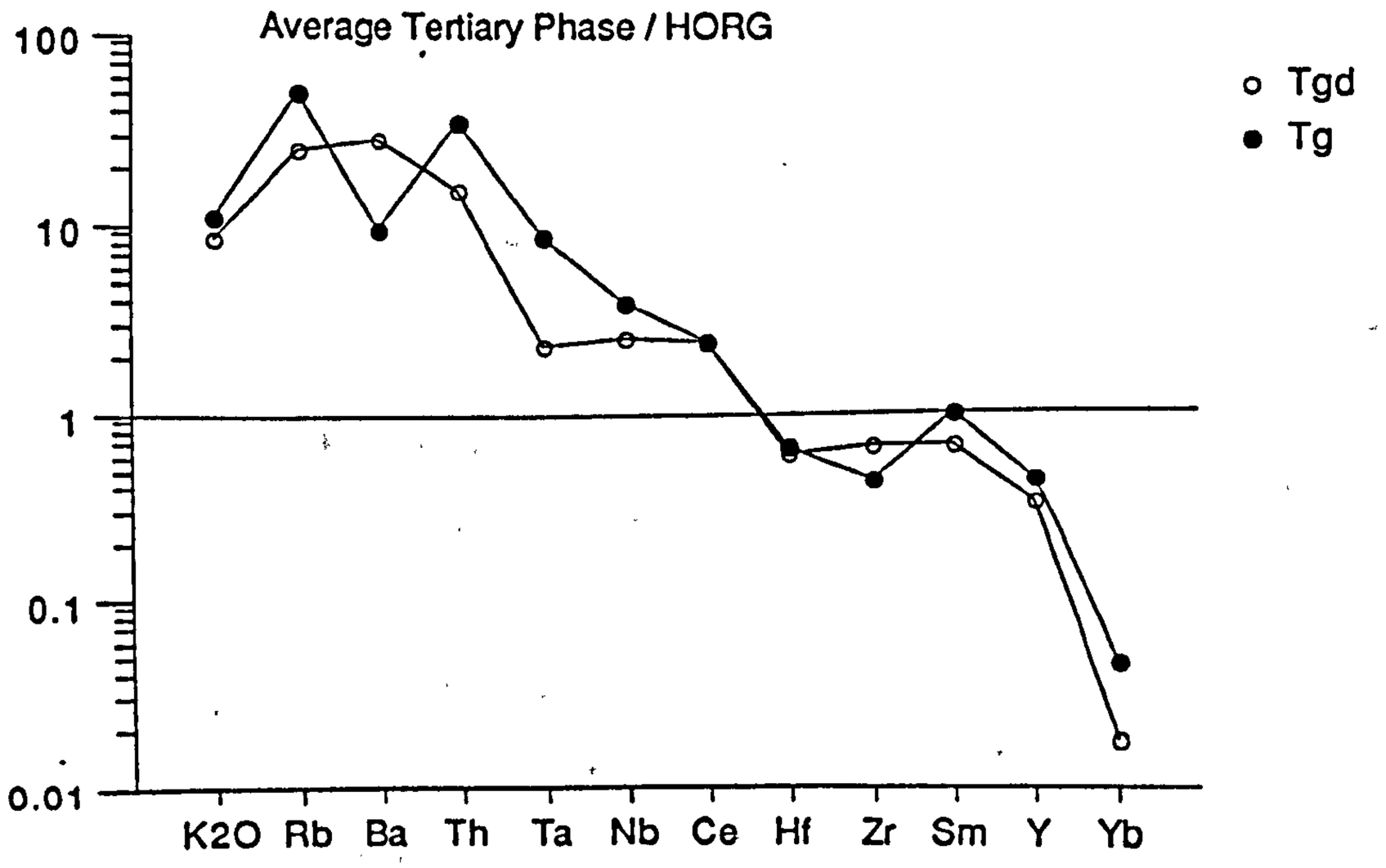

Figure 4.12 Hypothetical ocean ridge granite normalised trace element abundance "spider" diagrams for an average of the Tertiary dioritic suite and the Tertiary granitic suite.

The granitic suite has higher LILE contents with a distinct negative Ba anomaly (figure 4.12). The low concentrations of the alkaline earth elements which is also responsible for the high and variable Rb/Sr ratios in the granitic suite (to be seen in figure 4.14) reflecting the dominant control of alkali feldspar and plagioclase. The dioritic suite have variations of LILE similar to those of the Cretaceous phases with no significant anomalies.

The HFSE are enriched in the granitic suite relative to the dioritic suite and plot as a distinct group in the within plate granite field of granitoid tectonic discrimination diagrams Pearce et al. (1984) (figure 4.13).

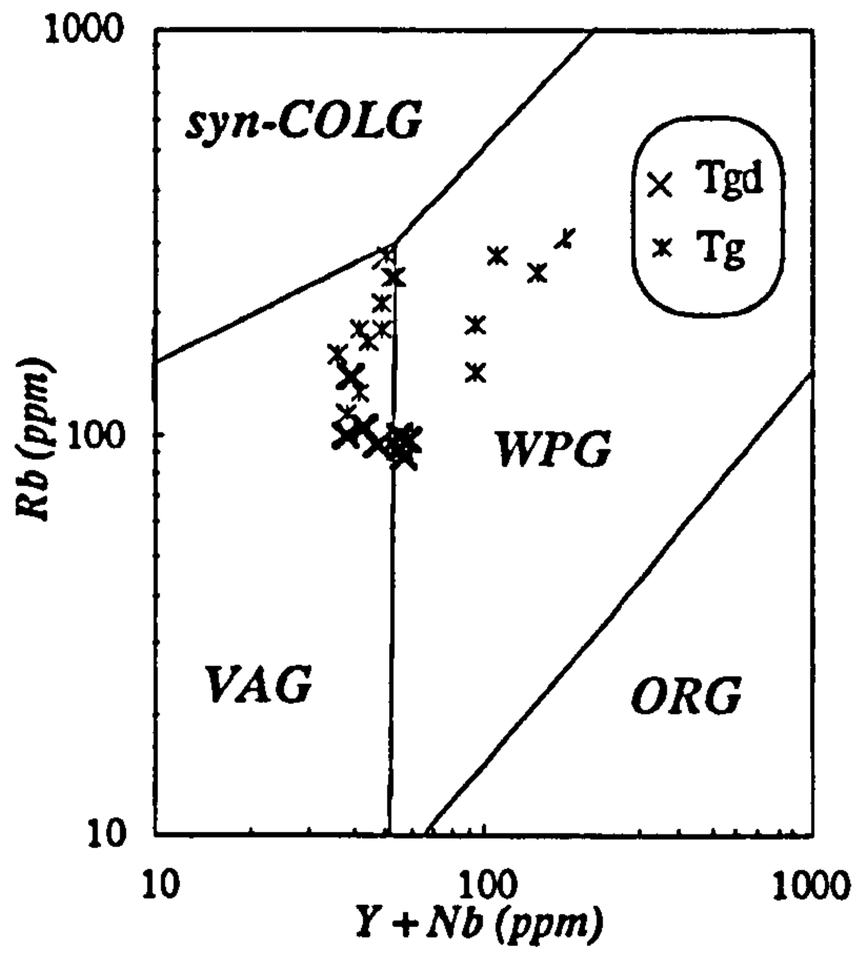

Figure 4.13 Granitoid tectonic discrimination diagram (Pearce et al., 1984) for the Tertiary bimodal suite.

Both Tertiary suites have slightly higher contents of LREE (Ce), Hf, and Zr than the Cretaceous rocks. The granitic suite has a weak negative Zr anomaly perhaps revealing the effect of residual zircon in these high silica magmas.

The dioritic suite has a strong depletion in HREE (Yb) which is nearly as extreme as that for the Cretaceous phases, whereas Yb is much less depleted in the granites. Y makes a reasonable analogue for Yb in all Tertiary and Cretaceous phases of the Idaho batholith, but its relative depletions and enrichments between groups is less extreme.

Low Rb/Sr ratios (≈0.1-0.2) which do not vary much with silica, are characteristic of the dioritic suite (figure 4.14). The granite suite, in contrast, have much higher and more variable Rb/Sr (≈ 0.2-100), and over a much smaller range in silica (figure 4.14).

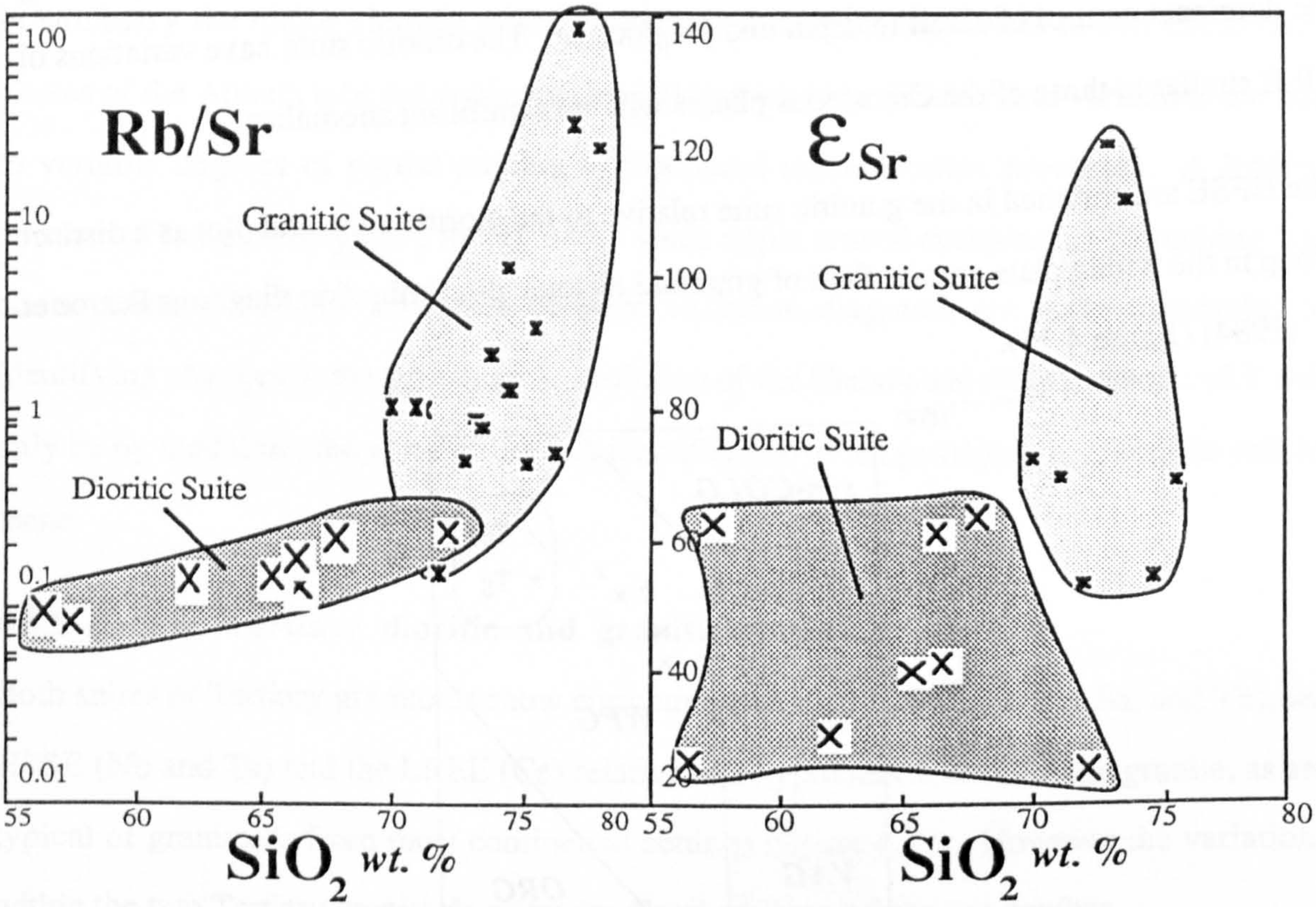

Figure 4.14 Log Rb/Sr versus SiO_2 wt. % and ε_{Sr} versus SiO_2 wt. % for the Tertiary bimodal suite.

The Sr isotope ratios of the two Tertiary suites are distinctly different. ε_{Sr} in the dioritic suite are lower (ε_{Sr} ≈ 20-65) and show a very scattered positive correlation with increasing SiO_2 (figure 4.14) alumina saturation, Rb/Sr etc... The granitic suite in contrast have higher and more variable Sr isotope ratios (ε_{Sr} ≈ 55-125) that do not correlate with SiO_2 (figure 4.14).

Although only a small number of samples of the two Tertiary granitoid suites have been analysed, their distinct characteristics suggest that they are not simply related to one another. This is in agreement with the preliminary conclusion drawn from field evidence and petrography.

4.6 Rare earth element geochemistry

A subset of representative samples have been analysed for the REE by INAA. The results are presented graphically on chondrite normalised diagrams (figure 4.15 and 4.16) for the Cretaceous and Tertiary phases respectively. The normalising values and the standard data are listed in Appendix A and analyses in Appendix B.

4.6.1 The Cretaceous phases

Each of the Cretaceous phases show strikingly similar REE patterns. In general they are LREE enriched and HREE depleted with smooth slightly concave upward patterns and only minor negative Eu anomalies (figure 4.15). The REE patterns are subparallel within and between the different rock types varying mainly in abundance rather than shape.

The tonalites are LREE enriched (Ce/Sm=1.71-3.54) and have a relatively large range in abundance from approximately 50-170 times chondrite. The HREE are depleted (Tb/Yb=1.67-3.11) with only minor negative to barely significant positive Eu anomalies (Eu/Eu*=0.71-1.04). All profiles within this magma type are subparallel except CBC87-55 which has a distinctly flatter LREE pattern (Ce/Sm=1.71).

The only hornblende-biotite granodiorite sample analysed has a slightly steeper LREE enriched pattern (Ce/Sm=3.31) than the tonalites, but similar HREE abundances and a minor negative Eu anomaly (Eu/Eu*=0.75).

The porphyritic granodiorites have LREE enriched patterns (3.02-3.85) with a very small range in abundance and a "cross-over" in patterns between Sm and Tb indicating some within magma type LREE/HREE fractionation. Minor negative Eu anomalies are observed (Eu/Eu*=0.70-0.79) in all samples.

The biotite granodiorites have LREE enriched patterns with LREE abundances of 80-200 times chondrite and Ce/Sm ranges from 3.08-4.43. As with the other phases the HREE

patterns are flatter (Tb/Yb=1.53-2.97) and show depleted HREE abundances (Yb<3 times chondrite). Eu anomalies are weakly positive to negative (Eu/Eu*=0.82-1.13).

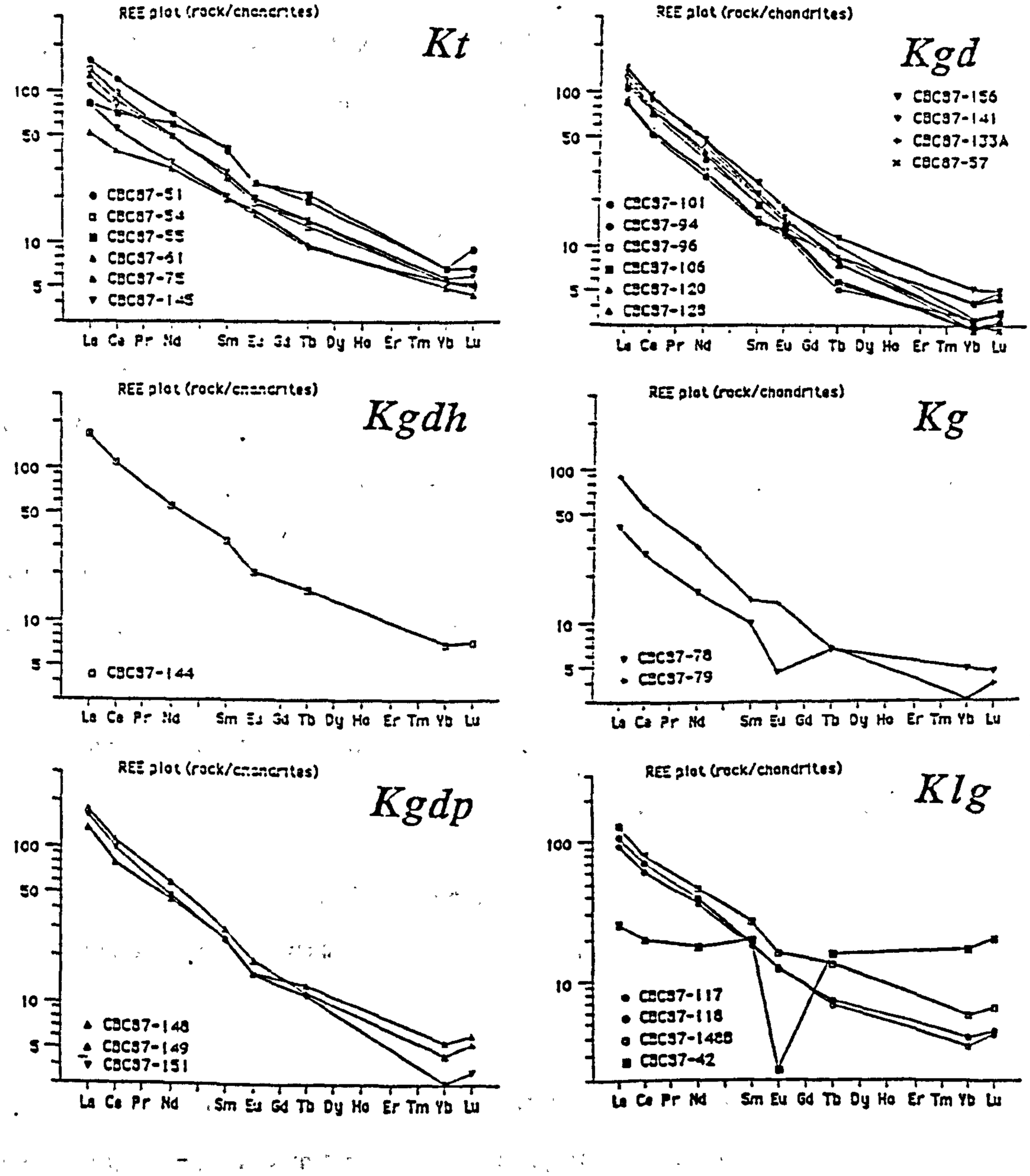

Figure 4.15 Chondrite normalised rare earth element abundance diagrams for the six Cretaceous phases of the Idaho batholith. Note the scales are logarithmic and lines are interpolated when there is no data for a particular REE.

The muscovite-biotite granites have marginally lower abundances of LREE (40-90 times chondrite) but the HREE are also depleted to 3-5 times chondrite, and so the patterns are still subparallel with the other phases (Ce/Sm=2.72-3.99 and Tb/Yb =1.3-2.2). The Eu anomalies are weakly positive to quite distinctly negative (Eu/Eu*=0.54-1.15) indicating some plagioclase and/or alkali feldspar fractionation within the suite. Moreover, a distinct "cross-over" in patterns at Tb is exhibited which supports some within suite fractionation of the REE.

The leucogranites have smooth LREE enriched patterns, but are slightly flatter than the other Cretaceous phases of the batholith (Ce/Sm=1.03-3.87, and Tb/Yb=0.94-2.32). Abundances of LREE are approximately 100 times chondrite and HREE are depleted to 3-5 times chondrite. Minor negative Eu anomalies are seen in all samples (Eu/Eu*≈0.9) except CBC87-42, a spessartine-bearing leucogranite with a flat REE profile at approximately 20 times chondrite and a large negative Eu anomaly (Eu/Eu*=0.13). The latter sample is similar to that seen in small volume, upper crustal partial melts in the Damara granitoids (McDermot, 1986).

In summary, the chondrite normalised REE diagrams for the various Cretaceous phases reveal no progressive changes in abundance or pattern except a slight decrease in abundance of Σ REE in the most evolved magmas. The most striking feature is the strong HREE depletion common to all phases. As it cannot be related to progressive fractionation between magma types, it must either be a feature shared by the sources or a process that occurs in all the sources during production of partial melts such as fractionation into a residual phase with high distribution coefficients for HREE, such as garnet.

4.6.2 The Tertiary bimodal suite

The chondrite normalised REE patterns for the dioritic and granitic suites are distinct from each other, and they differ from the Cretaceous phases in their higher abundances of HREE (figure 4.16).

The dioritic suite has smooth LREE enriched subparallel patterns with small negative Eu anomalies (Eu/Eu*=0.68-0.98). Abundances of LREE are in the range 100 to 300 times chondrite and are slightly steeper than the HREE profiles (Ce/Sm=2.63-2.73 and Tb/Yb=1.79-2.5). The within suite variation is mainly in differing abundances rather than changes in LREE/HREE fractionation.

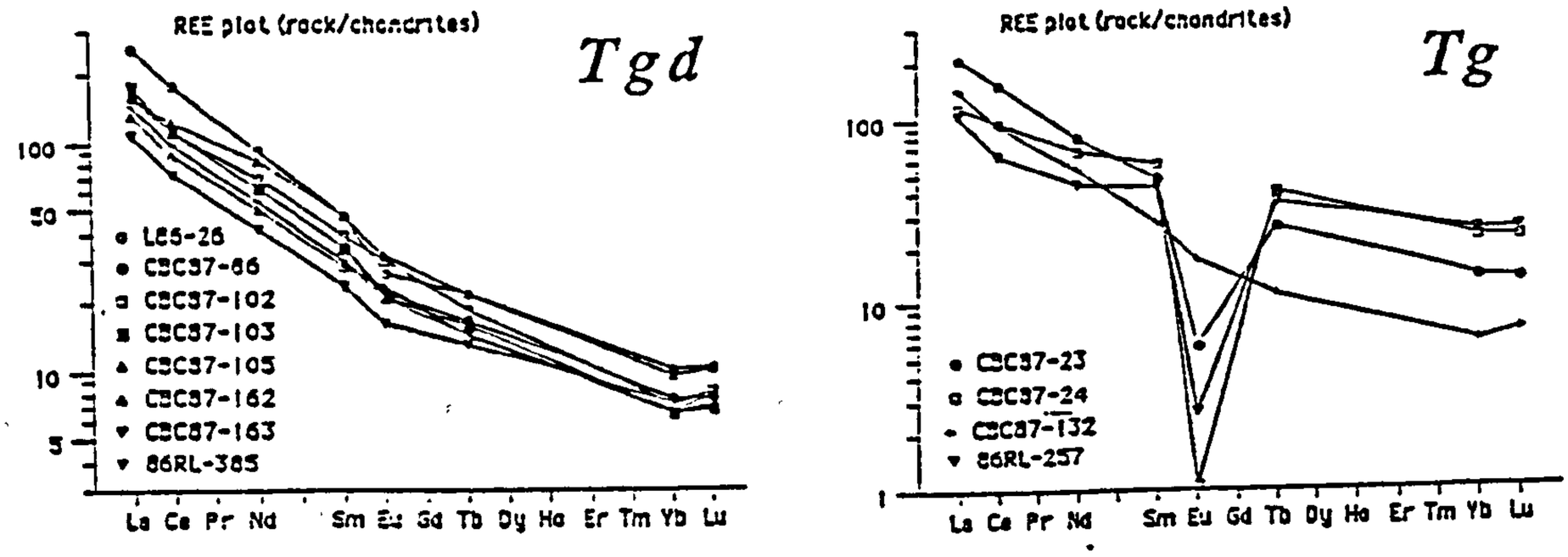

Figure 4.16 Chondrite normalised rare earth element abundance diagrams for the Tertiary bimodal suite of the Idaho batholith. Note the scales are logarithmic and that lines are interpolated when there is no data for a particular REE.

The granitic suite has smooth, but flatter, slightly concave downward REE profiles with steeper LREE enriched patterns relative to the HREE (Ce/Sm= 1.49-3.36 and Tb/Yb= 1.46-1.99). Weak to strong negative Eu anomalies (Eu/Eu*=0.02-0.75) are displayed which may have been the result of significant alkali feldspar and/or plagioclase control during either melting or crystallization processes. Abundances of HREE (10-50 times chondrite) are much greater than either the Tertiary dioritic suite or the Cretaceous phases. Modelling the effects of partial melting and crystallization processes on the REE is discussed in more detail in section 4.9.

4.7 Major element modelling

The aim of major element modelling is to ascertain the relative proportions of mineral phases that can account for the variation of the major elements within the Cretaceous and Tertiary granitoids of the Atlanta lobe. It allows the observed major element variations within a rock suite to be modelled in terms of the progressive removal (crystal fractionation) or progressive addition (partial melting) of specified mineral phases. Selection of the controlling mineral phases for fractional crystallization models can be taken simply from those present in the rock. To test whether removal of these mineral phases can account for the observed variations, or to evaluate which mineral phases contributed to the melt during partial melting, simple tie-line models are initially instructive.

CaO and Al_2O_3 are principally controlled by hornblende or plagioclase; MgO, Fe_2O_3 and TiO_2 can be controlled by various proportions of biotite, hornblende, clinopyroxene and perhaps garnet: and abundances of alkalis tend to be controlled by plagioclase alkali feldspar, biotite or muscovite.

Mixing calculations for natural rocks simply take into account the large number of components and elements. The relationship:

Unevolved magma = mineral components + evolved magma (for fractional crystallization);

Source = restite + melt (for partial melting);

was used by a computer program SUPERMIX based on the least squares method of Wright and Doherty (1970) to evaluate the major element variation. Mixing, fractional crystallization, and/or restite plus minimum melt processes can all be modelled by rearrangement of the above equation. The specific aim of modelling is to reproduce the composition of the least evolved liquid by mixing melted source phases and the most evolved liquid. The fit of the model to the data is measured in terms of the sum of the square of the residuals (ΣR^2). The lower the ΣR^2 value the better the fit.

A large number of assumptions and uncertainties are inevitably incorporated into such calculations and these include:

i) the assumption that analysed samples represent liquid compositions whereas in practice they may be mixtures of liquids and cumulates (McCarthy and Grooves,1979);

ii) the composition of the mineral phases were taken from the literature and listed in appendix A;

iii) the scatter of major element data about a straight line will introduce errors into the best fit approach;

iv) the mineral assemblages may vary regionally in the source region of a body as large as the Atlanta lobe of the Idaho batholith.

4.7.1 The Cretaceous granitoids

Modelling the major element results was undertaken in three steps in order to evaluate the change in controlling assemblages that may account for the observed inflexions in the major element trends at 69 wt.% SiO_2 and 72 wt.% SiO_2 (figure 4.2). The detailed results are given in appendix B and summarised below.

i) 54-69 wt.% SiO_2. The major element variation of the tonalite through to the least evolved biotite granodiorite requires that plagioclase and hornblende are the dominant controlling phases in an assemblage of 33.5% hornblende and 66% plagioclase + 0.5% apatite and minor amounts of sphene. The ratio of evolved liquid to crystalline solids used in this model is 26% evolved liquid to 74%solids.

ii) 69-72 wt.% SiO_2. The inflexions in the trends could be accounted for by biotite and alkali feldspar being the dominant controlling phases at 72 wt.% SiO_2 whereas at 69 wt.% SiO_2 plagioclase and hornblende are dominant. An assemblage of 26.5% hornblende + 25% plagioclase + 33.5% quartz + 12.5% biotite + 1% sphene + 1% apatite, using a ratio of 65% evolved liquid to 35% crystals can account for the variation in this portion of the trend.

iii) 72-79 wt.% SiO_2. The variation in major elements for the most evolved magmas can be controlled by an assemblage with approximately 50% plagioclase (oligoclase) + 22% alkali feldspar + 25% quartz + 2% biotite + 1% muscovite with minor amounts of apatite. The ratio of solid mineral phases to evolved liquid used is approximately 90% to 10%.

4.7.2 The Tertiary dioritic and granitic suites

Similar major element mixing calculations have been carried out for both the dioritic and granitic Tertiary suites. The same uncertainties and assumptions are incorporated into the calculations as noted above for the Cretaceous granitoids.

The major element variation within the dioritic suite can be accounted for by an assemblage of 43% plagioclase (andesine), 39% hornblende, 15% biotite and 1.5% sphene and minor apatite using a proportion of 35% evolved liquid to 65% crystalline phases. Clinopyroxene is not an important fractionating phase for this sample set, but Lewis (unpublished data) suggests that it may be in the more mafic end-members of this suite (≈ 52 wt. % SiO_2), although it is not observed as phenocrysts or in cumulate rocks.

The granitic suite, in contrast, has a range of major element compositions which can be accounted for by control of an assemblage consisting of 16% biotite + 35% plagioclase (oligoclase) + 47% alkali feldspar + 1% apatite. The proportions of 62% evolved liquid to 38% crystalline solids represent 38% fractional crystallization, but the degree of melting required for generation of the least evolved magma is clearly dependent on the source composition chosen.

4.8 Trace element modelling

4.8.1 The principles of LILE modelling for fractional crystallization and partial melting

Modelling the processes that may be responsible for the covariation between Sr, Ba and Rb has been carried out to assess the control of the major silicate mineral phases, into which these elements are preferentially partitioned in granitic systems. The reason for such modelling is :

i) to compare the proportions of phases with those inferred for the major elements;

ii) to begin to distinguish the effects of fractional crystallization from partial melting.

Comparison of the effects of fractional crystallization versus partial melting are modelled using Rayleigh fractional crystallization and batch equilibrium partial melting respectively. Rayleigh fractional crystallization is probably the most relevant method to model the physical separation of mineral phases from a magma as they are formed. The Rayleigh fractional crystallization equation is as follows:

$$C_l^i = C_{ol}^i F^{(D-1)}$$

C_l^i is the concentration of the trace element i in the final liquid;

C_{ol}^i is the concentration of the trace element i in the original liquid;

F is the weight proportion of liquid remaining;

D^i is the bulk distribution coefficient of the trace element i;

In contrast to this, batch equilibrium partial melting is a process where partial melts accumulate in equilibrium with the source rocks before separation as discrete batches. This is used as the preferred model for modal melting where:

$$C_l^i / C_o^i = 1 / (F + D - FD)$$

C_l^i is the concentration of trace element i in the batch of liquid;

C_o^i is the original concentration of trace element i in the source rock;

4.8.2 LILE modelling for the Cretaceous granitoids

LILE data are presented on logarithmic plots of Ba vs. Sr and Ba vs. Rb (figure 4.17). The Cretaceous phases are split into two groups merely for clarity. LILE covariation diagrams are instructive for gauging the effects of fractional crystallization in granitoid magmas because the minerals, plagioclase, alkali feldspar and biotite which commonly crystallize from such magmas at shallow levels have large and contrasting distribution coefficients (Kd values) for Ba, Sr and Rb (table 4.4). Trends generated in the LILE by fractional crystallization processes will contrast with those generated by partial melting from more mafic sources because the above mineralogy, and hence the bulk distribution coefficients are likely to be different. Moreover, removal of discrete batches of magma from a source region by for instance 30% batch equilibrium partial melting will produce trends of smaller

magnitude in the LILE than that of a "liquid line of descent" generated by the instant removal of solids from a liquid by 30% Rayleigh fractional crystallization.

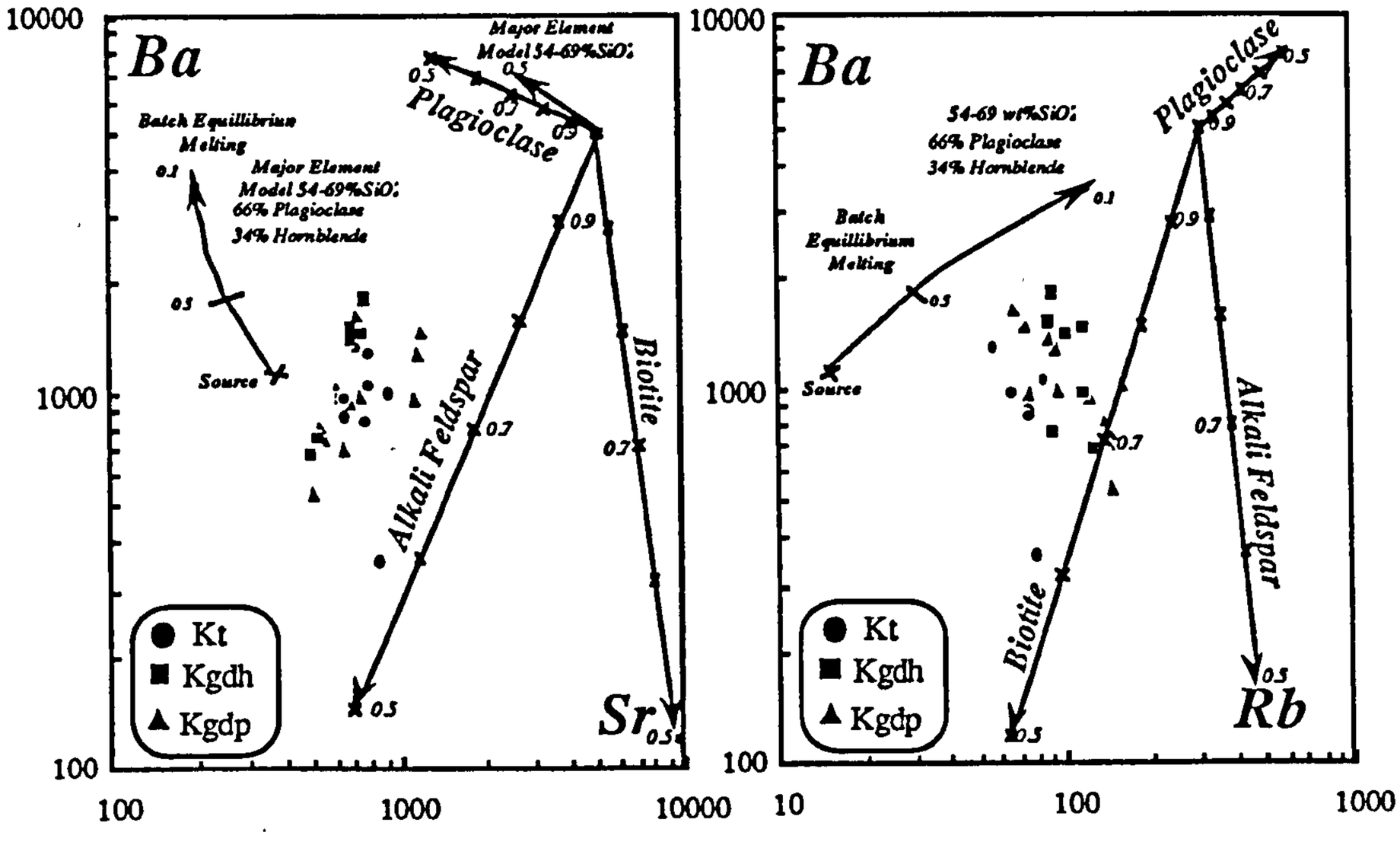

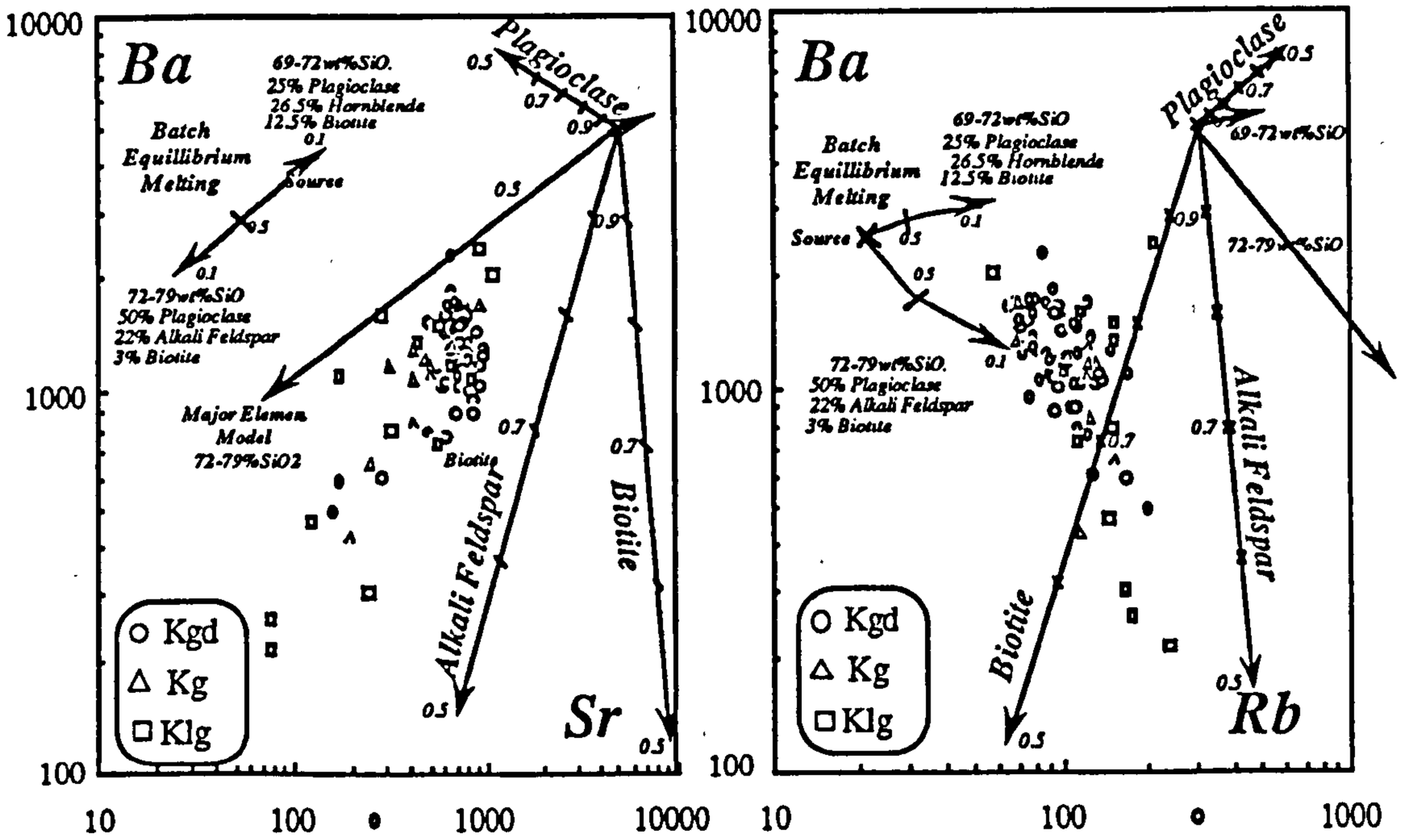

Figure 4.17 Logarithmic covariation diagrams of the LILE, (Ba vs. Rb, and Ba vs. Sr) for the Cretaceous granitoids. 4.17a shows the Kt, Kgdh and Kgdp while 4.17b shows the Kgd, Kg and Klg, the separation merely being made for the sake of clarity. Also shown are vectors for up to 50% Rayleigh crystallization of the major LILE host phases, plagioclase, alkali feldspar and biotite; vectors for batch equilibrium partial melting and Rayleigh fractional crystallization of the assemblages and degree of differentiation calculated from the major element variations. Numbers on vectors are F values and symbols for the Cretaceous phases are the same as all the previous diagrams

Vectors for up to 50% Rayleigh fractional crystallization of the above mineral phases and 10%-50% batch equilibrium partial melting are superimposed on figure 4.17 and illustrate the large trends generated by fractional crystallization and the relatively smaller trends generated by partial melting.

Variation diagrams (figure 4.7) indicate that Ba and Sr decrease and Rb increases with increasing silica in all Cretaceous phases of the Idaho batholith except the tonalites and the least evolved biotite granodiorites where Ba and Sr increase and Rb decreases. The LILE covariation trends for the more mafic Cretaceous rock types contrast with those for the more silicic granitoids. The tonalites, hornblende-biotite granodiorites, porphyritic granodiorites and all, but the most evolved biotite granodiorites, have short, rather scattered trends decreasing in Ba with increasing Rb and decreasing Sr. The muscovite-biotite granites, leucogranites and the more silicic biotite granodiorites show longer and much better defined trends, Ba and Sr decreasing together and Rb increasing.

In order to contrast the controlling mineral assemblages and the degree of differentiation suggested by major element modelling with the observed trends for the LILE, vectors are superimposed on figure 4.17 for the major element calculations, interpreted in terms of both Rayleigh fractional crystallization and equilibrium partial melting. Batch equilibrium partial melting models are realistically limited to degrees of 10%-50% by the ability of a viscous granitic melts to separate from the source at low degrees of partial melting (McKenzie,1985) and by total mobilisation of the source between 40%-50% partial melting (Wickham,1987). The bulk distribution coefficients for the partial melting model are those suggested from the the major element model, and trace element content of the the source is arbitrary because the effects of partial melting and fractional crystallization can be made by looking at their respective vectors on figure 4.17.

	Plagioclase	Alkali Feldspar	Biotite
Ba	0.36	6.12	6.36
Sr	2.94	3.87	0.12
Rb	0.05	0.34	3.26

Table 4.4 K_d values used for partial melting and fractional crystallization models after Arth and Hanson, 1975 and Hanson, 1978.

The major element model for the samples containing 54-69 wt. % SiO_2 is dominated by plagioclase and closely follows the plagioclase vector for both partial melting and fractional crystallization. Comparison of the models with the data in figure 4.17 shows no apparent fit because Ba is the only LILE which shows significant variation and no alkali feldspar or biotite, the major Ba hosting phases, were incorporated in the major element model.

This mismatch of the major element models with the LILE covariation trends in these least evolved magmas is to be expected where variable degrees of partial melting, source region heterogeneity and minor amounts of fractional crystallization all influence the composition of the magma. Moreover large errors are incorporated by the assumption of the mineral assemblages, the choice of Kd values and the instant removal of crystallized phases rather than the variable enrichment and depletion of the crystallizing mineral phases which may be more likely in highly viscous silicic magmas. The lack of sensitivity of major elements to different processes may only become apparent when the LILE are considered because, unlike major elements, they show extreme enrichments and depletions during fractional crystallization, but only mild changes for partial melting.

There appears to be a clearer correlation between the major element models and the LILE variations for the more evolved magmas (figure 4.17). The vector for Rayleigh fractional crystallization for the mineral proportions and degree of crystallization calculated in the major element model is similar to the observed inclination and degree of variation in the LILE data. Slightly higher proportions of alkali feldspar and/or biotite would produce a near perfect fit and could readily be tolerated within the margins of error incorporated in the major element model. The major element partial melting model vector is less extreme, but subparallel relative to the LILE trends, and while it appears to be unable to account for the more evolved rocks, it may explain some of the scatter in the LILE trends particularly at lower silica values as a result of differences in degree of partial melting.

Although the complicating factors and uncertainties mentioned for the less evolved rock types may be equally applicable here, fractional crystallization appears to have been the

dominant process and so the relationships are clearer. Thus the more silicic biotite granodiorites, muscovite-biotite granites and leucogranites are consistent with high degrees of fractional crystallization from parental magmas with some limited compositional variation and efficient removal of the solid phases from the system. The reason why Rayleigh fractional crystallization occurred only in the more silicic magmas is unclear, but could be a result of increasing concentration of volatiles reducing viscosity in the evolving melts as the earlier lower silica magmas crystallized.

In summary where significant degrees of fractional crystallization have occurred in a magma it appears to be readily distinguished from partial melting processes by the large variation in LILE. This is the case for the more silicic rock types and their LILE variations are consistent with the major element model. In contrast, when the effects of fractional crystallization are not dominant over those of partial melting and source region heterogeneities, rather scattered LILE trends occur, as for the more mafic rock types. The major element and LILE element variations in the more mafic rock types are poorly constrained, but they are consistent with variable degrees of partial melting from slightly heterogeneous source regions combined with minor amounts of fractional crystallization. Quantitative assessment of the effects of a partial melting process is difficult using the LILE, but may be better approached using elements such as the REE's which have high and variable distribution coefficients in likely source regions, but which are largely unaffected by fractional crystallization of the common liquidus phases of granitoid magmas (c.f. section 4.5.1).

4.8.3 Estimation of the possible degree of fractional crystallization by the calculation of relative bulk distribution coefficients (D values) for the Cretaceous granitoids

The following calculations were carried out in order to quantify the amount of fractional crystallization in a suite. They are most applicable to the muscovite-biotite granite and leucogranite whose trace element variations are probably dominated by fractional crystallization processes, but they have also been carried out for the more mafic rock types in

order to evaluate further the suggestion that high level crystallization processes are not significant for these magmas.

The approach taken was to assume that the least evolved sample from a comagmatic suite was representative of the parental liquid composition of that magma type, and that it was generated by partial melting processes in the source region. The variation within each suite was then taken to be a result of fractional crystallization processes during ascent and at the level of emplacement of the magmas, in order to estimate the maximum amount of fractional crystallization. Rayleigh fractional crystallization was used in preference to equilibrium fractional crystallization.

By assuming that Rayleigh fractional crystallization accounts for the variation between the least and most evolved samples within a magma suite the degree of crystallization required to produce the observed variation may be calculated. In order to calculate F, D must be estimated for each trace element. Allegre et al. (1977) showed that the Rayleigh fractional crystallization equation could be solved to give the bulk distribution coefficient of a compatible or mildly incompatible element if at least one element in a suite behaved as if D=0. Assuming the basic Rayleigh equation:

$$C_l^i = C_{ol}^i F^{(D-1)}$$

For a highly incompatible element (a hygromagmatophile element of Allegre et al.,1977), D « 1 therefore D - 1 ≈ -1 and the Rayleigh equation simplifies to:

$$C_l^H = C_{ol}^H F^{(D-1)} \approx C_l^H = C_{ol}^H / F$$

$$\text{or} \qquad F = C_{ol}^H / C_l^H$$

C_{ol}^H is the original liquid concentration of the hygromagmatophile element H

C_l^H is the final liquid concentration of the hygromagmatophile element H.

This can be substituted back into the Rayleigh equation, and thus allows D to be solved for any less incompatible element i:

$$C_l^i = C_{ol}^i (C_{ol}^H / C_l^H)^{(D-1)}$$

$$\log C_l^i = \log C_{ol}^i + (D^i - 1)(\log C_{ol}^H - \log C_l^H)$$

$$D^i = (\log C_l^i - \log C_{ol}^i) / (\log C_{ol}^H - \log C_l^H) + 1$$

These calculations yield average bulk D values for each trace element within the individual Cretaceous magma suites of the Atlanta lobe (table 4.5), and the degree of crystallization required to account for the variation. The calculations were carried out on each of the Cretaceous rock types to gauge the degree of fractionation within an individual magma type, although the trace element trends in the porphyritic granodiorite were too scattered to justify modelling. The more mafic biotite granodiorite and hornblende-biotite granodiorite, which fall between the two inflexion points at 69 wt. % SiO_2 and 72 wt. % SiO_2 (figure 4.7), show trace element behaviour inconsistent with Rayleigh fractional crystallization of the phases which typically crystallize from granitic magmas and thus they yield meaningless D values. Preliminary calculations showed that for these samples Sr most closely resembled the ideal hygromagmatophile behaviour and normally highly incompatible elements such as Rb, Th, and U had calculated relative bulk D values >5, and thus these have been discounted as unrealistic. The control of biotite appears to be significant in these samples, but there is no evidence to suggest that the comparatively rapid increase in Sr in these samples was due to plagioclase accumulation. The evidence above is taken to indicate that these samples are not representative of a liquid line of descent, but may merely reflect some scatter between the most evolved hornblende-biotite granodiorite magmas and the less evolved biotite granodiorites.

Similar calculations have been applied to the trace element variation of the suites of samples with silica contents above and below the inflexion points at 69 and 72 wt. % SiO_2, the same as those used during major element modelling, to facilitate comparison between the major and trace element models.

The choice of element having the closest behaviour to that of an ideal hygromagmatophile element in each suite (table 4.5) is in practice limited to those that define reasonably

unscattered trends. Therefore potentially highly incompatible elements like U and Th are discounted and yield negative relative bulk D values.

Magma Suite	Kt	Kt-Kgd	Kgd	Kg	Klg	Kgd-Klg
H Element	Ba	Ba	Rb	Rb	Rb	U
D_{Ba}			2.2	3.8	2.6	2.0
D_{Ce}		-	0.89	2.9		
D_{Nb}	0.66	0.46	0.91	-	0.93	0.93
D_{Pb}	0.58	0.014	0.84	-	0.85	0.78
D_{Rb}	1.1	0.31				0.41
D_{Sr}	1.1	1.4	2.5	4.2	2.9	2.1
D_{Th}	1.4	-	0.04	-	-	0.18
D_{U}	0.18	-	-	-	-	
D_{Zr}	0	0.23	1.4	2.6	0.96	1.1
D_{Y}	0.68	0.76	0.14	-	0.35	0.62
F Value	**0.43**	**0.33**	**0.35**	**0.61**	**0.24**	**0.13**

Table 4.5 Calculated D values assuming that for the most hygromagmatophile element D=0 (after Allegre et al., 1977). Negative values are indicated by -, and Ce is left blank for those suites where both end members have not been analysed by INAA.

The major problem with this technique in these rocks is the shortage of trace elements which are highly incompatible, exhibit coherent trends and are therefore make good fractionation indices. The error introduced because the chosen element is not totally incompatible is illustrated in figure 4.18. The validity of the approximation $F^{(D-1)} \approx 1/F$ is best for small degrees of crystallization ($F > 0.5$) and when the bulk distribution coefficient of the hygromagmatophile element approaches zero ($D < 0.05$).

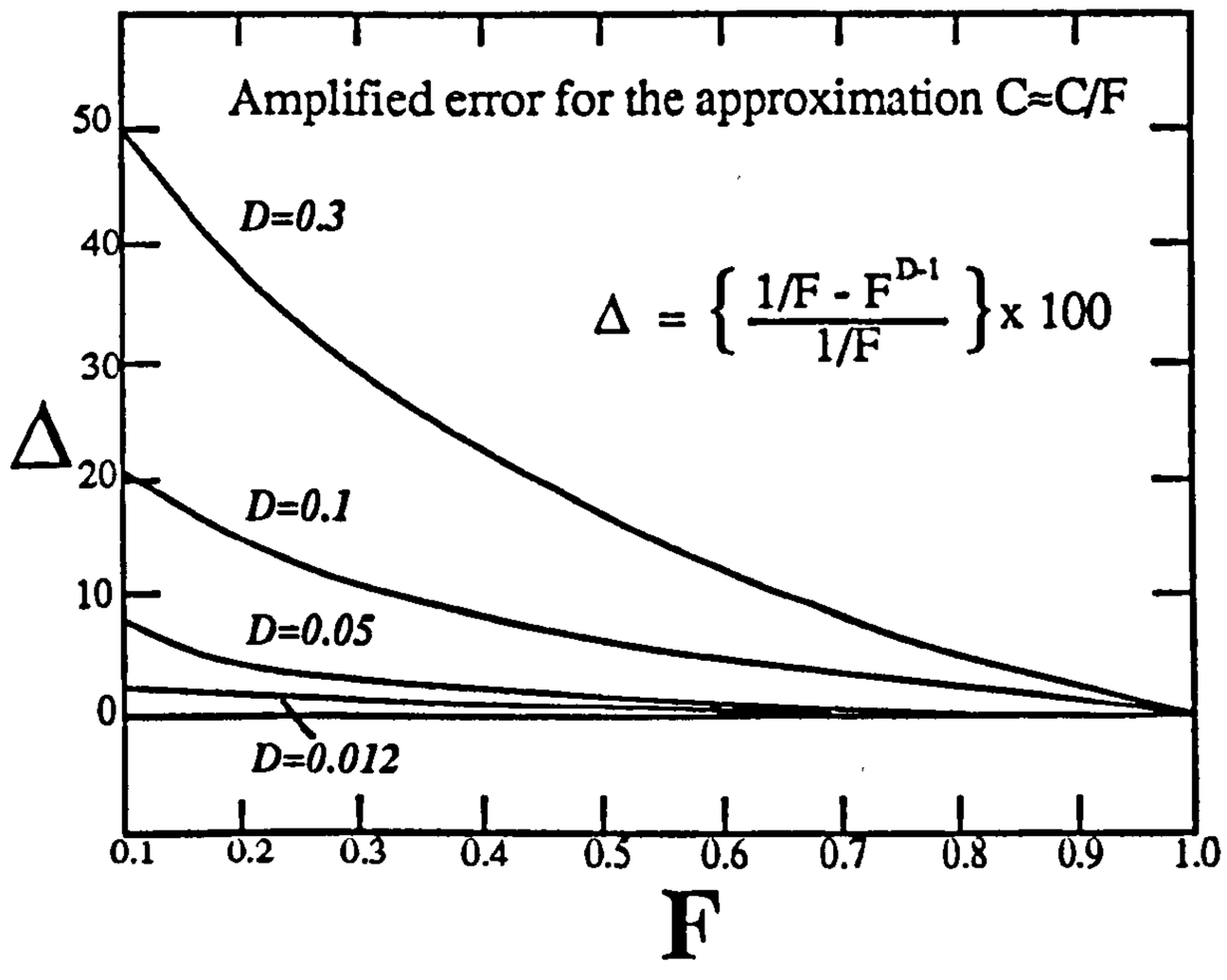

Figure 4.18 Error introduced by assuming D=0, so that $F^{(D-1)} \approx 1/F$ as a function the degree of crystallization and the true D value of the hygromagmatophile element.

In general the approximation causes an under-estimate of the amount of the residual liquid F and so an over estimate of the calculated bulk distribution coefficients. Although the relative D values are only semi-quantative (table 4.5) there are some results worth noting.

i) The tonalites behave differently from the remaining phases with all the trace elements behaving incompatibly apart from Rb, Sr and Th for which D≈1. Fractional crystallization of dominantly feldspars from granitic liquids cannot account for such element fractionation, and so the evolution of the magmas may involve larger proportions of hornblende and biotite than previously suggested by the major element modelling.

ii) The relative bulk D values for the variation between the tonalites and the least evolved biotite granodiorite (Kt-Kgd) contrast with those for the other rock types in that Zr has D<1 and Sr has a D value just greater than 1, indicating that alkali feldspar, and zircon fractionation are less important in the least evolved magmas. The degree of fractional crystallization required to go from the least evolved tonalite (54% SiO_2) to the least evolved biotite granodiorite (67% SiO_2) is approximately 67% and agrees well with the estimate from the major element model, and thus the Rayleigh fractional crystallization may control the within suite variation of the tonalites and hornblende-biotite granodiorites taken as a single suite.

iii) The relative bulk D values for the more evolved biotite granodiorite, the muscovite-biotite granite, the leucogranite and the three suites taken together, yield similar results as they all define colinear trends on trace element variation diagrams (figure 4.7). Ba, Sr and Zr have D>1 indicating the control of plagioclase, alkali feldspar and zircon fractionation. The required degree of crystallization of 65%, 39%, and 76% for the biotite granodiorite, muscovite-biotite granite and leucogranite respectively may be more realistic than the effective 88% fractional crystallization required to account for the variation of the combined suites on grounds that magmas cease to behave as fluids when they contain between 40-60% crystals (Wickham, 1987). However, the high degrees of crystallization for the combined suites agrees well with the estimates made from the major element modelling. It is

envisaged that the evolved liquids may separate from the crystallizing phases into higher level magma chambers so that taken as a single suite the overall estimates of the degrees of crystallization are high. The high degree of crystallization required by the leucogranite reflects their wide range in compositions and as remarked previously may be a result of limited partial melting of wall rocks (section 4.7).

4.8.4 LILE modelling the Tertiary bimodal Suite

Modelling of the LILE has also been carried out for both suites of Tertiary granitoids. Vectors for 50% Rayleigh fractional crystallization and batch equilibrium partial melting for plagioclase, alkali feldspar and biotite, (the major silicate mineral phases hosting LILE) are superimposed on the Ba vs. Sr and the Ba vs. Rb diagrams (figure 4.19) using the distribution coefficients listed in table 4.4. In addition, the vectors for Rayleigh fractional crystallization and batch equilibrium partial melting using the D and F values implied from the major element models are shown for the sake of comparison.

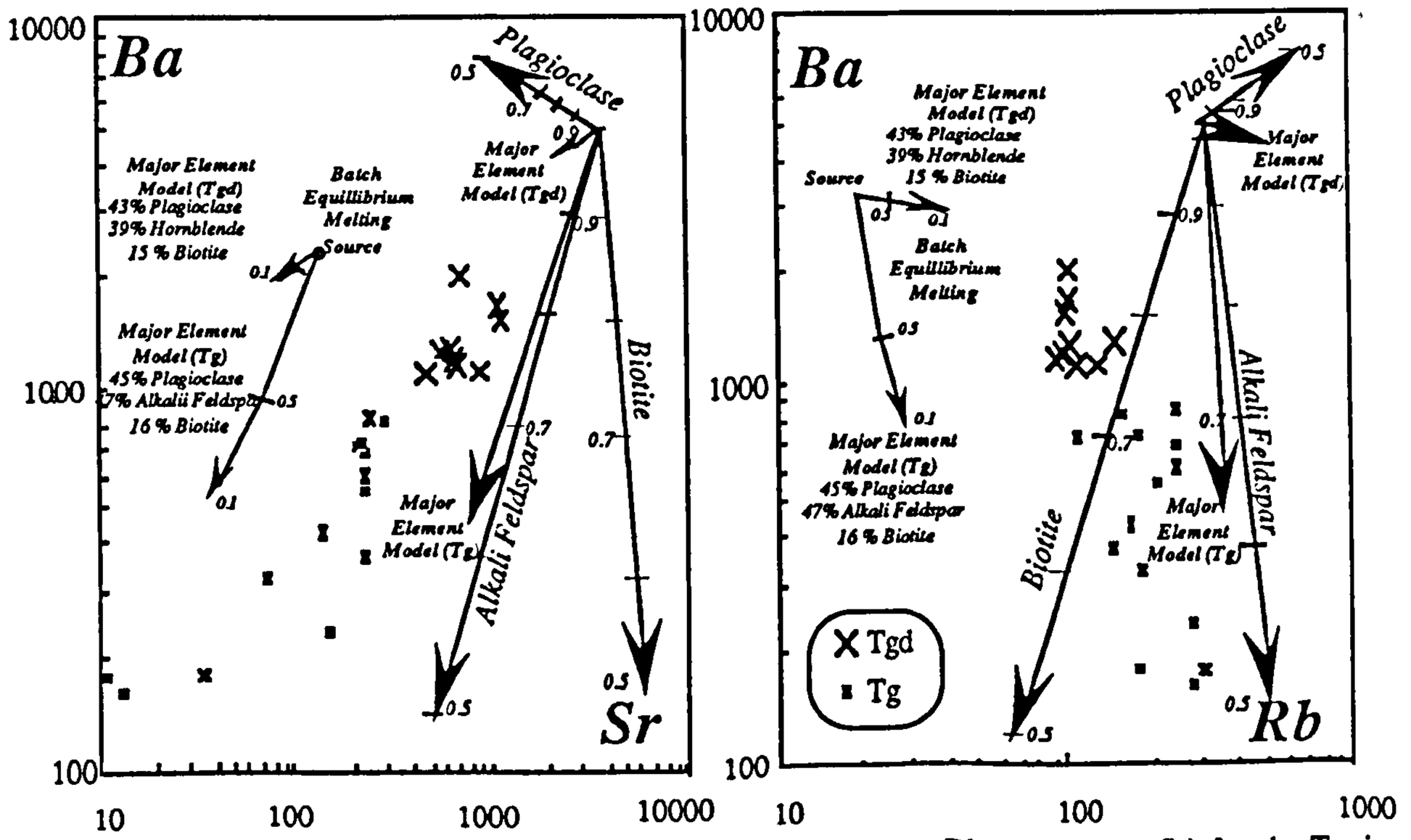

Figure 4.19 Logarithmic covariation diagrams of the LILE, (Ba vs. Rb, and Ba vs. Sr) for the Tertiary bimodal suite. Also shown are vectors for up to 50% Rayleigh crystallization of the major LILE hosting phases, plagioclase, alkali feldspar and biotite; vectors for batch equilibrium partial melting and Rayleigh fractional crystallization of the assemblages calculated from the major element variations are plotted.Large crosses represent the dioritic suite and asterisks the granitic suite. F values are indicated on model vectors.

The dioritic suite displays only minimal LILE variation and have therefore undergone only limited crystal differentiation of alkali feldspar or biotite. The major element model interpreted as fractional crystallization or partial melting produce parallel trends, but 50% fractional crystallization has much more effect on figure 4.19 than 50% partial melting. Both vectors are subparallel to the observed trend within the dioritic samples, but alone cannot produce the magnitude of the observed range in LILE composition. Therefore it is likely that earlier melting processes produced a small range in parental liquid compositions and/or source region heterogeneity produced a limited range in parental magmas which then underwent significant degrees of fractional crystallization of an assemblage similar to that calculated by major element modelling. An additional model approached with the aid of isotope data is that assimilation combined with fractional crystallization processes caused the variation within the dioritic suite.

The Tertiary granitic suite show large and coherent trends on the LILE covariation diagrams (figure 4.19) which are virtually parallel to and of the same magnitude as the Rayleigh fractional crystallization vector constrained by the major element model. Although the batch equilibrium partial melting vector is also parallel to the trend of the data, the magnitude is smaller than the observed variation and thus is discounted in favour of Rayleigh fractional crystallization as the dominant process.

In summary the LILE data from the Tertiary granitic suite are consistent with 38% Rayleigh fractional crystallization for the observed range of compositions. The dioritic suite, though not inconsistent with the major element model, does not appear to have such a simple origin and we must appeal to variable degrees of partial melting, source region heterogeneity or perhaps some limited mixing with the Tertiary granitic suite. As regards the clear bimodal distribution of the Tertiary granitoids observed in the field and bimodal age ranges, the LILE variation models alone certainly do not prohibit derivation of the granitic suite from the dioritic suite. However this is unlikely in view of the observed differences in Sr isotope ratios (figure 4.14). Mixing between the two Tertiary suites is investigated using isotopic evidence in Chapter 5.

4.8.5 Estimation of the degree of fractional crystallization for the Tertiary granitic and dioritic suites

The approach taken during the modelling of relative D values is to assume that Rayleigh fractional crystallization produced the most evolved magma from a homogeneous parental magma in order to gauge the possible effects of fractional crystallization on the liquid compositions. The mean relative bulk D values for the Tertiary granitoids were calculated for a range of trace elements using the method of Allegre et al. (1977) outlined in section 4.7.1i, and they are listed in table 4.6.

Rock Type	Dioritic Suite	Granitic suite	
H Element	U	Rb	Th
D_{Ba}	1.2	7.3	5.0
D_{Ce}	1.2	1.3	1.2
D_{Nb}	1.2	-	-
D_{Pb}	0.60	0.29	0.55
D_{Rb}	0.73		0.37
D_{Sr}	1.4	9.11	6.15
D_{Th}	0.26	-	
D_{U}		0.01	0.37
D_{Zr}	1.2	1.5	1.3
D_{Y}	1.4	-	-
F Value	0.25	0.50	0.33

Table 4.6 Calculated relative average bulk D values for the Tertiary dioritic and granitic suites using the approximation of Allegre et al. (1977) that D=0 for the most hygromagmatophile element.

U, Th and Rb are incompatible in the dioritic suite, but U most closely approaches the behaviour of an ideal hygromagmatophile trace element and it is thus used in subsequent calculations of bulk D and F. Nb and Y increase by the highest proportion in the granitic suite but do not show coherent variations with silica (figure 4.8). Therefore Rb was taken as the most hygromagmatophile element within the granites and Th, though more scattered, was used for comparison. Results are listed in table 4.6.

In the dioritic suite the relative bulk distribution coefficients calculated for Ba, Sr, Ce, Nb, Y, and Zr are all just greater than 1, suggesting only minor control by plagioclase, alkali feldspar and zircon. Pb, Rb, and Th are all incompatible as would be expected during crystallization in dioritic systems. The amount of crystallization required to produce the trace element variation within the dioritic suite is 75% of an assemblage that probably contains more mafic mineral phases than feldspars.

In the granitic suite Ba and Sr are the most compatible trace elements according to the calculated relative D values reflecting likely feldspar control. Zr is mildly compatible reflecting zircon crystallization, whereas Rb, Th and U all have D<1 within the suite. Rb and Th as the most hygromagmatophile elements yielded estimates of 50% and 75% Rayleigh fractional crystallization respectively which is approximately twice the estimate of 38% from major element modelling, but is consistent with the degree of fractionation required to cause the LILE covariation (figure 4.19).

In summary the LILE element variations of the dioritic suite demonstrate that fractional crystallization of biotite and alkali feldspar has not been an important process, but the large fall in CaO, TiO_2, MgO and Fe_2O_3, and the minimal change in trace element concentration except Sr suggest that plagioclase and hornblende controlled the chemical variations. The highly variable within-pluton modal mineralogies may suggest that this was a fractional crystallization rather than a partial melting effect. In the granitic suite, the contrasting highly variable LILE, Zr and the incompatible elements Rb, U, and Th are successfully modelled to be a result of high level crystallization processes of dominantly biotite, alkali feldspar and plagioclase.

4.9 Partial melting models and inferred source compositions

4.9.1 Recognition of partial melting trends versus fractional crystallization trends in the Cretaceous granitoids

Modelling the LILE in terms of fractional crystallization processes suggests that the more evolved rock types may have undergone significant degrees of fractional crystallization of plagioclase, alkali feldspar and biotite. The more mafic rock types (the tonalites through to the biotite granodiorites), in contrast, have not been modelled satisfactorily by fractional crystallization processes. Close inspection of the graphs of Sr and Y versus SiO_2 (figure 4.7) reveal that Y and Sr decrease through the biotite granodiorites, but in the more silicic biotite granodiorites, muscovite-biotite granites and leucogranites, Y does not continue to fall with increasing SiO_2, and yet Sr continues to decrease with silica. Figure 4.20 summaries the changes in Sr, Y and Sr/Y trends with silica with different symbols for the rocks with

70-73 wt.% SiO_2 generally comprising the biotite granodiorites and those with greater than 73 wt.% SiO_2 including the majority of the muscovite-biotite granites and leucogranites, and the more silicic biotite granodiorites. The Y concentration in the evolved rocks does not continue to fall and there is sharp decrease in Sr relative to the less evolved rocks. This change in Sr and Y is particularly well illustrated by the Sr/Y ratio (figure 4.20c). Although 73 wt. % SiO_2 is an arbitrary boundary, the samples with greater than 73 wt. % are those with the more extreme LILE fractionation which was modelled by variable but high degrees of fractional crystallization of a granitic assemblage.

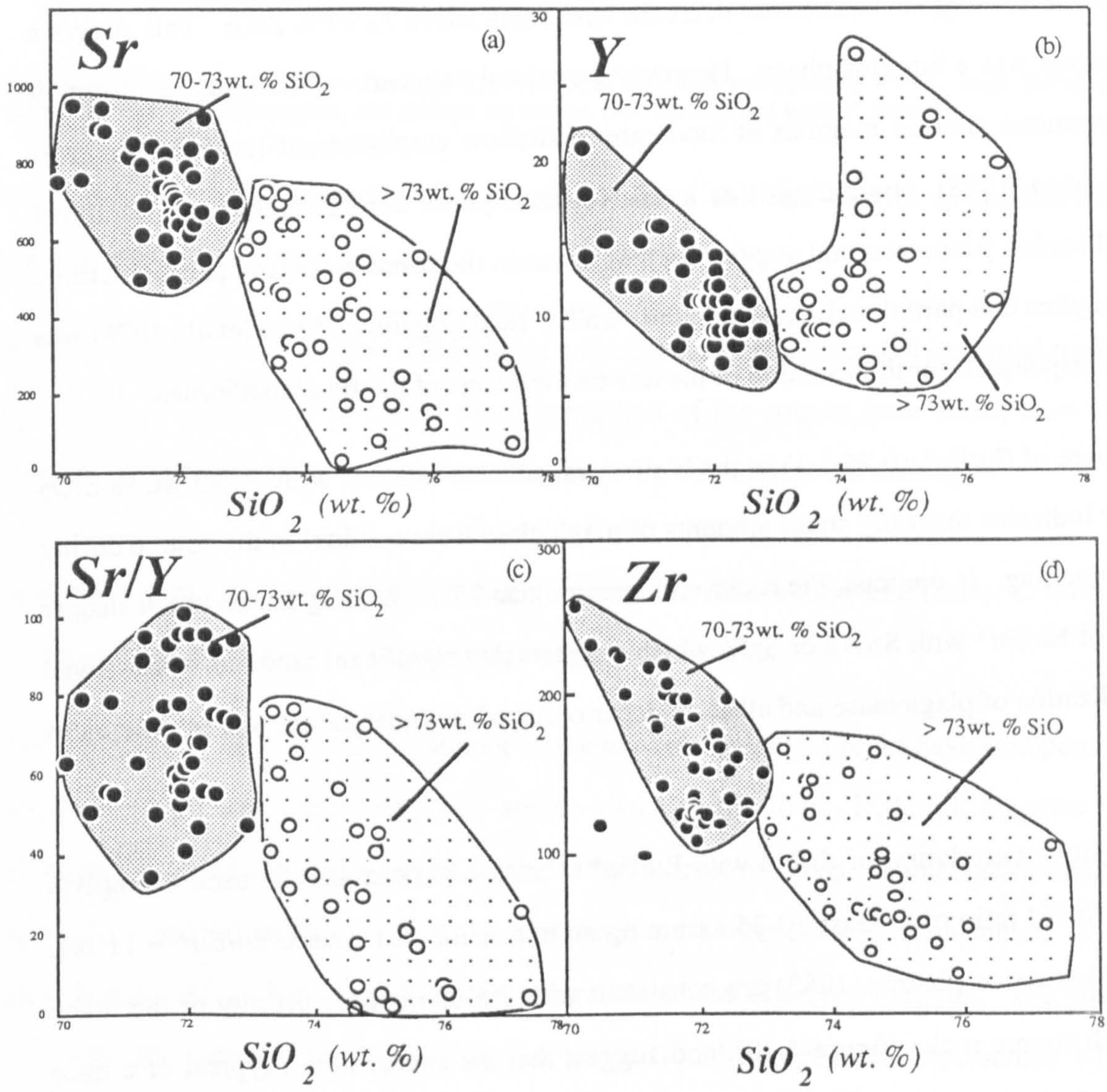

Figure 4.20 (a, b, c, & d) Sr, Y Sr/Y and Zr variations for rocks with greater than 73 wt. % silica that are implied to have undergone significant degrees of fractional crystallization (stippled field) and those with 70-73 wt. % silica that may represent parental liquids (dark shaded field). Notice that Y does not continue to fall with increasing silica continuously across the 73 wt. % boundary implying that a phase with high D_Y occurs on the liquidus for the less silicic samples.

Either a change in process (fractional crystallization or partial melting), or a change in the fractionating assemblage is implied at approximately 73 wt. % SiO_2 (figure 4.20).There are several geochemical characteristics of the more mafic biotite granodiorites (70-73 wt. % SiO_2) that suggest that partial melting processes gave rise to these less evolved magmas and help to constrain the controlling factors during the partial melting processes.

The key point is that HREE and Y are very depleted in the more mafic biotite granodiorites and they decrease with increasing silica until ≈73 wt.% SiO_2 (figure 4.20), where the trend stops, whereas zircon continues to decrease with silica above 73 wt.% SiO_2. This suggests that garnet was a liquidus phase. However garnet only appears on the liquidus of highly peraluminous granitic magmas at moderate to shallow emplacement levels in the crust (Thompson, 1988), precluding it as a near liquidus phase during mid-crustal fractional crystallization processes, and suggesting that it was in the residium during partial melting. This implies that partial melting within the stability field of garnet (Wyllie et al., 1976) was in part responsible for the variation of the less evolved suite of biotite granodiorites.

The range of Eu/Eu* (0.75-1.1) in the biotite granodiorite samples with 70-73 wt. % SiO_2 further indicates that only small amounts of plagioclase were residual in the source during partial melting. In contrast, the rocks with greater than 73 wt.% SiO_2 fall on much steeper trends of Eu/Eu* with Sr/Nd or Sr/Y which suggests that significant amounts of fractional crystallization of plagioclase and alkali feldspar occurred, and that garnet was not a liquidus phase.

The positive correlation of Sr/Nd with Eu/Eu* (figure 4.21) can also be used to imply a source Sr/Nd ratio of at least 30-35 assuming an unfractionated source Eu/Eu* ≈ 1± 0.1. These high ratios (Pearce, 1983) are consistent with the implied arc affinity of the Idaho batholith source rocks (figure 4.10), and suggest that the source is not typical of a trace element depleted lower crust of Taylor and McLennan (1985), but is relatively enriched and possibly of subduction related origin.

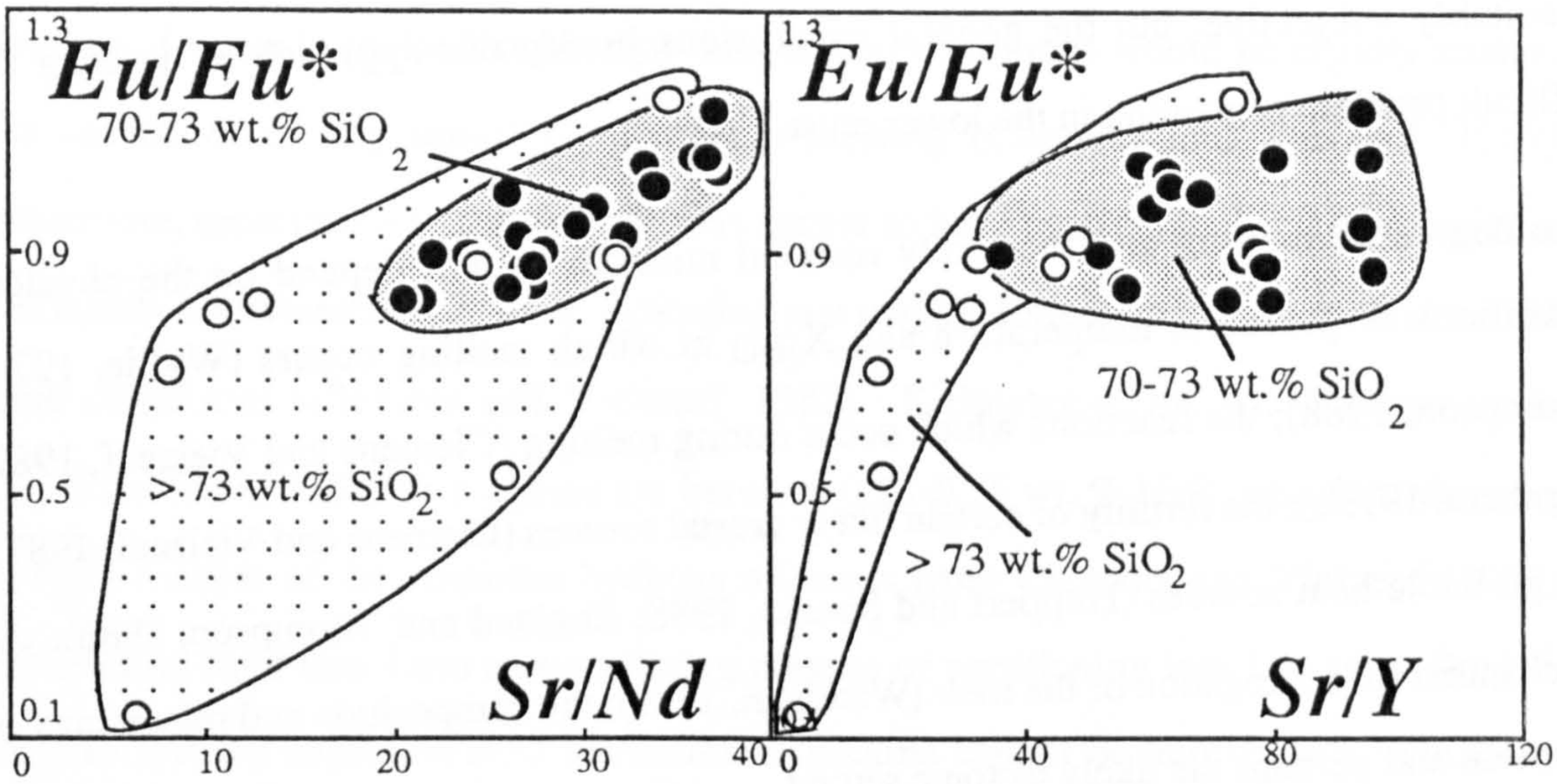

Figure 4.21 Eu/Eu* versus Sr/Nd and Sr/Y for the rocks with REE measured by INAA. High Sr/Nd ratios are implied for parental magmas and perhaps the source, with no inherited Eu/Eu* anomaly.

4.9.2 Modelling a probable source composition for the biotite granodiorites : an iterative approach.

Having suggested that the low silica biotite granodiorites were generated by partial melting processes, it is possible to model the composition of the source from which they were derived. Considering the equation for modal batch equilibrium partial melting:

$$C_0 = C_l (F + D - FD)$$

it is clear that the degree of melting, F and the bulk distribution coefficient D must be constrained in order to calculate the composition of the source.

In the region of the Idaho batholith none of the exposed basement rocks have isotope ratios suggesting that they represent likely source rocks to the Idaho batholith magmas (see Chapter 5) and so F and D must be arrived at by indirect methods. A qualitative-iterative approach was adopted in which several lines of evidence were considered in the development of a likely model for the generation of the observed magmas. The source composition was back-calculated from a given liquid composition represented by an unevolved granitoid from the biotite granodiorite suite using the inferred D and F values. The parameters of the model were then adjusted within the limits set by the independent evidence and a more likely source composition arrived at. Fine tuning of such a model is

inevitably subjective, but the general conclusions justify this approach to tackling the difficult problem of melting in the lower crust.

The degree of melting and the likely residual mineralogy will depend on the physical conditions of pressure, temperature and X_{H_2O} at which melting occurs (Wyllie, 1976; Thompson, 1988); the reactions which occur during melting (Clemens and Vielzeuf, 1987; Burnham, 1979a); the fertility of certain likely crustal sources (Clemens and Vielzeuf, 1987); the probable heat sources (Huppert and Sparks, 1988; England and Thompson, 1986); the mechanism for segregation of the melt (Wickham, 1987); the composition and mineralogy of the melts and perhaps the likely tectonic setting.

Several initial assumptions can be made in order to constrain the source characteristics for the biotite granodiorite. The magma is likely to have higher silica contents than the source from which it was generated, which brackets the source between gabbroic to more intermediate, tonalitic compositions. The source may be located towards the base of the crust; it is in the garnet stability field; it has undepleted trace element contents, and is required to melt to leave a mafic, granulitic residual mineralogy containing garnet and little or no plagioclase.

Experimental studies for basic to intermediate compositions (gabbro and tonalite) indicate that the dry solidi for anhydrous assemblages are probably at unreasonably high temperatures (1280°C-1150°C respectively) for partial melting to occur on a scale capable of producing batholithic proportions of magma within the crust, for the common range of conditions for high-grade metamorphism (upper amphibolite to granulite facies) (Burnham, 1979a). Therefore, in order for partial melting to occur in the lower crust a pervasive fluid phase and/or a given proportion of fluid within hydrated minerals, must exist to lower the solidus to more realistic temperatures.

In the lower crust, under high grade metamorphic conditions it is improbable that a large reservoir of a free fluid phase exists. If a likely pore space of < 0.1vol.% was filled with pure water then only 0.03 wt.% H_2O would exist as a free fluid phase. Moreover the high

solubility of water in melts dictates that fluid-absent conditions would be rapidly attained after the onset of any initial fluid-present melting (Clemens and Vielzeuf, 1987). Furthermore, most crustally derived magmas appear to have been crystallized from magmas significantly undersaturated in water indicating that magma formation took place under fluid-absent conditions (Clemens and Vielzeuf, 1987). Estimates of the wt. % water in the crystallized Idaho batholith magmas are between 0.25-0.75 wt. % H_2O, using the densities and H_2O content of the common hydrous minerals from Clemens and Vielzeuf (1987). Considerable fluid flux from a crystallizing magma or partitioning into late stage fluids is likely, so that the degree of H_2O saturation of magma cannot be implied from the rocks, although the absence of large amounts of pegmatite and the lower contents of hydrous minerals in the more evolved magmas, suggests that this was not an unduly large effect during emplacement of these Cretaceous magmas. Therefore fluid-absent melting is taken to be the most likely scenario, where the degree of melting is controlled by the temperatures and pressures at which reactions involving the breakdown of micas and amphiboles occur. Thus the source is constrained to be tonalitic to gabbroic, probably containing garnet in its subsolidus assemblage and possibly biotite if the source was of more intermediate in composition.

Rock Type	Modal Proportion Hydrous Phases	Weight Proportion Hydrous Phases	Weight % H_2O
Tonalite	9.2% Hb, 13.9% Bt	11% Hb, 15% Bt	0.75
Biotite Granodiorite	5.5% Bt	6.25% Bt	0.24
Muscovite-Biotite Granodiorite	2.2% Bt, 6.0% Ms	2.5% Bt, 6.3% Ms	0.38

Table 4.7 Average water content of the Cretaceous granitoids of the Atlanta lobe, where Hb=hornblende, Bt=biotite and Ms=muscovite. Specific gravity (gcm^{-3}) Hb=3.3, Bt=3 Ms=2.8, amphibolites=2.95 and quartzofeldspathic rocks=2.65. Wt.% H_2O Hb=2, Bt=3.9 and Ms= 4.5, after Clemens and Vielzeuf (1987).

Clemens and Vielzeuf (1987) have calculated the amount of melt produced by fluid-absent dehydration reactions for a range of likely source compositions and in this way the potential fertility of a given source can be gauged. Figure 4.22a,b shows the fertility of intermediate

and mafic rock types at 10kb for fluid-absent melting in terms of the volume of melt produced at a given temperature for the calculated wt. % H_2O in a source.

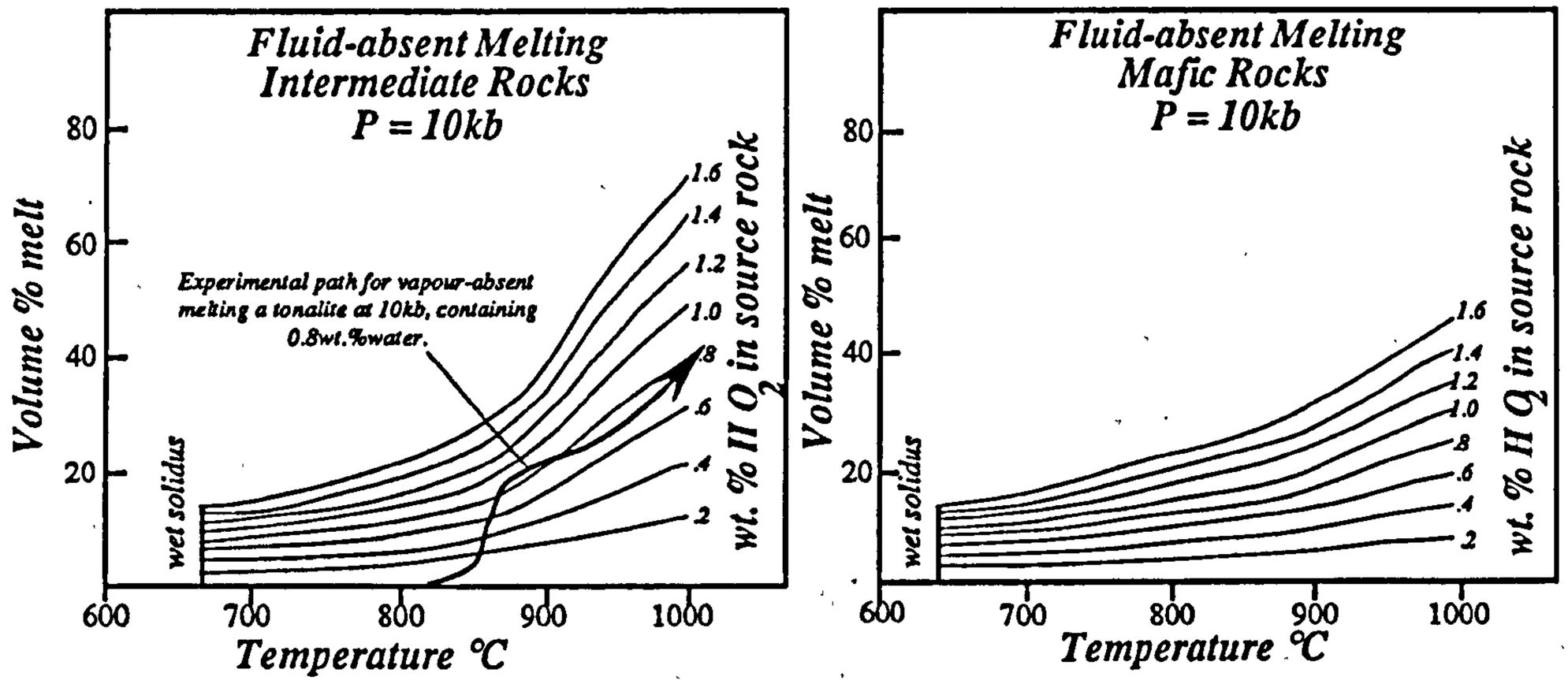

Figure 4.22 Diagram showing the amount of melt formed from fluid-absent reactions in intermediate and mafic rocks as a function of the water content and temperature of the source, after Clemens and Vielzeuf (1987). The graphs do not necessarily follow the amount of melt formed in a rock as a function of increasing temperature, but predict the amount of melt formed at the temperature that a known amount of hydrous minerals breakdown by dehydration reactions. The experimental path for vapour-absent melting tonalite at 10kb containing 0.8 wt. % H_2O stored in 12.5% biotite and 9% hornblende is superimposed from Rutter and Wyllie (1988). Between 825 and 900°C biotite dehydration produces 20% melt and by 1000°C hornblende has melted to produce 35% melt.

For intermediate compositions the dominant, and lowest temperature reaction by which melt is generated is by biotite breakdown, and this often takes the form of the following reaction:

$$Bt + Qz + Plg = Opx/Cpx \pm Grt/Crd + Kfs + Melt$$

(Clemens and Vielzeuf, 1987), and is constrained at a temperature of 870°C at 10kb by experimental studies (Naney, 1983; Hoschek, 1976 ; Rutter and Wyllie, 1988).

Hornblende breakdown occurs at higher temperatures in intermediate rocks by the reaction at 920°C:

$$Hb = Plg + Qz + Opx + Cpx + Melt$$

and in more mafic rocks by the following reaction at similar temperatures:

$$Hb + Plg = Grt + Qz + Cpx + Melt$$

(Naney, 1983; Rutter and Wyllie, 1988; Brown and Fyfe, 1970; Ellis and Thompson 1986).

The important conclusion from the point of view of this work is that plagioclase, biotite and hornblende are largely consumed in the vapour-absent dehydration reactions leaving a granulitic mineralogy essentially consisting of garnet, orthopyroxene and clinopyroxene.

The progressive changes in residual mineralogy for simulated dehydration-melting of the deep crust is shown in figure 4.23a for the same tonalite as shown in figure 4.22 at 10kb under vapour-absent conditions. For comparison a compilation of experimental results and calculations (Wyllie, 1976) for a range of compositions from gabbro to granite in temperature-X_{SiO_2} space at 10kb and X_{H_2O} = 2wt.% (although all vapour dissolves in the melt immediately above the solidus simulating vapour-absent conditions) is shown in figure 4.23b. For gabbroic compositions sodic-plagioclase reacts with hornblende to produce the first liquids, but the melting interval is dominated by the high temperature dissociation of hornblende. Hornblende and plagioclase are exhausted from the source at similar temperatures (≈1150°C) when 20%-30% by volume of melt exists. Any orthoclase is rapidly exhausted from a tonalitic source, followed by quartz and biotite, before hornblende and plagioclase are consumed at ≈ 1000°C when there is approximately 30%-40% melt.

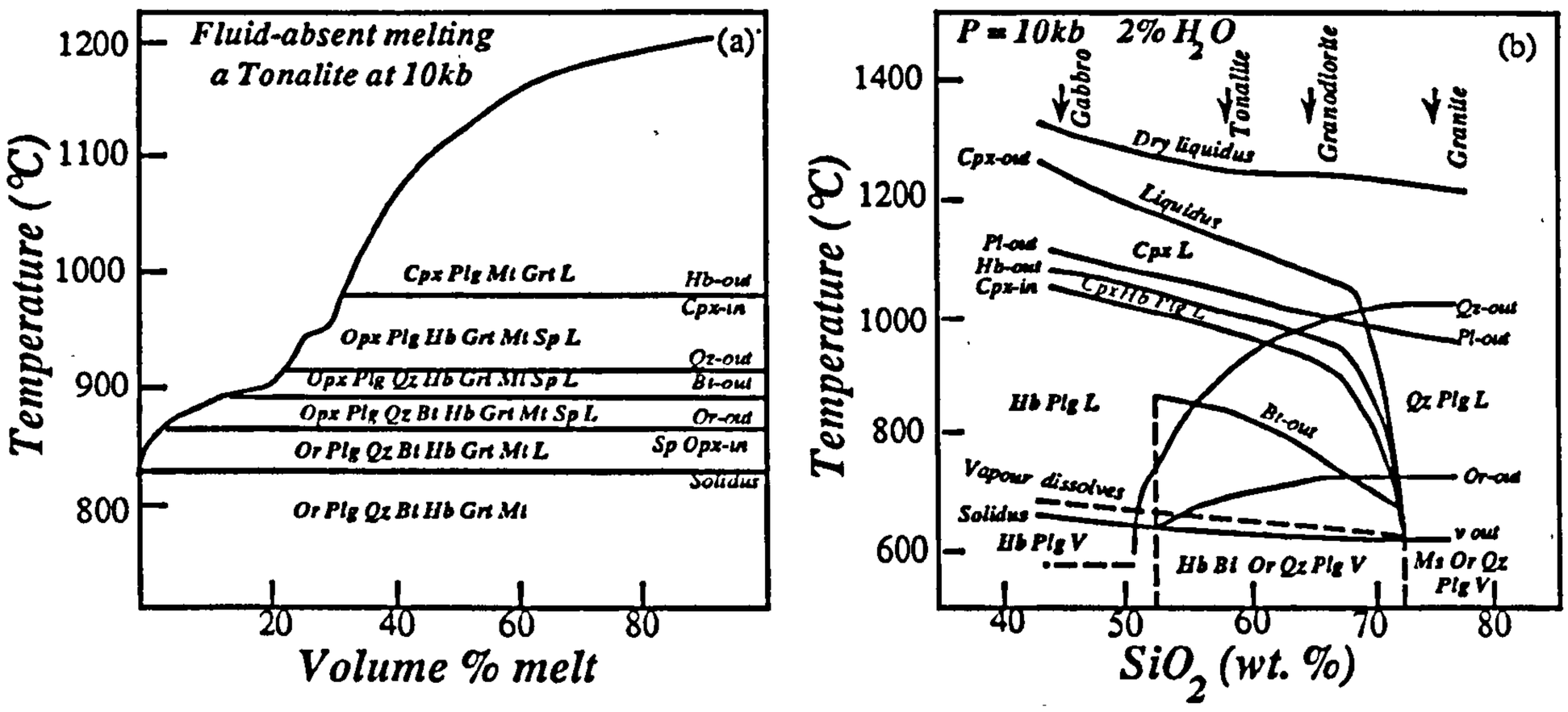

Figure 4.23 a) The effect of temperature on the melting interval of a tonalite from experimental results of Rutter and Wyllie (1988) indicating the progressive changes in residual mineralogy as minerals react and become exhausted within a source. b) Schematic temperature-composition diagram at 10kb in the presence of 2% H_2O indicating the differences in temperature of reaction for different compositions, after Wyllie (1976).

Although the actual volumes and temperatures at which melts are generated depends on the individual source rocks it is apparent that tonalitic rocks are more fertile for magma generation, but the plagioclase is only exhausted at about 40% melting, whereas in a gabbroic assemblage the plagioclase is exhausted at higher temperatures, but at lower degrees of melting.

Garnet is not consumed during melting reactions, but is commonly produced by such reactions (see previous section). Moreover garnet is reported to appear in the subsolidus assemblage during melting experiments using an initial garnet-free tonalite at pressures of 10kb (Rutter and Wyllie, 1989).

There are two commonly cited heat sources invoked to obtain the required temperatures, of up to 1000°C, for anatexis of crustal rocks: under-plating by high temperature basalts (Jaeger, 1957; Huppert and Sparks, 1988) and pressure, temperature, time paths (P,T,t paths) that intersect the solidi of common crustal rock types, by crustal thickening due to thrusting during compressive events (England and Thompson, 1986).

P,T,t paths that pass above the appropriate dehydration melting solidi only occur in cases that assume initial geothermal gradients that correspond to high surface heat flows (England and Thompson, 1986). In addition, during crustal thickening significant degrees of melting will only occur in the lower crust if large amounts of free water are introduced, unless an additional heat input is supplied (England and Thompson, 1986).

Additional heat may come from under-plating of hot basalts which have the potential to melt an equal volume of crustal material (Jaeger, 1957; Huppert and Sparks, 1988). Such bodies crystallize in relatively short time intervals (10^2-10^3a), which due to the slow diffusion of H_2O through melts (Thompson, 1988), does not allow a large H_2O contribution from even wet subduction-related basalts while the heat is available for melting (Thompson, 1988).

The tectonic environment just prior to the intrusion of the Idaho batholith (Chapter 2) favours generation of high temperatures in the lower crust due to both ponding of subduction-related magmas and crustal thickening related to the Sevier orogeny. Continuous injection and ponding of high temperature basalts at the base of the crust produced a high heat input and perhaps even some small fluid input, as a result of subduction of the Pacific slab beneath the Idaho batholith region at this time. Hyndman and Foster (1988) have cited this mechanism alone to account for the granitoids of the Bitteroot lobe, with evidence of the high temperature basalts manifested as synplutonic mafic dykes. There is an absence of

synplutonic mafic dykes in the Atlanta lobe, but ponding of basalt at the base of the lower crust is still feasible given the configuration of the subduction zone.

However, stacking of thrust plates during the Sevier orogeny in the Cretaceous to thicknesses of 50km provides a second mechanism by which melting could be triggered in the lower crust. Melting within the bottom 10km of crust is possible assuming a realistic geothermal gradient of 15°C/km and larger degree melts, by the breakdown of hornblende (at higher temperatures) as well as biotite in mafic-intermediate sources, could be attained by a combination of crustal thickening and under-plating without calling upon significant fluid flux from any under-plated basalts.

The timing of Sevier thrusting youngs to the east and is estimated at 119Ma in western Wyoming (Heller et al., 1986) and 100Ma in Nevada (Lawton, 1986). Immediately east of the Bitteroot lobe the thrusts are thought to be 80-85Ma old (Lewis, pers com., 1990) and the 85Ma White Clouds stock (Lewis et al., 1987), a satellite pluton east of the Atlanta lobe, cross cuts a Sevier thrust fault . An age of 100Ma for thrusting in the vicinity of the Atlanta lobe and a range of emplacement ages of the Atlanta lobe between 85-72Ma (Lewis et al., 1987) corresponds to the predicted time lag of "several tens of millions of years" between upper crustal thickening and attainment of the temperatures required for anatexis in the lower crust (Zen, 1989).

To summarise at this point it is probable that temperatures attained in the lower crust in the Idaho batholith region prior to intrusion of the batholith were consistent with generation of large volumes of granitoid melts by both biotite and hornblende fluid-absent dehydration reactions at up to at least 1000°C. Therefore the original source could either be basaltic or more intermediate in composition, the former bearing hornblende and the latter hornblende and biotite as the hydrous phases.

Further constraints can be placed on the original mineralogy and composition of the source from the mineralogy of the primary magma. Given that a primary magma was in equilibrium with the residual minerals in the source and is merely the product of partial melting and

separation from the source, it follows that its near liquidus minerals are likely to correspond to the minerals that are consumed in the source rock at the pressure and temperature of origin (Wyllie et al., 1976). Residual minerals with a reaction relationship do not crystallize on the liquidus of the separated liquid, but they are important for trace element fractionation and modelling. Biotite and plagioclase are the near liquidus phases of the less silicic biotite granodiorite being considered in detail here, whereas the more mafic rocks (considered later) have hornblende, biotite and plagioclase as near liquidus phases. The probable presence of biotite in the source of the biotite granodiorites argues for an intermediate composition lower crust and generation of the melts largely by biotite dehydration reactions.

Major element mass balance calculations using the inferred intermediate composition of the source and the probable undepleted, subduction related origin of the lower crust in the Idaho batholith region (see figures 4.10 and 4.20) allow limits to be placed on the probable degree of melting. Calculated degrees of melting for an assumed range of initial and residual residual compositions (Taylor and McLennan, 1985) and a liquid composition corresponding to two representative biotite granodiorites (CBC87-125, and CBC87-158) were carried out, where:

$$C_o = F\,C_l + (1-F)\,C_r \qquad \text{and so,} \qquad F = (C_o - C_r) / (C_l - C_r)$$

(C_o = original concentration; C_l = concentration in liquid; C_r = concentration in residium)

Sources either more basic and depleted, or more acidic, than a model andesite (Taylor and McLennan, 1985) yield unrealistically large (>50%) or small (<20%) degrees of melting respectively.

C_o	Andesite	Andesite	Andesite	Andesite	Bulk Crust	Bulk Crust
C_l	CBC87-125	CBC87-158	CBC87-125	CBC87-158	CBC87-125	CBC87-158
C_r	Lower crust	Lower crust	Meta-gabbro	Meta-gabbro	Lower crust	Lower crust
F_{SiO_2}	21%	21%	39%	40%	17%	18%
F_{TiO_2}	27%	32%	negative	negative	14%	16%
F_{FeO}	35%	36%	negative	negative	17%	18%
F_{K_2O}	33%	40%	32%	39%	22%	29%

Table 4.8 Results of mass balance calculations. Compositions of andesite, lower crust and meta-gabbro are from Taylor and McLennan (1985) and listed in appendix A. F is the percentage melt predicated for a particular major element.

In order that batholithic proportions of melt can separate from a residual garnet granulite assemblage Wickham (1987) has argued that melt proportions are limited within the range 30%-50% volume melts. Melt proportions of 30% on average are generated using the model andesite and lower crust of Taylor and McLennan (1985) for the original and residual source compositions respectively, and 25% melting for an original bulk crust. Calculated melt proportions are increased to 40%-50% for a depleted meta-gabbro residual composition (Bernard-Griffiths and Jahn, 1981).

A further constraint can be placed on the maximum degree of melting by the use of trace elements. By assuming that the source compositions are trace element enriched and arc related (figure 4.10) allows a model source composition to be used to examine how the bulk distribution coefficient of a particular trace element varies with the degree of melting for a given liquid composition. For batch equilibrium partial melting C_o / C_l is held constant and F and D varied. When a trace element curve on the F versus D diagram (figure 4.24) intersects the D=0 line this is the maximum amount of melting possible. The most incompatible element will intersect the D=0 line at the lowest F value and thus define the maximum amount of melting possible for a particular source. Although it must be stressed that this is a particularly circular line of reasoning to obtain a trace element signature of a source, the model andesite of Taylor and McLennan (1985) produces results between 27%-30% melting for the biotite granodiorites consistent with the major element calculations. Ba and Rb are almost equally the most incompatible elements (figure 4.24) consistent with biotite dehydration reactions. Sr is also incompatible (figure 4.24) suggesting that plagioclase is highly depleted from the source during melting. The use of a source more depleted in trace elements, such as the lower crust of (Taylor and McLennan, 1985), infers unreasonably small degrees of melting (<1%) and so further suggests that depleted sources can be discounted.

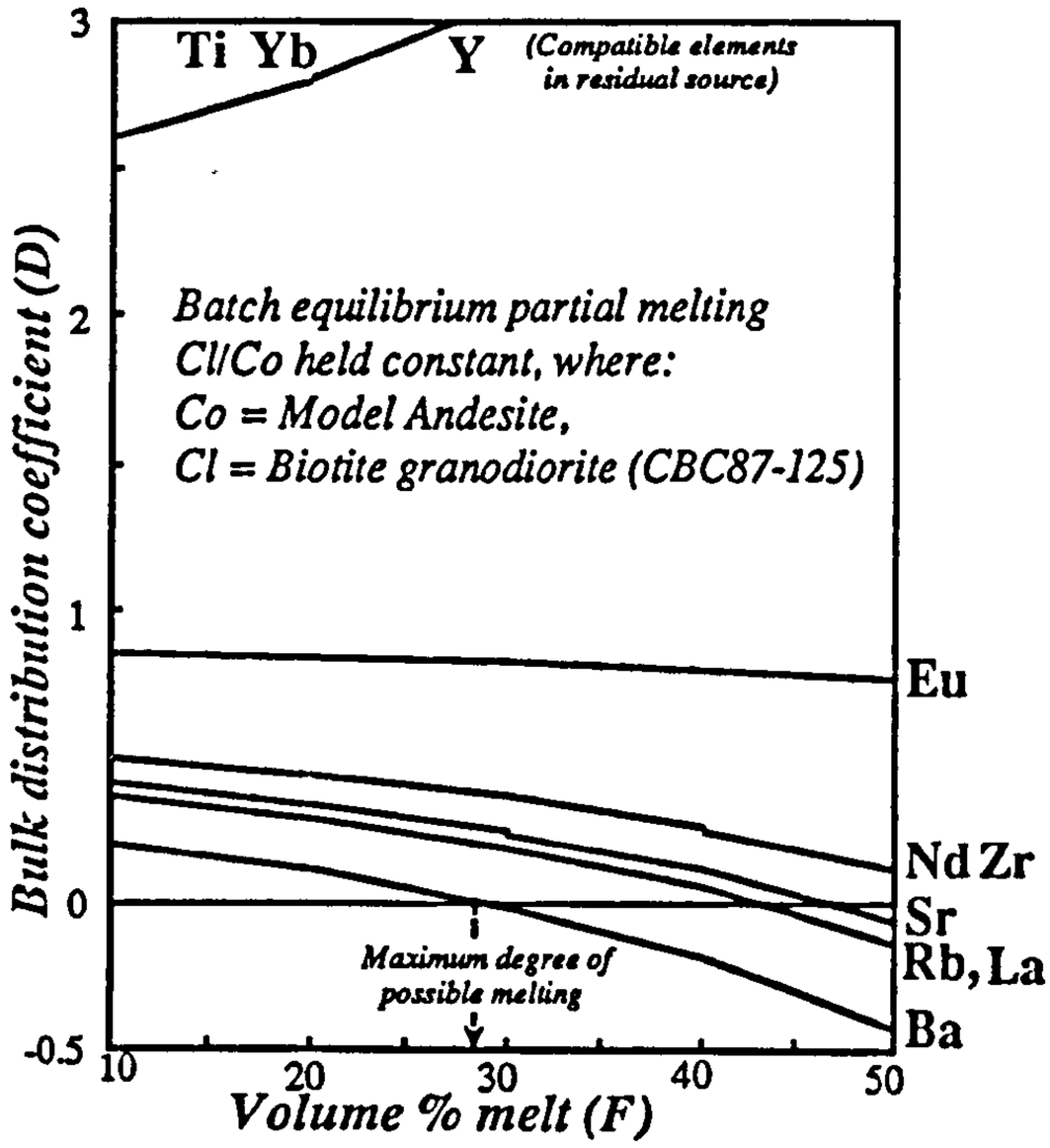

Figure 4.24 Diagram showing how the bulk distribution coefficient for a particular trace element varies with the degree of melting in order that Cl/Co remains constant. The maximum degree of melting is limited at approximately 30% melting by the most incompatible element, Ba in this case, for a given liquid composition (CBC87-125) and an andesitic source composition from Taylor and McLennan (1985).

The evidence discussed above suggests that the most feasible method of generating the biotite granodiorite is by approximately 30% melting of a biotite and hornblende-bearing source of intermediate composition, such as a tonalite, to leave a basic garnet granulite residium in the lower crust. For an initial intermediate composition containing 12.5% biotite, 9% hornblende, 4.4% alkali feldspar, 58.9% plagioclase, 13.1% quartz and 2% opaques (total H_2O=0.8 wt. %) 30 % melting is achieved at ≈960°C at 10kb (see figure 4.23, after Rutter and Wyllie, 1989). The biotite is exhausted at ≈880°C, and so the hornblende would be depleted by further dehydration reactions to generate the 30% volume melt required. The inferred residual mineralogy consists of only small amounts (≤20%) of plagioclase, 10% garnet, 28% orthopyroxene, 40% clinopyroxene and minor amounts of a Ti bearing opaque phase. However, in order to balance the large proportions of Al_2O_3 and CaO in the residue after extraction of the least evolved biotite granodiorite from the tonalitic starting composition there must be a residual phase or phases that contain significant amounts of Al_2O_3 and CaO. Hornblende and plagioclase are discounted because they are exhausted by mineral reactions, and trace element variations suggest that there were only minor amounts of residual phases with high Kd values for Sr, such as plagioclase.

Therefore, Al_2O_3 and CaO may be incorporated into calcic-clinopyroxene and grossular-rich garnet. Such assemblages are not aluminous enough to balance the liquid, source and residual proportions of Al_2O_3, but at extremely high crustal pressures (10-15kb) jadeite may become an important reservoir for Al_2O_3, due to the plagioclase-out jadeite-in reactions (Deer et al., 1966). Since Sevier thrusting thickened the crust in the region of the Idaho batholith prior to generation of the Cretaceous magmas, and garnet is another high pressure phase that played an unusually important role in generation of these magmas, the presence of jadeite may be justified in this case.

The original major element source composition is calculated to be tonalitic in composition by use of representative mineral analyses (Appendix A) consistent with the preferred source mineralogy. The approximate composition of the original source is therefore 59.8% SiO_2, 1.47% TiO_2, 19% Al_2O_3, 3.94% FeO, 2.5% MgO, 0.04% MnO, 6.5% CaO, 4.1% Na_2O and 2.1% K_2O consistent with an intermediate composition biotite and hornblende-bearing tonalite. This composition is weakly metaluminous suggesting the source had a magmatic origin consistent with the biotite granodiorites being I-type in the broad sense of the term (Section 4.2).

The trace element content of the source was then calculated using the residual mineral proportions identified above (and in appendix A) to give the bulk distribution coefficients (D), the preferred degree of melting (F), and the trace element composition of a representative parental liquid. The source composition is presented normalised to primordial mantle values in figure 4.25. The shaded field indicates the likely range of calculated source compositions calculated for different Kd values appropriate for intermediate to rhyolitic compositions (after Henderson, 1982). The favoured model is indicated in figure 4.25, in comparison to some representative crustal compositions; and the Kd and bulk D values for the preferred model are listed in table 4.9. The range of source compositions due to the uncertainties in the Kd values (shaded field) is greater than the differences in source compositions calculated for the two separate parental liquid compositions (CBC87-125 and CBC87-158).

	Ba	Rb	Th	K	Nb	Ta	La	Ce	Sr	Nd	Sm	Zr	Hf	Ti	Tb	Y	Yb
Cpx	0.06	0.09	0.05	0.01	0.8	0.4	0.6	0.9	0.14	2.1	2.7	0.6	0.34	0.7	3	1.5	2.1
Opx	0.01	0.09	0.15	0.00	0.8	0.05	0.6	0.46	0.05	0.62	0.7	0.2	0.04	0.4	1.2	0.9	1
Grt	0.02	0.01	0.01	0.02	2	0.5	0.3	0.62	0.02	0.63	2.2	1.2	0.5	1.2	5	18	28
Plg	0.36	0.05	0.04	0.19	0.06	0.05	0.32	0.24	2.94	0.19	0.13	0.1	0.07	0.05	0.15	0.1	0.08
Opq												10	25	100			
D	0.10	0.07	0.07	0.04	0.76	0.23	0.53	0.60	0.66	1.1	1.52	0.7	0.75	2.92	2.07	2.67	3.94

Table 4.9 Mineral Kd values and bulk distribution coefficient for the preferred residual mineralogy after 30% batch, equilibrium, modal, partial melting to produce the biotite granodiorite parental magma (CBC87-125 and CBC87-158). The residium contains 40% clinopyroxene (Cpx), 28% orthopyroxene (Opx), 10% garnet (Grt), 20% plagioclase (Plg) and 2% opaque and minor phases, principally sphene, magnetite and zircon (Opq). Kd values are from Henderson (1982) and references therein, and from Pearce and Norry (1979).

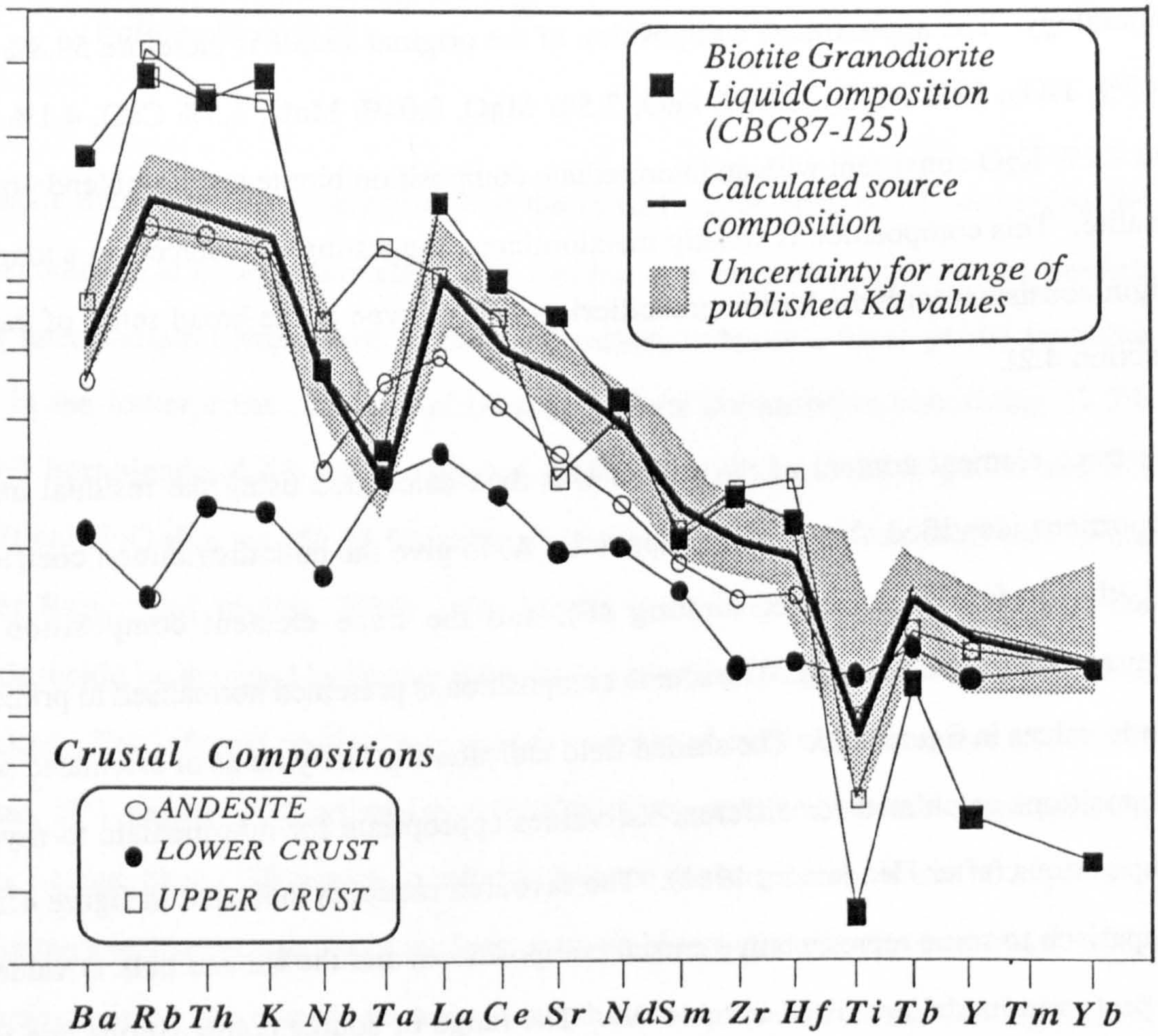

Figure 4.25 Calculated trace element composition of the biotite granodiorite source rock assuming 30% modal batch equilibrium partial melting. The shaded region represent the uncertainties for the range of possible Kd values (Henderson, 1982). The representative crustal compositions are merely for comparison (Taylor and McLennan, 1985) and the primordial mantle normalising factors are listed in Appendix A.

The trace element pattern of the calculated source has several characteristic features:

i) The high Ba/Nb and Sr/Nd ratios are typical of arc magmas (Pearce, 1983), suggesting that the lower crustal source rocks in the region of the Idaho batholith were generated by subduction related processes, if there has been no addition of mantle-derived material.

ii) The concentrations of Sr and the LREE are high, both in comparison with Rb, Ba, K, and Th and with the LREE and Sr contents of other subduction-related crustal magmas (c.f. model andesite of Taylor and McLennan, 1985 in figure 4.25). This is a result of Sr being efficiently mobilised from the source by extensive plagioclase melting so that Rb/Sr ratios are only increased by small amounts in the biotite granodiorite magmas relative to the original source composition. Rb/Sr ≈ 0.11 in the biotite granodiorite, whereas the calculated source Rb/Sr ≈ 0.07. Such melting processes have implications for the evolution and differentiation of the continental crust in terms of trace element composition and Sr isotopic signatures, where crustal reworking is often assumed to produce large changes in the Rb/Sr ratios.

iii) The garnet-bearing granulitic residual mineralogy inferred to account for the highly depleted Y and HREE contents of the Idaho batholith magmas has the potential to fractionate Sm/Nd ratios. Figure 4.25 shows that although the uncertainties due to the selection of Kd values are large, in the preferred model the Sm/Nd ratios are higher in the source than in the biotite granodiorite magmas. The time integrated effects of small changes in Sm/Nd ratios are significant in the context of model Nd age calculations and they are discussed in the light of Nd isotopic data and independent estimates of the age of the crust using Pb data in Chapter 5.

iv) The low Ta contents of the magma leads to unusually high Nb/Ta ratios calculated in the source. The source probably has higher Ta contents than the magma as a result of the presence of a stable Ta bearing phase in the residium reducing Ta in the biotite granodiorite magmas, much as the presence of residual rutile or magnetite has been implied to account for the low Ti concentrations in the biotite granodiorite magmas.

4.9.3 Within suite variation of the biotite granodiorites

The previous section summarised the effects of partial melting processes in the generation of two particular magma compositions (CBC87-125, CBC87-158). There are several possible processes by which the within-suite variations of the biotite granodiorites (figure 4.7) may be obtained. Among these are source region heterogeneity, small degrees of fractional crystallization, variable degrees of melting or mixing. The biotite granodiorites have Sr/Y (figure 4.20) and Nd/Yb ratios and concentrations of Sr, Y, Nd and Yb that systematically decrease with increasing evolution of the magmas gauged by increasing Rb or SiO_2 (c.f.figure 4.20 and figure 4.26).

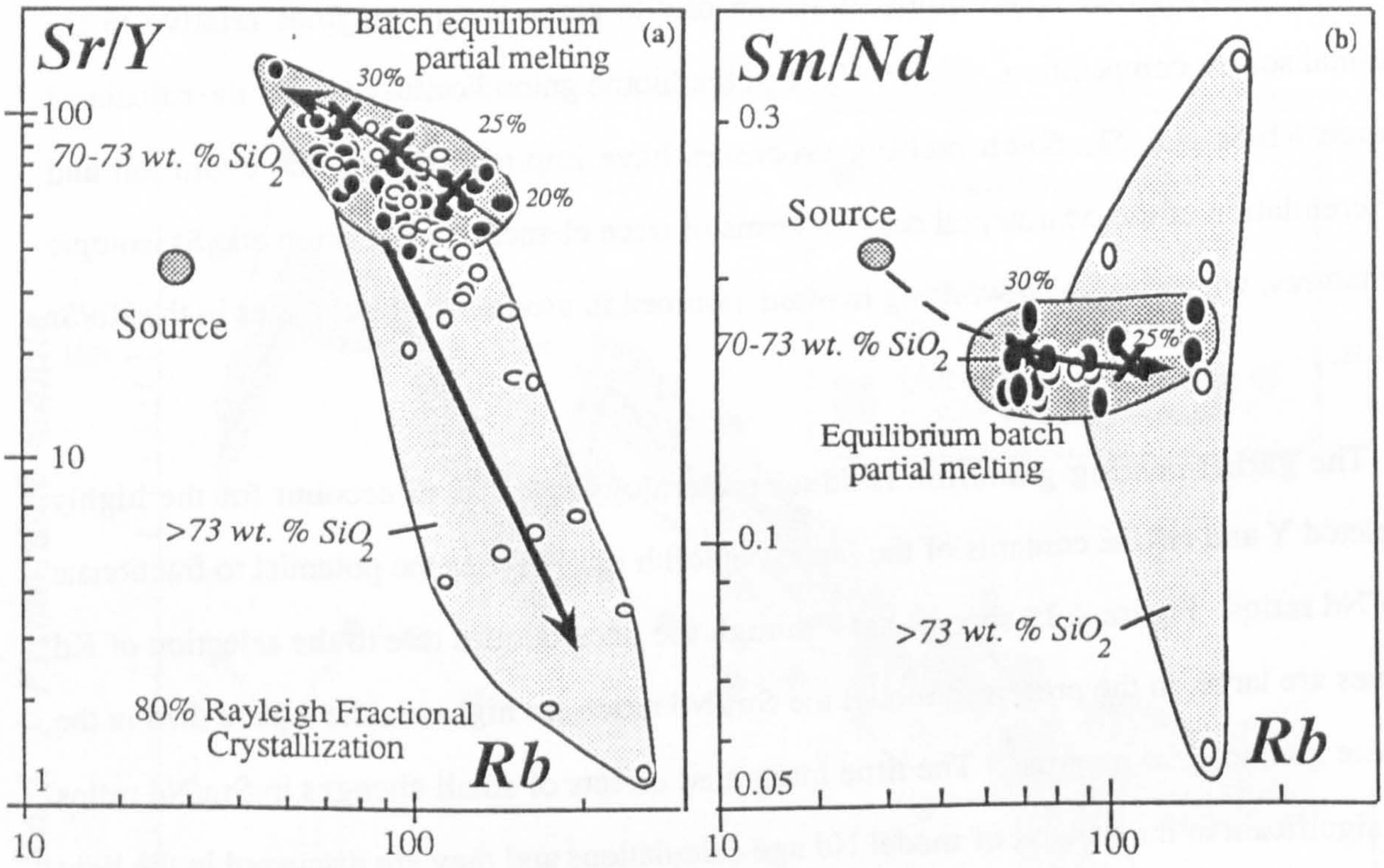

Figure 4.26 a) Variation of Sr/Y with Rb for the biotite granodiorites with ≈70-73 wt.% SiO_2 and the rocks of the Idaho batholith with greater than 73 wt. % SiO_2. Crosses for 20%, 25% and 30% equilibrium partial melting for residual assemblages progressively depleted in plagioclase are shown which successfully account for the within suite variation of the less silicic biotite granodiorites. The vector for Rayleigh fractional crystallization of the granitic mineral assemblage (calculated from major element modelling of the more evolved rocks) is shown and is of the correct order of magnitude and inclination to account for the data in the higher SiO_2 rocks. b) Variation of Sm/Nd with Rb for the limited sample set analysed by INAA. The superimposed vector for partial melting is not significantly effected by varying proportions of residual plagioclase.

These trends can be successfully modelled by increasing degrees of partial melting where the residual source assemblages are progressively depleted in plagioclase for degrees of melting

between approximately 20%-30%. This is consistent with plagioclase being gradually consumed by fluid-absent dehydration reactions at progressively higher temperatures. The changing compositions for variable degrees of partial melting (20%-30%) are superimposed on the diagram of log Sr/Y versus log Rb (crosses in figure 4.26a). The compositions were calculated for residual proportions of plagioclase of 15%-35%. The overall within suite trend for the rocks with 70-73wt.% SiO_2 can therefore be described by the line through each cross representing the continuous range of compositions generated for the range of partial melting and associated proportion of residual plagioclase. This contrasts with the trend for the rocks with greater than 73wt. % SiO_2 which are colinear with a vector for Rayleigh fractional crystallization of the granitic assemblage suggested by the major element modelling, also superimposed on figure 4.26a. The within-suite variation of Sm/Nd with Rb for the biotite granodiorites (figure 4.26b) is largely unaffected by changes in the proportion of residual plagioclase or even hornblende. Thus Sm/Nd remains near constant for the range of melt proportions but the smaller degrees of melting causing slightly greater enrichments of Rb in the magmas.

In summary the within-suite variation of the biotite granodiorites appears to have been dominantly controlled by reasonable variations in the degree of partial melting (20-30%) causing changes in the proportion of residual plagioclase. The difference in the volume of melt produced from a source is a function of temperature and/or the proportion of hydrous phases. It has been previously argued that the likely combination of basaltic underplating and crustal thickening may have produced temperatures of at least 1000°C, and so it is concluded that the degree of melting was more likely to have been limited by the proportion of hydrous phases in the source.

4.9.4 Within-suite variation of the muscovite-biotite granites and the leucogranites

The within-suite variation of the muscovite-biotite granites and leucogranites has already been largely attributed to high and variable degrees of fractional crystallization on the basis

of LILE element variation. Moreover, for closely related rocks, it can be demonstrated that the REE show systematic behaviour consistent with Rayleigh fractional crystallization.

CBC87-78 and CBC87-79 are two such closely related muscovite-biotite granites with a high LREE/HREE ratio and a positive Eu/Eu^* anomaly and a low LREE/HREE ratio and a negative Eu/Eu^* anomaly. Assuming that these rocks represent a relatively evolved liquid and a cumulate composition respectively, and that Rayleigh fractional crystallization was the dominate processes the bulk distribution coefficients (D) can be calculated using the equation:

$$C_{cumulate} = DC_{liquid}$$

D values can then be substituted back into the the Rayleigh fractional crystallization equation to obtain an internally consistent starting composition for a given degree of crystallization (30%). All the results are shown graphically in figure 4.27 including the calculated bulk D values which are compared with those estimated for a realistic fractionating assemblage containing plagioclase, alkali feldspar, quartz and muscovite and minor amounts of allanite, apatite and zircon.

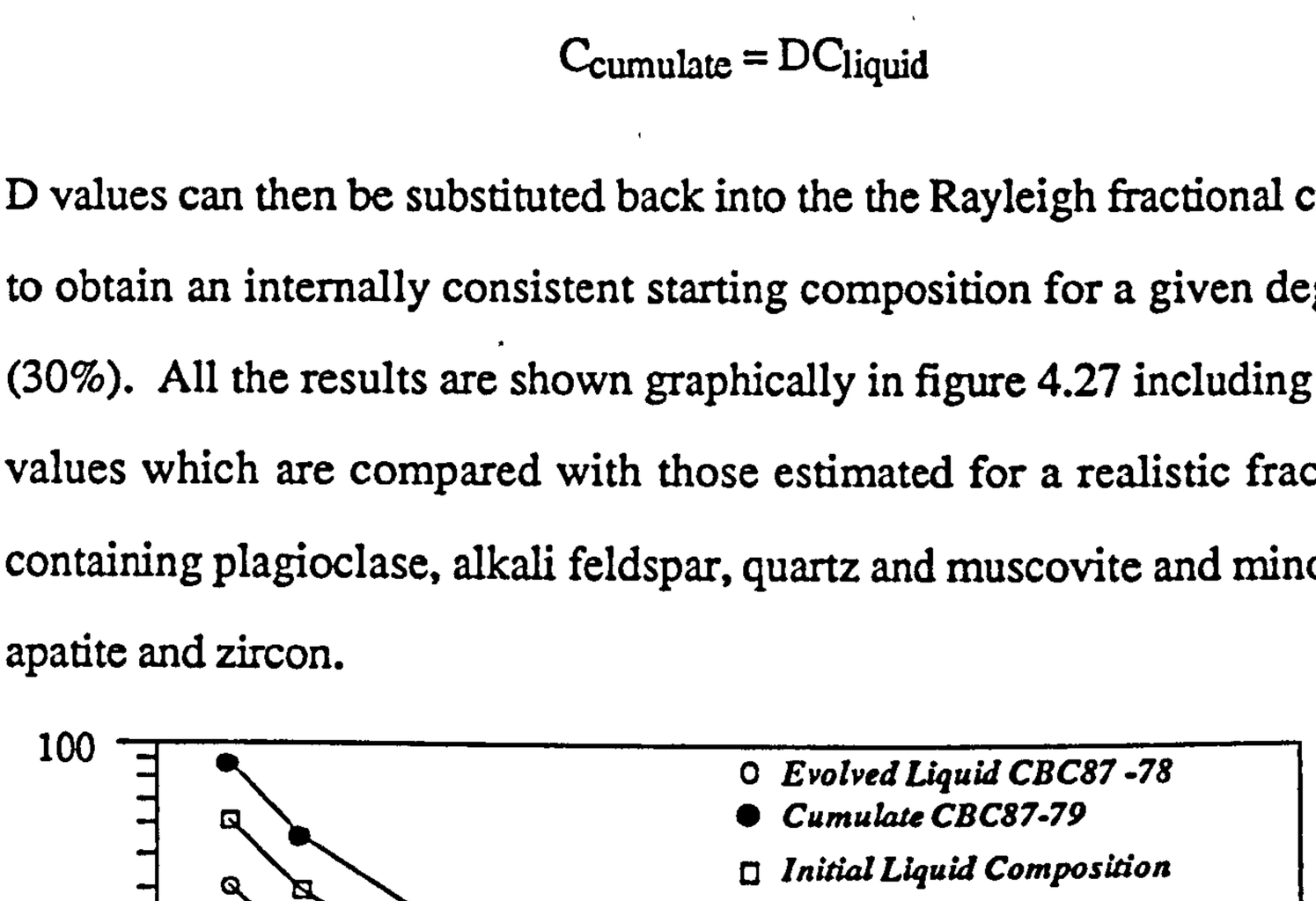

Figure 4.27 Internally consistent model for 30% Rayleigh fractional crystallization of the mineral assemblage in the cumulate rock CBC87-79 noted during petrographic studies. The proportions of the observed minor phases are taken to be 0.2% allanite, 0.1% apatite and 0.1% zircon.

The latter accessory phases were all noted during petrographic studies of CBC87-79 and they have distinctive high bulk distribution coefficients for the REE, described by Henderson, (1982). The only obvious discrepancy between the calculated D values are those for the middle order REE which could be accounted for by the presence of sphene, a commonly noted phase, but not recorded in CBC87-79. The initial assumption that, $C_{cumulate} = DC_{liquid}$, suggests that CBC87-79 consists of 100% cumulate phases, whereas in reality only a small proportion of the rock is composed of truly accumulated minerals. Thus the assumption would have been invalid until it was recognised that the majority of the REE budget would be contained in the fractionating minor and accessory phases which have extremely high REE contents.

Although fractional crystallization is certainly a dominant process in the more evolved rock types, rather scattered variations of Sm/Nd with Rb (figure 4.26) and the often variable Sr/Y ratios with silica (figure 4.23) may require some further explanation for the REE in the more evolved magmas. In addition to the variable REE contents of these rocks, certain leucogranites and a few of the muscovite-biotite granites have high initial $^{87}Sr/^{86}Sr$ ratios. Such rocks are thought to be the result of upper crustal melting where magmas are wholly derived from or become highly contaminated with the small degree melts that typically form small leucogranite stocks, dykes and veins. It has been suggested that the small leucogranite stocks represent the magmas which separated from the migmatites developed in the upper crustal country rocks on the margins of the batholith (Chapter 3). This is consistent with the inefficient extraction of highly viscous silicic magmas from source rocks at low degrees of melting so that only small granitic bodies rather than batholithic quantaties of magma may accumulate. Sample CBC87-42 is such a sample from close to the southwestern margin of the Atlanta lobe. It has a flat REE profile with high abundances, a large negative Eu/Eu^* anomaly (figure 4.15) and high initial $^{87}Sr/^{86}Sr$ and low $^{143}Nd/^{144}Nd$ ratios typical of ancient upper crustal rocks.

Previous workers have grouped the peraluminous granitoids of the Idaho batholith, the muscovite-biotite granites and the leucogranites, with the two-mica granites that form a

north-south trending belt collectively into the "inner cordilleran belt" (Miller and Bradfish, 1980). Included in this group are the two-mica granites of northeastern Washington (Asmerom et al.,1988), the Kern Mountains of northeast Nevada (Best et al., 1974) and the Ruby mountains of Nevada. It has been argued by the above authors that the two-mica granites are anatectic in origin and were generated as a result of crustal thickening during the Sevier orogeny (e.g. Miller and Gans, 1989). This is consistent with the coincidence of the north-south trending belt of granites with the hinterland of the Sevier thrust belt that has undergone high grades of Mesozoic and Cenozoic regional metamorphism.

Although it has been previously argued that crustal thickening is important to produce the high temperatures and the high pressures required for generation of the Idaho batholith magmas, it is thought that the large volumes of two-mica granites were not produced from a metasedimentary source at intermediate to shallow levels in the crust. The favoured interpretation is that the muscovite-biotite granites and the leucogranites represent the differentiates of the biotite granodiorites, because of their low initial $^{87}Sr/^{86}Sr$ ratios, the depleted HREE contents and the high LREE/HREE ratios. However, the presence of small stocks with high initial $^{87}Sr/^{86}Sr$ ratios, high and unfractionated REE abundances and high Nb+Y suggest that some small volumes of upper crustal melts have been generated and are probably related to the migmatite zones as noted above.

4.9.5 Melting models and source composition of the Tonalites and Hornblende-biotite granodiorites

In section 4.8.1 (LILE modelling) it was shown that the variation in composition of the tonalites through to the hornblende-biotite granodiorites can not satisfactorily be modelled simply by increasing degrees of fractional crystallization.

In this section the source compositions of the tonalites and the hornblende-biotite granodiorites are modelled using equilibrium partial melting models. The models were constrained and modified by the same iterative method used for the biotite granodiorites,

evaluating several lines of independent evidence to suggest realistic bulk distribution coefficients (D) and the degrees of melting (F).

The models were developed by assuming that the source compositions were more mafic than the least evolved sample from each suite: CBC87-145 for the tonalites and CBC87-144 for the hornblende-biotite granodiorites. The moderate to low Y and HREE concentrations in the magmas (figure 4.7 and 4.30) suggest that garnet was a residual phase in the source; that melting occurred at elevated temperatures in the lower crust, and that the magma was extracted to leave a granulitic residual mineralogy. Crustal thickening and ponding of basalts likely at the time of formation of the Idaho batholith (previous section) allow the extreme conditions of temperature of metamorphism required for large degrees of melting. Fluid-absent conditions are thought to be most likely in the lower crust, as stated previously, and so melting was taken to occur by fluid-absent dehydration reactions, although some small fluid flux is possible if continuous upwelling and ponding of subduction related basalts occurred.

The tonalites and hornblende-biotite granodiorites are enriched in Sr (figure 4.7), they have high LILE/HFSE ratios and fall into the volcanic arc field of Pearce et al. (1984) in figure 4.11. The positive correlation between Eu/Eu* and Sr or Sr/Nd ratios, in the magmas, suggest that parental magmas with Eu/Eu* anomalies of ≥1 have extremely high Sr/Nd ratios of at least 35, typical of magmas generated by suduction-related processes. Thus the source is thought to be enriched in trace elements similar to that of the biotite granodiorites, typical of a crust generated by subduction-related processes rather than a lower crust depleted in trace elements by a history of crustal reprocessing events.

Estimates of the degree of melting were deduced by trace element modelling, assuming that the maximum possible degree of melting was limited by the point at which the most incompatible element was finally depleted from a given source composition and concentrated in the magma. The same procedure was followed as that for the biotite granodiorites, holding Co/Cl constant and plotting the variation of D with F, where Co is the model andesite of Taylor and McLennan (1985).

The results are graphically illustrated in figure 4.28a and b for the tonalites and hornblende-biotite granodiorites respectively. Rb and Sr are the most incompatible elements for the tonalite, limiting the maximum degree of melting to ≈47%, while the maximum degree of melting for the least evolved hornblende-biotite granodiorite is limited to 35% by Ba which behaves most incompatibly. The high concentrations of Sr in these two parental liquids are consistent with a lack of residual plagioclase and consistent with the experimental results which suggest that plagioclase is exhausted at higher temperatures, but lower degrees of melting in mafic sources (Wyllie, 1976).

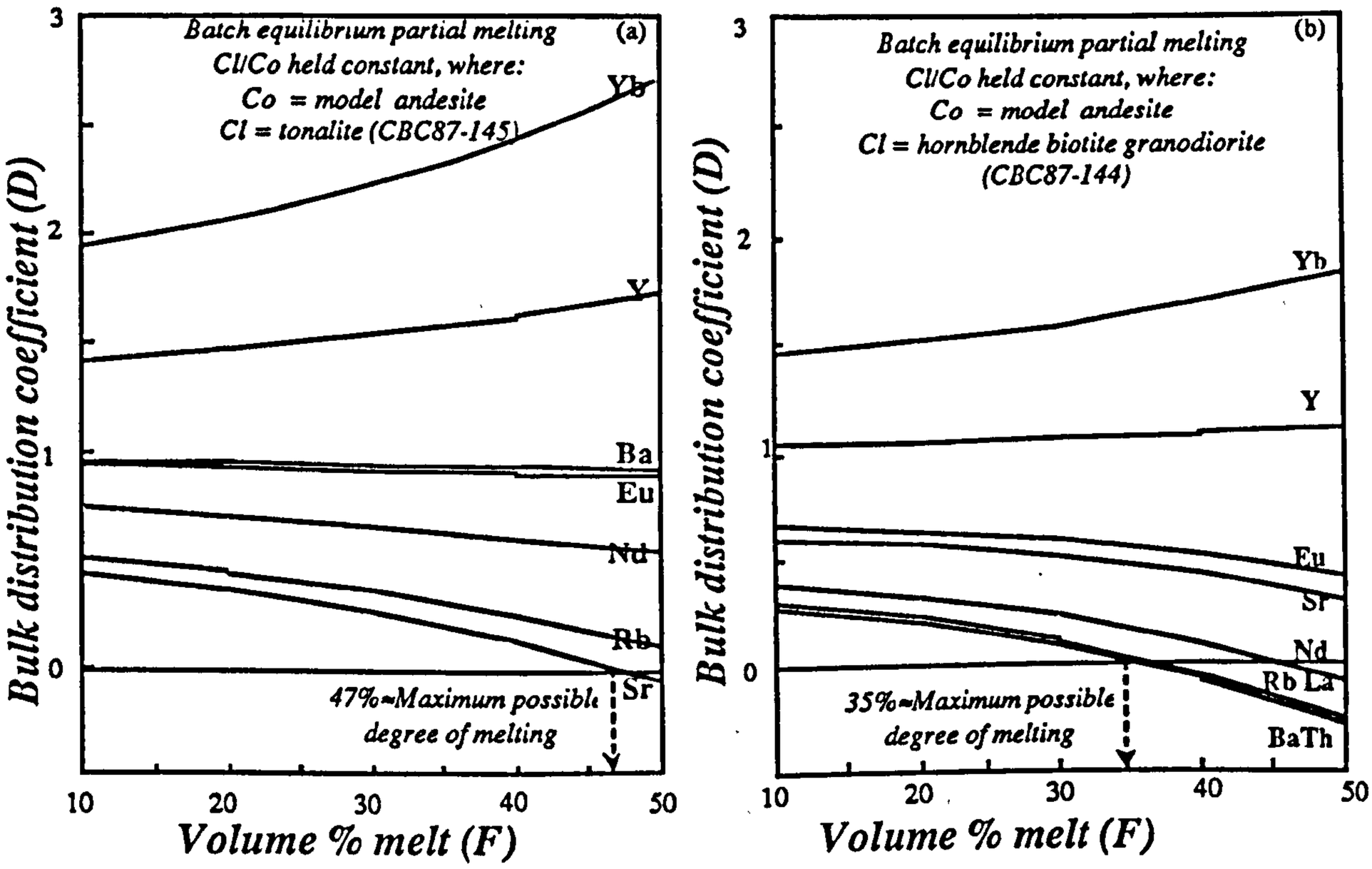

Figure 4.28 a) Diagram showing how the bulk distribution coefficient for a particular trace element varies with the degree of melting in order that Cl/Co remains constant. The maximum degree of melting is limited at approximately 45% melting for the tonalites by the most incompatible element, in this case, Rb and Sr for a given liquid composition (CBC87-145) and an andesitic source composition from Taylor and McLennan (1985). b) The same diagram for the hornblende-biotite granodiorites where melting is limited by Ba and Th to a maximum of 35% .

Clemens and Vielzeuf (1987) have shown that the potential fertility of mafic rocks for a given hydrous mineral content, under fluid-absent conditions, is less than that for more intermediate compositions (see figure 4.22). The need for a source of more mafic composition than the parental magmas at 54 and 64 wt. % SiO_2 for the tonalites and hornblende-biotite granodiorites respectively implies that the source had a high proportion of

hydrous phases. Hornblende was probably the only modally significant hydrous phase in mafic source rocks and is present as the dominant hydrous mineral and crystallizes as a near liquidus phase in the tonalites and the hornblende-biotite granodiorites. Biotite is less likely to be present in mafic sources and only crystallizes as a late phase in the tonalites and hornblende-biotite granodiorites.

35% and 45% melting requires 1.2 and 1.6 wt.% H_2O at 1000°C in mafic rocks under fluid-absent conditions at 1000°C and 10kb, which implies that the sources contained 60 and 80 wt. % hornblende for the hornblende-biotite granodiorites and tonalites respectively. The common range of hydrous mineral content for the major mafic metamorphosed rock types is 36-80 wt.% hornblende (Clemens and Vielzeuf, 1987) which makes the above hypothesis just plausible. Assuming that melting occurs by hornblende dehydration reactions, (as indicated for the biotite granodiorites section 4.9.1) suggests that plagioclase would be largely consumed, and so Sr would be highly incompatible and concentrated in the magmas. The major element composition of the original source can either be assumed to be that of a published gabbroic composition or calculated for mineral assemblages containing 60 and 80 wt.% hornblende necessary for the melting reactions. Either way, mass balance calculations then allow the major element composition of the residual source region (C_r) to be calculated

where: $C_o = FC_l + (1-F)C_r$

and so $C_r = (C_o - FC_l) / (1-F)$

Calculated compositions for the preferred residual mineralogies can then be compared with the residual source compositions calculated above. Results are listed in table 4.9 and show that the oxides Fe_2O_3, MgO, TiO_2 are very similar in both calculated residual compositions and the small discrepancies can easily be accounted for by small changes in the proportion of minor phases such as magnetite or sphene. The alkalis are also balanced between their concentration in the magma, the original source and the residium. However, the high concentrations of Al_2O_3 and CaO in the residium after extraction of the least evolved tonalite and hornblende-biotite granodiorite are not consistent with granulitic assemblages dominated by clinopyroxene and orthopyroxene and minor amounts of plagioclase and garnet.

	Residual composition of source (C_r) after 45% melting to produce the tonalite CBC87-145 (C_l)		Preferred residual mineralogy of tonalite	Residual composition of source (Cr) after 35% melting to produce the Kgdh (CBC87-144)		Preferred residual mineralogy of Kgdh
	C_o=Gabbro	C_o=80%Hb + 20%Plg	20%Plg+10 %Gt+30%Cpx+40%Opx	C_o=Gabbro	C_o=60%Hb+ 40%Plg	25%Plg+5% Gt+30%Cpx +40%Opx
SiO_2	38.8	40	55	38.8	43	55
Al_2O_3	13.9	10	9	13.9	16.6	10
TiO_2	1.22	1.6	0.5	1.22	1.11	.5
Fe_2O_3	14.21	20.6	18	14.21	14.4	17
MgO	10.6	12	11	10.6	8.4	10
CaO	16.8	14	3.3	16.8	14.3	3
Na_2O	1.13	1.07	1.76	1.13	2.16	2
K_2O	-1.15	-0.25	0.4	-1.15	-0.4	0.5

Table 4.10 Results of mass balance calculations showing the problem in balancing the high concentrations of Al_2O_3 and CaO in the source and those in the preferred granulitic residual mineralogies when plagioclase and hornblende have largely been consumed by dehydration reactions.

Therefore an alumina and lime-bearing phase must be residual in the source. Hornblende may be ruled out since it is probably entirely consumed by dehydration reactions to produce the required amounts of melting; large amounts of plagioclase are discounted by the need to enrich the magmas in Sr; and large amounts of residual garnet are inconsistent with the moderate depletions of the HREE in the tonalites and the hornblende-biotite granodiorites. Kyanite or sillimanite are ruled out because they are only likely to be stable in highly peraluminous rocks such as metapelites.

Alternatively the starting composition may have lower concentrations of Al_2O_3 and CaO than assumed implying that there may have been little plagioclase in the initial source rocks and that the high Sr anomaly in the magmas is merely inherited from a high concentration of Sr in the source. The preferred explanation is a compromise where calcic-clinopyroxene and grossular rich garnet together with up to 20% plagioclase, 5% garnet and 10% hornblende may remain in the residium and account for the alumina and lime concentrations. Such a model would be facilitated by influx of sub-crustal fluids, so that less hornblende is required in the initial source for dehydration reactions.

Moreover, a model which assumes a lack of plagioclase cannot specifically be limited to crustal sources, but must take into account the possibility that magmas, or components of the magmas, may have been derived from the sub-continental mantle lithosphere.

Traditionally, extrusive and intrusive andesites and diorites have been interpreted to be the product of differentiation of mantle-derived basaltic magmas, such as the classic examples from the Andes (Thorpe,1984). In the western United States cordillera the large amounts intrusive gabbros to granites are interpreted to be the products of either mixing or assimilation/fractional crystallization of such mantle-derived basalts or their andesitic fractionates with crustal components. Therefore the possibility that the tonalites are either fractionated basaltic mantle-derived melts, or at least contain a significant component of mantle-derived material must be considered and investigated isotopically in Chapter 5.

Fleck and Criss (1985) argued that mixing of high Sr, low initial $^{87}Sr/^{86}Sr$ mantle derived magmas with low Sr, high initial $^{87}Sr/^{86}Sr$ Precambrian metasediments accounted for the range of intermediate Sr concentrations and initial $^{87}Sr/^{86}Sr$ ratios of the tonalites and granodiorites intruded across the suture zone between old Proterozoic lithosphere to the east and the young oceanic island-arc accreted terranes to the west of the northern Atlanta lobe.

In summary, the trace elements may be explained without a contribution from a mantle-derived component, and so it is consistent that the tonalites and hornblende-biotite granodiorites were derived by ≈35% and ≈45% dehydration melting of mafic amphibolites in the lower crust to leave granulitic mineralogies with only minor amounts of residual plagioclase and hornblende. The trace element compositions of the calculated sources of the tonalites and hornblende-biotite granodiorites and the preferred residual mineralogies are shown in figure 4.29 and figure 4.30 respectively.

Following the procedure in section 4.9.2, a residual mineralogy of 20% plagioclase, 5% garnet, 30% clinopyroxene, 40% orthopyroxene and 5% hornblende was used to calculate the primordial mantle normalised trace element abundance patterns (figure 4.29). Small adjustments to the values of D_{Ti} and D_K were made by inferring some residual magnetite and phlogopite because of the low concentrations of Ti and K in the tonalitic magmas.

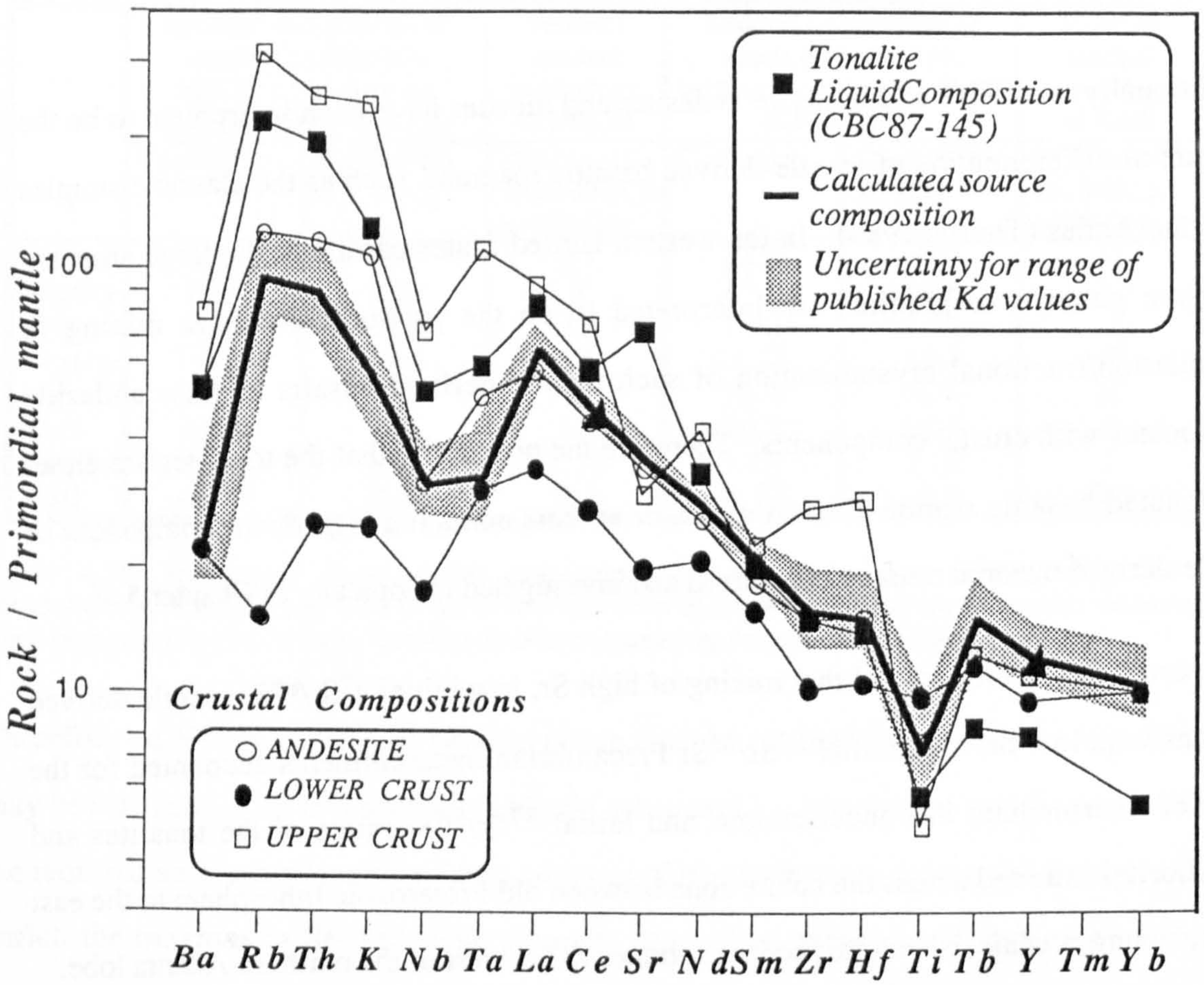

Figure 4.29 Calculated trace element composition of the tonalite source rock assuming 40% batch equilibrium melting. Shaded region are the likely uncertainties for the range of possible Kd values (Henderson, 1982), the representative crustal compositions are merely for comparison (Taylor and McLennan, 1985) and they and the primordial mantle normalising factors are listed in Appendix A.

The dominant trace element characteristics of the tonalite source are:

i) High LILE/HFSE ratios typical of magmas generated in magmatic arcs by subduction related processes (Pearce, 1983).

ii) The trace element abundances are similar to the model andesite of Taylor and McLennan (1985), apart from the LILE elements which appear to be less abundant. The unusually low LILE/LREE ratios are probably the result of the high published Kd values for the LREE in ortho- and clinopyroxenes in equilibrium with intermediate composition magmas and their high concentration in the residual mineralogy.

iii) Potassium is lower in the tonalitic magmas than the other granitoids, and if it is assumed to be similar in relative concentration to the other LILE in the source, it suggests that small amounts of phlogopite may have been present in the source.

iv) Sr is highly incompatible with the result that Rb/Sr ratios in the source and magma are 0.078 and 0.092 respectively, which is an unusually small fractionation for a major magmatic crustal reprocessing event.

iv) Sm/Nd ratios are only slightly higher in the source rocks than the least evolved tonalite due to the small amount of residual garnet used in the model.

The trace element abundances in the source of the hornblende-biotite granodiorites are calculated using a residual mineralogy of 25% plagioclase, 3% garnet, 30% clinopyroxene and 40% orthopyroxene and minor amounts of magnetite, rutile and phlogopite (figure 4.30). The high LILE/HFSE ratios similar to that of the tonalitic magmas again suggest that the source rocks were generated by subduction-related magmatic processes.

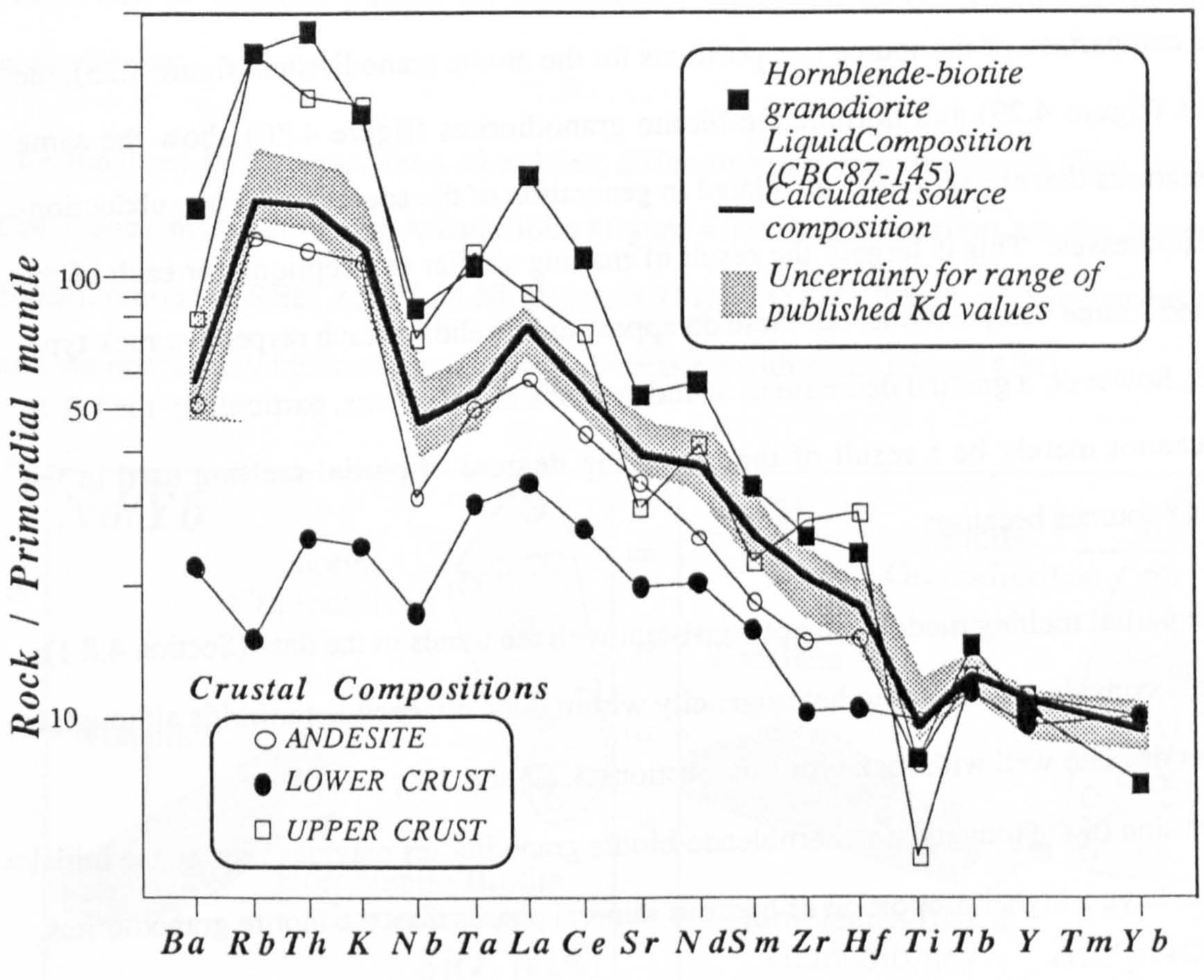

Figure 4.30 Calculated trace element composition of the hornblende-biotite granodiorite source rock assuming 35% batch equilibrium melting. Shaded region are the likely uncertainties for the range of possible Kd values (Henderson, 1982), the representative crustal compositions are merely for comparison (Taylor and McLennan, 1985) and they and the primordial mantle normalising factors are listed in Appendix A.

The slightly higher LILE/LREE ratios in the source of the hornblende-biotite granodiorites with respect to the source of the tonalites are due to the lower LILE/LREE ratios in the magmas which in turn are a result of the LREE/HREE being less fractionated by residual garnet in the hornblende-biotite granodiorites. Only small amounts of garnet are necessary to account for the depletion of Yb in the magmas and over 20% residual plagioclase is consistent with the small increase in Sr from source to magma. Thus larger Rb/Sr and smaller Sm/Nd source to magma fractionation occurs in these rocks than in the tonalites or the biotite granodiorites (Rb/Sr_{source} =0.1, Rb/Sr_{magma}= 0.18 and Sm/Nd_{source} = 0.224, Sm/Nd_{magma} = 0.19). The positive Th anomaly is largely removed from the source composition by invoking small amounts of residual phlogopite.

Overall comparison of the source compositions for the biotite granodiorites (figure 4.25), the tonalites (figure 4.29) and hornblende-biotite granodiorites (figure 4.30) show the same major features that are argued to be related to generation of the source rocks by subduction-related processes. This is largely the result of making similar assumptions for each of the calculated source compositions, but these do appear to be valid for each respective rock type. There is, however, a gradual decrease in abundance of trace elements, particularly the LILE, which cannot merely be a result of the increasing degrees of partial melting used in the modelling sources because:

i) simple partial melting models are not consistent with the trends in the data (Section 4.8.1);

ii) there is considerable isotopic heterogeneity within the Cretaceous granitoids although it does not correlate well with rock type (see sections 5.2.2 and 5.4);

iii) generation of the tonalitic and hornblende-biotite granodiorites magmas require the initial sources to have a higher proportion of hydrous mineral phases than the biotite granodiorites.

The reduced trace element abundances in the source of the tonalites, for example, with flatter primordial mantle normalised patterns are thought to be derived from a differentiated lower crust where the more mafic source rocks have lower trace element abundances and lower LILE/REE ratios.

4.9.6 Within-suite variation of the tonalites and hornblende-biotite granodiorites

The within suite trace element variation of the tonalites and hornblende-biotite granodiorites is difficult to assess due to the small number of samples and the large scatter within the trends, probably reflecting the large geographical separation of the samples.

Figure 4.7 shows that the trace element variations in the hornblende-biotite granodiorites often follow similar trends to the biotite granodiorites, but at slightly lower silica values. This may be due to variable degrees of partial melting because of differences in the amount of hornblende in the original source rock, the degree of melting being limited by the proportion of hydrous phases for dehydration reactions, as described for the biotite granodiorites.

The tonalites in contrast, tend to exhibit different trace element trends than the other Cretaceous magmas of the Atlanta lobe (figure 4.7). Most apparent are the increasing concentrations of REE, Zr, Y and Nb (figure 4.7) and the ratio Nd/Yb with increasing silica and the less steeply inclined trend of Sr/Y decreasing with silica (figure 4.31).

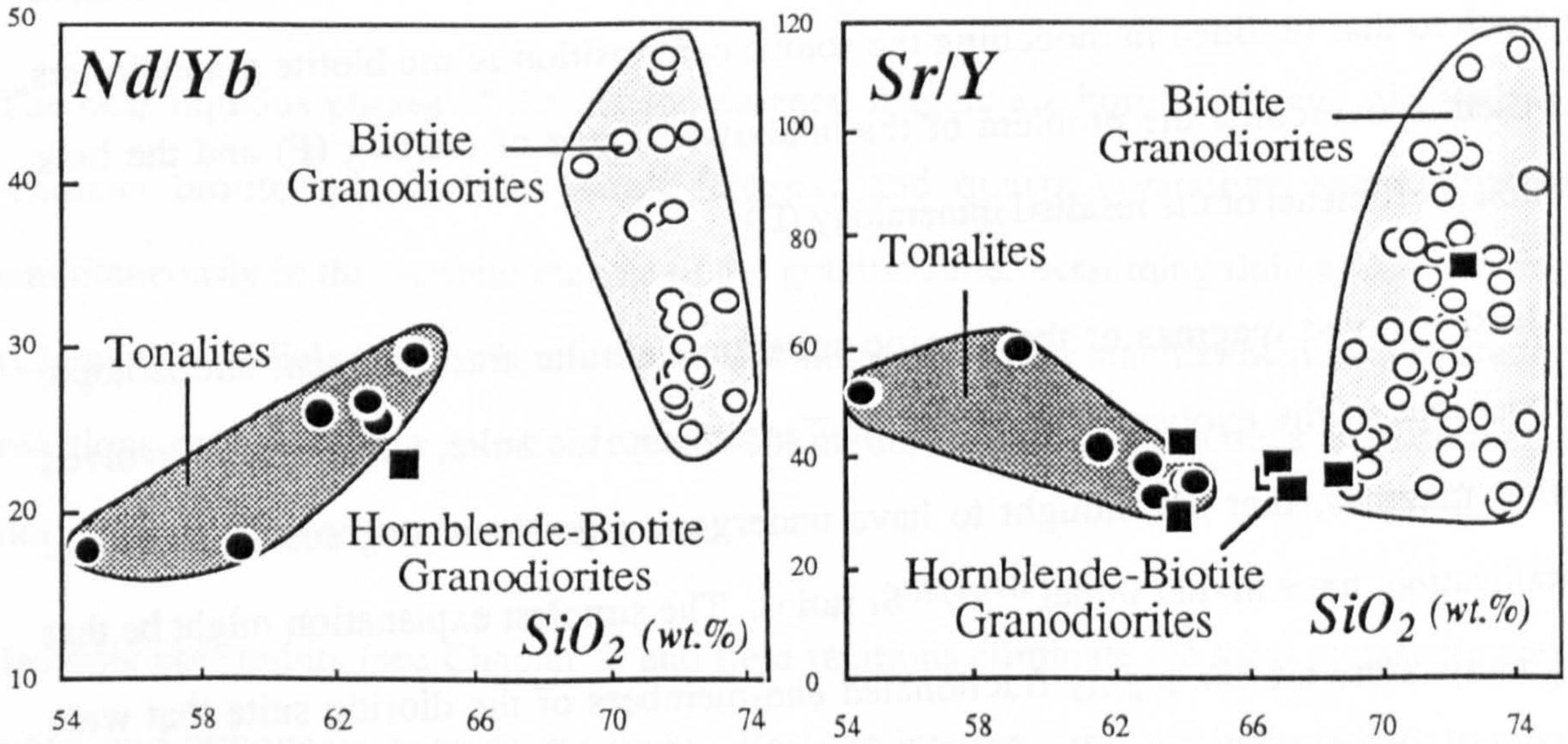

Figure 4.31 Nd/Yb and Sr/Y ratios of the tonalites, hornblende-biotite granodiorites and less evolved biotite granodiorites.

These variations and the increasing concentrations of the generally incompatible trace elements Rb, La, Ce, Th, and the decreasing concentrations of Sr, Al_2O_3, CaO, Fe_2O_3 and MgO are consistent with limited fractional cystallization of hornblende and plagioclase dominated assemblages. Initial increases in the concentration of TiO_2, Fe_2O_3 and P_2O_5 before gradual decreases within the trend of the tonalites (figure 4.2) are thought to be the result of the mafic magmas being initially undersaturated in TiO_2, Fe_2O_3 and P_2O_5 for magnetite and apatite to crystallize, but in more silicic magmas at higher concentrations of the above elements crystallization occurs.

4.9.7 Partial melting models and source composition of the Tertiary dioritic suite and granitic suite

The within-suite major and trace element variations of the dioritic suite have been convincingly modelled by fractional crystallization of plagioclase and hornblende-dominated assemblages. The granitic suite, however was modelled by high degrees of fractional crystallization of biotite, alkali feldspar, plagioclase and quartz.

In this section the parental magmas of the dioritic suite are modelled by batch equilibrium partial melting to obtain a likely source composition for the magmas. A similar iterative approach to that outlined in modelling the source composition of the biotite granodiorites was used to overcome the problem of the unknown degree of melting (F) and the bulk partition coefficients of the residual mineralogy (D).

The least evolved magmas of the granitic suite have similar trace element and isotopic compositions to the evolved samples of the Tertiary dioritic suite, but the more evolved granitic magmas, that are thought to have undergone significant degrees of fractional crystallization, have higher initial $^{87}Sr/^{86}Sr$ ratios. The simplest explanation might be that the granitic suite are the highly fractionated end-members of the dioritic suite that were separated and emplaced at shallow levels in the crust, where they underwent some upper crustal contamination to account for the isotopic differences. There are several reasons to doubt this hypothesis including the field evidence which indicates that rocks are distinctly

bimodal with no gradations of one suite into the other; there are highly evolved granitic magmas that have intermediate initial $^{87}Sr/^{86}Sr$ ratios; and the two suites are not always contemporaneous. The approach taken here is to model a source composition for the least evolved sample of the granitic suite to test whether it may have been generated from a plausible source composition by a realistic melting process. In addition the granulitic residue after extraction of the Cretaceous magmas is demonstrated to be an unrealistic source for the Tertiary granitic magmas despite suggestions to the contrary (Bennett and Knowles, 1985).

The least evolved magma from the Tertiary dioritic and granitic suites, CBC87-105 and CBC87-132 respectively are assumed to be parental magmas. Both rocks have high LILE/HFSE ratios, undepleted HREE abundances significantly higher than those of the Cretaceous magmas, metaluminous and weakly peraluminous compositions respectively, high Sr concentrations and no Eu/Eu* anomalies. Similar lines of evidence were used to imply that the Cretaceous magmas were derived from enriched crustal sources typical of crust generated by igneous processes related to subduction. Such inferences are probably valid here, but the undepleted HREE and smaller LREE/HREE ratios are used to imply that residual garnet was not present and that melting occurred at shallower levels due to crustal attenuation than the Cretaceous melting event.

The near liquidus phases of the dioritic parental magma are hornblende and plagioclase, whereas biotite, plagioclase, alkali feldspar and quartz crystallize approximately simultaneously in the parental magma of the granitic suite. Assuming fluid-absent melting (Clemens and Vielzeuf, 1987), the above assemblages suggest that hornblende-dehydration reactions gave rise to the dioritic magmas, but biotite-dehydration reactions were dominant during production of the granitic magmas.

Isotopic constraints (see Chapter 5) and field relations eliminate the local metasediments, para- and orthogneisses as source rocks. Basic to intermediate, and intermediate to more acidic, compositions in the lower levels of the crust are taken to be the most likely precursors to the dioritic and granitic suites respectively for these crustal melting models. Clemens and Vielzeuf (1987) have shown that the volume of magma produced during fluid-absent melting

at a given temperature, and the hydrous mineral content, are both higher at the intermediate crustal pressures envisaged for the Tertiary granitoids than for pressures at the base of thickened continental crust. For melt proportions limited to approximately 30%-50% by viscosity considerations (Wickham, 1987), mafic sources would be required to have between 0.8 wt. % H_2O corresponding to 35-54% by volume hornblende and intermediate sources 0.4-0.7 wt. % H_2O corresponding to 18-31% by volume hornblende or 9.8-16% by volume biotite.

The maximum degree of melting required to produce the parental liquids of the dioritic and granitic suites was estimated in the same way as that for the Cretaceous biotite granodiorites, by holding constant the trace element concentration ratio of the liquid and of the assumed andesitic source . A similar model can be used to test whether the granitic suite can be generated at reasonable degrees of partial melting from the granulite residue after Cretaceous magmatism. Results are shown graphically in figure 4.32 with the trace element composition of the residium (C_r) after the Cretaceous melting event, calculated from the inferred bulk distribution coefficient (D) and the trace element composition of the biotite granodiorites (C_l) using the equation: $C_r = D.C_l$.

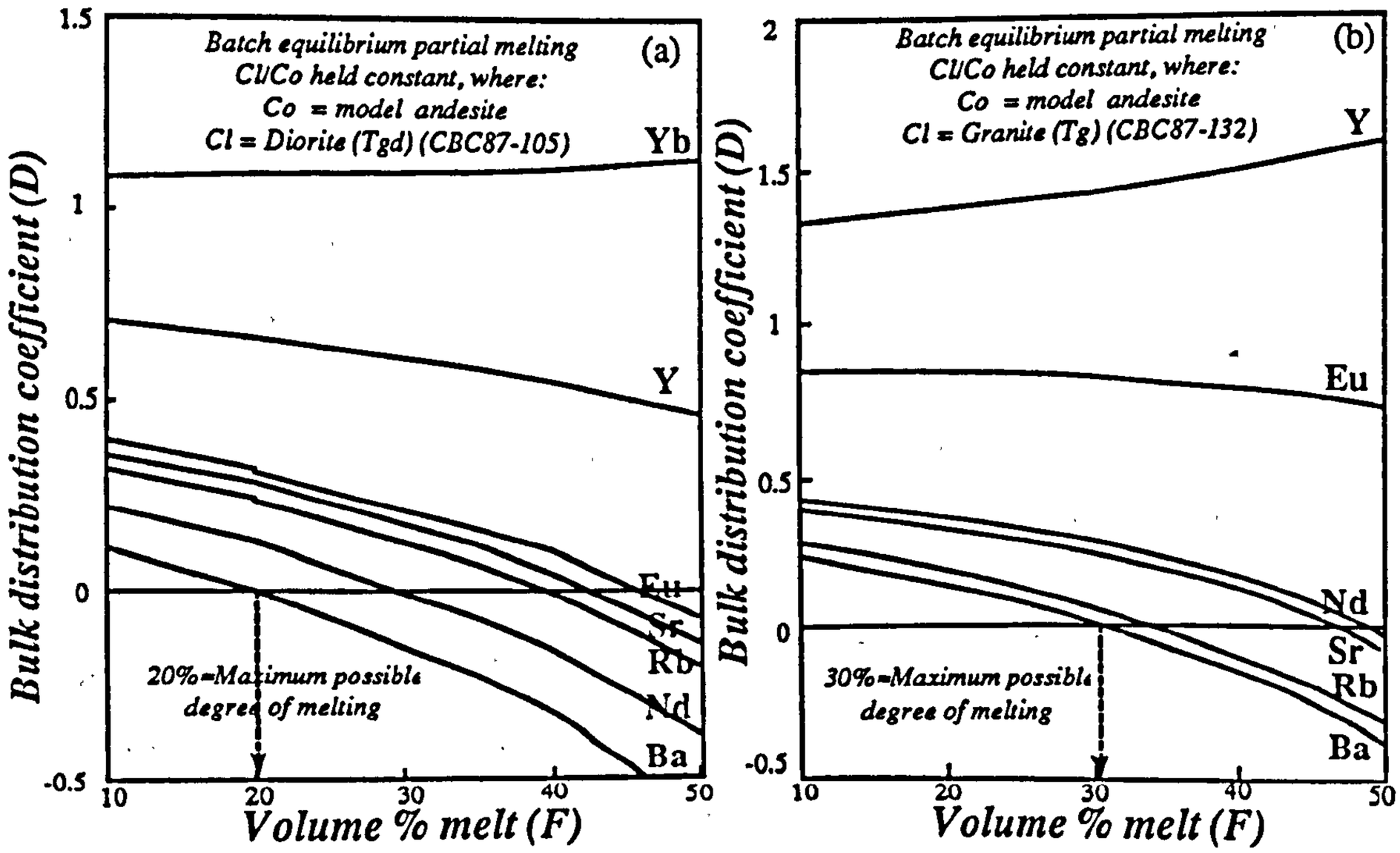

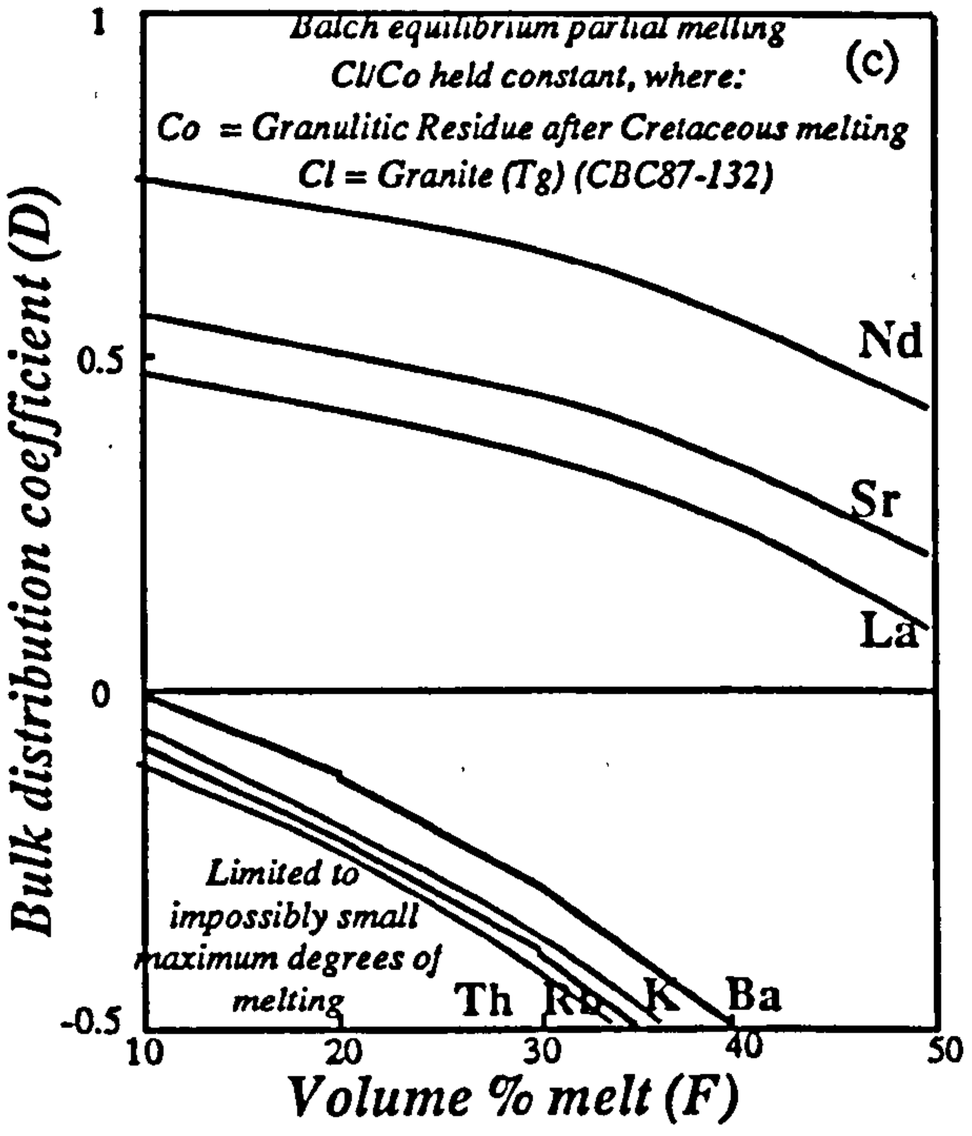

Figure 4.32 Diagram showing how the bulk distribution coefficient for a particular trace element varies with the degree of melting in order that Cl/Co remains constant. a) The maximum degree of melting is limited at approximately 20% melting by the most incompatible element, Ba, for the parental magma of the dioritic suite and an andesitic source composition from Taylor and McLennan (1985). b) The maximum degree of melting is limited at approximately 30% by Ba and Rb for the parental magma of the granitic suite for the same andesitic source. c) The maximum degree of melting is limited to unreasonably small degree melts (<1%) by the LILE Th, Rb and K for the calculated trace element composition of the granulitic residium after melting the Cretaceous biotite granodiorites. This disproves the suggestion by Bennett and Knowles (1985) that the granitic suite were generated from the same source as the Cretaceous magmas, but after extraction and depletion by the Cretaceous magmatic event.

The maximum degree of melting is limited by Ba, the most incompatible element, at only 20% for the dioritic suite (figure 4.32a). Extraction of such small degree melts to form plutons in which significant degrees of fractional crystallization occurred may be difficult over short time periods. There are, however several features which may give credibility to the existence of such unusually small degree crustal melts: the diorites are mafic and have high hydrous mineral contents, which correspond to 5 wt.% H_2O for CBC87-105, both of which reduce the viscosity of the magmas (Wickham, 1987). Also the diorites have high abundances of trace elements even compared with the model upper crust of Taylor and McLennan (1985), and that favours small degrees of melting (see figure 4.33), and the diorites only form small plutonic bodies perhaps consistent with small scale melting. Moreover, there are large margins for error in the Ba concentration of the preferred source composition, especially when it is observed that Rb would limit the degree of melting to up to 40%, and so it must be stressed that such calculations can only give an approximation of the degree of melting for probable source compositions.

The maximum degree of melting is limited to a plausible 30% melting by Ba and Rb for the model andesite and the parental magma of the granitic suite (figure 4.32b). Furthermore, the hypothesis that the granitic magmas were generated by melting granulitic residues after

previous magma extraction (Bennett and Knowles, 1985) is disproved by the improbably small degree melts (<1%) required to produce the observed LILE concentrations in the granitic suite out of such depleted granulites (figure 4.32c).

Using values of 20%-30% and 30% melting for the dioritic and granitic suites respectively and approximate temperatures of 900-1000°C and 800-900°C and 5kb, requires 25-50% volume hornblende in intermediate to mafic sources and 9-30% volume biotite in quartzofeldspathic to intermediate sources. However, these rather wide limits put only minor constraints on the original major element compositions of the sources such that mass balance calculations may be performed to constrain the models further. At least as meaningful results can be obtained for published average major element compositions of crustal rock types. Mass balance calculations show that extraction of 20-30 % of a dioritic magma with the composition of CBC87-105 from a gabbroic source leaves a residual composition that is consistent with the likely granulitic assemblage of 60% ortho- and clinopyroxene, 30% plagioclase and 10% hornblende. The bulk distribution coefficients can be calculated from this preferred assemblage and their relative proportions adjusted to produce reasonable inferred source compositions. The same reasoning was applied to the granitic suite, using a tonalitic source composition to leave a granulite of intermediate composition containing plagioclase and pyroxene.

Although the compositions of the Tertiary source rocks are not well constrained, the procedure usefully demonstrates that both the dioritic suite and the granitic suite need trace element enriched sources compatible with crustal melting of a source region generated by subduction-related processes that has not subsequently undergone any significant reprocessing event. The calculated source compositions are illustrated on primordial mantle normalised trace element abundance diagrams shown in figure 4.33. The source composition of the dioritic suite has high abundances of the REE, high Sr and low LILE. The low LILE abundances are a product of the small degree of melting (20%) used during modelling, which was directly dependent on the high Ba content of the dioritic magmas.

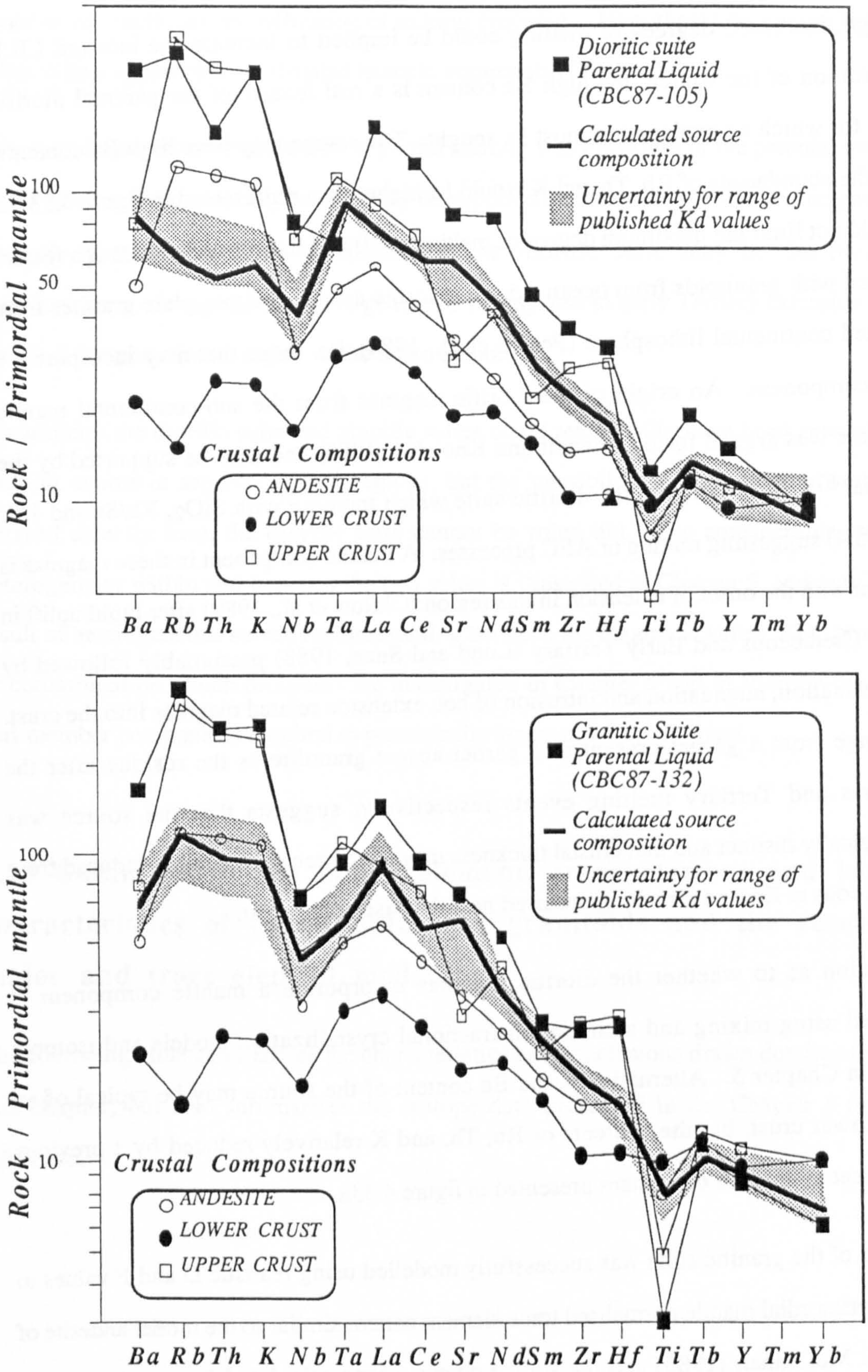

Figure 4.33 Calculated trace element composition of the dioritic suite and granitic suite source rocks, assuming 20% and 30% batch equilibrium melting. Shaded region are the likely uncertainties for the range of possible Kd values (Henderson, 1982), the representative crustal compositions are merely for comparison (Taylor and McLennan, 1985) and the primordial mantle normalising factors are listed in Appendix A.

Although, increased degrees of melting could be implied to increase the inferred LILE concentration of the source, the high Ba content is a real feature of the parental dioritic magma for which an explanation must be sought. The source may have high Ba contents, so that the abundances of Rb, Th and K would be higher than represented in figure 4.33 i.e. Ba would not limit the maximum degree of melting to 20%. High Ba abundance is a feature correlated with granitoids from ocean ridges, volcanic arcs and within-plate granites from attenuated continental lithosphere (Pearce et al., 1984), i.e. those that may incorporate a mantle component. An origin of the dioritic magmas from the sub-continental mantle lithosphere was argued for by Bennett and Knowles (1985) and may be supported by the low initial $^{87}Sr/^{86}Sr$ ratios in the dioritic suite which increase with SiO_2, Rb/Sr and 1/Sr (section 5.4) suggesting mixing or AFC processes. A mantle component in these magmas is consistent with the onset of extension in this region (Oldlow et al., 1989) after rapid uplift in the Late Cretaceous and Early Tertiary (Lund and Snee, 1988) presumably followed by crustal relaxation, attenuation and intrusion of hot, extension related magmas into the crust. The change from a garnet present to a garnet absent granulite as the residue after the Cretaceous and Tertiary melting events respectively, suggests that the source was mineralogically distinct and that crustal thickness may have been considerably reduced from the Cretaceous to Eocene if melting occurred near the base of the crust.

The question as to whether the dioritic magmas incorporate a mantle component is approached using mixing and assimilation-fractional crystallization models and isotopic evidence in Chapter 5. Alternatively, the Ba content of the source may be typical of an enriched lower crust, but the contents of Rb, Th, and K relatively reduced by a previous melting event to produce the pattern presented in figure 4.33a.

The source of the granitic suite was successfully modelled using realistic D and F values to produce a primordial mantle normalised trace element pattern similar to the model andesite of Taylor and McLennan (1985) and the source compositions calculated for the Cretaceous phases (figure 4.33b). The plausible process and a realistic calculated source composition therefore fails to suggest that the granitic suite was necessarily derived from the dioritic

magmas by fractional crystallization or mixing processes. Hypotheses on mixing between suites is best approached by detailed isotopic arguments (Chapter 5).

However the need for a heat source, if partial melting was the origin of the parental magmas of the granitic suite, can only realistically be supplied from hot mantle-derived magmas for normal continental crustal thicknesses. The dioritic suite may be the modified representatives of magmas that were generated in response to early Tertiary extension of the mantle-lithosphere in the region of the Idaho batholith.

In summary the dioritic suite and granitic suites could realistically have been generated by melting events in separate source regions, but the possibility that the granitic suite was derived directly from the dioritic suite cannot be ruled out. The considerable isotopic heterogeneity within and between the two suites is illustrated in Chapter 5 and may be the result of heterogeneous source regions, mixing between the magmatic suites, AFC processes or contamination. Such processes are investigated in Chapter 5 and in addition the likely end-member components required to generate the magmas are constrained.

4.10 Summary of the major element, trace element and isotope characteristics of the Atlanta lobe granitoids and the results of major and trace element modelling

The following table summarises the characteristics and conclusions drawn dominantly from this chapter, but also summarises the isotope data presented in the Chapter 5 for easy reference.

Rock Type	Kt Kgdh Tonalite and Hb-Bt granodiorite	Kgd Bt granodiorite	Kg Mu-Bt granite	Klg Leucogranite	Tgd Dioritic suite	Tg Granitic suite
Major elements	Metaluminous	Metaluminous Peraluminous	Peraluminous	Peraluminous	Metaluminous	Peraluminous
Trace elements	High Sr, Ba, LILE/HFSE. Low P, Ti, K	High Sr, Ba, LILE/HFSE. Low P, Ti. Small LILE variation.	High Rb, Rb/Sr LILE/HFSE. Low P, Ti. Large LILE variation.	High Rb, Rb/Sr, Rb/Zr. Low P, Ti. Large LILE variation.	High Sr, Ba. Low HFSE, Rb,P, Ti. Small LILE variation.	Low Ba, Sr. Mod HFSE. High Rb,U,Th. Large LILE variation.
Rare earth elements	High LREE/HREE. Low Yb. Minor+ve, -ve Eu/Eu*.	High LREE/HREE. Low Yb. Minor+ve, -ve Eu/Eu*.	High LREE/HREE. Variable abundances. Moderate+ve, -ve Eu/Eu*.	Low LREE/HREE. High abundances. Large -ve Eu/Eu*.	High LREE/HREE. Minor+ve, -ve Eu/Eu*.	Moderate LREE/HREE. Large -ve Eu/Eu*.
ε_{Sr}	35 to 70	35 to 99	50 to 120	50 to 160	25 to 65	54 to 120
ε_{Nd}	-5.8 to -10.8	-4.9 to -11.6	-7 to -11	-12 to -22	-4 to -11.8	-8.1 to -15.4
T_{DM}^{Nd}	1.4-1.8Ga	≈1.45Ga	≈1.5Ga	2.1-2.7Ga	1.0-1.7Ga	1.2-1.6Ga
Crystal Fraction-ation	Small degrees of within suite Hb and Pg fractionation	Little within suite crystal fractionation	Up to 50% Ksp, Qz, Mu, Bt and Pg from Bt granodiorite parental magma	Some limited crystal fractionation limited by quenching at high levels.	AFC process Hb and Pg crystallize. Parental magma mantle-derived andesite. Assimilant old continental crust.	Up to 40% Ksp, Qz, and Pg at high levels
Partial Melting	35-45% melting a Hb-Bt bearing tonalitic to gabbroic source to leave a garnet poor mafic granulite.	25-35% melting a Hb-Bt bearing tonalitic source to leave a garnet mafic granulite.		Upper crustal small volume (<20%) partial melts.	60-70% assimilation required at mid- to upper crustal levels.	30% melting a Bt bearing tonalite source to leave a mafic granulite at the base of a thinned crust.

Table 4.11 Summary of the geochemical and isotope characteristics of the Atlanta lobe granitoids and conclusions from trace element modelling.

CHAPTER 5

Isotope Geochemistry

5.1 Introduction

In this chapter new Sr, Nd and Pb isotopic data are presented for the Cretaceous and Tertiary granitoids of the eastern, central and southern regions of the Atlanta lobe of the Idaho batholith. There has been much previous Rb-Sr, K-Ar and Ar-Ar geochronological work within the Idaho batholith (see section 3.3), and some limited studies addressing the isotopic signature of the western Atlanta lobe and Bitteroot lobe granitoids and their possible sources (Fleck and Criss, 1985). Pb isotopes have been analysed in zircons and for whole rocks from the northeastern Bitteroot lobe by Chase et al. (1978) and by Shuster and Bickford (1985), but there have been no such studies on the granitoids of the Atlanta lobe. This chapter attempts to combine the evidence from the different isotope systems, Rb-Sr, Sm-Nd, Th-Pb and U-Pb with that from the major and trace element geochemistry data on the same samples to approach the following objectives:

i) to characterise the isotopic compositions of the granitoids;

ii) to model the age and composition of the possible source rocks and their evolution;

iii) to further develop a model for formation of the Idaho batholith granitoids in the light of new isotope results;

iv) to comment upon previously suggested petrogenetic models that have been applied to the southern and central Atlanta lobe by comparison with other western United States cordilleran granitoids;

v) to define more accurately the boundaries of the crustal age formation boundaries in the northwestern United States cordillera using Nd model ages and Pb-Pb model ages;

The advantage this work has over previous studies is the good field control, the combination of major, trace element and Sr, Nd and Pb isotope ratios, and a stand-point from which previous ideas were taken into account but not adhered to by a long tradition of study in the region.

5.2 Sr isotope variations

5.2.1 Previous work

There is a large amount of previously published Sr isotope data from the Idaho batholith, but this was generally obtained from the western border zone and the Bitteroot lobe. Armstrong et al. (1977) analysed samples from the accreted terranes in eastern Oregon and granitoids from the western border zone of the Atlanta lobe. They recognised an age independent step in initial $^{87}Sr/^{86}Sr$ ratios from ≤0.704 in the west to ≥0.706 in the east, and suggested this reflected the suture between Precambrian crust and Permian-Jurassic accreted island arc terranes in the basement rocks. They also recognised that the Idaho batholith was largely intruded between 75Ma-100Ma, but that the Tertiary igneous episode caused much resetting particularly of the K/Ar ages. Shuster and Bickford (1985) and Chase et al. (1978) published Sr isotopic data from the northeastern Bitteroot lobe on both granitoids, metasediments and country rock xenoliths and concluded that the granitoids included a "significant contribution from a lower crustal source region", but that upper crustal contamination produced the relatively high whole-rock initial $^{87}Sr/^{86}Sr$ ratios for the low Rb/Sr granitoids. Criss and Fleck (1983, 1987) and Fleck and Criss (1985) reconfirmed the sharp increase in initial $^{87}Sr/^{86}Sr$ across the suture zone previously recognised by Armstrong et al. (1977). Criss et al. (1982) recognised that initial $^{87}Sr/^{86}Sr$ appears to be unaffected by to the large Tertiary hydrothermal systems and they developed a petrogenetic model whereby the Cretaceous granitoids near the border of the Precambrian sialic crust represent simple mixtures of upper Precambrian wall-rocks (initial $^{87}Sr/^{86}Sr \approx 0.752$) and magmas derived from the upper mantle or subducted oceanic lithosphere (initial $^{87}Sr/^{86}Sr \approx 0.7035$). For granitoid samples further away from the border zone in the Bitteroot lobe they recast their model as mixtures between a lower crustal end member (initial $^{87}Sr/^{86}Sr \approx 0.708$) and upper crustal Precambrian wall-rocks. Manduca (1988) used similar mixing models with end members of "lithospheric oceanic arc derived magma" (initial $^{87}Sr/^{86}Sr \approx 0.7035$) with spillitised oceanic crust in the accreted terranes and upper continental metasedimentary crust for the granitoids close to the suture zone. For the granitoids in the

internal portions of the Atlanta lobe, a third end-member of basaltic lower crust or upper mantle was used by Manduca (1988) to account for the intermediate initial $^{87}Sr/^{86}Sr$ ratios and $\partial^{18}O$ values. These models are discussed in the context of the Sr isotope results from this study in the next section.

A number of Sr isotopic measurements were also made by Fleck and Criss (1985) on the Eocene epizonal granites of the Bitteroot lobe, which are equivalent to the Tertiary granitic suite from the Atlanta lobe. They concluded that the constant initial $^{87}Sr/^{86}Sr$ ratios ($\approx$ 0.708) with decreasing Sr concentration and increasing Rb/Sr ratio in the Tertiary granites suggest that they do not contain any Precambrian Upper crustal component, but that the Sr, Rb and Sr isotope results are consistent with either assimilation of large amounts of Cretaceous batholithic material by mantle-derived magmas, or from magmas derived from Precambrian lower crust.

A commonly noted feature by previous authors and from this study is that whole-rock isochrons with small errors are not preserved from even closely related rocks in the Cretaceous granitoids. This has plausibly been attributed to source region heterogeneity, to mixing of components with heterogeneous initial $^{87}Sr/^{86}Sr$ and limited local ranges in Rb/Sr. However, a small number of Rb/Sr isochrons on mineral separates and whole rock pairs produce consistent results between 75Ma-100Ma (Chase et al., 1978 and Armstrong et al., 1977).

The available published Sr isotope data is compared with the data generated during this study on histograms of initial $^{87}Sr/^{86}Sr$ ratios calculated at 80Ma (figure 5.1). The distribution of initial $^{87}Sr/^{86}Sr$ ratios differs markedly between this and previous studies. There are no granitoids from this study with initial $^{87}Sr/^{86}Sr$ ratios <0.704) in contrast with the peak of samples from previous studies with initial $^{87}Sr/^{86}Sr \approx 0.7035$ tailing off to 0.706. However initial $^{87}Sr/^{86}Sr$ ratios <0.704 are only recorded in samples from the western border zone and accreted terranes, and no samples were collected from these areas during this study. It is widely accepted that these low initial ratios (<0.704) reflect the isotopic signature of young accreted oceanic arc mantle-lithosphere, from which the granitoids are thought to be

largely derived (Armstrong et al., 1977; Fleck and Criss, 1985). Manduca (1988) further argues the $\partial^{18}O$ values of the accreted terrane granitoids indicate that there has been some contribution of spillitised oceanic-derived crustal material by assimilation/ fractional crystallization processes.

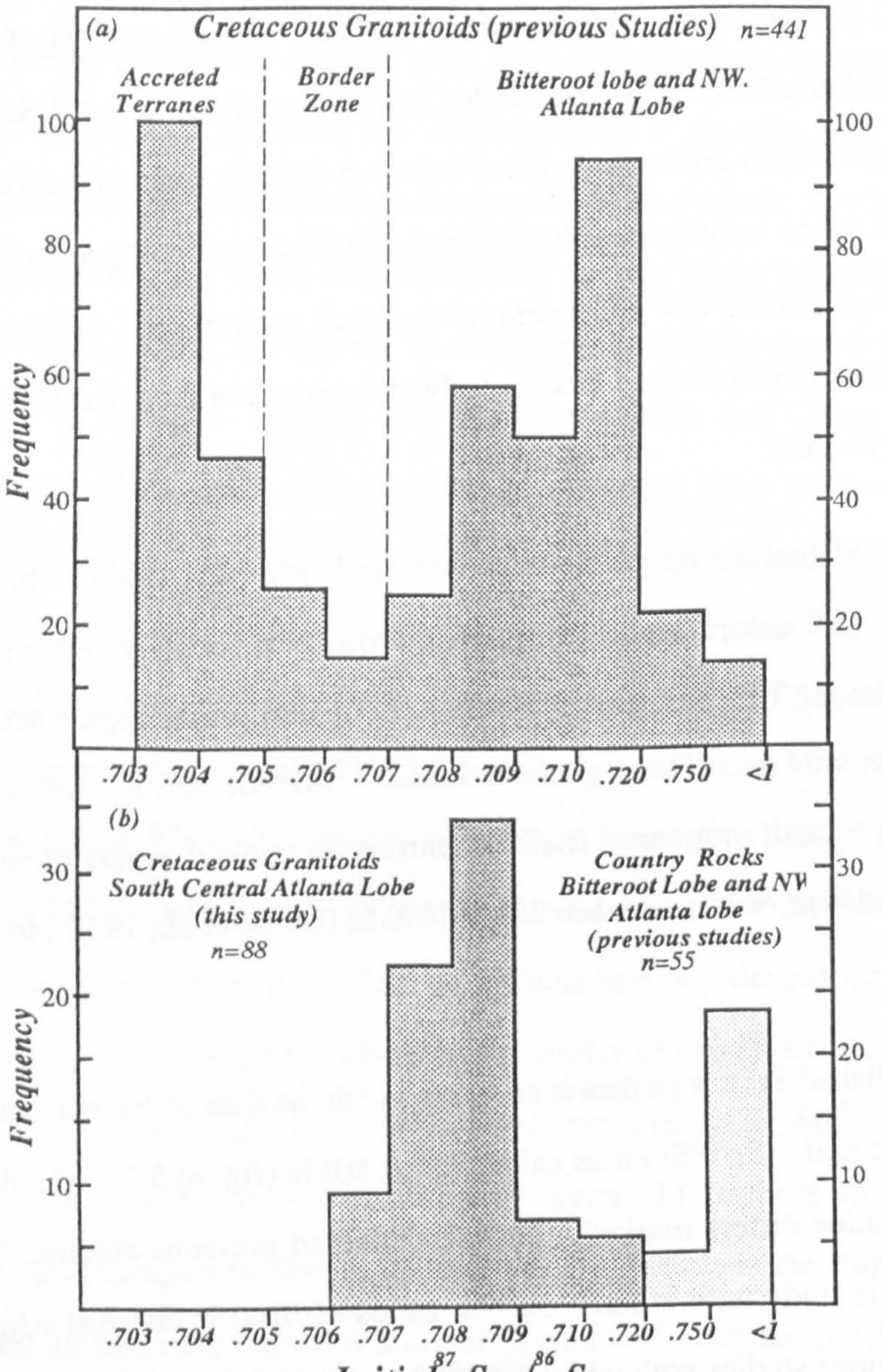

Figure 5.1 a) Histogram of initial $^{87}Sr/^{86}Sr$ ratios calculated at 80Ma for previously published data on granitoids from the Idaho batholith and The Blue Mountains oceanic island arc accreted terrane in eastern Oregon and western Idaho. Rock types are gabbros, quartz diorites, granodiorites and granites. Data are taken from Armstrong et al. (1977); Criss and Fleck (1987), Manduca (1988) and Shuster and Bickford (1985).
b) Histogram of all initial $^{87}Sr/^{86}Sr$ ratios for all the Cretaceous granitoids from this study and the Sr isotope ratios of the Precambrian country rocks both calculated at 80Ma. Country rock data from Shuster and Bickford (1985) and Criss and Fleck (1987).

Intermediate initial $^{87}Sr/^{86}Sr$ ratios ≈ 0.705-0.706 have only been recorded in samples from the western border of the Atlanta lobe in the vicinity of the suture zone, and they have been attributed to mixing between components from oceanic arc mantle-lithosphere, oceanic arc basaltic crust, Precambrian upper crust and old continental basement (Armstrong et al., 1977; Fleck and Criss, 1985 and Manduca, 1988). In this study initial $^{87}Sr/^{86}Sr$ ratios in the range 0.7060-0.7079 are recorded throughout the Atlanta lobe in most Cretaceous rock types and they do not show any decrease towards the western margins of the Atlanta lobe.

Comparison of figures 5.1a and 5.1b shows that there is a peak at values of initial $^{87}Sr/^{86}Sr$ ≈ 0.708 in this and previous studies, whereas only in the studies of Fleck and Criss (1985) and Shuster and Bickford (1985) is there also a peak at ≈ 0.710-0.72. Also illustrated on figure 5.1b are the high initial $^{87}Sr/^{86}Sr$ ratios of the Precambrian upper crustal metasediments and orthogneisses which have initial $^{87}Sr/^{86}Sr \geq 0.72$. It was argued by Fleck and Criss (1985) that mixing between such old upper crustal components and oceanic arc mantle-lithosphere derived magmas caused the Sr isotopic variation across the western border zone while mixing a similar upper crustal component with lower crustal rocks corresponding to the initial $^{87}Sr/^{86}Sr \approx 0.708$ peak (in figure 5.1a and 5.1b) caused the variation within the interior of the Bitteroot lobe.

Arguments based on major and trace element modelling (chapter 4) have been put forward which suggest that only several of the highly peraluminous leucogranites and muscovite-biotite granites, from this study, with high ε_{Sr} and distinctive flat REE profiles with large negative europium anomalies possibly contain a significant upper crustal component. Most of the evolved rocks appear to have been derived as fractionates from the less silicic rocks with no evidence of an upper crustal component.

The granitoids collected from the northern Atlanta lobe and the Bitteroot lobe which have high initial $^{87}Sr/^{86}Sr$ ratios (>0.710) were noted to be those adjacent to screens or pendants of Precambrian rocks and/or contained abundant country rock xenoliths (Fleck and Criss, 1985; and Shuster and Bickford, 1985). Although country rock xenoliths and screens are virtually absent in the southern Atlanta lobe, and pendents are present, but rare, care was

taken to collect samples away from such rocks during this study and to use only the freshest samples for isotope analysis so that the composition of the rocks could be ascertained without unravelling the effects of localised wall-rock contamination. Comparison of figures 5.1a and 5.1b illustrates that the above sampling procedure has tended to eliminate the peak of granitoids with initial $^{87}Sr/^{86}Sr > 0.710$ in the Atlanta lobe.

A further preliminary consideration is the possible effect of hydrothermal systems on the Rb-Sr isotope systematics. Criss and Fleck (1987) noted that hydrothermal transport processes have the potential to disturb whole rock Rb-Sr isotope systematics by subsolidus changes in either the initial $^{87}Sr/^{86}Sr$ ratio, the Rb/Sr ratio or both. Hydrothermal circulation systems were active during the emplacement of the Cretaceous and Tertiary plutons (Criss and Taylor, 1983). Deep, large scale circulation of high $\partial^{18}O$ metamorphic-hydrothermal fluids reset the $\partial^{18}O$ values in a concentric pattern increasing away from the margins of the batholith in the metasedimentary rocks north of the Bitteroot lobe during the Cretaceous intrusive event (Criss and Fleck, 1987).

In the Eocene large depletions in ∂D and $\partial^{18}O$ occurred due to shallow level meteoric hydrothermal circulation of low-∂D, low-$\partial^{18}O$ heated fluids centred upon the the Tertiary epizonal granites of the Bitteroot lobe. Criss and Fleck (1987) argued that for their Bitteroot lobe granitoid sample set, which contained both fresh and hydrothermally altered rocks, "hydrothermal alteration systems do not seem to have profoundly influenced initial $^{87}Sr/^{86}Sr$ ratios". Altered rocks were recognised as those with highly depleted $\partial D \leq -120‰$ and in extreme cases small depletions in $\partial^{18}O$, but these did not correlate with variations in initial $^{87}Sr/^{86}Sr$ ratios. Moreover, Criss and Fleck (1987) further argue that the initial $^{87}Sr/^{86}Sr$ ratios would be unlikely to have been perturbed much in altered rocks anyway because:

i) the Sr concentrations in continental meteoric fluids are low compared with those in submarine hydrothermal systems and in the granitoids themselves;
ii) the Sr in the circulating fluids was probably largely derived from Cretaceous and Tertiary granitoids and so it would have had Sr isotope ratios similar to those of the granitoids themselves;

iii) the Sr in the Precambrian wall-rocks was a potential source of heterogeneous Sr isotopic ratios, but they were discounted due to their low Sr concentrations (185ppm) and minimal contact with Tertiary magmas.

The first two points are probably valid, but the third point may be questioned because the highest initial $^{87}Sr/^{86}Sr$ ratios occur in granitoids spatially related to Precambrian wall-rocks; although Fleck and Criss (1985) argue this to be due to melting rather than hydrothermal alteration.

The areal extent, depth and $\partial^{18}O$ values of the meteoric-hydrothermal systems centred on Tertiary plutons in the Atlanta lobe (see figure 5.6) are larger, deeper, and much more depleted than those in the Bitteroot lobe (Criss and Taylor, 1983; Criss and Fleck, 1987). Criss and Taylor (1983) argued that the relative ages and thus temperatures, between the Cretaceous granitoids and the Tertiary granitoids were higher in the Atlanta lobe than the Bitteroot lobe, and so higher lateral temperature gradients developed with the result that the hydrothermal circulation was more focused and intense in the Atlanta lobe. The higher water/rock ratios then caused the greater depletions in ∂D, but particularly in $\partial^{18}O$, and also resulted in a greater potential for mass transport and perturbation of other isotope systems in these granitoids.

There are several questions posed for the internal Atlanta lobe granitoids by the previous studies in adjacent areas which will be addressed in the following section.

i) Are the initial $^{87}Sr/^{86}Sr$ ratios of the Atlanta lobe also largely unaffected by hydrothermal circulation?

ii) Is there evidence of mixing components during magmatism similar to those proposed for the Border zone or Bitteroot lobe granitoids in the Atlanta lobe?

iii) What was the likely source region for the Atlanta lobe granitoids?

5.2.2 Sr isotope variation of the Cretaceous granitoids of the Atlanta lobe

A histogram of the initial $^{87}Sr/^{86}Sr$ ratios for the different Cretaceous rock types analysed here is shown in figure 5.2. The biotite granodiorites are the most abundant rock type and their initial $^{87}Sr/^{86}Sr$ ratios range from 0.7069-0.711, with a distinct peak at 0.708. The tonalites range from 0.7069-0.710 with an even distribution, while the porphyritic granodiorites and hornblende-biotite granodiorites (grouped together in this diagram) range from 0.7064-0.7079. Although relatively few of the muscovite-biotite granites and leucogranites (grouped here) were analysed, half the analyses are restricted between 0.708-0.709 whereas the remainder have initial $^{87}Sr/^{86}Sr$ between 0.710-0.715.

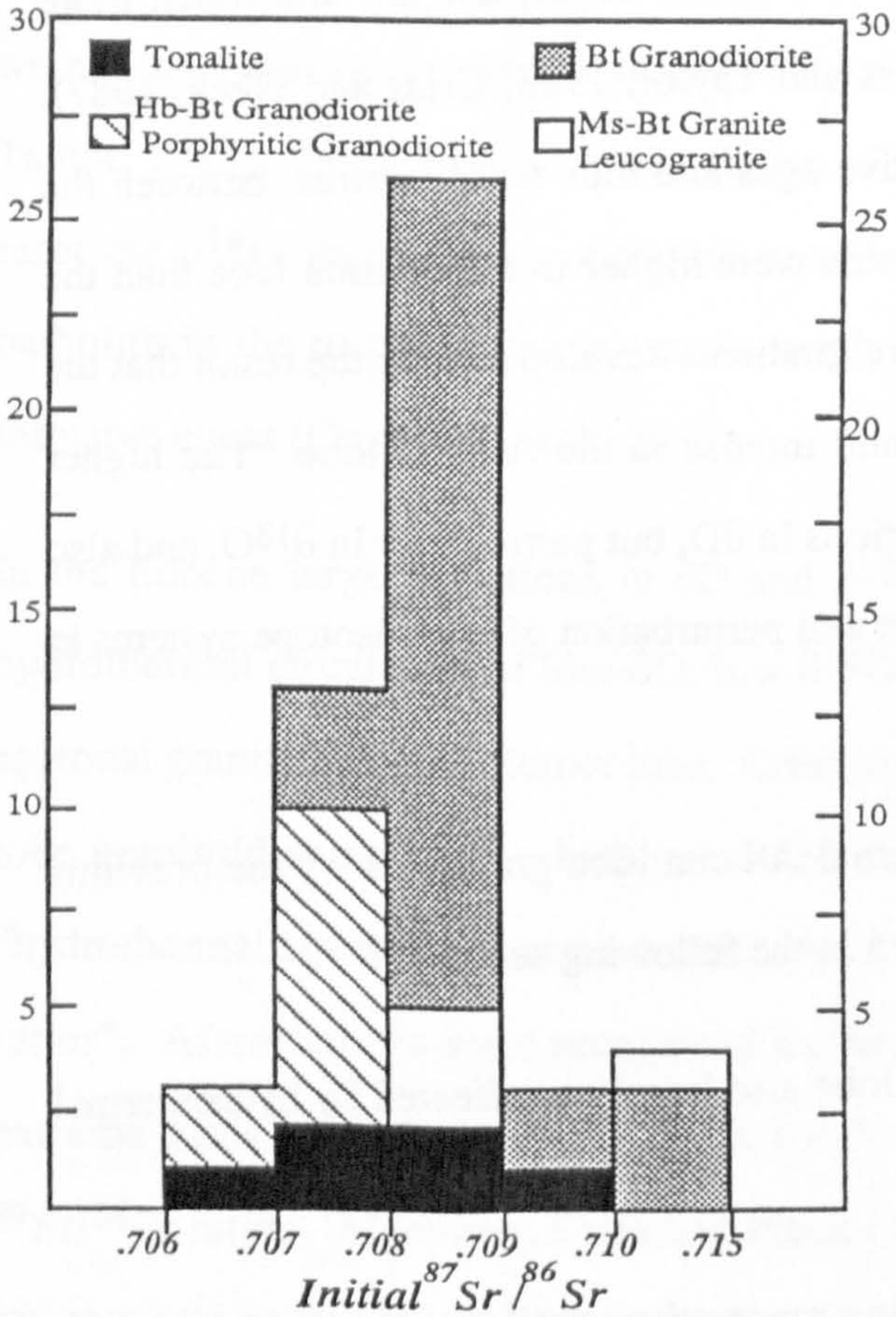

Figure 5.2 Histogram of initial $^{87}Sr/^{86}Sr$ ratios for the Cretaceous rock types of the Atlanta lobe calculated at 80Ma. The porphyritic granodiorites and hornblende-biotite granodiorites are grouped together as are the muscovite-biotite granites and leucogranites.

This diagram indicates that there is no clear correlation between initial $^{87}Sr/^{86}Sr$ and rock type as previously demonstrated in figure 4.11. The only exception to this are the few highly peraluminous leucogranites, muscovite-biotite granites and biotite granodiorites collected from the southern border of the Atlanta lobe northwest of Mountain Home (see

figure 1.3) which have high initial $^{87}Sr/^{86}Sr$ ratios and REE and trace element signatures which suggest that they contain a significant contribution from upper crustal materials.

Discounting these samples there appears to be a near normal distribution around a peak at 0.708 (figure 5.2), which neither suggests significant contributions from low-$^{87}Sr/^{86}Sr$ (0.7035) oceanic arc-derived magmas or high-$^{87}Sr/^{86}Sr$ (>0.715) upper crustal rocks. The lack of correlation of initial $^{87}Sr/^{86}Sr$ with rock type (figure 5.2), silica (figure 4.11) or regional distribution suggests that isotopic heterogeneities in the range of initial $^{87}Sr/^{86}Sr \approx$ 0.706-0.713 may exist on a small scale (0.1km-1km) within the granitoid source regions. Moreover, the mean value of initial $^{87}Sr/^{86}Sr \approx 0.708$ is the same as that suggested by Fleck and Criss (1985) and Manduca (1988) for their respective lower crustal and deep continental basement components respectively. The above arguments are in agreement with major and trace element modelling (Chapter 4) which suggested that the Cretaceous granitoids were derived from lower crustal sources and so presumably the isotope variation was inherited from, and already existed within the source regions.

5.2.3 Sr isotope evidence for the absence of mixing source components to generate the Cretaceous granitoids

Mixing processes have commonly been invoked to account for the isotope variations within the western United States cordilleran batholiths. The Idaho batholith was suggested by Armstrong (1977) and Fleck and Criss (1985) to have been generated by mixing significant amounts of upper crustal country rocks with either low-$^{87}Sr/^{86}Sr$ oceanic-arc, mantle-derived magmas for the western border zone, or with old Proterozoic or Archaean lower crust-derived magmas for the internal Bitteroot lobe. These hypotheses were tested by various mixing models to assess the significance of these processes for the Cretaceous magmas from the Atlanta lobe of this study.

Fleck and Criss (1985) used the South Fork of the Clearwater River (SFCR) sample traverse from the accreted terranes across the suture zone (figures 1.2 and 1.3) to infer simple mixing between Precambrian wall-rocks and oceanic-arc, mantle-derived magmas. Figure 5.3a

shows the simple mixing model of Fleck and Criss (1985) for initial $^{87}Sr/^{86}Sr$ plotted against 1/Sr for the SFCR granitoids. The end member compositions are:

Upper crust Precambrian wall-rocks: Sr≈185ppm Rb≈135ppm $^{87}Sr/^{86}Sr_{(80Ma)}$≈0.752
"Primary" orogenic arc magmas: Sr≈1200ppm Rb≈20ppm $^{87}Sr/^{86}Sr_{(80Ma)}$≈0.7035

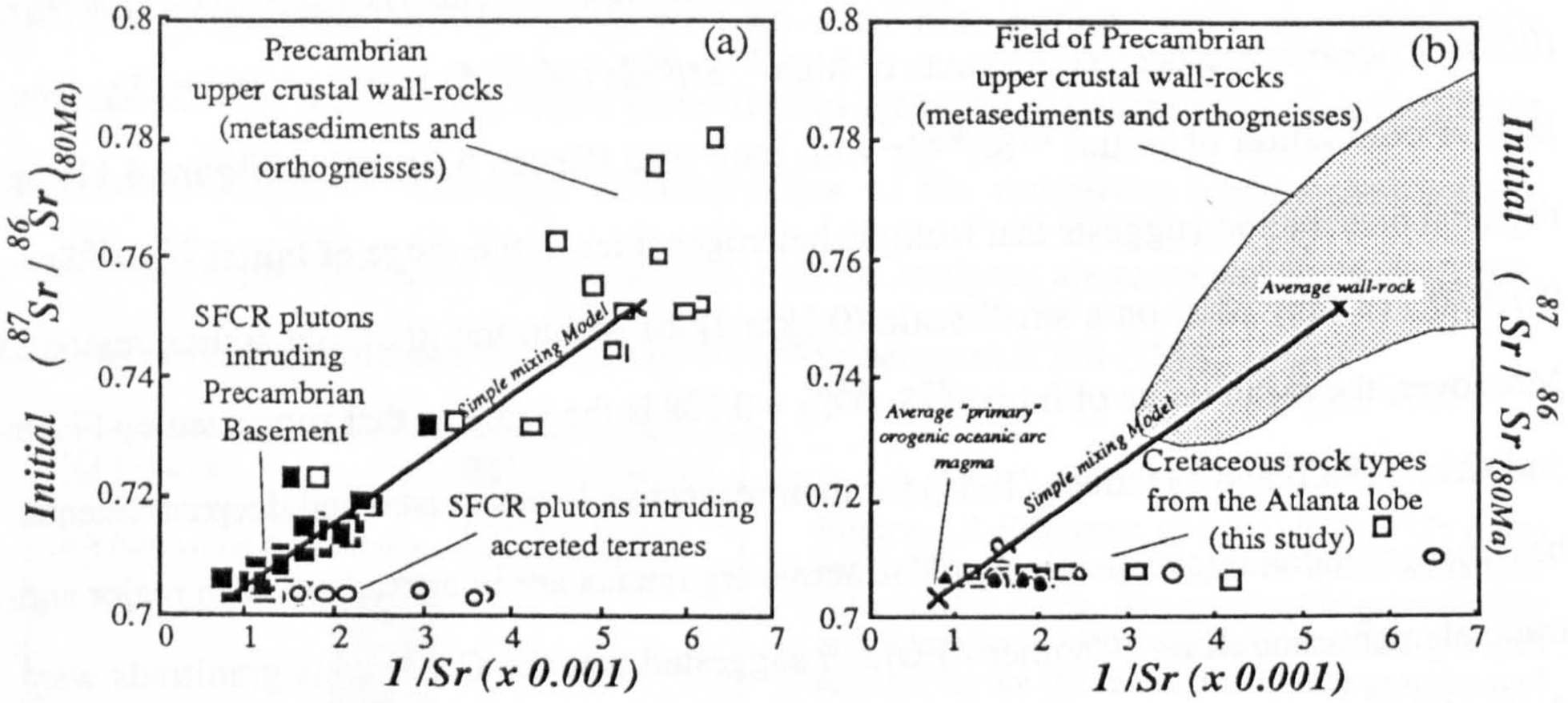

Figure 5.3 **a)** Graph of initial $^{87}Sr/^{86}Sr$ versus 1/Sr for the plutons of the SFCR traverse across the suture zone in the northwestern Atlanta lobe, the granitoids intruding the accreted terranes and selected metasediments and Precambrian country rocks from the Salmon River arch and to the north of the Bitteroot lobe. **b)** Graph of initial $^{87}Sr/^{86}Sr$ versus 1/Sr for the Cretaceous granitoids of the Atlanta lobe from this study with standard symbols for rock types.

Figure 5.3a shows two distinct trends, the SFCR magmas intruding Precambrian basement lie on a simple mixing line between the above end-member compositions and the SFCR magmas intruding the accreted terranes lie on a flat trend of constant $^{87}Sr/^{86}Sr$ ratios with variable Sr (1200-200ppm). The latter trend is interpreted to represent fractional crystallization of the orogenic arc derived magmas, dominated by plagioclase to reduce the Sr concentration, but the $^{87}Sr/^{86}Sr$ ratios remain constant in the granitoids because any assimilated material from the accreted terranes would have similar $^{87}Sr/^{86}Sr$ ratios to the magmas.

The Cretaceous rock types from this study are shown in figure 5.3b with initial $^{87}Sr/^{86}Sr$ plotted against 1/Sr with the mixing trajectory of Fleck and Criss(1985) superimposed. It clearly demonstrates that the granitoids from the Atlanta lobe from this study do not lie on

the mixing trajectory of Fleck and Criss (1985), but define a short flat trend with little change in initial $^{87}Sr/^{86}Sr$ with decreasing Sr abundances.

Figure 5.4 is an enlarged version of figures 5.3 a and b, plotting initial $^{87}Sr/^{86}Sr$ against 1/Sr for the granitoids from the accreted terranes (open circles), the SFCR granitoids (open triangles), the unfractionated near primary melt granitoids from this study (closed circles) and the evolved granitoids which show major and trace element evidence for significant degrees of fractional crystallization (closed triangles).

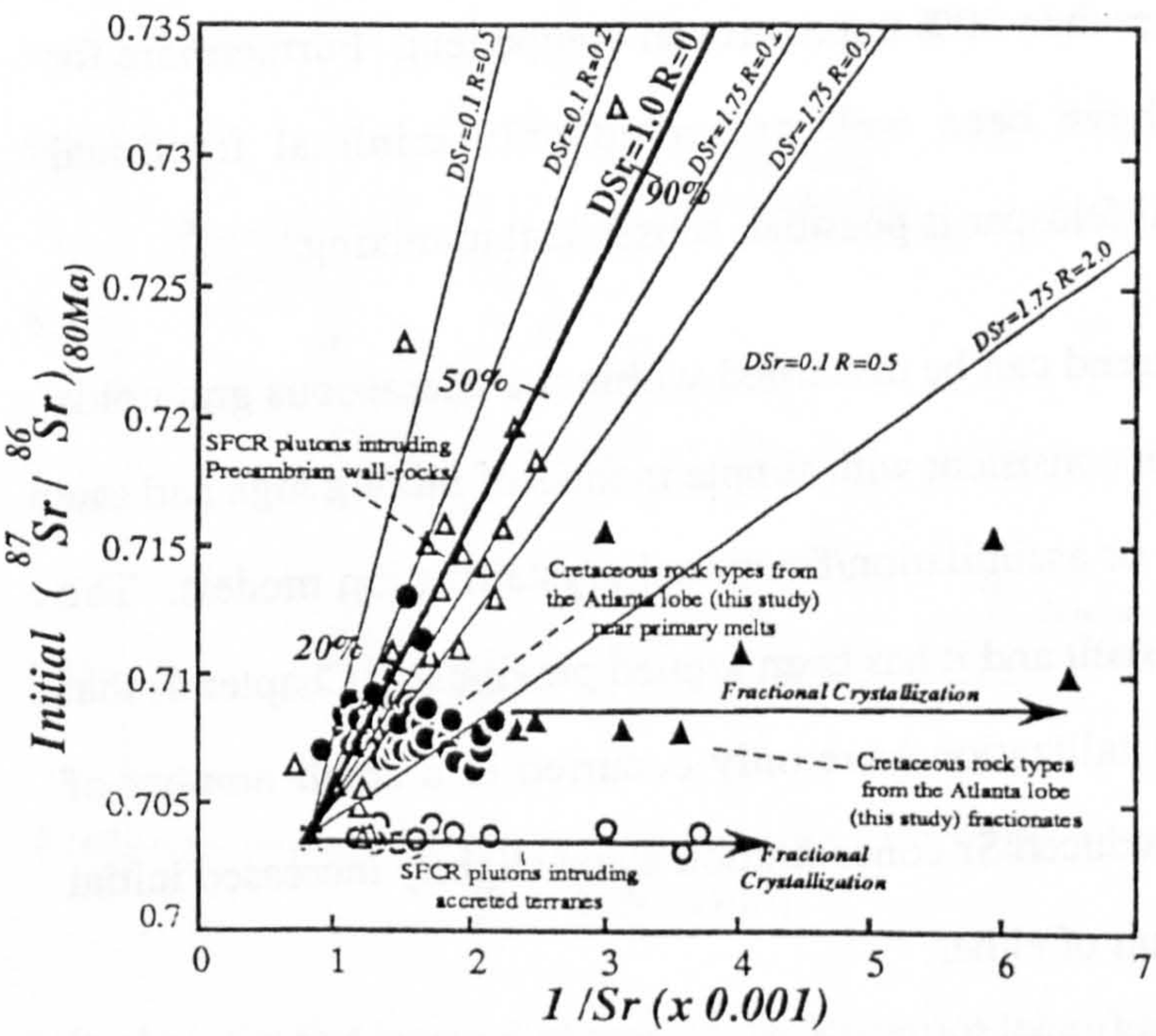

Figure 5.4 Initial $^{87}Sr/^{86}Sr$ versus 1/Sr for the granitoids from the accreted terranes (open circles), the SFCR granitoids (open triangles), the unfractionated near primary melt granitoids from this study (closed circles) and the evolved granitoids which show major and trace element evidence for significant degrees of fractional crystallization (closed triangles). The bold line is Fleck and Criss (1985) preferred simple mixing model, the tin lines are various AFC models whereas the arrows represent fractional crystallization without assimilation.

Superimposed on figure 5.4 is the preferred mixing model of Fleck and Criss (1985) and also several different assimilation/fractional crystallization models (DePaolo, 1981) which suggests that the SFCR magmas most closely correspond to simple mixtures. Using the equation of DePaolo (1981) in the form:

$$\frac{(^{87}Sr/^{86}Sr)_m - (^{87}Sr/^{86}Sr)_i}{(^{87}Sr/^{86}Sr)_a - (^{87}Sr/^{86}Sr)_i} = \frac{(1/Sr)_m - (1/Sr)_i}{(k/Sr)_a - (1/Sr)_i}$$

where: $k = [1 + R(D_{Sr} - 1)]$

R = ratio of the rate of fractional crystallization to the rate of assimilation

subscripts: i = initial magma, a = assimilated material m = resultant magma

it can be shown that simple mixing is only a specific case of AFC, i.e. mixing trajectories only trend towards the composition of the assimilated material from the initial composition when k = 1, i.e. either $D_{Sr} = 1$ or R = 0. Fleck and Criss (1985) argue that if R « 1, assimilation exceeds fractional crystallization and so the mass proportion of magma (F) will increase as mixing occurs. By regarding their preferred simple mixing model as a specific case of AFC they concluded that the granitoids of the SFCR are simple mixtures of Precambrian upper crust and primary arc magmas that occurred within a melting rather than a crystallization regime which helps to account for the granitoids with the highest initial $^{87}Sr/^{86}Sr$ ratios which require greater than 80% upper crustal component. Furthermore for the the mixing relationships to have been well preserved only minimal fractional crystallization of plagioclase or alkali feldspar is possible, subsequent to mixing.

Even in more detail (figure 5.4) no trend can be discerned within the Cretaceous granitoids of the Atlanta lobe and so they are not consistent with simple models of mixing high and low $^{87}Sr/^{86}Sr$ crustally derived magmas or assimilation/fractional crystallization models. The initial $^{87}Sr/^{86}Sr$ ratios are nearly constant and it has been argued previously (Chapter 4) that significant degrees of fractional crystallization have only occurred in a small number of samples. Some of the samples with reduced Sr concentration show slightly increased initial $^{87}Sr/^{86}Sr$ ratios which may be the result of either:

i) greater inaccuracy of the calculated initial ratios for high-Rb/Sr samples, although no unexpectedly low ratios are recorded;

ii) the reduced Sr content of these magmas make them more sensitive to the effects of incorporation of small amounts of upper crustal material. Such processes differ significantly from the mixing model of Fleck and Criss (1985) because the former would be implied to have occurred at high levels after significant degrees of fractional crystallization rather than in a melting regime with near primary magmas;

iii) these rocks represent the upper crustal melts with high Rb/Sr ratios, and distinctive flat REE profiles with negative Eu/Eu* anomalies.

Figure 5.5 shows the variation of initial $^{87}Sr/^{86}Sr$ with 1/Sr for the internal or "main phase" Bitteroot lobe granitoids which Fleck and Criss (1985) regarded as mixtures between an old lower crustal component ($^{87}Sr/^{86}Sr_{(80Ma)}$=0.708 and upper crustal components.

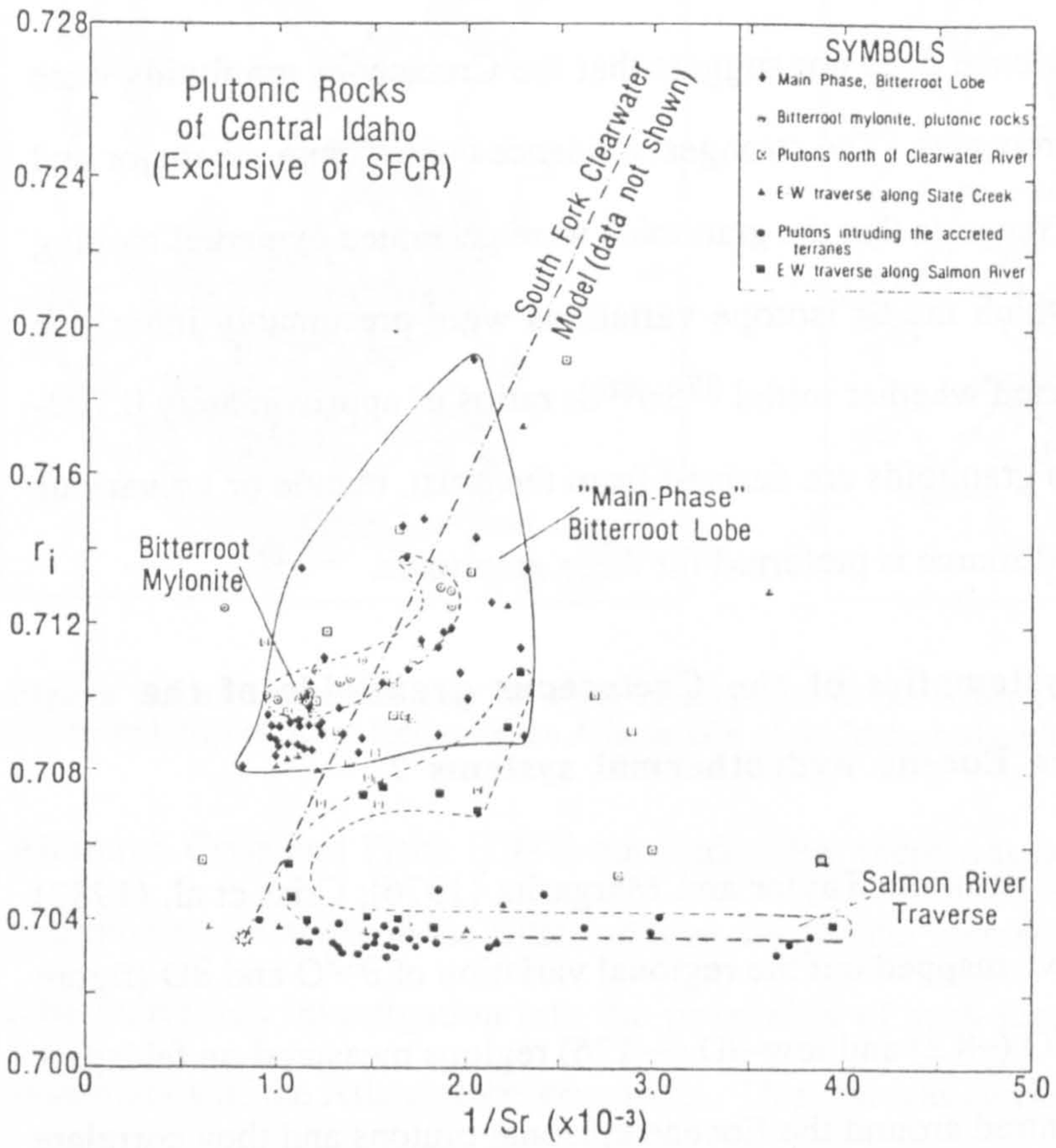

Figure 5.5 Initial $^{87}Sr/^{86}Sr$ versus 1/Sr for the Bitteroot lobe granitoids in comparison with those from the accreted terranes, and the model for the SFCR pluton traverse. After Fleck and Criss (1985).

It is clear for the internal phases of the Bitteroot lobe that there is a cut off with no samples with $^{87}Sr/^{86}Sr_{(80Ma)}$<0.708 and that there is a concentration of samples with $^{87}Sr/^{86}Sr_{(80Ma)}$ ≈0.708-0.709 and 1/Sr (x10^{-3}) ≈1-1.5 (Sr =1000-650ppm) similar to the samples from the Atlanta lobe from in study (figure 5.4). This suggests that similar source regions may have existed in the Bitteroot lobe and the Atlanta lobe and have been a major source component for the granitoids. Fleck and Criss (1985) and Manduca (1988) suggest that the lower crust was the most likely source region and the lower crust was the preferred source for the Atlanta lobe granitoids based on major and trace element modelling in chapter 4. Upper crustal materials are generally not incorporated into the magmas of the Atlanta lobe apart from on a localised scale near Precambrian wall-rocks. It is suggested that more

careful sampling away from wall-rocks and altered zones in the Bitteroot lobe may well reveal lower and more restricted initial $^{87}Sr/^{86}Sr$ ratios (0.708-0.709) consistent with the volume of upper crustal material incorporated into the Cretaceous magmas, in either lobe of the Idaho batholith, being quite small.

In summary the Sr isotope evidence does not suggest that the Cretaceous granitoids were generated by mixing or AFC processes. The strongest evidence comes from the major and trace element modelling which suggests that the granitoids were generated by partial melting a lower crustal source from which the Sr isotope variations were presumably inherited. Because it cannot be distinguished whether initial $^{87}Sr/^{86}Sr$ ratios of approximately 0.708-0.709 typical of the Cretaceous granitoids are derived from the crust, mantle or by various mixing processes a lower crustal source is preferred for these granitoids.

5.2.4 Are the Sr isotope systematics of the Cretaceous granitoids of the Atlanta lobe affected by the Eocene hydrothermal systems ?

In the Atlanta lobe of the Idaho batholith Taylor and Margaritz (1976); Criss et al. (1982) and Criss and Taylor (1983) have mapped out the regional variation of $\partial^{18}O$ and ∂D (figure 5.6a, b). Anomalously low-$\partial^{18}O$ (~8.2) and low-∂D (~-176) regions measured on feldspars and biotites respectively are centred around the Eocene epizonal plutons and they correlate with reductions in K-Ar dates and loss of K_2O from biotite (Criss et al., 1982 and references therein). The above authors argued that the reductions were due to extensive ($1500km^2$) circulation systems of meteoric fluids with low-∂D (≈-120) and low-$\partial^{18}O$ (≈-16) at temperatures of 150°-400°C that laterally spread 25-50km and circulated to depths of 5-7km, driven by the Tertiary epizonal plutons. The most intense hydrothermal activity was marked by low-$\partial^{18}O$ zones on the margins of the Eocene plutons such as the Sawtooth batholith (figure 5.6a), where there is a ring zone of low-$\partial^{18}O$ coincident with the high-permeability ring fracture zone of the ancient Sawtooth caldera system (Criss and Taylor, 1983).

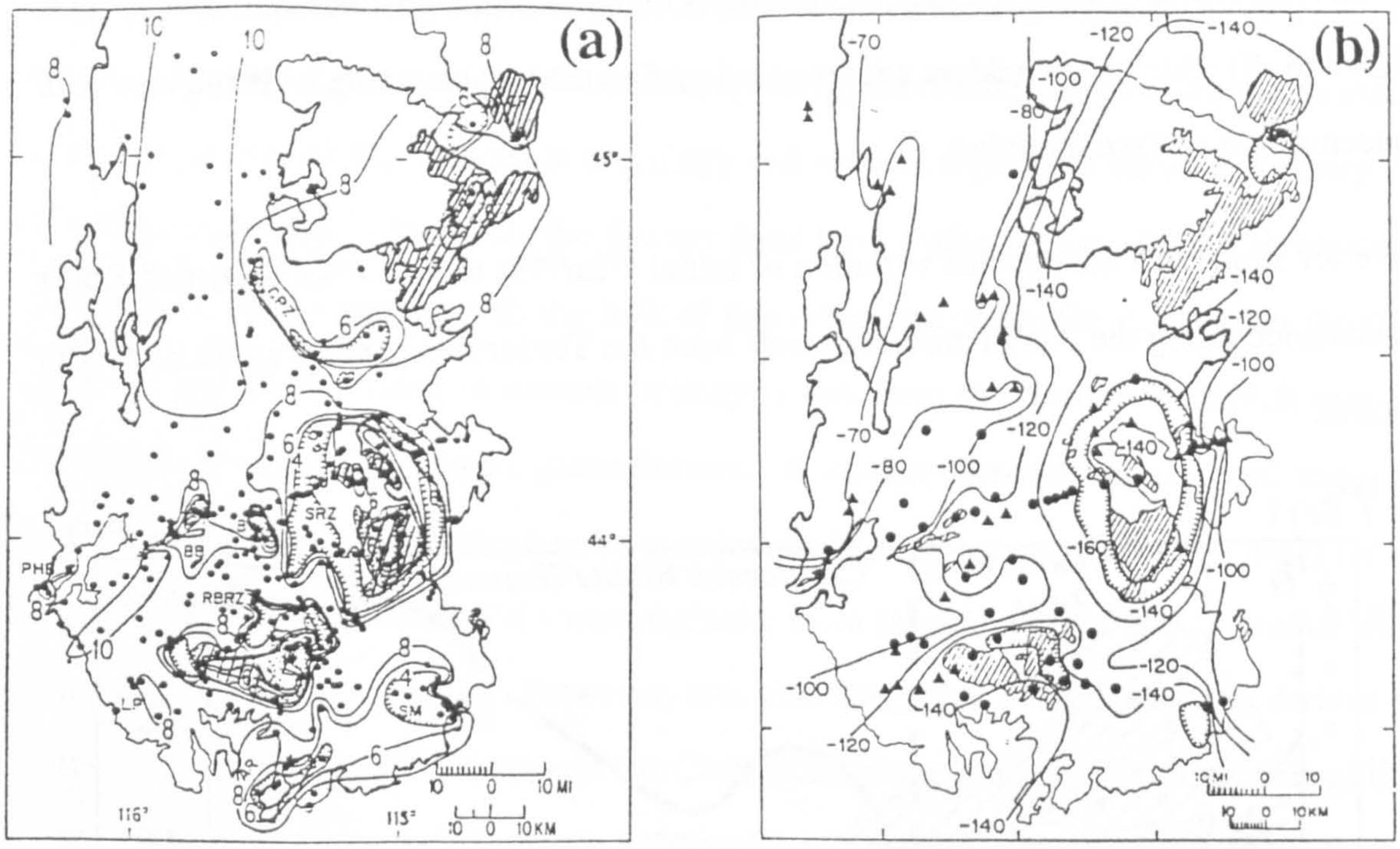

Figure 5.6 a) Contoured map of $\partial^{18}O$ of feldspars in the Atlanta lobe of the Idaho batholith. **b)** Contoured map of ∂D of biotites in the Atlanta lobe of the Idaho batholith. After Criss and Taylor (1983).

Although Criss and Fleck (1977) concluded that there was no change in $^{87}Sr/^{86}Sr$ due to hydrothermal activity in the Bitteroot lobe, the greater intensity of circulation in the Atlanta lobe warranted investigation into the possibility of such process affecting the Sr isotope systematics of the Atlanta lobe granitoids. This test was carried out by making two detailed traverses across established hydrothermally altered zones. The Alice Lake to Vienna Mining district traverse (ALVT) was made away from the southern margin of the large Tertiary epizonal granite batholith across the Sawtooth Ring Zone (SRZ) of low-$\partial^{18}O$ and low-∂D (Criss and Taylor 1983) (see figure 3.4c and 5.6a). The Long Gulch Pluton traverse (LGPT) (figure 3.4b) is across a much smaller dioritic pluton on the north margin of the low-$\partial^{18}O$ anomaly of Boise Basin (figure 5.6a), that has also been intruded by a Tertiary dyke swarm.

The detailed contoured map of $\partial^{18}O$ around the Sawtooth batholith has allowed accurate correlation of Criss and Taylor's (1983) measured $\partial^{18}O$ values with the whole rock samples of the ALVT traverse and thus with the major element, trace element and Sr isotopic data. The ALVT traverse crosses the SRZ of extremely depleted, but highly variable $\partial^{18}O$ values

The ALVT traverse crosses the SRZ of extremely depleted, but highly variable $\partial^{18}O$ values ($\partial^{18}O \approx 4$ to -8) which is coincident with the ancient Sawtooth caldera ring fault and also with a concentration of Tertiary dykes.

Figure 5.7 illustrates the detailed variation of initial $^{87}Sr/^{86}Sr$ ratios, $\partial^{18}O$, SiO_2 and Rb/Sr with distance along the ALVT traverse away from the Tertiary epizonal granitic Sawtooth batholith.

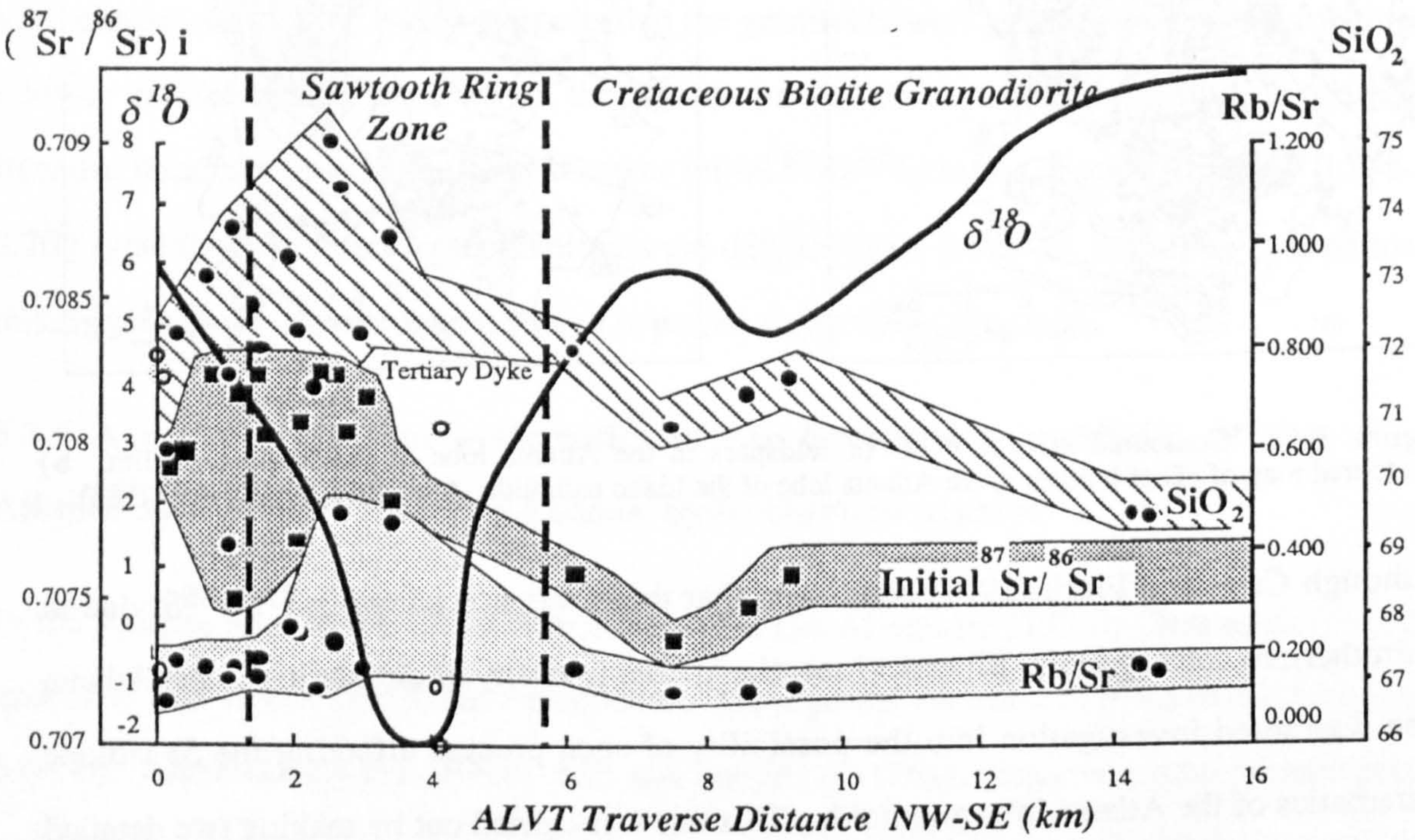

Figure 5.7 Diagram of the variation of initial $^{87}Sr/^{86}Sr$ ratios, $\partial^{18}O$, SiO_2 and Rb/Sr with distance along the ALVT traverse away from the Sawtooth batholith. $\partial^{18}O$ was from Criss and Taylor (1983) and where uncontoured within the SRZ, it is arbitrarily drawn down to -2.3 which is the nearest measured value from within the SRZ. The fields for variation of the Cretaceous phases are shaded around the filled symbols and the two open symbols are from the Sawtooth batholith and a Tertiary dyke respectively.

The initial $^{87}Sr/^{86}Sr$ ratios, the silica content and the Rb/Sr ratios (figure 5.7) are near constant across the southeastern portion of the traverse furthest from the Tertiary batholith, although $\partial^{18}O$ falls systematically from +8 to +4‰. However, on the inner margin of the SRZ where Criss and Taylor (1983) report extremely low, but highly variable $\partial^{18}O$ values, SiO_2 and initial $^{87}Sr/^{86}Sr$ are also more variable and Rb/Sr ratios exhibit a small increase in variation (figure 5.8). There does not appear to be any systematic correlation between Sr isotope initial ratios and $\partial^{18}O$, but there is some indication that initial $^{87}Sr/^{86}Sr$, SiO_2 and Rb/Sr may have been disturbed slightly and increased rather than reduced from background

levels. This suggests that circulating fluids incorporated Sr with higher $^{87}Sr/^{86}Sr$, higher silica and higher Rb/Sr than the Cretaceous biotite granodiorite surrounding the Sawtooth batholith. Although the contrast in chemistry and isotopic signatures between Tertiary and Cretaceous granitoids is small, the former does have higher values for all three above parameters. This together with the lack of any other source for the material in the fluid suggests that the direction of material transport was from the Tertiary batholith into the surrounding cooler Cretaceous granodiorites. A similar direction of material transport causing perturbation of Sr isotope ratios was invoked by Farmer and DePaolo (1987) for the hydrothermal circulation around a monzogranite stock intruding Precambrian granite wall-rocks at San Manuel, Arizona. However, it is also likely that SiO_2, Rb and Sr derived by hydrothermal fluid circulation through the Cretaceous biotite granodiorite were concentrated in the fluid and redeposited within the highly altered zones. Field and petrographic studies (Chapter 3) have shown that most of the granitoids on the ALVT traverse, even within the SRZ, remain fresh apart from weak seritisation of feldspar and biotite reacting to chlorite. It has also been shown that strong alteration is confined to small fracture or shear zones, typically on a meter scale.

In summary the coincidence of the low-$\partial^{18}O$ values, variable SiO_2 and initial $^{87}Sr/^{86}Sr$ ratios and the ancient Tertiary caldera fracture zone suggests that even within regions of the most intense hydrothermal circulation, the fluid flow, material carried with it and associated alteration were not pervasive, but controlled by fractures. The extremely high flow rates required for the large volumes of fluid argued for by Criss and Taylor (1983) are only consistent by flow along fractures rather than by slower diffusion. Moreover diffusion or flow along micro-fractures might be expected to have caused a more pervasive alteration to the rock that is unobserved in this case. It is concluded that the Sr isotopic variations are not altered pervasively and that undisturbed Sr isotope systems have been sampled by avoiding the highly localised fracture controlled alteration zones.

The variations of initial $^{87}Sr/^{86}Sr$, SiO_2 and Rb/Sr across the Long Gulch dioritic pluton are shown in figure 5.8 in comparison with the low-$\partial^{18}O$ anomaly of Criss and Taylor (1983).

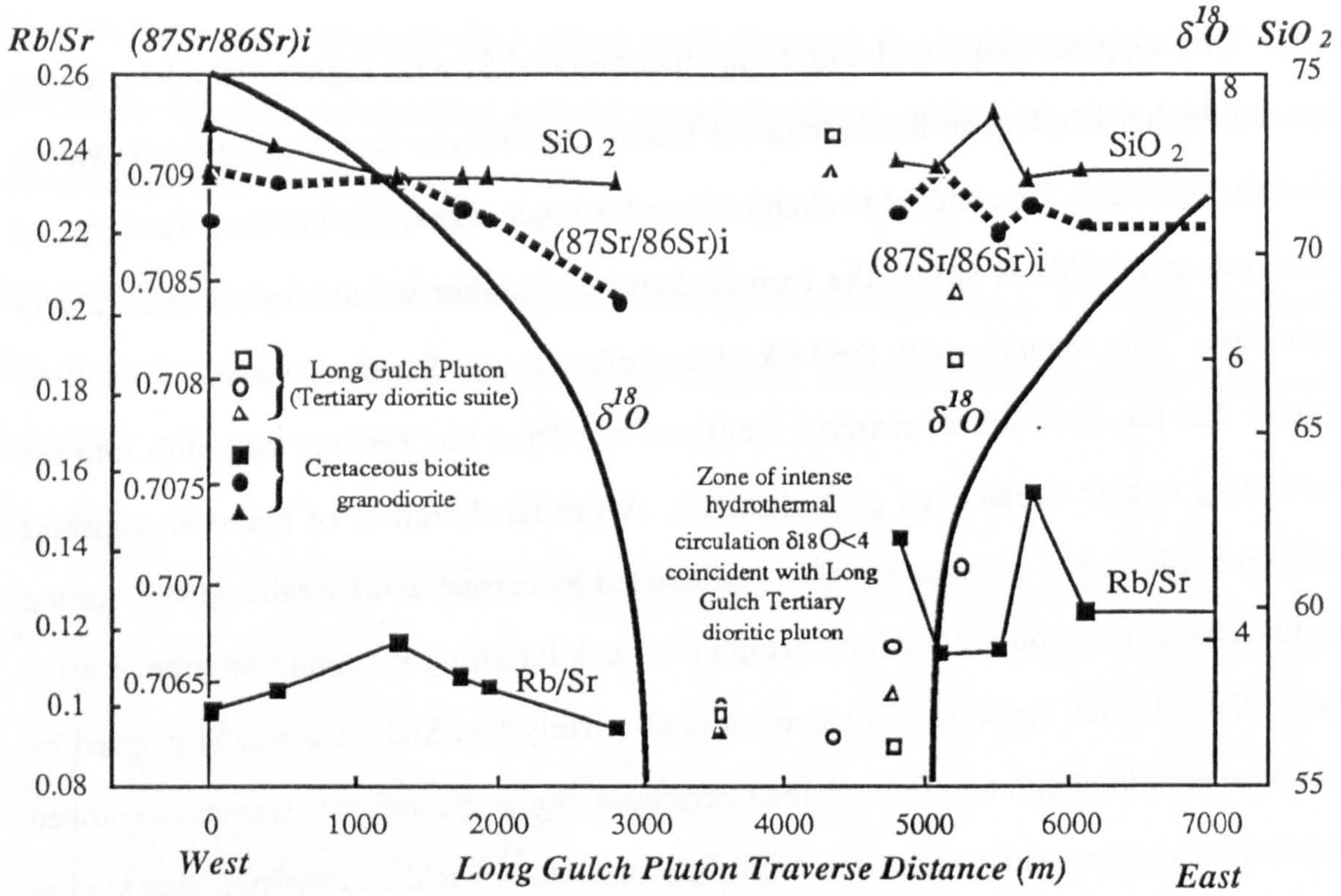

Figure 5.8 Diagram of the variation of initial $^{87}Sr/^{86}Sr$ ratios, $\partial^{18}O$, SiO_2 and Rb/Sr with distance along the LGPT traverse across a Tertiary dioritic stock. $\partial^{18}O$ values were extrapolated from those from Criss and Taylor (1983).

There is no obvious change or increased variation of initial $^{87}Sr/^{86}Sr$, SiO_2 or Rb/Sr within the Cretaceous biotite granodiorites which is consistent with field and petrographic observations of sharp intrusive contacts with little alteration. Unlike the ALVT traverse there are no Cretaceous granitoids within the area of the most extreme depletion of $\partial^{18}O$ values because it is very localised and centred on the dioritic stock. The Tertiary diorites taken from within this stock are fresh and show minimal variation of initial $^{87}Sr/^{86}Sr$ between 0.706-0.7065, which is similar to other Tertiary dioritic plutons. In addition the correlation of higher silica with higher Rb/Sr contents in the dioritic samples, which has previously been argued to be the result of within-pluton fractional crystallization (section 4.8), are preserved and thus presumably undisturbed by the hydrothermal circulation.

In conclusion, the intense hydrothermal circulation of fluids in the Atlanta lobe has not significantly altered the $^{87}Sr/^{86}Sr$ ratios, or the major and trace element geochemistry of the Cretaceous granitoids or the Tertiary dioritic and granitic suites. The exception to this are highly altered rocks confined to fracture or shear zones which are effectively mapped out by

the largely disused Au, Ag and Pb mines or prospects and the extremely low-$\partial^{18}O$ values (Criss and Taylor, 1983).

5.2.5 Sr isotope variations of the Tertiary dioritic and granitic suites

Few previous Sr isotope analyses have been carried out on the Tertiary bimodal granitoids of the Idaho batholith. Fleck and Criss (1985) and Criss and Fleck (1987) report $^{87}Sr/^{86}Sr$ ratios from the Bitteroot lobe, but have either not analysed any dioritic end members or have failed to divide them from the Tertiary granites.

Figure 5.9, a histogram of initial isotope ratios for the dioritic and granitic suites from this study, calculated at 50Ma and 45Ma respectively shows that the dioritic suite generally has lower initial $^{87}Sr/^{86}Sr$ ratios than the granitic suite. Initial $^{87}Sr/^{86}Sr$ in the dioritic suite ranges from 0.7062-0.7089, whereas the granitic suite ranges from 0.7083-0.7130.

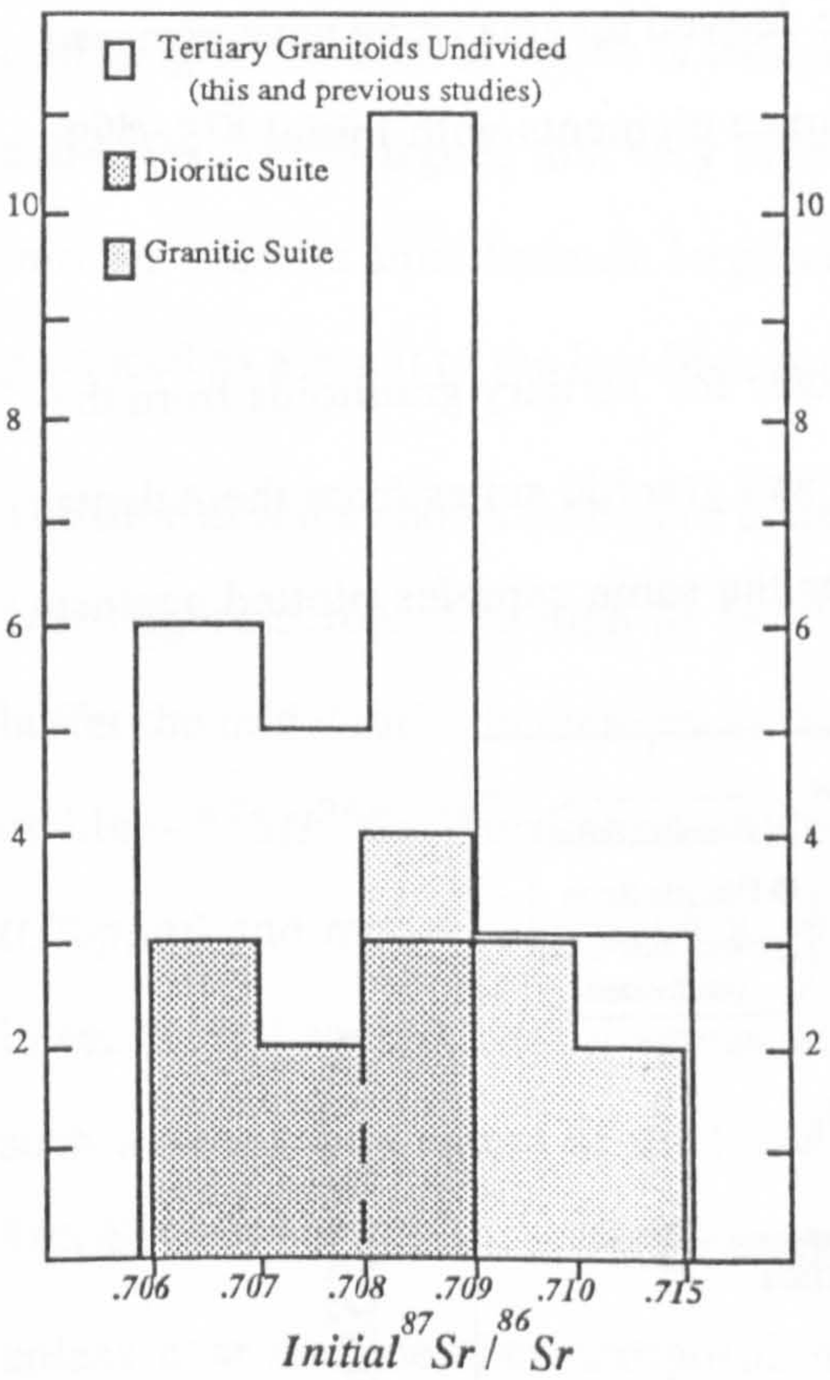

Figure 5.9 Histogram of initial Sr isotope ratios of the Tertiary dioritic and granitic suites from this study and the entire sample set of undivided Tertiary granitoids from this and previous studies.

The entire sample set of undivided Tertiary granitoids including those of Criss and Fleck (1987) are also shown in figure 5.9. Although the total number of analyses is small there is a peak at 0.708 where the dioritic and granitic suites overlap and where most of the samples

from Criss and Fleck (1987) plot. The distribution of samples tails off to higher initial $^{87}Sr/^{86}Sr$ ratios (>0.709), but there is a weak peak at $^{87}Sr/^{86}Sr$=0.7065.

There are several previously alluded to mixing processes which can account for a weak bimodal distribution of the Sr isotopic ratios which also vary systematically with major and trace elements (see figure 4.14). The wall-rocks and presumably the basement through which the Tertiary plutons were intruded are almost exclusively the Cretaceous granitoids with only minor contacts with Precambrian rocks as rare roof pendents as for example in the Sawtooth batholith. Contamination or mixing with Precambrian upper crustal rocks was improbable and likely to be restricted to small volumes of rock close to the roof pendants. The similar inferred trace element patterns of the source of the Cretaceous granitoids and Tertiary granites (section 4.8) and the similar range of $^{87}Sr/^{86}Sr$ ratios, with an average ≈0.708 suggests that a likely source may have been isotopically heterogeneous lower crust. Limited mixing with subcontinental mantle-lithosphere derived magmas may have occurred to account for the systematic variation of major and trace elements with initial $^{87}Sr/^{86}Sr$ ratios in the dioritic suite.

Figure 5.10a shows initial $^{87}Sr/^{86}Sr$ plotted against Rb/Sr for Tertiary granitoids from the Bitteroot lobe (Fleck and Criss, 1985) and the dioritic and granitic suites from the Atlanta lobe, whereas figure 5.10b shows initial $^{87}Sr/^{86}Sr$ for the same samples plotted against 1/Sr.

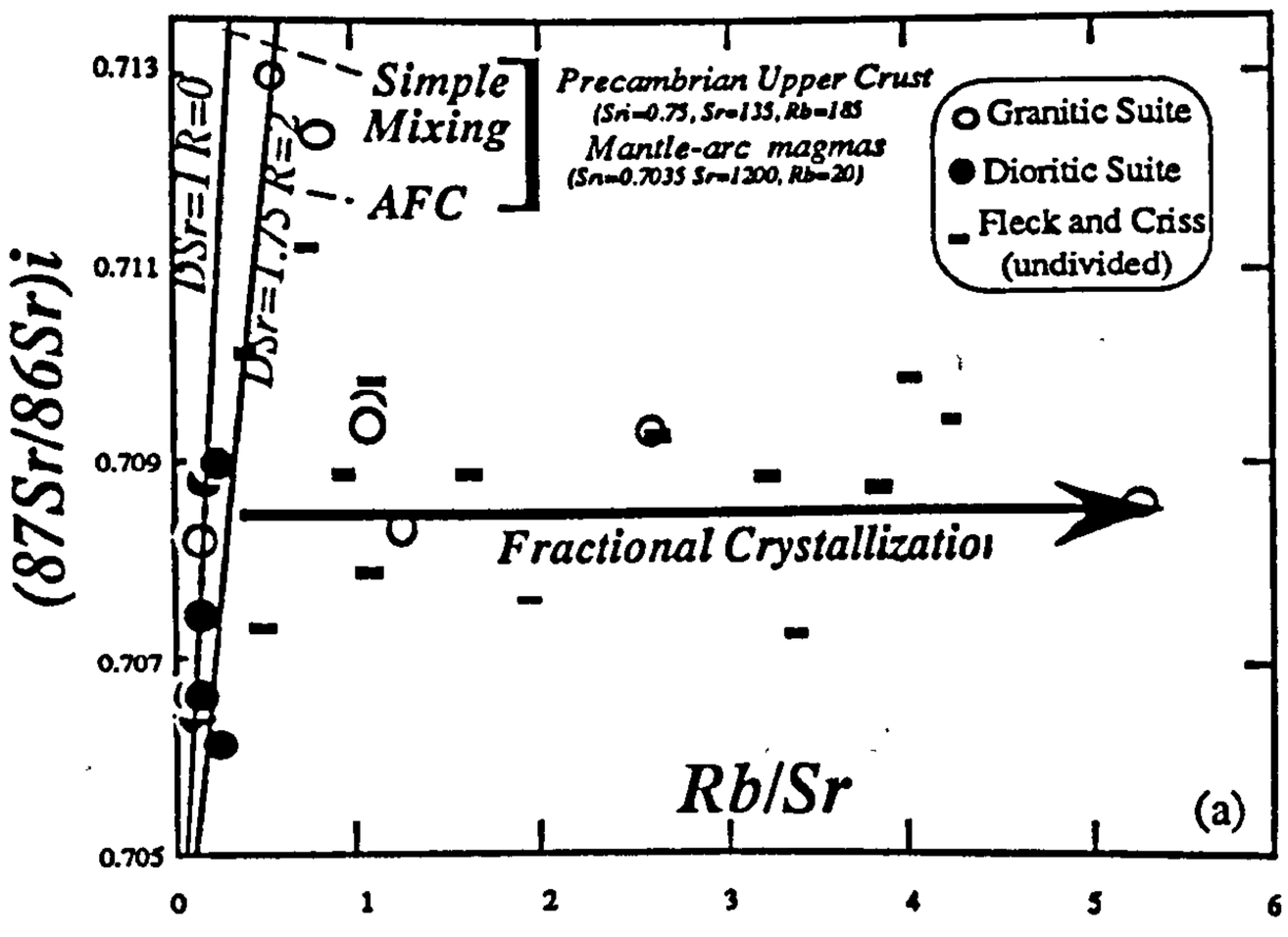

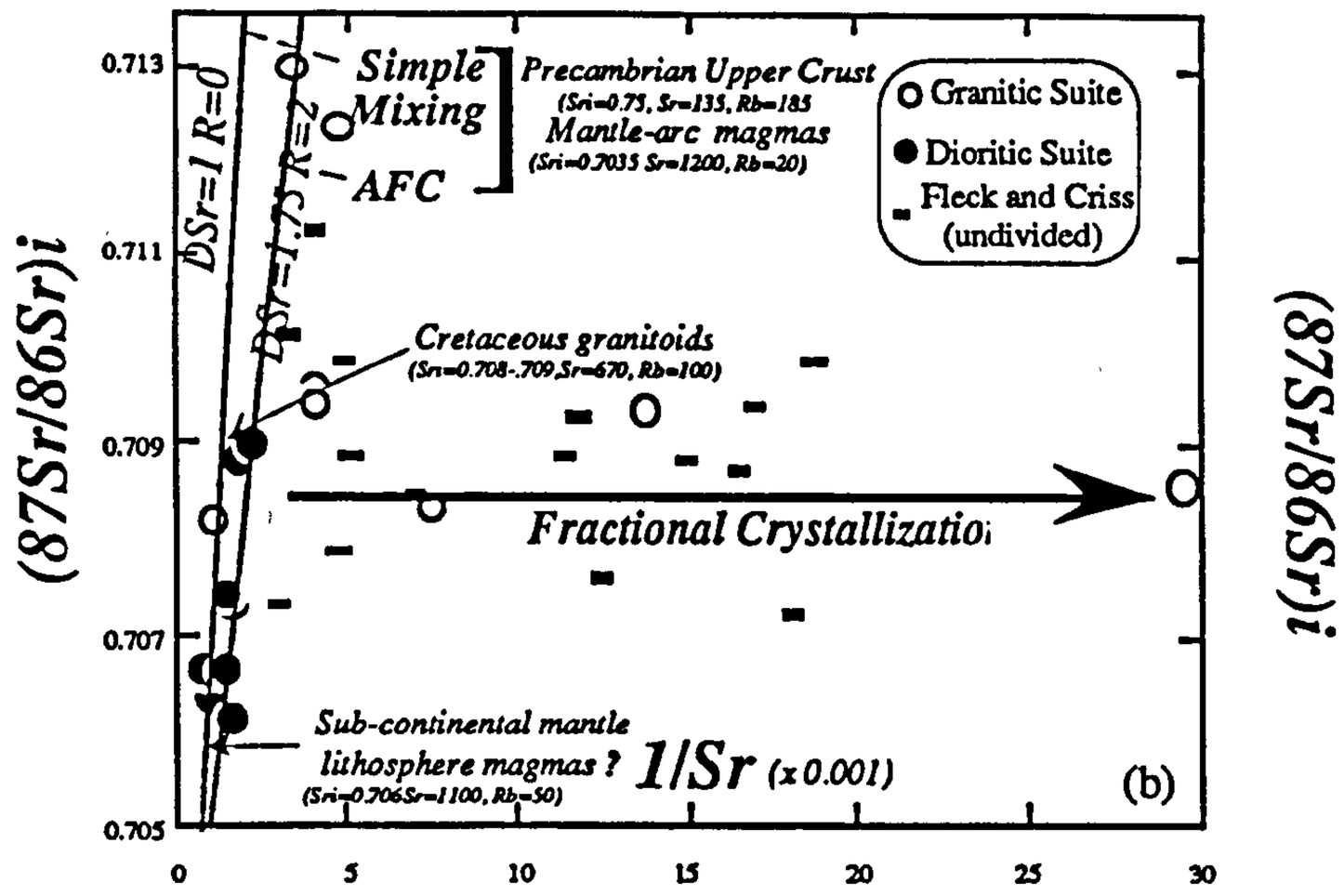

Figure 5.10 a) Graph of initial $^{87}Sr/^{86}Sr$ versus Rb/Sr for the Tertiary dioritic and granitic suites and the Tertiary granites from the Bitteroot lobe (Criss and Fleck, 1977). b) Graph of initial $^{87}Sr/^{86}Sr$ versus 1/Sr for the same samples.

The granitic suite like the Bitteroot lobe granites show constant initial $^{87}Sr/^{86}Sr$ with changing Rb/Sr or 1/Sr which is thought to be the result of fractional crystallization. Fleck and Criss (1985) argued that very little Precambrian material could have been incorporated into the granitic suite because large variations in initial $^{87}Sr/^{86}Sr$ ratios would have been produced as a result of the low Sr contents of the granitoids.

The dioritic suite shows a trend of increasing initial $^{87}Sr/^{86}Sr$ over a small range in Rb/Sr or 1/Sr (figure 5.10). The high Sr (≈1100ppm) contents of the dioritic suite would tend to buffer the initial ratios in these rocks from the effects of incorporation of quite large amounts of high- $^{87}Sr/^{86}Sr$ Precambrian material. However, mixing of material with high Sr (670ppm) and moderate initial $^{87}Sr/^{86}Sr$ ≈0.708, similar to the Cretaceous granitoids or a lower crustal source, with magmas with high Sr and low initial $^{87}Sr/^{86}Sr$ could produce such a trend. The nature of the low $^{87}Sr/^{86}Sr$ material is constrained by the fact that no $^{87}Sr/^{86}Sr$ ratios of even the most mafic of the dioritic suite are less than 0.706. Therefore unless near end-member compositions with lower initial $^{87}Sr/^{86}Sr$ are unseen, the low $^{87}Sr/^{86}Sr$, perhaps mantle-derived component, was taken to have $^{87}Sr/^{86}Sr$≈0.706.

Figure 5.10a and 10b clearly shows that within the scatter of the trend of the dioritic suite it cannot be resolved whether the end members during mixing processes are more likely to be partial melts of Precambrian upper crust ($^{87}Sr/^{86}Sr$=0.752, Sr=185), oceanic arc mantle-derived material ($^{87}Sr/^{86}Sr$=0.7035, Sr=20), a component of sub-continental lithospheric mantle ($^{87}Sr/^{86}Sr$≈0.706, Sr≈1000), lower crust ($^{87}Sr/^{86}Sr$=0.708, Sr≈750, or the Cretaceous granitoids ($^{87}Sr/^{86}Sr$=0.708, Sr=650).

Previous arguments suggest that upper crust is unlikely to be involved as it does not interact with the dioritic magmas and major and trace element modelling suggested that a large contribution of material from a lower crustal source was incorporated into the dioritic suite. Therefore, heterogeneous lower crust, the Cretaceous granitoids or old sub-continental lithospheric mantle are the most likely end members.

Moreover due to the small number of samples and considerable scatter within the trend it can not resolved whether simple mixing or AFC processes occurred, but the evidence for within pluton fractional crystallization (Chapter 3 and 4) and general arguments about the latent heat of crystallization needed for assimilation suggests AFC is more likely.

In summary the evolution of the Tertiary bimodal suite was likely to have been related to early Tertiary extension and intrusion of low-$^{87}Sr/^{86}Sr$ (≤0.706) mantle-derived magmas, at least as a source of heat. Trace element modelling suggests that melting could have occurred in the lower crust to produce dioritic magmas with initial $^{87}Sr/^{86}Sr$ ≈0.706, but the old underlying sub-continental mantle-lithosphere could plausibly have such ratios and the extensional regime may have aided rapid passage and emplacement of these into the upper crust without ponding and melting in the lower crust.

Whatever the origin, the extensional tectonic setting and attenuated nature of the crust allowed these hot, mafic magmas to reach moderate to upper crustal levels, where cooling crystallization and assimilation of old continental crust wall-rocks occurred to produce the trends of increasing SiO_2 and Rb/Sr with initial $^{87}Sr/^{86}Sr$ (Figure 5.10). The granitic suite, which has been successfully modelled by high degrees of fractional crystallization of a

mineralogy similar to that observed in the rocks, could either be derived from the high $^{87}Sr/^{86}Sr$ members of the dioritic suite which separated and fractionated after the parental magmas cooled sufficiently to prohibit further assimilation, or be partial melts of lower crustal material by dioritic magmas that were trapped lower in the crust. The former model may be unlikely because the dioritic magmas would be nearly solid by the time material was no longer assimilated, preventing separation of granitic magmas and fractional crystallization observed in the granitic plutons. In addition the granitic plutons are spatially and temporally separated from the dioritic suite. The preferred model is that the dioritic magmas acted as a heat source for melting the lower crust to produce the granitic magmas, which because of their low density and the extensional tectonic regime were emplaced high in the crust at temperatures too low to assimilate upper crustal material.

5.3 Nd isotope geochemistry

No previous Nd isotope geochemistry has been published on the Atlanta lobe granitoids, although some limited $^{143}Nd/^{144}Nd$ analyses of the SFCR granitoids, the accreted terranes and Precambrian upper crustal wall-rocks were carried out by Fleck and Criss (in press). The $^{143}Nd/^{144}Nd$ ratios determined on selected granitoids from the Atlanta lobe during this study are listed in appendix B.

The measured $^{143}Nd/^{144}Nd$ ratios of the Cretaceous and Tertiary granitoids are presented on histograms in figure 5.11. An age correction has not been applied to the suite in order that all $^{143}Nd/^{144}Nd$ ratios could be presented including those without measured Sm/Nd ratios. The average age of 80Ma and the generally low Sm/Nd ratios, however would produce only small reduction in the $^{143}Nd/^{144}Nd$ ratios, typically in the order of 0.00005 for an Sm/Nd ratio of 0.2 which is a change of only 0.009% of the measured value.

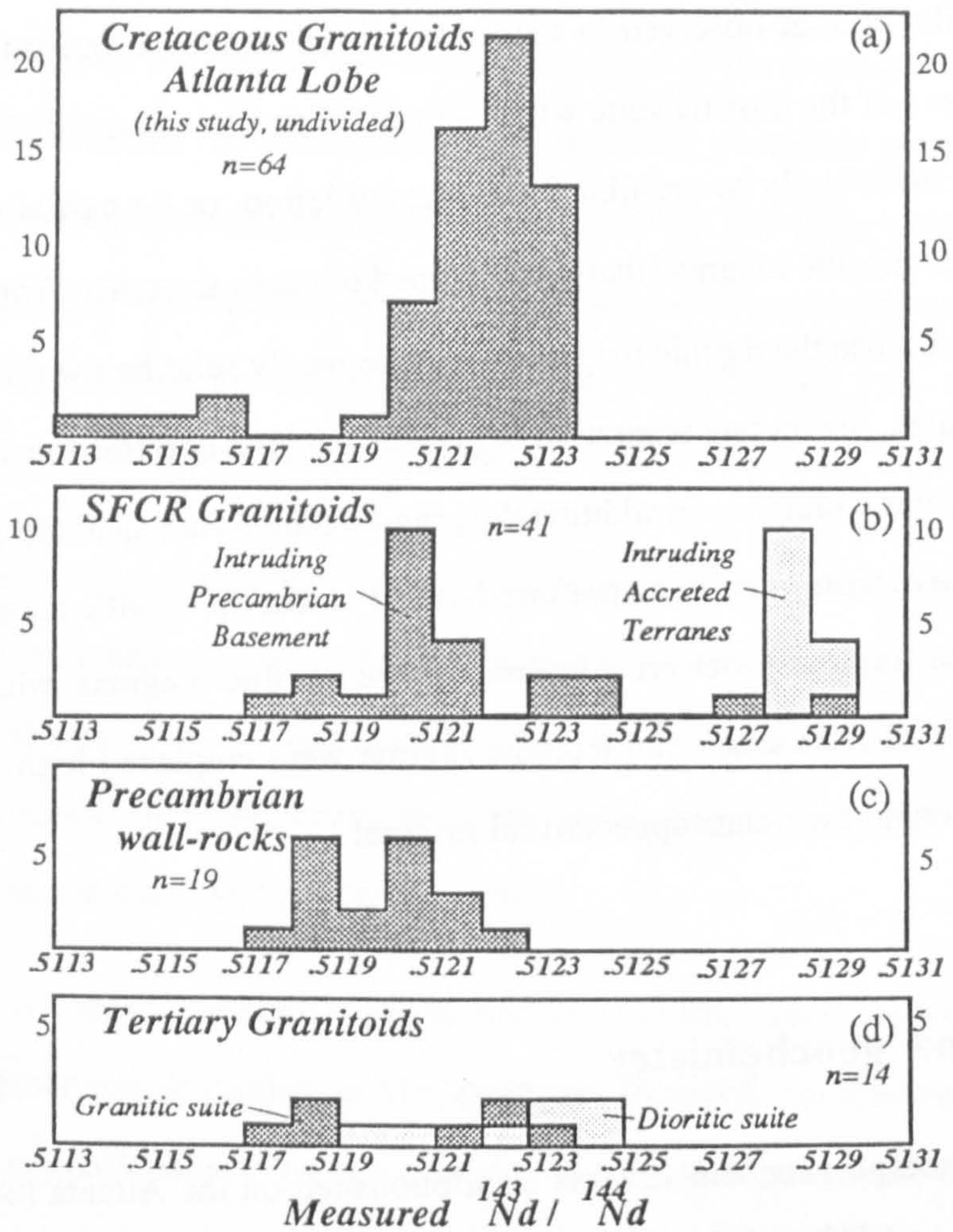

Figure 5.11 Histogram of measured $^{143}Nd/^{144}Nd$ ratios from the region of the Idaho batholith. a) Cretaceous granitoids from this study, b) SFCR granitoids Fleck and Criss (unpublished); c) Precambrian wall-rocks; d) Tertiary granitoids.

The Cretaceous granitoids range from $^{143}Nd/^{144}Nd = 0.5119\text{-}0.5124$ with an average value of 0.5122. Five analyses with very low $^{143}Nd/^{144}Nd$ between 0.5113-0.5117 are leucogranites and high silica biotite granodiorites which have been previously demonstrated to be upper crustal melts, although they have lower $^{143}Nd/^{144}Nd$ ratios than the Precambrian wall-rocks (Fleck and Criss, unpublished data) suggesting considerable differences in age and chemical heterogeneity within the upper crustal rocks of the region.

The Cretaceous granitoids from this study have generally lower and a smaller range in $^{143}Nd/^{144}Nd$ than the SFCR granitoids, the latter which have been previously argued to be mixtures between Precambrian upper crustal wall-rocks and mantle derived magmas, on the

basis of Sr isotope evidence. This may again suggest that the Cretaceous magmas from the Atlanta lobe were not derived by such mixing processes.

The high measured $^{143}Nd/^{144}Nd$ ratios of the plutons intruding the accreted terranes are consistent with evolution in a source region that had high time integrated Sm/Nd ratios, unlike those of old continental crust or old LREE enriched sub-continental mantle-lithosphere, but consistent with a depleted-mantle reservoir.

The few Tertiary granitoids analysed do not exhibit a clear bimodal distribution of $^{143}Nd/^{144}Nd$ ratios between the Tertiary granitic and dioritic suites (figure 5.11). The range of measured values is 0.5117-0.5125, but more samples of the granitic suite have lower ratios than the dioritic suite. This is consistent with the dioritic suite incorporating a component with higher time integrated Sm/Nd ratios than the granitic suite, possibly from the mantle.

The observed range of $^{143}Nd/^{144}Nd$ ratios in the Atlanta lobe granitoids are suggested by trace element modelling (chapter 4) to have been generated in and inherited from a lower crustal source. Assuming that Sm/Nd has not been appreciably fractionated during intra-crustal processes (McCulloch and Wasserburg, 1978) an average continental crustal value of Sm/Nd allows an estimate of the time it has taken to generate the observed range of $^{143}Nd/^{144}Nd$ within the crustal reservoir. The Cretaceous granitoids yield a range of source ages of 1.1Ga-1.8Ga assuming that the crust was extracted from a depleted mantle reservoir and the crust had an average value of Sm/Nd of 0.2. The Cretaceous granitoids with anomalously low $^{143}Nd/^{144}Nd$ yield source ages of 2.13Ga-2.72Ga. The Tertiary granitoids yield a source ages in the range 0.93Ga-2.13Ga for the same parameters used above. These results broadly indicate that the lower crust which is sampled by the Cretaceous granitoids is Proterozoic, but that there is a broad range in age of the source regions. The anomalous Cretaceous granitoids and the Tertiary granitoids possibly contain material of Archaean age consistent with old source ages.

The Nd model ages of individual granitoids are considered in more detail in section 5.6 in the light of Pb-Pb model ages and taking into account evidence from trace element modelling which suggests that Sm/Nd may have been fractionated during partial melting to generate the granitoids in the lower crust.

5.4 Combined Sr and Nd isotope evolution

In order to address the Sr and Nd isotope evolution of the Idaho batholith and its respective source regions and compare this with other granitoid batholiths and source rocks of different ages the ε_{Nd} and ε_{Sr} notation was used. The ε_{Nd} notation (see appendix A 7.1 for equation) compares the $^{143}Nd/^{144}Nd$ ratio at the time of granitoid emplacement with that of the bulk earth at the same time. Samples with negative ε_{Nd} values result from low time-integrated Sm/Nd ratios. Sm/Nd ratios are generally unfractionated during intra-crustal processes (McCulloch and Wasserburg, 1978), but crustal formation by extraction of magmas from the mantle reduces Sm/Nd ratios. Therefore granitoids with negative ε_{Nd} may either be derived from ancient crustal rocks or old, LREE enriched, continental mantle lithosphere. Similarly samples with positive ε_{Sr} result from rocks which have had high time-integrated Rb/Sr ratios. Rb/Sr ratios are increased slightly from mantle to crust during crust formation, but they can also be increased by intra-crustal or within-mantle processes so that positive ε_{Sr} may be derived from either old enriched mantle or old continental crustal sources.

The ε_{Nd} versus ε_{Sr} diagram (figure 5.12a) shows that the ε_{Nd} values of the Cretaceous granitoids from this study range from -4 to -15 and ε_{Sr} from 30 to 160, and so all the granitoids analysed here plot in the enriched, high-Rb/Sr, low-Sm/Nd quadrant of the diagram. For comparison granitoids from the SFCR in the northwestern Atlanta lobe, the accreted terranes (Fleck and Criss, unpublished data) and granitoids from the Sierra Nevada and Peninsular Ranges (DePaolo, 1981), are presented in figure 5.12b. Precambrian wall-rocks (Fleck and Criss, unpublished data) basalts and Archaean xenoliths from the Snake River Plain (Leeman et al., 1985) are shown in relation to all the previous data on an ε_{Nd} versus ε_{Sr} diagram of much reduced scale in figure 5.12c.

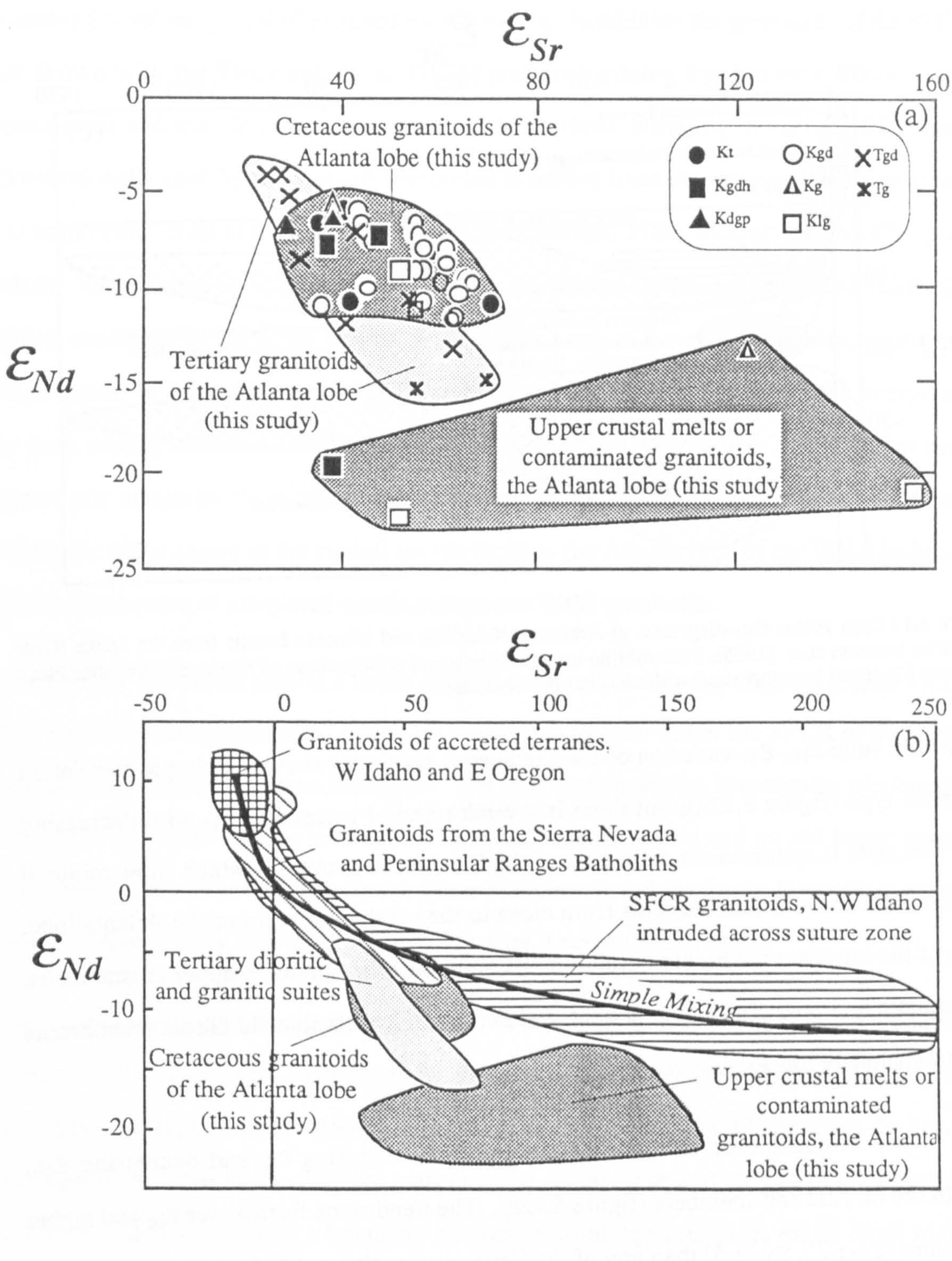

Figure 5.12 ε_{Nd} versus ε_{Sr} diagrams. a) Cretaceous and Tertiary granitoids of the Atlanta lobe from this study. b) Granitoids of the SFCR and accreted terranes after Fleck and Criss (in press), and granitoids of the Sierra Nevada and Peninsular Ranges after DePaolo (1981) in comparison with the Atlanta lobe granitoids.

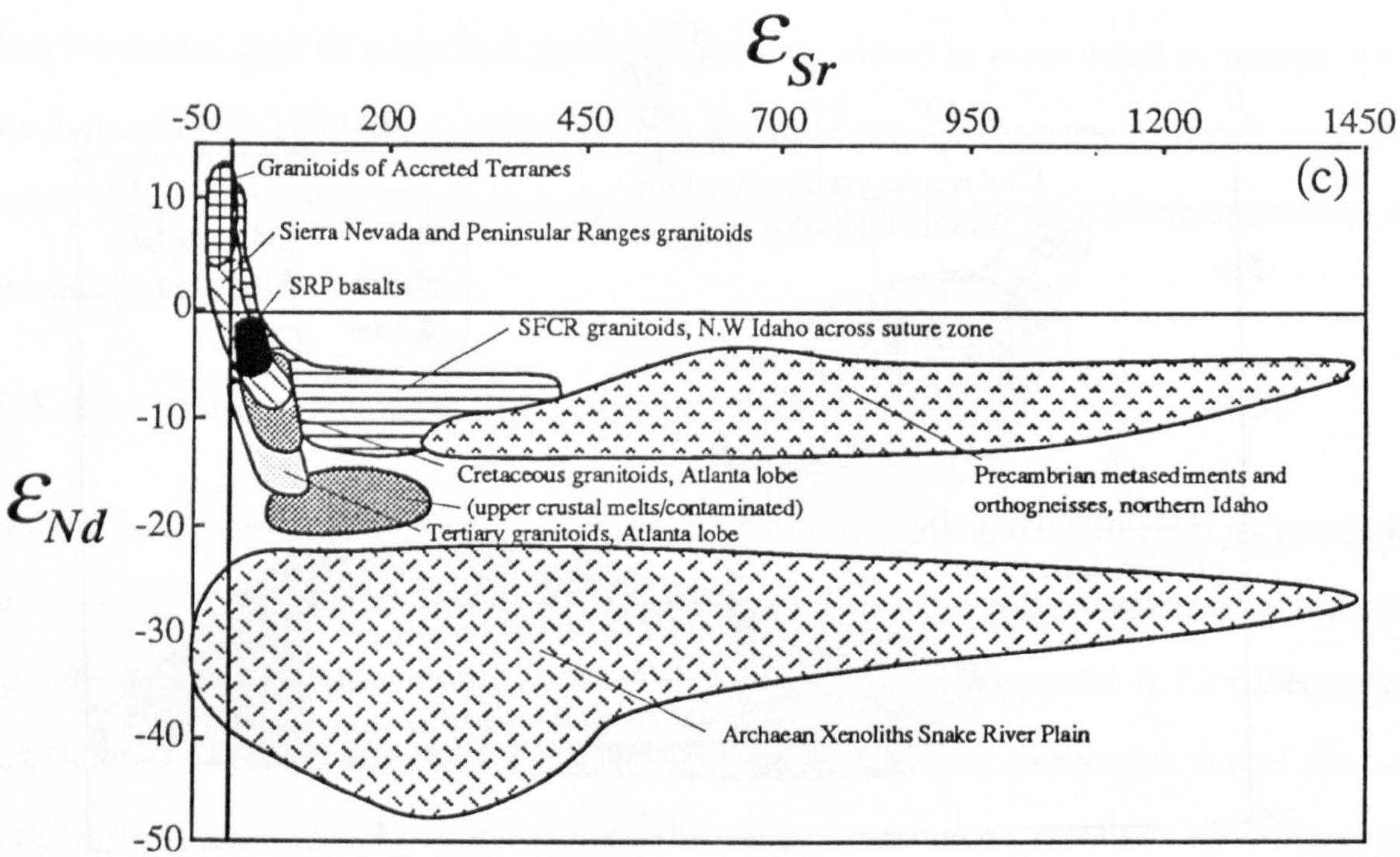

Figure 5.12 ε_{Nd} versus ε_{Sr} diagrams. c) Archaean Xenoliths and Miocene basalts from the Snake River Plain after Leeman et al. (1985), Precambrian metasediments and orthogneisses of northern Idaho after Fleck and Criss (in press) in comparison with all other previous data.

The within suite ε_{Nd}-ε_{Sr} variation of the Cretaceous granitoids shows no simple correlation with rock type (figure 5.12a), but there is a weak trend of increasing ε_{Sr} with decreasing ε_{Nd}. The suite is split into the main bulk of the Cretaceous granitoids which show minimal isotopic variation and four samples from close to the southern margin of the Atlanta lobe. Three of the latter are the highly peraluminous granitoids thought to be upper crustal melts, or to contain an upper crustal component, and the fourth is a hornblende-biotite granodiorite with anomalously low ε_{Nd}.

The Tertiary bimodal suite exhibits a steep trend of increasing ε_{Sr} and decreasing ε_{Nd} through the dioritic end-members (figure 5.12a). The trend starts from lower ε_{Sr} and higher ε_{Nd} values ($\varepsilon_{Sr} \leq 25$, $\varepsilon_{Nd} \geq -5$) than any of the Cretaceous rock types and projects towards the granitic suite end-members which have restricted ε_{Sr} and ε_{Nd} values of -16 and 50-60 respectively.

The ε_{Nd}-ε_{Sr} diagram is expanded in figure 5.12b to include the granitoids of the accreted terranes (Fleck and Criss, in press) which lie within the mantle array, with positive ε_{Nd} and

negative ε_{Sr} values typical of depleted mantle source. In addition the granitoids of the SFCR are shown with the Fleck and Criss' (1985) preferred mixing line between Precambrian upper crust and mantle derived magmas similar to those intruding the accreted terranes. Conventionally such hyperbolae are interpreted as mixing lines between depleted mantle and old continental crust end-members (Allegre and Othman, 1980; McCulloch and Chappell, 1982). The granitoids of the Sierra Nevada and the Peninsular Ranges batholiths (DePaolo, 1981), shown on figure 5.12b, exhibit a hyperbolic array of isotopic compositions between those typical of depleted mantle and young continental crust and they have been interpreted by such mixing models. The Cretaceous granitoids of the Atlanta lobe do not define such hyperbolic arrays as these other granitoids, and they have lower ε_{Nd} values. This may reflect the older nature of the crustal source rocks in the Atlanta lobe of the Idaho batholith and/or the absence of a depleted mantle component in the granitoids.

The Tertiary granitoids exhibit a better defined trend on the ε_{Nd}-ε_{Sr} diagram (figure 5.12b) than the Cretaceous granitoids, which is steeper than that for either the SFCR or the Sierra Nevada and Peninsular Ranges batholiths. The next section section investigates whether this trend may represent mixing between an enriched-mantle source and an old lower-crustal component, perhaps similar to a Snake River Plain basalt and the Snake River Plain crustal xenoliths respectively (shown in figure 5.12c after, Leeman et al., 1985).

The "upper crustal melt granitoids" typically have much lower ε_{Nd} values than the granitoids of the SFCR, which were interpreted by Fleck and Criss (1985) to contain a significant component of upper crustal material. This may reflect a significant difference in the age of the upper crust between the southern margin of the Atlanta lobe and the rest of the batholith, and so be the first hint that a boundary between crustal age provinces exists close to the southern margin of the Atlanta lobe. Such an old crustal source may be represented by the Archaean xenoliths from the Snake River Plain and metasediments which are exposed further to the south in the Albion Range (figure 5.12c, data from Leeman et al., 1985).

The Miocene tholeiitic basalts of the Snake River Plain are shown on figure 5.12c and have previously been interpreted as uncontaminated partial melts from old enriched spinel

lherzolite mantle ($^{87}Sr/^{86}Sr$ >0.7058, $^{143}Nd/^{144}Nd$ <0.51252) which contained at least a component of 2.5Ga material (Menzies et al., 1984). Such a mantle component is similar to that suggested for the mantle-derived end-member for the trend of the dioritic suite (figure 5.12b) and is investigated further in the following section.

5.4.1 Binary mixing and combined assimilation fractional crystallization (AFC) models

It was demonstrated above that the majority of the Cretaceous granitoids of the Atlanta lobe do not lie on simple mixing or AFC trajectories between depleted mantle sources and Precambrian upper crustal rocks of northern Idaho (section 5.3). This together with the absence of a hyperbolic trend on ε_{Nd}-ε_{Sr} diagrams (figures 5.12a and 5.12b) suggests that these processes were unimportant in their generation and are not further considered in this section. However, the four Cretaceous granitoids from near the southern margin of the lobe which have anomalously low ε_{Nd} and moderate to high ε_{Sr}, also do not contain a component similar to the Precambrian metasediments and orthogneisses of northern Idaho (figures 5.12b and 5.12c). They appear to be derived from or contain a significant component of old, low-ε_{Nd} material similar to Archaean sediments to the south of the Snake River Plain, or the Archaean crustal xenoliths from within the Snake River Plain. The above hypotheses cannot be distinguished for the few samples available and the argument is curtailed here. In summary the anomalous Cretaceous granitoids appear likely to have been derived by mixing moderate to high proportions of a component similar to the Archaean crustal xenoliths of the Snake River Plain and an Idaho batholith granitoids. The scatter of the low ε_{Nd} granitoids does not allow binary mixing processes to be distinguished from AFC processes, but suggests that the end-members, particularly the Archaean component were isotopically heterogeneous.

The Tertiary dioritic suite exhibits a steep trend on figures 5.12a,b and c, which is clearly inconsistent with the combination of Precambrian country rocks of northern Idaho and depleted mantle end-members such as those suggested by Fleck and Criss (1985) to account for the SFCR granitoids (figures 5.12a and b). This section investigates whether the

variation in the dioritic suite is consistent with mixing or AFC processes between an old enriched sub-continental, mantle-derived component and a low-ε_{Nd} Archaean crustal component.

Binary mixing models for the Tertiary dioritic (figure 5.13) suite have been calculated using both the least evolved dioritic granitoid and a mantle component equivalent to an average Snake River Plain basalt, as high ε_{Nd} end-members and a group of Archaean xenoliths as low ε_{Nd} components. The compositions of the end-members are listed in table 5.1.

End-Member Samples	Sr (ppm)	Nd(ppm)	ε_{Sr}	ε_{Nd}
Unevolved Cretaceous Granitoid	677	38.01	37	-5.5
Least Evolved Tertiary Diorite	1010	52	30	-4.9
Average Snake River Plain Basalt	281	19.7	29	-3.9
Archaean Xenolith (CK1-1)	210.9	13.51	410	-41.8
Archaean Xenolith (70-40)	324.4	9.75	149.7	-42.6
Archaean Xenolith (B1)	220	16.4	15.5	-22.9
Archaean Metasediment (YAG799)	115	19	1437.5	-22.9
Archaean Xenolith (Preferred)	324.4	9.75	80	-42.6

Table 5.1 All end-member compositions used in mixing and AFC calculations. Xenoliths data after Leeman et al (1985) and average Snake River Plain basalt from Lum et al. (1989).

Binary mixing to produce the trend within the dioritic suite (figure 5.13) is inconsistent with Archaean rocks with high ε_{Sr}, but good trends were fitted through the data for Archaean crustal components with low ε_{Nd} <-40 and ε_{Sr} ≈80-350. The proportion of Archaean material required for mixing with the Snake River Plain basalt was 0-40% whereas the least evolved dioritic magma required 0-60% addition of Archaean material, due to the higher concentrations of Sr and Nd in the latter. Two samples of the Tertiary granitic suite fall at the low end of the dioritic suite trend, with lower ε_{Nd} than the Cretaceous granitoids (compare figure 5.12a and figure 5.13) suggesting that the Tertiary granites may have been derived from the dioritic suite rather than a source isotopically similar to the granitic suite. However, this is thought to be unlikely as there is no evidence of systematic variation of ε_{Sr} or ε_{Nd} within the granitic suite. The preferred explanation is that the observed range in ε_{Sr} and ε_{Nd} was inherited from a heterogeneous source region.

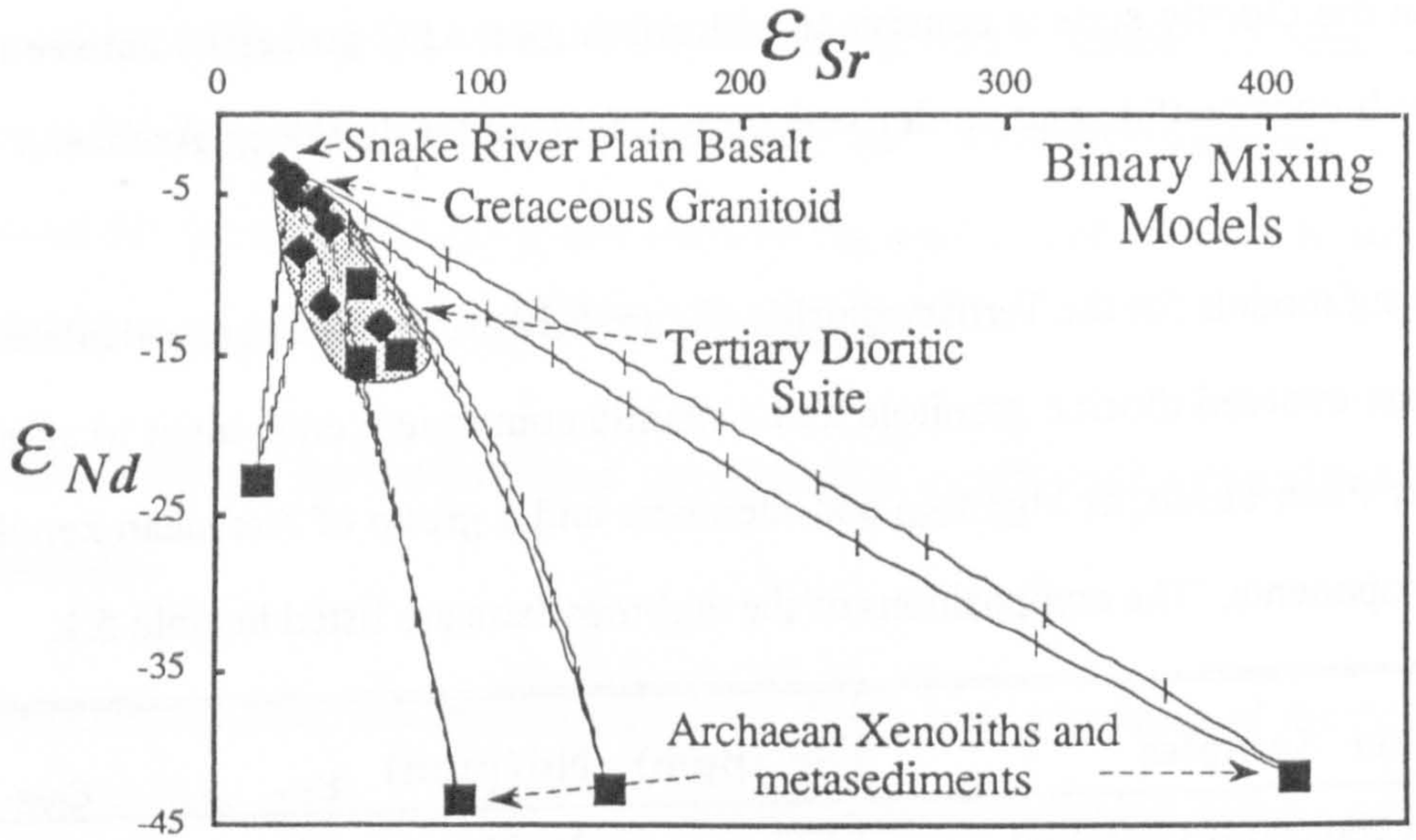

Figure 5.13 Binary mixing lines for the Tertiary dioritic suite. End-member compositions are listed in table 5.1

There is no evidence for a source with ε_{Nd} intermediate between the Archaean component and the main phase Cretaceous granitoids. The need for a component with low ε_{Nd} to generate the trend within the dioritic suite and perhaps the granitic suite, which outcrop throughout the eastern and central Atlanta and Bitteroot lobes suggests that isotopically heterogeneous lower crust exists throughout the Idaho batholith region. AFC trajectories for the dioritic suite, using the same end-members as those for mixing above and listed in table 5.1 are presented on figure 5.14. AFC processes were modelled using the equation of DePaolo, 1981 in the form:

$$\varepsilon_m = \frac{(r/r\text{-}1)\,(C_a/Z)\,(1\text{-}F^{-Z})\,\varepsilon_a + C_m^o\,F^{-Z}\,\varepsilon_m^o}{(r/r\text{-}1)\,(C_a/Z)\,(1\text{-}F^{-Z}) + C_m^o\,F^{-Z}}$$

ε_m = isotope ratio of final magma.

ε_m^o = isotope ratio of original magma.

ε_a = isotope ratio of assimilated material.

C_m^o = concentration of element in original magma.

C_a = concentration of element in assimilated material.

F = mass proportion of magma remaining.

$Z = r + D - 1/r\text{-}1$; where D is the bulk distribution coefficient of element

r = Ma/Mc ; ratio of the mass rate of assimilation to the mass rate of fractional crystallization.

The r value used during AFC modelling is critical. Taylor (1980) showed that 5g of granitoid magma at 850°C was required to assimilate 1g of country rock at 150°C. This suggests that a geologically realistic value of $r \approx 0.2$ for granitoid magmas. However values of up to $r = 0.5$ are plausible for hotter tonalitic to basaltic initial magmas or where the ambient temperature of the wall-rocks was significantly higher than 150°. The bulk distribution coefficients of Sr and Nd were also assumed during AFC modelling and trajectories are drawn for a range of values. These and other parameters used for each of the AFC models presented in figures 5.14a, b, c,d and e are listed on the individual diagrams.

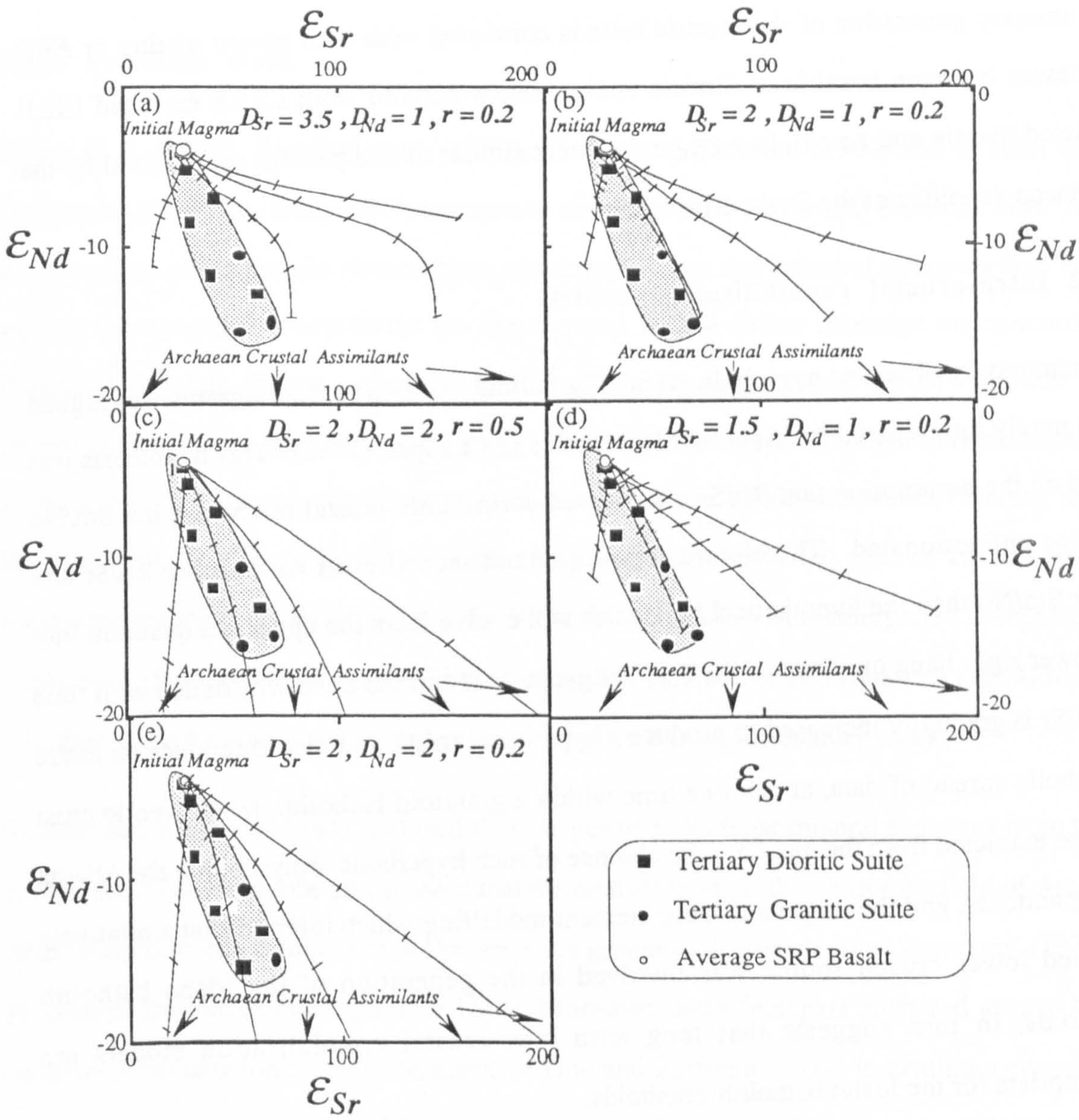

Figure 5.14 AFC trajectories graduated in 10% steps for the Tertiary dioritic suite and old Archaean crustal components. End member compositions are listed in table 5.1 and r, D_{Sr} D_{Nd} values indicated on individual diagrams.

An envelope around the data is best generated by Archaean end-members with ε_{Sr}≈80-350 and ε_{Nd}≈-40, for values of r between 0.2-0.5 and D_{Sr}=D_{Nd}≈2. The higher concentrations of Sr and Nd in the initial dioritic magma rather than a magma equivalent to an average Snake River Plain basalt does not change the position of the trajectories appreciably, but requires a larger proportion of assimilant. The preferred low D_{Nd} values are consistent with the intermediate magma compositions which are less likely to precipitate accessory phases with high D_{REE}.

In summary generation of the dioritic suite is consistent with both binary mixing or AFC processes between basaltic to dioritic end-members derived from LREE enriched LILE depleted mantle and an old, low ε_{Nd} component similar to and perhaps represented by the Archaean xenoliths of the Snake River Plain.

5.4.2 Intra-crustal remobilisation models

The commonly observed hyperbolic trend of granitoids on ε_{Nd} vs ε_{Sr} diagrams was argued to be purely intra-crustal in origin by McCulloch and Chappell (1982). This hypothesis was based on the assumption that Rb/Sr is increased during intra-crustal reworking but Sm/Nd remains unfractionated. Therefore a segment of continental crust with higher Rb/Sr and lower Sm/Nd than the hypothetical bulk earth will evolve from the upper left quadrant into the lower right hand quadrant of the ε_{Nd} vs ε_{Sr} diagram and the trend will flatten with time as Rb/Sr is gradually increased to produce a hyperbolic array. In order to produce an entire hyperbolic spread of data, at any one time within a granitoid batholith, new juvenile crust must be extracted from the mantle. The absence of such hyperbolic arrays within the Atlanta lobe granitoids, and the major and trace element modelling which inferred that a relatively enriched lower crustal source was involved in the generation of the Idaho batholith granitoids, in turn suggests that long term intra-crustal remobilisation models are inappropriate for the Idaho batholith granitoids.

5.5 Pb isotope geochemistry

Pb isotope ratios have been determined on a limited number of Cretaceous and Tertiary whole-rock granitoid samples from the Atlanta lobe and the results listed in appendix B. In addition, a number of K-feldspar mineral separates were analysed and the results listed in table 5.2. K-feldspars were analysed for Pb isotopes because they have low U/Pb ratios so that their measured Pb isotope ratios are likely to be similar to those of the magmas from which they crystallized (Patterson and Tatsumoto, 1964).

5.5.1 Previous work

Chase et al. (1978), Bickford et al. (1980), Shuster and Bickford (1984) and Grauert and Hofmann (1973) have analysed Pb isotopes in zircons in the northeastern Bitteroot lobe. All these authors noted that the zircons have xenocrystic cores and euhedral overgrowths. The age of the euhedral overgrowths are represented by the lower intercept on concordia diagrams and date the time of crystallization of the Cretaceous and Tertiary granites at approximately 70Ma and 45Ma respectively. The upper intercept is thought to represent the mean age of the xenocrystic zircon and falls in the range 1700Ma-2349Ma (Shuster and Bickford, 1984). These xenocrystic zircon ages are similar to the ages of zircons from metasedimentary xenolith suites from the Bitteroot lobe and so were interpreted to represent wall-rocks (Bickford et al., (1980), but later argued by Shuster and Bickford (1984) to be inherited from the source region rather than assimilated from the country rocks.

Shuster and Bickford (1984) analysed Pb isotopes of K-feldspar mineral separates from the northeastern Bitteroot lobe and showed that the data all fell into the Pb isotope field of Area I (that thought to be underlain by a Precambrian granulitic lower crust) of Zartmans' (1974) Pb isotope provinces (see figure 15.16b). Moreover these feldspars clustered around the orogene plumbotectonic evolution curve of Doe and Zartman (1979) indicating a complex multi-stage evolution for the Pb isotopes, but one dominated by a lower crustal source (Shuster and Bickford, 1984).

Few Pb isotope analyses have been carried out on the granitoids of the Atlanta lobe, but Norman and Leeman (1989) published several analyses on representative whole-rock and K-feldspar mineral separates from near the southern margin of the lobe and these are listed with the K-feldpsar data from this study in table 5.2.

Sample	$^{206}Pb/^{204}Pb$	$^{207}Pb/^{204}Pb$	$^{208}Pb/^{204}Pb$
CBC87-79 (Kg)	19.232	15.721	39.543
CBC87-57 (Kgd)	19.578	15.726	39.522
CBC87-101 (Kgd)	19.024	15.686	39.398
CBC87-94 (Kgd)	19.159	15.688	39.395
CBC87-106 (Kgd)	19.047	15.691	39.433
CBC87-134 (Kgd)	19.682	15.726	39.525
CBC87-146 (Kgd)	19.662	15.727	39.522
CBC87-148 (Kgdp)	19.959	15.750	39.668
L82-9 (K, whole rock)	19.409	15.687	39.274
84-13 (K, whole rock)*	19.021	15.617	39.773
84-14 (K, whole rock)*	19.224	15.658	39.082
LC72-1F (K)*	19.56	19.34	39.45
LC72-4F (K)*	19.34	15.69	39.23

Table 5.2 K-feldspar Pb isotope data and L82-9 from this study and the four samples from Norman and Leeman (1989) are marked with asterisks.

5.5.2 Pb isotopes of the Cretaceous granitoids

Cretaceous whole-rock samples have present day $^{206}Pb/^{204}Pb$, $^{207}Pb/^{204}Pb$ and $^{208}Pb/^{204}Pb$ ratios in the range 17.33-20.34, 15.62-15.88 and 38.78-40.16 respectively, and they are presented on $^{207}Pb/^{204}Pb$ versus $^{206}Pb/^{204}Pb$ and $^{208}Pb/^{204}Pb$ versus $^{206}Pb/^{204}Pb$ diagrams in figure 5.15a and 5.15b.

The Pb isotopes results are all presented as measured ratios rather than time corrected in order to avoid complication in the sample set where U and Th have not been analysed by INAA and where Pb was measured by XRF only. In addition U and Th are notoriously mobile in upper crustal systems and exhibit large amount of scatter on variation diagrams (see figure 4.7). However, because the rocks are only 80Ma old and they have average U/Pb and Th/Pb ratios of 0.13 and 0.75 respectively, the average age corrections are only, 0.1, 0.005 and 0.2 for the $^{206}Pb/^{204}Pb$, $^{207}Pb/^{204}Pb$ and $^{208}Pb/^{204}Pb$ ratios respectively. These changes represent minor shifts on $^{207}Pb/^{204}Pb$ versus $^{206}Pb/^{204}Pb$ and $^{208}Pb/^{204}Pb$ versus $^{206}Pb/^{204}Pb$ diagrams (figure 5.15). Also shown on these diagrams are Stacey and

Kramers' two-stage terrestrial Pb isotope evolution curve, the lower crust, orogene and upper crust plumbotectonic Pb isotope evolution curves generated by the model of Zartman and Doe (1981) and the Pb isotope fields of Zartmans' (1974) Pb isotopic provinces in the western United States cordillera.

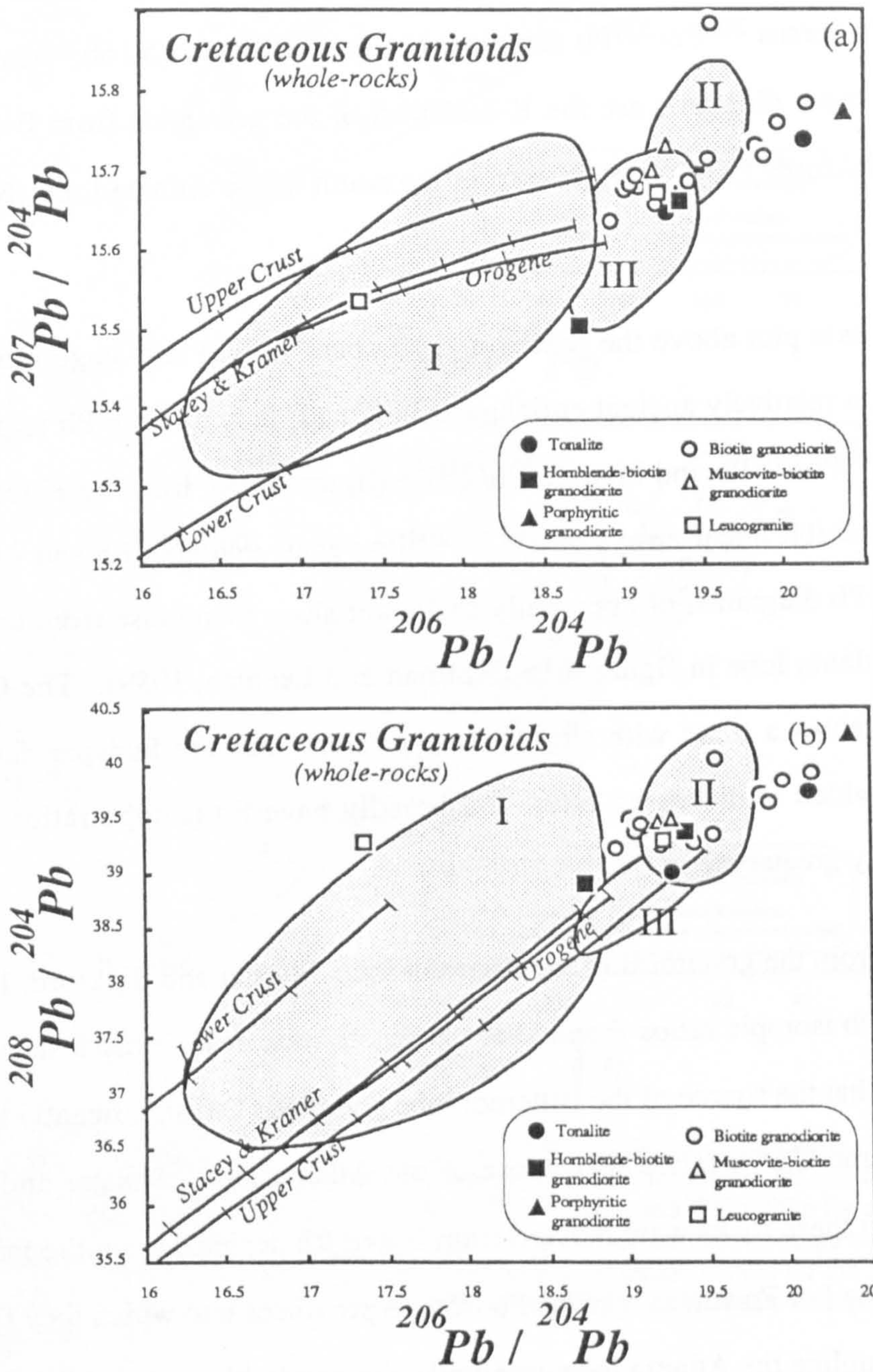

Figure 5.15 a) Graph of $^{207}Pb/^{204}Pb$ versus $^{206}Pb/^{204}Pb$ for the Cretaceous whole-rock samples from this study. **b)** Graph of $^{208}Pb/^{204}Pb$ versus $^{206}Pb/^{204}Pb$ for the Cretaceous whole-rock samples from this study. Also shown are the two-stage terrestrial Pb model growth curve of Stacey and Kramers (1975) and the plumbotectonic evolution curves for the lower crust, upper crust and orogene (Zartman and Doe, 1981). The fields of Zartmans' (1974) Pb isotopic provinces in the western United States cordillera are indicated where: area I Pb derived from crust underlain by Precambrian lower crustal basement, area II.Pb derived from isotopically homogenised sedimentary rocks eroded from Precambrian upper crust and area III Pb derived from material of eugeosynclinal or subduction-related origin.

Discounting the uppercrustal melt granitoid, CBC87-42 and two granitoids from the most southern Atlanta lobe (86RL-387 and 86RL -219), the Cretaceous granitoids show a coherent linear array and plot above any of the model Pb isotope growth curves.

The new K-feldspar mineral separate data are presented on $^{207}Pb/^{204}Pb$ versus $^{206}Pb/^{204}Pb$ and $^{208}Pb/^{204}Pb$ versus $^{206}Pb/^{204}Pb$ diagrams in figure 5.16a and 5.16b. Also shown for comparison on these diagrams are the K-feldspars of the granitoids from Bitteroot lobe (Shuster and Bickford, 1984) and those from the south of the Atlanta lobe (Norman and Leeman, 1989).

The K-feldspar data plot above the Stacey and Kramers' (1975) two-stage model growth curve indicating a relatively ancient enrichment in U and Th relative to Pb to produce the observed high $^{207}Pb/^{204}Pb$ and high $^{208}Pb/^{204}Pb$ (figure 5.16a, b). The K-feldspar data from this study exhibit linear arrays on $^{207}Pb/^{204}Pb$ versus $^{206}Pb/^{204}Pb$ and $^{208}Pb/^{204}Pb$ versus $^{206}Pb/^{204}Pb$ diagrams, of apparently shallower slope than those from the southern margin of the Atlanta lobe in figure 5.16 (Norman and Leeman, 1989). The Cretaceous whole-rock data show a trend with slightly steeper slope than the feldspar data, the age significance of which is discussed later, and broadly have Pb isotope ratios of similar values, but slightly greater range.

The K-feldspars from the granitoids of the Bitteroot lobe (Shuster and Bickford, 1984) have markedly lower Pb isotopic ratios than either the whole-rock or K-feldspar data from this study, indicating that the source of the Bitteroot lobe granitoids had significantly lower time integrated U/Pb and Th/Pb ratios than those of the Atlanta lobe. Shuster and Bickford (1984) argued that these rocks were derived from U and Rb depleted granulite facies lower crust typical of area I of Zartmans' (1974) Pb isotope provinces into which they fall (figure 5.16). However, unlike the Atlanta lobe granitoids, the granitoids analysed for Pb isotopes by Shuster and Bickford (1985) from the Bitteroot lobe contain abundant metasedimentary xenoliths and typically have high initial $^{87}Sr/^{86}Sr$ ratios (average ≈ 0.710) thought to be due to mixing material from the lower crust and upper crustal metasedimentary material (Fleck and Criss (1985).

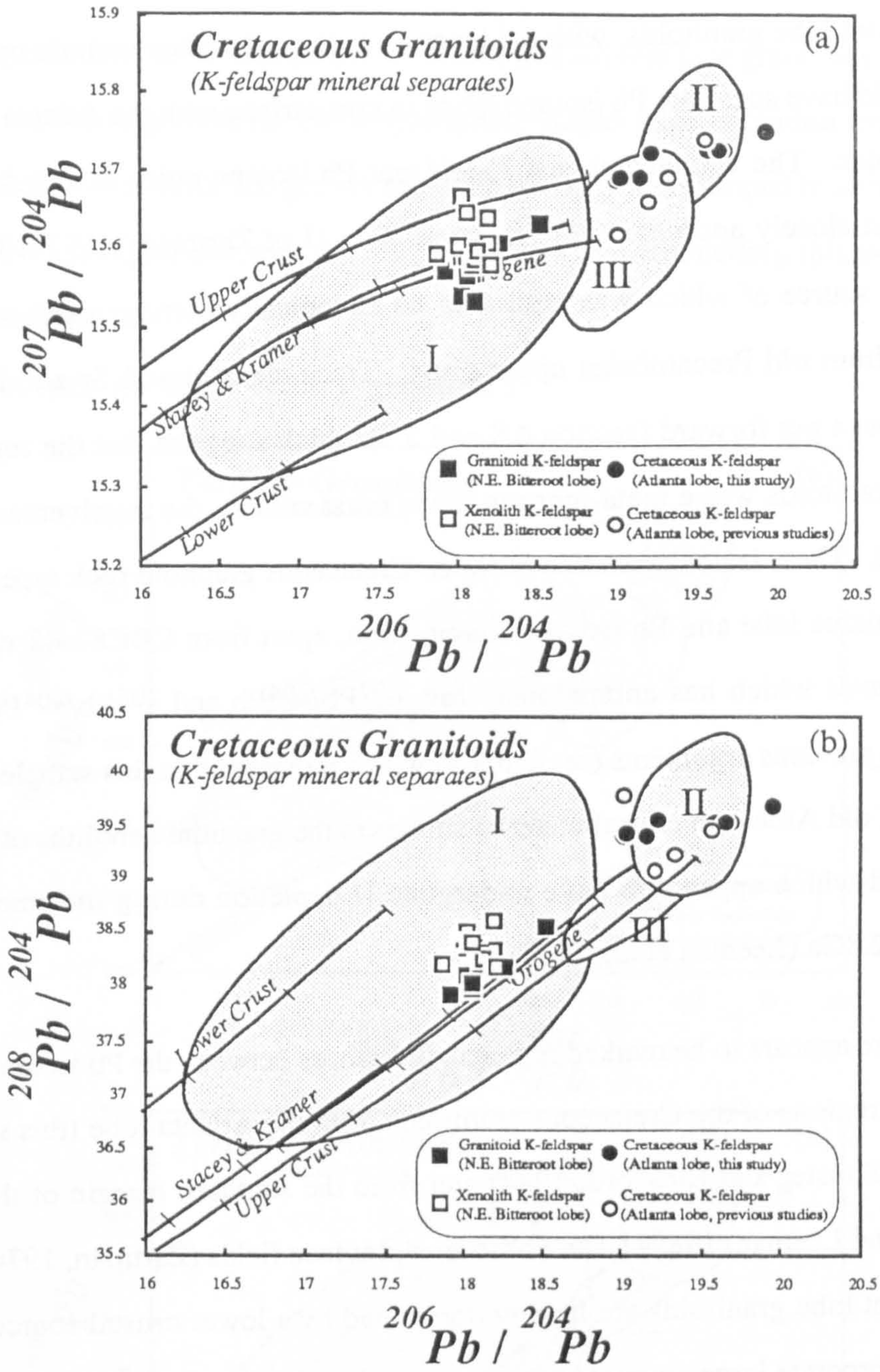

Figure 5.16 a) Graph of $^{207}Pb/^{204}Pb$ versus $^{206}Pb/^{204}Pb$ for the Cretaceous K-feldspar samples from this study, those from the Bitteroot lobe (Shuster and Bickford, 1984) and those from the southern margin of the Atlanta lobe (Norman and Leeman, 1989). **b)** Graph of $^{208}Pb/^{204}Pb$ versus $^{206}Pb/^{204}Pb$ for the Cretaceous K-feldspar samples. Data from the same sources as above. Also shown are the two-stage terrestrial Pb model growth curve of Stacey and Kramers (1975), the plumbotectonic evolution curves for the lower crust, upper crust and orogene (Zartman and Doe, 1981) and the fields of Zartmans' (1974) Pb isotopic provinces in the western United States cordillera.

In addition the Pb isotope data of the Bitteroot lobe granitoids, in contrast with those from the Atlanta lobe, do not lie on linear arrays indicating that the Pb isotopes may have been subject to open system behaviour. This suggests that variable degrees of contamination by the isotopically heterogeneous metasediments may have occurred. It still remains intriguing

that the Bitteroot lobe granitoids, with evidence to suggest that they contain upper crustal material, should have such low Pb isotope ratios in comparison with the Atlanta lobe lower crustal granitoids. The whole-rock and K-feldspar Pb isotope ratios of the Atlanta lobe granitoids most closely approximate to those of Area II of Zartmans' (1974) Pb isotopic provinces, the source of which was argued to be isotopically homogenised sedimentary rocks eroded from old Precambrian upper crust. Trace element and Sr and Nd isotope evidence has been put forward (section 4.8 and 5.3) which suggests that the source of the Atlanta lobe granitoids was a meta-igneous lower crust without the involvement of upper crustal material. There is no correlation between Cretaceous granitoid rock types from this study in the Atlanta lobe and Pb isotope composition, apart from CBC87-42 which is an upper crustal melt which has anomalously low $^{207}Pb/^{204}Pb$ and $^{206}Pb/^{204}Pb$. This is consistent with previous arguments (section 5.3) which indicated that this sample contained a component of old Archaean crustal material similar to the granulite xenoliths of the Snake River Plain and which appears to have undergone U depletion during metamorphism at approximately 2.8Ga (Leeman et al., 1985).

In summary there appears to be marked regional differences between the Pb isotope data and thus the source regions of the Cretaceous granitoids from the Atlanta lobe (this study), the Bitteroot lobe (Shuster and Bickford, 1984) and from the southern margin of the Atlanta lobe (Norman and Leeman, 1989). The Pb isotope province fields (Zartman, 1974) suggest that the Bitteroot lobe granitoids are largely dominated by a lower crustal source and that they did not incorporate large amounts of upper crustal material contrary to what Fleck and Criss (1985) argued for on the basis of Sr isotopes. Moreover the Atlanta lobe granitoids fall into the field of eroded upper crustal Precambrian rocks, despite having been shown to have been derived from lower crustal, meta-igneous sources (section 4.8). Therefore the Pb isotope provinces of Zartman (1974) appear to be inconsistent with the Pb isotopic signatures of the likely source regions of the Idaho batholith granitoids. The relatively high Pb isotopic signatures of Atlanta lobe granitoids, however, suggest that they were generated from undepleted sources which either had higher time integrated U/Pb ratios than Bitteroot lobe granitoids or were derived from older source regions.

It is most probable that the Pb isotope evolution of these Atlanta lobe granitoids has occurred by a complex multi-stage process and inappropriate single-stage evolution models are not considered here. A model for the growth of the Pb isotopes is developed in section 5.7 after considering the age significance of the Pb isotope data and reconciling this with evidence from Nd model ages.

5.5.3 Pb isotopes of the Tertiary granitoids

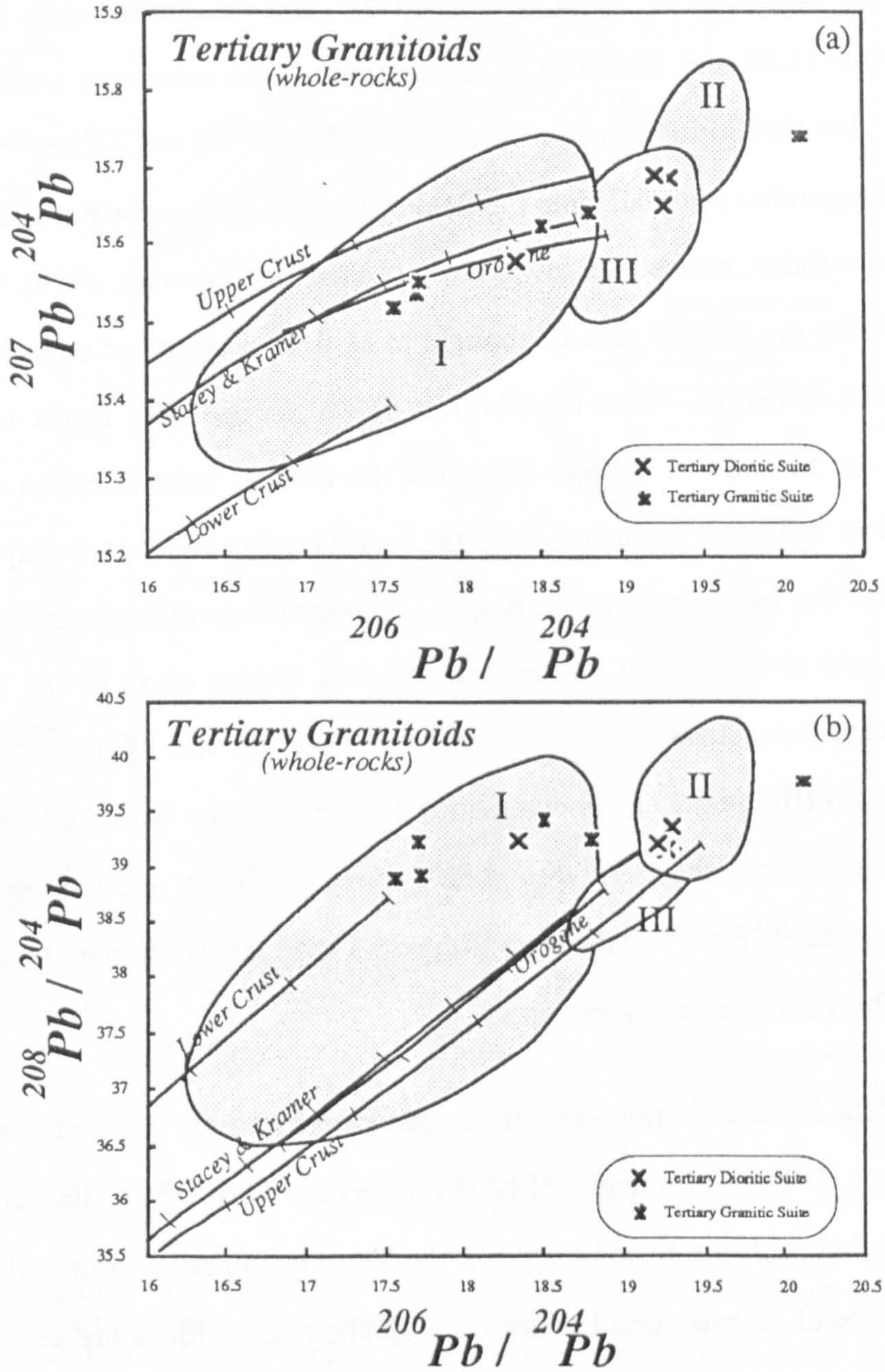

Figure 5.17 **a)** Graph of $^{207}Pb/^{204}Pb$ versus $^{206}Pb/^{204}Pb$ for the Tertiary whole-rock samples from this study. **b)** Graph of $^{208}Pb/^{204}Pb$ versus $^{206}Pb/^{204}Pb$ for the Tertiary whole-rock samples from this study. Also shown are the two-stage terrestrial Pb model growth curve of Stacey and Kramers (1975), the plumbotectonic evolution curves for the lower crust, upper crust and orogene (Zartman and Doe, 1981) and the fields of Zartmans' (1974) Pb isotopic provinces in the western United States cordillera.

Pb isotope ratios have been measured on 5 samples of the Tertiary granitic suite and four samples of the dioritic suite, and the present day values are plotted on diagrams of $^{207}Pb/^{204}Pb$ versus $^{206}Pb/^{204}Pb$ and $^{208}Pb/^{204}Pb$ versus $^{206}Pb/^{204}Pb$ (figure 5.17a and b) and listed in appendix B.

The dioritic suite has $^{206}Pb/^{204}Pb$, $^{207}Pb/^{204}Pb$ and $^{208}Pb/^{204}Pb$ ratios in the ranges, 18.30-19.28, 15.54-15.65 and 39.01-39.22 respectively, and the granitic suite has ratios of 17.53-18.79, 15.48-15.60 and 38.72-39.26 respectively. The suite as a whole defines a good linear trend, but the dioritic samples have higher $^{206}Pb/^{204}Pb$ and $^{207}Pb/^{204}Pb$ than the granitic suite. The granitic suite falls into the field of Pb isotope compositions thought to be derived from Precambrian, crystalline, lower crustal basement (Zartman, 1974), whereas the dioritic suite fall into the field of area III thought to be from material of eugeosynclinal or subduction related in origin. This distribution of Pb isotope data again suggests, in agreement with the Sr and Nd isotope data, that the dioritic suite contains material of isotopically distinct character compared with the granitic suite and that it may have been derived from either the lower crust or the mantle. The granitic suite appears to have been derived from an old lower crustal source and the data cluster close to the Stacey and Kramers' two-stage terrestrial Pb model growth curve on the $^{207}Pb/^{204}Pb$ versus $^{206}Pb/^{204}Pb$ diagram (figure 5.17a), in contrast to the dioritic suite which falls above such growth curves. Significantly the granitic suite falls above the Stacey and Kramers' curve on the $^{208}Pb/^{204}Pb$ versus $^{206}Pb/^{204}Pb$ diagram (figure 5.17b) suggesting that U was depleted in preference to Th in the source of these rocks.

The K-feldspar data for the Tertiary granitoids are listed in table 5.3 and presented on $^{207}Pb/^{204}Pb$ versus $^{206}Pb/^{204}Pb$ and $^{208}Pb/^{204}Pb$ versus $^{206}Pb/^{204}Pb$ diagrams (figure 5.18 a and b) together with published result on the Tertiary intrusive granitoids from the southern Atlanta lobe of Norman and Leeman (1989).The compositions are very similar to the whole rock samples with $^{206}Pb/^{204}Pb$, $^{207}Pb/^{204}Pb$ and $^{208}Pb/^{204}Pb$ in the ranges, 17.59-19.15, 15.47-15.65 and 38.85-38.97 respectively. The range, slope and values of

the Tertiary K-feldspar Pb isotope data are similar to those for the Tertiary granitoids from Norman and Leeman (1989) from the southern part of the Atlanta lobe.

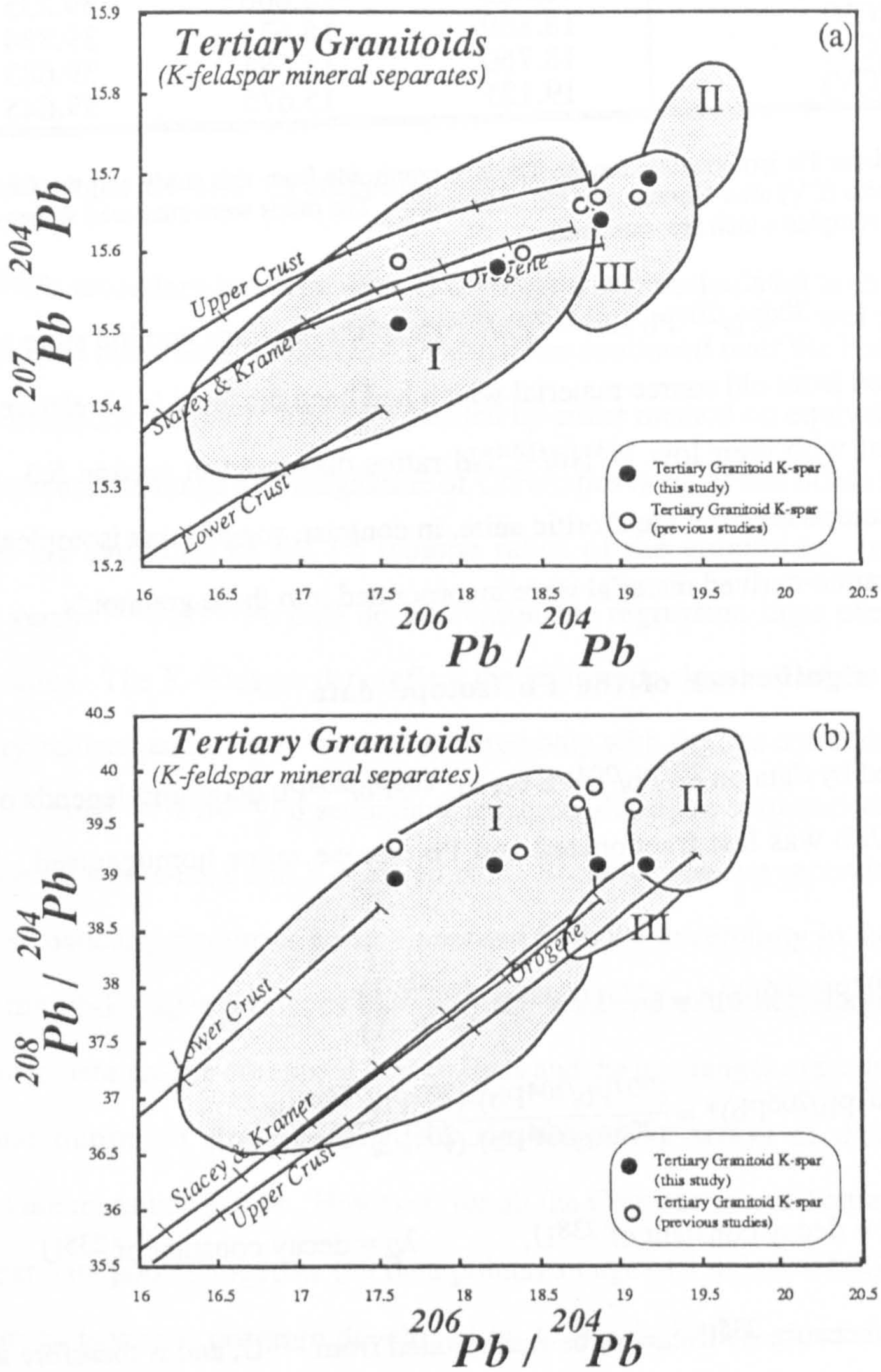

Figure 5.18 a) Graph of $^{207}Pb/^{204}Pb$ versus $^{206}Pb/^{204}Pb$ for the Tertiary K-feldspar samples from this study and those from the Atlanta lobe (Norman and Leeman, 1989). **b**) Graph of $^{208}Pb/^{204}Pb$ versus $^{206}Pb/^{204}Pb$ for the Tertiary K-feldspar samples. Data from the same sources as above. Also shown are the two-stage terrestrial Pb model growth curve of Stacey and Kramers (1975), the plumbotectonic evolution curves for the lower crust, upper crust and orogene (Zartman and Doe, 1981) and the fields of Zartmans' (1974) Pb isotopic provinces in the western United States cordillera.

Sample	$^{206}Pb/^{204}Pb$	$^{207}Pb/^{204}Pb$	$^{208}Pb/^{204}Pb$
CBC87-23 (Tg)	17.622	15.509	39.976
CBC87-132 (Tg)	18.890	15.641	39.090
CBC87-86 (Tgd)	19.184	15.693	39.104
CBC87-162 (Tgd)	18.232	15.581	39.103
L70-14 (Tg)	17.633	15.600	39.308
TM 71-2S(CV)	18.403	15.606	39.235
L73-1S (CV)	18.869	15.671	39.834
L71-2S (CV)	18.760	15.664	39.683
L72-1S (CV)	19.121	15.675	39.645

Table 5.3 K-feldspar Pb isotope data for the Tertiary granitoids from this study and the Challis intrusive and Challis volcanics (CV) after Norman and Leeman (1989). The ratios were measured values on orthoclase except for the CV samples which are sanidines.

In summary the low $^{206}Pb/^{204}Pb$ and $^{207}Pb/^{204}Pb$ of the Tertiary granitic suite suggest that they were derived from old source material which had been depleted in U relative to Pb, and that is consistent with their low $^{143}Nd/^{144}Nd$ ratios discussed in section 5.3. The more radiogenic Pb isotope ratios of the dioritic suite, in contrast, suggest that isotopically distinct lower crust or mantle-derived material were incorporated into these granitoids.

5.5.4 The age significance of the Pb isotope data

The slope defined by data on $^{207}Pb/^{204}Pb$ versus $^{206}Pb/^{204}Pb$ diagrams depends on the time elapsed since U/Pb was last fractionated and Pb isotope ratios homogenised. Using the equation:

$$(^{207}Pb/^{206}Pb)^* = (^{235}U/^{238}U)\,\frac{(e^{\lambda 1 t}-1)}{(e^{\lambda 2 t}-1)}$$

where:
$$(^{207}Pb/^{206}Pb)^* = \frac{(^{207}Pb/^{204}Pb)-(^{207}Pb/^{204}Pb)i}{(^{206}Pb/^{204}Pb)-(^{206}Pb/^{204}Pb)i}$$

and: λ_1 = decay constant of ^{238}U, λ_2 = decay constant of ^{235}U

it is apparent that because ^{235}U cannot be fractionated from ^{238}U, and is therefore a constant equal to 1/137.88, '^{207}Pb-^{206}Pb secondary isochron' dates can be calculated solely on the basis of the isotopic composition of Pb in the mineral or whole rock, without having to know its abundance. The range of $^{238}U/^{204}Pb$ (μ values) controls the distribution along such isochrons, whereas the approximation to a straight line is largely dependent on the degree of homogenisation of the Pb isotope ratios at the beginning of the last stage of

evolution. The above equation is transcendental and cannot be solved by algebraic methods, but Stacey and Stern (1973) produced a table of compatible values of t and $(^{207}Pb/^{206}Pb)^*$. Thus the above procedure arguably offers the most powerful method of obtaining model ages in order to evaluate the age of magma source regions.

5.5.4 i) Pb-Pb ages of the Cretaceous granitoids

The '^{207}Pb-^{206}Pb secondary isochron' ages (Pb-Pb ages) were calculated both ignoring and taking into account the effects of decay of U which has continued over the last 80Ma in the Cretaceous whole-rock samples. The ages yielded by either method on equivalent suites are very similar because the range and magnitude of U/Pb ratios is small and 80Ma is a relatively short time in the evolution of the Pb isotope ratios of the granitoids. In general the $^{207}Pb/^{204}Pb$ versus $^{206}Pb/^{204}Pb$ data define reasonable regression lines over a spread in $^{206}Pb/^{204}Pb$ ratios. The K-feldspar data reflect the Pb isotope signature of the magma from which they crystallized and so they were considered only with the age corrected whole-rock data. The calculated '^{207}Pb-^{206}Pb secondary isochron' dates are summarised in table 5.4 for the Cretaceous whole-rock and K-feldspar data. Because these are secondary isochrons, to propagate statistically rigourous errors (inherited from the uncertainty in the gradients of the lines) to the Pb-Pb ages produces both unlikely ages and extremely large errors. The results presented here are the computed best fit lines and the age ranges are calculated for the maximum and minimum slopes defined by the respective arrays of data taking into consideration the measured errors. However, for all the Cretaceous and Tertiary whole rock and K-feldspar data pooled together (49 data points) an age of 1.4Ga ± 0.02Ga is produced by the rigourous isochron program developed by D.Wright which gives more weight to those analyses with the best errors. Although the error on this age may be unrealistically small, if it is reasonable to group all the data together it suggests that the Tertiary and Cretaceous granitoids are largely derived from sources of approximately the same age.

Sample Suite	No.	Slope	Fit R^2	Age	Age Range
All Cretaceous whole-rocks	22	0.111	0.472	1.8 Ga	1.25-2.0 Ga
All Cretaceous whole-rocks + K-feldspar	35	0.095	0.581	1.53 Ga	1.2-1.65 Ga
Biotite granodiorite whole-rocks	13	0.091	0.736	1.45 Ga	0.9-1.8 Ga
Biotite granodiorite whole-rock + K-feldspar	18	0.087	0.827	1.40 Ga	0.8-1.55 Ga
Cretaceous K-feldspar	8	0.062	0.870	0.70 Ga	0.6-1.1 Ga
Cretaceous K-feldspar (previous studies)	4	0.230	0.997	3.05 Ga	2.8-3.3 Ga

Table 5.4 '207-206 secondary isochron' ages for the Cretaceous granitoids of the Atlanta lobe. Data from this study and Norman and Leeman (1989) from the southern Atlanta lobe.

The calculated Pb-Pb K-feldspar age of 0.7Ga (table 5.4) is anomalously low compared with the results from the other suites, and with the Nd model ages considered later in section 5.6. This is likely to be due to the small number of K-feldspar samples and the more restricted range of $^{207}Pb/^{204}Pb$ and $^{206}Pb/^{204}Pb$ ratios (see figure 5.16a).

The Cretaceous suite, as a whole, have Pb-Pb ages of 1.65Ga-1.8Ga, but the closely related suite of biotite granodiorites have Pb-Pb ages of 1.45Ga. This suggests that the source of the Atlanta lobe granitoids was Proterozoic in age, and that it therefore lay to the west of the Archaean craton and to the north of the Archaean Snake River Plain crustal province (see figure 2.2). However, the Pb-Pb age of the Cretaceous granitoids of Norman and Leeman (1989) from the southern margin of the Atlanta lobe is 3.05Ga which suggests that these granitoids at least contain a component of Archaean crustal material. Thus it may be inferred that a terrane boundary, initially suggested by Leeman (1985), between the Archaean Snake River Plain crustal province and the Proterozoic aged basement province of the Idaho batholith is located just within the southern margin of the Atlanta lobe. The change from fertile Proterozoic lower crust in the north (section 4.8), to more depleted Archaean basement to the south (Leeman et al., 1985) may have been a controlling factor in the locating the extent of the southern margin of the Atlanta lobe.

5.5.4 ii) Pb-Pb ages of the Tertiary granitoids :

The '^{207}Pb-^{206}Pb secondary isochron ages' for the Tertiary granitoids are given in table 5.5 using the same procedures as for the Cretaceous granitoids outlined above.

Sample Suite	No.	Slope	Fit R^2	Age	Age Range
Tertiary Bimodal Suite whole-rocks	8	0.088	0.953	1.40 Ga	1.1-1.45 Ga
Dioritic Suite whole-rocks	4	0.102	0.873	1.65 Ga	1.1-2.1 Ga
Dioritic Suite whole-rocks + K-feldspars	6	0.104	0.95	1.7 Ga	1.2-1.95 Ga
Granitic Suite whole-rocks	5	0.095	0.981	1.55 Ga	1.2-1.8 Ga
Granitic Suite whole-rocks + K-feldspars	7	0.095	0.952	1.55 Ga	1.33-1.7 Ga
Tertiary Bimodal Suite K-feldspars	4	0.112	0.989	1.85 Ga	1.45-1.9 Ga
Tertiary K-feldspars (previous studies)	5	0.059	0.833	0.60 Ga	0.50-1.0 Ga

Table 5.5 '207-206 secondary isochron' ages for the Tertiary granitoids of the Atlanta lobe. Data from this study and Norman and Leeman (1989) from the southern Atlanta lobe.

The Tertiary whole-rock granitoid data yield Pb-Pb ages of 1.65Ga-1.7Ga and 1.55Ga for the dioritic and granitic suites respectively, whereas when considered together they yield an age of 1.4 Ga. The limited K-feldspar data yield an older age of 1.85Ga. Although difficult to assess, the errors on these ages are likely to be large due to the small number of samples analysed. The ages produced are however, similar and consistent with each other and similar to the Pb-Pb ages of the Cretaceous granitoids suggesting that they have been largely derived from Proterozoic source regions.

It is important to note that mixing has been demonstrated to be a likely process for the generation of the dioritic suite (section 5.4.1) and whether this destroyed any meaningful '^{207}Pb-^{206}Pb secondary isochrons' is unknown. The Pb isotope results on the granitic suite are, however consistent with earlier conclusions based on trace element and Sr and Nd isotope evidence, that they were derived by melting in the lower crust of similar nature to the source of the Cretaceous granitoids.

5.6 Nd model ages

The Nd model age of a crustal rock is taken to represent the time of crustal residence since extraction from the mantle (McCulloch and Wasserburg, 1978). There are two major premises upon which the above hypothesis is based:

i) that crustal rocks have lower Sm/Nd than the mantle, and that the major Sm/Nd fractionation occurred when the crust was extracted from the mantle;

ii) that Sm/Nd ratios remain relatively constant and unaffected by intra-crustal processes.

Before presenting the Nd model ages of the Idaho batholith rocks the validity of these assumptions is discussed. Miller (1988) has shown that the mantle to crust flux in continental subduction zones, the accepted major sites of continental growth since the Archaean (Taylor, 1967), has moderately low Sm/Nd ratios (average Sm/Nd=0.21) similar to that of the bulk crust of Taylor and McLennan (1985) (average Sm/Nd=0.22). Miller (1988) also argues that these values are intrinsic to calc-alkali magmatism in both continental and "oceanic" arcs, and that they are inherited from enriched source regions in the sub-continental lithospheric mantle. Thus it appears that the initial premise that Sm/Nd is fractionated by extraction from the mantle to the crust may be incorrect, the dominant Sm/Nd fractionation occurring by minor trace element enrichment processes in the uppermost mantle.

However, comparison of Sm/Nd ratios of various crustal reservoirs (figure 5.19) shows that upper crust typically has a significantly lower and more restricted range of Sm/Nd (average Sm/Nd≈0.19) than the flux from the mantle taken to be represented by continental calc-alkali arcs (average Sm/Nd=0.21) as shown in figure 5.19. This indicates that extraction from the mantle is not the only cause of Sm/Nd fractionation, and it implies that certain intra-crustal processes have the ability to fractionate Sm/Nd ratios.

Sm/Nd ratios are unlikely to be fractionated within fine grained rocks by upper crustal sedimentary and metamorphic processes (Menzies et al., 1979), because the REE budget is dominantly controlled by clay minerals which tend to homogenise initial differences in Sm/Nd and to produce a restricted range of Sm/Nd ratios (Frost and Wilson, 1987).

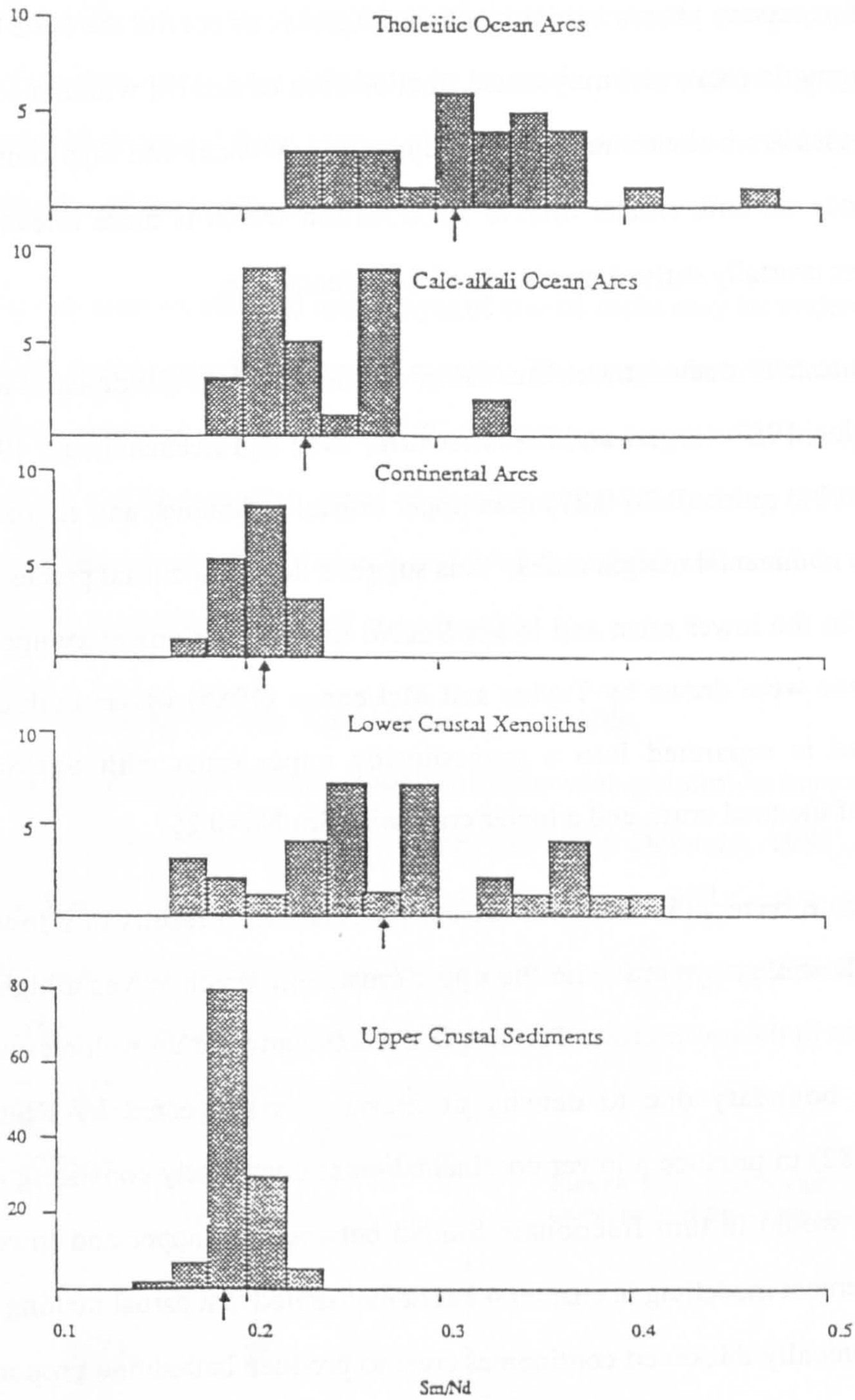

Figure 5.19 Histograms of Sm/Nd for basalts and basaltic andesites divided by crustal setting and major element chemistry with mean values indicated by arrows, after Miller (1988) and references therein. The calc-alkali continental and oceanic arcs have average Sm/Nd significantly higher than the upper crust thought to be inherited from their source regions. The lower crustal xenoliths have high Sm/Nd as a result of intra-crustal reprocessing reducing Sm/Nd in the upper crust.

In coarse grained sediments the REE budget is controlled by heavy minerals of magmatic origin which when concentrated or depleted due to density fractionation can change the

Sm/Nd of a sediment (Frost and Wilson 1987). Similarly, relative depletions and concentrations of accessory phases in highly silicic magmas can control the REE budget of upper crustal magmatic rocks and may cause fractionation of Sm/Nd within a rock suite. The above processes are however restricted to upper crustal rocks and thus cannot be an important influence on bulk crustal Sm/Nd fractionation which is more relevant to the intermediate, lower crustally derived granitoids of the Atlanta lobe.

Inspection of figure 5.19 demonstrates that lower crustal xenoliths (Rudnick et al., 1986; Rudnick and Taylor, 1987; Rogers and Hawkesworth, 1982 and Leeman et al., 1985) tend to have higher Sm/Nd ratios (0.26-0.27) than upper crustal sediments, and slightly higher Sm/Nd ratios than continental margin rocks. This suggests that intra-crustal processes result in higher Sm/Nd in the lower crust and lower Sm/Nd in the complementary upper crust. Similar conclusions were drawn by Taylor and McLennan (1985) whose bulk crust has Sm/Nd= 0.22 and is separated into a granodioritic upper crust with Sm/Nd=0.173 comprising 25% of the total crust, and a lower crust with Sm/Nd=0.25.

There must therefore be a common lower crustal process which results in a low Sm/Nd intermediate to silicic flux upwards into the upper crust, and which leaves a high Sm/Nd more mafic fraction in the lower crust. Ponding and fractionation of up-welling magmas at the crust mantle boundary due to density contrasts was suggested by Rogers and Hawkesworth (1982) to produce a lower continental crust dominantly consisting of mafic cumulates, which would in turn fractionate Sm/Nd between the upper and lower crust. Major and trace element modelling in chapter 4 has demonstrated that partial melting towards the base of a tectonically thickened continental crust to produce batholithic proportions of intermediate magma with a garnet-bearing mafic residue also has the ability to fractionate Sm/Nd ratios significantly between the upper and lower crust.

In summary Sm/Nd is likely to be fractionated twice during passage from the mantle to the upper crust; the first by crustal extraction from an enriched upper mantle and the second by intra-crustal processes as material is remobilised from the lower to the upper crust. Thus allowances must be made for this if a realistic estimate of crustal residence time is to be

obtained from the Nd model ages. This is particularly relevant for the Cretaceous magmas of the Atlanta lobe, but accurate modelling of the trace element composition of the source (section 4.8) allows such considerations to be made in the following section. If such corrections for intra-crustal fractionation of Sm/Nd are not made the Nd model ages would underestimate the crustal residence times.

There are further reasons why Nd model ages of crustal rocks may be underestimates of the actual time of crustal extraction from the mantle. The mantle from which they are derived may have been depleted relative to CHUR, but this can be allowed for by assuming the depleted mantle model evolution curve of Jacobsen and Wasserburg (1979) and DePaolo (1981). In addition any mixing of mantle and crustal material will result in a Nd model age which will be younger than the crustal component.

5.6.1 Nd model ages of the Cretaceous granitoids

Nd model ages were first calculated for the Cretaceous granitoids assuming a depleted mantle reservoir (Jacobsen and Wasserburg, 1979 and DePaolo, 1981), and using the measured Sm/Nd and Nd isotope ratios. The Nd model ages (T_{DM}^{Nd}) results are presented on a histogram (figure 5.20), and although the individual rock types are distinguished there is no clear correlation between T_{DM}^{Nd} and rock type.

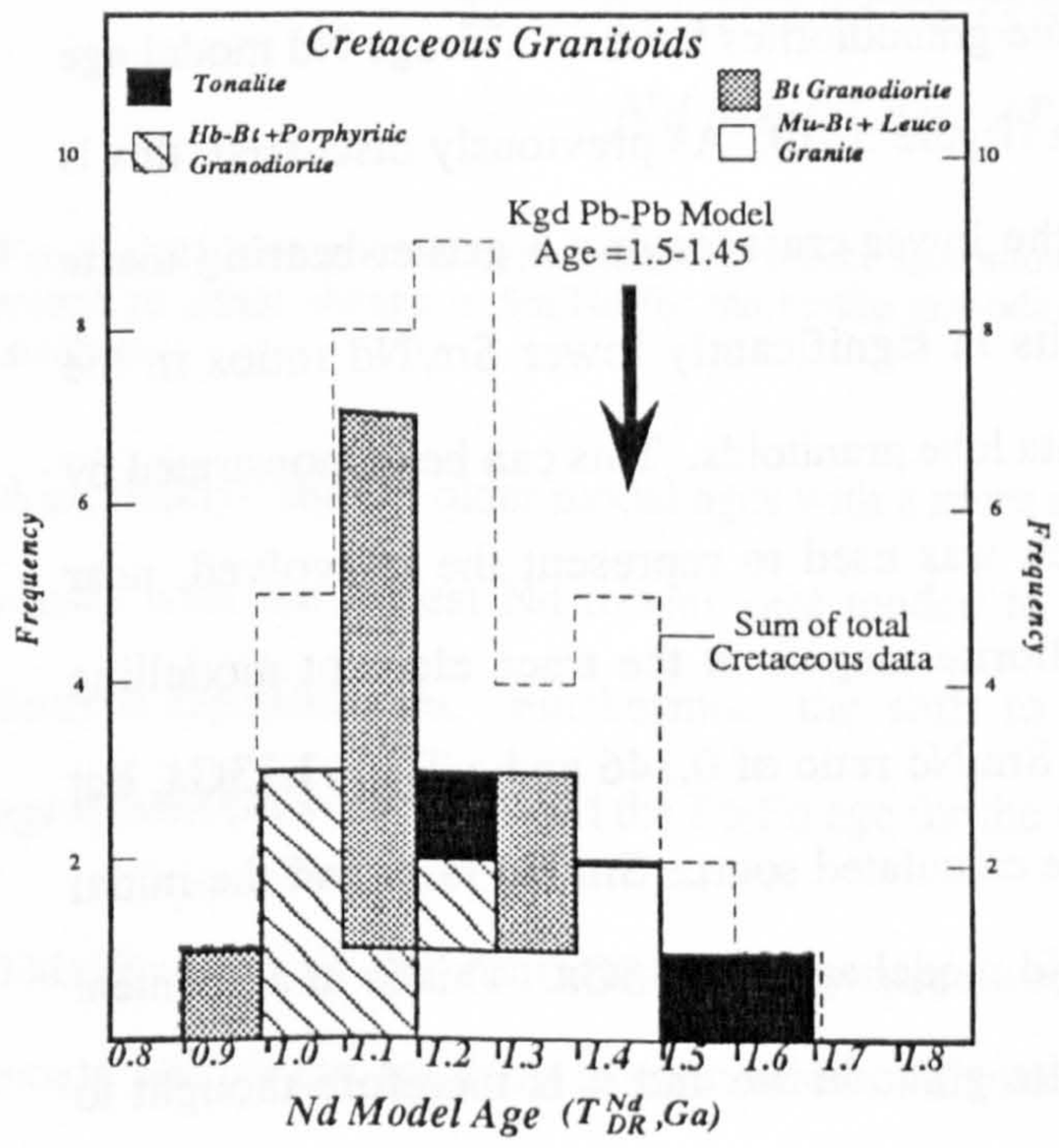

Figure 5.20 Histogram of depleted mantle model ages of the Cretaceous granitoids.

The exception to this are the leucocratic upper crustal melts which either yield anomalously old ages (e.g. T_{DM}^{Nd} L86-60 = 2.7Ga), or do not project back to an intersection with the model mantle evolution curve and so are not plotted in figure 5.20. This may be due to the incorporation of old Archaean upper crustal material with low $^{143}Nd/^{144}Nd$, and/or to exceptionally high Sm/Nd ratios produced by upper crustal partial melting. Approximate Nd model ages can be obtained for these granitoids by using initial $^{143}Nd/^{144}Nd$ ratios and the Sm/Nd of either average upper crust. Such Nd model ages fall in the range 2.1Ga-2.7Ga which may either be the true age of the material from which the granitoids were derived or a hybrid value as a result of mixing either in the granitoid magmas and/or the sedimentary sources. This is significantly older than the other granitoid model ages and suggests that Archaean aged sedimentary material was incorporated into the upper crustal melt granitoids from the southern margin of the Atlanta lobe.

The remaining T_{DM}^{Nd} range from 0.8Ga-1.6Ga with an average Nd model age of 1.2Ga for the whole suite, whereas the biotite granodiorites have an average age of 1.15Ga (figure 5.20). As expected, for these lower crustal melt granitoids the Nd model ages are significantly older than the average age of emplacement of 80Ma (Lewis et al., 1987). The most striking feature of the histogram in figure 5.20 is the discrepancy between the preferred Pb-Pb age and the Nd model age. The biotite granodiorites have an average Nd model age of 1.15Ga, but have a Pb-Pb age of 1.45Ga (figure 5.20). As previously discussed, this is interpreted in terms of partial melting in the lower crust leaving a garnet-bearing mafic granulite residual mineralogy which results in significantly lower Sm/Nd ratios in the intermediate magmas emplaced as the Atlanta lobe granitoids. This can be demonstrated by considering CBC87-125, the sample which was used to represent the unevolved, near primary composition of the biotite granodiorite magma in the trace element modelling (section 4.8). CBC87-125 has a measured Sm/Nd ratio of 0.146 and a T_{DM}^{Nd}=1.13Ga, but recalculation of the Nd model age using the calculated source Sm/Nd ratio and the initial $^{143}Nd/^{144}Nd$ calculated at 80Ma yields a Nd model age of 1.45Ga. This is in agreement with the Pb-Pb age of 1.45Ga for the biotite granodiorite and it is therefore thought to

represent the average age of the lower crustal source of the Cretaceous Atlanta lobe biotite granodiorites. Similar corrections have been made for the other Cretaceous granitoid magmas using the average source to magma changes in Sm/Nd for the biotite granodiorites, hornblende-biotite granodiorites and tonalites calculated in section 4.8. The results of this are shown on a histogram in which Nd model ages corrected for Sm/Nd fractionation are compared with the initially calculated Nd model ages (figure 5.21).

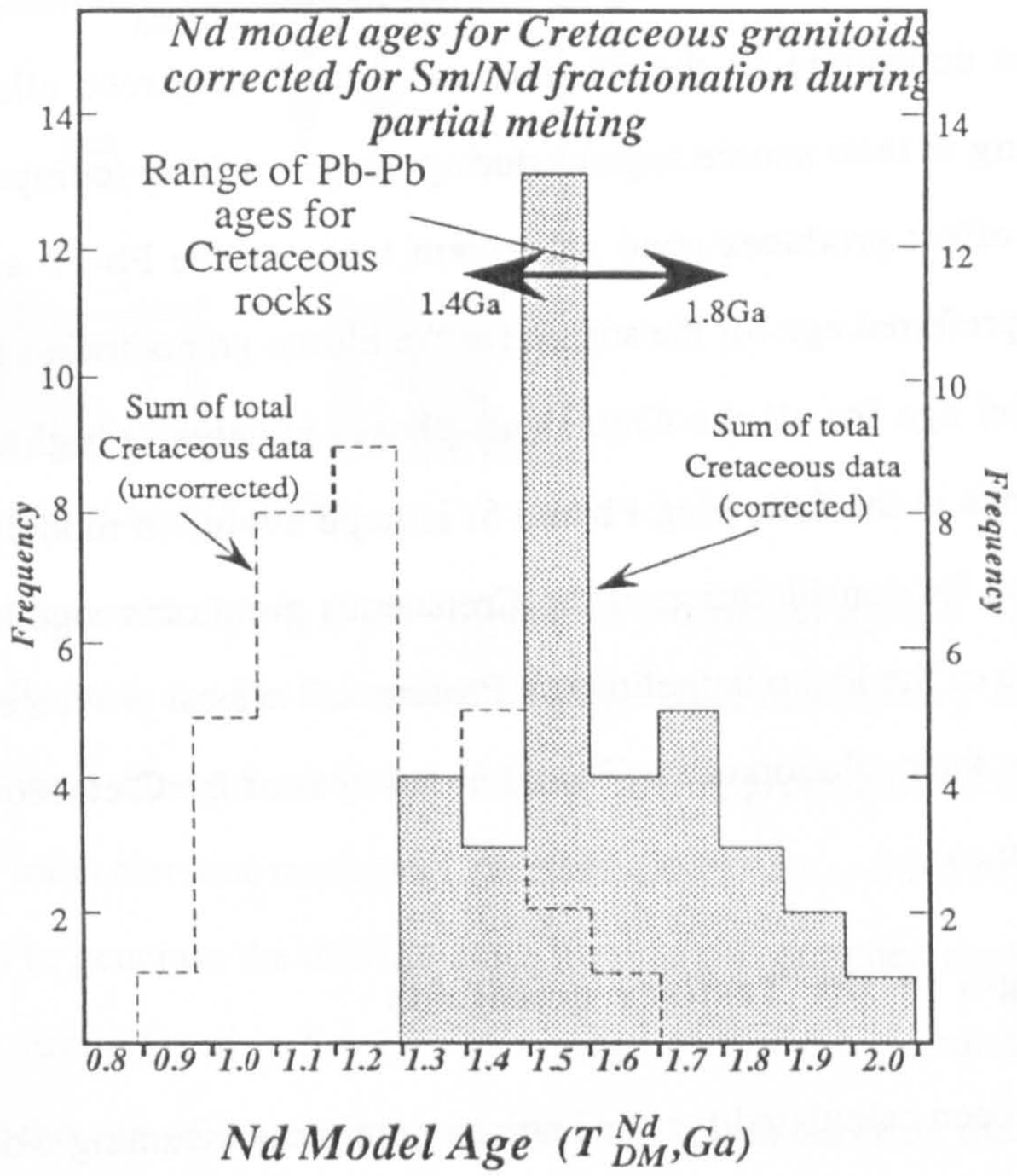

Figure 5.21 Histogram of depleted mantle model ages allowing for Sm/Nd fractionation tawing an average source to liquid change in Sm/Nd for the biotite granodiorites, hornblende-biotite granodiorites and the tonalites.

A significant shift to older model ages with a more restricted range is observed because those rocws with the lowest Nd model ages tended to be those with greatest source-to-liquid Sm/Nd fractionation. Furthermore the shift to older Nd model ages produces better agreement between these and the Pb-Pb age for the total Cretaceous suite.

This Proterozoic age confirms previous speculations that a major age province boundary exists within the southern margin of the Atlanta lobe (see figure 2.2) between crust of

Proterozoic age to the north, in the region of the Idaho batholith, and an Archaean province to the south, in the region of the Snawe River Plain (Leeman et al., 1985). In addition, a crustal formation age province boundary is implied to exist between the Wyoming Archaean province and the Proterozoic crustal province into which the Idaho batholith is intruded, somewhere to the east of the Atlanta lobe (figure 2.2).

In summary, it is argued that the Nd model ages of the Cretaceous granitoids variably reflect Sm/Nd fractionation depending on the proportions of residual garnet, clinopyroxene and hornblende remaining in their source regions during partial melting (compare section 4.8). Correction for this effect produces good agreement between the Pb-Pb ages and the Nd model ages and the preferred age for the source for the biotite granodiorites is ~1.45Ga. An average Pb-Pb model age for all the Cretaceous phases is actually higher than this, but mawes little difference in the following Pb and Sr isotope evolution models so an average age of 1.5 Ga is used for consideration of the Cretaceous granitoids together. Moreover, this confirms the area of the Idaho batholith as a Proterozoic crustal province and constrains models developed for the evolution of the Pb and Sr isotopes of the Cretaceous granitoids in the following sections.

5.6.2 Nd model ages of the Tertiary granitoids

Nd model ages have been calculated for the Tertiary granitoids assuming a depleted mantle reservoir (Jacobsen and Wasserburg, 1979 and DePaolo, 1981) and using the measured Sm/Nd and Nd isotope ratios. The results are presented on a histogram (figure 5.22) and have an overall range from 1.0Ga-1.7Ga. The granitic suite has a more restricted range of ages between 1.2-1.6Ga whereas the dioritic suite has a peaw of samples with a Nd model of 1.0Ga and range up to 1.7Ga.

It was previously argued (section 4.9.7) that Sm/Nd was unliwely to have been fractionated from source to liquid during partial melting and production of the granitic suite. Thus the Nd model ages are thought to represent the age of the source region and the range of ages reflect some source region isotopic heterogeneity and the small range in Sm/Nd ratios. This

conclusion is confirmed by the Pb-Pb age of 1.45Ga which corresponds to the average Nd model age of the Tertiary granitic suite.

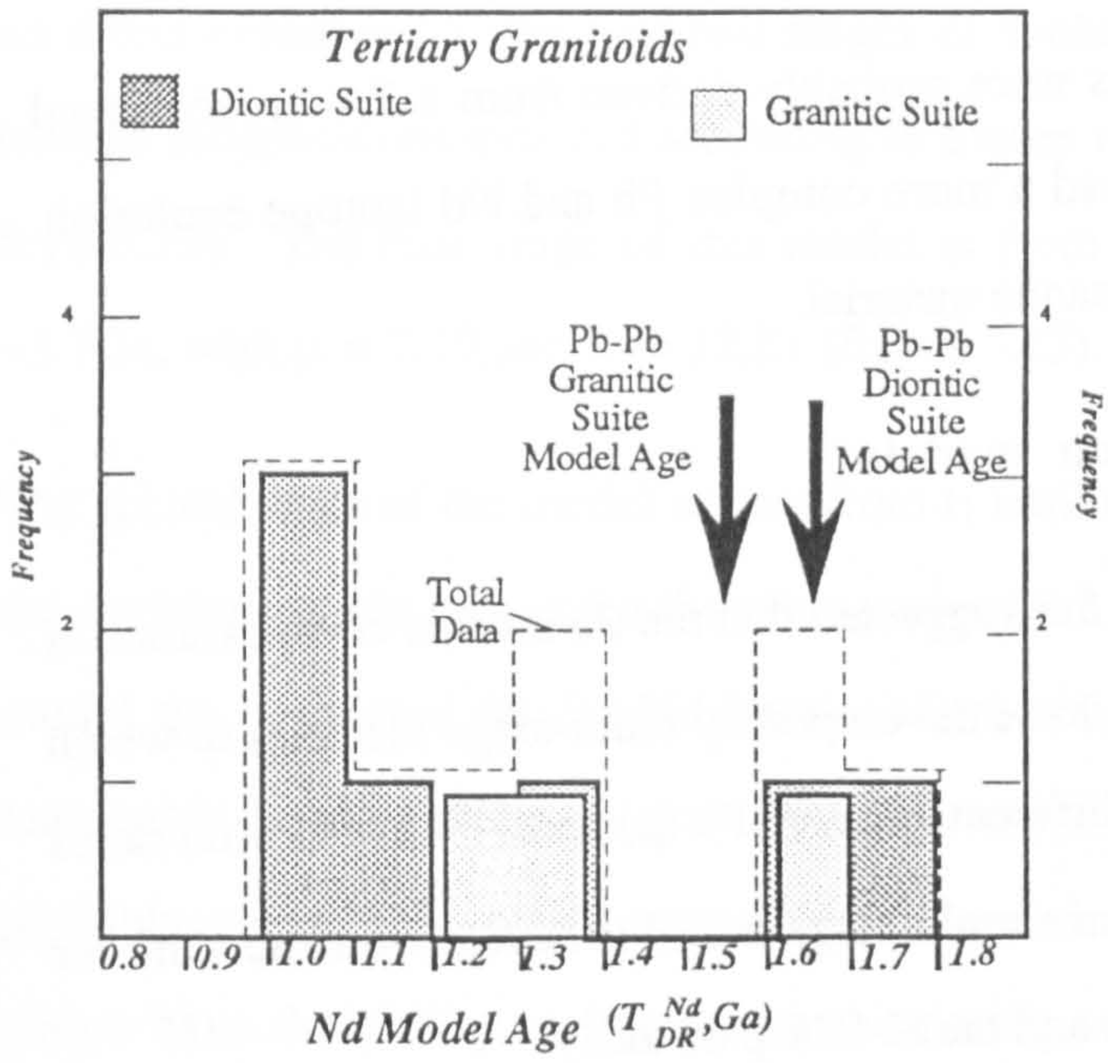

Figure 5.22 Histogram of depleted mantle model ages for the Tertiary granitic and dioritic suites.

The dioritic suite however, has a distinct peaw of Nd model ages at 1.0Ga-1.1Ga which contrasts marwedly with the Pb-Pb age of 1.65Ga. This discrepancy is unliwely to have been the result of intra-crustal Sm/Nd fractionation during production of the dioritic magmas as argued for by trace element modelling (section 4.9.7). Sr and Nd isotope evidence for mixing processes to generate the dioritic suite from LREE enriched mantle and old crustal material is quite strong (section 5.4.1). This suggests that the Nd model ages will be an underestimate of the age of the crustal end-member and in addition that the '^{207}Pb-^{206}Pb secondary isochron' is in fact a mixing line.

It is possible to carry out calculations to estimate the proportion of crustal to mantle end members which could account for the range of Nd model ages displayed by the dioritic suite, but there are several reasons why such calculations become unrealistic over-simplifications. The liwely end-members are poorly constrained, and the crustal components may have either been Archaean material similar to crustal xenoliths from the Snawe River Plain or Proterozoic material similar to the source of the granitic suite. The mantle component might be similar to the Snawe River Plain basalts (see section 5.4.1) and so have negative ε_{Nd} with

the result that model ages are difficult to interpret. Moreover the small number of analyses does not allow within suite variations to removed by using average values.

In summary, while the granitic magmas were probably derived from a Proterozoic aged lower crustal source, the dioritic suite had a more complex Pb and Nd isotope evolution, perhaps involving mixing of crustal and mantle material.

5.7 Multi-stage Pb isotope evolution models

The Pb isotope data presented in section 5.5 suggested that the Pb isotope compositions of the Atlanta lobe granitoids were likely to have developed by multi-stage histories in which the Pb isotopes evolved in systems with different $^{238}U/^{204}Pb$ (μ) and $^{232}Th/^{204}Pb$(ω) ratios for variable lengths of time. In this section a multi-stage model is developed to account for the Pb isotope ratios observed in the rocks and the K-feldspars today.

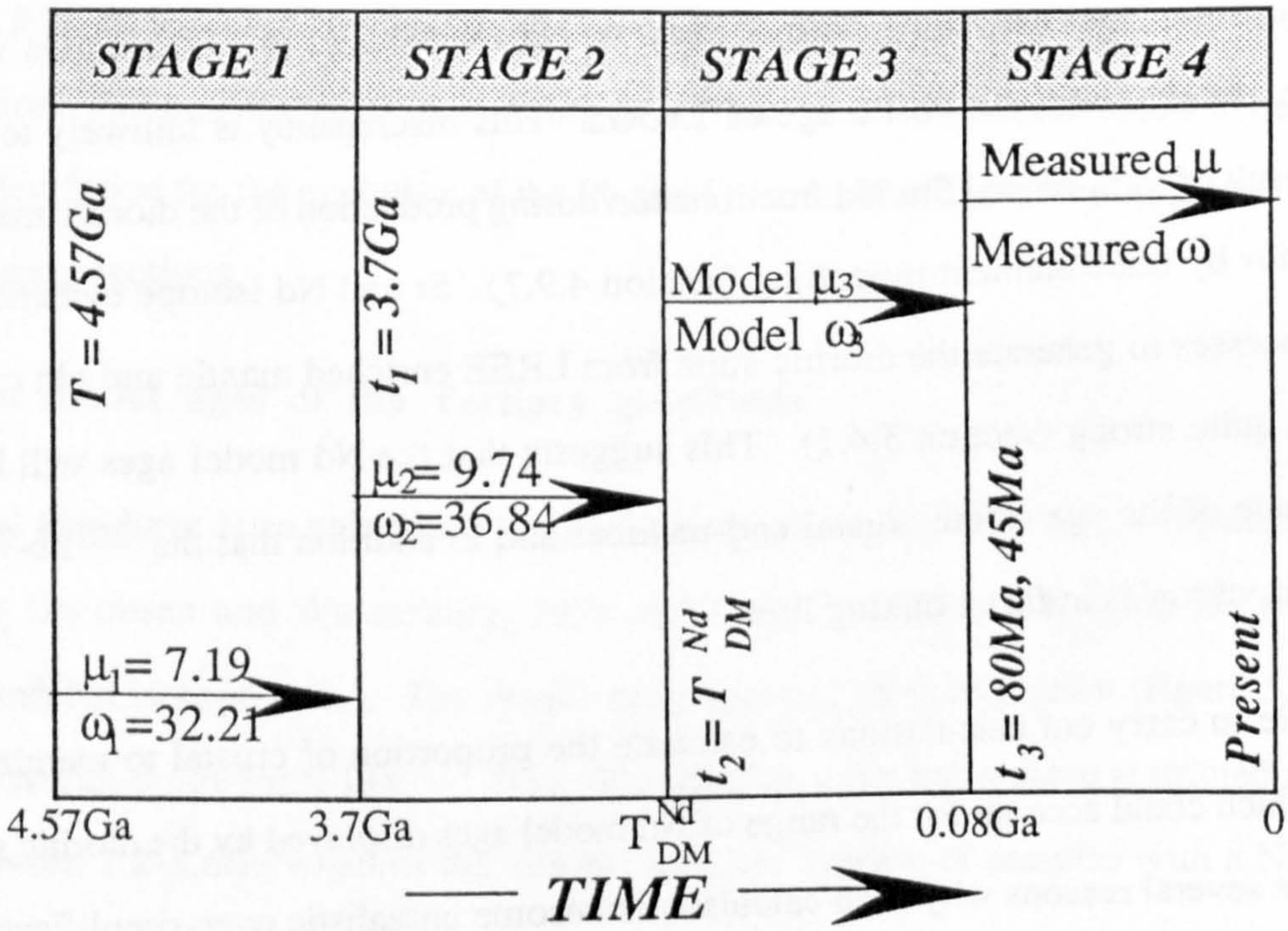

Figure 5.23 Schematic diagram of four-stage Pb isotope evolution applicable to the Cretaceous granitoids and the Tertiary granitic suite. The parameters for the first two stages are after Stacey and Kramers' (1975) terrestrial model Pb isotopic evolution.

It is assumed that the Pb isotopes of the whole-rock samples evolved in four stages, separated by orogenic events, each for specified periods of time characterised by different μ and ω values for each stage. The K-feldspars, in contrast, developed in three stages,

because the Pb isotope compositions were effectively frozen when the Pb was incorporated into the K-feldspars during crystallization, because of their low μ_1 and ω_1 values. There is no direct evidence for the first two stages of evolution, and so it is assumed that the Pb isotope compositions evolved according to Stacey and Kramers' (1975) model (see figure 5.16-5.19). The first stage of this model is from the age of the earth T≈4.57Ga, to t_1 =3.7Ga, with $\mu = 7.19$ and $\omega = 32.21$ (figure 5.23).

The second stage of the model occurs from t_1 until the time of extraction of the crust from the depleted mantle (t_2), and it therefore varies from sample to sample depending on the Nd model age (corrected for Sm/Nd fractionation) and the Pb-Pb age. This is a geologically reasonable time to change the μ and ω values and to homogenise the Pb isotopic ratios, as it probably represented a major orogenic event involving magmatic and metamorphic processes which have the ability to fractionate the parent nuclide ratios and homogenise isotopic compositions of large volumes of material.

The third stage of the model Pb isotope evolution is from the Nd model age (t_2) to the emplacement age of the granitoid (t_3) when the whole-rocks and the K-feldspars crystallized. The emplacement ages are taken to be 80Ma for the Cretaceous granitoids and 45Ma for the Tertiary granitic suite. The μ_3 and ω_3 values for the third stage of evolution of the model may be calculated by using:

i) the T, t_1, t_2 and t_3 time parameters (figure 5.23);

ii) the decay constants for ^{238}U, ^{235}U and ^{232}Th, λ_1, λ_2 (Steiger and Jäger (1977) , and λ_3 (Lederer et al., 1967), listed in appendix A;

iii) the measured K-feldspar and whole-rock age corrected $^{206}Pb/^{204}Pb$, $^{207}Pb/^{204}Pb$ and $^{208}Pb/^{204}Pb$ ratios.

The model μ_3 and ω_3 values are listed in table 5.6.

The fourth stage of Pb isotope growth concerns the whole-rocks only and occurs from 80Ma and 45Ma to the present day for the Cretaceous and Tertiary whole-rocks respectively, for which the μ_4 and ω_4 values are those measured in the samples.

		Whole-rocks				K-feldspars			
Sample	Rock Type	μ_3 $^{206}Pb/^{204}Pb$	μ_3 $^{207}Pb/^{204}Pb$	ω_3	Th/U	μ_3 $^{206}Pb/^{204}Pb$	μ_3 $^{207}Pb/^{204}Pb$	ω_3	Th/U
CBC-79	Kg	11.6	12.0	46.5	4.0	12.0	12.8	49.0	4.0
CBC-57	Kgd	13.1	13.6	44.9	3.4	14.0	14.4	51.5	3.6
CBC-94	Kgd	11.59	11.9	46.4	4.0	12.0	12.3	48.6	4.0
CBC-128	Kgd	10.4	9.9	46.1	4.5				
CBC-134	Kgd	14.3	14.1	50.4	3.6	14.2	14.0	50.8	3.6
CBC-146	Kgd	15.2	14.3	51.8	3.5	14.5	14.7	52.0	3.6
CBC-141	Kgd	16.1	16.9	53.7	3.3				
CBC-158	Kgd	15.0	15.8	52.1	3.4				
CBC-101	Kgd	11.2	11.6	46.0	4.0	11.3	11.8	47.5	4.1
CBC-106	Kgd	11.4	12.1	46.8	4.0	11.4	12.1	48.4	4.1
86RL-219	Kgd	13.7	23.9*	50.8*	3.3				
86RL-249	Kgd	12.6	12.0	45.8	3.7				
L82-9	Kgd	12.1	11.8	43.7	3.7				
86RL309	Kgdh	11.3	10.3	42.53	4.0				
86RL-387	Kgdh	10.0	4.5*	40.2	6.5				
CBC-148	Kgdp	16.5	15.9	57.8	3.6	15.3	15.1	52.9	3.5
CBC042	Klg	6.8	8.5	42.3	5.6				
CBC-117	Klg	11.8	11.3	44.4	3.8				
CBC-55	Kt	11.6	10.3	40.6	3.7				
CBC-145	Kt	14.2	12.7	46.3	3.5				
L84-13	K	13.5	9.0	72.4*	6.7				
L84-14	K	15.1	14.2	53.0	3.6				
Average	K	12.7	12.6	46.7	3.7				
CBC-23	Tg	6.3	6.6	42.4	6.6	6.1	5.8	41.9	7.1
CBC-132	Tg	10.0	10.2	45.9	4.5	10.7	10.7	45.7	4.3
86RL-257	Tg	9.0	9.5	43.6	4.7				
Average	Tg	8.4	8.8	44.0	5.1				

Table 5.6 Model μ_3 and ω_3 values for the Cretaceous granitoids and Tertiary granitic suite, whole-rocks and K-feldspar mineral separates. The μ_3 values calculated from both the $^{206}Pb/^{204}Pb$ and $^{207}Pb/^{204}Pb$ ratios are listed and the inferred model Th/U ratios are also presented. Asterisks denote anomalous values discounted in any models and averages.

Before discussing the model μ_3 and ω_3 values, a summary of the assumed conditions for the model is listed below:

i) The time at which the system became closed with respect to the transport of Pb and U across its boundaries and had homogeneous U/Pb ratios and homogeneous U, Th and Pb isotopic compositions, was at 4.57Ga.

ii) The system evolved according to the Stacey and Kramers' (1975) model from T to t_1 (4.57Ga-3.7Ga).

iii) At t_1 (3.7 Ga) it is assumed that an orogenic event occurred over a relatively short time period in which differentiation resulted in closed system fractionation of U/Pb and Th/Pb ratios, but without any isotopic fractionation of the compositions of U, Th or Pb (see Stacey

and Kramers, 1975). This assumption is tawen to be the case for all subsequent events which resulted in U/Pb and Th/Pb fractionation.

iv) For each stage of Pb isotopic evolution, the system evolved isotopically as a series of sub-systems with different μ and ω values to produce a range of Pb isotopic compositions with time. At subsequent differentiation events the diverse isotopic compositions between the individual sub-systems were homogenised. Furthermore, a new range of U/Pb ratios were generated so that a new series of sub-systems developed, each characterised by different μ and ω values, which again resulted in a range of isotopic compositions with time.

The Cretaceous granitoids are characterised by high model μ_3 (average = 12.63) and ω_3 values (average = 46.70) for the time period representative of the evolution of the source region within the crustal environment (t_1-t_2 in figure 5.23). The upper crustal melt granitoids are characterised by CBC87-42 (table 5.6) which has relatively low μ_3 and ω_3 values, confirming that the source of these granitoids was liwely to have been Archaean material which underwent early U depletion as was suggested by Leeman (1985) for the Archaean Snawe River Plain crustal xenolith analogues. An additional feature of these results (table 5.7) is that the model μ_3 and ω_3 values of the K-feldspars are in agreement with those of the age corrected whole-rock data, for the same samples, suggesting that the measured U/Pb and Th/Pb ratios may not have been perturbed since crystallization. However, such calculations are fairly insensitive because of the relatively short period of time (80Ma) that the whole-rock systems have existed with different U/Pb and Th/Pb than the K-feldspars.

The model μ_3 and ω_3 values can be simply translated to give estimates of the elemental U/Pb, Th/Pb and Th/U ratios of the source of the Cretaceous granitoids (table 5.7). The values of 0.2 and 0.70 for the U/Pb and Th/Pb ratios of the Cretaceous whole-rocks respectively, are extremely high compared with any of the average crustal rocks types of Taylor and McLennan (1985) (table 5.7) and they are curiously higher than the measured ratios in the rocks today or those calculated for the source by trace element modelling (listed in table 5.7 from section 4.8).

Rock Suite Averages (and method of estimate)	U/Pb	Th/Pb	Th/U
Cretaceous whole-rocks (from model μ_3 and ω_3 values)	0.20	0.70	3.58
Cretaceous K-feldspar (from model μ_3 and ω_3 values)	0.21	0.79	3.86
Cretaceous whole rocks (measured today)	0.154	0.68	4.89
Cretaceous Biotite granodiorite suite (measured today)	0.132	0.57	4.63
Cretaceous source rocks (from trace element modelling)	0.06	0.25	4.46
Biotite granodiorite source (from trace element modelling)	0.08	0.4	5.0
Tertiary granitic suite (from model μ_3 and ω_3 values)	0.13	0.66	5.23
Tertiary granitic K-spar (from model μ_3 and ω_3 values)	0.13	0.67	5.4
Tertiary granitic suite (measured today)	0.308	1.25	4.04
Tertiary granitic suite source (trace element modelling)	0.148	0.475	3.36
Bulw Crust (Taylor and McLennan, 1985)	0.114	0.438	3.85
Upper Crust (Taylor and McLennan, 1985)	0.14	0.535	3.82
Lower Crust (Taylor and McLennan, 1985)	0.07	0.265	3.79
Andesite Model crust (Taylor and McLennan, 1985)	0.125	0.647	6.052
CBC87-42 (from model μ_3 and ω_3 values)	0.107	0.647	6.052
CBC87-42 (measured today)	0.24	0.30	1.21

Table 5.7 Comparison of average U/Pb, Th/Pb and Th/U ratios measured in the samples, estimated from model μ and ω values and calculated in the source by trace element modelling for the Cretaceous granitoids (section 4.8) and the Tertiary granitic suite (section 4.9.7). In addition the upper crustal melt, CBC87-42 and average values for bulw, upper, andesite and lower crust are given for comparison. The measured Th and U values are by INAA and Pb by XRF.

The model U/Pb and Th/Pb ratios are model dependent and so these discrepancies may indicate that the model for Pb isotope evolution has been oversimplified. The assumption that the crustal source evolved since 1.5Ga ago to 80Ma with a constant U/Pb and Th/Pb ratio in a lower crustal environment is probably unliwely and intra-crustal processing may be responsible for reductions of U/Pb and Th/Pb in the source rocks to produce unsupported Pb isotope ratios. These problems and evolution of the source are addressed and further discussed using Sr isotope data and the calculation of time integrated Rb/Sr ratios (see section 5.8).

The relative differences between the model U/Pb and Th/Pb of the Cretaceous granitoids and the Tertiary granitic suite, however, are model independent and direct comparisons may be drawn between these results (table 5.7). The Tertiary rocks have significantly lower model U/Pb (average = 0.13) and Th/Pb (average = 5.23) than the Cretaceous rocks and higher

Th/U ratios suggesting that the source of the Tertiary granitic suite reflect relatively low time integrated U/Pb and Th/Pb ratios. This would be in agreement with combined Nd and Sr isotopic evolution models which suggested that the Tertiary granitic suite were derived from a relatively old source with low time integrated Rb/Sr ratios (section 5.4). Moreover, the measured U/Pb and Th/Pb ratios are higher than the model values, suggesting, as would be expected, that U and Th were enriched relative to Pb in the magmas of the granitic suite during the last partial melting event which was responsible for generation of the granitic magmas. The U/Pb and Th/Pb ratios calculated for the source of the Tertiary granitic suite (section 4.9) are in close agreement with the model U/Pb and Th/Pb ratios, but still high compared with those of average lower crust (table 5.7) indicating that the source was not depleted by any previous magma production.

In summary the four stage Pb isotope evolution model appears to be a good approximation for the Tertiary granitic suite which is characterised by low Pb isotope ratios reflecting relatively low time integrated U/Pb and Th/Pb ratios. In contrast, the model U/Pb and Th/Pb ratios of the Cretaceous granitoids are actually higher than those measured in the rocks today suggesting a more complex Pb isotope evolution.

5.8 Model Rb-Sr isotope evolution

In the preceding sections, the time of crustal formation, in which the source regions of the Atlanta lobe granitoids were generated, was constrained to be in the range 1.3Ga-2.0Ga ago, but on average has a crustal residence time of ~1.5Ga. These dates were based on Pb-Pb secondary isochron ages and depleted mantle model ages allowing for Sm/Nd fractionation during the last melting event and production of the Atlanta lobe granitoids. In this section the evolution of the source regions is discussed in terms of Rb-Sr isotope systematics, particularly because Rb/Sr fractionation is typically sensitive to the effects of intra-crustal recycling processes.

There are several lines of evidence upon which models are based and these include:

i) The age of the source region allows calculation of the time integrated Rb/Sr ratio of a granitoid protolith from the initial $^{87}Sr/^{86}Sr$ ratio of a granitoid sample.

ii) Independent estimates of the source Rb/Sr ratios at the time of generation of the Cretaceous granitoid magmas (80Ma ago) have been made by trace element modelling.

iii) T_{DM}^{Sr} model ages may be calculated in the same way as T_{DM}^{Nd} ages, but they tend not to have the same age significance, because it is liwely that Rb/Sr has been increased by intra-crustal processes. However, comparison of T_{DM}^{Sr} model ages calculated using various estimates of source Rb/Sr (as outlined above) with T_{DM}^{Nd} model ages may yield useful information on the evolution of the source regions.

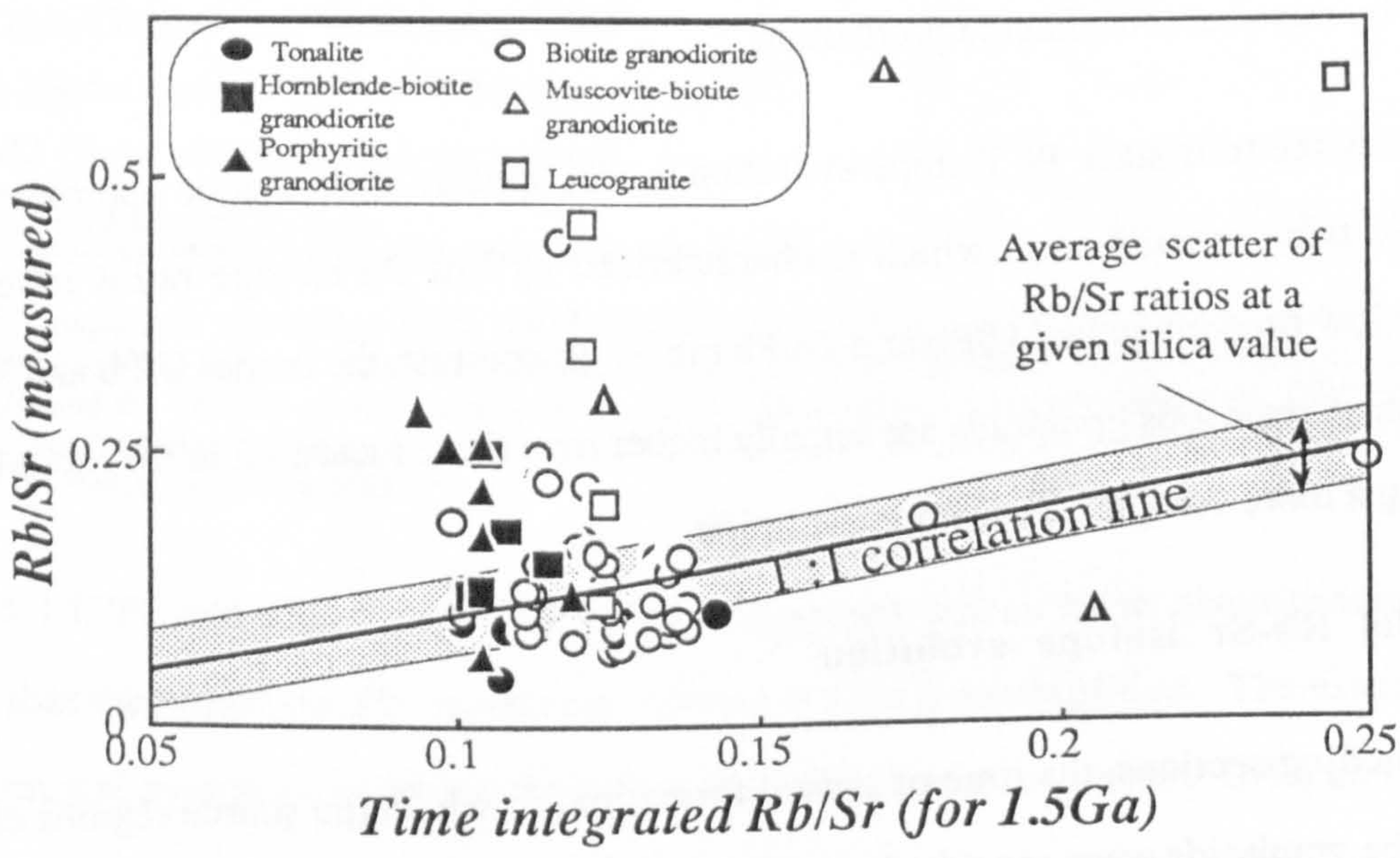

Figure 5.24 Graph of measured Rb/Sr versus time integrated Rb/Sr ratio assuming an average model age of 1.5Ga to allow for the Sm/Nd fractionation thought to have occurred during the generation of the Cretaceous granitoids (section 5.6). The shaded field represents the average scatter of Rb/Sr ratios at a given silica value.

The measured Rb/Sr ratios of the Cretaceous granitoids are plotted against the calculated time integrated Rb/Sr ratios for source regions with the preferred average age (section 5.6) of 1.5Ga (figure 5.24). The more evolved biotite granodiorites, muscovite-biotite granites and leucogranites have measured Rb/Sr ratios which are significantly higher than their time integrated Rb/Sr ratios (figure 5.24). This is to be expected because Rb/Sr is increased, both from source to melt during partial melting, and in the evolved liquid during fractional

crystallization, and these granitoids were those demonstrated to have undergone significant degrees of fractional crystallization (section 4.8.1) or are small % upper crustal melts. The hornblende-biotite and porphyritic granodiorites also generally have higher measured Rb/Sr ratios than the time integrated ratios, but the most startling feature of this diagram (figure 5.24) is that most of the biotite granodiorites and tonalites have lower or approximately equal measured Rb/Sr ratios and time integrated Rb/Sr ratios. This implies that intra-crustal processes over the time of crustal residence, including the last melting event responsible for the generation of the Cretaceous granitoids, have not acted so as to increase the Rb/Sr ratios in the granitoids with respect to their time integrated source compositions.

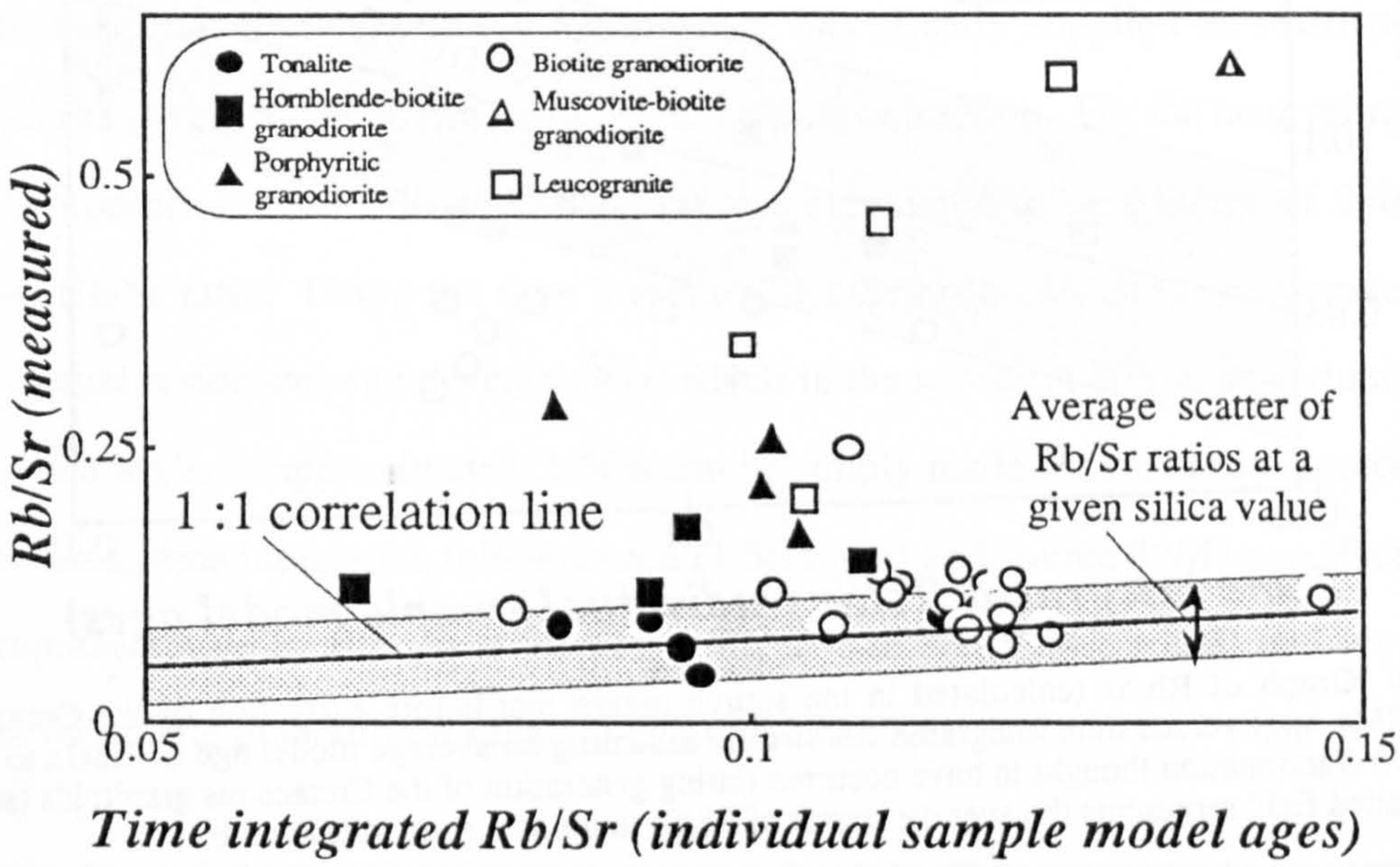

Figure 5.25 Graph of measured Rb/Sr versus time integrated Rb/Sr ratio calculated for individual sample model ages corrected the Sm/Nd fractionation thought to have occurred during generation of the Cretaceous granitoids (section 5.6). The shaded field represents the average scatter of Rb/Sr ratios at a given silica value.

A similar comparison was made between the measured Rb/Sr ratios of the granitoids and the time integrated Rb/Sr ratios of their protoliths, but this time individual sample model ages (corrected for Sm/Nd fractionation) were used to allow for some source region variation of the model ages and presented in figure 5.25. Although this procedure considerably reduces the effective sample set to those with measured $^{143}Nd/^{144}Nd$, it also reduces the number of samples, particularly the tonalites which have the oldest T_{DM}^{Nd} model ages, that have lower

Rb/Sr measured today than the time integrated Rb/Sr ratios of their source regions (figure 5.25).

The calculated source Rb/Sr ratios at 80Ma (from trace element modelling) are plotted against time integrated Rb/Sr in figure 5.26, and do not fall into the shaded field for the scatter of the Rb/Sr data indicating that Rb/Sr was lower in the lower crustal source 80Ma ago than the average over the previous 1.5Ga.

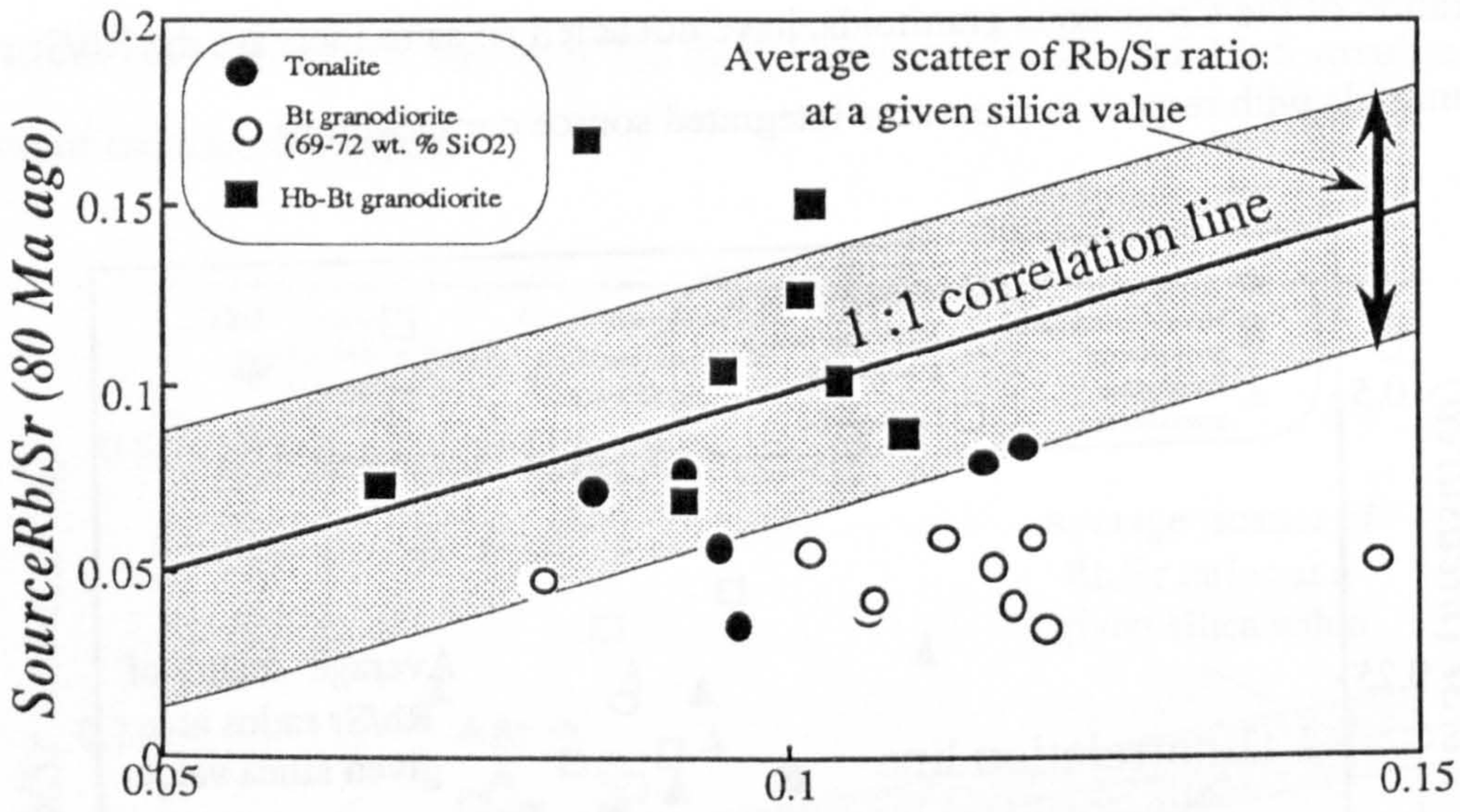

Figure 5.26 Graph of Rb/Sr (calculated in the source region just before extraction of the Cretaceous granitoids 80Ma ago) versus time integrated Rb/Sr ratio assuming an average model age of 1.5Ga to allow for the Sm/Nd fractionation thought to have occurred during generation of the Cretaceous granitoids (section 5.6). The shaded field represents the average scatter of Rb/Sr ratios at a given silica value.

This represents a significant problem in that a large number of samples, especially the least evolved biotite granodiorites, which have relatively high time integrated Rb/Sr, but low Rb/Sr measured today and even lower Rb/Sr ratios in the source at 80Ma, and thus fall below the 1:1 correlation line (figures 5.25 and 5.26). There are two simple arguments which can account for the unexpectedly high time integrated Rb/Sr ratios relative to those measured and those inferred in the source at 80Ma; the first that the simple source evolution outlined above is unjustified, and the second suggests that the scatter of the analytical data gives the appearance that some measured Rb/Sr ratios are low.

i) In model one the relatively high initial $^{87}Sr/^{86}Sr$ of the Atlanta lobe granitoids is tawen as evidence that their source regions had relatively high Rb/Sr, but that this was then subsequently reduced by intra-crustal processes to leave unsupported $^{87}Sr/^{86}Sr$ ratios. A consequence of this would be that the calculated time integrated Rb/Sr ratios of the source may be higher than the actual Rb/Sr ratios in the source at 80Ma ago when partial melting occurred. In extreme cases, when reduction of Rb/Sr was high and increase of Rb/Sr from source to liquid was minor, due to a small amount of residual plagioclase, such as in this case, the measured Rb/Sr ratios of the granitoids may also be lower than the time integrated values.

Trace element modelling (section 4.8) however, has already supplied an estimate of the Rb/Sr ratio of the source at 80 Ma just prior to magma extraction. For the near primary melt biotite granodiorites the Rb/Sr of the source was calculated to be a factor of 0.46 of the measured Rb/Sr ratio. Using the time integrated Rb/Sr ratio (which is an average for the time of crustal residence) and the calculated Rb/Sr in the source at 80Ma, an estimate of the initial source Rb/Sr at approximately 1.5Ga can be simply made for the biotite granodiorites. The measured, time integrated, initial source (1.5Ga ago) and source 80Ma ago Rb/Sr ratios of the representative biotite granodiorites (CBC87-125 and CBC87-158) and an average value for the biotite granodiorite suite are given in table 5.8.

Sample	CBC87-125	CBC86-158	Average Kgd
Measured Rb/Sr	0.114	0.076	0.127
Source Rb/Sr (80Ma ago)	0.052	0.035	0.058
Time integrated Rb/Sr (1.5Ga)	0.116	0.120	0.113
Time integrated Rb/Sr (T_{DM}^{Nd})	0.116	0.118	0.112
Initial source Rb/Sr (1.5Ga)	0.18	0.201	0.166
Change in Rb/Sr over 1.42Ga	0.128	0.166	0.108
Rate of decrease of Rb/Sr per 500Ma	1.5x	1.75x	1.25x

Table 5.8 The measured, time integrated, initial source and source at 80 Ma Rb/Sr ratios of the representative biotite granodiorites (CBC87-125 and CBC87-158) and an average value for the biotite granodiorite suite.

The inferred initial Rb/Sr ratios range from 0.17-0.2, which is higher than the average bulk crust (Rb/Sr=0.125) of Taylor and McLennan (1985), but significantly lower than their average upper crust estimate (Rb/Sr=0.32), and is thus thought to be a realistic ratio for juvenile crust extracted from the mantle.

In addition the initial source Rb/Sr ratio allows calculation of the average rate at which Rb/Sr has been reduced in the source during its crustal residence time of approximately 1.42Ga (before generation of the biotite granodiorites. Reduction of Rb/Sr was calculated to have occurred at the rate of 1.5x - 1.75x per 500Ma for the lower crustal source of the biotite granodiorites. Although the validity of such rates are difficult to assess quantitatively, previous estimates have been made on the rate of increase of Rb/Sr in the upper crust using crustal melt granitoids and sediments (Martin and Meybecw, 1979; Davies et al., 1985; McDermott, 1986 and Miller, 1988). The rates of increase of Rb/Sr for similar periods of crustal residence, estimated by the above authors range from 1.2x - 6x per 500Ma for the upper crust which is the same order of magnitude, but generally higher than the estimate of Rb/Sr decrease in the lower crust made here. This is in agreement with previous arguments (section 5.6) which suggested that the upper and lower crust were complementary to one-another, with lower crustal melts enriched in LILE and LREE emplaced at higher levels, whereas the lower crust was enriched in residual mafic material with reduced Rb/Sr and increased Sm/Nd ratios. The slower rates of Rb/Sr reduction in the lower crust compared to the rate of Rb/Sr increase in the upper crust may suggest that the upper crust represents a smaller proportion of the total continental crust, but mass balance estimates of the amount of material undergoing lower to upper crustal processing are rather beyond the scope of these preliminary speculations.

ii) The second line of reasoning suggests that the samples, mainly of biotite granodiorite, which tend to have lower measured Rb/Sr and lower source Rb/Sr (at 80Ma) than time integrated Rb/Sr ratios (figure 5.24, 5.25 and 5.26) are merely a consequence of scatter within the data (figure 4.11). The range of variation of Rb/Sr within the least evolved biotite granodiorites (69-73 wt.% SiO_2), at a given silica value, is at least 0.08-0.1 (figure 4.11).

In figure 4.24 and 4.25 the shaded field represents the range of scatter of Rb/Sr at any given silica value and it can be seen that most samples fall within this range and thus the samples below the 1:1 correlation line (in figures 5.24 and 5.25) could in reality fall on it. However, as previously noted the calculated source Rb/Sr ratios at 80Ma (from trace element modelling) plotted against time integrated Rb/Sr in figure 5.26 do not fall into the shaded field for the scatter of the Rb/Sr data indicating that Rb/Sr was lower in the lower crustal source 80Ma ago than 1.5Ga ago.

In summary it would appear that there has been a reduction of Rb/Sr in the source region of the biotite granitoids during its crustal residence time, but the actual rate of reduction would be difficult to assess due to scatter in the data. Typically Rb/Sr is thought to be reduced during discrete events, the timing of which would be critical to any Sr isotope evolution model for the source region. The later the intra-crustal depletion event occurred, during evolution of the source region, the smaller the initial Rb/Sr ratio in the source is required to be and thus the smaller the amount by which Rb/Sr was reduced in the depletion event prior to partial melting. Similar intra-crustal processes as these, which caused relatively small depletions of Rb with respect to Sr in the source region of the biotite granodiorites could cause U and Th depletion. This may account for the high time integrated U/Pb and Th/Pb ratios calculated for the source of the Cretaceous in comparison with the lower source at 80Ma (section 4.8) and the measured U/Pb and Th/Pb ratios in the rocks today (compare section 5.7).

Selective depletion of the LILE, but particularly U, Rb and Th, is a commonly observed characteristic of high grade granulite terrains (Heier and Thorensen, 1970; Heier, 1973; Newton and Hansen, 1986), and lower crustal granulite xenoliths (Leeman, 1985). There have been two mechanisms proposed for the selective depletion of U, Th and Rb during granulite metamorphism either:

i) Partial melting where U, Th and Rb are concentrated in melts resulting in relative depletions of the residue. Selective enrichment and depletion of very incompatible from mildly incompatible elements is most effective at very low degrees of melting so that

although the rock may become dehydrated the abundances of all but the most incompatible trace elements are not significantly reduced.

ii) An advective fluid flux may also have the ability to selectively deplete a region of lower crust of the most incompatible elements (Newton and Hansen, 1986).

By which ever mechanism these processes occurred, it is liwely that the lower crustal source regions of the Idaho batholith underwent high grade granulite facies metamorphism and thus selective depletions of these elements in the lower crust appears to be geologically realistic.

Furthermore, the normalised trace element abundance diagrams for the calculated source of the Cretaceous granitoids (section 4.8, figures 4.25, 4.28 and 4.29) indicate that the source rocks are not depleted liwe the lower crust of Taylor and McLennan (1985), but have trace element abundances more similar to the model andesite composition of Taylor and McLennan (1985). However, the tonalites and especially the biotite granodiorites, have significantly lower LILE/LREE ratios than the model andesite of Taylor and McLennan (1985) suggesting, in agreement with previous arguments that some relative depletion of the LILE (K,U,Th and Rb) relative to the LREE (La, Ce and Nd) and Sr occurred. Since the parent nuclides of the radioactive U-Pb, Th-Pb and Rb-Sr systems were selectively reduced in the source region during its evolution unsupported radiogenic isotope ratios were generated resulting in high time integrated parent to daughter ratios, specifically Rb/Sr, U/Pb and U/Th.

5.9 Summary of the conclusions from the isotope geochemistry

i) The Cretaceous granitoids of the Atlanta lobe have initial Sr, Nd and Pb isotope signatures consistent with derivation from a lower crustal source with moderate Rb/Sr and U/Pb and low Sm/Nd ratios.

ii) There is no evidence for mixing processes for generation of the Cretaceous granitoids, and no evidence of a recently derived mantle component incorporated into the magmas.

iii) Upper crustal material was only incorporated into the small volumes of highly leucocratic, peraluminous granitoids with anomalously high $^{87}Sr/^{86}Sr$ ratios. The upper

crustal melts from the southern margin of the Atlanta lobe, are thought to be derived from Archaean aged metasediments.

iv) The Sr, Nd and Pb isotope ratios of the Cretaceous and Tertiary granitoids are thought to be have been little affected by the large the large Tertiary hydrothermal circulation systems, except along discrete fracture and shear zones.

v) The Pb-Pb age of the Cretaceous granitoids is on average ~1.5Ga, which is in agreement with T_{DM}^{Nd} model ages allowing for source to magma fractionation of Sm/Nd.

vi) The Idaho batholith was generated in a crustal province of Proterozoic age with the boundary with the Archaean Snawe River Plain province just within the southern margin of the Atlanta lobe, and another boundary with the Wyoming Archaean craton somewhere to the east of the batholith.

vii) Time integrated U/Pb, Th/Pb and Rb/Sr ratios suggest that the lower crustal source of the Cretaceous granitoids was slightly depleted in highly incompatible elements, specifically U, Th and Rb during its crustal residence time of 1.42Ga. This is tentatively attributed to granulite metamorphism.

viii) The Tertiary dioritic suite is thought to have been generated by AFC processes, with old continental crust as the assimilant and the initial mafic magmas probably derived from enriched sub-continental lithosphere.

ix) The Tertiary granitic suite was probably derived by melting of the lower crust as a consequence of ponding hot, mafic, parental magmas of the dioritic suite, but differentiation from the dioritic suite cannot be totally dismissed.

x) The Tertiary granitic suite was derived from a Proterozoic source, the T_{DM}^{Nd} model ages were unaffected by source to liquid Sm/Nd fractionation and the source region was of a similar age to the source regions of the Cretaceous granitoids, but evolved as an isotopically isolated system.

CHAPTER 6

Summary, Conclusions and Synthesis

6.1 Introduction

This chapter summarises the geochemical characteristics of the Cretaceous and Tertiary granitoid suites of the Atlanta lobe, and highlights aspects of their petrogenesis and the inferred source region characteristics. This is followed by a brief section on the models for inducing crustal anatexis. The available data are then used to develop a geotectonic model for generation of the Idaho batholith granitoids in context of the crustal evolution of the northwestern United States cordillera and the implications for crustal evolution on a global scale are evaluated. Such features are then compared and contrasted with granitoids and inferred source regions from other areas of the western United States cordillera, and with granitoids from other orogenic belts.

6.2 Summary of granitoid petrogenetic studies

6.2.1 The biotite granodiorites

The biotite granodiorites are the dominant phase of the calc-alkaline, Cretaceous granitoids of the Atlanta lobe and the large sample set for this rock type has facilitated the development of more quantitative geochemical models for their petrogenesis. Such models have then provided a basis for evaluating the petrogenesis of the more subordinate rock types.

The biotite granodiorites are characterised by weakly peraluminous major element geochemistry; low HFSE, HREE, P and Ti abundances; high Ba and Sr; and ε_{Sr} and ε_{Nd} of -4.9 to -11.6 and 35 to 99 respectively. There is relatively little within suite variation in LILE abundances, but notably Yb falls with increasing silica which suggests that garnet was an important residual phase during partial melting, under high pressure conditions, and that the magma compositions were not significantly changed by any subsequent fractional crystallization processes. The biotite granodiorites have been successfully modelled as 25%-35% partial melts of a tonalitic lower crustal source in equilibrium with a garnet-bearing

granulite residue. The within-suite variation was modelled as increasing proportions of plagioclase entering the melt during partial melting, which was likely to have occurred under fluid absent conditions by dehydration breakdown of biotite and hornblende. Sr and Nd isotope compositions suggest that these rocks were largely derived from a lower-crustal source with little or no mantle or upper crustally derived material involved. Partial melting models reveal that Rb/Sr and U/Pb ratios are only increased by moderate degrees from source to liquid, but Sm/Nd is reduced by proportions large enough to significantly reduce the depleted-mantle Nd model ages. Correcting for the estimated source to liquid Sm/Nd fractionation, Nd model ages are on average 1.45Ga and agree well with the Pb-Pb ages of whole-rocks and K-feldspar mineral separates.

6.2.2 The silica rich biotite granodiorites, muscovite-biotite granites and leucogranites

The more silica rich biotite granodiorites (≥73 wt.%SiO_2), the muscovite-biotite granites and certain leucogranite samples which together outcrop more commonly in the interior regions of the Atlanta lobe are characterised by peraluminous to highly peraluminous major element compositions. They have highly variable LILE abundances, Ba and Sr decrease and Rb increases systematically with silica. They have been modelled as the products of up to 50% fractional crystallization of a granitic mineral assemblage from a biotite granodiorite parental magma.

Although the REE abundances become increasingly variable due to the effects of minor and accessory phase fractional crystallization at higher silica contents, specifically above 73 wt.% SiO_2, the systematic decrease in HREE observed in the biotite granodiorites is discontinued. This has allowed distinction of the biotite granodiorite suite dominated by the effects of partial melting with garnet as a liquidus phase, and the silicic biotite granodiorite, muscovite-biotite granite and leucogranite suite dominated by the effects of fractional crystallization processes. However, certain rocks have systematic depletions and enrichments of the REE with positive and negative Eu/Eu* anomalies respectively, which have been modelled by internally consistent fractional crystallization processes.

The Sr, Nd and Pb isotope signatures of this suite are similar to those of the biotite granodiorite magmas from which they are derived, but a subset of dominantly leucogranites (some of which contain muscovite) are distinguished by their anomalously high ε_{Sr} values. In addition these high ε_{Sr} rocks can be distinguished from the other highly silicic phases of the Idaho batholith by their high Rb/Zr ratios and flat REE profiles (figure 4.15): these are thought to reflect the unusually efficient separation of small volume, upper crustal, partial melts where residual accessory phases in the source (e.g. zircon) retain the REE and Zr. Furthermore they are emplaced as small stocks and dykes and thus are thought to be the products of small volume melt regimes, in contrast with the other larger volume melt granitoids of the Idaho batholith (further discussed in section 6.4 - crustal anatexis).

6.2.3 The tonalites, hornblende-biotite granodiorites and porphyritic granodiorites

The tonalites and hornblende-biotite granodiorites are characterised by metaluminous major element compositions; they are enriched in Sr, have high LILE/HFSE and LREE/HREE ratios and ε_{Sr} and ε_{Nd} of 35 to 70 and -5.8 to -10.5 respectively. They have been modelled as 35%-45% partial melts of mafic amphibolites in the lower crust, by fluid-absent biotite and hornblende dehydration melting reactions to leave a garnet-bearing mafic granulite residue. The hornblende-biotite granodiorites exhibit minimal within-suite trace element variations and are thought to represent unevolved magma compositions in contrast to the moderate variations in the tonalites which reflect the effects of small degrees of hornblende and plagioclase fractional crystallization.

The porphyritic granodiorites contain large alkali-feldspar megacrysts and have major and trace element compositions which exhibit much unsystematic variation (figures 4.3 and 4.5), but they are thought to be members of both the tonalite and hornblende-biotite granodiorite suites which crystallized alkali feldspar very late from volatile-rich final magmas (section 3.2.2).

These three suites cannot be distinguished from the biotite granodiorites on the basis of Sr, Nd and Pb isotope ratios, and show no evidence for mixing or AFC processes with material derived from either the upper crust or the mantle. Similar arguments to those proposed for the biotite granodiorites can be used to identify the nature of their source regions (discussed in section 6.3), but the principal conclusion made here is that the tonalite, hornblende-biotite granodiorite and biotite granodiorite suites on geochemical grounds probably represent separate yet near coeval intrusive phases unrelated to one another by fractional crystallization processes. The differences between the suites are thus thought to be inherited from their source regions (see section 6.3).

6.2.4 The Tertiary dioritic suite

The Tertiary dioritic suite -the more mafic rocks of the Tertiary bimodal suite, are diorites to granodiorites and they are characterised by metaluminous major element compositions, low HFSE and HREE abundances, high Sr and Ba, and ε_{Sr} and ε_{Nd} of 25 to 65 and -4.1 to -11.8 respectively. Distinctively they exhibit minimal within-suite trace element variation, but Sr and Ba decrease, while Rb/Sr and ε_{Sr} increase with increasing silica, which is thought to be the result of AFC type processes (section 5.4.1). The initial magmas appear to have been the evolved fractionates of magmas derived from enriched, subcontinental-mantle lithosphere, whereas the likely assimilant is old, low ε_{Nd} continental crustal material similar to the Archaean xenoliths of the Snake River Plain (Leeman et al., 1985) or the source rocks from which the granitic suite was derived. The small dioritic stocks were emplaced at epizonal levels and exhibit sharp within-pluton variations in mineralogy suggesting that the AFC processes occurred at these levels during crystallization of assemblages dominated by plagioclase and hornblende.

6.2.5 The Tertiary granitic suite

The peraluminous, epizonal Tertiary granitic suite are granites (*sensu-stricto*) distinguished from the other granites of the Atlanta lobe by their low Ba and Sr, moderate HFSE and HREE and high Rb, U and Th abundances, and several additional features similar to A-type

granites (Collins et al.,1982). The large and systematic variation in the LILE, the alkalis and the large negative Eu/Eu* anomalies have been successfully modelled by up to 40% fractional crystallization of mineral assemblages similar to those in the rocks themselves. The parental magma of the granitic suite was modelled by 30% partial melting of tonalitic source rocks at lower pressures than the chemically similar source of the Cretaceous granitoids, so that garnet was not an important residual phase and notably Sm/Nd was not significantly fractionated from source to liquid. It was further argued that the mafic granulitic residue after extraction of the Cretaceous granitoids, and the Cretaceous granitoids themselves, were unsuitable source rocks. The range in ε_{Nd} and ε_{Sr} is -8.1 to -15.4 and 54 to 120 respectively; ε_{Sr} is similar to the Cretaceous granitoids, but ε_{Nd} is slightly lower as are the Pb isotope compositions suggesting that these granitoids may have been derived from an isotopically distinct source region. Although derivation of the granitic suite from the evolved magmas of the dioritic suite cannot be totally ruled out, on isotopic or trace element grounds, the preferred origin is by lower crustal anatexis where the parental magmas of the dioritic suite acted as a heat source and emplacement in the upper crust was aided by the extensional tectonic regime.

6.3 The nature of the source regions of the Atlanta lobe granitoids

The combination of major element, trace element and Sr, Nd and Pb isotope modelling has been used to infer the composition, mineralogy, rock type (metasedimentary or meta-igneous), the age and evolution of the source regions of the various granitoids of the Atlanta lobe.

6.3.1 The source of the biotite granodiorites

The source of the biotite granodiorites and their evolved differentiates (the muscovite-biotite granites and some of the leucogranites) which together probably comprise 75% of the currently exposed Atlanta lobe (figure 3.2), were tonalitic, biotite- and hornblende-bearing amphibolites in the lower crust. At pressures greater than 10kb garnet may have appeared in

the subsolidus assemblage, or it may have been generated during biotite and hornblende dehydration reactions (section 4.9.2). The generation of the biotite granodiorite magmas is inferred to have left a residual mafic granulite assemblage of 40% clinopyroxene, 28% orthopyroxene, 10% garnet, 20% plagioclase and 2% opaque phases.

The estimated trace element composition of the source is similar to the model andesite of Taylor and McLennan (1985), being relatively enriched in incompatible elements compared with model lower crust (see figure 4.25). The source was characterised by high LILE/HFSE ratios, moderate LILE/LREE ratios, low Ti and higher Sm/Nd ratios than the biotite granodiorite magmas. The high LILE/HFSE ratios indicate that the source regions were themselves generated by subduction-related processes (Pearce et al., 1984). This subduction signature has been passed on to the biotite granodiorite magmas and although they were derived by partial melting the lower crust, they fall into the volcanic arc granite field on granitoid tectonic discrimination diagrams (see figure 4.10). The various characteristics of the biotite granodiorites similar to the features of I-type granites (table 4.1) and an origin of the source region by subduction suggests that the source rocks are dominantly meta-igneous.

The source is Proterozoic in age with Nd depleted mantle model ages (corrected for Sm/Nd fractionation) of, on average, ~1.5Ga which is in agreement with the more durable Pb-Pb ages which are unaffected by U/Pb fractionation. Thus it is concluded that the Idaho batholith region lies in a Proterozoic crust formation age province and bounded to the south and east by the Snake River Plain and Wyoming Archaean provinces respectively.

The calculated source LILE/LREE ratios are notably low (figure 4.25), but there is some suggestion that the LILE may have been depleted during evolution of the source region prior to magma production at 80Ma. The initial Sr, Pb and Nd isotope compositions are typical of a source with high Rb/Sr, U/Pb, Th/Pb and low Sm/Nd ratios. However, the initial Sr and Pb isotopic ratios are unsupported by the inferred source Rb/Sr, U/Pb and Th/Pb ratios, such that time integrated Rb/Sr, U/Pb and Th/Pb are higher. It is thus concluded that geochemical evolution of the source region since 1.5Ga has been minimal except for small

depletions of the most incompatible trace elements (Rb, U and Th) under high grade metamorphic conditions.

The substantial range in isotope composition of the biotite granodiorites suggests that there were localised heterogeneities in the trace element composition of the lower crust in this region, and comparison of the major element source compositions of the tonalites, hornblende-biotite granodiorites (section 6.3.2) further indicates that the major element composition also varies. This is taken to suggest that in regions where there has been little lower crustal reprocessing initial chemical heterogeneities obtained during crustal formation are preserved and it is likely that large scale, lower crustal partial melting events act to generate a more uniform, trace element-depleted lower crust.

6.3.2 The source of the tonalites and hornblende-biotite granodiorites

The major conclusion on the inferred source regions of the tonalites and hornblende-biotite granodiorites is that they had many similarities with those of the biotite granodiorites. The former are Proterozoic in age (T_{DM}^{Nd} = 1.2Ga-1.7Ga), they have high LILE/HFSE ratios and low LILE/LREE ratios, are meta-igneous and have similar isotopic compositions to the biotite granodiorites. Thus the source regions of the tonalites and the hornblende-biotite granodiorites are assumed to have had a similar evolutionary history to that of the biotite granodiorites.

The source regions of the tonalites and hornblende-biotite granodiorites were distinguished by being more mafic in composition (tonalitic to gabbroic), containing higher proportions of hornblende than biotite or plagioclase, they yielded higher degree partial melts with more plagioclase and less garnet in the mafic granulite residue, and this resulted in greater Rb/Sr and less Sm/Nd source to liquid fractionation. In addition the primordial mantle-normalised trace element abundance patterns are lower and slightly flatter than those of the biotite granodiorite source regions (compare figures 4.25 and 4.29), which is concluded to be the result of igneous differentiation during production of the source regions. The more mafic source rocks were less enriched in incompatible trace elements and these characteristics have

been passed on to the Cretaceous granitoids because it was ultimately the major element chemistry, at the particular pressure and temperature conditions which governed the partial melting processes.

6.3.3 The source of the Tertiary dioritic and granitic suites

In many respects the crustal source regions of the granitic and dioritic suites are similar to those of the Cretaceous granitoids. The Tertiary granitoid source regions are thought to have been tonalitic to gabbroic, meta-igneous in origin, contain biotite and hornblende, be relatively enriched in trace elements with high LILE/HFSE ratios, be Proterozoic in age and to have been partially melted in the lower crust to leave a mafic granulite residue.

The Tertiary source regions only differ significantly from the Cretaceous granitoid source regions by having undergone partial melting at lower pressures where cordierite may have been produced during biotite dehydration reactions in preference to garnet (see reaction in section 4.9.2) due to lithospheric attenuation. The granitic suite is however, isotopically distinct from the Cretaceous granitoids having lower ε_{Nd}, $^{206}Pb/^{204}Pb$ and $^{207}Pb/^{204}Pb$. Though the source of the granitic suite is of the same age and presumably generated during the same crustal formation event as the Cretaceous granitoids, it was not involved in production of the Cretaceous granitoids and it appears to have evolved in isolation from the Cretaceous source regions as witnessed by the differences in isotope composition. This again suggests that the fertile, unprocessed lower crust in this region is chemically heterogeneous.

The high Ba abundances and low initial Sr isotope ratios which vary systematically with trace element composition reflect incorporation of mantle-derived material in the dioritic suite. The old Nd model ages and the Pb-Pb age suggest that the continental mantle lithosphere in this region may have attained its characteristically low Sm/Nd and high Rb/Sr ratios during the same subduction-related orogenic event as the lower crust, from which the other granotoids were generated.

6.3.4 The source of the upper crustal melt leucogranites

The leucogranites from the southern margin of the Atlanta lobe have anomalously high initial $^{87}Sr/^{86}Sr$ ratios, low ε_{Nd}, $^{206}Pb/^{204}Pb$ and $^{207}Pb/^{204}Pb$ and have Nd depleted mantle model ages of 2.1Ga-2.8Ga. This is thought to reflect derivation from Archaean upper crustal sedimentary source rocks similar to the Archaean Albion range metasediments that outcrop to the south of the Snake River Plain, in south central Idaho (Armstrong and Hills,1967). This suggests that the boundary between the 1.5Ga Proterozoic age province of the Idaho batholith region, and the Archaean Snake River Plain province may be accurately located just within the southern margin of the Atlanta lobe. However, the upper crustal metasedimentary precursors to these leucogranites may have been transported by sedimentary processes to their present position from the adjacent Archaean provinces. In order to define better this boundary deep crustal anatectic granitoids or dykes with undisputed Archaean signatures need to be identified by future work near the boundary region.

6.4 Models for inducing crustal anatexis

With the exception of the Tertiary dioritic suite all the granitoids of the Atlanta lobe are largely derived from material that had been resident in the crust for approximately 1.5Ga. The large volume of Atlanta lobe granitoids thus emphasizes that pure crustal anatexis has been an important aspect of intra-crustal evolution and differentiation on a cordilleran and a global scale. It is necessary to understand the mechanisms which induce crustal anatexis both so that its effects may be better understood, and so that where crustal anatexis has played a key role in crustal evolution can be better recognised by a set of required or associated tectonic characteristics. This section reviews some of the current ideas of how crustal anatexis is induced and assesses the applicability of these ideas to the Atlanta lobe of the Idaho batholith. It compliments section 4.9.2 which dealt with the specific mechanisms and their geochemical effects for lower crustal anatexis to produce the Atlanta lobe granitoids.

There are currently four mechanisms by which crustal anatexis is thought to be induced, all of which have recently been invoked to account for the granitoids of the western United States Cordilleran Interior.

i) Advective heating as a result of intrusion of mantle-derived magmas into the crust (Huppert and Sparks, 1988), proposed for the granitoids of the Cordilleran Interior by Hyndman and Foster (1988).

ii) Tectonic thickening of the crust (England and Thompson, 1986) proposed for the Cordilleran Interior by Patiño Douce et al. (1990).

iii) Lithospheric thinning in response to subduction, with or without advective heating by sub-crustal derived magmas (Barton, 1990).

iv) Mantle-derived water rich fluid fluxes passing upwards into the crust (Hoisch and Hamilton, 1990).

Foster and Hyndman (1990) cite direct evidence for the presence of mantle-derived, mafic rocks associated with anatectic granitoids in the Bitteroot lobe of the Idaho batholith, given the accepted thermal arguments for generation of granitoid magmas by intrusion of basaltic magma into the crust (Huppert and Sparks, 1988). Hyndman (1981) argues that the Bitteroot lobe was emplaced at levels ≥20km, not far above the level of magma generation and that it is associated with diorite and tonalite plutons, dioritic to tonalitic gneissic sheets structurally below the granitoids, syn-plutonic basaltic dykes associated with quartz-diorite complexes and syn-plutonic gabbros. Moreover it is argued that these are all mantle-derived magmas generated by subduction-related processes, associated with basaltic under-plating and the advective heat source responsible for generation of the granitoids. This model is thought by Foster and Hyndman (1990) to be applicable to most of the granitoids of the Cordilleran Interior because:

i) All of western North America lay above a subduction zone in the Late Cretaceous to Early Tertiary;

ii) The level of exposure of most Cordilleran Interior granitoids is too high to reveal the presence of these proposed voluminous mafic rocks;

iii) The proportion of metaluminous granitoids increases with depth of emplacement (Farmer and DePaolo, 1981) which it is argued, suggest that, although these granitoids contain a large proportion of old crust, they probably contain a significant proportion of juvenile mantle-derived material.

There are, however, several objections to these arguments principally in regard to the timing of the various intrusive events. The tonalites are probably too early to be realistic heat sources (Patiño Douce et al., 1990), the syn-plutonic mafic dykes require that the granitoids were already in existence and, at least in the Atlanta lobe, the large dyke swarms are associated with the Eocene dioritic plutons which post-date the main Cretaceous intrusive phases. In addition it has been argued here that the tonalites in the Atlanta lobe are probably wholly crustal anatectic melts and therefore not heat sources for crustal melting.

Although there is little evidence for intrusion of syn- or pre-plutonic mafic magmas in the Atlanta lobe, the ponding of subduction associated mafic magmas at the crust/mantle interface (due to density contrasts; Rogers and Hawkesworth, 1982) and advection of heat, (including the latent heat of crystallization) offers an efficient method to produce melting in the lower crust as opposed to melting at mid-crustal levels produced by crustal thickening (Patiño Douce et al.,1990). Moreover, the identification of a mantle derived component in the Tertiary dioritic suite and the association of mafic dyke swarms with these stocks indicates that advection of heat by sub-crustal magmas was likely to have been an important process in the generation of the Tertiary dioritic and granitic suite granitoids.

Patiño Douce et al. (1990), argue that given an idealised pre-Mesozoic lithospheric section of the Cordilleran Interior, with defined thermal properties, a fertile window of quartzofeldspathic metapsammites and metapelites can be identified from which large volume, mobile, granitoid magmas may be generated (presumably of S-type nature), by tectonic crustal thickening alone. Simulation of the pressure-temperature conditions for crustal thickening events demonstrate that:

i) the mid-crustal temperature increases as a result of the insulating effect of added crust, but dominantly due to the increased thickness of crust rich in heat producing elements;

ii) the energy required for anatexis is provided by normal heat flow through the mantle and radiogenic heat production;

iii) the scale of melting is large, a 10km thick layer of granitoid magma derived as a 40% melt fraction of a metapsammite can be produced 20Ma after a crustal thickening event;

iv) rapid deformation produces post-kinematic granitoids whereas slow or semi-continuous deformation produces syn-kinematic granitoids.

v) the metamorphic pressure and temperature gradients produced by such events are typically those of the Barrovian facies series.

The importance of the pre-existing crustal structure is paramount to this model, and arguments cited against it by Foster and Hyndman (1990) are the unrealistically high proportion of hydrous phases required, the high radiogenic heat production figures used in the model and typically where Proterozoic middle crust is exposed it is dominantly orthogneisses, not fertile metapsammites.

The applicability of inducing anatexis by the crustal thickening model alone for the Atlanta lobe granitoids appears to be good because it is situated in the tectonically thickened hinterland of the Sevier orogeny of the early Cretaceous, there is no geochemical or isotope evidence for the involvement of mantle-derived material and the predicted association of Barrovian facies metamorphic assemblages are preserved to the north of the Bitteroot lobe.

However, crustal thickening cannot have been the sole cause generation of the Atlanta lobe granitoids since it has been demonstrated that the precursors to the Atlanta lobe granitoids are not mid-crustal metapsammites, but tonalitic, meta-igneous amphibolites situated near the base of a tectonically thickened crust (section 4.9.2). The Barrovian metamorphic facies to the north of the Bitteroot lobe appear to be unrelated to the main phases of the Atlanta lobe, but overprinted during emplacement of the Bitteroot lobe which was generated at deeper levels (Hyndman, 1981). The important role that crustal thickening played in generation of the voluminous Atlanta lobe granitoids was indeed to raise the ambient temperature of the

crust, but for lower crustal melting the insulating effect was probably more significant. In addition the compressional tectonic regime leading to crustal thickening placed the source region within the stability field of garnet and also may have encouraged ponding rather than rapid passage through the crust of mantle derived magmas.

Crustal anatexis of the mid- to upper crust by crustal thickening appears likely to be responsible for generation of the leucogranite upper crustal melts of the Atlanta lobe. They are small volume stocks and dykes associated with migmatites which post-date the other Cretaceous granitoids of the Atlanta lobe. A temporal evolution of anatectic granitoids containing increasing proportions of mid- upper crustal metasedimentary material has been noted by Barton (1990), but, as thought to be the case here, Patiño Douce et al. (1990) suggest that this represents the change from wholly anatectic granitoids generated at deep crustal levels to those generated at mid-crustal levels.

Thus it appears that there were two distinct melting regimes during generation of the Atlanta lobe granitoids:

i) low volume partial melting (<20%) induced largely by crustal thickening at mid-crustal levels to produce the leucogranites;

ii) higher volume partial melting (≈30%-40%) dominantly the result of basaltic underplating, but also due to crustal thickening resulting in generation of the tonalites, hornblende-biotite granodiorites and biotite granodiorites.

The high viscosity of small volume granitic partial melts (Wickham, 1986) generated by high grade metamorphic conditions does not allow efficient extraction and separation of these melts from their matrices. Upward expulsion of the low-density melt by the more dense compacting matrix is improbable unless the volatile content is high and the matrix grain size is large, hence the common association of high grade metamorphic conditions with migmatite terrains (Richter and McKenzie, 1985 and Richter, 1986). It is only with the aid of regional scale deformation that such granitoids may be forced out to form mobile granitoid magmas. The compressional tectonic regime associated with Sevier crustal shortening and

thickening could perhaps provide the mechanism whereby the Atlanta lobe leucogranites were extracted.

Barton (1990) suggests that the increase of the basal crustal heat flux, due to thinning of the sub-crustal lithosphere, with or without intrusion of sub-crustal magmas, could raise the temperature to induce crustal anatexis. He also suggested that the mantle-derived magmas made up a larger proportion of granitoids early in the evolution of the Cordilleran Interior and the proportion of sedimentary material increased due to heating of the crust by prolonged injection of basaltic magmas. Objections to this model for the generation of the Atlanta lobe granitoids are similar to those against advective heating, but in addition it is suggested that:

i) a crustal thickening event is unlikely to be associated with thinning of the lithosphere, but may be apt for the Tertiary bimodal suite where there is evidence for extension;
ii) that lithospheric attenuation would be more likely to cause melting within the mantle itself and heat transfer by advection rather than merely by conduction would be more efficient.

The above model is the preferred mechanism for generation of the Tertiary bimodal suite where sub-crustal magmas generated as a result of lithosphere extension were intruded into the crust to generate the dioritic suite by advection of heat and AFC processes. In contrast the granitic suite was generated later after the temperature of the lower crust was raised sufficiently by ponding and crystallization of the mantle derived magmas to form pure crustal anatectic melts. Evidence for extension and lithospheric thinning are the Eocene extensional fault-bounded horst and graben systems (Bennett and Knowles, 1985), the change from lower crustal melts in the Cretaceous to the granitic suite without residual garnet and emplacement of the dioritic and granitic suites at epizonal levels presumably aided by extensional fractures. The change from the earlier dioritic suite with incorporation of mantle-derived material to the later granitic suite with no mantle-derived material is similar to the observations made by Barton (1990) for the cordilleran granites in general.

Finally, Hoisch and Hamilton (1990) suggest that dehydration of underplated metasedimentary rocks in the subducted plate resulted in pervasive flushing of the crust with

H_2O rich fluids to induce anatexis in southeastern California. At the depths of 10kb-20kb suggested by Hoisch and Hamilton (1990) dehydration melting rather than subsolidus dehydration would be more likely to occur, whereupon any free fluid phase would be immediately dissolved in the melt (Clemens and Vielzeuf, 1987). Such mechanisms may be more prevalent for upper crustal melting where pore space is greater and can accommodate the relatively large volumes of fluid required (Hoisch and Hamilton, 1990), and where fluids are not immediately dissolved in the melts.

In summary it is important to note that the above processes are not mutually exclusive so that one or number of the following list of mechanisms capable of inducing crustal anatexis may be used together with other evidence to suggest the occurrence of crustal anatexis throughout the geological record. Crustal anatexis may occur associated with:
i) active subduction; ii) tectonically thickened crust; iii) intrusion of mantle derived mafic magmas; iv) crustal/lithospheric extension and v) subcretion of rocks rich in hydrous phases.

A final synthesis of the geotectonic evolution of the northwestern United States cordillera (section 6.5) links the development of these suggested tectonic environments to develop a model for the generation of the Atlanta lobe granitoids.

6.5 Geotectonic model for the generation of the Atlanta lobe granitoids and the evolution of the northwestern United States cordillera

A simplified model for evolution of the western United States cordillera is proposed which brings together the conclusions from all aspects of this study and seeks to account for the following key observations.
i) The suture between the Precambrian North American continent and the accreted island arc terranes and the isotopic discontinuity of the Cretaceous granitoids intruded across this boundary.

ii) Moderate pressure and high temperature pre-plutonic episode of Barrovian metamorphism of the Precambrian country rocks to the north of the Atlanta lobe which may have originally extended further south.

iii) Generation of large volumes of tonalitic to granitic Cretaceous magmas from the lower crustal with little or no incorporation of mantle-derived material.

iv) Emplacement of the Cretaceous granitoids at mid- to lower crustal depths and the probable absence of large volumes of mafic or felsic, Cretaceous, volcanic products.

v) Generation of chemically distinct upper crustal leucogranite melts after the main Cretaceous phases of the Atlanta lobe.

vi) Rapid, Late Cretaceous to Eocene, post-emplacement uplift of the Idaho batholith and the surrounding region.

vii) The generation of the Tertiary dioritic suite containing mantle-derived material and the anatectic Tertiary granitic suite derived from lower continental crust, but at depths shallower than the partial melting event which produced the Cretaceous granitoids.

viii) Emplacement of the Tertiary dioritic and granitic suites at epizonal levels in association with their equivalent volcanic products.

The Proterozoic crust of the northwestern United States cordillera underwent substantial tectonic crustal thickening by basement thrusting between 120Ma-100Ma as a result of the Sevier orogeny (Heller, 1986; Lawton, 1986; Oldow et al., 1989). Specifically in the Atlanta lobe region at least two major northeast directed basement thrust sheets of Early Proterozoic metasediments and meta-igneous rocks overode the Middle Proterozoic rocks of the Belt Basin (Skipp, 1987 and figure 6.1). The cause of this major compressional event was related to eastward subduction of the Pacific oceanic plate beneath the North American continent, with either shallow subduction causing interaction with the overlying lithosphere (Lipman, 1971) and/or the coeval docking of the allocthonous Blue Mountain oceanic island arc terrane on the western border of the current Atlanta lobe (figure 6.1). The final docking of the island arc terrane was dated at 118Ma by Sutter et al. (1984), and it occurred by transpressive motion along a north-south strike slip fault to produce a sharp vertical suture with the North American continent, ultimately as a response to the oblique angle of

subduction (Lund and Snee,1988: Snee et al., 1989; Manduca, 1988) as illustrated in figures 2.10 and 6.1.

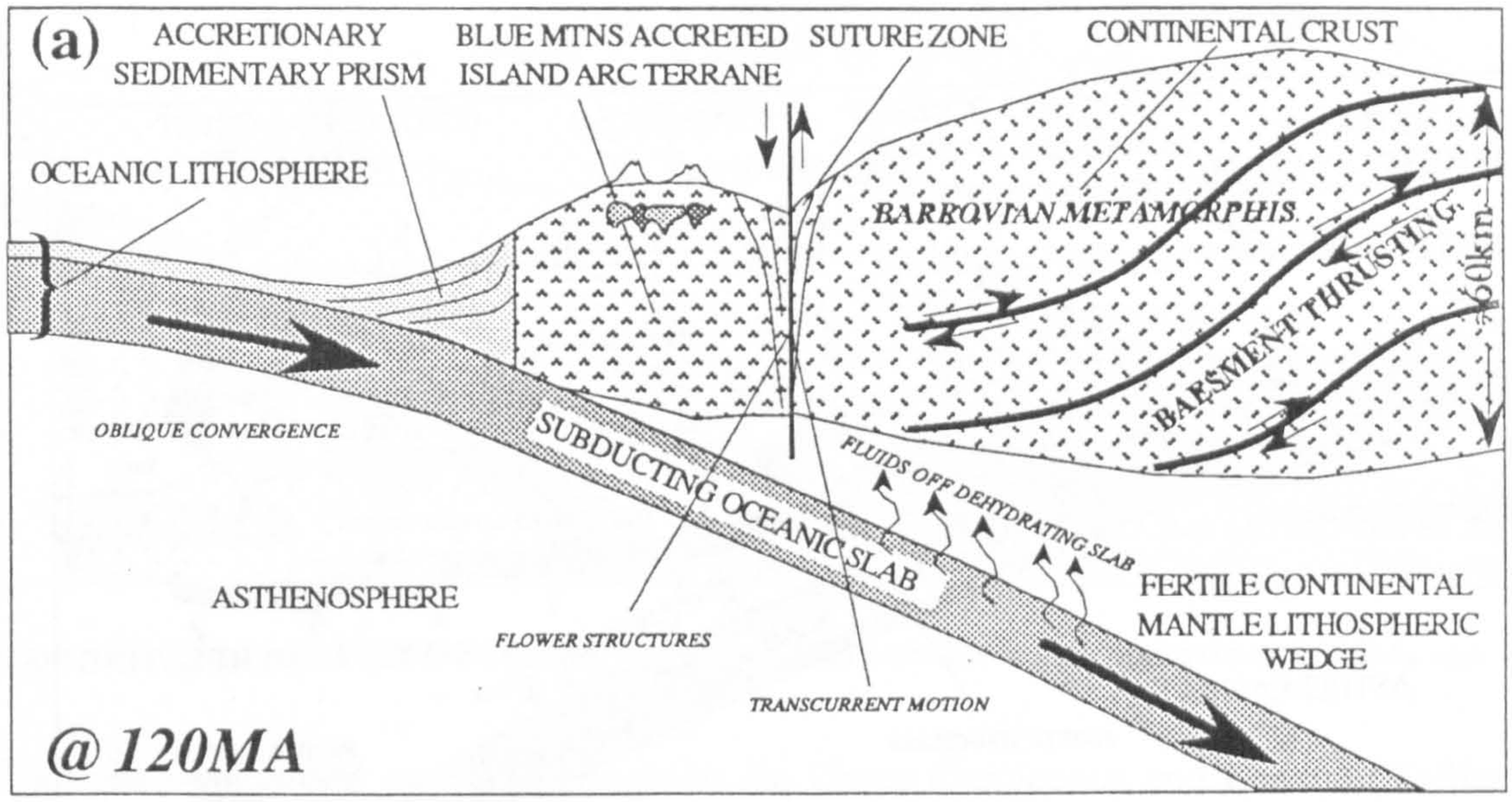

Figure 6.1 Schematic east-west cross-section of the Idaho batholith region approximately 120Ma ago.

The combination of continued subduction and thickened continental crust caused ponding of subduction related basaltic magmas generated in the mantle wedge, at ≈ 60km at the crust mantle interface, due to density contrasts (figure 6.2). The increased lower crustal heat flow due to advection of these magmas (Huppert and Sparks, 1988) and the insulating effect of the increased thickness of overlying crust (England and Thompson, 1986) caused large scale partial melting of the lower crust and production of large volumes of granitoid magmas represented by the main Cretaceous phases of the Atlanta lobe (figure 6.2). The granitoids intruded to the west of the suture zone inherited the isotope signatures of the oceanic-island-arc lithosphere, whereas those intruded into continental basement inherited the isotope signature of the Proterozoic lower crust (figure 6.2).

The emplacement depths of the Cretaceous granitoids are estimated to be at least 25km (Zen and Hammarstrom, 1984), and this is attributed to the thickness of the overlying low density crust and, the compressional tectonic regime which would tend to hinder the diapiric or dyke controlled rise of granitoid magmas (figure 6.2). This suggests that the lack of Cretaceous volcanic products or their sedimentary derivatives is because the Cretaceous magmas were

trapped at deep crustal levels, rather than the removal of any such volcanics by uplift and erosion.

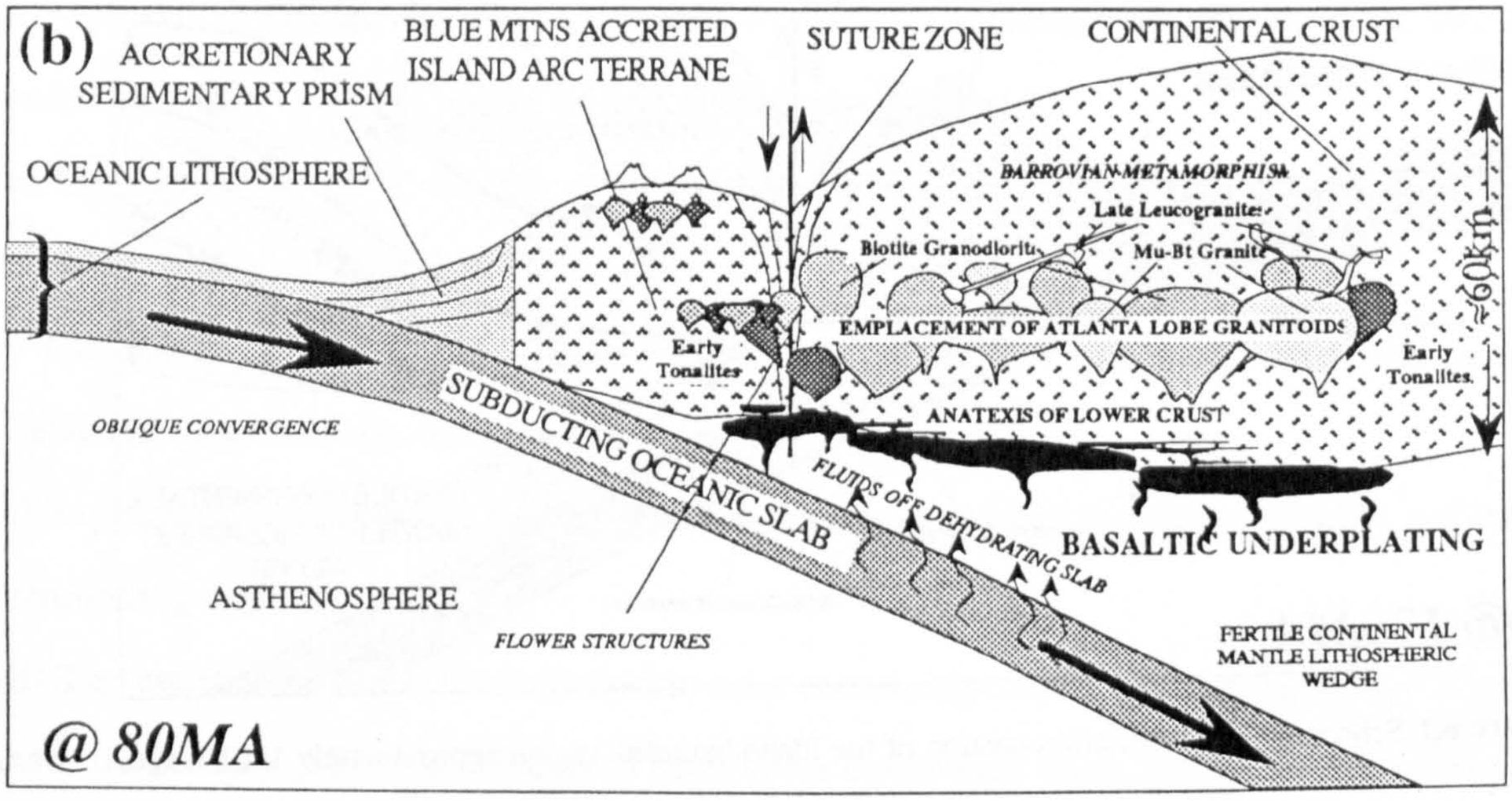

Figure 6.2 Schematic east-west cross-section of the Idaho batholith region approximately 80Ma ago.

The increased thicknesses of crust rich in heat producing elements was thought to have caused the mid-crustal Barrovian metamorphism of the northern Bitteroot lobe and in extreme cases production of the migmatites, some of which separated to produce the leucogranite stocks (figure 6.2). Patiño Douce et al. (1990) argued that lower crust levels will reach their maximum temperatures earlier than shallower levels, which is consistent with the leucogranites being the youngest Cretaceous phase and being derived from melting mid- to upper crustal metasediments.

The tectonically and magmatically thickened crust under went rapid syn- to post-plutonic isostatic uplift at rates of 4mm/yr from 84Ma-81Ma and 2mm/yr from 81-78Ma (Lund and Snee, 1984; Snee et al., 1989) suggesting that the latter granitoids, and specifically the leucogranites, may have been emplaced at shallower crustal levels (figure 6.3).

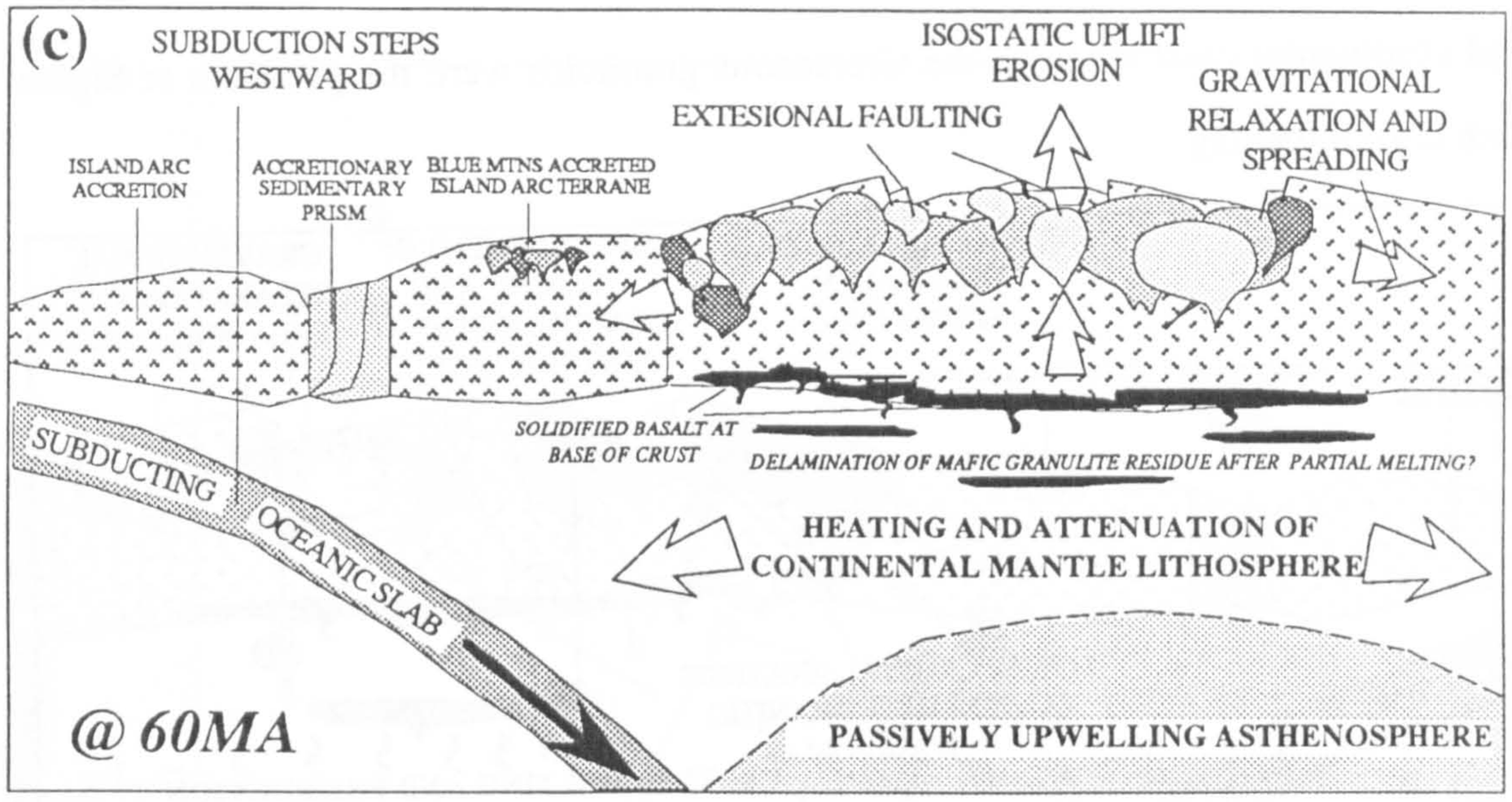

Figure 6.3 Schematic east-west cross-section of the Idaho batholith region approximately 60Ma ago.

Continued uplift and erosion throughout the Upper Cretaceous and Eocene (Vallier and Brooks, 1987) combined with thermal and gravitational relaxation led to post orogenic thinning and intra-continental extension (Gaudemer et al., 1988) as shown in figure 6.3. The extensional tectonic regime is accentuated by a step in subduction to the west (Duncan, 1982) which resulted in the Atlanta lobe region being in more of a back-arc setting.

Passive upwelling of asthenospheric mantle below the region of lithospheric thinning caused melting of the continental mantle lithosphere to produce the parental magmas of the Tertiary dioritic suite (figure 6.4). The Tertiary dioritic magmas assimilated large amounts of continental crustal material during emplacement at epizonal levels with the rapid passage to high levels in the crust facilitated by the extensional tectonic regime. However, it is postulated that some mantle-derived magmas ponded at the base of the crust which increased the already high temperature, due to lithosphere thinning, sufficiently to cause crustal anatexis of the lower crust and production of the Tertiary granitic magmas (figure 6.4). Both the granitic and dioritic magmas were emplaced into extensional fault controlled structures and were associated with dyke swarms which reached the surface to produce the Tertiary andesitic to rhyolitic Challis volcanics. The Tertiary anatectic granitoids differ significantly from the Cretaceous granitoids because they were generated at the base of a

thinned continental crust whereas the Cretaceous granitoids were the products of higher pressure crustal melting.

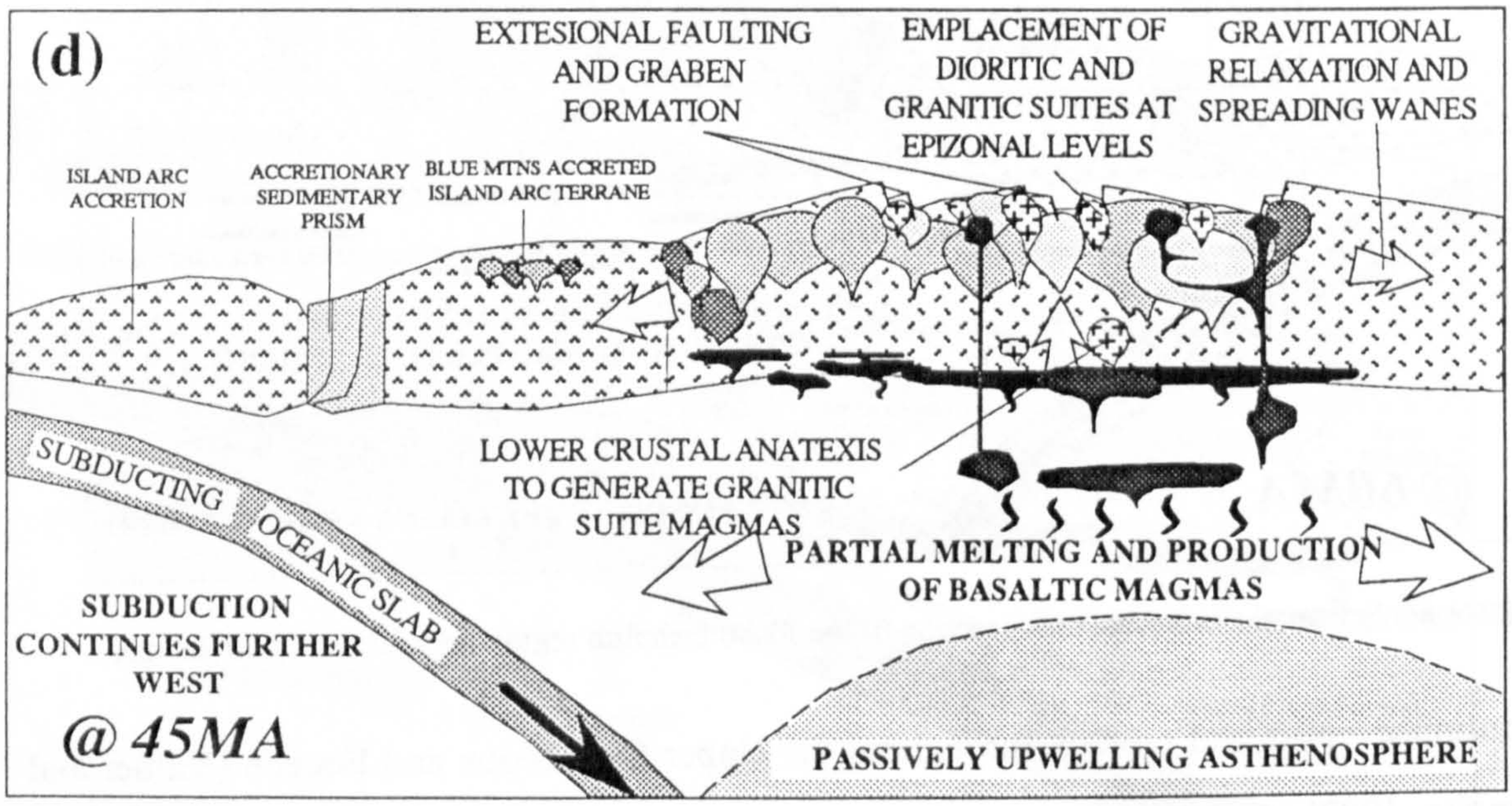

Figure 6.4 Schematic east-west cross-section of the Idaho batholith region approximately 45Ma ago.

An important corollary to this is the near spatial coincidence of the focus of Cretaceous to Tertiary granitoid magmatism, which suggests that the region of maximum crustal thickening in the Cretaceous, marked by generation of the main phases of the Atlanta lobe, underwent the maximum amounts crustal thinning, marked by the extensional fault horst and graben system (Bennett, 1986 and figure 3.5), and in turn was coincident with the region of thinnest lithosphere, marked by the Tertiary anatectic granitoids. This suggests that rifting was symmetrical and that it may have been in part triggered by the previous tectonic thickening of the region.

6.6 Comparison of the Atlanta lobe granitoids with the Andean and Mesozoic North American granitoids: implications for the growth of the continental crust.

A brief comparison of the characteristics of the lower crustal anatectic granitoids of the Atlanta lobe of the Idaho batholith with the upper crustal melt granitoids of the central Andes and the Mesozoic Peninsular Ranges mantle derived granitoids is made and their relevance to continental growth assessed.

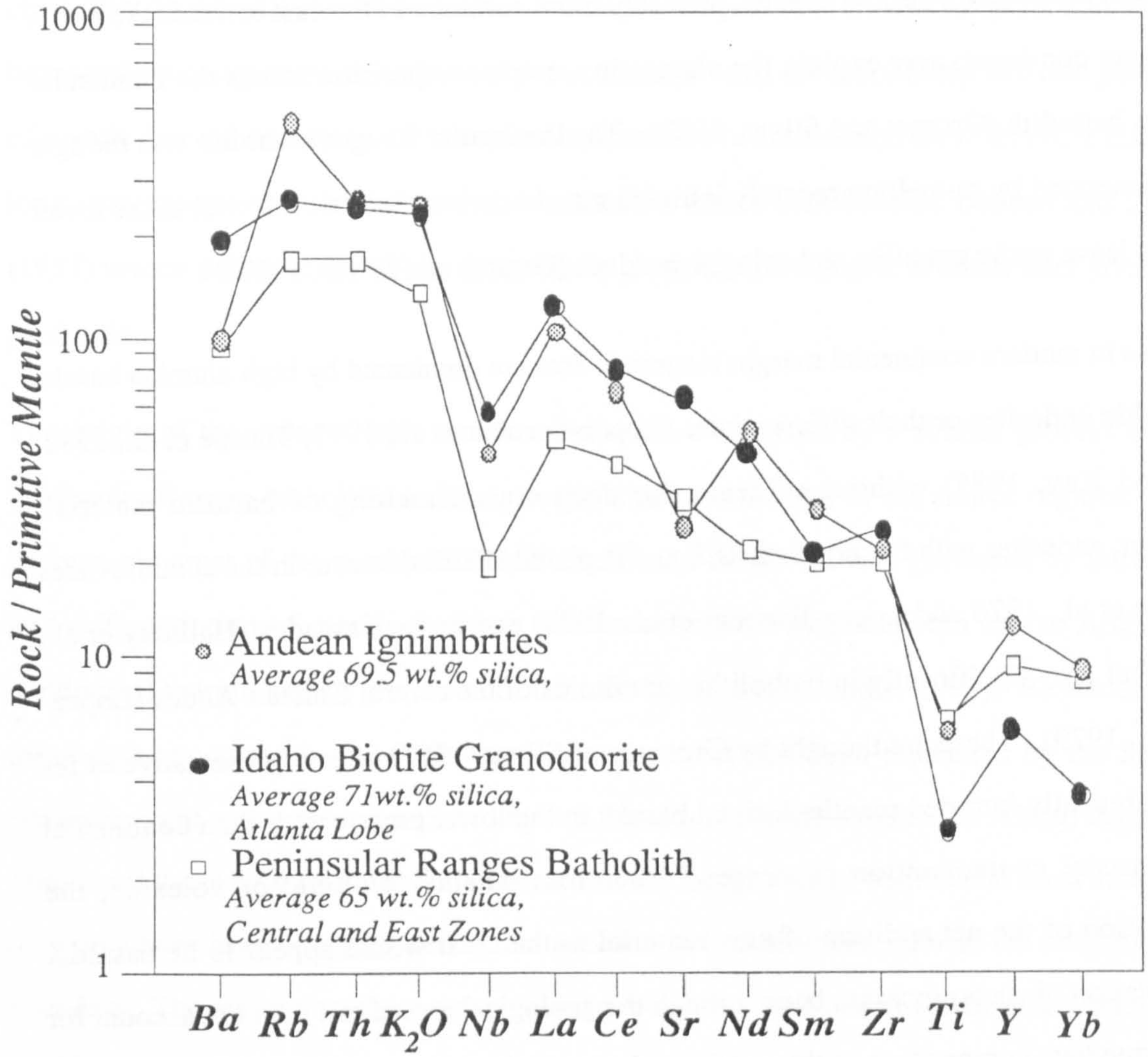

Figure 6.5 Primordial mantle normalised trace element variation diagram comparing the average composition of the biotite granodiorites from the Atlanta lobe of the Idaho batholith with the Andean upper crustal continental margin ignimbrites (De Silva, 1987) and the lower crustal melt Peninsular Ranges Batholith (Gromet and Silver, 1987).

The central Andes upper crustal melt granitoids (DeSilva, 1988, and Rogers, 1985) can be distinguished by their high Rb/Ba ratios, low Sr, and relatively undepleted Y and HREE abundances (figure 6.5). The Peninsular Ranges batholith (figure 6.5) has depleted Y, low Sr, low Rb/Ba and moderate LREE/HREE ratios (Gromet and Silver, 1987; Silver and Chappell, 1988). The latter better resemble the Atlanta lobe biotite granodiorites than the upper crustal Andean granitoids, but can be distinguished by their lower LREE/HREE (i.e. higher Sm/Nd ratios) and low Sr (figure 6.5). Moreover, the isotope signatures of the Peninsular Ranges granitoids suggest that the source regions are dominated by recently intruded, continental margin, subduction-related, mantle-derived basalts, although old

subcreted metasediments and basalts, probably more common in the east towards the North American continent, may explain the change in isotope composition across the Peninsular Ranges batholith (Gromet and Silver, 1987). The Peninsular Ranges batholith was thought to be generated by re-melting recently intruded mantle-derived basaltic material in the lower crust to leave mafic granulite and eclogite residues (Gromet and Silver, 1987).

Magmas in modern continental margin magmatic arcs are dominated by high alumina basalts to basaltic andesites or their differentiates (Lopez-Escobar et al., 1977; Thorpe et al., 1982; Kay and Kay, 1985) without evidence for deep crustal melting of basaltic material. However, andesites with fractionated REE and depleted HREE do occur in the central Andes (Thorpe et al., 1976 and Lopez-Escobar et al., 1977) and in the Cascades (Halliday et al., 1983), but also significantly in batholithic granitoids of the central Chilean Andes (Lopez-Escobar, 1979). These are thought by Gromet and Silver (1987) to be representative of re-melting recently intruded mantle-derived basalts in the lower crust, rather than continental lower crustal contamination processes. Therefore whether plutonic or volcanic, the composition of the net addition of new material to the crust would appear to be basaltic. Extrapolation of such processes back through the geological record can then not account for the intermediate composition of the continental crust and an alternative explanation must be sought.

Gromet and Silver (1987) suggest that the Peninsular Ranges batholith could be representative of an important continental margin differentiation process whereby recently intruded subduction related mantle derived magmas are re-melted in the lower crust and contribute a sialic fraction to the continental crust. These are represented by, for instance, the dominant Mesozoic to Recent batholithic components of the central Andes (Thorpe, 1981) and thus represent significant growth of the continental crust (Weaver and Tarney, 1982).

The circum-Pacicific cordilleran batholiths from mature continental margin magmatic arcs have a dominance of tonalitic to granodioritic magmas compared with the less mature oceanic arcs, which was thought by Pitcher (1978) and Roddick (1983) to indicate that pre-existing continental margins represent a more favourable tectonic environment for generation of new

crust than do oceanic island arcs. Gromet and Silver's (1987) model suggests that this is because density contrasts at the base of the continental crust are more likely to cause ponding of mantle derived basalts at the crust/mantle interface in continental arcs. In order that the long term contribution to the crust is intermediate rather than basaltic Gromet and Silver (1987) invoke delamination of the dense mafic granulite and eclogite residues after granitoid production.

The origin of the Atlanta lobe was thought to have occurred by a similar process to the Peninsular Ranges batholith, and only really differs in the age of the source regions. The Proterozoic crust of the north western United States cordillera was generated by intrusion and differentiation of mantle-derived, subduction-related magmas both on the Archaean continental margin and by accretion of oceanic island arcs (Condie, 1987). Re-melting of these rocks occurred in the Cretaceous after the crust had been thickened by the Sevier orogenic event and then under-plated by hot, basaltic, juvenile subduction related magmas. Thus the Atlanta lobe magmas do not represent any net growth of continental crust although they may have been accompanied by the addition of basaltic material near the crust/mantle boundary. The reason that there was a delay in re-melting the Proterozoic basaltic material in the Idaho batholith region as opposed to immediate re-melting proposed for the Peninsular Ranges and the Andes may have been the result of the coincidence of thickened crust and an advective heat source existing in the latter regions, whereas coincidence of tectonically thickened crust and a sub-crustal heat source only occurred in the late Cretaceous in the Idaho batholith region. Processes similar to these appear to have occurred in the eastern or continental side of the Peninsular Ranges batholith.

In summary lower and upper crustal anatectic granitoid melts can be distinguished by differences in HREE depletion and Rb/Ba ratios, whereas granitoids derived from old and juvenile lower crustal sources are best recognised isotopically. Although significant continental growth may occur by intrusion of mantle-derived batholithic material along destructive boundaries at continental margins, large subduction-related continental margin batholiths such as the Atlanta lobe may represent no net addition of material to the crust.

However, batholiths such as these represent sites of major lower to upper crustal recycling and differentiation.

6.7 Concluding remarks and future work

The preceding sections have outlined the major conclusions drawn from this study of the geochemistry of the Cretaceous and Tertiary granitoids of the Atlanta lobe of the Idaho batholith. These are important in the context of constraining the geotectonic evolution of the continental crust of the western United States cordillera and particularly the generation of the 'Inner Cordilleran' granitoids. In addition constraints have been placed on the nature of the lower crust, granitoid magmagenesis and crustal recycling processes at continental destructive plate margins which may have global significance for continental crustal evolution. The following key points should be emphasised:

i) There is little direct, detectable evidence for crustal growth during the generation of the Cretaceous granitoids and only minor amounts of mantle-derived material have been inferred in the Tertiary dioritic suite. This may be because evolved magmas from an enriched sub-continental mantle lithosphere are difficult to distinguish from intermediate lower crustal melts. The preferred explanation, however, is that the high temperatures required for lower crustal anatexis are attained by tectonic crustal thickening which both insulates the lower crust and promotes ponding of mantle-derived basaltic magmas at the base of the crust increasing the heat flow and leading to anatexis. It is postulated that the crust may grow by the addtion of dominatly basaltic material from the underlying, sub-continental mantle lithosphere, but the bulk crust retains an intermediate to granodioritic composition by remobilisation of the basaltic material with the less dense silicic magmas retained in the crust and the mafic granulitic to eclogitic residues returned to the mantle, perhaps by some form of delamination.

ii) Combined major and trace element partial melting models demonstrate that the Cretaceous granitoids were generated at the base of a tectonically thickened crust leaving a garnet-bearing mafic granulite residue.

iii) The inferred composition of the source regions was intermediate to basic (tonalitic to gabbroic), biotite and hornblende-bearing rocks of meta-igneous origin. The source regions were trace element enriched with an inherited volcanic arc signature (high LILE/HFSE ratios), presumably attained during generation of the source regions at an ancient subduction zone.

iv) Melting models indicate that Sm/Nd was significantly reduced from source to magma during lower crustal partial melting, indicating that intra-crustal recycling may be responsible for generation of upper crust with low Sm/Nd ratios. Correcting for Sm/Nd fractionation the depleted mantle model Nd ages are similar to the Pb-Pb ages of approximately 1.5Ga.

v) The inferred source trace element abundances suggest that little intra-crustal recycling occurred in the source regions during their time of crustal residence since, the Proterozoic. The high Sr and Pb isotope ratios of the granitoids, however, suggest that the exception to this may have been minor depletions of the most incompatible trace elements during granulite metamorphism postulated to have occurred prior to the Cretaceous magmatic event.

v) The Proterozoic aged source region indicates that major age province boundaries within the western United States cordillera are located along the southern margin of the Atlanta lobe with the Snake River Plain Archaean province and to the east of the Idaho batholith with the Wyoming Archaean province.

vi) The Tertiary granitoids are generated from crustal sources of similar age and composition as those of the Cretaceous granitoids, except that melting occurred at lower pressures due to late Cretaceous to early Tertiary crustal attenuation and with an absence of residual garnet. Uplift and thermal and gravitational relaxation of the thickened crust led to attenuation of the crust and mantle lithosphere and increased heat flow due to passively upwelling asthenosphere. Magmas derived by melting in the upper mantle were the parental magmas of the dioritic suite generated by AFC processes, whereas advective heating of the lower crust caused crustal anatexis and production of the granitic suite. The temporal change from production of anatectic granitoids associated with crustal thickening and ponding of mantle derived magmas at the base of the crust, to crustal thinning and emplacement of epizonal

granitoids with increasing mantle components and associated volcanics may be a feature that could be recognised in ancient orogenic belts.

Clearly there is considerable scope for future work on the nature of the lower crust from granitoid and xenolith studies. Within this region of the western United States cordillera several lines of investigation standout as priorities for future studies:

i) The identification of a similar lower crustal component from any of the numerous small Mesozoic 'Inner Cordilleran' granitoid batholiths by combined isotope and trace element studies.

ii) More extensive work on the Tertiary granitoids, but particularly the Tertiary dioritic suite, the mafic dyke swarms and the genetically related andesites of the Challis volcanics is needed in order to constrain better the nature of the sub-continental mantle lithosphere in this region so that mantle and crustal-derived magmas may be better distinguished. Related to this would be detailed trace element and isotope studies of the Cretaceous syn-plutonic mafic dykes of the Bitteroot lobe which were suggested by Hyndman and Foster (1988) to be the manifestation of the subcrustally derived basaltic magmas acting as an advective heat source for crustal anatexis and generation of the Bitteroot lobe granitoids. By constraining the petrogenesis of these dykes, both the nature of the sub-continental mantle lithosphere and whether they represent a significant and plausible heat source, may be ascertained.

iii) The crustal age province boundaries within this region of the western United States cordillera could be more accurately constrained by detailed trace element and isotope studies of granitoids. The northern margin of the Archaean Province could be better located by detailed work on the southern margin of the Atlanta lobe. The boundary with the Wyoming Archaean province could be better located by trace element and isotope analyses of the Boulder batholith to the east of the Idaho batholith (figure 1.3). Further evidence of this boundary may be gleaned from work on the more easterly Challis volcanics and on rocks from the Absaroka volcanic field. Work on crustally derived granitoids such as the Atlanta lobe granitoids and mantle-derived volcanics from the same region may suggest whether the crust and sub-continental mantle lithosphere evolved as a coupled system or whether mantle enrichment processes and crustal growth events are temporally and spatially separated.

REFERENCES

Aitken, J.D. and McMechan, M.E. (1989) Chapter 5, Middle Proteozoic assemblages. *in, Gabrielse, H., and Yorath, eds., The Cordilleran orogen, Canada, Geological Survey of Canada, Geology of Canada.* **no.4**

Allegre, C.J. and Minster, J.F. (1973) Quantative models of trace element behaviour in magmatic processes. *Earth Planet. Sci. Lett.* **v. 38** p. 1-25

Allegre, C.J., Treuil, M., Minster, J. F., Minster, B. and Albarede, F. (1977) Systematic use of trace elements in igneous processes: Part1 Fractional crystallization processes in volcanic suites. *Contrib. Mineral. Petrol.* **v. 60** p. 57-75

Allegre, C.J. and Othman, D.B. (1980) Nd-Sr isotopic relationship in granitoid rocks and continental crust development: a chemical approach to orogenesis. *Nature* **v. 286** p. 335-341

Allman and Lawrence (1972) Geological laboratory methods. *Longman.*

Anderson, A. L. (1982) Multiple emplacement of the Idaho batholith. *Jour. Geol.* **v. 60 no. 3** p. 255-265

Armstrong, R. L. (1975a) Precambrian (1500 m.y. old) rocks of central Idaho-the Salmon River Arch and its role in Cordilleran sedimentation and tectonics. *American Journal of Science* **v. 275-A** p. 437-467

Armstrong, R. L. (1975b) Geochronometry of Idaho. *Isochron West* **no. 14** 50 p.

Armstrong, R.L (1977) Cenozoic igneous history of the U.S. cordillera from lat 42° to 49°N. *Geol. Soc. Am. Mem.* **v.152** p. 265-282

Armstrong, R. L. (1982) Cordilleran metamorphic core complexes-from Arizona to southern Canada. *Ann. Rev. Earth Planet. Sci.* **v. 10** p. 129-154

Armstrong, R. L. (1988) Mesozoic and early Cenozoic magmatic evolution of the Canadian cordillera. *in, Clark, S.P., Burchfiel, B.C., and Suppe, J., eds., Processes in continental lithosphere deformation, Geol. Soc. Am. Special Paper* **218** p. 55-92

Armstrong, R.L. and Oriel, S.S. (1965) Tectonic developement of Idaho-Wyoming thrust belt. *A.A.P.G.* **v.49** p. 1847-1856

Armstrong, R.L. and Hills, F. A. (1967) Rb-Sr and K-Ar geochronologic studies of mantled gneiss domes, Albion Range, southern Idaho, U.S.A. *Earth Planet. Sci. Lett.* **v. 3** p.114-124

Armstrong, R.L., Leeman, W.P., and Malde, H.E. (1975) K-Ar dating, Quaternary and Neogene volcanic rocks of the Snake River Plain Idaho. *American Journal of Science.* **v. 275** p. 225-251

Armstrong, R. L., Taubeneck, W. H. and Hales, P.O. (1977) Rb-Sr and K-Ar geochronology of Mesozoic granitic rocks and their Sr isotopic composition, Oregon, Washington, and Idaho. *Geol. Soc. Am. Bull.* **v. 88** p. 397-411

Asmerom, Y., Ikramuddin, M., and Kinart, K. (1988) Geochemistry of late Cretaceous granitoids from northeastern Washington: implications for genesis of two-mica cordilleran granites. *Geology* **v. 16** p. 431-435

Avé Lallemant, H.G., Phelps, D.W., and Sutter, J.F. (1980) 40Ar/39Ar ages of some pre-Tertiary plutonic and metamorphic rocks of eastern Oregon and their geologic relationships. *Geology* **v. 8** p. 371-374

Avé Lallemant, H.G. (1989) Pre-Cretaceous tectonic evolution of thr Blue Mountains province, northeast Oregon. *U.S. Geol. Surv. Prof. Paper.* **1438**

Barton, M. D. (1990) Cretaceous magmatism, metamorphism and metallogeny in the east-central Great Basin. *in, Anderson, J. L. ed., The Nature and Origin of Cordilleran Magmatism, Gel. Soc. Am. Mem.* **v. 174**

Bennett, E. H. (1980) Granitic rocks of the Idaho batholith and their relation to mineralisation. *Econ. Geol.* **v.75** p. 278-288

Bennett, E. H. and Knowles, C.R. (1985) Tertiary plutons and related rocks in central Idaho. *in, McIntyre, D.H., ed., Symposium on the geology and mineral deposits of the Challis 1° x 2° quadrangle, Idaho: U.S. Geol. Survey Bull.* **1658** p.81-95

Bennett, E.H. (1986) Relationship of the trans-Challis fault system in central Idaho to Eocene and Basin and Range extensions. *Geology* **v. 14** p. 481-484

Bennett, V.C. and DePaulo, D.J. (1987) Proterozoic crustal history of the western United States as determined by neodymium isotopic mapping *Geol. Soc. Am. Bull.* **v. 99** p. 674-685

Bernard-Griffiths, J. and Jahn, B. M. (1981) REE geochemistry of eclogites and associated rocks from Sauviat-sur Vige, Massif Central, France. *Lithos* **v. 14** p. 263

Best, M.G., Armstrong, R.L., Graustein, W.C., Embree, G.F. and Ahlborn, R.C. (1974) Mica granites of the Kern Mountains pluton, eastern White Pine County , Nevada : remobilised basement of the cordilleran miogeosyncline. *Geol. Soc. Am. Bull.* **v. 185** p. 1277-1286

Bickford, M.E. (1988) The formation of continental crust: Part1. A review of some principles; Part 2. An application to the Proterozoic evolution of southern North America. *Geol. Soc. Am. Bull.* **v. 100** p. 1375-1391

Bickford, M.E., Chase, R.E., Nelson, B.K., Shuster, R.D., and Arruda, E.C. (1981) U-Pb studies of Zircon cores and overgrowths, and monazite: implications for age and petrogenesis of the northeastern Idaho batholith. *Jour. Geol.* **v. 89** p. 433-457

Bird, P., (1984) Laramide crustal thickening even in the Rocky Mountain foreland and great Plains. *Tectonics* **v. 3** p. 741-758

Bittner, E. (1987) Migmatite zones in the Bitteroot lobe of the Idaho batholith. *U.S. Geol. Sur. Prof. Paper.* **1436** p. 73-93

Bonnichensen, B. (1987) Pre-Cenozoic geology of the West Mountain-Council Mountain-New Meadows area, west-central Idaho *U.S. Geol. Sur. Prof. Paper.* **1436** p. 151-169

Bowden, A., Batchelor, R. A., Chappell, B. W., Didier, J. and Lameyre, J. (1984) Petrological and geochemical source criteria for the classification of granitic rocks : a discussion. *Physics of the Earth and Planetary Interiors.* **v. 35** p. 1-11

Brown, G.C. and Fyfe, W. S. (1970) Production of granitic melts during ultrametamorphism *Contrib. Mineral. Petrol.* **v. 28** p. 310-318

Brown, C. G., Thorpe, R. S., and Webb, P. C. (1984) The geochemical characteristics of granitoids in contrasting arcs and comments on magma sources. *J. Geol. Soc. London*. **v. 141** p. 413-426

Brown, G.C. (1987) The changing pattern of batholith emplacement during Earth history. *in Atherton, M.P. and Tarney, J., eds, The origin of granite batholiths geochemical evidence*. p. 106-115

Burchfield, B.C. and Davis, G.A. (1975) Nature and controls of Cordilleran orogenesis, western United States - extensions of an earlier synthesis. *American Journal of Science* **v. 275A** p. 363-396

Burnham, C. W. (1979a) Magmas and hydrothermal fluids. *in, Barnes, H. L., ed., Geochemistry of hydrothermal ore deposits; New York: Hott, Rhinehart and Winston*. **2nd edition** p. 34-67

Burnham, C. W. (1979b) The importance of volatile constituents. *in, Yoder, H. S., ed., The evolution of the Igneous rocks; Fiftieth anniversary perspectives, Princeton, N. J.* p. 34-67

Catanzaro, E. J., Murphy, T. J., Shields, W. R. and Garner, E. L. (1968) Absolute isotope abundance ratios of common, equal atom, and radiogenic lead isotopic standards *Jour. Res. Nat. Bur. Stand. (US)* **v. 72A** p. 261-267

Carlson, R.W. and Hart, W.K. (1987) Crustal genesis on the Oregon Plateau. *Jour. Geophysical. Res.* **v. 92** p. 6121-6206

Chadwick, R.A. (1985) Overview of Cenozoic volcanism in the west-central United States. *in, Flores, R.M. and Kaplan, S.S., eds., Rocky mountain section-S.E.P.M., Cenozoic paleogeography of west-central United States* p. 359-382

Chappell, B. W. and White, A. J. R. (1974) Two contrasting granite types. *Pacific Geology*. **v. 8** p. 173-178

Chappell, B. W., White, A. J. R., and Wyborn,D. (1987) The importance of residual source material (restite) in granite petrogenesis. *J. Pet.* **v. 28** p. 1111-1138

Chappell, B.W. and Stephens,W.E. (1988) Origin of infracrustal (I-type)granite magmas. *Trans. R. Soc. Edinburgh. Earth Science*. **v. 79** p. 71-86

Chase, R.B., Bickford, M.E., and Tripp, S.E. (1978) Rb-Sr and U-Pb isotopic studies of the northeastern Idaho batholith and border zone. *Geol. Soc. Am. Bull.* **v. 89** p. 1325-1334

Chase, R.B., Bickford, M.E., and Arruda, E.C. (1983) Tectonic implications of Tertiary intrusion and shearing within the Bitteroot dome, northeastern Idaho batholith. *Jour. Geol.* **v. 91** p. 462-470

Chayes, F. (1952) Staining of potash feldspars with sodium cobaltinitrite. *American Mineralogist*.. **v.37** p. 337-340

Chen, J.H. and Moore, J.D. (1982) Uranium-lead isotopic ages from the Sierra Nevada batholith, California *Jour. Geophysical. Res.* **v. 87** p. 4761-4784

Christiansen, R.L. and Lipman, P.W. (1972) Cenozoic volcanism and plate-tectonic evolution of the western United States. II Late Cenozoic. *Phil. Trans. R. Soc. Lond A*. **v. 271** p.249-284

Christiansen, R.L. and McKee, E.H. (1977) Late Cenozoic volcanic and tectonic evolution of the Great Basin and Columbia Intermontane regions. *Geol. Soc. Am. Mem.* **v. 152** p. 283-311

Clemens, J.D., Holloway, J.R., and White, A.J.R. (1986) Origin of an A-type granite: Experimental constraints *American Mineralogist* **v. 71** p. 317-324

Clemens, J.D. and Vielzeuf, D. (1987) Constraints on melting and magma production in the crust. *Earth Planet. Sci. Lett.* **v. 86** p. 287-306

Clemens, J.D. and Wall, V.J.. (1981) Origin and crystallization of some peraluminous (S-type) granitic magmas *Canadian Mineralogist.* **v. 19** p. 111-131

Clemens, J.D. and Wall, V.J.. (1988) Controls on the mineralogy of S-type volcanic and plutonic rocks. *Lithos*. **v. 21** p. 53-66

Cocherie, A: (1986) Systematic use of trace element distribution patterns in log-log diagrams for plutonic suites. *Geochim. Cosmochim. Acta* **v. 50** p. 2517-2522

Collins, W. J., Beams, S. D., White, A. J. R., and Chappell,B. W. (1982) Nature and origin of A-type granite with particular reference to southeastern Australia. *Contrib. Mineral. Petrol.* **v. 80** p. 189-200

Condie, K.C. (1982) Plate-tectonics model for Proterozoic continental accretion in the southwestern United States. *Geology* **v. 10** p. 37-42

Criss, R. E. (1981) An $^{18}O/^{16}O$ D/H and K/Ar study of the southern half of the Idaho batholith. *California Institute of Technology, Pasaadena.* **Ph.D. dissertation** 401p.

Criss, R.E., Champion, D.E., and McIntyre, D.H. (1985) Oxygen isotope, aeromagmatic, and gravity anomalies associated with hydrothermally alterred zones in the Yanke Fork mining district, Custer County, Idaho. *Econ. Geol.* **v. 80** p. 1277-1296

Criss, R.E., and Fleck, R.J. (1987) Petrogenesis, geochronology, and hydrothermal sysyems of the northern Idaho batholith and adjacent areas based on $^{18}O/^{16}O$, D/H, $^{87}Sr/^{86}Sr$, K-Ar, and ^{40}Ar-^{39}Ar studies, in Vallier, T.L., and Brooks, H.C., eds. *U.S. Geol. Surv. Prof. Paper.* **1436** p. 95-137

Criss, R. E.,and Lanphere, M. A., and Taylor,H. P., Jr. (1982) Effects of regional uplift, deformation, and meteoric-hydrothermal metamorphism on K-Ar ages of biotites in the southern half of the Idaho batholith. *Jour. Geophysical. Res.* **v. 87, no. B8.** p. 7029-7046

Criss, R. E., and Taylor, H. P. Jrn. (1983) An $^{18}O/^{16}O$ and D/H study of Tertiary hydrothermal systems in the southern half of the Idaho batholith. *Geol. Soc. Am. Bull.* **v. 94** p. 640-663

Daniel, F. and Berg, R.B., (1981) Radiometric dates of rocks in Montana *Mont. Bur. Mines Geology Bull.* **v. 114** 136 p.

Davies, G., Gledhill, A. and Hawkesworth, C. (1985) Upper crustal recycling in southern Britain: evidence from Nd and Sr isotopes. *Earth Planet. Sci. Lett.* **v. 75** p. 1-12

Davis, G.A., Monger, J.W.H., and Burchfiel, B.C. (1988) Mesozoic construction of the cordilleran "collage" central British Columbia to central California.

Deer, W.A., Howie, R.A. and Zussman, J. (1986) An introduction to the rock forming minerals *Longman Group Limited.*

Deniel, C., Vidal,P., Fernandez, A., LeFort, P., and Peucat, J.-J. (1987) Isotopic study of the Mansalu granite (Himalaya, Nepal): inferences on the age and source of Himalyan leucogranites. *Contrib. Mineral. Petrol.* **v. 96** p. 78-92

DePaolo, D.J. (1981a) Trace element and isotopic effects of combined wallrock assimilation and fractional crystallization. *Earth Planet. Sci. Lett.* **v. 53** p.189-202

DePaolo, D.J. (1981b) A Neodymium and Strontium Isotopic Study of the Mesozoic Calc-Alkaline Granitic Batholiths of the Sierra Nevada, and Peninsular Ranges, California. *Jour. Geophysical. Res.* **v. 86, no. B11** p.10470-10488

DePaolo, D.J. (1981c) Nd Isotopic Studies: some new perspectives on Earth structure and evolution. *Eos.* **v.62, no. 14** p.137-140

DePaolo, D.J. (1988) Age dependence of the composition of continental crust: evidence from Nd isotopic variations in granitic rocks *Earth Planet. Sci. Lett.* **v. 90** p. 263-271

DePaolo, D.J. and Farmer, G. L. (1984) Isotopic data bearing on the origin of Mesozoic and Tertiary granitic rocks in the western United States *Phil. Trans. R. Soc. Lond A.* **v. 310** p. 745-753

DeSilva, S. L. (1987) Large volume explosive silicic volcanism in the Central Andes of Northern Chile. *Unpub. PhD. Thesis, Open University, Milton Keynes, England.*

Dickinson, W.R. (1977) Palaeozoic plate tectonics and the evolution of the cordilleracontinental margin. *in, Stewart, J.H., Stevens, C.H., and Fitsch, A.E., eds., Palaeozoic palaeogeography of the western United States, Pacific Section, Society of Economic and Paleontologists and Mineralogists, Pacific coast Palaeogeography symposium 1.* p. 137-155

Doe, B.R. and Zartman, R. E. (1979) Chapter 2. Plumbotectonics I, the Phanerozoic. *in, Barnes, H. L., ed. Geochemistry of hydrothermal ore deposits. 2nd ed., Willey-Interscience, New York.* p.22-77

Doe, B.R. and Delevaux, M.H. (1985) Lead isotope characteristics of ore systems in central Idaho *in, McIntyre, D.H., ed., Symposium on the geology and mineral deposits of the Challis 1° x 2° quadrangle, Idaho: U.S. Geol. Survey Bull.* **1658** p. 181

Doe, B.R., Leeman, W.P., Christiansen, R.L., and Hedge, C.E. (1982) Lead and strontium isotopes and related trace elements as genetic tracers in the Upper Cenozoic rhyolite-basalt association of the Yellowstone plateau volcanic field. *Jour. Geophysical. Res.* **v. 87, no. B6** p. 4785-4806

Downes, H. and Duthou, J.-L. (1988) Isotopic and trace element arguments for the lower-crustal origin of Hercynian granitoids and pre-Hercynian orthogneisses, Massif Central (France). *Chem. Geol.* **v. 68** p. 291-308

Ekren, E.B. (1985) Eocene cauldron-related volcanic events in the Challis Quadrangle. *in, McIntyre, D.H., ed., Symposium on the geology and mineral deposits of the Challis 1° x 2° quadrangle, Idaho: U.S. Geol. Survey Bull.* **1658** p.43-58

Ellam, R.M. and Hawkesworth, C.J. (1988) Is average continental crust generated at subduction zones? *Geology* **v. 16** p. 314-317

Ellis, D. J. and Thompson, A. B. (1986) Subsolidus partial melting melting reactions in the quartz excess $CaO+MgO+Al_2O_3+SiO_2+H_2O$ system under water excess and water

deficient conditions at 10kb. Some implications for the origin of peraluminous melts from mafic roccks. *J. Pet.* **v. 27, part 1** p. 91-121

Engebretson, D.C., Cox A., and Thompson, G.A. (1984) Correlation of plate motions with continental tectonics: Laramide to Basin-Range. *Tectonics* **v. 3** p. 115-119

Engebretson, D.C., Cox A., and Gordon, R.G. (1985) Relative motions between oceanic and continental plates in the Pacific basin. *Geol. Soc Am. Special paper* **v. 206** 59 p.

England, P. C. and Thompson, A. B. (1984) P-T-t paths of regional metamorphism. 1 Heat transfer during the evolution of thickened continental crust *J. Pet.* **v. 25** p. 929-955

England, P. C. and Thompson, A. B. (1986) Some thermal and tectonic models for crustal melting in continental collision zones. *in, Coward, M. P. and Ries, A. C., eds., Collision tectonics, Geol. Soc. Special Pub.* **No. 19** p. 83-94

Ernst, W.G. (1988) Metamorphic terranes, isotopic provinces, and implications for crustal growth of the western United States. *Jour. Geophysical. Res.* **v. 93, no. B7** p. 7634-7642

Evans, K.V. and Fischer, L.B. (1986) U-Pb geochronology of two augen gneiss terranes, Idaho -New data and tectonic implications. *Can. J. Earth Science.* **v. 23** p. 1919-1927

Evans, K.V. and Zartman, R.E. (1988) Early Paleozoic alkalic plutonism in east-central Idaho *Geol. Soc. Am. Bull.* **v. 100** p.1981-1987

Farmer, G.L. and DePaulo, D.J. (1983) Origin of Mesozoic and Tertiary granite in the western United States and implications for pre-Mesozoic crustal structure: 1. Nd and Sr isotopic studies in the geocline of the northern Great Basin. *Jour. Geophysical. Res.* **v. 88 no. B4** p.3379-3401

Farmer, G.L. and DePaulo, D.J. (1987) Nd and Sr Isotope Study of Hydrothermally Altered Granite at San Manuel, Arizona: Implications for Element Migration Paths during the Formation of Porphyry Copper Ore Deposits. *Econ. Geol.* **v. 82** p. 1142-1151

Faure, G. (1977) Principles of Isotope geology, J. Wliey and Sons, Chichester , England.

Fenn, P.M. (1977) The nucleation and growth of alkali feldspars from hydrous melts. *Can. Mineral.* **v. 15** p.135-161

Fischer, F.S., Mc Intyre, D.H. and Johnson, K.M. (in Press) Geologic map of the Challis 1° x 2° quadrangle,Idaho. *U.S. Geol. Sur. Open File Report* **83-253** 41p.

Fischer, F.S., Mc Intyre, D.H. and Johnson, K.M. (in Press) Geologic map of the Challis 1° x 2° quadrangle,Idaho. *Geol. Soc. Am. Bull.* **I-1819**

Fleck, R. J., and Criss, R. E. (1985) Strontium and Oxygen isotopic variations in Mesozoic and Tertiary plutons of central Idaho. *Contrib. Mineral. Petrol.* **v. 90** p. 291-308

Fleck, R.J. (1987) Nd, Sr and Trace element evidence of large-scale crustal contamination of magmas of the Idaho batholith. *In Press.*

Flynn, R. T. and Burnham, C. W. (1978) An experimental determination of rare earth element co-efficients between a chloride containing vapour phase and silicate melts. *Geochim. Cosmochim. Acta* **v. 42** p. 685-701

Foster, D. A. and Hyndman, D. W. (1990) Large-Scale Crustal Anatexis: The Importance of subcrustal Magma Intrusion. *EOS* **Feb.** p. 299-300

Frost, C. D. and Winston, D. (1987) Nd isotope systematics of coarse- and fine-grained sediments: examples from the middle Proterozoic Belt Purcell Supergroup. *Jour. Geol.* **v. 95** 309-327

Frost, T.P. and Mahood, G.A. (1987) Field, chemical, and physical constraints on mafic-felsic magma interaction in the Lamarck Granodiorite, Sierra Nevada, California. *Geol. Soc. Am. Bull.* **v. 99** p. 272-291

Gans, P.B. (1987) An open system, two-layer crustal stretching model for the eastern Great Basin. *Tectonics* **v. 6, No. 1** p. 1-12

Gaudemer, Y., Jaupart, C. and Tapponnier, P. (1988) Thermal control on post-orogenic extension in collision belts. *Earth Planet. Sci. Lett.* **v. 89** p. 48-62

Ghiorso, M.S. (1985) Chemical mass transfer in magmatic processes. I. Thermodynamic relations and numerical algorithms. *Contrib. Mineral. Petrol.* **v. 90** p. 107-120

Ghiorso, M.S. and Carmichael, I.S.E. (1985) Chemical mass transfer in magmatic processes. II. Applications in equillibrium crystallization, fractionation and assimilation.. *Contrib. Mineral. Petrol.* **v. 90** p. 121-141

Goldstein, S.L. (1988) Decoupled evolution of Nd and Sr isotopes in the continental crust and the mantle. *Nature* **v. 336** p. 733-738

Goranson, R. W. (1931) The solubility of water in granite magmas. *American Journal of Science*. **v. 22** p. 481-502

Green T. H. and Ringwood, A. E. (1968) Genesis of calc-alkaline igneous rock suite. *Contrib. Mineral. Petrol.* **v. 18** p. 105-162

Gromet, L. P., Dymek, R. F., Haskin, L. A. and Korotev, R. L. (1984) The 'North American Shale Composite': its compilation, major and trace element characteristics. *Geochim. Cosmochim. Acta* **v. 48** p. 2469-2482

Gromet, L.P. and Silver, L.T. (1987) REE in the Peninsular Ranges batholith *J. Pet.* **v. 28** p. 75-125

Grove, T.L. and Baker, M.B. (1984) Phase equillibrium controls on the tholeiitic versus cala-alkaline differentiation trends. *Jour. Geophysical. Res.* **v. 89, no. B5** p. 3253-3274

Halliday, A.N. and five others (1983) The isotopic and chemical evolution of Mount St. Helens. *Earth Planet. Sci. Lett.* **v. 63** p. 241-256

Hammarstom, J.M. and Zen, E-an. (1986) Aluminium in hornblende: an empirical igneous geobarometer. *American Mineralogist* **v. 71** p. 1297-1313

Hamilton, W. (1969) The volcanic Andes-A modern model for the Cretaceous batholiths and tectonics of western North America.

Hamilton, W. (1976) Tectonic history of west-central Idaho (abs). *Geol. Soc Am. Abs. Progs.* **v. 8** p. 379

Hamilton, W. (1988) Tectonic setting and variations with depth of some Cretaceous and Cenozoic structural and magmatic systems of the western United States *in, Ernst,*

W.G., ed., Metamorphism and crustal evolution of the western United Srares Rubey volume7, Englewood Cliffs, New Jersey, Prentice-Hall.

Hardyman, R.F. and Fischer, F.S. (1985) Rhyolite intrusions and associated mineral deposits in the Challis volcanic field Challis quadrangle. *in, McIntyre, D.H., ed., Symposium on the geology and mineral deposits of the Challis 1° x 2° quadrangle, Idaho: U.S. Geol. Survey Bull.* **1658** p.167-177

Harley, S.L. (1987) Origin and growth of continents *Nature* **v. 329** p. 108-109

Harris, N.B.W., Pearce, J.A., and Tindle, A.G. (1986) Geochemical characteristics of collision zone magmatism. *in, Coward, M.P. and Ries, A.C., eds, Collision tectonics, Geological Society Special Publication* **no. 19** p. 67-81

Hart, W.K. (1985) Chemical and isotopic evidence for mixing between depleted and enriched mantle, northwestern U.S.A. *Geochim. Cosmochim. Acta* **v. 49** p. 131-144

Hawkesworth, C.J. (1986) 143Nd/144Nd, 87Sr/86Sr and trace element characteristics of magmas along destructive plate margins. *in Atherton, M.P. and Tarney, J., eds, The origin of granite batholiths geochemical evidence.* p. 76-89

Hawkesworth, C.J. and Ellam, R.M. (1989) Chemical fluxes and wedge replenishment rates along recent destructive plate margins. *Geology* **v. 17** p. 46-49

Hawkesworth, C.J., Van Calsteren, P. C. W. (1983) Radiogenic Isotopes-some geological applications. *in, Henderson, P., ed, Rare earth element geochemistry. Developments in geochemistry, Elsevier Science Publishers, Amsterdam.* **v. 2** p. 375-421

Hawkesworth, C.J., Van Calsteren, P., Rogers, N.W., and Menzies, M.A. (1985) Isotope variations in recent volcanics: a trace element perspective. *in, Menzies, M.A., Mantle Metasomatism*

Hawkesworth, C.J., Kempton, P.D., Mattey, D.P., Palacz, Z.A., Rogers, N.W., and van Calsteren, P.W.C. (1989) Intra-mantle fractionation versus lithosphere recycling: evidence from the sub-continental mantle. *in, Hart, S.R. and Gulen, L., eds., Crust/mantle recycling at convergent zones.* p. 227-237

Hayes. R.J. and Klugman, M.A. (1957) Feldspar staining methods. *J. Pet.* **v. 29** p. 227-232

Hedge, C. E. (1987) Correlation of Precambrian rocks of the western United States and Mexico. *Geol. Soc Am. Memoir*

Heier, K.S. (1973) Geochemistry of granulite facies rocks and problems of their origin. *Phil. Trans. R. Soc. Lond A.* **v. 273** p. 429-422

Heier, K.S. and Thoresen (1970) Geochemistry of high grade metamorphic rocks, Lofoten-Veterålen, North Norway. *Geochim. Cosmochim. Acta* **v. 35** p.89-99

Heller, P.L. and 7 others (1986) Time of initial thrusting in the Sevier orogenic belt, Idaho, Wyoming and Utah. *Geology* **v. 14** p. 388-391

Helz, R. T. (1976) Phase relations of basalts in their melting ranges at P_{H2O} = 5Kb : PartII. *J. Pet.* **v. 17** p. 139-193

Henderson, P. (1982) General geochemical proporties and Abundances of the REE. *in, Henderson, P. (ed.), Rare earth element geochemistry. Elsevier Publishing.* p. 12-35

Henderson, P. (1984) Inorganic Geochemistry. *Pergammon press.*

Hietanen, A. (1969) Distribution of Fe and Mg between garnet, staurolite and biotite in aluminium rich schist in various metamorphic zones of the Idaho batholith. *American Journal of Science.* **v. 9** p. 422-456

Hildreth, W., and Moorbath,S. (1988) Crustal contributions to arc magmatism in the Andes of Central Chile. *Contrib. Mineral. Petrol.* **v. 98** p. 455-489

Hodges, K.V., LeFort, P., and Pecher, A. (1988) Possible thermal buffering by crustal anatexis in collisional orogens: Thermobarometric evidence from the Nepalese Himalaya. *Geology* **v. 16** p. 707-710

Hofmann, A.W., Jochum, K.P., Seufert, M., and White, W.M. (1986) Nd and Pb in oceanic basalts: new constraints on mantle evolution. *Earth Planet. Sci. Lett.* **v. 79** p. 33-45

Hofmann, A.W. (1988) Chemical differentiation of the Earth: the relationship between mantle, continental crust, and oceanic crust. *Earth Planet. Sci. Lett.* **v. 90** p. 297-314

Hoisch, T. D. and Hamilton, W. (1990) Latest Cretaceous metamorphism in southeastern California by fluids from subducted schist. *EOS.* **May** p694-696

Holder, M.T. (1987) An emplacement mechanism for post-tectonic granites and its implications for their geochemical features. *in Atherton, M.P. and Tarney, J., eds, The origin of granite batholiths geochemical evidence.* p. 116-128

Holloway, J. R. and Ford, C. E. (1975) Fluid-absent melting of the fluoro-hydroxy pargasite to 35kbars. *Earth Planet. Sci. Lett.* **v.25** p. 44-49

Holloway, J. R. and Burnham, C. W. (1972) Melting relations of basalt with equillibrium water pressure less than total pressure. *J. Pet.* **v. 10** p. 131-129

Holmes, A. (1964) The Principles of Geology.

Honjo, N. and Leeman, W.P. (1987) Origin of hybrid ferrolatite lavas from Magic Reservoir eruptive centre, Snake River Plain, Idaho. *Contrib. Mineral. Petrol.* **v. 96** p.163-177

Hoschek, G. (1976) Melting relations of biotite + plagioclase + quartz. **v. 1976** p. 79-83

Howe, S.S. and Hall, W.E. (1985) Light-stable-isotope characteristics of ore systems in central Idaho. *in, McIntyre, D.H., ed., Symposium on the geology and mineral deposits of the Challis 1° x 2° quadrangle, Idaho: U.S. Geol. Survey Bull.* 1658 p. 183-192

Huppert, H.E. and Sparks, R.S.J. (1985) Cooling and contamination of mafic and ultramafic magmas during ascent through continental crust. *Earth Planet. Sci. Lett.* **v.74** p. 371-386

Huppert, H.E. and Sparks, R.S.J. (1988) The generation of granitic magmas by intrusion of basalt into continental crust. *J. Pet.* **v. 29** p. 599-624

Hyndman, D. W. (1981) Controls on source, and depth of emplacement of granitic magma. *Geology.* **v. 9** p. 244-249

Hyndman, D. W. (1983) The Idaho batholith and associated plutons, Idaho and western Montana. *Geol. Soc. Am. Memoirs.* **v. 159** p. 213-240

Hyndman, D. W. (1984) A petrographic and chemical section through the northern Idaho batholith. *Jour. Geol.* **v. 92** p. 83-102

Hyndman, D. W., and Foster, D. A. (1988a) The role of tonalites and mafic dykes in the generation in the Idaho batholith. *Jour. Geol.* **v. 96** p. 31-46

Hyndman, D. W. Alt, D. L. and Sears, J. W. (1988b) Post-Archean metamorphic and tectonic evolution of western Montana and northern Idaho *in, Ernst, W.G., ed., Metamorphism and crustal evolution of the western United States Rubey volume7, Englewood Cliffs, New Jersey, Prentice-Hall.* **v. 7** p. 333-361

Irvine, T. N. and Barager, N. R. A. (1971) A guide to the chemical classification of the common volcanic rocks. *Can. J. Earth. Sci.* **v. 8** p. 523-548

Jacobsen, S.B. (1988) Isotopic constraints on crustal growth and recycling. *Earth Planet. Sci. Lett.* **v. 90** p. 315-329

Jacobsen, S.B. and Wasserburg, G.H. (1979) The mean age of mantle and crustal reservoirs. *Jour. Geophysical. Res.* **v. 84** p. 7411-7426

Jaeger, J. C. (1957) The temperature in the neighborhood of a cooling intrusive sheet. *American Journal of Science.* **v. 255** p. 306-318

Johnson, K. M., Lewis, R. S., Romett, E. H., and Kiilsgaard, T. H. (1988) Cretaceous and Tertiary Intrusive rocks of south-central Idaho. *Idaho. Geol. Surv. Bull.* **v. 27** p. 55-86

Jones, D.L., Silberling, N.J., and Hillhouse, J. (1977) Wrangellia- a displaced terrane in northwestern North America. *Can. J. Earth. Sci.* **v. 14** p. 2565-2577

Kay, S. M. and Kay, R. W. (1985) Aleutian tholeitic and calc-alkaline magma series, I: The mafic phenocrysts. *Contrib. Mineral. Petrol.* **v. 90** p. 276-290

Kiilsgaard, T. H., Freeman, V. L. and Coffman, J. S. (1970) Mineral resources of the Sawtooth Primitive area, Idaho. *U.S. Geol. Surv. Bull.* **1319-D** 174p.

Kiilsgaard, T. H., and Bennett, E.H. (1985) Mineral deposits in the southern part of the Atlanta lobe of the Idaho batholith and their genetic relationship to Tertiaty intrusive rocks and to faults. **1658** p.153-165

Kiilsgaard, T. H., Fischer, F. S., and Bennett, E.H. (1986) The trans-Challis fault system and associated precious metal deposits. *Econ. Geol.* **v. 81** p. 721-724

Kiilsgaard T. H., and Lewis, R. S. (1985) Plutonic rocks of Cretaceous age and faults in the Atlanta lobe of the Idaho batholith. *in, McIntyre, D.H., ed., Symposium on the geology and mineral deposits of the Challis 1° x 2° quadrangle, Idaho: U.S. Geol. Survey Bull.* **1658** p. 29-42

Kistler, R.W. (1974) Phanerozoic batholiths in western North America. *Ann. Rev. Earth. planet. Sci.* **v. 2** p.403-418

Kistler, R.W., and Peterman, Z.E. (1978a) Reconstruction of crustal blocks of California on the basis initial Sr isotopic compositions of Mesozoic plutons. *U.S. Geol. Surv. Prof. Paper.* **1061** 27 p.

Kistler, R.W., and Peterman, Z.E. (1978b) A study of regional variations of initial strontium isotopic composition of Mesoxzoic granitic rocks in Calfornia *U.S. Geol. Surv. Prof. Paper.* **1071** 17 p.

Kistler, R.W., and Ghent, E.D., and O'Neil (1981) Petrogenesis of garnet two-mica granites in the Ruby Mountains, Nevada. *Jour. Geophysical. Res.* **v. 86, no. B11** p. 10591-10606

Kushiro, I. S. and Yoder, H. S. (1972) Origin of calc-alkaline peraluminous andesites and dacites. *Carnegie Inst., Washington D. C.* **Yearbook 1971** p. 411-413

Langmuir, C.H., Vocke Jrn.,R.D., Hanson, G.N., and Hart, S.R. (1978) A general mixing equation with applications to icelandic basalts. *Earth Planet. Sci. Lett.* **v. 37** p. 380-392

Larsen, E. S. Jr. (1945) Batholith and associated rocks of Corona, Elsinore and San Luis Rey quadrangles, southern Calfornia. *Geol. Soc. Am. Memoirs.* **v. 29** 182p.

LaTour, T.E. and Barnett, R.L. (1987) Mineralogical changes accompanying mylonitization in the Bitteroot dome of the Idaho batholith: Implications for timing of deformation. *Geol. Soc. Am. Memoirs.* **v. 98** p. 356-363

Lawton, C. (1986) Sevier Thrusting?

Lederer, C.M., Hollander J.M. and Perlman, I. (1967) Table of isotopes, Sixth edition. *J. Wiley, New York.* 594p.

Leeman, W. P. (1982) Developement of the Snake River Plain - Yellowstone Plateau Province, Idaho and Wyoming. An overview and petrologic model. *Idaho Bureau of Mines and Geology Bull.* **v. 26** p. 1-15

Leeman, W. P. (1982) Geology of the Magic Reservoir area, Snake River Plain, Idaho. *Idaho Bureau of Mines and Geology Bull.* **v. 26** p. 369-376

Leeman, W.P. and Hawkesworth, C.J. (1986) Open magma systems: trace element and Isotopic constraints. *Jour. Geophysical. Res.* **v. 91, no. B6** p. 5901-5912

Leeman, W.P., Menzies, M.A., Matty, D.J., and Embree, G.F. (1985) Strontium, neodymium and lead isotopic compositions of deep crustal xenoliths from the Snake River Plain: evidence for archean basement. *Earth Planet. Sci. Lett.* **v. 75** p. 354-368

LeFort, P. (1981) Manasalu leucogranite : a collision signature of the Himalaya, a model for its genesis and emplacement. *Jour. Geophysical. Res.* **v. 86** p. 10545-10568

Lewis, R. S. (1984) Geology of the Cape Horn Lakes Quadrangle, south-central Idaho. *University of Washington.* **M.S. Thesis** 91p.

Lewis, R. S., Kiilsgaard, T. H., Bennett, E.H., and Hall, W. (1987) Lithological and chemical characteristics of the central and southeastern part of the southern lobe of the Idaho batholith. *U.S. Geol. Sur. Prof. Paper.* **1436** p. 171-196

Lewis, R.S. and Kiilsgaard,T.H. (1988) In Press

Link, P.K. and 6 others (1988) Structural and stratigraphic transect of south-central Idaho. *in, Link, P. K. and Hackett, W. R. eds., Guidebook to the geology of central and southern Idaho: Idaho Geol. Surv. Bull.* **v. 27** p. 5-42

Lipman, P.W. (1980) Cenozoic volcanism in the western United States: implications for continental tectonics. *in, Continental Tectonics, National Acamedy of Sciences.* p. 821-825

Lipman, P.W., Prostka, H.J., and Christiansen, R.L. (1971) Cenozoic volcanism and plate-tectonic evolution of the western United States. I Early and Middle Cenozoic. *Phil. Trans. R. Soc. Lond A.* **v. 271** p. 217-248

Loiselle, M. C. and Wones, D.R. (1979) Characteristics and origin of anorogenic granites. *Geol. Soc. Am. Abs. Progs.* **v. 11, no. 7** p. 468

Lopez, D. A. (1982) Constraints on the shape and position of the Yellowjacket (Proterozoic Y) depositional basin. *Geol. Soc. Am. Abs. Progs.* **v. 14. no. 6.** p. 320

Lopez-Escobar, L., Frey, F.A.,Oyarzun, J. and Vergara, M. (1977) Andesites and high alumina basalts from the central-south Chile high Andes: geochemical evidence on their petrogenesis. *Ibid* **v. 63** p. 199-228

Lopez-Escobar, L., Frey, F.A., and Oyarzun, J. (1979) Geochemical characteristics of central Chile (33°-34° S) granitoids. *Contrib. Mineral. Petrol.* **v. 70** p. 439-450

Lum, C. C. L., Leeman, W. P., Foland, K. A., Kargel J. A. and Fitton, J. G. (1989) Isotopic Variaitons in Continental Basaltic Lavas as Indicators of Mantle Heterogeneity: Examples from the Western U. S. Cordillera. *Jour. Geophysical. Res.* **v. 94, no. B6** p. 7871-7884

Lund, K. W. (1984) The continent-island juncture in west-central Idaho a missing link in cordilleran tectonics. *Geol. Soc. Am. Abs. Progs.* **v. 16. no. 6** p. 580

Lund, K. W. and Snee, L.W. (1988) Metamorphism, structural developement, and geology of the continent : island arc juncture in West Central Idaho. *in, Ernst, W.G., ed., Metamorphism and crustal evolution of the western United States Rubey volume7, Englewood Cliffs, New Jersey, Prentice-Hall.* **v.7** p. 296-331

Mabey, D.R. and Webring, M.W. (1985) Regional geophysical studies in the Challis quadrangle. *in, McIntyre, D.H., ed., Symposium on the geology and mineral deposits of the Challis 1° x 2° quadrangle, Idaho: U.S. Geol. Survey Bull.* **1658** p. 69-79

Mahood, G. and Hildreth, W. (1983) Large partition coefficients for trace elements in high silica rhyolites. *Geochim. Cosmochim. Acta* **v. 47** p. 11-30

Manduca, C.A.A. (1988) Geology and geochemistry of the oceanic arc-continent boundary in the western Idaho batholith near McCall. *Ph.D. Thesis, California Institute of Technology*

Manning, D. C. A. (1980) The effect of fluorine on liquidus phase relations in the system Qz-Ab-Or with excess H2O at 1Kb. *Contrib. Mineral. Petrol.* **v. 76** p. 206-215

Martin, H. and Meybeck, M. (1979) Elemental mass-balance of material carried by major world rivers. *Marine Chem.* **v.7** p. 173-206

McCarthy, T. S. and Groves, D. I. (1979) The Blue Tier Batholith northeastern Tasmania: a cumulate-like product of fractional crystallization. *Contrib. Mineral. Petrol.* **v. 71** p. 193-209

McCulloch, M.T. and Wasserburg, G. J. (1978) Sm-Nd, and Rb-Sr chronology of continental crust formation. *Science* **v. 200** p. 1003-1011

McCulloch, M.T. and Chappell, B.W. (1982) Nd isotopic characteristics of S- and I-type granites. *Earth Planet. Sci. Lett.* **v. 58** p. 51-64

McDermott, P.F. (1986) Granite petrogenesis and crustal evolution studies in the Damara Pan-African orogenic belt. *Unpub. PhD. Thesis, Open University, Milton Keynes, England.* 303p.

McKenzie, D. (1984) The generation and compaction of partially molten rock. *J. Pet.* **v. 25** p. 713-765

McKenzie, D. (1985) The extraction of magma from the crust and mantle. *Earth Planet. Sci. Lett.* **v. 74** p. 81-91

McKenzie, D. and Bickle, M.J. (1988) The volume and composition of melt generated by extension of the lithosphere. *J. Pet.* **v. 29, part 2**

McIntyre, D.H., Ekren, E.B., and Hardyman, R.F. (1982) Stratigraphic and structural framework of the Challis volcanics in the eastern half of the Challis 1° x 2° quadrangle, Idaho. *in, Bonnichsen, B. and Breckenridge, R.M., eds., Cenozoic geology of Idaho: Idaho Bureau of mines and geology bulletin.* **v. 26** p. 3-22

Meade (1974) Methods of mineral staining.

Menzies, M.A., Seyfried, W.Jrn., and Blanchard, D. (1979) Experimental evidence of rare earth element immobilty in greenstones. *Nature* **v. 282** p.398

Menzies, M.A., Leeman, W.P., and Hawkesworth, C.J. (1983) Isotope geochemistry of Cenozoic volcanic rocks reveals mantle heterogeneity below western U.S.A. *Nature* **v. 303** p. 205-209

Menzies, M.A., Leeman, W.P., and Hawkesworth, C.J. (1984) Geochemical and isotopic evidence for the origin of continental flood basalts with particular reference to the Snake River Plain Idaho, U.S.A. *Phil. Trans. R. Soc. Lond A.* **v. 310** p. 643-660

Miller, C. F. (1985) Are strongly peraluminous magmas derived from pelitic sedimentary sources. *Jour. Geol.* **v. 193** p. 673-689

Miller, C. L. and Bradfish, L. J. (1980) An Inner Cordilleran belt of muscovite-bearing plutons. *Geology* **v. 8** p. 412-416

Miller, C. F. and Mittelfehldt, D. W. (1982) Depletion of the light rare earth elements in felsic magmas. *Geology* **v. 10** p. 129-133

Miller, E. F., Gans, P. B., Wright, J. E. and Sutter, J. F. (1988) Metamorphic history of the east-central Basin and Range Province: Tectonic setting and relationship to magmatism. *in, Ernst, W.G., ed., Metamorphism and crustal evolution of the western United Srares Rubey volume7, Englewood Cliffs, New Jersey, Prentice-Hall.* **v. 7** p. 649-682

Miller, J. F. (1988) Granite Petrogenesis in the Cordillera Real, Boliva and Crustal Evolution in the Central Andes. *Unpub. PhD. Thesis, Open University, Milton Keynes, England.* p. 106

Miller, J. F. and Harris, N.B.W. (1989) Evolution of continental crust in the central Andes; constraints from Nd and Sr isotope systematics. *Earth Planet. Sci. Lett.* .

Monoz, J. L. and Ludington, S. D. (1974) Fluoride-hydroxyl exchange in biotite. *American Jour. Sci.* **v. 274** p.396-413

Moore, J. G. (1959) The quartz diorite boundary line in the western United States. *Jour. Geol.* **v. 67** p. 198-210

Morgan, J. P. (in, Shagam, R. ed., Studies in Earth and Space sciences, Hess volume) Plate motions and deep mantle convection, *Geol. Soc. Am. Mem.* **v. 132** p. 711

Mueller, P.A. and Wooden, J.L. (1988) Evidence for Archean subduction and crustal recycling, Wyoming province. *Geology* **v.16** p. 871-874

Nakamura, N. (1974) Determination of Rare earth elements, Ba, Fe, Mg, Na and K in carbonaceous and ordinary meteorites. *Earth Planet. Sci. Lett.*

Naney, M.T. (1983) Phase equillibria of rock-forming ferromagnesian silicates in granitic systems *American Jour. Sci.* **v. 283** p. 993-1033

Naney, M.T, and Swanson, S. E. (1980) The effect of Fe and Mg on crystallization in granitic systems. *American Mineralogist* **v.65** p. 639-653

Nash, W.P. and Crecraft, H.R. (1985) Partition coefficients for trace elements in silicic magmas. *Geochim. Cosmochim. Acta* **v. 49** p. 2309-2322

Navon, O. and Stopler, E. (1987) Geochemical consequences of melt percolation: The upper mantle as a chromatographic column. *Jour. Geol.* **v. 95** p.285-307

Nelson, B.K. and DePaulo, D.J. (1985) Rapid production of continental crust 1.7 to 1.9 b.y. ago: Nd isotopic evidence from the basement of the North American Mid-continent. *Geol. Soc. Am. Abs. Progs.* **v.96** p.746-754

Newton, R. C. and Hansen, E. C. (1986) The South India-Sri Lanka high-grade terrain as a possible deep-crust secretion. *in, Dawson, J. B. ed., The Nature of the Lower Continental Crust, Geological Society Special publication.* **No. 25** p. 297-306

Norman, M. D. and Leeman, W. P. (1989) Geodynamic evolution of magmatism and tectonic setting, northwestern, U.S.A. *Earth Planet. Sci. Lett.*

Onash, C.M (1987) Temporal and spatial relations between folding, intrusion, metamorphism, and thrust faulting in the Riggins area, west-central Idaho. *U.S. Geol. Sur. Prof. Paper.* **1436** p. 139-149

O'Neill, R.L. and Pavlis, T.L. (1988) Superposition of Cenozoic extension on Mesozoic compressional structures in the Pioneer Mountains metamorphic core complex, central Idaho. *Geol. Soc. Am. Abs. Progs.* **v. 100** p. 1833-1845

O'Nions, R.K., Evensen, N.M., and Hamilton, P.J. (1979) Geochemical modeling of mantle differentiation and crustal growth. *Jour. Geophysical. Res.* **v. 84, no. B11** p. 6091-6101

Ormerod, D.S., Hawkesworth, C.J., Rogers, N.W., Leeman, W.P., and Menzies, M.A. (1988) Tectonic and magmatic transitions in the western Great Basin, U.S.A. *Nature* **v. 333** p. 349-353

Oxburgh, E.R. and McRae, T. (1984) Physical constraints on magma contamination in the continental crust: an example, the Adamello complex. *Phil. Trans. R. Soc. Lond A.* **v. 310** p. 457-472

Patiño-Douce, A. E., Johnston, A. D. and Humphreys, E. D. (1990) Closed System Anatexis in the Cordilleran Interior: The Importance of initial lithologic structure. *EOS.* **Feb,** p. 298-299

Patiño-Douce, A. E., Humphreys, E. D. and Johnston, A. D. (1990) Anatexis and metamorphism in tectonically thickened continental crust exemplified by the Sevier hinterland, western North America. *Earth Planet. Sci. Lett.* **v. 97** p. 290-315

Paterson, C. and Tatsumoto, S. (1964) The significance of lead isotopes in detrital feldspar with respect to chemical differentiatrion within the Earths' mantle. *Geochim. Cosmochim. Acta* **v. 28** p. 1-22

Peacock, M. A. (1931) Classification of igneous rock series *Jour. Geol.* **v. 39** p. 65-67

Pearce, J. A. (1983) The role of sub-continental lithosphere in magma genesis at active continental margins. *in, Hawkesworth, C. J. and Norry, M. J. (eds), Continental basalts and mantle xenoliths. Shiva publishing Ltd.* p. 236-249

Pearce, J. A. and Norry, M. J. (1979) Petrogenetic Implications of Ti, Zr, Y, and Nb Variations in Volcanic rocks. *Contrib. Mineral. Petrol.* **v. 69** p. 33-47

Pearce, J. A., Harris,N. B. W., and Tindle, A. G. (1984) Trace element discriminationation diagrams for the tectonic interpretation of granitic rocks. *J. Pet.* **v. 25** p. 956-983

Pitcher, W.S. (1978) The anatomy of a batholith. *J. Geol. Soc. London.* **v. 135** p. 157-182

Pitcher, W.S. (1987) Granite: Typology, geological environment and melting relationships. *in Atherton, M.P. and Tarney, J., eds, The origin of granite batholiths geochemical evidence.* p. 277-285

Potts, P.J., Thorpe, O.W., and Watson, J.S. (1981) Determinationation of REE abundances in 29 international rock standards by instrumental neutron activation analysis: a critical appraisal of calibration errors. *Chem. Geol.* **v. 34** p. 331-352

Potts, P.J., Thorpe, O.W., Issacs, M.C., and Wright, D.W. (1985) High precision instrumental neutron_activation analysis of geological samples employing simultaneous counting with both planar and coaxial detectors. *Chem. Geol.* **v. 38** p. 145-155

Reid, R.R. (1963) Reconnaissance geology of the Sawtooth range *Idaho Bureau of Mines and Geology Pamphlet* **v. 129** 37p.

Reid, R.R. (1987) Structural geology and petrology of a part of the Bitteroot lobe of the Idaho batholith. *U.S. Geol. Sur. Prof. Paper.* **1436** p. 37-57

Richter, F.M. (1986) Simple models for trace element fractionation during melt segregation. *Earth Planet. Sci. Lett.* **v. 77** p. 333-344

Richter, F.M. and McKenzie, D. (1984) Dynamic models for melt segregation from a deformable matrix. *J. Geol.* **v. 92** p. 729-740

Roddick, J.A. (1983) Geophysical review and composition of the Coast Plutonic Complex, south of latitude 55° N *Geol. Soc. Am. Memoirs.* **v. 159** p. 195-211

Roddick, J.A. (1983) Circum-Pacific plutonic terranes: An overview. *Geol. Soc. Am. Memoirs.* **v. 159** p. 1-3

Rogers, G. (1985) A geochemical traverse across the North Chilean Andes. *Unpub. Open University PhD. Thesis*

Rogers, G. and Hawkesworth, C.J. (1989) A geochemical traverse across the North Chilean Andes: evidence for crust generation from the mantle wedge. *Earth Planet. Sci. Lett.* **v. 91** p.271-285

Rogers, N.W. (1977) Granulite xenoliths from Lesotho kimberlites and the lower continental crust. *Nature* **v. 270, no. 5639** p. 681-684

Rogers, N.W. and Hawkesworth, C.J. (1982) Proterozoic age and cumulate origin for the granulite xenoliths, Lesotho. *Nature* **v. 299, no. 5882** p. 409-413

Ross, C. P. (1928) Mesozoic and Tertiary granitic rocks in Idaho. *Jour. Geol.* **v. 36 no. 8** p. 673-693

Ross, C. P. (1934) Geology and ore deposits of the Castro quadrangle, Idaho. *U.S. Geol. Surv. Bull.* **877** 161 p.

Rudnick, R. L. and Taylor, S.R. (1987) The composition and petrogemesis of the lower crust: a xenolith study. *Jour. Geophysical. Res.*

Ruppel, E.T. (1975) Precambrian and Lower Ordovician rocks in east-central Idaho. *U.S. Geol. Sur. Prof. Paper.* **889** 34 p.

Rutter, M.J. and Wyllie, P.J. (1988) Melting of vapour-absent tonalite at 10Kbar to simulate dehydration-melting in the deep crust. *Nature* **v. 331** p.159-160

Ryerson, F.J. and Watson, E.B. (1987) Rutile saturation in magmas: implications for Ti-Nb-Ta depletion in island-arc basalts. *Earth Planet. Sci. Lett.* **v. 86** p. 225-239

Saleeby, J.B., Sams, D.B., and Kistler, R.W. (1987) U/Pb zircon, Sr and O isotopic and geochronological study of the southernmost Sierra Nevada batholith, California. *Jour. Geophysical. Res.* **v.92** p. 3831-3848

Sawka, W.N., Chappell, B.W., and Norrish, K. (1984) Light-rare-earth element zoning in sphene and allanite during granitoid fractionation. *Geology* **v. 12** p. 131-134

Schmidt, S. (1964) Reconnaissance petrographic cross-section of the Idaho batholith in Adams and Valley Counties, Idaho. *U.S. Geol. Sur. Bull.* **v. 1181-G** 50p.

Shand, S. J. (1951) Eruptive Rocks *J. Wiley, N. York*

Shuster, R.D. and Bickford, M.E. (1985) Chemical and isotopic evidence for the petrogenesis of the northeastern Idaho batholith. *Jour. Geol.* **v. 93** p. 727-724

Silver, L.T. and Chappell, B.W. (1988) The Peninsular Ranges Batholith: an insight into the evolution of the Cordilleran batholiths of southwestern North America. *Trans. R. Soc. Edinburgh. Earth Science.* **v. 79** p. 105-121

Skipp, B. (1987) Basement thrust sheets in the Clearwater orogenic zone, central Idaho and western Montana. *Geology* **v. 15** p. 220-224

Smith, I.E.M., White, A.J.R., Chappell, B.W., and Eggleton, R.A. (1988) Fractionation in a zoned mozonite pluton: Mount Dromedary, southeastern Australia. *Geol. Mag.* **v. 125** p. 273-284

Smitherton, J. R. (1985) Geology of the stibnite roof pendant, Valley county, Idaho. *Univ. Idaho. M.S. Thesis.*

Snee, L.W. and Lund, K. (1984) Age and depth of formation of gold deposits using 40Ar/39Ar age-spectrum techniques: geologic implications in central Idaho. *Geol. Soc. Am. Abs. Progs.* **v. 16, no. 6**

Snee, L.W., Sutter, J.F., Lund, K., Balcer, D.E., and Evans, K.V. (1986) 40Ar/39Ar age spectrum data for metamorphic and plutonic rocks from west-central Idaho. *Geol. Survey Open File*. **OF87-0052** 20 p.

Snyder, W.S., Dickson, W.R., and Silberman (1976) Tectonic implications of space-time patterns of Cenozoic magmatism in the western United States. *Earth Planet. Sci. Lett.* **v. 32** p. 91-106

Sparks, R.S.J., Huppert, H.E., and Turner, J.S. (1984) The fluid dynamics of evolving magma chambers. *Phil. Trans. R. Soc. Lond A.* **v. 310** p. 511-534

Speed, R.C. (1979) Collided Paleozoic microplate in the western United States. *Jour. Geol.* **v.32** p. 279-292

Steiger, R.H. and Jaeger, E. (1977) Subcommission on geochronology: conventiation on the use of decay constants in geo- and cosmochronology. *Earth Planet. Sci. Lett.* **v. 36** p.30-35

Stern, C. R. and Stern, T. W. (1973) Revised table for the calculation of lead isotope ages. *Natl. Tech. Inform. Service, Springfield, Virginia 22151, USA.* 35p.

Stacey, J. S. and Kramers, J. D. (1975) Approximation of Terrestrial Lead Isotope Evolution by a Two-Stage Model. *Earth Planet. Sci. Lett.* **v. 26** p. 207-221

Stern, C. R. and Wyllie, P. J. (1978) Phase compositions through crystallization intervals in andesite-basalt-H2O at 30Kb with implications for subduction zone magmas. *American Mineralogist.* **v. 63** p. 641-663

Streikeisen, A. L. and others. (1973) Plutonic rocks - classification and nomenclature recommended by the IUGS Subcommision on the Systematicsof igneous rocks. *Geotimes.* **V. 18** p. 223-226

Sutter, J. F., Snee, L. W., and Lund, K. W. (1984) Metamorphic, plutonic, and uplift history of a continent-island arc suture zone, west-central Idaho. *Geol. Soc. Am. Abs. Progs.* **v.16. no. 6** p. 670-671

Swanberg, C. A. (1972) Vertical distribution of heat generation in the Idaho batholith. *Jour. Geophysical. Res.* **v. 77. no. 14** p. 2508-2513

Swanberg, C.A., and Blackwell, D. D. (1973) Areal distribution and geophysical significance of heat generation in the Idaho Batholith and Adjacent intrusions in eastern Oregon and western Montana *Geol. Soc. Am. Bull.* **v. 84** p. 1261-1282

Swanson, S. E. (1977) Relation of nucleation and crystal growth rate to the development of granitic textures. *American Mineralogist.* **v. 62** p. 966-978

Tarney, J. and Saunders, A.D. (1987) Trace element constraints on the origin of cordilleran batholiths. *in Atherton, M.P. and Tarney, J., eds, The origin of granite batholiths geochemical evidence.* p. 90-105

Taubeneck, W.H. (1971) Idaho batholith and its southern extension. *Geol. Soc. Am. Bull.* **v. 82** p. 1899-1928

Taylor, H. P. Jr., and Magaritz, M. (1976) An oxygen and hydrogen isotope study of the Idaho batholith (abs.) *EOS.* **v. 57** p. 350

Taylor, H. P. Jr., and Magaritz, M. (1978) An oxygen and hydrogen studies of the cordilleran batholiths of western North America, in Robinson, B. W. ed. Stable

isotopes in the earthsciences. *N. Zealand. Sci. and Indust. Res. Bull.* **v. 220** p.151-173

Taylor, H. P. Jr. (1980) The effects of assimilation of country rocks by magmas on $^{18}O/^{16}O$ and 87Sr/86Sr systematics in igneous rocks. *Earth Planet. Sci. Lett.* **v.47** p. 243-254

Taylor S. R. (1967) The origin and growth of the continents. *Tectonophysics.* **v. 4** p.17

Taylor S. R. and McLennan (1985) The continental crust: its composition and evolution. *Blackwell Scientific Publications; Geosciences Texts* 312p.

Thompson, R. N. and Morrison, M. A. (1983) Continental flood basalts...arachnids rule O.K.? *in, Hawkesworth, C. J. and Norry, M. J. (eds), Continental basalts and mantle xenoliths. Shiva publishing Ltd.* p. 211

Thompson, A. B. (1988) Dehydration melting of Crustal Rocks. *Rendiconti Soc. Italiana Mineral. Pet.* **v.43** p. 41-60

Thorpe, R.S., Potts, P. J. and Francis, P. W. (1976) Rare earth data and petrogenesis of andesite from the north Chilean Andes. *Contrib. Mineral. Petrol.* **v. 54** p. 65-78

Thorpe, R.S., Francis, P.W., and Moorbath, S. (1979) Rare earth and strontium isotope evidence concerning thepetrogenesis of northern Chilean ignimbrites. *Earth Planet. Sci. Lett.* **v. 42** p. 359-367

Thorpe, R.S., Francis, P.W.,Hammill, M., and Baker, M. C. W. (1982) The Andes. *in, Thorpe, R. S.ed., Andesites. Chichester: John Wiley and Sons.* p. 187-205

Toth, M.I. (1987) Petrology and origin of the Bitteroot lobe of the Idaho batholith. *U.S. Geol. Sur. Prof. Paper.* **1436** p. 9-35

Tuttle, P. F. and Bowen, N. L. (1958) Origin of granite in the light experimental studies in the system NaAlSi3O8-KalSi3O8-H2O *Mem. Geol. Soc. Am.* **v. 74** 45p.

Vallier, T. L., Brooks, H.C., and Thayer, T.P. (1977) Paleozoic Rocks of eastern Oregon and western Idaho. p. 455-

Vallier, T. L., and Brooks, H.C. (1987) The Idaho batholith and its border zone - a regional perspective. *U.S. Geol. Sur. Prof. Paper.* **1436** p. 1-7

Van der Molen, I. and Paterson, M.S. (1979) Experimental deformation of partially melted granite. *Contrib. Mineral. Petrol.* **v. 70** p. 299-318

Villien, A., and Kligfield, R.M., (1986) Thrusting and synorogenic sedimentation in central Utah. *in, Peterson, J.A., ed., Palaeotectonics and sedimentation in the Rocky Mountain region, United States, Am. Ass. Pet. Geol. Mem.* **v. 41** p. 353-370

Von Platen, H. (1965) Experimental anatexis and genesis of migmatites. *in, Pitcher, W. G. amd Flinn, G. W. eds. Controls of metamorphism. Pub. Oliver and Boyd, Edinburgh.* p. 202-218

Wall, V.J., Clemens,J.D., and Clarke, D.B. (1987) Models for evolution and source compositions. *Jour. Geol.* **v. 95, no. 6** p. 731-749

Watson, E.B. (1979) Zircon saturation in felsic liquids : Experimental results and applications to the trace element geochemistry. *Contrib. Mineral. Petrol.* **v. 70** p. 407-419

Watson, E.B. and Harrison T.M. (1983) Zircon saturation revisted: temperature and composition effects in a variety of crustal magma types. *Earth Planet. Sci. Lett.* v. 64 p. 295-304

Watson, E.B. and Harrison T.M. (1984) Accessory minerals and the geochemical evolution of crustal magamtic systems : A summary and prospectus of experimental approaches. *Physics of the Earth and Planetary Interiors.* v. 35 p. 19-30

Weaver, B.L. and Tarney, J. (1980) Continental crust composition and nature of the lower crust: constraints from mantle Nd-Sr isotope correlation. *Nature* v. 286 p. 342-346

Weaver, B.L. and Tarney, J. (1982) Andesite magmatism and continental growth. *in, Thorpe, R. S.ed., Andesites. Chichester: John Wiley and Sons.* p. 639-661

White, A.J.R. and Chappell, B.W. (1988) Some supracrustal (S-type) granites of the Lachlan fold belt. *Trans. R. Soc. Edinburgh. Earth Science.* v. 79 p. 169-181

White, A.J.R., Clemens, J.D., Holloway, J.R., Silver, L.T. Chappell, B.W., and Wall, V.J. (1986) S-type granites and their probable absence in southwestern North America. *Geology* v. 14 p. 115-118

White, R.S. and McKenzie, D.P. (1989) Magmatism at rift zones: The generation of volcanic continental margins and flood basalts. *Jour. Geophysical. Res.* v. 94 p.32-56

Whitney, J.A. (1988) The origin of granite: the role and source of water in the evolution of granitic magmas. *Geol. Soc. Am. Bull.* v. 100 p. 1886-1897

Wickham, S. M. (1987) The segregation and emplacement of granitic magmas. *Contrib. Mineral. Petrol.* v. 98 p. 455-489

Wickham, S. M. and Oxburgh (1985) Continental rifts as a setting for regional metamorphism. *Nature* v. 318 p. 330-333

Winkler, H. C. F. (1974) Petrogenesis of metamorphic rocks (Std. Edn). *Pub. Springer Verlag : Berlin, Heidelberg, New York.* 320p.

Winston, D. (1986) Sedimentation and tectonics of the Middle Proterozoic belt basin and their influence on Phanerozoic compression and extension in western Montana and northern Idaho. *in, Peterson, J.A., ed., Paleotectonics and sedimentation in the Rocky Mountain region, United States, A.A.P.G.Memoir* 41 p. 3-20

Wiswall, C.G. (1979b) Structure and petrography below the Bitteroot dome, Idaho batholith near Paradise Idaho. *University of Montana, Missoula, Montana.* Ph.D. dissertation 129p.

Wiswall, C.G. and Hyndman, D.W. (1987) Emplacement of the main plutons of the Bitteroot lobe of the Idaho batholith. *U.S. Geol. Sur. Prof. Paper.* 1436 p. 59-72

Wooden, J.L. and Mueller, P.A. (1988) Pb, Sr, and Nd isotopiccompositions of a suite Late Archean igneous rocks, eastern Beartooth Mountains: Implications forcrust-mantle evolution. *Earth Planet. Sci. Lett.* v. 87 p. 59-72

Wright, T. L. and Doherty, P. C. (1970) A linear programming and least squares computer method for solving petrologic mixing problems. *Bull. Geol. Soc. Am.* v.81 p. 1995-2008

Wyborn, D. and Chappell, B.W. (1986) The petrogenetic significance of chemically related plutonic and volcanic rock units. *Geol. Mag.* **v. 123** p. 619-628

Wyllie, P.J. (1976) Crustal Anatexis: An experimental review *in, Green, D. H., ed., Experimental petrology related to extreme metamorphism; Tectonophysics.* **v. 43** p.41-71

Wyllie, P.J., Huang, W., Stern, C.R., and Maaloe, S. (1976) Granitic magmas: possible and impossible sources, water contents, and crystallization sequences. *Can. J. Earth. Sci.* **v.13** p.1007-1019

Wyllie, P.J. (1987) Experimental studies on biotite- and muscovite granites and some crustal magmatic sources. *in Atherton, M.P. and Tarney, J., eds, The origin of granite batholiths geochemical evidence.*

Zartman, R.E. (1974) Lead isotopic provinces in the cordillera of the western United States and their geologic significance. *Econ. Geol.* **v. 69** p. 792-805

Zartman, R.E. and Doe, B. R. (1981) Plumbotectonics-The Model *Tectonophysics* **v. 75** p. 135-162

Zeitler, P.K., (1985) Cooling history of the N.W. Himalaya, Pakistan *Tectonics* **v.4** p. 127-157

Zen, E-an. (1985) Implications of magmatic epidote-bearing plutons on crustal evolution in the accreted terranes of northwestern North America. *Geology* **v. 13** p. 266-269

Zen, E-an. (1988) Tectonic significanceof high pressure plutonic rocks in the western cordillera of North America. *in, Ernst, W.G., ed., Metamorphism and crustal evolution of the western United States Rubey volume7, Englewood Cliffs, New Jersey, Prentice-Hall.* **v.7** p. 42-63

Zen, E-an. and Hammarstrom, J.M. (1984) Magmatic epidote and its petrologic significance *Geology* **v. 12** p. 515-518

Zindler (1986) Chemical geodynamics *Ann. Rev. Earth Planet. Sci.* **v. 14** p. 493-571

APPENDIX A

Sample Preparation, Analytical Techniques and Data Presentation

A 1 Sample powder preparation

Granitoid samples of 4-7 kg and smaller samples of uncommon or fine grained material, such as inclusions and dykes were collected. Only fresh material, often from recent road cuttings was taken. All samples were split into ≈ 2 cm cubes using a hydraulic splitter and any weathered material removed. At least 2 kg of these pieces were crushed in a hardened steel jaw crusher to <5 mm pieces. A representative 150g portion of this crushate was taken using cone and quartering techniques. This sample was powdered in an agate lined tema mill for approximately 15 minutes to produce a powder of less than 200 mesh grain size.

A 1.1 Alkali feldspar separation and preparation

Samples selected for alkali feldspar separation were put through the hardened steel jaw crusher until at least 75% of the sample was <2mm. This fraction was then selectively sieved and the fraction >100μm, but <0.5mm was collected and repeatedly washed in distilled water until all the dust had been removed as indicated by the water remaining clear.

A staining procedure combining techniques outlined by Allman and Lawerence (1972) and Meade (1974) was employed to differentiate plagioclase feldspar from alkali feldspar. The method outlined below leaves the plagioclase crystals red and the alkali feldspar crystals unaffected The details of the technique including etching and immersion times are only approximate as the technique was slightly varied between samples to obtain the best results.

A 5g sample was etched in 5ml of 20% HF for 10 seconds in a teflon beaker and then rinsed in QD water several times. The sample was then immersed and agitated in a saturated solution of Barium Chloride ($BaCl_2$: 15g/250ml) for 30 seconds and the excess solution poured off and rinsed once with QD water. The sample was then immersed and agitated in red Rhodizonate solution (0.05g/20ml) or red Amaranth solution (F.D. & C. Ltd. Red no.

2) for up to 1 minute. The excess is poured off and the sample is repeatedly rinsed with QD water and finally washed in an ultrasonic bath. The sample is dried overnight leaving the plagioclase red-pink, and was stored ready to be hand-picked under a binocular microscope.

After hand picking about 500mg of pure alkali feldspar the sample was leached in 15M HNO_3 for 10 minutes and then extensively washed in QD water. The sample was then crushed to a fine powder with an agate pestle and mortar and stored for analysis, from here on following the same procedure as that for whole rock Pb isotope analysis.

A 2 XRF sample preparation

Two separate preparation techniques were followed to obtain elemental concentrations; pressed powder pellets were prepared for trace element analyses and glass discs, for major element analyses.

To form pellets ≈8 g of rock powder and a Moviol binder were mixed and pressed into 3 cm diameter pellets using a hydraulic press. The pellets were dried in an oven at 110°C overnight before analysis.

Glass discs were formed from a flux of 4:1 mixture of lithium metaborate:tetraborate mixture (Spectraflux 100B) in a 6:1 ratio with pre-dried rock powder. The mixture was fused in a platinum-gold alloy crucible in a muffle furnace at 1100 °C for fifteen minutes. The resulting glass was poured into a 3 cm mould and cast to form a glass disc. A correction for flux volatilization was applied to each batch of beads. Loss on ignition data was calculated for each sample by heating the sample to 1000°C for twenty minutes and measuring the percentage mass loss.

A 3 XRF Analysis

All XRF analysis was carried out at Nottingham University on a wavelength dispersive XRF spectrometer (WDXRF).

A 3.1 Major elements

For major element analyses, glass beads were counted in duplicate for 500 seconds at 10KV, 0.2mA with no primary beam filter. Instrument drift was monitered by analysis of USGS AGV-1.

A 3.2 Trace elements

Trace elements Ba, Ce, Co, Cr, Hf, La, Ni, Nb, Pb, Rb, Sr, Ta, Th, U,V, Zr ,Y were analysed at Nottingham University on a Phillips PW1400 wavelength dispersive X-ray fluorescence spectrometer. Analyses were carried out on pressed pellets prepared at Nottingham University. A rhodium X-ray tube was used for all wavelength dispersive analyses. Operating conditions are shown in Table 1.2. Detection limits are about 3ppm. Rb and Sr were determined separately from other trace elements. Both elements were analysed at 75KV, 40mA using a LiF 220 crystal. A detailed account of the technique is given by Harvey and Atkin (1981).

Element	KV	mA	Crystal	Ct (peak)[A1]	Ct (bkd)[A1]
Ba	50	60	LiF220	20	10
Co	60	50	LiF220	20	20
Cr	50	60	LiF220	20	8
Ni	70	40	LiF220	10	4
Nb	75	40	LiF220	10	8
Y	75	40	LiF220	20	16
Zr	75	40	LiF220	20	20

Table A.1 Operating conditions for Nottingham University WDXRF system

[A1] Ct (peak) and Ct (bkd) are normal counting times for peak and background positions respectively.

All WDXRF results are tabulated in Appendix B. Detection limits for the major elements are generally 0.05 wt% except for the light elements Na, Mg, Al, and Si for which the detection limits are between 0.2 wt% (Si) and 0.96 wt% (Na). Precision is better than 1% relative (at a 2 sigma certainty level) except Al (2%), Mg (3%), and Na (10%). Trace element detection limits are 6 ppm for Rb, Sr, Y, Nb and Ni, 15 ppm for Zr, and 31 ppm for Ba. Precision for all trace elements is about 2% at 100 ppm level.

A 4 Instrumental neutron activation analysis (INAA)

INAA was carried out on 36 samples to determine the concentrations of the rare earth elements (REE) as well as Th, U, Co, Sc, Ta and Hf.

0.3 g of pre-dried rock powder was accurately weighed into a polythene capsule and sealed. The capsules were stacked into a cylinder with a pre-weighed lacquered iron foil between each capsule to monitor the neutron flux along the length of the cylinder. Each cylinder contained 9 samples and 2 standards. The two standards used were the irradiation standard AC (OURS) and a sample of Whin Sill, which was used as an internal standard.

Samples were irradiated in a core tube at the Imperial College reactor centre, Silwood Park, Ascot, in a thermal flux of 5×10^{12} n cm^2 sec-1 for 24-30 hours. Following irradiation the samples were allowed to 'cool' for about a week to allow the short lived radioisotopes to decay. The samples were 'counted' at the Open University using two detectors on either side of the sample capsule; a planar low energy photon spectrometer (LEPS) and a coaxial Ge(Li) detector. Each sample was 'counted' for 800 sec on the LEPS detector for Sm, and on the coaxial detector for La, Co, and Sc. The other elements were determined by counting each sample for 2.5×10^4 to 5×10^4 sec using the LEPS detector. The iron foils were 'counted' using the coaxial detector for 300 sec each, to assess the variations in the neutron flux. Data were processed using spectroscopy amplifiers and a multichannel analyser. Photopeak data were corrected for neutron flux variations calculated using the iron foil data. Details of counting conditions, peak fitting, calibration, and corrections are given in Potts et

al. (1981) and Potts et al. (1985). The data was normalized to Chondritic values using the values of Nakamura (1974), see Table A4.1.

Element	Chondrite Normalising value	Element	Primordial Mantle Normalising Value
La	0.328	Ba	6.9
Ce	0.805	Rb	0.35
Nd	0.630	Th	0.042
Sm	0.203	K	116
Eu	0.077	Nb	0.35
Gd	0.276	Ta	0.02
Tb	0.052	Sr	11.8
Ho	0.780	Zr	6.840
Tm	0.034	Hf	0.2
Yb	0.220	Ti	617
Lu	0.0339	Y	2

Table A.2 Chondrite normalizing values from Nakamura (1974) and Primordial mantle normalising values from Thompson (1973).

A 5 Radiogenic isotope analysis: chemistry

All isotopic analyses and preparation were carried out in a clean-air laboratory in which a positive air pressure was maintained. All solutions were made up with either twice quartz distilled or Milli-Q reverse osmosis purified, water. Sample dissolutions were carried out in teflon beakers for Sr and teflon bombs for Nd, both were normally opened only in laminar air flow cupboards.

Bombs and beakers were cleaned between batches by washing in QD or Milli-Q water and soaking in 15 M $HN0_3$ (aq) at 80 °C overnight, washed in pure water overnight and allowed to dry inverted on tissue paper.

Total procedural blanks for Sm and Nd are <1 ng, for Pb ≈ 1 and 8 ng for Sr.

A 5.1 Sr chemistry

Approximately 100 mg of rock powder was weighed into a teflon beaker to which approximately 2 ml of 15 M $HN0_3$ (aq) was added and then 5 ml of 40% HF (aq). The solution was covered and allowed to stand cold for several hours, then it was evaporated to near dryness under evaporating lamps in a laminar flow cupboard. A further 2 ml of 15 M $HN0_3$ (aq) was added and evaporated to near dryness. Approximately 6 ml of 6 M HCI (aq) was added and warmed under the evaporating lamps, at this stage total dissolution has occurred and a clear yellow-orange solution should result. If total dissolution was not achieved the solution was evaporated to near dryness and the last two acid stages repeated till total dissolution was achieved. Accessory phases were occasionally observed in the solutions and proved insoluble by this method, this was not considered an important problem for Sr isotope studies. The final solution was evaporated to near dryness and re-dissolved in 1 ml of 2.5 M HCI (aq), any residue was centrifuged off.

Sr separation was carried out using columns of 10 ml of pre-conditioned Bio-rad AG50W x8, 200-400 mesh resin. The sample was loaded on to the resin with the minimum disturbance. The sample was slowly washed on to the resin with two 1 ml aliquots of 2.5 M HCI (aq), each aliquot was allowed to soak into the resin before the second was added. If the Rb fraction was needed 26 ml of 2.5 M HCI (aq) was eluted and the Rb fraction was collected in 10 ml of 2.5 M HCI (aq) and 12 ml of 2.5 M HCI (aq) eluted. If the Rb fraction was not needed 48 ml of 2.5 M HCI (aq) was then eluted through the resin. The Sr fraction was collected in 10 ml of 2.5 M HCl (aq). The Rb and Sr solutions were evaporated to dryness and stored for analysis.

A 5.2 Nd and Sm chemistry

Dissolutions were carried out in teflon bombs to ensure total dissolution of REE rich accessory phases. Approximately 150 mg of rock powder was weighed into a teflon bomb and 2 ml of 15 M $HN0_3$ (aq) followed by 5 ml of 40% HF (aq) added. The mixture was allowed to stand cold for several hours in sealed bombs. Each bomb was then placed in a tight polythene sleeve to hold the top in place; the assembly was then placed in a monel

jacket and placed in an oven at 180 °C overnight. After cooling the bomb was removed from the casing and the solution evaporated under lamps to near dryness. 2 ml of 15 M $HN0_3$ (aq) was added and evaporated to near dryness and 6 ml of 6 M HCI (aq) added. If total dissolution was not achieved at this stage then the bomb was reassembled and returned to the oven for a further 24 hours. When total dissolution was achieved the MREE were separated on the Sr columns, following the procedure for Sr, as described above, but after the Sr fraction had been collected 22 ml of 3 M $HN0_3$ (aq) was eluted through the columns and the MREE fraction was collected in a further 24 ml of 3 M $HN0_3$ (aq). This fraction was evaporated to dryness and re-dissolved in 1 ml of 0.25 M HCl (aq). The MREE fraction was loaded on to pre-conditioned reverse chromatography columns, composed of 1g of teflon powder (Voltalef 300LD PL micro) with 100 mg DEP ((Di(2-ethylhexyl) phosphate). The sample was washed in with 2 x 1 ml of 0.25 M HCI (aq), a further 8 ml of 0.25 M HCl (aq) eluted through the columns and the Nd collected in 4 ml of 0.25 M HCl (aq) which was evaporated to dryness and stored for analysis. If the Sm was needed 6 ml of 0.5 M HCI (aq) was eluted and the Sm fraction collected in 4 ml of 0.5 M HCl (aq) which was evaporated to dryness and stored for analysis.

A 5.3 Pb chemistry

About 20 mg of sample is weighed into a sevalex bomb in batches of five samples. About 1 ml of TD $HN0_3$ followed by 2-3 mls of TD HF are added to each sample. This mixture is allowed to stand cold overnight and then evaporated down under the evaporating lamps. When dry, a further 2 mls of TD $HN0_3$ are added which are also evaporated to dryness. After evaporation, 3mls of 6M HCl are added and evaporated to dryness. 1 ml of 1 M HBR is then added and this is allowed to stand cold overnight. The solution is then ready for ion exchange columns.

Ion exchange columns consist of polythene pipette tips loaded with 3-4 drops of Dowex 200-400 mesh anion exchange resin. The pipette tips are taken from a sealed container in which they have been immersed overnight in hot 6M HCl. The columns are placed in a covered perspex rack in a laminar flow unit and are flushed through with 16M $HN0_3$

followed by 1 column volume (c.v.) of QD H_20. The resin is added at this stage (3-4 drops) followed by successive 1 c.v. washes of CD 6M HCl, QD H_20 and 6M HCl and 2 c.v. washes of TD H_20 and using a clean pipette tip, 1ml of HBr which contains the sample lead is carefully transferred from a sevalex bomb to the column taking care not to disturb the column resin. When the HBr has eluted into the resin 1c.v. of HBr is slowly added to the column. This is followed by the addition of three successive column volumes of HBr. When the HBr has eluted through the resin Pb is collected in a clean sevalex bomb by eluting the column with three c.v. of TD H_20 and collecting the elutant. A few drops of TD 6M $HN0_3$ are added to this solution before evaporating to dryness under lamps.

All Pb chemistry was carried out in a laboratory which is used exclusively for Pb chemistry. Special precautions were taken to ensure low Pb blanks which were in the range 0.7-1.1 ng during this study.

A 6 Radiogenic isotope analysis: Mass spectrometry

A 6.1 Sample loading

Most samples were run on a Vacuum Generators Isomass 54E solid source, mass spectrometer (VG MS) interfaced with a HP 9845T computer using software designed by D.W.Wright and P.W.C. Van Calsteren. Pb analyses and several Nd analyses were run on an Finnigan M80 261, solid source, multi-collector mass spectrometer (FM MS) interfaced with a HP 9836 computer using software designed by D.W.Wright and P.W.C. Van Calsteren.

Filaments for both machines were out-gassed before use. Single filaments were out-gassed for 5 minutes at 4.5 A in a vacuum better than 10-6 torr. Triple filaments were out-gassed at 4.5 A at 10-5 torr for 5 minutes allowed to cool and further outgassed at 4.5 A for 5 minutes at 10-6 torr.

Sr and Nd are analysed on outgassed single Ta and triple Re/Ta filaments (Re centre filament) respectively. The Sr fraction is redissolved in about O.5ml H_20 and loaded into a

drop of H_3P0_4 on the centre of a single Ta filament using a micro-pipette. A current is allowed to pass through the filament and is gradually increased until a dull red glow is observed. The current is increased very slowly to prevent the solution from spreading on the filament. When the filament begins to glow the phosphoric acid fumes off and the sample should remain close to the filament centre as it dries down.

Nd fractions are redissolved in a small drop of QD H_20 and carefully loaded on to the side filaments (Ta) of a triple filament. The current is increased slowly to dry down the solution.

Pb is loaded by dissolving the dried down sample in a small drop of phosphoric acid. Using a pipette tip a small drop of silica gel is placed on the centre of a single Re filament and the current is increased to about 0.45A. The silica gel is allowed to evaporate until it appears mushy, but not dry. The drop of phosphoric acid in which the sample has been dissolved is now loaded on to the silica gel and excess phosphoric acid is driven off by slowly increasing the current. When the filament begins to glow the current is slowly turned down. The filament is now ready for loading in the sample turret.

All sample loading is carried out in a laminar flow unit in a clean air laboratory. The loaded samples were placed in a 6 sample turret for the VG MS or a 13 sample magazine for the Finnigan MS. The VG MS turret was allowed to stand overnight in a vacuum oven at 80 °C over night before use. All analyses took place at $<10^{-7}$ torr and an accelerating potential of 8 kV.

A 6.2 Sr isotope measurement

Sr isotope abundances were measured with a beam intensity of 15 pA at a filament current of 2.5 A. Peaks were counted for four periods of 1.28 sec after which the magnet stepped to the next peak. The measurement cycle was 88, 87, 86, 85.5, 85, and 84. The 84 peak was eliminated after the first set of results and the 85 peak after the Rb contribution to the 87 peak was less than 0.01%. Peak intensities were measured using a double interpolation algorithm (Dobson, 1978) and were corrected for zero, dynamic memory, and Rb interferences where necessary. Mass fractionation was corrected for, by assuming that $^{86}Sr/^{88}Sr$=O.1194 and

that there is a linear dependence of mass fractionation on mass difference. The isotope ratios were stored as sets of 10 and mean and standard deviation of each set calculated. Sets which did not satisfy Chauvenet's criterion were rejected. Sets with total errors (1σ) of 100 ppm or more were rejected, those with error (1σ) in excess of 500 ppm were ignored. Chauvenet's criterion was then applied to all the accepted and rejected sets and the running mean calculated. The analysis continued till at least 100 ratios had been excepted and the error (1σ) was 20 ppm or less. Repeat analyses of NBS 987 standard were carried out and during this study averaged; $^{86}Sr/^{87}Sr$=0.710167, 1 std. deviation = 0.00053, 1 std. error = 0.000005. Total blanks for the period of this study were 1.6ng/g Sr.

A 6.3 Nd isotope measurement

Nd measurements were made on both the VG MS and the Finnigan MS. On the VG MS Nd measurements and data reduction was similar to that for Sr. Measurements were made with a 144 beam intensity of 7 pA with a centre filament current of 3.9 A and a side filament current of 2 A. The measuring cycle was 146, 144, 143, 142.5, 142, and 147. The 142 peak was eliminated after the first set and the 147 peak was eliminated when Sm contribution to the 144 peak was less than 0.01%. Mass fractionation was corrected by assuming linear dependence on mass difference and that $^{146}Nd/^{144}Nd$=0.7219. Sets were rejected when the error (1σ) was 100 ppm or worse and ignored when it was greater than 500 ppm. Analysis was continued until at least 200 ratios were accepted and the error (1σ) was 10 ppm or less.

On the Finnigan MS simultaneous measurements of the intensities of the 143, 144, 146, and 147 peaks were made. Data collection was initiated once the 144 beam intensity reached 5 pA. Data was collected in sets of 10 isotope ratios to which the Dixon rejection test was applied up to 1 group of ratios was dropped from the set if the test was failed. Ten sets were collected. A running value and associated error was calculated on the accumulated sets. Final values and associated errors are the product of between 90 and 100 measurements of the isotope ratios.

The standard J&M Std. was used as to correct instrumental drift on both machines and all FM MS (J&M Std.= 0.51) data was corrected to a J&M Std. value of 0.51 for the period of study for the VG MS. Average total Nd blanks for the period of this study were 2.97ng/g Nd.

A 6.4 Pb isotope measurement

Pb analyses using the FM MS are carried out in static mode (as opposed to the peak switching of the VG MS), and at a fixed temperature of 1100°C. No correction for fractionation is made to the $^{206}Pb/^{204}Pb$, $^{207}Pb/^{204}Pb$ and $^{208}Pb/^{204}Pb$ ratios during the run. Fractionation was monitored and amended by repeated measurement of the NBS 981 standard and normalising values to $^{206}Pb/^{204}Pb = 16.937$,$^{207}Pb/^{204}Pb = 15.491$ and $^{208}Pb/^{204}Pb = 36.700$. A run is terminated when at least 60 ratios are accumulated and the error is < 100ppm (2σ) on $^{207}Pb/^{204}Pb$.

A 7 Data presentation

For the principals of isotope systematics, the reader is referred to Faure (1977) and Hawkesworth and van Calsteren (1984).

A 7.1 Sr and Nd isotope data presentation

Age corrections to obtain the initial $^{87}Sr/^{86}Sr$ and $^{143}Nd/^{144}Nd$ isotope ratios ($(^{87}Sr/^{86}Sr)_o$ and $(^{143}Nd/^{144}Nd)_o$) have been made using the isochron equation below:

$$(^{87}Sr/^{86}Sr)_o = (^{87}Sr/^{86}Sr) - (e^{\lambda t} - 1)\ ^{87}Rb/^{86}Sr$$

$$(^{143}Nd/^{144}Nd)_o = (^{143}Nd/^{144}Nd) - (e^{\lambda t} - 1)\ ^{147}Sm/^{143}Nd$$

In several diagrams Sr and Nd data have been reported using the ε notation of DePaolo and Wasserberg (1976), defined as:

$$\varepsilon_{Nd} = \left\{(^{143}Nd/^{144}Nd)_t / (^{143}Nd/^{144}Nd)_{CHUR,\,t} - 1\right\} \times 10^4$$

$$\varepsilon_{Sr} = \left\{ (^{87}Sr/^{86}Sr)_t / (^{87}Sr/^{86}Sr)_{B.E.,\,t} - 1 \right\} \times 10^4$$

Model ages are reported relative to a depleted mantle (DM):

$$T_{DM}^{Nd} = 1/\lambda \ln \left\{ \frac{^{143}Nd/^{144}Nd_{sample} - ^{143}Nd/^{144}Nd_{DM}}{^{147}Sm/^{144}Nd_{sample} - ^{147}Sm/^{144}Nd_{DM}} + 1 \right\}$$

$$T_{DM}^{Sr} = 1/\lambda \ln \left\{ \frac{^{87}Sr/^{86}Sr_{sample} - ^{87}Sr/^{86}Sr_{DM}}{^{87}Rb/^{86}Sr_{sample} - ^{87}Rb/^{86}Sr_{DM}} + 1 \right\}$$

Where:

$\lambda^{147}Sm$	=	$6.54 \times 10^{-12}\ a^{-1}$	$\lambda^{87}Rb$	=	$1.42 \times 10^{-11}\ a^{-1}$
$^{143}Nd/^{144}Nd_{CHUR}$	=	0.51264	$^{87}Sr/^{86}Sr_{B.E.}$	=	0.7047
$^{147}Sm/^{144}Nd_{CHUR}$	=	0.1967	$^{87}Rb/^{86}Sr_{B.E.}$	=	0.0847
$^{143}Nd/^{144}Nd_{DM}$	=	0.51310	$^{87}Sr/^{86}Sr_{DM}$	=	0.70306
$^{147}Sm/^{144}Nd_{DM}$	=	0.2238	$^{87}Rb/^{86}Sr_{DM}$	=	0.0487

A 7.2 Presentation of Pb isotope data

The three decay schemes that result in Pb isotopes and their decay constants are as follows:

U^{238} decays to ^{206}Pb	$\lambda_1 = 1.55125 \times 10^{-10}$
U^{235} decays to ^{207}Pb	$\lambda_2 = 9.8485 \times 10^{-10}$
Th^{236} decays to ^{207}Pb	$\lambda_3 = 4.475 \times 10^{-11}$

A 7.2.1 Age correction

Initial ratios are calculated knowing the U, Th, and Pb concentrations using the three isochron equations below:

$$(^{206}Pb/^{204}Pb)_o = (^{206}Pb/^{204}Pb) - (e^{\lambda_1 t} - 1)\ ^{238}U/^{204}Pb$$

$$(^{207}Pb/^{204}Pb)_o = (^{207}Pb/^{204}Pb) - (e^{\lambda_2 t} - 1)\ ^{235}U/^{204}Pb$$

$$(^{208}Pb/^{204}Pb)_o = (^{208}Pb/^{204}Pb) - (e^{\lambda_3 t} - 1)\ ^{232}Th/^{204}Pb$$

In order to use these equations, it is necessary to calculate $^{238}U/^{204}Pb$, $^{235}U/^{204}Pb$, and $^{232}Th/^{204}Pb$. The equations for these ratios are:

$$^{238}U/^{204}Pb = (Uppm / Pbppm) \times (\text{atomic wt.Pb}/238.03) \times (99.27 / \%\ ^{204}Pb)$$

where 238.03 is the atomic wt. of U and 99.27 is the percentage of ^{238}U.

$$^{235}U/^{204}Pb = (^{238}U/^{204}Pb) / 137.88$$

$$^{232}Th/^{204}Pb = (Thppm/Pbppm).(\text{atomic wt.Pb}/232.038).(99.27 / \%\ ^{204}Pb)$$

where 232.038 is the atomic wt. of Th and 100 is the percentage of 232Th.

Clearly, the percentage of ^{204}Pb in each sample must be calculated. Using the fractionation corrected $^{206}Pb/^{204}Pb$, $^{207}Pb/^{204}Pb$ and $^{208}Pb/^{204}Pb$ ratios, it is possible to calculate the percentages of ^{204}Pb, ^{206}Pb,^{207}Pb and ^{208}Pb.

Strictly, because the atomic weight of Pb depends on the abundances of the isotopes (which of course changes from sample to sample), calculation of the atomic weight of the lead in each sample is made, although the difference is likely to be within error.

A 7.2.2 Fractionation correction

Two types of error are introduced into the measured $^{206}Pb/^{204}Pb$, $^{207}Pb/^{204}Pb$ and $^{208}Pb/^{204}Pb$ lead ratios obtained by mass spectrometry. The first is caused by mass fractionation and the second by the small size of the 204 peak relative to the 206, 207 and 208 peaks.

Mass fractionation can be approximated by the linear relation:

$$R = Rm\ (1 + \varepsilon\delta m)$$

where: R = the true value (of say $^{208}Pb/^{204}Pb$)

Rm = the measured value

ε = a mass discrimination coefficient per mass unit

δm = the mass difference between the two isotopes (e.g. 208-204 = 4)

Mass fractionation occurs during the measurement of Sr and Nd isotopic ratios as well, but these were normalised to a fixed ratio (e.g. $^{86}Sr/^{88}Sr = 0.1194$). With Pb this was not possible, so the standard (NBS 981) was measured numerous times and the average displacement from the true values of $^{206}Pb/^{204}Pb$, $^{207}Pb/^{204}Pb$ and $^{208}Pb/^{204}Pb$ was calculated. The amount of displacement from the true value varies from person to person, but consistent loading results in a reasonably tight cluster of points as illustrated below.

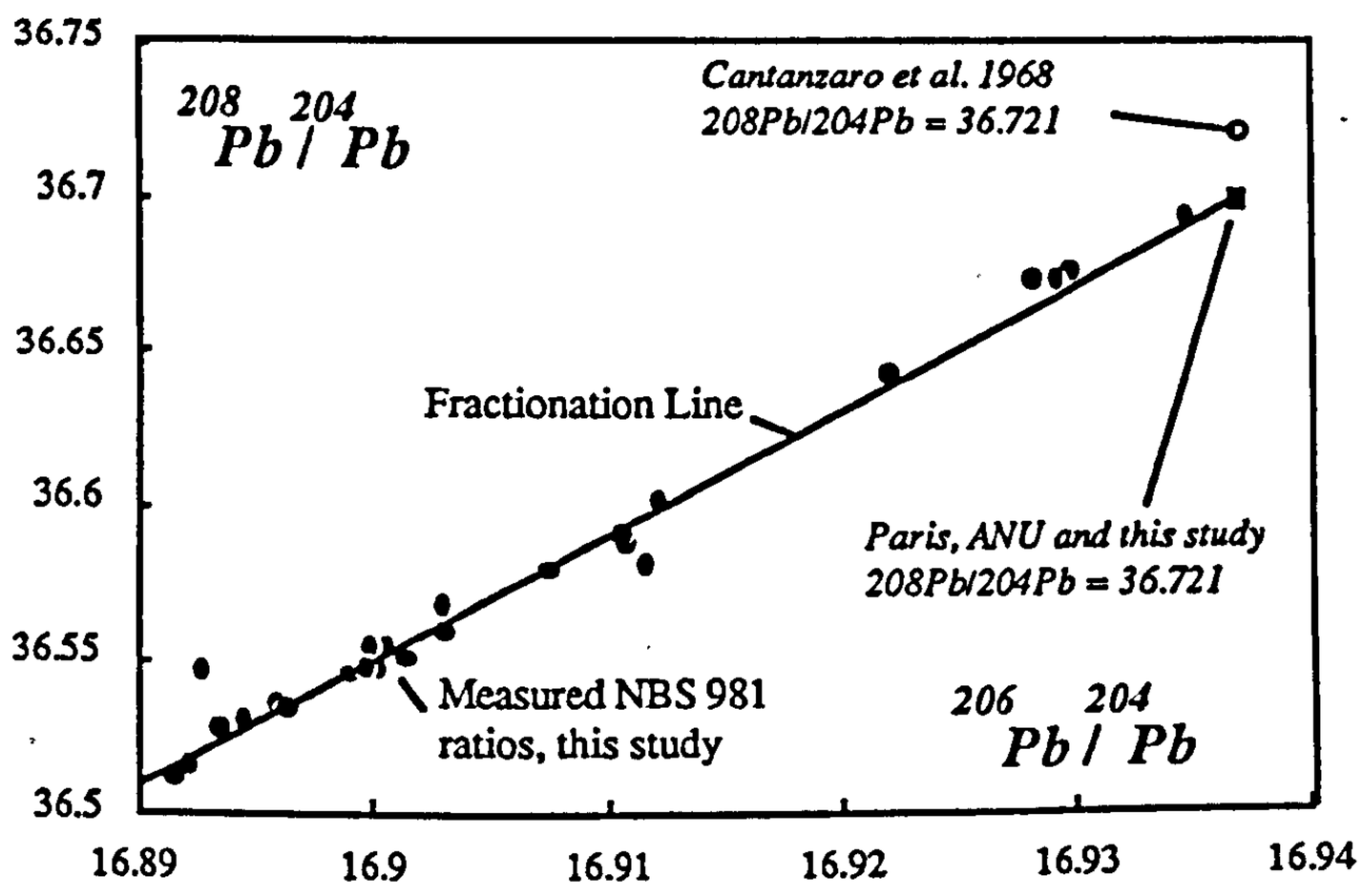

Figure A.1. The measured NBS 981 analyses from this study and the fractionation line from the value of $^{208}Pb/^{204}Pb$ from Cantanzaro et al. (1968) and the value used in this study.

This factor was then used to correct the ratios of the samples assuming that they behaved in the same way. The slope of the fractionation line is a function of the mass difference between the ratios and the absolute values of the ratios. Therefore the mass difference and $^{208}Pb/^{204}Pb$ ratio compound to produce a fractionation slope of approximately 4 (i.e. slope = R1/R2 x δm1/δm2, which for $^{208}Pb/^{204}Pb$ (R1 = 36.721, δm1 = 4) versus $^{206}Pb/^{204}Pb$ (R2 = 16.937, δm2 = 2) gives: 4.34). In contrast, the $^{207}Pb/^{204}Pb$ ratio is almost 1 so the slope of the fractionation line on a $^{207}Pb/^{204}Pb$ versus $^{206}Pb/^{204}Pb$ diagram is simply the ratio of the mass differences ie. ~3/2. Given the dependence of the slope of the fractionation line on the values of $^{206}Pb/^{204}Pb$, $^{207}Pb/^{204}Pb$ and $^{208}Pb/^{204}Pb$, each sample will fractionate along a line of different slope. The standard NBS 981 used was prepared to give

ratios that simulate those of a geologically reasonable sample. The slight variation in slope for different samples is negligible and such small differences can be ignored (see figure A1).

The value of ε in the equation above gives the measure of fractionation from the true value. Each time NBS 981 was measured there was the potential to gain 3 estimates of this coefficient for a particular run. Solution of the equation above for each ratio on every standard run produces equal values for ε based on $^{206}Pb/^{204}Pb$, $^{208}Pb/^{204}Pb$, but lower values based on $^{207}Pb/^{204}Pb$.

However it has been recognised that the values for NBS 981 quoted in the above calculations from Cantanzaro et al. (1968), are incorrect. Two labs (Paris University and the Australian National University) suggest that the $^{208}Pb/^{204}Pb$ ratio of the standard is closer to 36.700 rather than 36.721 originally quoted by Catanzaro et al (1968). Given that this is possibly true, recalculation of the ε values of the standard run data produces near equal values of ε based on all three of the ratios $^{206}Pb/^{204}Pb$, $^{207}Pb/^{204}Pb$ and $^{208}Pb/^{204}Pb$. Therefore the use of $^{208}Pb/^{204}Pb = 36.700$ is justified and adopted in this study. Only the ε value based on $^{206}Pb/^{204}Pb$ is slightly high indicating that perhaps the measured $^{206}Pb/^{204}Pb$ is a little low (figure A 2).

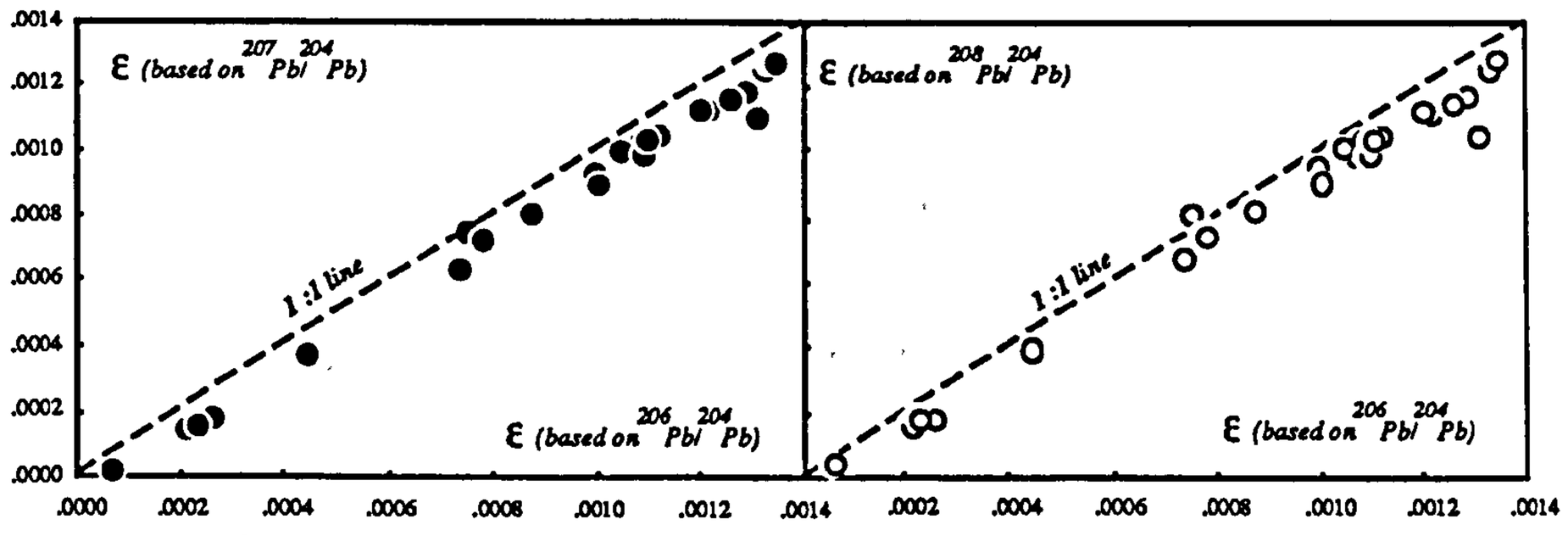

Figure A.2. Diagram of mass discrimination coefficient per unit mass unit for each of the measured Pb isotope ratios showing that the $^{206}Pb/^{204}Pb$ ratios may be a little high.

Having checked the above arguments, in practise, it was more convenient simply to normalise the measured standard ratios to the true values giving factors that were used to correct the measured ratios of the samples.

	Quoted values	Average NBS 981	Fractionation Correction
$^{206}Pb/^{204}Pb$	16.937	16.9064	1.001811
$^{207}Pb/^{204}Pb$	15.4405	15.4530	1.002462
$^{208}Pb/^{204}Pb$	36.721	36.5779	1.003338

Table A.3 Fractionation factors used to correct measured Pb isotopic ratios, after Cantanzaro et al. (1968).

The second type of error associated with Pb data was caused by the small size of the 204 peak relative to 206, 207 and 208 peaks. If the beam intensity is low, then the measurement of 204 is subject to larger errors and therefore the $^{206}Pb/^{204}Pb$, $^{207}Pb/^{204}Pb$ and $^{208}Pb/^{204}Pb$ ratios will inherit this error. Because the heavier isotopes are divided by 204, when we plot diagrams of $^{207}Pb/^{204}Pb$ and $^{208}Pb/^{204}Pb$ versus $^{206}Pb/^{204}Pb$, the errors are correlated and define a line. If the beam is too low, the 204 peak will be subject to large uncertainties that will be inherited into the the measured ratios. Therefore runs with low and variable beam intensity are discarded from the data set.

A 7.2.3 The age significance of Pb data

The fundamental relationship between time and the slope of a line defined by data on a $^{207}Pb/^{204}Pb$ versus $^{206}Pb/^{204}Pb$ diagram may be illustrated by consideration of the following equations. The equation of an isochron on a $^{207}Pb/^{204}Pb$ versus $^{206}Pb/^{204}Pb$ diagram is:

$$\frac{^{207}Pb/^{204}Pb - (^{207}Pb/^{204}Pb)_o}{^{206}Pb/^{204}Pb - (^{206}Pb/^{204}Pb)_o} = \frac{1}{137.8} x \frac{e^{\lambda_2 tn-1} - e^{\lambda_2 n}}{e^{\lambda_1 tn-1} - e^{\lambda_1 n}}$$

where o refers to the initial lead isotopic compositions and λ_1 and λ_2 are the decay constants of U^{238} and U^{235} respectively. The slope of the line (isochron) is defined by:

$$\frac{1}{137.8} x \frac{e^{\lambda_2 tn-1} - e^{\lambda_2 n}}{e^{\lambda_1 tn-1} - e^{\lambda_1 n}}$$

however,

$$\frac{^{207}Pb/^{204}Pb - (^{207}Pb/^{204}Pb)_o}{^{206}Pb/^{204}Pb - (^{206}Pb/^{204}Pb)_o} = (^{207}Pb/^{206}Pb)^*$$

where $(^{207}Pb/^{206}Pb)^*$ is the ratio of radiogenic ^{206}Pb.

Therefore: $$(^{207}Pb/^{206}Pb)^* = \frac{1}{137.8} \times \frac{e^{\lambda_2 tn-1} - e^{\lambda_2 n}}{e^{\lambda_1 tn-1} - e^{\lambda_1 n}}$$

Compatible values of t and $(^{207}Pb/^{206}Pb)^*$ have been deduced by Stacey and Stern (1973) so that t can be calculated from the slope of the isochron.

A.8 Standard rock and mineral analyses

A.8.1 Major element mineral compositions used in modelling

The following mineral analyses were taken from the literature as representative of those occurring in the Idaho batholith magmas and those assumed for the sources of the magmas. Care was taken to use compositions from solid-solution series most applicable to the paragenesis of the mineral in question.

	Lab	And	Oli	Ksp	Bt	Hb	Gt	Cpx	Opx	Sph	Mgt	Ilm	Apa
SiO_2	52.96	58.1	64.1	65.58	37.17	44.99	38.69	48.9	50.08	30.44	0.27	0.051	
Al_2O_3	29.72	26.4	22.66	19.58	14.60	11.21	18.17	3.86	1.23		0.21		
TiO_2					3.14	1.46	0.55	0.12	0.64	39.66		50.02	
FeO	0.84	0.19	0.2	0.21	30.6	16.5	9.48	29.32	2.34	0.14	99.98	46.37	0.21
MgO		0.03	0.25	0.12	4.23	10.41	0.76	6.87	15.78			0.46	0.54
CaO	12.28	7.84	3.26	0.49	0.17	12.11	31.76	7.96	1.44	27.20		0.71	52.4
Na_2O	4.21	6.48	9.89	5.9	0.15	0.97		0.58	0.05	0.37			
K_2O	0.13	1.1	0.05	7.88	8.25	0.76		0.2	0.02				
MnO					0.06	0.31	0.64	0.51	0.85	0.05		1.44	1.52
P_2O_5													40.98

Table A.4 Major element compositions of minerals used in major element modelling and mass-balance calculations. Analyses are all taken from Deer et al. (1966) for the rocks types and tables listed below:

Labradorite (Lab)	(Table 31, 5)	Basalt, Utah.
Andesine (And)	(Table 31, 4)	Antiperthite, two pyroxene granulite, Madras.
Oligoclase (Oli)	(Table 31, 3)	Pegmatite, Kenya.
Alkali feldspar (Ksp)	(Table 30, 5)	Microcline, perthite, nepheline syenite, Korea.
Biotite (Bt)	(Table18, 6)	Biotite granite, Southern California.
Hornblende (Hb)	(Table 15, 7)	Hornblende tonalite Idaho.
Garnet (Gt)	(Table 4, 3)	Brownish red grossular, garnet gneiss Madras.
Clinopyroxene (Cpx)	(Table 13, 9)	Sub-calcic ferroaugite, andesite, Japan.
Orthopyroxene (Opx)	(Table 13, 2)	Ferrohypersthene-diopside-plagioclase hornfels, Norway.
Sphene (Sph)	(Table 3, 1)	Nepheline syenite, USSR.
Magnetite (Mgt)	(Table 46, 5)	Titaniferous magnetite, gabbro, Skaergaard.
Ilmenite (Ilm)	(Table 44,1)	Fayalite ferrogabbro, Skaergaard.
Apatite (Ap)	(Table 50,1)	Quartz diorite, Japan.

A.8.2 Major and trace element composition of average rock types used in modelling

The average rock compositions in Table A.5 are after Taylor and Mclennan (1985).

	Andesite	Bulk Crust	Upper Crust	Lower Crust	Oceanic Crust
SiO_2	58	57.3	66	54.4	49.5
TiO_2	0.8	0.9	0.5	1	1.5
Al_2O_3	18	15.9	15.2	16.1	16
FeO	7.5	9.1	4.5	10.6	10.5
MgO	3.5	5.3	2.2	6.3	7.7
CaO	7.5	7.4	4.2	8.5	11.3
Na_2O	3.5	3.1	3.9	2.8	2.8
K_2O	1.5	1.1	3.4	0.34	0.15
Li	10	13	20	11	10
Be	1.5	1.5	3	1	0.5
B		10	15	8.3	4
Na	2.6	2.3	2.89	2.08	2.08
Mg	2.11	3.2	1.33	3.8	4.64
Al	9.5	8.41	8.04	8.52	8.47
Si	27.1	26.77	30.8	25.42	23.1
K	1.25	0.91	2.8	0.28	1250
Ca	5.36	5.29	3	6.07	8.08
Sc	30	30	11	36	38
Ti	4800	5400	3000	0.6	0.9
V	175	230	60	285	250
Cr	55	185	35	235	270
Mn	1100	1400	600	1670	1000
Fe	5.83	7.07	3.5	8.24	8.16
Co	25	29	10	35	47
Ni	30	105	20	135	135
Cu	60	75	25	90	86
Zn		80	71	83	85
Rb	42	32	112	5.3	2.2
Sr	400	260	350	230	130
Y	22	20	22	19	32
Zr	100	100	190	70	80
Nb	11	11	25	6	2.2
Ag		80	50	90	26
Sn		2.5	5.5	1.5	1.4
Cs	1.7	1	3.7	0.1	30
Ba	350	250	550	150	25
La	19	16	30	11	3.7
Ce	38	33	64	23	11.5
Pr	4.3	3.9	7.1	2.8	1.8
Nd	16	16	26	12.7	10
Sm	3.7	3.5	4.5	3.17	3.3
Eu	1.1	1.1	0.88	1.17	1.3
Gd	3.6	3.3	3.8	3.13	4.6
Tb	0.64	0.6	0.64	0.59	0.87
Dy	3.7	3.7	3.5	3.6	5.7
Ho	0.82	0.78	0.8	0.77	1.3
Er	2.3	2.2	2.3	2.2	3.7
Tm	0.32	0.32	0.33	0.32	0.54
Yb	2.2	2.2	2.2	2.2	5.1
Lu	0.3	0.3	0.32	0.29	0.56
Hf	3	3	5.8	2.1	2.5
Ta		1	2.2	0.6	0.3
Au		3	1.8	3.4	0.23
Pb	10	8	20	4	0.8
Th	4.8	3.5	10.7	1.06	0.22
U	1.25	0.91	2.8	0.28	0.1

Table A.5 Average rock compositions after Taylor and McLennan (1985).

APPENDIX B

Major element, Trace element, Rare-earth element, Isotope analyses and Granite Norm Data

This section contains all the analytical data (with the exception of the Pb isotope analysis on alkali feldspar mineral separates) that has been generated during this study. The samples are arranged into groups of similar rock types which are coded as follows:

Cretaceous Granitoids

Kt	Tonalite
Kgdh	Hornblende-biotite granodiorite
Kgdp	Porphyritic granodiorite
Kgd	Biotite granodiorite
Kg	Muscovite-biotite granodiorite
Klg	Leucogranite

Tertiary Granitoids

Tgd	Dioritic suite
Tg	Granitic suite

Sample locations are given in degrees, minute and second notation (X°, Y', Z") latitude (north) and longitude (west) and the name of the locality or sample traverse given some of which are coded as follows:

ALVT	Alice Lake Sawtooths to Vienna mining district traverse.
LGPT	Long Gulch Pluton traverse, South Fork of the Payette River.
EFSR	East Fork of the Salmon River, East of Stanley.
NW	Northwest Atlanta lobe.

The major elements are expressed as oxides with totals and loss on ignitions (LOI). The degree of alumina saturation (A/CNK) is expressed as mol% (Al_2O_3 / $CaO+Na_2O+K_2O$). The trace elements are expressed as parts per million (ppm) with those measured by XRF (Ba-Y) listed above those measured by INAA. The Sr, Nd and Pb isotope ratios are the measured values uncorrected for age, but the Pb results are corrected for mass fractionation (see appendix A).

Sample names prefixed by: "CBC87-" were collected during this study. Those prefixed by: "L86-" were whole rocks kindly donated by W. P. Leeman and those designated "86RL-" were supplied by Reed Lewis as whole rocks and powders.

The second section of the appendix B contains the results of the Grannorm calculations written by N. B. W. Harris which gives a fair representation of the modal mineralogy of each granitoid sample.

Sample	CBC87-145	CBC87-40	CBC87-51	CBC87-54	CBC87-55	CBC87-61	CBC87-75
Rock type	Kt	Kt	Kt	Kt	Kt	Kt	Kt
Locality	EFSR	Jumbo.Crk.	Banks	Payette Lk.	LickCrk.Rd.	Fischer Crk.	LickCrk.Rd.
Lat.(°N)	44°13'50"	43°36'00"	44°10'00"	45°01'40"	45°01'00"	45°05'15"	44°55'00"
Long.(°W)	114°42'00"	115°02'30"	116°38'15"	116°03'00"	115°57'00"	116°01'20"	115°59'30"
SiO_2	54.58	64.05	64.24	61.53	63.25	59.17	62.9
Al_2O_3	21.18	16.18	16.44	16.36	16.36	18.44	16.97
TiO_2	0.59	0.73	0.88	0.89	0.89	0.81	0.83
Fe_2O_3	4.85	4.73	4.79	6.07	6.07	5.75	5.33
MgO	3.67	2.16	1.9	2.94	2.94	3.04	2.12
CaO	9.64	4.8	4.67	5.67	5.67	6.47	5.44
Na_2O	2.24	3.86	3.8	3.18	3.18	3.91	3.22
K_2O	1.72	2.04	2.21	2.08	2.08	1.48	1.85
MnO	0.08	0.11	0.07	0.1	0.1	0.07	0.1
P_2O_5	0.14	0.23	0.28	0.25	0.25	0.24	0.27
LOI	0.96	0.69	0.59	0.71	0.71	0.59	0.87
Total	99.66	99.56	99.86	99.76	99.76	99.96	99.9
A/CNK	0.92	0.94	0.96	0.92	0.92	0.93	0.99
Ba	363	875	850	976	1309	1020	1067
Ce	19	56	82	54	55	7	67
Co	14	10	14	12	11	15	14
Cr	11	30	342	13	30	15	16
Cu	9	4	14	3	1	5	4
La	19	30	40	32	30	18	15
Nb	18	24	24	15	14	10	18
Nd	8	22	31	18	34	12	24
Ni	7	6	8	4	6	8	4
Pb	7	11	10	13	10	15	13
Rb	77	73	73	65	55	41	83
Sm	3	7	14	11	18	15	15
Sr	833	646	746	638	766	902	779
Th	10	7	7	14	2	3	7
U	1	1	2	1	1	1	1
V	76	83	80	127	93	97	95
Zn	51	83	100	89	97	85	103
Zr	101	174	238	154	131	136	224
Y	16	18	21	15	23	15	20
La	26.52		52.75	46.48	27.67	17.21	40.98
Ce	49.22		104.5	83	61.35	35.39	75.34
Nd	20.99		44.27	31.98	37.95	19.44	31.68
Sm	4.016		8.05	5.51	8.408	3.827	5.354
Eu	1.162		1.89	1.41	1.905	1.269	1.407
Gd	6.752				43.01		67.61
Tb	0.4328		0.89	0.603	1.005	0.4525	0.6547
Ho				1.444			1.49
Tm				0.264	0.3081	0.2127	
Yb	1.19		1.49	1.22	1.482	1.091	1.189
Lu	0.1785		0.299	0.175	0.2273	0.1496	0.1678
Th	8.219		8.83	11.74	1.945	0.9869	6.128
U	2.408		1.03	0.796	0.8497	0.568	2.22
Ta	1.181		1.763	0.674	0.5873	0.3906	1.072
Hf	2.744		6.7	5.15	4.221	3.656	5.76
Cs	3.369		0.775	1.15	0.9022	0.7463	2.744
$^{87}Sr/^{86}Sr$	0.70761±3		0.70718±3	0.70884±4	0.70856±3	0.70740±3	0.70969±3
$^{143}Nd/^{144}Nd$	0.51206±5		0.51221±2	0.51218±3	0.51220±2	0.51230±4	0.51204±2
$^{206}Pb/^{204}Pb$	20.0850±51				19.2828±72		
$^{207}Pb/^{204}Pb$	15.7006±40				15.6568±58		
$^{208}Pb/^{204}Pb$	39.6216±90				39.033±15		

Sample	CBC87-144	L86-42	CBC87-39	86RL-309	86RL-387	CBC87-157	CBC87-69
Rock type	Kgdh	Kgdh	Kgdh	Kgdh	Kgdh	Kgdh	Kgdh
Locality	EFSR	EFSR	Dollarhide.	Soldier Mtn	Soldier Mtn	EFSR	Ddwd Mine
Lat.(°N)	44°14'00"	44°15'40"	43°36'45"	43°35'8"	43°33'55"	44°21'25"	44°28'20"
Long.(°W)	114°42'00"	114°46'50"	114°44'00"	114°57'55"	114°50'4"	114°44'00"	115°34'40"
SiO_2	63.85	64.06	66.52	66.86	67.28	68.63	72.4
Al_2O_3	15.75	16.43	14.86	15.31	15.78	14.51	14.45
TiO_2	0.82	0.8	0.6	0.81	0.75	0.53	0.34
Fe_2O_3	4.81	4.59	3.83	4.49	4.18	3.22	2.2
MgO	2.24	1.81	1.62	1.86	1.63	1.48	0.59
CaO	4.43	4.51	3.99	4.13	3.9	3.07	2.55
Na_2O	3.23	3.35	3.24	3.69	3.32	3.35	3.61
K_2O	3.26	2.75	3.1	2.51	2.77	3.39	3.19
MnO	0.08	0.07	0.08	0.07	0.06	0.07	0.04
P_2O_5	0.27	0.39	0.17	0.38	0.37	0.16	0.07
LOI	0.82		1.92			1.42	0.43
Total	99.75	100.49	99.92	100.7	100.53	99.83	99.89
A/CNK	0.93	0.98	0.93	0.94	1.01	0.98	1.03
Ba	983	1461	774	1513	1816	698	1408
Ce	77		46			28	48
Co	15	19	11	18	17	11	4
Cr	17	53	13	53	53	17	5
Cu	3	5	1	5	5	3	4
La	57		45			28	27
Nb	29	29	18	23.6	25.4	21	18
Nd	33		21			13	18
Ni	8	7	9	7	7	8	2
Pb	12	17	16	16	17	19	23
Rb	113	112	88	86	90	123	99
Sm	8		6			8	13
Sr	621	735	516	670	749	489	676
Th	17	23	16	15	11	18	14
U	2	4	1	3	3	4	1
V	88		74			71	20
Zn	68	87	63	87	81	47	65
Zr	172	236	133	250	236	132	198
Y	21	17	14	17	22	13	9

La	55.31
Ce	94.22
Nd	35.41
Sm	6.677
Eu	1.568
Gd	6.469
Tb	0.747
Ho	
Tm	
Yb	1.554
Lu	0.2421
Th	15.03
U	2.758
Ta	2.09
Hf	4.625
Cs	3.131

$^{87}Sr/^{86}Sr$	0.70790±4	0.70822±8	0.70749±3	0.70735±3	0.70792±3
$^{143}Nd/^{144}Nd$	0.51221±1	0.51222±2	0.51160±2	0.51220±3	0.51231±1
$^{206}Pb/^{204}Pb$					
$^{207}Pb/^{204}Pb$					
$^{208}Pb/^{204}Pb$					

Sample	CBC87-155	CBC87-150	CBC87-149	CBC87-159	CBC87-152	CBC87-62	CBC87-148
Rock type	Kgdp	Kgdp	Kgdp	Kgdp	Kgdp	Kgdp	Kgdp
Locality	EFSR	EFSR	EFSR	EFSR	EFSR	CapeHn.Rd	EFSR
Lat.(°N)	44°16'00"	44°16'00"	44°16'00"	44°19'06"	44°17'15"	44°21'30"	44°16'12"
Long.(°W)	114°49'45"	114°46'20"	114°46'40"	114°43'30"	114°47'20"	115°13'00"	114°44'30"
SiO_2	65.56	67.21	68.04	68.3	69.32	71.3	71.41
Al_2O_3	15.57	14.77	14.77	14.08	16.88	15.42	14.08
TiO_2	0.74	0.72	0.58	0.66	0.29	0.25	0.43
Fe_2O_3	3.94	3.73	3.04	3.74	1.99	1.7	2.7
MgO	1.45	1.44	1.16	1.91	0.5	0.39	0.92
CaO	4.28	3.55	3.42	3.25	2.29	1.88	2.32
Na_2O	3.14	3.62	3.52	2.97	5.47	4.46	3.57
K_2O	2.99	3.16	3.46	4.1	2.32	3.67	3.64
MnO	0.04	0.07	0.07	0.08	0.04	0.03	0.08
P_2O_5	0.23	0.25	0.18	0.18	0.08	0.09	0.16
LOI	2.21	1.06	1.44	0.66	0.71	0.61	0.43
Total	100.13	99.57	99.68	99.93	99.89	99.8	99.74
A/CNK	0.96	0.93	0.94	0.92	1.08	1.05	1.00
Ba	1360	722	942	824	964	1280	541
Ce	97	105	88	80	101	69	61
Co	9	9	4	8	2	2	3
Cr	17	11	11	38	18	5	7
Cu	1	1	3	1	6	1	1
La	57	60	43	54	50	54	38
Nb	30	29	28	30	33	16	35
Nd	37	33	37	30	32	24	22
Ni	3	6	4	7	2	3	6
Pb	18	15	16	18	12	22	21
Rb	87	139	120	137	74	92	144
Sm	14	14	13	1	8	14	12
Sr	707	638	677	532	1123	1157	497
Th	15	34	18	29	19	6	20
U	4	6	2	4	2	2	3
V	70	64	48	68	20	25	37
Zn	64	62	43	54	31	41	39
Zr	214	231	177	159	217	183	142
Y	16	14	12	22	12	13	15
La			57.83				43.07
Ce			96.06				69.37
Nd			38.01				29.39
Sm			6.09				5.384
Eu			1.45				1.196
Gd			61.76				
Tb			0.57				0.6281
Ho							
Tm							
Yb			1.03				1.241
Lu			0.187				0.2144
Th			23.78				32.04
U			4.54				7.302
Ta			1.95				2.515
Hf			5.07				4.383
Cs			3.03				3.737
$^{87}Sr/^{86}Sr$	0.70832±2	0.70780±4	0.70763±4	0.70757±3	0.70729±4		0.70739±2
$^{143}Nd/^{144}Nd$	0.51224±1	0.51227±2	0.51231±2		0.51219±1		0.51225±1
$^{206}Pb/^{204}Pb$							20.3885±11
$^{207}Pb/^{204}Pb$							15.7854±9
$^{208}Pb/^{204}Pb$							40.3254±22

Sample	CBC87-50	CBC87-151	CBC87-68	L86-45	CBC87-63	CBC87-35	CBC87-74
Rock type	Kgdp	Kgdp	Kgdp	Kgdh	Kgdh	Kgd	Kgd
Locality	W.Lowman.	EFSR	DeerCrk.Rd.	EFSR	Cape Horn	DeerCrk.Rd.	McCall
Lat.(°N)	44°05'00"	44°11'30"	44°24'30"	44°15'45"	44°21'00"	43°31'30"	44°45'00"
Long.(°W)	115°38'15"	114°45'30"	115°34'30"	114°46'00"	115°16'30"	114°28'00"	115°55'30"
SiO_2	71.98	72.45	73.43	66.73	71.48	66.98	67.32
Al_2O_3	15.1	13.15	14.98	15.95	15.25	14.99	15.92
TiO_2	0.19	0.46	0.17	0.71	0.25	0.66	0.64
Fe_2O_3	1.56	2.43	1.1	3.84	1.8	3.97	3.59
MgO	0.32	0.99	0.35	1.27	0.39	1.89	1.25
CaO	1.94	2.5	1.78	2.93	2.01	3.14	4.12
Na_2O	4.66	3.06	4.3	3.28	4.02	3.31	3.47
K_2O	2.94	3.76	3.1	3.75	3.62	3.95	2.41
MnO	0.02	0.06	0.03	0.06	0.05	0.08	0.05
P_2O_5	0.06	0.16	0.06	0.33	0.06	0.2	0.22
LOI	0.74	1.17	0.61		0.59	0.81	0.79
Total	99.51	100.18	99.92	100.22	99.52	99.97	99.77
A/CNK	1.05	0.96	1.10	1.08	1.08	0.97	1.01
Ba	1624	750	992	1024	1461	1107	1591
Ce	45	62	17		61	105	80
Co	2	9	6	17	2	15	9
Cr	5	21	5	52	5	14	9
Cu	2	2	1	5	4	10	5
La	18	48	4		38	76	45
Nb	16	19	13	32	8	33	16
Nd	16	19	6		26	28	22
Ni	2	10	2	8	3	14	2
Pb	20	21	18	16	26	21	15
Rb	66	143	93	155	72	167	70
Sm	5	5	1		1	1	10
Sr	706	550	724	608	1181	562	790
Th	3	21	5	32	16	37	11
U	1	5	1	7	1	6	1
V	9	40	15		27	65	48
Zn	41	45	39	70	34	68	82
Zr	126	153	92	249	201	239	243
Y	7	10	12	16	6	21	12
La	52.28						
Ce	85.3						
Nd	31.36						
Sm	5.2						
Eu	1.18						
Gd							
Tb	0.537						
Ho							
Tm							
Yb	0.677						
Lu	0.125						
Th	24.08						
U	5.327						
Ta	1.49						
Hf	4.59						
Cs	2.25						
$^{87}Sr/^{86}Sr$	0.70792±4	0.70846±12					0.70915±4
$^{143}Nd/^{144}Nd$	0.51229±2	0.51220±4					0.51215±2
$^{206}Pb/^{204}Pb$							
$^{207}Pb/^{204}Pb$							
$^{208}Pb/^{204}Pb$							

Sample	CBC87-99	CBC87-116	86RL-219	86RL-249	CBC87-87	CBC87137A	CBC87-147
Rock type	Kgd	Kgd	Kgd	Kgd	Kgd	Kgd	Kgd
Locality	LGPT	Wapiti Crk.	SoldierMtn	SoldierMtn	Sacajawa	ALVT	EFSR
Lat.(°N)	44°03'40"	44°08'15"	43°36'3"	43°33'10"	44°10'00"	43°50'20"	44°14'45"
Long.(°W)	114°44'45"	114°13'40"	114°58'40"	114°50'50"	115°11'00"	114°51'30"	114°42'15"
SiO_2	68.75	69.1	69.19	69.23	69.36	69.38	69.41
Al_2O_3	15.04	15.48	15.85	16.03	15.76	15.37	15.37
TiO_2	0.55	0.53	0.49	0.5	0.41	0.47	0.54
Fe_2O_3	2.76	2.86	2.93	3.12	2.76	2.7	2.89
MgO	1.15	0.9	0.83	0.79	0.74	0.8	1.08
CaO	2.4	3	3.01	3.03	3.17	2.78	3.14
Na_2O	4.18	3.9	3.45	3.9	4.09	3.73	3.62
K_2O	3.76	3.04	3.63	2.73	2.95	3.49	3.03
MnO	0.11	0.07	0.04	0.06	0.06	0.05	0.05
P_2O_5	0.2	0.18	0.24	0.26	0.14	0.15	0.17
LOI	1.19	0.48			0.54	0.69	0.61
Total	100.09	99.54	99.66	99.65	99.99	99.62	99.91
A/CNK	0.98	1.02	1.05	1.08	1.01	1.03	1.03
Ba	1284	767	1739	1410	1283	1491	1051
Ce	67	94			72	66	49
Co	10	3	15	15	4	6	8
Cr	9	9	52	50	7	8	10
Cu	38	2	5	5	1	4	4
La	37	44			51	49	35
Nb	16	30	19.5	16.3	23	23	20
Nd	27	32			30	33	25
Ni	14	9	7	7	2	4	2
Pb	17	20	17	17	15	16	10
Rb	146	121	89	67	80	109	83
Sm	9	2		19	6	11	4
Sr	774	612	690	776	706	719	902
Th	14	15	17	19	21	11	7
U	7	3	3	3	3	3	3
V	40	48			35	44	49
Zn	156	71	64	67	65	57	65
Zr	180	198	251	254	226	238	211
Y	9	18	15	13	18	16	21
La			75.41				
Ce			127.8				
Nd			47.82				
Sm			7.336				
Eu			1.685				
Gd							
Tb			0.6309				
Ho							
Tm							
Yb			1.161				
Lu			0.1669				
Th			18.47				
U			2.264				
Ta			2.265				
Hf			6.682				
Cs			1.049				
$^{87}Sr/^{86}Sr$	0.70741±2		0.70786±2	0.70778±3			0.70935±3
$^{143}Nd/^{144}Nd$			0.51229±2	0.51225±1			0.51216±1
$^{206}Pb/^{204}Pb$			19.544±7	19.3812±4			
$^{207}Pb/^{204}Pb$			15.881±58	15.6757±3			
$^{208}Pb/^{204}Pb$			40.053±100	39.3982±4			

Sample	CBC87-138	CBC87-81	CBC87-160	CBC87-126	CBC87-92	CBC87-136	CBC87-158
Rock type	Kgd	Kgd	Kgd	Kgd	Kgd	Kgd	Kgd
Locality	ALVT	Wt.Hrse.Rp	EFSR	ALVT	Wapiti Crk.	ALVT	EFSR
Lat.(°N)	43°50'30"	44°47'15"	44°17'30"	43°54'10"	44°8'50"	43°53'15"	44°19'10"
Long.(°W)	114°52'00"	115°32'15"	114°51'30"	114°54'55"	115°11'55"	114°55'50"	114°44'50"
SiO_2	69.42	69.83	70.13	70.37	70.5	70.73	70.81
Al_2O_3	15.34	14.77	15.73	15.51	15.91	15.4	15.3
TiO_2	0.47	0.45	0.41	0.37	0.12	0.36	0.38
Fe_2O_3	2.66	2.64	2.2	2.48	0.87	2.31	2.2
MgO	0.83	0.93	0.65	0.68	.0.1	0.65	0.77
CaO	2.8	2.93	2.69	2.43	1.65	2.41	2.63
Na_2O	3.76	3.12	4.1	4.22	5.48	4.22	3.95
K_2O	3.36	3.92	2.96	3.24	3.62	3.18	2.88
MnO	0.06	0.04	0.04	0.05	0.05	0.05	0.05
P_2O_5	0.14	0.13	0.13	0.12	0.03	0.12	0.12
LOI	0.71	1.01	0.74	0.51	1.63	0.54	0.77
Total	99.55	99.77	99.79	100	99.95	99.98	99.86
A/CNK	1.03	1.00	1.06	1.04	1.00	1.04	1.06
Ba	1250	1462	1160	1307	1655	1192	1243
Ce	81	87	78	93	20	73	91
Co	5	7	2	2	2	2	2
Cr	7	6	10	4	6	5	24
Cu	5	3	5	1	1	1	1
La	56	40	60	49	26	56	50
Nb	23	23	26	19	41	23	18
Nd	32	31	28	37	11	31	36
Ni	4	3	2	3	2	4	2
Pb	11	11	13	16	12	14	10
Rb	112	108	99	78	96	90	72
Sm	10	8	19	8	14	10	5
Sr	692	653	752	952	760	893	945
Th	17	20	18	13	10	14	12
U	1	4	3	2	3	1	2
V	57	45	28	33	7	34	42
Zn	57	43	41	53	34	59	45
Zr	230	170	256	233	117	228	223
Y	18	15	12	12	15	16	12
La			65.99				51.64
Ce			112.7				86.53
Nd			44.39				34.83
Sm			6.451				5.387
Eu			1.57				1.418
Gd							6.272
Tb			0.5453				0.4803
Ho							
Tm			0.2635				
Yb			1.044				0.9319
Lu			0.1628				0.1093
Th			12.12				7.333
U			1.484				1.609
Ta			1.061				1.006
Hf			6.025				5.509
Cs			0.812				1.089
$^{87}Sr/^{86}Sr$		0.70864±4	0.70819±4				0.70863±5
$^{143}Nd/^{144}Nd$		0.51222±2	0.51215±1			0.51221±1	0.51219±1
$^{206}Pb/^{204}Pb$							19.9710±22
$^{207}Pb/^{204}Pb$							15.7698±18
$^{208}Pb/^{204}Pb$							39.8972±45

Sample	CBC87-91	CBC87-135	CBC87-125	CBC87-161	CBC87-134	CBC87133A	CBC87-141
Rock type	Kgd	Kgd	Kgd	Kgd	Kgd	Kgd	Kgd
Locality	Wapiti Crk.	ALVT	ALVT	EFSR	ALVT	ALVT	EFSR
Lat.(°N)	44°8'30"	43°52'30"	43°55'06"	44°14'15"	43°53'40"	43°52'00"	44°15'00"
Long.(°W)	115°12'00"	114°54'30"	114°56'00"	114°54'30"	114°52'00"	114°55'00"	114°37'00"
SiO_2	70.88	71.23	71.34	71.43	71.46	71.5	71.63
Al_2O_3	15.2	14.92	15.09	14.87	14.94	14.79	14.95
TiO_2	0.32	0.32	0.27	0.18	0.33	0.31	0.33
Fe_2O_3	2.23	2.15	1.82	1.42	2.12	2.01	1.95
MgO	0.56	0.52	0.48	0.25	0.54	0.55	0.55
CaO	2.53	2.48	1.91	1.74	2.45	2.4	2.4
Na_2O	3.9	3.95	4.18	4.15	3.96	3.66	4.01
K_2O	3.41	3.36	3.82	3.62	3.52	3.678	3.04
MnO	0.06	0.04	0.06	0.03	0.04	0.04	0.02
P_2O_5	0.11	0.11	0.08	0.05	0.1	0.1	0.11
LOI	0.56	0.87	0.59	2.32	0.35	0.92	0.82
Total	99.76	99.94	99.63	100.04	99.82	99.96	99.8
A/CNK	1.03	1.02	1.04	1.07	1.01	1.03	1.05
Ba	1458	1244	1210	1702	1032	1101	970
Ce	84	99	61	48	65	60	75
Co	4	6	2	3	2	2	3
Cr	6	9	6	4	6	6	8
Cu	14	3	1	1	2	3	4
La	45	45	35	31	45	45	38
Nb	23	22	19	25	23	20	18
Nd	26	39	27	23	26	24	31
Ni	5	2	4	4	6	2	2
Pb	17	18	17	19	16	17	15
Rb	111	87	97	120	96	89	76
Sm	12	14	11	1	5	13	19
Sr	885	816	854	615	797	695	847
Th	14	11	16	12	14	13	14
U	1	3	1	2	2	1	1
V	28	25	23	16	27	28	33
Zn	53	50	42	17	47	48	43
Zr	201	217	181	143	220	208	197
Y	16	13	9	18	11	14	11
La		44.48		59.29	47.93	43.88	
Ce		76.58		100.5	77.79	75.78	
Nd		28.91		39.01	31.37	30.37	
Sm		4.24		5.7	5.162	4.47	
Eu		1.25		1.412	1.387	1.2	
Gd							
Tb		0.483		0.529	0.4761	0.371	
Ho							
Tm							
Yb		0.759		0.8323	0.7352	0.636	
Lu		0.122		0.1294	0.1223	0.113	
Th		10.12		11.94	11.38	8.15	
U		1.36		2.875	1.976	2.64	
Ta		0.69		0.9929	0.9172	0.979	
Hf		4.57		5.537	5.181	4.97	
Cs		1.307		1.325	2.207	1.73	
$^{87}Sr/^{86}Sr$	0.70783±3	0.70863±3	0.71201±5	0.70798±3	0.70791±4	0.70865±3	
$^{143}Nd/^{144}Nd$	0.51219±2	0.51212±3	0.51170±1	0.51207±2	0.51223±1	0.51212±2	
$^{206}Pb/^{204}Pb$				19.8387±26			
$^{207}Pb/^{204}Pb$				15.7415±21			
$^{208}Pb/^{204}Pb$				39.7643±53			

Sample	CBC87-106	CBC87-56	CBC87-111	CBC87-156	CBC87-109	CBC87-93	CBC87-97
Rock type	Kgd	Kgd	Kgd	Kgd	Kgd	Kgd	Kgd
Locality	LGPT	LickCrk.Rd.	LGPT	EFSR	LGPT	LGPT	LGPT
Lat.(°N)	44°03'35"	44°59'00"	44°03'30"	44°17'20"	44°03'50"	44°03'30"	44°03'25"
Long.(°W)	115°43'00"	115°57'20"	115°45'00"	114°43'20"	115°42'30"	114°40'00"	114°42'15"
SiO_2	71.73	71.73	71.8	71.83	71.85	71.88	71.89
Al_2O_3	15.41	15.11	14.89	14.89	15.35	15.47	15.39
TiO_2	0.18	0.31	0.16	0.29	0.18	0.19	0.17
Fe_2O_3	1.42	1.95	1.48	1.74	1.47	1.51	1.45
MgO	0.31	0.61	0.33	0.5	0.3	0.33	0.33
CaO	1.9	2.62	1.69	1.91	1.87	2	1.97
Na_2O	4.88	3.97	4.56	4.05	4.65	4.82	4.72
K_2O	3.05	2.69	3.63	3.77	3.28	3.17	3.23
MnO	0.04	0.03	0.05	0.06	0.04	0.04	0.04
P_2O_5	0.05	0.07	0.04	0.08	0.03	0.05	0.05
LOI	0.74	0.61	1.15	0.76	0.81	0.54	0.38
Total	99.72	99.71	99.78	99.87	99.84	99.99	99.63
A/CNK	1.04	1.06	1.03	1.05	1.05	1.03	1.04
Ba	1527	1372	1599	1229	1702	1701	1477
Ce	24	51	54	48	35	50	31
Co	5	4	2	2	4	2	2
Cr	6	7	10	6	5	8	7
Cu	4	3	18	2	1	2	3
La	28	34	26	43	32	23	26
Nb	20	15	17	24	18	20	19
Nd	16	19	13	24	16	16	20
Ni	5	4	4	2	2	2	2
Pb	20	15	21	15	17	17	15
Rb	70	78	93	104	73	69	71
Sm	11	8	5	3	2	1	5
Sr	743	776	602	793	704	701	667
Th	11	11	10	10	7	7	9
U	1	1	2	5	1	1	1
V	10	22	14	21	11	12	14
Zn	43	37	19	52	46	35	45
Zr	124	184	116	165	124	136	129
Y	8	11	10	14	8	9	7

La	35.09	28.1	40.61
Ce	61.36	46.7	69.01
Nd	23.11	19.6	30.67
Sm	3.773	3.15	5.26
Eu	1.059	0.93	1.35
Gd	5.061		
Tb	0.3663	0.3	0.541
Ho			2.63
Tm			
Yb	0.7008	0.7	1.136
Lu	0.1244	0.15	0.17
Th	6.967	6.3	10.13
U	1.635	3.36	3.01
Ta	0.8643	0.94	1.41
Hf	3.871	3.21	4.1
Cs	2.515	1.4	1.21

$^{87}Sr/^{86}Sr$	0.70868±2	0.70936±4	0.70914±4	0.70735±6	0.70738±4	0.70919
$^{143}Nd/^{144}Nd$	0.512047±1	0.51206±1	0.51219±4			0.51225±5
$^{206}Pb/^{204}Pb$	19.0778±3					
$^{207}Pb/^{204}Pb$	15.7022±3					
$^{208}Pb/^{204}Pb$	39.4875±6					

Sample	CBC87-127	CBC87-96	CBC87-124	CBC87-47	L86-20	CBC87-114	CBC87-112
Rock type	Kgd	Kgd	Kgd	Kgd	Kgd	Kgd	Kgd
Locality	ALVT	LGPT	ALVT	MFBR	Soldier Mtn	LGPT	LGPT
Lat.(°N)	43°53'45"	44°03'20"	43°55'20"	43°47'15"	43°28'20"	44°02'00"	44°03'35"
Long.(°W)	114°54'15"	114°41'55"	114°56'30"	115°25'30"	114°45'30"	115°45'00"	115°45'20"
SiO_2	71.9	71.9	71.93	71.96	71.96	72.03	72.04
Al_2O_3	14.71	15.18	15.02	14.71	15.35	15.46	15.13
TiO_2	0.26	0.18	0.24	0.21	0.33	0.19	0.17
Fe_2O_3	1.91	1.45	1.36	1.8	2.01	1.44	1.34
MgO	0.47	0.33	0.34	0.5	0.58	0.34	0.35
CaO	1.88	1.83	1.56	1.85	2.05	1.56	1.6
Na_2O	3.97	4.7	4.17	4.49	3.99	4.66	4.55
K_2O	3.8	3.22	4.28	3.23	3.8	3.35	3.65
MnO	0.04	0.02	0.04	0.07	0.06	0.06	0.05
P_2O_5	0.09	0.04	0.06	0.06	0.18	0.05	0.05
LOI	0.51	0.69	0.79	0.64		0.66	1.02
Total	99.54	99.53	99.8	99.52	100.31	99.8	99.94
A/CNK	1.05	1.04	1.05	1.03	1.07	1.09	1.05
Ba	1246	1535	1371	1542	1003	1723	1725
Ce	52	50	41	32		27	21
Co	6	2	3	9	13	2	2
Cr	5	6	5	6	50	10	6
Cu	1	1	1	2	73	2	4
La	45	19	28	24		33	16
Nb	25	18	22	30	18.2	20	18
Nd	17	10	14	14		15	12
Ni	2	2	2	9	7	2	4
Pb	19	17	14	17	33	17	21
Rb	112	75	124	100	128	76	79
Sm	6	6	8	3		6	7
Sr	731	648	720	488	555	670	640
Th	12	10	15	9	24	4	11
U	3	1	2	2	7	1	1
V	21	5	18	15		16	11
Zn	44	29	35	39	60	51	71
Zr	186	127	154	108	165	126	120
Y	14	11	13	12	9	7	10
La	47.36	29.5				28.4	28.68
Ce	79.19	47.9				46.8	48.02
Nd	30.8	19.5				18.3	18.93
Sm	4.592	3.02				2.89	3.023
Eu	1.233	0.95				0.91	0.8989
Gd							
Tb	0.4162	0.27				0.25	0.2392
Ho		0.71					
Tm							
Yb	0.8047	0.62				0.64	0.7137
Lu	0.1657	0.11				0.11	0.1267
Th	10.96	5.29				6.37	6.031
U	2.994	1.81				1.65	1.719
Ta	1.194	0.78				0.95	0.9191
Hf	4.888	3.25				3.19	3.061
Cs	1.551	1.5				1.6	1.542
$^{87}Sr/^{86}Sr$	0.70808±3	0.70935±6	0.70861±5		0.70836±7	0.70916±8	0.70916±3
$^{143}Nd/^{144}Nd$	0.51215±2	0.51233±9			0.51205±20	0.51200±4	0.51204±2
$^{206}Pb/^{204}Pb$						19.0238±4	
$^{207}Pb/^{204}Pb$						15.6881±3	
$^{208}Pb/^{204}Pb$						39.5296±8	

Sample	CBC87-100	CBC87-119	CBC87131A	CBC87-122	CBC87-146	CBC87-101	CBC87-57
Rock type	Kgd	Kgd	Kgd	Kgd	Kgd	Kgd	Kgd
Locality	LGPT	ALVT	ALVT	ALVT	EFSR	LGPT	LickCrk.Rd.
Lat.(°N)	44°03'45"	43°54'52"	43°55'50"	43°55'10"	44°14'45"	44°03'40"	45°03'20"
Long.(°W)	115°44'40"	114°55'30"	114°57'00"	114°56'20"	114°42'00"	115°44'30"	115°55'10"
SiO_2	72.1	72.14	72.15	72.19	72.24	72.28	72.29
Al_2O_3	15.38	14.93	14.24	14.83	14.55	15.13	14.47
TiO_2	0.16	0.24	0.26	0.25	0.29	0.17	0.31
Fe_2O_3	1.47	1.58	2.03	1.68	1.72	1.41	2.19
MgO	0.27	0.42	0.47	0.39	0.44	0.31	0.68
CaO	1.81	1.39	1.35	1.52	2.24	1.56	2.57
Na_2O	4.77	4.29	4.74	3.96	4.16	4.39	3.63
K_2O	3.25	3.79	3.79	4.08	3.13	3.86	2.77
MnO	0.03	0.03	0.06	0.06	0.04	0.05	0.03
P_2O_5	0.05	0.06	0.08	0.08	0.09	0.05	0.07
LOI	0.66	0.86	0.8	1.03	0.61	0.64	0.51
Total	99.96	99.75	99.97	100.08	99.5	99.86	99.51
A/CNK	1.05	1.09	0.99	1.08	1.02	1.06	1.06
Ba	1591	897	1107	1063	887	1848	1669
Ce	21	53	58	76	69	29	57
Co	2	2	2	2	2	4	6
Cr	5	5	6	7	9	19	10
Cu	1	1	1	1	1	7	4
La	26	25	39	31	41	19	27
Nb	16	21	24	15	23	16	14
Nd	15	23	27	23	30	6	26
Ni	2	5	4	2	4	4	7
Pb	16	19	20	17	18	22	15
Rb	78	105	132	136	93	92	65
Sm	9	7	4	5	9	7	2
Sr	690	681	792	613	839	644	767
Th	8	11	8	13	9	9	16
U	1	1	5	4	1	1	3
V	17	17	22	16	27	25	34
Zn	32	39	30	64	40	42	48
Zr	124	152	170	169	175	119	168
Y	11	10	17	9	15	8	8
La	28.11			39.49	43.92	28.6	47.41
Ce	47.78			65.98	74.35	45.5	81.23
Nd	18.58			23.55	30.66	17.9	28.81
Sm	3.02			3.492	4.853	2.89	4.301
Eu	0.942			1.062	1.237	0.91	1.132
Gd							
Tb	0.282			0.3379	0.44	0.25	0.4087
Ho				2.267			0.8802
Tm						0.18	
Yb	0.673			0.7884	0.9654	0.72	0.6714
Lu	0.134			0.1385	0.1592	0.12	0.0956
Th	5.77			9.221	9.36	5.99	10.89
U	1.34			2.434	3.327	1.7	0.9557
Ta	0.821			0.9008	1.314	0.9	0.5511
Hf	3.16			4.407	4.68	3.41	4.292
Cs	1.47			2.373	2.394	2.2	0.8497
$^{87}Sr/^{86}Sr$	0.70941±4	0.70867±3	0.70853±3	0.70882±4	0.70869±2	0.70929±4	0.70897±3
$^{143}Nd/^{144}Nd$	0.51210±1	0.51211±2	0.51217±3	0.51211±4	0.51222±1	0.51199±2	0.51214±10
$^{206}Pb/^{204}Pb$		19.2151±14			19.8975±10	19.0509±5	19.5494±93
$^{207}Pb/^{204}Pb$		15.6703±12			15.7299±8	15.6927±4	15.7264±70
$^{208}Pb/^{204}Pb$		39.2864±30			39.6822±20	39.4114±11	39.378±20

Sample	CBC87-128	CBC87-94	CBC87130A	CBC87-64	CBC87123B	CBC87-110	CBC87-49
Rock type	Kgd	Kgd	Kgd	Kgd	Kgd	Kgd	Kgd
Locality	ALVT	LGPT	ALVT	Fir Crk. Rd.	ALVT	LGPT	Pikes Fork.
Lat.(°N)	43°55'25"	44°03'35"	43°55'40"	44°25'05"	43°55'15"	44°03'55"	43°57'45"
Long.(°W)	114°58'40"	114°41'30"	114°56'50"	115°17'15"	114°56'20"	115°42'40"	115°34'10"
SiO_2	72.56	72.73	72.95	73.1	73.28	73.32	73.57
Al_2O_3	14.77	15.03	14.39	14.07	13.64	14.88	14.83
TiO_2	0.26	0.16	0.23	0.24	0.21	0.14	0.11
Fe_2O_3	1.72	1.29	1.55	1.52	0.99	1.18	1.11
MgO	0.47	0.31	0.38	0.33	0.49	0.26	0.16
CaO	1.7	1.83	1.73	1.82	1.43	1.37	1.25
Na_2O	4.34	4.59	4.02	3.13	4.92	4.38	4.64
K_2O	3.39	3.12	3.88	4.68	2.89	3.78	3.74
MnO	0.04	0.06	0.05	0.04	0.05	0.04	0.05
P_2O_5	0.09	0.04	0.1	0.04	0.06	0.03	0.03
LOI	0.71	0.45	0.51	0.76	1.61	0.54	0.48
Total	100.03	99.61	99.76	99.74	99.58	99.91	99.96
A/CNK	1.06	1.05	1.03	1.04	0.99	1.08	1.06
Ba	913	1623	1044	1041	801	1710	1238
Ce	48	7	50	29	58	7	40
Co	5	2	2	4	2	7	2
Cr	10	5	7	4	25	8	8
Cu	1	4	1	3	1	1	4
La	24	20	48	25	42	21	14
Nb	21	16	19	9	18	18	36
Nd	9	8	21	17	27	12	16
Ni	2	2	5	4	3	2	2
Pb	16	14	17	18	17	17	19
Rb	110	68	108	130	111	87	104
Sm	14	5	6	6	4	7	6
Sr	821	661	703	579	484	609	474
Th	7	11	12	12	15	9	11
U	4	1	1	1	5	1	1
V	28	14	16	22	17	12	9
Zn	41	48	34	26	22	50	34
Zr	161	131	151	115	166	95	98
Y	11	7	15	5	12	8	10
La	38.01	28				35.09	
Ce	65.87	46.1				61.36	
Nd	26.23	17.84				23.11	
Sm	4.254	2.91				3.773	
Eu	1.145	1				1.059	
Gd	7.726					5.061	
Tb	0.407	0.28				0.3663	
Ho							
Tm	0.266	0.2					
Yb	0.9212	0.63				0.7008	
Lu	0.1532	0.11				0.1244	
Th	9.965	5.26				6.967	
U	2.939	1.24				1.635	
Ta	1.209	0.67				0.8643	
Hf	4.12	3.31				3.871	
Cs	1.246	1.44				2.515	
$^{87}Sr/^{86}Sr$	0.70868±3	0.70931±6	0.70875±4		0.70844±4	0.70936±4	
$^{143}Nd/^{144}Nd$	0.51226±10	0.51211±2	0.51211±1		0.51213±2	0.51198±3	
$^{206}Pb/^{204}Pb$	18.9320±6	19.1072±7					
$^{207}Pb/^{204}Pb$	15.6465±5	15.6905±6					
$^{208}Pb/^{204}Pb$	39.2583±14	39.4663±16					

Sample	CBC87-120	CBC87-76	CBC87-98	L86-43	CBC87-129	L86-59	L86-39
Rock type	Kgd	Kgd	Kgd	Kgd	Kgd	Kgd	Kgd
Locality	ALVT	LickCrk.Rd.	LGPT	EFSR	ALVT	NW.Mtn.H.	Elk Creek
Lat.(°N)	43°54'45"	45°02'30"	44°03'38"	44°15'40"	43°55'30"	43°23'30"	44°17'15"
Long.(°W)	114°55'20"	115°56'00"	114°44'50"	114°46'50"	114°56'45"	115°49'50"	115°9'30"
SiO_2	73.59	73.65	73.68	73.69	73.71	73.75	74.49
Al_2O_3	13.71	14.22	14.66	14.21	14.17	15.87	14.05
TiO_2	0.23	0.22	0.16	0.28	0.21	0.13	0.26
Fe_2O_3	1.54	1.53	1.38	1.68	1.53	1.28	1.65
MgO	0.36	0.4	0.3	0.32	0.38	0.32	0.37
CaO	1.74	2.14	1.77	1.88	1.57	1.67	1.66
Na_2O	2.71	3.54	4.59	3.12	3.64	4.93	3.54
K_2O	3.42	3.55	2.87	4.1	3.8	2.76	4.05
MnO	0.04	0.03	0.04	0.03	0.03	0.05	0.03
P_2O_5	0.07	0.06	0.06	0.16	0.07	0.16	0.13
LOI	2.88	0.51	0.59		0.84		
Total	100.28	99.86	100.09	99.47	99.95	100.92	100.23
A/CNK	1.21	1.05	1.06	1.09	1.09	1.12	1.06
Ba	607	1542	1310	892	1044	974	1943
Ce	36	20	20		56		
Co	5	3	2	12	2	11	12
Cr	7	5	6	46	15	48	50
Cu	1	1	4	5	1	4	5
La	41	28	27		31		
Nb	20	15	20	13.5	16	29.7	10
Nd	16	17	11		21		
Ni	4	3	2	6	2	6	6
Pb	10	20	16	26	16	30	22
Rb	125	111	73	122	114	82	111
Sm	10	10	6		8		
Sr	283	691	643	461	720	337	709
Th	12	16	12	11	10	2	9
U	5	3	3	3	2	2	3
V	17	14	11		18		
Zn	44	36	38	38	26	48	41
Zr	147	139	124	133	146	45	149
Y	9	9	9	7	11	10	6
La	36.03						
Ce	63.94						
Nd	24.96						
Sm	3.78						
Eu	0.9553						
Gd							
Tb	0.4047						
Ho							
Tm							
Yb	0.9403						
Lu	0.1687						
Th	11.63						
U	2.86						
Ta	1.318						
Hf	4.024						
Cs	5.274						
$^{87}Sr/^{86}Sr$	0.70927±6	0.70948±2	0.70910±3	0.70915±4	0.70869±2	0.71645±3	0.70954±2
$^{143}Nd/^{144}Nd$	0.51227±3	0.51218±3					
$^{206}Pb/^{204}Pb$							
$^{207}Pb/^{204}Pb$							
$^{208}Pb/^{204}Pb$							

Sample	CBC87-70	CBC87-45	CBC87108B	CBC87-84	CBC87-60	CBC87-66	CBC87-79
Rock type	Kgd	Kgd	Kgd	Kgd	Kgd	Kg	Kg
Locality	Deadwood S.	MFBR	LGPT	Wthwk.Mtn.	McCall	DeerCrk.Rd.	EFSFSR
Lat.(°N)	44°32'40"	43°43'00"	44°03'40"	44°16'45"	45°01'20"	44°24'20"	44°56'45"
Long.(°W)	115°33'45"	115°37'30"	115°42'50"	115°32'10"	116°02'00"	115°31'55"	115°35'40"
SiO_2	74.63	74.65	74.81	75	75.95	72.43	72.73
Al_2O_3	14.36	12.79	14.25	13.75	12.84	15.22	14.79
TiO_2	0.14	0.22	0.04	0.07	0.11	0.21	0.17
Fe_2O_3	1.13	1.68	0.42	0.94	1.19	1.41	1.52
MgO	0.24	0.32	0.09	0.12	0.15	0.42	0.35
CaO	1.52	1.13	1.16	0.92	1.17	2.32	2.52
Na_2O	3.94	3.53	3.73	4.49	3.34	4.38	3.98
K_2O	3.45	4.42	4.87	3.88	4.53	2.65	2.78
MnO	0.05	0.04	0.01	0.05	0.04	0.05	0.02
P_2O_5	0.02	0.06	0.02	0.04	0.02	0.06	0.05
LOI	0.48	0.89	0.43	0.28	0.3	0.59	0.61
Total	99.96	99.73	99.83	99.53	99.65	99.74	99.53
A/CNK	1.11	1.01	1.05	1.04	1.03	1.07	1.05
Ba	1434	592	2303	423	493	1688	1343
Ce	25	75	36	10	56	26	14
Co	2	2	2	2	2	3	2
Cr	5	7	4	7	5	5	6
Cu	1	1	6	1	1	1	1
La	20	31	23	12	41	20	20
Nb	17	33	6	212	22	13	16
Nd	15	20	20	14	21	14	13
Ni	2	4	2	9	4	2	2
Pb	21	23	22	28	20	15	14
Rb	98	164	85	114	196	70	69
Sm	6	5	9	6	17	5	12
Sr	595	168	641	194	154	917	663
Th	5	30	6	12	19	7	8
U	1	3	1	4	6	2	1
V	7	11	5	2	11	13	13
Zn	45	42	12	32	20	46	34
Zr	89	163	59	61	94	134	125
Y	13	27	7	43	22	10	9
La							29.18
Ce							48.77
Nd							19.13
Sm							2.866
Eu							1.039
Gd							
Tb							0.3316
Ho							
Tm							0.1969
Yb							0.6775
Lu							0.1312
Th							7.137
U							0.799
Ta							0.6313
Hf							3.285
Cs							0.8073
$^{87}Sr/^{86}Sr$						0.71434±3	0.71336±5
$^{143}Nd/^{144}Nd$						0.51217±2	0.51191±2
$^{206}Pb/^{204}Pb$							19.1840±7
$^{207}Pb/^{204}Pb$							15.7102±6
$^{208}Pb/^{204}Pb$							39.5139±14

Sample	CBC87-48	CBC87-77	CBC87-53	CBC87-78	CBC87-73	CBC87-71	CBC87-83
Rock type	Kg	Kg	Kg	Kg	Kg	Kg	Kg
Locality	NFBR	LickCrk.Rd.	McCall	LickCrk.Rd.	TrailCrk.Rd.	Summit Lk.	Wthwk.Mtn.
Lat.(°N)	43°54'15"	45°05'37"	44°58'00"	45°00'30"	44°38'10"	44°38'45"	44°18'00"
Long.(°W)	115°26'15"	115°49'30"	116°10'20"	115°41'40"	115°43'50"	115°35'15"	115°37'50"
SiO_2	73.94	74.34	74.54	74.64	74.72	74.93	74.93
Al_2O_3	14.19	14.57	14.47	14.31	14.06	13.74	13.92
TiO_2	0.08	0.09	0.07	0.06	0.12	0.1	0.1
Fe_2O_3	0.88	1.06	0.7	0.81	1.05	1.1	1.02
MgO	0.11	0.24	0.15	0.14	0.21	0.18	0.14
CaO	1.26	1.74	1.36	1.04	1.56	1.32	1.18
Na_2O	4.15	3.8	4.25	3.72	3.76	3.72	4.02
K_2O	3.71	3.55	3.38	4.3	3.7	3.98	3.92
MnO	0.04	0.05	0.04	0.05	0.05	0.04	0.07
P_2O_5	0.03	0.03	0.04	0.04	0.03	0.03	0.04
LOI	1.14	0.48	0.59	0.64	0.43	0.56	0.48
Total	99.53	99.97	99.58	99.76	99.69	99.69	99.83
A/CNK	1.08	1.10	1.10	1.13	1.08	1.07	1.07
Ba	1179	1120	843	657	1175	1087	1316
Ce	12	10	7	17	17	35	7
Co	5	4	5	2	2	2	5
Cr	5	7	6	7	4	5	10
Cu	1	1	1	1	2	3	1
La	11	20	17	10	9	23	12
Nb	21	13	10	14	14	18	28
Nd	10	12	3	6	11	16	7
Ni	2	2	4	2	4	2	3
Pb	24	22	21	25	20	18	18
Rb	131	100	124	151	122	120	122
Sm	1	7	10	3	5	12	6
Sr	313	506	407	250	500	410	407
Th	4	7	5	10	12	10	12
U	3	1	1	3	1	1	1
V	3	7	6	6	2	5	15
Zn	34	43	23	34	47	50	45
Zr	64	65	63	63	96	86	75
Y	9	9	13	14	17	10	10

La	13.53
Ce	23.59
Nd	9.777
Sm	2.033
Eu	0.3665
Gd	3.293
Tb	0.3194
Ho	1.201
Tm	
Yb	1.089
Lu	0.1606
Th	4.203
U	0.8921
Ta	0.9865
Hf	1.632
Cs	2.458

$^{87}Sr/^{86}Sr$	0.70925±3	0.71297±4
$^{143}Nd/^{144}Nd$		
$^{206}Pb/^{204}Pb$		19.2680±74
$^{207}Pb/^{204}Pb$		15.7380±51
$^{208}Pb/^{204}Pb$		39.509±17

Sample	CBC87-115	CBC87-36	CBC87143*	CBC87-89	CBC87-118	CBC87-72	L86-44
Rock type	Klg	Klg	Klg	Klg	Klg	Klg	Klg
Locality	Wapiti Crk.	Bdman.Crk.	EFSR	CanyonCrk.	ALVT	TrailCrk.Rd.	EFSR
Lat.(°N)	44°07'10"	43°36'50"	44°15'20"	44°10'20"	43°55'00"	44°38'10"	44°15'40"
Long.(°W)	115°15'00"	114°57'15"	114°41'50"	115°14'45"	114°55'45"	115°43'50"	114°46'50"
SiO_2	69.43	71.19	71.8	73.83	74.25	74.59	74.74
Al_2O_3	16.06	15.9	14.94	14.77	13.93	14.64	14.38
TiO_2	0.17	0.15	0.31	0.07	0.22	0.02	0.1
Fe_2O_3	1.39	1.19	1.83	0.72	1.4	0.61	0.62
MgO	0.23	0.41	0.49	0.06	0.34	0.02	0.14
CaO	1.36	1.96	2.14	1.07	0.86	0.41	1.22
Na_2O	4.06	5.34	3.99	5.1	2.86	4.56	3.35
K_2O	5.81	2.84	3.31	3.71	4	3.91	5.1
MnO	0.04	0.04	0.05	0.04	0.05	0.19	0.02
P_2O_5	0.05	0.05	0.09	0.02	0.07	0.06	0.07
LOI	1.32	0.56	0.81	0.25	1.88	0.51	
Total	99.92	99.61	99.75	99.63	99.87	99.51	100.97
A/CNK	1.04	1.03	1.06	1.03	1.31	1.17	1.09
Ba	2420	2039	1088	1195	812	40	1355
Ce	31	7	106	20	50	10	
Co	2	2	6	2	1	2	9
Cr	4	7	11	7	288	7	45
Cu	4	1	1	2	1	1	4
La	27	11	52	4	31	7	
Nb	16	21	22	31	24	40	6
Nd	15	11	32	12	22	6	
Ni	7	3	6	2	6	3	6
Pb	38	22	11	23	11	9	25
Rb	108	57	94	103	148	252	150
Sm	7	1	11	5	6	1	
Sr	891	1058	828	643	322	24	431
Th	15	7	11	13	19	5	4
U	2	1	2	2	2	6	3
V	7	10	25	2	20	2	
Zn	34	29	48	28	35	69	17
Zr	126	99	198	81	151	39	101
Y	14	8	12	9	12	19	6
La					35.9		
Ce					60.7		
Nd					24.8		
Sm					3.78		
Eu					0.92		
Gd							
Tb					0.34		
Ho							
Tm					0.14		
Yb					0.88		
Lu					0.15		
Th					14.36		
U					1.66		
Ta					1.26		
Hf					4.23		
Cs					5.1		
$^{87}Sr/^{86}Sr$		0.70858±4		0.70956±4		0.70917±31	
$^{143}Nd/^{144}Nd$				0.51213±2		0.51142±12	
$^{206}Pb/^{204}Pb$							
$^{207}Pb/^{204}Pb$							
$^{208}Pb/^{204}Pb$							

Sample	CBC87-117	CBC87-42	L86-60	CBC87148B	CBC87-88	CBC87-82	CBC87-41
Rock type	Klg	Klg	Klg	Klg	Klg	Klg	Klg
Locality	ALVT	N.W.Mtn.H.	N.W.Mtn.H.	EFSR	Grandjean	Wthwk Mtn.	N.W.Mtn.H.
Lat.(°N)	43°55'03"	43°24'00"	43°23'30"	44°16'12"	44°10'15"	44°18'00"	43°24'25"
Long.(°W)	114°55'50"	115°51'25"	115°49'50"	114°44'30"	115°12'05"	115°37'50"	115°51'25"
SiO_2	74.95	75.16	75.35	75.53	75.83	76.01	77.17
Al_2O_3	13.23	13.46	14.51	13.24	13.49	13.52	13.04
TiO_2	0.19	0.03	0.04	0.07	0.04	0.05	0.06
Fe_2O_3	1.27	0.66	0.53	1.12	0.34	0.71	0.66
MgO	0.18	0.08	0.13	0.07	0.11	0.05	0.09
CaO	1.35	0.58	1.09	0.41	1.07	0.68	0.96
Na_2O	3.94	3.6	4.59	3.34	2.65	3.72	3.76
K_2O	3.62	5.14	4.07	5.49	6.11	4.22	3.96
MnO	0.05	0.12	0.03	0.02	0.02	0.05	0.04
P_2O_5	0.05	0.03	0.14	0.01	0.01	0.01	0.02
LOI	0.86	0.52		0.51	0.33	0.71	0.4
Total	99.7	99.81	100.71	99.8	99.8	99.72	100.16
A/CNK	1.03	1.07	1.04	1.09	1.04	1.13	1.07
Ba	741	257	1114	301	1500	465	1601
Ce	52	11		10	7	29	10
Co	4	2	8	3	2	2	2
Cr	8	6	42	7	6	5	3
Cu	1	1	30	1	2	1	1
La	32	6		4	4	11	4
Nb	23	57	15	31	3	37	25
Nd	23	5		3	7	6	1
Ni	2	6	7	3	4	4	4
Pb	17	39	39	19	27	21	25
Rb	112	172	100	163	149	144	114
Sm	5	4		2	7	5	2
Sr	546	76	169	240	559	125	283
Th	12	13	6	12	7	10	5
U	1	8	2	11	2	3	2
V	15	4		6	2	4	5
Zn	35	12	23	4	9	17	27
Zr	125	51	58	44	25	55	56
Y	12	39	8	14	6	23	11
La	30.9	8.5		43.07			
Ce	53.1	17.1		69.37			
Nd	22.5	11.12		29.39			
Sm	3.6	3.88		5.384			
Eu	0.95	0.18		1.196			
Gd		4.6					
Tb	0.32	0.74		0.6281			
Ho							
Tm		0.19					
Yb	0.76	3.6		1.241			
Lu	0.14	0.66		0.2144			
Th	9.94	11.5		32.04			
U	3.16	9.45		7.302			
Ta	1.18	5.44		2.515			
Hf	3.42	3.22		4.383			
Cs	1.8	2.24		3.737			
$^{87}Sr/^{86}Sr$	0.70892±4		0.71733±4				
$^{143}Nd/^{144}Nd$	0.51202±1	0.51135±7	0.51153±3	0.51225			
$^{206}Pb/^{204}Pb$	19.2112±90	17.3601±3		20.3794±11			
$^{207}Pb/^{204}Pb$	15.5716±75	15.5356±3		15.7749±12			
$^{208}Pb/^{204}Pb$	39.296±18	39.2743±7		40.2898±22			

Sample	86RL-386	CBC87-105	CBC87-102	L86-26	CBC87-162	CBC87-163	CBC87-86
Rock type	Klg	Tgd	Tgd	Tgd	Tgd	Tgd	Tgd
Locality	Soldier Mtn	LGPT	LGPT	Soldier Mtn	Jackson Pk.	Marsh Crk.	Sacajawa
Lat.(°N)	43°32'38"	44°03'40"	44°03'40"	43°32'35"	44°6'30"	44°26'45"	44°09'55"
Long.(°W)	114°52'40"	115°43'30"	115°44'20"	114°48'45"	115°24'45"	115°14'18"	115°10'30"
SiO_2	77.26	56.23	57.23	61.86	65.14	66.02	66.16
Al_2O_3	13.28	16.37	16.3	15.94	14.9	14.9	15.4
TiO_2	0.17	1.31	1.17	0.99	0.65	0.58	0.72
Fe_2O_3	1.2	7.75	7.47	6.15	4.46	4.18	3.94
MgO	0.23	3.9	3.61	2.99	2.18	2	1.59
CaO	0.64	5.76	5.15	4.7	3.35	3.67	4.2
Na_2O	3.76	3.66	3.64	4.21	4.06	3.39	3.5
K_2O	4.9	3.39	3.25	3.11	3.66	3.59	3.04
MnO	0.03	0.11	0.14	0.1	0.09	0.08	0.06
P_2O_5	0.16	0.62	0.54	0.42	0.24	0.19	0.22
LOI		0.89	1.5		0.96	1.09	0.88
Total	102.01	99.99	100	101.11	99.71	99.7	99.72
A/CNK	1.05	0.81	0.86	0.85	0.89	0.92	0.92
Ba	215	1731	1615	2071	1251	1317	1206
Ce		108	87		59	65	72
Co	10	22	20	21	12	7	8
Cr	42	18	26	80	42	57	8
Cu	4	27	17	80	7	1	1
La		43	45		25	29	48
Nb	23.1	28	25	28.1	35	16	30
Nd		53	33		26	25	30
Ni	6	13	13	22	14	10	5
Pb	27	11	18	23	16	18	12
Rb	235	98	95	99	92	100	88
Sm		8	17		4	18	3
Sr	75	1010	1059	674	612	535	649
Th	38	5	10	22	13	15	12
U	8	1	4	3	4	1	3
V		153	143		74	65	77
Zn	18	110	120	90	52	56	73
Zr	105	248	273	351	171	169	204
Y	20	30	22	27	19	21	26
La		5.294	52.13	84.78	43.61	35.85	54.7
Ce		10.74	96.89	153	77.22	63.34	100.1
Nd		5.2	44.54	58.25	31.55	26.41	39.81
Sm		0.9585	7.873	9.626	5.749	4.678	7.139
Eu		0.2394	2.295	2.012	1.779	1.23	1.673
Gd		6.068	7.396		9.733	8.654	
Tb		0.1023	0.8689	1.012	0.6797	0.6183	0.78
Ho		0.2085	4.915	4.502			
Tm							
Yb		0.2061	1.536	2.157	1.434	1.581	1.628
Lu		0.0335	0.2718	0.3463	0.2606	0.269	0.2534
Th		0.6467	8.94	25.38	12.11	12.7	14.05
U		0.1768	2.392	4.06	2.711	1.686	3.079
Ta		0.1377	1.4	1.683	2.529	1.157	2.933
Hf		0.6463	7.091	9.809	5.03	5.078	5.553
Cs		0.2616	2.817	1.489	1.362	2.314	1.128
$^{87}Sr/^{86}Sr$	0.7173±12	0.70656±3	0.706674±1	0.70694±8	0.70763±4	0.70921±8	0.70768±3
$^{143}Nd/^{144}Nd$		0.51240±5	0.51234±2	0.51218±7	0.51201±2	0.51194±2	0.51225±3
$^{206}Pb/^{204}Pb$		19.2330±31			18.3446±7		19.3192±7
$^{207}Pb/^{204}Pb$		15.7008±24			15.5894±6		15.6959±26
$^{208}Pb/^{204}Pb$		39.2408±61			39.2604±16		39.3845±64

Sample	86RL-385	CBC87-103	L86-32	L86-33	CBC87-90	CBC87-132	86RL-384
Rock type	Tgd	Tgd	Tg	Tg	Tg	Tg	Tg
Locality	Soldier Mtn	LGPT	BoulderMtn	BoulderMtn	PrieCrk.Rd.	Sawtooth	Soldier Mtn
Lat.(°N)	43°32'10"	44°03'35"	43°49'35"	43°49'35"	43°47'00"	43°56'00"	43°30'45"
Long.(°W)	114°56'15"	115°44'00"	114°34'40"	114°34'40"	114°40'00"	114°57'00"	114°52'20"
SiO_2	67.62	71.96	69.91	70.86	71.24	71.76	72.82
Al_2O_3	15.39	13.79	14.71	14.56	14.21	14.65	14.87
TiO_2	0.57	0.36	0.35	0.26	0.3	0.31	0.31
Fe_2O_3	3.97	2.2	2.44	2.09	2.5	2.03	1.96
MgO	1.82	0.75	0.45	0.45	0.56	0.51	0.53
CaO	3.13	1.34	1.55	1.02	1.07	1.71	1.81
Na_2O	4.28	4.51	3.55	3.56	3.43	4.06	4.06
K_2O	3.53	4.16	5.77	5.43	5.27	3.78	3.76
MnO	0.07	0.03	0.05	0.04	0.05	0.03	0.05
P_2O_5	0.31	0.14	0.15	0.13	0.09	0.09	0.17
LOI		0.48			0.84	0.61	
Total	101.44	99.72	99.82	99.46	99.56	99.533	100.96
A/CNK	0.93	0.96	0.99	1.07	1.07	1.06	1.06
Ba	1156	1338	685	594	852	1153	834
Ce		79			99	71	
Co	27	3	23	13	8	2	12
Cr	52	6	48	46	10	6	49
Cu	52	5	6	5	5	1	4
La		39			66	42	
Nb	22.9	22	27.2	25.7	27	25	18.8
Nd		36			45	24	
Ni	17	5	7	11	10	4	7
Pb	24	19	42	29	31	14	32
Rb	106	142	245	246	243	124	155
Sm		10			7	1	
Sr	444	581	237	238	245	858	282
Th	22	14	36	35	34	12	23
U	5	4	8	10	9	4	6
V		35			31	25	
Zn	56	26	44	37	43	23	41
Zr	209	183	218	197	249	179	133
Y	19	17	27	29	26	17	17
La		58.2				47.21	
Ce		98.3				80.36	
Nd		39.6				33.21	
Sm		6.88				5.617	
Eu		1.6				1.285	
Gd						12.3	
Tb		0.75				0.5289	
Ho		1.7					
Tm							
Yb		1.4				1.335	
Lu		0.23				0.2345	
Th		17.08				11.16	
U		3.9				3.495	
Ta		1.72				1.854	
Hf		5.86				5.33	
Cs		2.5				2.116	
$^{87}Sr/^{86}Sr$	0.70949±45	0.70668±2	0.71149±8	0.71130±2		0.70851±2	0.71394±3
$^{143}Nd/^{144}Nd$		0.51240±1				0.51207±2	0.51166±8
$^{206}Pb/^{204}Pb$		19.2835±9				18.8297±13	17.7197±35
$^{207}Pb/^{204}Pb$		15.6621±8				15.6499±11	15.5497±32
$^{208}Pb/^{204}Pb$		39.1734±20				39.2628±27	38.8729±79

Sample	CBC87-34	86RL-338	L86-51	L86-38	CBC87-19	CBC87-44	CBC87-23
Rock type	Tg	Tg	Tg	Tg	Tg	Tg	Tg
Locality	Lt.FallsCrk.	Soldier Mtn	MackeyPk.	Sawtooth	Sawtooth	MFBR	Sawtooth
Lat.(°N)	43°50'30"	43°29'	43°52'20"	44°17'15"	44°12'20"	43°40'00"	44°10'25"
Long.(°W)	114°15'00"	114°58'	113°40'00"	115°9'30"	115°05'54"	115°43'30"	115°01'05"
SiO_2	73.24	73.41	73.73	74.4	74.49	75.09	75.45
Al_2O_3	13.37	14.03	13.64	12.76	13.12	13.2	12.73
TiO_2	0.27	0.37	0.26	0.1	0.19	0.19	0.14
Fe_2O_3	1.78	2.27	1.98	1.29	1.81	1.26	1.66
MgO	0.45	0.76	0.49	0.13	0.22	0.34	0.12
CaO	1.54	1.7	1.69	0.6	0.53	1.19	0.6
Na_2O	3.39	3.62	4	4.03	3.53	3.9	3.83
K_2O	4.65	4.16	4.6	4.42	5.12	4.11	4.78
MnO	0.04	0.05	0.04	0.03	0.05	0.06	0.04
P_2O_5	0.09	0.22	0.14	0.07	0.04	0.03	0.03
LOI	0.84				0.54	0.48	0.45
Total	99.66	101.11	101.17	97.83	99.63	99.86	99.85
A/CNK	1.00	1.04	0.93	1.02	1.07	1.01	1.01
Ba	550	722	231	180	425	712	318
Ce	67				48	42	53
Co	6	14	12	11	3	3	5
Cr	8	50	45	42	7	7	6
Cu	15	5	6	5	1	1	1
La	34				38	14	47
Nb	30	23.1	61	28.2	27	21	59
Nd	25				19	11	25
Ni	9	12	6	7	5	2	10
Pb	26	27	43	30	22	21	24
Rb	208	179	276	179	168	111	187
Sm	8				4	14	13
Sr	237	224	148	34	135	213	72
Th	41	33	53	48	22	18	27
U	9	6	6	4	6	3	4
V	28				13	7	9
Zn	37	42	55	32	38	36	44
Zr	132	182	212	112	171	102	173
Y	19	19	49	22	18	18	37
La		7					69.81
Ce		17					131.4
Nd		67					49.82
Sm							9.642
Eu							0.4532
Gd							
Tb							1.259
Ho							
Tm							
Yb							2.902
Lu							0.4366
Th							27.62
U							5.854
Ta							4.253
Hf							5.993
Cs							1.731
$^{87}Sr/^{86}Sr$	0.71383±2		0.718230±6	0.71061±4			0.71414±4
$^{143}Nd/^{144}Nd$	0.51226±2		0.51197±50	0.51181±2			0.51185±2
$^{206}Pb/^{204}Pb$	17.5620±35						17.7232±6
$^{207}Pb/^{204}Pb$	15.5183±30						15.5481±6
$^{208}Pb/^{204}Pb$	38.8443±76						39.2223±18

Sample	CBC87-65	86RL-257	CBC87-24	L86-37	CBC87-94B	CBC87150B	CBC87-96A
Rock type	Tg	Tg	Tg	Tg	Td(M)	Td(P.M)	Td(P.M)
Locality	DeerCrk.Rd.	Soldier Mtn	Sawtooth	Sawtooth	LGPT	EFSR	LGPT
Lat.(°N)	44°24'25"	43°29'	44°10'25"	44°17'15"	44°03'30"	44°16'00"	44°03'20"
Long.(°W)	115°27'45"	114°58'	114°56'40"	115°9'30"	115°41'50"	115°46'20"	115°41'55"
SiO_2	76.28	76.97	77.11	77.96	49.98	52.6	63.52
Al_2O_3	13.55	13.29	12	13.43	15.07	13.99	15.66
TiO_2	0.03	0.1	0.07	0.06	1.79	1.46	0.69
Fe_2O_3	0.43	0.84	1.11	0.93	8.46	11.74	5.01
MgO	0.05	0.13	0.04	0.22	5.87	5.57	2.37
CaO	1.05	0.48	0.47	0.46	7.25	9.15	3.99
Na_2O	3.47	4.35	4	4.17	3.19	2.57	3.67
K_2O	4.85	4.38	4.51	4.5	1.87	1.27	3.6
MnO	0.02	0.08	0.03	0.03	0.16	0.18	0.07
P_2O_5	0.02	0.1	0.01	0.12	0.6	0.4	0.3
LOI	0.05		0.51		5.98	1.24	0.64
Total	99.79	101.01	99.85	102.11	100.2	100.19	99.52
A/CNK	1.05	1.04	0.97	1.07	0.74	0.63	0.91
Ba	367	177	14	161	860	694	1364
Ce	7		58		84	84	63
Co	2	9	2	9	27	44	7
Cr	6	42	7	41	208	38	19
Cu	1	4	1	7	24	35	7
La	4		34		42	36	53
Nb	46	107.8	86	28.6	33	13	24
Nd	2		30		35	42	31
Ni	4	9	10	6	98	49	12
Pb	34	31	23	37	32	11	21
Rb	143	301	249	276	33	21	97
Sm	1		11		11	8	14
Sr	238	11	3	13	979	295	771
Th	19	42	36	37	10	4	15
U	9	9	8	5	2	2	3
V	2		2		181	247	79
Zn	7	34	26	25	78	102	87
Zr	52	111	128	47	216	197	201
Y	48	68	63	23	25	39	16

La	34.98	38.4
Ce	53.94	81.95
Nd	27.11	41.46
Sm	8.506	11.5
Eu	0.2026	0.0815
Gd		
Tb	1.655	1.893
Ho		
Tm	0.4698	0.259
Yb	5.205	4.891
Lu	0.8352	0.7502
Th	43.66	37.86
U	11.15	8.764
Ta	10.59	9.014
Hf	6.147	6.686
Cs	5.837	3.734

$^{87}Sr/^{86}Sr$		
$^{143}Nd/^{144}Nd$	0.51222±5	0.51216±3
$^{206}Pb/^{204}Pb$	18.5206±3	
$^{207}Pb/^{204}Pb$	15.6240±3	
$^{208}Pb/^{204}Pb$	39.3878±8	

Sample	CBC87-67	CBC87103A	CBC87-121	CBC87141B	CBC87-95	CBC8799B	CBC87108C
Rock type	Td(P.I)	Td(M)	Td(P.I)	Td(P.I)	Td(P.F)	Td(F)	Td(P.F)
Locality	DeerCrk.Rd.	LGPT	Sawtooth	EFSR	LGPT	LGPT	LGPT
Lat.(°N)	44°15'15"	44°03'35"	43°54'20"	44°15'00"	44°03'30"	44°03'40"	44°03'40"
Long.(°W)	115°33'40"	115°44'00"	114°55'08"	114°37'00"	115°41'50"	115°44'45"	115°42'50"
SiO_2	63.66	66.06	66.84	69.73	72.28	72.56	72.84
Al_2O_3	15.03	15	15.83	14.61	13.04	14.86	13.07
TiO_2	0.78	0.68	0.49	0.24	0.21	0.15	0.28
Fe_2O_3	4.77	4.04	3.17	2.24	1.4	1.34	1.77
MgO	2.21	1.91	0.51	0.5	0.45	0.31	0.67
CaO	3.08	3.45	1.29	2.4	1.35	1.75	1.26
Na_2O	3.51	3.64	4.35	3.55	4.55	4.52	3.73
K_2O	4.09	3.93	6.04	3.52	4	3.32	4.39
MnO	0.09	0.05	0.08	0.08	0.04	0.06	0.07
P_2O_5	0.36	0.3	0.15	0.09	0.07	0.04	0.1
LOI	2.15	0.79	1.26	2.81	2.27	0.84	1.56
Total	99.75	99.85	100.01	99.76	99.68	99.75	99.75
A/CNK	0.95	0.91	0.99	1.04	0.91	1.05	0.99
Ba	1459	1297	1411	1531	688	1642	654
Ce	74	62	131	61	21	29	35
Co	15	8	2	6	3	2	2
Cr	16	20	16	17	8	14	8
Cu	5	7	2	2	3	3	4
La	48	37	58	37	27	26	34
Nb	22	22	48	13	17	17	21
Nd	34	35	49	24	20	14	18
Ni	10	15	3	2	7	2	8
Pb	21	13	13	33	25	17	22
Rb	119	121	144	99	158	79	191
Sm	20	13	11	18	4	5	13
Sr	1044	814	228	802	349	679	351
Th	14	18	18	13	25	9	26
U	4	2	5	2	11	1	6
V	81	74	24	16	24	8	28
Zn	82	61	42	38	49	19	45
Zr	211	100	632	137	124	121	145
Y	20	18	31	11	10	8	11
La			78.57				
Ce			144.5				
Nd			56.86				
Sm			8.956				
Eu			1.711				
Gd							
Tb			1.031				
Ho							
Tm			0.5596				
Yb			2.298				
Lu			0.3626				
Th			15.74				
U			3.409				
Ta			2.637				
Hf			12.14				
Cs			2.124				
$^{87}Sr/^{86}Sr$		0.70931±5	0.70938±3				
$^{143}Nd/^{144}Nd$		0.51235±2	0.51200±2				
$^{206}Pb/^{204}Pb$							
$^{207}Pb/^{204}Pb$							
$^{208}Pb/^{204}Pb$							

Sample	CBC87104B
Rock type	Td(F)
Locality	LGPT
Lat.(°N)	44°03'35"
Long.(°W)	115°43'50"
SiO_2	76.7
Al_2O_3	12.66
TiO_2	0.08
Fe_2O_3	0.64
MgO	0.13
CaO	0.3
Na_2O	4.2
K_2O	4.81
MnO	0.04
P_2O_5	0.01
LOI	0.51
Total	100.06
A/CNK	1.00
Ba	51
Ce	36
Co	3
Cr	5
Cu	1
La	18
Nb	47
Nd	19
Ni	3
Pb	22
Rb	150
Sm	8
Sr	55
Th	18
U	3
V	6
Zn	26
Zr	85
Y	27
La	
Ce	
Nd	
Sm	
Eu	
Gd	
Tb	
Ho	
Tm	
Yb	
Lu	
Th	
U	
Ta	
Hf	
Cs	
$^{87}Sr/^{86}Sr$	
$^{143}Nd/^{144}Nd$	
$^{206}Pb/^{204}Pb$	
$^{207}Pb/^{204}Pb$	
$^{208}Pb/^{204}Pb$	

Sample	CBC87-66	CBC87-79	CBC87-77	CBC87-48	CBC-73	CBC87-53	CBC87-78	CBC87-83	CBC87-71
Rock type	Kg	Kg	Kg	Kg	Kg	Kg	Kg	Kg	Kg
Quartz	32.4	34.2	35.2	33.5	35.7	34.4	34.6	34.4	35.7
Orthoclase	11.5	13.2	16.4	18.5	18.1	15.6	20.2	19.8	20.2
Albite	37.6	34.2	32.4	35.8	32.1	36.4	31.8	34.3	31.8
Anorthite	11.3	12.4	8.5	6.2	7.6	6.6	5	5.6	6.4
Hornblende	0	0	0	0	0	0	0	0	0
Biotite	4.5	4.4	3.1	2.3	3	2	2.2	2.7	2.9
Muscovite	2.4	1.3	4.2	3.6	3.2	4.9	6	2.9	2.7
Magnetite	0	0	0	0	0	0	0	0	0
Haematite	0.2	0.2	0.2	0.2	0.2	0.1	0.1	0.2	0.2
Ilmenite	0.1	0	0	0	0	0	0	0	0
Apatite	0.1	0.1	0.1	0.1	0.1	0.1	0.1	0.1	0.1

Sample	L86-45	CBC87-35	CBC87-74	86RL-219	86RL-249	CBC87-99	CBC87-87	CBC87-116	CBC87-147
Rock type	Kgdp	Kgd	Kgd	Kgd	Kgd	Kgd	Kgd	Kgd	Kgd
Quartz	28.6	26.8	30.3	29.8	30.7	25.9	28.2	29.4	31
Orthoclase	13.2	14.4	7.3	15.2	8.5	16.4	12.7	12.7	12.2
Albite	28.4	28.3	29.9	29.6	33.4	35.9	35	33.6	31.1
Anorthite	12.7	14.4	19.3	13.5	13.5	10.8	15	13.9	14.7
Hornblende	0	0	0	0	0	0	0	0	0
Biotite	12.5	15	11.9	8.9	9.2	10	8.3	9.2	9.8
Muscovite	2.7	0	0	1.7	3.3	0	0	0	0
Magnetite	0	0.3	0	0	0	0	0	0	0
Haematite	0.5	0.1	0.4	0.4	0.5	0.3	0.4	0.4	0.3
Ilmenite	0.5	0.2	0.4	0.3	0.3	0.3	0.2	0.4	0.3
Apatite	0.8	0.5	0.5	0.6	0.6	0.5	0.3	0.4	0.4

Sample	CBC87-137A	CBC87-138	CBC87-81	CBC87-126	CBC87-160	CBC87-136	CBC87-91	CBC87-158	CBC87-92
Rock type	Kgd	Kgd	Kgd	Kgd	Kgd	Kgd	Kgd	Kgd	Kgd
Quartz	29.4	29.7	31.3	29	30	29.6	30.5	32	21.7
Orthoclase	15.9	15.1	18.2	14.4	12.3	14.2	16.3	11.6	20.5
Albite	32.2	32.4	26.9	36.2	35.3	36.2	33.5	34	47.2
Anorthite	13.1	13.2	13.9	11.4	12.7	11.3	12	12.5	8.1
Hornblende	0	0	0	0	0	0	0	0	0
Biotite	8.4	8.5	8.8	7.5	6.8	7.1	6.6	7.3	2.2
Muscovite	0	0	0	0.7	2	0.8	0.4	1.7	0
Magnetite	0	0	0	0	0	0	0	0	0
Haematite	0.4	0.4	0.3	0.3	0.3	0.3	0.3	0.3	0.2
Ilmenite	0.3	0.3	0.2	0.2	0.3	0.2	0.1	0.2	0.1
Apatite	0.4	0.3	0.3	0.3	0.3	0.3	0.3	0.3	0.1

Sample	L86-20	CBC87-134	CBC87-135	CBC87-125	CBC87-133A	CBC87-63	CBC87-93	CBC87-141	CBC87-56
Rock type	Kgd	Kgd	Kgd	Kgd	Kgd	Kgd	Kgd	Kgd	Kgd
Quartz	30.4	30.3	30.9	29	31.8	30.5	27.8	32.3	33.4
Orthoclase	16.8	17.3	16.4	19	18.3	16.8	15.9	13.7	11.2
Albite	33.9	33.8	33.9	35.9	31.5	34.6	41.2	34.5	34.1
Anorthite	9	11.6	11.8	9.1	11.4	9.7	9.7	11.4	12.7
Hornblende	0	0	0	0	0	0	0	0	0
Biotite	6.2	6.2	6.3	5.5	6.1	5.1	4.3	5.9	6.2
Muscovite	2.9	0	0	1	0.2	2.8	0.6	1.4	1.7
Magnetite	0	0	0	0	0	0	0	0	0
Haematite	0.3	0.3	0.3	0.3	0.3	0.3	0.2	0.3	0.3
Ilmenite	0.2	0.2	0.2	0.1	0.2	0.1	0.1	0.2	0.1
Apatite	0.4	0.2	0.3	0.2	0.2	0.1	0.1	0.3	0.2

Sample	CBC87-97	CBC87-156	CBC87-106	CBC87-109	CBC87-127	CBC87-100	CBC87-114	CBC87-124	CBC87-96
Rock type	Kgd	Kgd	Kgd	Kgd	Kgd	Kgd	Kgd	Kgd	Kgd
Quartz	28.3	30.4	28.1	28.7	31	28.5	29.2	28.5	28.9
Orthoclase	16.2	18.5	14.9	16.1	18.6	15.8	14.7	22	16
Albite	40.4	34.8	41.9	39.9	34.1	40.8	39.9	35.8	40.4
Anorthite	9.6	9.1	9.2	9.2	8.9	8.8	7.5	7.5	9
Hornblende	0	0	0	0	0	0	0	0	0
Biotite	4.2	5.4	4	4.1	5.6	4	4.2	4	4.1
Muscovite	1	1.2	1.3	1.6	1.2	1.8	4	1.7	1.3
Magnetite	0	0	0	0	0	0	0	0	0
Haematite	0.2	0.2	0.2	0.2	0.3	0.2	0.2	0.2	0.2
Ilmenite	0	0.2	0.1	0.1	0.1	0	0.1	0.2	0
Apatite	0.1	0.2	0.1	0.1	0.2	0.1	0.1	0.1	0.1

Sample	CBC87-131A	CBC87-47	CBC87-111	CBC87-112	CBC87-101	CBC87-122	CBC87-119	CBC87-57	CBC87-128
Rock type	Kgd	Kgd	Kgd	Kgd	Kgd	Kgd	Kgd	Kgd	Kgd
Quartz	27.7	30.2	28.4	28.7	29.1	30.9	30.3	35.9	31.3
Orthoclase	19.1	16	19.1	18.1	19	19.2	17.4	11.7	15.6
Albite	40.5	38.7	39.3	39.1	37.6	34	36.9	31.3	37.2
Anorthite	6.2	8.9	8.3	7.7	7.5	7.1	6.6	12.5	7.9
Hornblende	0	0	0	0	0	0	0	0	0
Biotite	5.9	5.6	4.3	4.1	4	4.9	4.8	6.9	5.2
Muscovite	0	0.2	0.2	2	2.4	3.3	3.6	1.1	2.2
Magnetite	0	0	0	0	0	0	0	0	0
Haematite	0.3	0.2	0.2	0.2	0.2	0.3	0.2	0.3	0.2
Ilmenite	0.1	0	0	0	0	0.1	0.1	0.1	0.1
Apatite	0.2	0.1	0.1	0.1	0.1	0.2	0.1	0.2	0.2

Sample	CBC87-146	L86-59	CBC87-161	CBC87-94	CBC87-130A	CBC87-110	CBC87-64	CBC87-49	CBC87-98
Rock type	Kgd	Kgd	Kgd	Kgd	Kgd	Kgd	Kgd	Kgd	Kgd
Quartz	32	31	30.6	30.6	31.7	30.7	33.7	29.8	32.6
Orthoclase	15.7	9.3	17.7	15	19.9	18.3	24.9	18.8	13.3
Albite	35.8	41.5	36.1	39.3	34.4	37.4	26.9	39.6	39.2
Anorthite	10.7	7.2	8.5	8.9	8	6.7	8.9	6.1	8.5
Hornblende	0	0	0	0	0	0	0	0	0
Biotite	5.1	3.8	3.8	3.8	4.6	3.4	4.3	2.9	3.9
Muscovite	0	6.7	2.8	1.9	0.8	3.2	0.8	2.6	2.1
Magnetite	0	0	0	0	0	0	0	0	0
Haematite	0.2	0.2	0.2	0.2	0.2	0.2	0.2	0.2	0.2
Ilmenite	0.2	0	0.1	0	0.1	0	0.2	0	0
Apatite	0.2	0.4	0.1	0.1	0.2	0.1	0.1	0.1	0.1

Sample	L86-43	CBC87-76	L86-39	CBC87-129	CBC87-123B	CBC87-70	CBC87-108B	CBC87-45	CBC87-120
Rock type	Kgd	Kgd	Kgd	Kgd	Kgd	Kgd	Kgd	Kgd	Kgd
Quartz	36.5	35.4	35.2	35.2	31.4	35.5	32.2	35.5	42.3
Orthoclase	18.6	17.6	19.4	17.5	15.2	15.6	26.4	23.8	12.2
Albite	26.6	30.3	30	31.2	42.5	33.6	31.8	30.3	23.6
Anorthite	8.4	10.3	7.4	7.4	6.7	7.5	5.7	5.3	8.4
Hornblende	0	0	0	0	0.2	0	0	0	0
Biotite	4.5	4.6	4.6	4.5	3.7	3.2	1.2	4.6	4.5
Muscovite	4.5	1.3	2.6	3.7	0	4.3	2.6	0	8.4
Magnetite	0	0	0	0	0	0	0	0	0
Haematite	0.3	0.2	0.3	0.2	0.1	0.2	0.1	0.3	0.2
Ilmenite	0.2	0.1	0.2	0.1	0.1	0	0	0.1	0.1
Apatite	0.4	0.1	0.3	0.2	0.1	0	0	0.1	0.2

Sample	CBC87-84	CBC87-60	CBC87-144	L86-42	86RL-309	86RL-387	CBC87-39	CBC87-157	CBC87-69
Rock type	Kgd	Kgd	Kgdh	Kgdh	Kgdh	Kgdh	Kgdh	Kgdh	Kgdh
Quartz	32.5	37.1	24.1	26.1	28.1	30.5	28.1	30.7	34.4
Orthoclase	20.8	25.1	10.4	6.8	5.5	7.8	12.8	13	15.1
Albite	38.4	28.5	27.5	28.9	31.2	28.4	27.7	28.9	30.9
Anorthite	4.3	5.7	18.6	20.2	17.7	17.1	16.5	14.5	12.3
Hornblende	0	0	3	0	0.4	0	4.1	0	0
Biotite	2.4	3	15	16.1	15.3	14.4	9.7	12.1	6.6
Muscovite	1.4	0.3	0	0	0	0	0	0	0
Magnetite	0	0	0.2	0	0	0	0.1	0.2	0
Haematite	0.2	0.2	0.3	0.5	0.5	0.5	0.3	0.2	0.3
Ilmenite	0	0	0.4	0.4	0.4	0.4	0.3	0.1	0.2
Apatite	0.1	0	0.6	0.9	0.9	0.9	0.4	0.4	0.2

Sample	CBC87-155	CBC87-150	CBC87-159	CBC87-149	CBC87-152	CBC87-62	CBC87-148	CBC87-50	CBC87-151
Rock type	Kgdp	Kgdp	Kgdp	Kgdp	Kgdp	Kgdp	Kgdp	Kgdp	Kgdp
Quartz	28	27.4	28.9	27.8	24.2	27.9	32.6	30.1	35.7
Orthoclase	10.2	12.8	18.2	16.5	8.2	17.9	16.4	13.9	17.6
Albite	27.1	30.9	25	30.1	46.9	38.2	30.6	40.1	26.1
Anorthite	19.9	14.4	12.3	13.9	11	8.9	10.6	9.4	11
Hornblende	0.4	2.8	4.4	3.4	0	0	0	0	0.7
Biotite	13	10.1	10.3	7.1	.5.9	4.9	8.9	4.3	7.9
Muscovite	0	0	0	0	3.2	1.7	0	1.7	0
Magnetite	0	0	0.2	0	0	0	0	0	0
Haematite	0.5	0.4	0.1	0.3	0.3	0.3	0.3	0.2	0.3
Ilmenite	0.5	0.6	0.4	0.5	0.1	0.1	0.2	0.1	0.3
Apatite	0.5	0.6	0.4	0.4	0.2	0.2	0.4	0.1	0.4

Sample	CBC87-68	CBC87-115	CBC87-36	CBC87-143*	CBC87-89	L8644	L8660	CBC87-72	CBC87-118
Rock type	Kgdp	Klg	Klg	Klg	Klg	Klg	Klg	Klg	Klg
Quartz	33.2	21.2	25.6	32.1	27.9	33.3	30.9	32.5	41.3
Orthoclase	13.4	31.7	14.1	15	20.3	26.1	21	16.4	13.1
Albite	36.8	35	45.8	34.3	43.5	28.5	38.7	39	24.8
Anorthite	8.5	6.5	9.5	10.2	5.2	5.6	4.5	1.7	3.9
Hornblende	0	0	0	0	0	0	0	0	0
Biotite	3.5	3.7	4	5.6	1.7	1.8	1.6	1.8	4.2
Muscovite	4.3	1.5	0.8	2.2	1.2	4.4	2.9	8.4	12.3
Magnetite	0	0	0	0	0	0	0	0	0
Haematite	0.1	0.2	0.1	0.3	0.1	0.1	0.1	0.1	0.2
Ilmenite	0.1	0.1	0	0.2	0	0.1	0	0	0.1
Apatite	0.1	0.1	0.1	0.2	0	0.2	0.3	0.1	0.2

Sample	CBC87-117	86RL-386	CBC87-42	CBC87-148B	CBC87-88	CBC87-82	CBC87-41	CBC87-145	CBC87-61
Rock type	Klg	Klg	Klg	Klg	Klg	Klg	Klg	Kt	Kt
Quartz	35.9	35.2	33.7	34.5	34.9	37	38.2	14	16.9
Orthoclase	19.3	24.8	27.4	29	34.3	20.2	20.6	1.4	0
Albite	33.8	31.4	30.9	28.5	22.5	31.8	31.9	18.1	32
Anorthite	6.5	2.1	2.7	2	5.3	3.3	4.6	41	27
Hornblende	0	0	0	0	0	0	0	9.2	4.5
Biotite	3.3	3.2	1.9	2.5	1.1	1.7	1.7	13.9	13.6
Muscovite	0.7	2.6	3.2	3.3	1.9	5.7	2.7	0	0
Magnetite	0	0	0	0	0	0	0	2	5.1
Haematite	0.2	0.2	0.1	0.2	0	0.1	0.1	0	0
Ilmenite	0.1	0.1	0	0	0	0	0	0	0.3
Apatite	0.1	0.4	0.1	0	0	0	0	0.3	0.5

Sample	CBC87-54	CBC87-55	CBC87-75	CBC87-51	CBC87-40	L86-32	CBC87-90	L86-33	CBC87-132
Rock type	Kt	Kt	Kt	Kt	Kt	Tg	Tg	Tg	Tg
Quartz	23.6	24.9	26.7	24.8	24.3	24.6	29.7	28.1	30.8
Orthoclase	1.4	1.3	0	3.2	3.5	30.6	26.4	27.4	18.1
Albite	26.8	26.3	27.7	32.4	32.8	30.4	29.6	30.8	34.9
Anorthite	23.6	23.2	25.6	21.4	20.5	6.8	4.8	4.3	8
Hornblende	5	5	0	0.1	3.4	0	0	0	0
Biotite	18.1	17.7	18.3	16.5	14.3	6.6	7.2	5.9	6
Muscovite	0	0	0	0	0	0	1.7	2.8	1.5
Magnetite	0.7	0.7	0.6	0	0.4	0	0	0	0
Haematite	0	0	0.2	0.5	0.2	0.4	0.4	0.3	0.3
Ilmenite	0.2	0.2	0.3	0.5	0.3	0.2	0.1	0.1	0.2
Apatite	0.6	0.6	0.6	0.7	0.5	0.4	0.2	0.3	0.2

Sample	86RL-384	86RL-338	L86-51	CBC87-34	CBC87-19	CBC87-44	CBC87-23	L86-38	86RL-257
Rock type	Tg	Tg	Tg	Tg	Tg	Tg	Tg	Tg	Tg
Quartz	31.5	33.5	29.2	33.2	33.8	34.5	34	33.8	33.9
Orthoclase	17	19.5	26.1	24.7	26.8	22.2	26.3	24.6	23
Albite	34.4	30.7	33.3	29.1	30.3	33.3	32.7	35	36.6
Anorthite	7.9	7	4.9	7.2	2.4	5.8	2.8	2.6	1.7
Hornblende	0	0	4	0	0	0	0	0	0
Biotite	5.9	7.3	1.7	5.3	4.5	3.9	3.8	3.1	2.3
Muscovite	2.5	1	0	0	1.8	0	0	0.5	2
Magnetite	0	0	0	0	0	0	0	0	0
Haematite	0.3	0.3	0.2	0.3	0.3	0.2	0.3	0.2	0.1
Ilmenite	0.2	0.2	0.3	0.1	0.1	0.1	0	0	0
Apatite	0.4	0.5	0.3	0.2	0.1	0.1	0.1	0.2	0.2

Sample	CBC87-65	L86-37	CBC87-24	CBC87-105	CBC87-102	L86-26	CBC87-162	CBC87-86	CBC87-163
Rock type	Tg	Tg	Tg	Tgd	Tgd	Tgd	Tgd	Tgd	Tgd
Quartz	35.4	35.2	35.7	10.5	13.9	15.7	20.8	25.8	25.3
Orthoclase	26.4	22.2	26.6	10.5	6.8	11.1	16.1	12.6	14.7
Albite	29.5	34.7	33.9	30.2	30.7	34.6	34.2	29.6	28.7
Anorthite	5.1	1.5	1.2	15.8	17.4	13.3	10.4	16.7	14.2
Hornblende	0	0	1.9	14	7.8	11.3	7.6	4.6	4.7
Biotite	1.1	2.6	0.5	16	20.9	11.8	9.5	9.2	11.2
Muscovite	2.4	3.4	0	0	0	0	0	0	0
Magnetite	0	0	0	0.4	0.7	0.3	0.5	0	0.6
Haematite	0.1	0.1	0.2	0.2	0.1	0.1	0	0.4	0
Ilmenite	0	0	0.1	0.9	0.5	0.7	0.3	0.6	0.2
Apatite	0	0.3	0	1.5	1.3	1	0.6	0.5	0.4

Sample	86RL-385	CBC87-103
Rock type	Tgd	Tgd
Quartz	23.1	27.5
Orthoclase	13.4	21.3
Albite	35.8	38.4
Anorthite	11.8	4.9
Hornblende	2.5	1.4
Biotite	12	5.7
Muscovite	0	0
Magnetite	0.4	0
Haematite	0.1	0.3
Ilmenite	0.1	0.2
Apatite	0.7	0.3

APPENDIX C

Thin Section Descriptions

This section contains brief descriptions of all the thin sections made during this study and gives estimated modal compositions where: Qz-quartz; Ksp-alkali feldspar; Pg-plagioclase; Bt-biotite; Hb-hornblende and An40- anorthite composition of the plagioclase in mol %.

Tonalites (Kt)

CBC87-40 Tonalite Strongly foliated, equigranular mesocratic rock with early chloritised hornblende and later near poikilitic plagioclase (An40). Mode:Qz:20%, Ksp:10%, Pg:35%, Bt:15%, Hb:20% Accessories:Epidote, zircon, apatite and opaques.

CBC87-51 Tonalite Hypidiomorphic granular rock with large euhedral sphene and associated epidote. Minor deformation produces undulose extinction in quartz and distortion of plagioclase twins. Mode:Qz:25%, Pg:45%, Bt:15%, Sphene:15% Accessories:Epidote, apatite and opaques.

CBC87-55 Tonalite Coarse-grain, hypidiomorphic, inequigranular freshly preserved rock except rarely chloritised hornblende. Plagioclase (An35). Mode:Qz:25%, Pg:50%, Bt:10%, Hb:15% Accessories:Epidote, zircon, apatite and opaques.

CBC87-61 Tonalite Gneissic foliated mesocratic rock with layers of hornblende with biotite; and plagioclase (An35)with quartz. Mode:Qz:20%, Pg:40%, Bt:20%, Hb:20% Accessories:Epidote, zircon, apatite and opaques.

CBC87-75 Tonalite Foliated, fresh mesocratic rock with interlocking texture. Plagioclase appears late and is subhedral (An40). Mode:Qz:20%, Pg:50%, Bt:20%, Hb:10% Accessories:Epidote, zircon, apatite and opaques.

CBC87-145 Tonalite Coarse grain, granular, melanocratic rock with euhedral, zoned plagioclase phenocrysts (cores An55, rims An 35). Mode:Qz:5%, Ksp:10%, Pg:35%, Bt:15%, Hb:20% Accessories:Epidote, zircon, apatite, allanite and opaques.

Hornblende-biotite granodiorites (Kgdh)

CBC87-39 Hornblende-biotite granodiorite Coarse grain, equigranular, hypidiomorphic rock with rare, zoned plagioclase phenocrysts (cores An38, rims An 35). Hornblende altered to chlorite, epidote and opaques. Mode:Qz:20%, Ksp:20%, Pg:40%, Bt:10%, Hb:10% Accessories:Epidote, zircon, apatite, chlorite and opaques.

CBC87-144 Hornblende-biotite granodiorite Medium grain, hypidiomorphic rock with euhedral plagioclase phenocrysts (An35-40). Hornblende altered to chlorite, epidote and opaques. Mode:Qz:25%, Ksp:10%, Pg:45%, Bt:10%, Hb:10% Accessories:Epidote, zircon, allanite, apatite, chlorite and opaques.

CBC87-144 Hornblende-biotite granodiorite Medium grain, hypidiomorphic rock with euhedral plagioclase phenocrysts (An35-40). Hornblende altered to chlorite,

epidote and opaques. Mode:Qz:25%, Ksp:10%, Pg:45%, Bt:10%, Hb:10% Accessories:Epidote, zircon, allanite, apatite, chlorite and opaques.

L86-42 Hornblende-biotite granodiorite Coarse grain, granular unfoliated rock with unzoned plagioclase (An36). Hornblende altered to chlorite, epidote and opaques and sphene oxidised. Mode:Qz:20%, Ksp:15%, Pg:45%, Bt:10%, Hb:10% Accessories:Sphene, zircon, apatite, epidote and opaques.

86RL-309 Hornblende-biotite granodiorite Coarse grain, equigranular unfoliated rock with euhedral plagioclase (An34). Hornblende altered and sphene coarse grained and euhedral. Mode:Qz:20%, Ksp:20%, Pg:40%, Bt:10%, Hb:10% Accessories:Sphene, zircon, apatite, epidote and opaques.

86RL-387 Hornblende-biotite granodiorite Coarse grain, equigranular unfoliated rock with plagioclase (An35). Hornblende altered and sphene coarse grained and euhedral. Mode:Qz:20%, Ksp:20%, Pg:40%, Bt:10%, Hb:10% Accessories:Sphene, zircon, apatite, allanite and opaques.

86RL-387 Hornblende-biotite granodiorite Coarse grain, equigranular unfoliated rock with plagioclase (An35). Hornblende altered and sphene coarse grained and euhedral. Mode:Qz:20%, Ksp:20%, Pg:40%, Bt:10%, Hb:10% Accessories:Sphene, zircon, apatite, allanite and opaques.

Porphyritic granodiorites (Kgdp)

CBC87-62 Porphyritic granodiorite Coarse grain, inequigranular, with euhedral and poikilitic alkali feldspar megacrysts. Plagioclase (An35). . Mode:Qz:25%, Ksp:25%, Pg:35%, Bt:15% Accessories:Zircon, apatite, sphene and opaques.

CBC87-101 Porphyritic granodiorite Coarse grain, inequigranular, leucocratic rock with euhedral, white alkali feldspar megacrysts. Plagioclase (An35). . Mode:Qz:25%, Ksp:25%, Pg:35%, Bt:15% Accessories:Zircon, apatite, sphene and opaques.

CBC87-150 Porphyritic granodiorite Coarse grain, inequigranular, melanocratic rock with many euhedral and common poikilitic alkali feldspar megacrysts. Plagioclase (An37) and contains rare hornblende. Mode:Qz:20%, Ksp:30%, Pg:35%, Bt:15% Accessories:Zircon, apatite, sphene and opaques.

CBC87-152 Porphyritic granodiorite Coarse grain, inequigranular, melanoocratic rock with few euhedral and common poikilitic alkali feldspar megacrysts. Plagioclase (An35) and contains common hornblende. Mode:Qz:25%, Ksp:25%, Pg:35%, Bt:10%, Hb:5% Accessories:Zircon, apatite, allanite, sphene and opaques.

CBC87-152 Porphyritic granodiorite Coarse grain, inequigranular, melanoocratic rock with few euhedral and common poikilitic alkali feldspar megacrysts. Plagioclase (An35) and contains common but altered hornblende. Mode:Qz:25%, Ksp:25%, Pg:35%, Bt:10%, Hb:5% Accessories:Zircon, apatite, allanite, sphene and opaques.

L86-41 Porphyritic granodiorite Coarse grain, inequigranular, mesocratic rock with few euhedral and common poikilitic alkali feldspar megacrysts. Plagioclase (An30). Mode:Qz:25%, Ksp:30%, Pg:35%, Bt:10% Accessories:Zircon, apatite, sphene and opaques.

L86-45 Porphyritic granodiorite Coarse grain, inequigranular, mesocratic rock with few euhedral and common poikilitic alkali feldspar megacrysts with inclusions and resorbed margins. Plagioclase (An33). Mode:Qz:25%, Ksp:30%, Pg:35%, Bt:10% Accessories:Zircon, apatite, sphene and opaques.

L86-46 Porphyritic granodiorite Coarse grain, inequigranular, mesocratic rock with few euhedral and common poikilitic alkali feldspar megacrysts with inclusions and resorbed margins. Plagioclase (An33) and large areas of free quartz. Mode:Qz:0%, Ksp:30%, Pg:30%, Bt:10% Accessories:Zircon, apatite, sphene and opaques.

Biotite granodiorites (Kgd)

CBC87-57 Biotite granodiorite Medium-coarse grain, equigranular-porphyritic, mesocratic rock with plagioclase (An25) and contains rare and altered hornblende and muscovite. Mode:Qz:30%, Ksp:25%, Pg:35%, Bt:10%, Accessories:Zircon, apatite, allanite, sphene, monazite and opaques.

CBC87-60 Biotite granodiorite Medium grain, equigranular, mesocratic rock with plagioclase (An20). Mode:Qz:30%, Ksp:20%, Pg:4%, Bt:10%, Accessories:Zircon, apatite, sphene and opaques.

CBC87-81 Biotite granodiorite Coarse grain, hypidiomorphic granular leucocratic rock with plagioclase (An25) and contains rare edidote and chlorite as alteration products. Mode:Qz:30%, Ksp:25%, Pg:35%, Bt:10%, Accessories:Apatite, allanite, sphene, and opaques.

CBC87-94 Biotite granodiorite Coarse grain, equigranular-porphyritic, mesocratic rock with plagioclase (An20) and contains rare orthoclase megacrysts. Mode:Qz:30%, Ksp30%, Pg:30%, Bt:10%, Accessories:Zircon, apatite, sphene,and opaques.

CBC87-106 Biotite granodiorite Medium grain, equigranular, leucocratic rock with plagioclase (An20) and contains rare chlorite after biotite and minor sericitization. Mode:Qz:25%, Ksp:30%, Pg:35%, Bt:10%, Accessories:Zircon, apatite, sphene, monazite and opaques.

CBC87-119 Biotite granodiorite Coarse grain, equigranular, leucocratic rock with plagioclase (An25) and contains rare muscovite and is weakly sericitized. Mode:Qz:30%, Ksp:25%, Pg:35%, Bt:10%, Accessories:Zircon, apatite, sphene,and opaques.

CBC87-124 Biotite granodiorite Medium grain, hypidiomorphic granular, mesocratic rock with plagioclase (An25) and has biotite oxidised to opaques and chlorite. Mode:Qz:30%, Ksp:30%, Pg:35%, Bt:5%, Accessories:Apatite, sphene, monazite and opaques.

CBC87-128 Biotite granodiorite Medium-grain, equigranular, mesocratic rock with plagioclase (An25) and has fresh appearance. Mode:Qz:30%, Ksp:30%, Pg:30%, Bt:10%, Accessories:Zircon, apatite,, sphene, and opaques.

CBC87-134 Biotite granodiorite Coarse grain, equigranular, leucocratic rock with plagioclase (An28). Mode:Qz:30%, Ksp:20%, Pg:40%, Bt:10%, Accessories:Zircon, apatite, sphene and opaques.

CBC87-143 Biotite granodiorite Coarse grain, equigranular rock containing plagioclase (An20) with sericitized cores and minor hornblende. Mode:Qz:25%, Ksp:20%, Pg:40%, Bt:15%, Accessories:Zircon, apatite, sphene and opaques.

CBC87-146 Biotite granodiorite Coarse grain, equigranular rock containing zoned plagioclase (An20-An25) with sericitized cores and granophyric textures. Mode:Qz:30%, Ksp:30%, Pg:30%, Bt:10%, Accessories:Zircon, apatite, sphene and opaques.

CBC87-147 Biotite granodiorite Coarse grain, porphyritic rock containing large euhedral biotite and plagioclase (An25) with sericitized cores and concentric inclusions of apatite. Mode:Qz:20%, Ksp:20%, Pg:40%, Bt:20%, Accessories:Zircon, apatite, sphene and opaques.

CBC87-158 Biotite granodiorite Coarse grain, equigranular, leucocratic rock with early euhedral plagioclase zoned from (An28-An35) and contains common chlorite and rare muscovite. Mode:Qz:30%, Ksp:30%, Pg:30%, Bt:10%, Accessories:Apatite, sphene and opaques.

L86-20 Biotite granodiorite Medium grain, equigranular leucocratic rock with plagioclase (An25) and contains rare muscovite. Mode:Qz:30%, Ksp:25%, Pg:35%, Bt:10%, Accessories:Zircon, apatite, sphene and opaques.

L86-30 Biotite granodiorite Coarse grain, hypidiomorphic granular leucocratic rock with plagioclase (An20). Mode:Qz:30%, Ksp:25%, Pg:35%, Bt:10%, Accessories:Zircon, apatite, allanite, sphene and opaques.

L86-30A Biotite granodiorite Medium-fine grain, equigranular melanocratic inclusion with plagioclase (An40) and biotite. Mode:Pg:60%, Bt:40%, Accessories:Sphene and opaques.

L86-39 Biotite granodiorite Coarse grain, equigranular leucocratic rock with plagioclase (An20) and contains rare chlorite and muscovite as alteration products. Mode:Qz:30%, Ksp:30%, Pg:30%, Bt:10%, Accessories:Zircon, apatite, allanite, sphene and opaques.

L86-59 Biotite granodiorite Medium grain, equigranular, leucocratic rock with zoned plagioclase (An25-An20) and contains rare muscovite. Mode:Qz:40%, Ksp:25%, Pg:30%, Bt:5%, Accessories:Zircon, apatite, allanite, sphene, monazite and opaques.

86RL-219 Biotite granodiorite Medium-coarse grain, equigranular-porphyritic, mesocratic rock with euhedral plagioclase (An25) and contains rare and altered hornblende. Mode:Qz:30%, Ksp:25%, Pg:35%, Bt:10%, Accessories:Apatite, sphene and opaques.

86RL-249 Biotite granodiorite Coarse grain, equigranular-porphyritic, mesocratic rock with euhedral plagioclase (An25) and contains rare and altered hornblende. Mode:Qz:30%, Ksp:25%, Pg:35%, Bt:10%, Accessories:Apatite, sphene and opaques.

Muscovite-biotite granodiorite (Kg)

CBC87-48 Muscovite-biotite granite Coarse grain, equigranular, leucocratic rock with sericitized plagioclase (An25), biotite is chloritised and muscovite both primary and secondary. Mode:Qz:35%, Ksp:30%, Pg:25%, Bt:5%, Mu:5% Accessories:Zircon, apatite, allanite and monazite.

CBC87-53 Muscovite-biotite granite Coarse grain, poikilitic alkali feldspar, leucocratic rock with sericitized plagioclase (An25), biotite is chloritised and primary muscovite present. Mode:Qz:35%, Ksp:30%, Pg:25%, Bt:5%, Mu:5% Accessories:Apatite.

CBC87-66 Muscovite-biotite granite Medium grain, equigranular, leucocratic rock with granophyric alkali feldspar. Biotite is chloritised, muscovite both primary and secondary and quartz has undulose extinction and concertal grain boundaries. Mode:Qz:30%, Ksp:30%, Pg:30%, Bt:7%, Mu:3% Accessories:Zircon, apatite and opaques.

CBC87-73 Muscovite-biotite granite Coarse grain, porphyritic leucocratic rock containing euhedral alkali feldspar megacrysts, with sericitized and zoned plagioclase (An25-An20) and undulose quartz. Mode:Qz:30%, Ksp:35%, Pg:25%, Bt:5%, Mu:5% Accessories:Zircon and apatite.

CBC87-77 Muscovite-biotite granite Coarse grain, hypidiomorphic granular, leucocratic rock with fresh appearance. Plagioclase (An20) is subhedral with biotite and muscovite primary. Mode:Qz:35%, Ksp:30%, Pg:25%, Bt:5%, Mu:5% Accessories:Apatite, allanite and monazite.

CBC87-78 Muscovite-biotite granite Coarse grain, equigranular, leucocratic rock with plagioclase (An20) and poikilitic alkali feldspar. Biotite is chloritised, muscovite is both primary and secondary and quartz intercertal. Mode:Qz:35%, Ksp:30%, Pg:25%, Bt:5%, Mu:5% Accessories:Zircon, apatite, allanite and monazite.

Leucogranites (Klg)

CBC87-36 Leucogranite Fine to medium grain, equigranular, leucocratic rock with anhedral interlocking texture. Feldspars are sericitized, biotite is chloritised, and rare muscovite is secondary and quartz intercertal. Mode:Qz:35%, Ksp:35%, Pg:25%, Mu:5% Accessories:Zircon, epidote, apatite, sphene and opaques.

CBC87-42 Leucogranite Fine to medium grain, allotriomorphic, leucocratic rock with anhedral interlocking texture. Feldspars are sericitized, rare muscovite is secondary, quartz intercertal and small (0.5mm), subhedral red garnet grains are present. Mode:Qz:35%, Ksp:35%, Pg:30% Accessories:Zircon and garnet.

CBC87-161 Leucogranite Fine to medium grain, equigranular, leucocratic rock with anhedral interlocking texture. Feldspars are sericitized, biotite is chloritised and completely replaced by muscovite and opaques. Mode:Qz:35%, Ksp:35%, Pg:30% Accessories:Zircon, chlorite, apatite, muscovite and opaques.

L86-40 Leucogranite Fine to medium grain, equigranular, leucocratic rock with anhedral interlocking texture. Feldspars are sericitized, biotite is chloritised, and rare muscovite is secondary and quartz intercertal. Mode:Qz:35%, Ksp:35%, Pg:25%, Mu:5% Accessories:Zircon, epidote, apatite, sphene and opaques.

L86-43 Leucogranite Fine grain, equigranular, leucocratic rock with anhedral interlocking texture. Feldspars are sericitized, muscovite is secondary, quartz is intercertal and rare garnet grains. Mode:Qz:40%, Ksp:35%, Pg:25% Accessories:Zircon, apatite, sphene and opaques.

L86-44 Leucogranite Fine to medium grain, equigranular, leucocratic rock with anhedral interlocking texture. Feldspars are sericitized, biotite is chloritised, and rare muscovite is secondary and quartz intercertal. Mode:Qz:35%, Ksp:35%, Pg:25%, Mu:5% Accessories:Zircon, epidote, apatite, sphene and opaques.

L86-60 Leucogranite Fine to medium grain, equigranular, leucocratic rock with anhedral interlocking texture. Feldspars are sericitized, biotite is chloritised, and rare muscovite is secondary and quartz intercertal. Mode:Qz:35%, Ksp:35%, Pg:25%, Mu:5% Accessories:Garnet, apatite and zircon.

L86-61 Pegmatite Megacrysts of perthitic microcline, quartz and rarer biotite in a vein cutting above rock. Mode:Qz:25%, Ksp:70%, Bt:5% Accessories:

86RL-386 Leucogranite Fine to medium grain, equigranular, leucocratic rock with anhedral interlocking texture. Feldspars are sericitized, biotite is absent, and rare muscovite is secondary, quartz is intercertal and garnet present. Mode:Qz:35%, Ksp:35%, Pg:25%, Mu:5% Accessories:Zircon, garnet, apatite, sphene and opaques.

Tertiary Dioritic Suite (Tgd)

CBC87-86 Dioritic suite (quartz-monzodiorite) Coarse-medium grain, seriate to porphyritic, melanocratic rock with euhedral, complex zoned plagioclase phenocrysts (cores An35, rims An 30) and subhedral hornblende and biotite grains with quartz and alkali feldspar subordinate and interstitial. Mode:Qz:25%, Ksp:20%, Pg:35%, Bt:10%, Hb:10% Accessories:Sphene, epidote, apatite and opaques.

CBC87-102 Dioritic suite (quartz-monzodiorite) Coarse grain, seriate to porphyritic, melanocratic rock with euhedral, plagioclase (An 35), hornblende and biotite ophitically in alkali feldspar and altered cores of clinopyroxene. Mode:Qz:5%, Ksp:25%, Pg:25%, Bt:20%, Hb:25% Accessories:Sphene, epidote, apatite and opaques.

CBC87-103 Dioritic suite (quartz-monzodiorite) Coarse grain, porphyritic, melanocratic rock with euhedral, zoned plagioclase (An 30), hornblende and biotite ophitically in alkali feldspar and altered cores of clinopyroxene. Mode:Qz:15%, Ksp:20%, Pg:35%, Bt:10%, Hb:20% Accessories:Sphene, epidote, zircon, apatite and opaques.

CBC87-105 Dioritic suite (quartz-monzodiorite) Coarse grain, porphyritic, melanocratic rock with euhedral and subophitic plagioclase phenocrysts (cores

An40, rims An 35) and subhedral hornblende and biotite grains with quartz and alkali feldspar subordinate and interstitial. Mode:Qz:5%, Ksp:10%, Pg:50%, Bt:15%, Hb:20% Accessories:Sphene, epidote, apatite and opaques.

CBC87-162 Dioritic suite (quartz-monzodiorite) Coarse-medium grain, hypidiomorphic granular, mesocratic rock with euhedral, complex zoned plagioclase phenocrysts (cores An35, rims An 30) and subhedral hornblende and biotite grains with quartz and alkali feldspar subordinate and interstitial. Mode:Qz:25%, Ksp:30%, Pg:30%, Bt:5%, Hb:10% Accessories:Sphene, apatite and opaques.

CBC87-163 Dioritic suite (quartz-monzodiorite) Coarse grain, hypidiomorphic granular, mesocratic rock with euhedral, complex zoned plagioclase phenocrysts (cores An45, rims An 35) and subhedral hornblende and altered biotite grains with quartz and alkali feldspar subordinate and interstitial. Mode:Qz:20%, Ksp:5%, Pg:55%, Bt:10%, Hb:10% Accessories:Sphene, apatite and opaques.

L86-26 Dioritic suite (quartz-monzodiorite) Coarse grain, seriate to porphyritic, melanocratic rock with euhedral, plagioclase (An 35), hornblende and biotite ophitically in alkali feldspar and altered cores of clinopyroxene. Mode:Qz:25%, Ksp:20%, Pg:35%, Bt:10%, Hb:10% Accessories:Sphene, epidote, apatite and opaques.

86RL-339 Dioritic suite (quartz-monzodiorite) Coarse-medium grain, seriate to porphyritic, melanocratic rock with euhedral, complexley zoned plagioclase phenocrysts (cores An35, rims An 30) and subhedral hornblende and biotite grains with quartz and alkali feldspar subordinate and interstitial. Mode:Qz:15%, Ksp:20%, Pg:35%, Bt:10%, Hb:20% Accessories:Sphene, epidote, apatite and opaques.

86RL-385 Dioritic suite (quartz-monzodiorite) Coarse grain, hypidiomorphic granular, mesocratic rock with euhedral, complex zoned plagioclase phenocrysts (cores An45, rims An 35) and subhedral hornblende and altered biotite grains with quartz and alkali feldspar subordinate and interstitial. Mode:Qz:20%, Ksp:5%, Pg:55%, Bt:10%, Hb:10% Accessories:Sphene, apatite and opaques.

86RL-388 Dioritic suite (quartz-monzodiorite) Coarse grain, porphyritic, melanocratic rock with euhedral and subophitic plagioclase phenocrysts (cores An40, rims An 35) and subhedral hornblende and biotite grains with quartz and alkali feldspar subordinate and interstitial. Mode:Qz:25%, Ksp:20%, Pg:35%, Bt:10%, Hb:10% Accessories:Sphene, epidote, apatite and opaques.

Tertiary Granitic Suite (Tg)

CBC87-23 Granitic suite Coarse grain, hypidiomorphic granular, leucocratic rock with antiperthitic plagioclase (An20) and dominant perthitic alkali feldspar. Biotite and rare hornblende chloritised and quartz is coarse grain, but intercertal. Mode:Qz:35%, Ksp:40%, Pg:15%, Bt:5%, Hb:5% Accessories:Zircon, allanite, apatite and opaques.

CBC87-132 Granitic suite Coarse grain, hypidiomorphic granular, leucocratic rock with plagioclase (An20) sericitized and megacrysts of perthitic alkali feldspar. Biotite and rare hornblende chloritised and quartz intercertal. Mode:Qz:35%, Ksp:40%, Pg:20%, Bt:5% Accessories:Zircon, allanite, apatite and opaques.

L86-32 Granitic suite Coarse grain, hypidiomorphic granular, leucocratic rock with subhedral plagioclase (An20) and dominant perthitic alkali feldspar and quartz. Biotite chloritised and quartz is intercertal. Mode:Qz:35%, Ksp:40%, Pg:20%, Bt:5% Accessories:Zircon, allanite, apatite and opaques.

L86-33 Granitic suite Coarse grain, hypidiomorphic granular, leucocratic rock with plagioclase (An20) and perthitic alkali feldspar. Biotite and rare hornblende chloritised and quartz is intercertal. Mode:Qz:30%, Ksp:45%, Pg:15%, Bt:5%, Hb:5% Accessories:Zircon, allanite, apatite and opaques.

L86-37 Granitic suite Coarse grain, hypidiomorphic granular, leucocratic rock with dominant perthitic alkali feldspar, subhedral plagioclase (An20) and biotite (often chloritised). Quartz is late, coarse grain, but intercertal. Mode:Qz:35%, Ksp:35%, Pg:25%, Bt:5% Accessories:Zircon, allanite, monazite, apatite and opaques.

L86-38 Granitic suite Coarse grain, hypidiomorphic granular, leucocratic rock with dominant perthitic alkali feldspar, subhedral plagioclase (An20) and biotite (often chloritised). Quartz is late, coarse grain, but intercertal. Mode:Qz:35%, Ksp:35%, Pg:25%, Bt:5% Accessories:Zircon, allanite, monazite, apatite and opaques.

L86-51 Granitic suite Fine grain, sugary, leucocratic rock with subhedral plagioclase (An20), dominant perthitic alkali feldspar and quartz. Biotite is rare. Mode:Qz:35%, Ksp:45%, Pg:20%, Bt:<1% Accessories:Apatite and opaques.

86RL-257 Granitic suite Medium grain, hypidiomorphic granular, leucocratic rock with dominant perthitic alkali feldspar, plagioclase (An20) and intercertal quartz. Biotite and rare hornblende are chloritised. Mode:Qz:35%, Ksp:40%, Pg:15%, Bt:5%, Hb:5% Accessories:Zircon, apatite and opaques.

86RL-384 Granitic suite Coarse grain, hypidiomorphic granular, leucocratic rock with subhedral plagioclase (An15) and dominant perthitic alkali feldspar. Quartz is coarse grain and intercertal and biotite unusually fresh. Mode:Qz:35%, Ksp:40%, Pg:20%, Bt:5% Accessories:Zircon, sphene, apatite and opaques.

86RL-388 Granitic suite Coarse grain, granular, leucocratic rock with plagioclase (An20) and dominant perthitic alkali feldspar. Biotite and rare hornblende chloritised and quartz is coarse grain, but intercertal. Mode:Qz:35%, Ksp:40%, Pg:15%, Bt:5%, Hb:5% Accessories:Zircon, apatite and opaques.

APPENDIX D

Parameters and Results of Modelling

This section contains the compositions of the rocks used and the results of the major element modelling. In addition the Nd model age data, both corrected and uncorrected for Sm/Nd fractionation is listed.

D1 Major element models

D1.1 Cretaceous granitoids

i) 54-69 wt. % SiO_2

Unevolved Magma		Evolved Magma		Fractionated assemblage	Sum of square of residuals	Ratio evolved liquid to solids
CBC87-145		CBC87-157			1.99	26% : 74%
54.58	SiO_2	68.63	SiO_2	66% Plagioclase		
21.18	Al_2O_3	14.5	Al_2O_3	33.5% Hornblende		
0.59	TiO_2	0.53	TiO_2	0.5% Apatite		
4.85	Fe_2O_3	3.22	Fe_2O_3			
3.67	MgO	1.48	MgO			
9.64	CaO	3.07	CaO			
2.24	Na_2O	3.35	Na_2O			
1.72	K_2O	3.39	K_2O			
0.08	MnO	0.07	MnO			
0.14	P_2O_5	0.16	P_2O_5			

ii) 69-71 wt. % SiO_2

Unevolved Magma		Evolved Magma		Fractionated assemblage	Sum of square of residuals	Ratio evolved liquid to solids
CBC87-157		CBC87-92			1.17	65% : 35%
68.63	SiO_2	70.5	SiO_2	25% Plagioclase		
14.5	Al_2O_3	15.9	Al_2O_3	26.5% Hornblende		
0.53	TiO_2	0.12	TiO_2	12.5% Biotite		
3.22	Fe_2O_3	0.87	Fe_2O_3	33.5% Quartz		
1.48	MgO	0.1	MgO	1% Sphene		
3.07	CaO	1.65	CaO	1% Apatite		
3.35	Na_2O	5.48	Na_2O			
3.39	K_2O	3.62	K_2O			
0.07	MnO	0.05	MnO			
0.16	P_2O_5	0.03	P_2O_5			

iii) 71-76 wt. % SiO_2

Unevolved Magma		Evolved Magma		Fractionated assemblage	Sum of square of residuals	Ratio evolved liquid to solids
CBC87-92		CBC87-148B			0.02	10% : 90%
72	SiO_2	75.5	SiO_2	50% Plagioclase		
15.9	Al_2O_3	13.24	Al_2O_3	22% Alkali feldspar		
0.12	TiO_2	0.07	TiO_2	2% Biotite		
0.87	Fe_2O_3	1.12	Fe_2O_3	35% Quartz		
0.1	MgO	0.07	MgO	1% Muscovite		
1.65	CaO	0.41	CaO	<1% Apatite		
5.48	Na_2O	3.34	Na_2O			
3.62	K_2O	5.49	K_2O			
0.05	MnO	0.02	MnO			
0.03	P_2O_5	0.01	P_2O_5			

D1.1 Tertiary granitoids

i) Dioritic suite

Unevolved Magma		Evolved Magma		Fractionated assemblage	Sum of square of residuals	Ratio evolved liquid to solids
CBC87-105		CBC87-103			1.02	35% : 65%
56.23	SiO_2	71.96	SiO_2	43% Plagioclase		
16.37	Al_2O_3	13.79	Al_2O_3	39% Hornblende		
1.31	TiO_2	0.36	TiO_2	15% Biotite		
7.75	Fe_2O_3	2.22	Fe_2O_3	1.5% Sphene		
3.9	MgO	0.75	MgO	<1% Apatite		
5.76	CaO	1.34	CaO			
3.66	Na_2O	4.51	Na_2O			
3.39	K_2O	4.16	K_2O			
0.11	MnO	0.03	MnO			
0.62	P_2O_5	0.14	P_2O_5			

ii) Granitic suite

Unevolved Magma		Evolved Magma		Fractionated assemblage	Sum of square of residuals	Ratio evolved liquid to solids
L86-32		CBC87-24			1.51	62% : 38%
69.91	SiO_2	77.11	SiO_2	35% Plagioclase		
14.71	Al_2O_3	12.0	Al_2O_3	47% Alkali feldspar		
0.35	TiO_2	0.07	TiO_2	16% Biotite		
2.44	Fe_2O_3	1.11	Fe_2O_3	1% Apatite		
0.45	MgO	0.04	MgO			
1.55	CaO	0.47	CaO			
3.55	Na_2O	4.00	Na_2O			
5.77	K_2O	4.51	K_2O			
0.05	MnO	0.03	MnO			
0.15	P_2O_5	0.01	P_2O_5			

D 2 Nd model Ages

The following table lists the Nd model ages of the Cretaceous and Tertiary granitoids of the Atlanta lobe for those samples which have had both the $^{143}Nd/^{144}Nd$ isotope ratio and the Sm and Nd concentrations measured. Nd model ages are listed for the previously depleted reservoir model T_{DM}^{Nd} of Jacobsen and Wasserburg (1979) and the chondritic uniform reservoir T_{CHUR}^{Nd} of DePaolo and Wasserburg (1976).

In addition a correction has been applied to the depleted reservoir model ages to allow for the source to magma fractionation of Sm/Nd calculated from the melting models listed in section 4.9 and listed under the heading T_{DM}^{Nd} (corrected). The correction is applied assuming each rock type suite underwent a certain degree of Sm/Nd fractionation and then the modified value of Sm/Nd propagated through the Nd model age calculations.

Sample	Rock Type	T^{Nd}_{DM} (Ga)	T^{Nd}_{DM} (Ga) (corrected)	T^{Nd}_{CHUR} (Ga)
CBC87-79	Kg	1.42	1.79	1.05
86RL-219	Kgd	0.96	1.21	0.52
86RL-249	Kgd	1.07	1.41	0.61
CBC87-126	Kgd	1.02	1.06	0.61
CBC87-158	Kgd	1.09	1.39	0.67
CBC87-125	Kgd	1.13	1.40	0.73
CBC87-134	Kgd	1.19	1.47	0.80
CBC87-141	Kgd	1.13	1.40	0.73
CBC87-106	Kgd	1.33	1.76	0.93
CBC87-111	Kgd	1.32	1.66	0.92
CBC87-156	Kgd	1.19	1.61	0.74
CBC87-127	Kgd	1.10	1.37	0.69
CBC87-96	Kgd	0.91	1.15	0.45
CBC87-114	Kgd	1.30	1.63	0.90
CBC87-112	Kgd	1.36	1.75	0.97
CBC87-100	Kgd	1.25	1.64	0.83
CBC87-122	Kgd	1.15	1.43	0.75
CBC87-146	Kgd	1.08	1.38	0.64
CBC87-101	Kgd	1.39	1.81	0.99
CBC87-57	Kgd	1.12	1.40	0.71
CBC87-128	Kgd	1.05	1.36	0.59
CBC87-94	Kgd	1.24	1.63	0.82
CBC87-110	Kgd	1.27	1.64	0.87
CBC87-120	Kgd	0.97	1.21	0.53
L86-42	Kgdh	1.09	1.28	0.64
L86-45	Kgdh	1.08	1.38	0.65
86RL-387	Kgdh	1.18	1.42	0.73
86RL-309	Kgdh	2.17	2.71	1.85
CBC87-144	Kgdh	1.28	1.59	0.79
CBC87-149	Kgdp	0.97	1.13	0.51
CBC87-151	Kgdp	1.02	1.20	0.55
CBC87-148	Kgdp	1.18	1.45	0.68
CBC87-118	Klg	1.16	1.47	0.75
CBC87-117	Klg	1.34	1.73	0.94
L86-44	Klg	1.39	1.47	1.15
L86-60	Klg	2.71	5.07	2.41
CBC87-148B	Klg	1.18	1.54	0.69
CBC87-51	Kt	1.15	1.57	0.66
CBC87-61	Kt	1.20	1.74	0.66
CBC87-54	Kt	1.21	1.59	0.75
CBC87-75	Kt	1.38	1.80	0.96
CBC87-55	Kt	1.62	2.89	1.07
CBC87-145	Kt	1.54	2.21	1.09
CBC87-132	Tg	1.22	1.22	0.82
CBC87-19	Tg	1.34	1.34	1.02
CBC87-23	Tg	1.64	1.64	1.27
CBC87-24	Tg	1.31	1.31	-5.41
86RL-257	Tg	1.22	1.22	0.00
CBC87-163	Tgd	1.70	1.70	1.29
CBC87-162	Tgd	1.56	1.56	1.13
L86-26	Tgd	1.30	1.30	0.83
CBC87-86	Tgd	1.15	1.15	0.66
CBC87-102	Tgd	1.01	1.01	0.51
CBC87-103	Tgd	0.97	0.97	0.43
CBC87-105	Tgd	0.97	0.97	0.43